

2

DTIC FILE COPY

TECHNICAL REPORT GL-88-12



US Army Corps of Engineers

AD-A199 281

EXPERIMENTAL EVALUATION OF VARIABLES AFFECTING THE TESTING OF PAVEMENTS BY THE SPECTRAL-ANALYSIS-OF-SURFACE-WAVES METHOD

by

Dennis R. Hiltunen

Department of Civil Engineering
University of Michigan
2340 GG Brown Building
Ann Arbor, Michigan 48109

DEPARTMENT OF THE ARMY
Waterways Experiment Station, Corps of Engineers
PO Box 631, Vicksburg, Mississippi 39180-0631



August 1988

Final Report

Approved For Public Release Distribution Unlimited

DTIC
ELECTE
SEP 15 1988
S E D

Prepared for DEPARTMENT OF THE ARMY
US Army Corps of Engineers
Washington, DC 20314-1000

Monitored by Geotechnical Laboratory
US Army Engineer Waterways Experiment Station
PO Box 631, Vicksburg, Mississippi 39180-0631

88 9 14 215



**Destroy this report when no longer needed. Do not return
it to the originator.**

**The findings in this report are not to be construed as an official
Department of the Army position unless so designated
by other authorized documents.**

**The contents of this report are not to be used for
advertising, publication, or promotional purposes.
Citation of trade names does not constitute an
official endorsement or approval of the use of
such commercial products.**

Unclassified

SECURITY CLASSIFICATION OF THIS PAGE

REPORT DOCUMENTATION PAGE				Form Approved OMB No. 0704-0188	
1a. REPORT SECURITY CLASSIFICATION Unclassified		1b. RESTRICTIVE MARKINGS			
2a. SECURITY CLASSIFICATION AUTHORITY		3. DISTRIBUTION / AVAILABILITY OF REPORT Approved for public release; distribution unlimited.			
2b. DECLASSIFICATION / DOWNGRADING SCHEDULE		5. MONITORING ORGANIZATION REPORT NUMBER(S) Technical Report GL-88-12			
4. PERFORMING ORGANIZATION REPORT NUMBER(S)		7a. NAME OF MONITORING ORGANIZATION USAEWES Geotechnical Laboratory			
6a. NAME OF PERFORMING ORGANIZATION Department of Civil Engineering University of Michigan		6b. OFFICE SYMBOL (if applicable)		7b. ADDRESS (City, State, and ZIP Code) PO Box 631 Vicksburg, MS 39180-0631	
6c. ADDRESS (City, State, and ZIP Code) 2340 GG Brown Building Ann Arbor, MI 48109		9. PROCUREMENT INSTRUMENT IDENTIFICATION NUMBER See reverse			
8a. NAME OF FUNDING / SPONSORING ORGANIZATION See reverse		8b. OFFICE SYMBOL (if applicable) See reverse		10. SOURCE OF FUNDING NUMBERS	
8c. ADDRESS (City, State, and ZIP Code) See reverse		PROGRAM ELEMENT NO.	PROJECT NO.	TASK NO.	WORK UNIT ACCESSION NO.
11. TITLE (Include Security Classification) Experimental Evaluation of Variables Affecting the Testing of Pavements by the Spectral-Analysis-of-Surface-Waves Method					
12. PERSONAL AUTHOR(S) Hiltunen, Dennis R.					
13a. TYPE OF REPORT Final report		13b. TIME COVERED FROM 1985 TO 1988		14. DATE OF REPORT (Year, Month, Day) August 1988	15. PAGE COUNT 324
16. SUPPLEMENTARY NOTATION Available from National Technical Information Service, 5285 Port Royal Road, Springfield, VA 22161					
17. COSATI CODES			18. SUBJECT TERMS (Continue on reverse if necessary and identify by block number)		
FIELD	GROUP	SUB-GROUP	See reverse		
19. ABSTRACT (Continue on reverse if necessary and identify by block number) ➤ The spectral-analysis-of-surface-waves (SASW) method is a testing procedure for determining in situ stiffness profiles of multi-layered elastic systems, e.g., soil, pavements. The method is nondestructive, is performed from the surface, and requires no boreholes. Measurements are made at strain levels below 0.001 percent, where elastic properties are considered independent of strain amplitude. The key elements in SASW testing are generation and measurement of surface waves, i.e., Rayleigh waves. A number of case studies have been conducted employing the SASW method. The results have been compared with the results from crosshole tests performed independently at the same location. Generally, the shear wave velocity and modulus profiles from the two methods compare closely. The major disadvantage of the method at this time is that the testing and data reduction procedures are too time-consuming.					
(Continued)					
20. DISTRIBUTION / AVAILABILITY OF ABSTRACT <input type="checkbox"/> UNCLASSIFIED/UNLIMITED <input checked="" type="checkbox"/> SAME AS RPT. <input type="checkbox"/> DTIC USERS			21. ABSTRACT SECURITY CLASSIFICATION Unclassified		
22a. NAME OF RESPONSIBLE INDIVIDUAL			22b. TELEPHONE (Include Area Code)		22c. OFFICE SYMBOL

DD Form 1473, JUN 86

Previous editions are obsolete.

SECURITY CLASSIFICATION OF THIS PAGE
Unclassified

Unclassified

SECURITY CLASSIFICATION OF THIS PAGE

8a. NAME OF FUNDING/SPONSORING ORGANIZATION (Continued).

US Army Corps of Engineers
US Air Force Engineering and Services Center
Federal Aviation Administration

8b. OFFICE SYMBOL (Continued).

CEEC-EG
AFESC-RDCP
APM-740

8c. ADDRESS (Continued).

Washington, DC 20314-1000
Tyndall, AFB, FL 32403-6001
Washington, DC 20591

9. PROCUREMENT INSTRUMENT IDENTIFICATION NUMBER (Continued).

FAD 88080013
MIPR No. N87-27
IAA No. DTFA01-81-Y-10555

18. SUBJECT TERMS (Continued).

Elastic moduli
Inversion
Nondestructive evaluation
Pavement systems
Rayleigh wave dispersion curve

SASW
Seismic field methods
Spectral-analysis-of-surface-waves
➤ Wave propagation
Young's moduli

19. ABSTRACT (Continued).

The purpose of this research was to further the development of the SASW method toward a practical technique for in situ investigation of pavement systems. It is envisioned that eventually an automated testing procedure will be developed to enable one to quickly collect the necessary field data. It was felt that the development of a multiple transducer testing procedure was an important step towards the development of an automated testing method. In particular, this research examined the influence of source and receiver geometry, source-to-near-receiver distance, and source type in the context of a multiple transducer testing procedure at two asphaltic concrete pavement sites.

The first major conclusion of the research was that the test results are independent of the source and receiver geometry. Second, the source-to-near-receiver distance is critical to obtaining good data during SASW testing. It was found that the ratio of the source-to-near-receiver distance to the receiver spacing should be less than or equal to two for best results. Third, phase velocity measurements are independent of source-to-near-receiver distance if wavelengths larger than twice the receiver spacing are filtered from the data. Fourth, two sources, one comparable to a 4 oz. ball peen hammer, the other similar to an 8 lb sledge hammer, are sufficient for defining the dispersion curve. The implication of these findings is that the common receivers midpoint (CRMP) geometry currently used in SASW testing is not appropriate for a multiple transducer configuration. A common source (CS) geometry is recommended.

Unclassified

SECURITY CLASSIFICATION OF THIS PAGE

PREFACE

The work reported herein was performed for the US Army Engineer Waterways Experiment Station (WES) under Intergovernmental Personnel Act 85-30-M with the University of Michigan during the period 1 July 1985 to 30 June 1988. The work was jointly funded by the Office, Chief of Engineers, US Army, US Air Force Engineering and Services Center, and the Federal Aviation Administration. The work was conducted and report prepared by Dr. Dennis R. Hiltunen as partial fulfillment of the requirements for the degree of Doctor of Philosophy (Civil Engineering), University of Michigan.

Dr. A. J. Bush III and Mr. D. R. Alexander, Pavement Systems Division (PSD), Geotechnical Laboratory (GL), WES, were the Principal Investigators. The study was conducted under the general supervision of Dr. W. F. Marcuson III, Chief, GL; Messrs. H. H. Ulery, Jr., Chief, PSD, GL; J. W. Hall, Jr., Chief, Engineering Investigations, Testing, and Validation Group, PSD, GL; and R. W. Grau, Chief, Prototype Testing and Evaluation Unit, PSD, GL.

The Commander and Director of WES during the period of this study was COL Dwayne G. Lee, EN. The Technical Director was Dr. Robert W. Whalin.

Approved for	
DTIC (P&M)	<input checked="" type="checkbox"/>
DTIC (A&S)	<input type="checkbox"/>
DTIC (S&D)	<input type="checkbox"/>
DTIC (S&I)	
DTIC (S&E)	
DTIC (S&C)	
DTIC (S&B)	
DTIC (S&A)	
DTIC (S&R)	
DTIC (S&O)	
DTIC (S&N)	
DTIC (S&M)	
DTIC (S&L)	
DTIC (S&K)	
DTIC (S&J)	
DTIC (S&I)	
DTIC (S&H)	
DTIC (S&G)	
DTIC (S&F)	
DTIC (S&E)	
DTIC (S&D)	
DTIC (S&C)	
DTIC (S&B)	
DTIC (S&A)	
DTIC (S&R)	
DTIC (S&Q)	
DTIC (S&P)	
DTIC (S&O)	
DTIC (S&N)	
DTIC (S&M)	
DTIC (S&L)	
DTIC (S&K)	
DTIC (S&J)	
DTIC (S&I)	
DTIC (S&H)	
DTIC (S&G)	
DTIC (S&F)	
DTIC (S&E)	
DTIC (S&D)	
DTIC (S&C)	
DTIC (S&B)	
DTIC (S&A)	
DTIC (S&R)	
DTIC (S&Q)	
DTIC (S&P)	
DTIC (S&O)	
DTIC (S&N)	
DTIC (S&M)	
DTIC (S&L)	
DTIC (S&K)	
DTIC (S&J)	
DTIC (S&I)	
DTIC (S&H)	
DTIC (S&G)	
DTIC (S&F)	
DTIC (S&E)	
DTIC (S&D)	
DTIC (S&C)	
DTIC (S&B)	
DTIC (S&A)	
DTIC (S&R)	
DTIC (S&Q)	
DTIC (S&P)	
DTIC (S&O)	
DTIC (S&N)	
DTIC (S&M)	
DTIC (S&L)	
DTIC (S&K)	
DTIC (S&J)	
DTIC (S&I)	
DTIC (S&H)	
DTIC (S&G)	
DTIC (S&F)	
DTIC (S&E)	
DTIC (S&D)	
DTIC (S&C)	
DTIC (S&B)	
DTIC (S&A)	
DTIC (S&R)	
DTIC (S&Q)	
DTIC (S&P)	
DTIC (S&O)	
DTIC (S&N)	
DTIC (S&M)	
DTIC (S&L)	
DTIC (S&K)	
DTIC (S&J)	
DTIC (S&I)	
DTIC (S&H)	
DTIC (S&G)	
DTIC (S&F)	
DTIC (S&E)	
DTIC (S&D)	
DTIC (S&C)	
DTIC (S&B)	
DTIC (S&A)	
DTIC (S&R)	
DTIC (S&Q)	
DTIC (S&P)	
DTIC (S&O)	
DTIC (S&N)	
DTIC (S&M)	
DTIC (S&L)	
DTIC (S&K)	
DTIC (S&J)	
DTIC (S&I)	
DTIC (S&H)	
DTIC (S&G)	
DTIC (S&F)	
DTIC (S&E)	
DTIC (S&D)	
DTIC (S&C)	
DTIC (S&B)	
DTIC (S&A)	
DTIC (S&R)	
DTIC (S&Q)	
DTIC (S&P)	
DTIC (S&O)	
DTIC (S&N)	
DTIC (S&M)	
DTIC (S&L)	
DTIC (S&K)	
DTIC (S&J)	
DTIC (S&I)	
DTIC (S&H)	
DTIC (S&G)	
DTIC (S&F)	
DTIC (S&E)	
DTIC (S&D)	
DTIC (S&C)	
DTIC (S&B)	
DTIC (S&A)	
DTIC (S&R)	
DTIC (S&Q)	
DTIC (S&P)	
DTIC (S&O)	
DTIC (S&N)	
DTIC (S&M)	
DTIC (S&L)	
DTIC (S&K)	
DTIC (S&J)	
DTIC (S&I)	
DTIC (S&H)	
DTIC (S&G)	
DTIC (S&F)	
DTIC (S&E)	
DTIC (S&D)	
DTIC (S&C)	
DTIC (S&B)	
DTIC (S&A)	
DTIC (S&R)	
DTIC (S&Q)	
DTIC (S&P)	
DTIC (S&O)	
DTIC (S&N)	
DTIC (S&M)	
DTIC (S&L)	
DTIC (S&K)	
DTIC (S&J)	
DTIC (S&I)	
DTIC (S&H)	
DTIC (S&G)	
DTIC (S&F)	
DTIC (S&E)	
DTIC (S&D)	
DTIC (S&C)	
DTIC (S&B)	
DTIC (S&A)	
DTIC (S&R)	
DTIC (S&Q)	
DTIC (S&P)	
DTIC (S&O)	
DTIC (S&N)	
DTIC (S&M)	
DTIC (S&L)	
DTIC (S&K)	
DTIC (S&J)	
DTIC (S&I)	
DTIC (S&H)	
DTIC (S&G)	
DTIC (S&F)	
DTIC (S&E)	
DTIC (S&D)	
DTIC (S&C)	
DTIC (S&B)	
DTIC (S&A)	
DTIC (S&R)	
DTIC (S&Q)	
DTIC (S&P)	
DTIC (S&O)	
DTIC (S&N)	
DTIC (S&M)	
DTIC (S&L)	
DTIC (S&K)	
DTIC (S&J)	
DTIC (S&I)	
DTIC (S&H)	
DTIC (S&G)	
DTIC (S&F)	
DTIC (S&E)	
DTIC (S&D)	
DTIC (S&C)	
DTIC (S&B)	
DTIC (S&A)	
DTIC (S&R)	
DTIC (S&Q)	
DTIC (S&P)	
DTIC (S&O)	
DTIC (S&N)	
DTIC (S&M)	
DTIC (S&L)	
DTIC (S&K)	
DTIC (S&J)	
DTIC (S&I)	
DTIC (S&H)	
DTIC (S&G)	
DTIC (S&F)	
DTIC (S&E)	
DTIC (S&D)	
DTIC (S&C)	
DTIC (S&B)	
DTIC (S&A)	
DTIC (S&R)	
DTIC (S&Q)	
DTIC (S&P)	
DTIC (S&O)	
DTIC (S&N)	
DTIC (S&M)	
DTIC (S&L)	
DTIC (S&K)	
DTIC (S&J)	
DTIC (S&I)	
DTIC (S&H)	
DTIC (S&G)	
DTIC (S&F)	
DTIC (S&E)	
DTIC (S&D)	
DTIC (S&C)	
DTIC (S&B)	
DTIC (S&A)	
DTIC (S&R)	
DTIC (S&Q)	
DTIC (S&P)	
DTIC (S&O)	
DTIC (S&N)	
DTIC (S&M)	
DTIC (S&L)	
DTIC (S&K)	
DTIC (S&J)	
DTIC (S&I)	
DTIC (S&H)	
DTIC (S&G)	
DTIC (S&F)	
DTIC (S&E)	
DTIC (S&D)	
DTIC (S&C)	
DTIC (S&B)	
DTIC (S&A)	
DTIC (S&R)	
DTIC (S&Q)	
DTIC (S&P)	
DTIC (S&O)	
DTIC (S&N)	
DTIC (S&M)	
DTIC (S&L)	
DTIC (S&K)	
DTIC (S&J)	
DTIC (S&I)	
DTIC (S&H)	
DTIC (S&G)	
DTIC (S&F)	
DTIC (S&E)	
DTIC (S&D)	
DTIC (S&C)	
DTIC (S&B)	
DTIC (S&A)	
DTIC (S&R)	
DTIC (S&Q)	
DTIC (S&P)	
DTIC (S&O)	
DTIC (S&N)	
DTIC (S&M)	
DTIC (S&L)	
DTIC (S&K)	
DTIC (S&J)	
DTIC (S&I)	
DTIC (S&H)	
DTIC (S&G)	
DTIC (S&F)	
DTIC (S&E)	
DTIC (S&D)	
DTIC (S&C)	
DTIC (S&B)	
DTIC (S&A)	
DTIC (S&R)	
DTIC (S&Q)	
DTIC (S&P)	
DTIC (S&O)	
DTIC (S&N)	
DTIC (S&M)	
DTIC (S&L)	
DTIC (S&K)	
DTIC (S&J)	
DTIC (S&I)	
DTIC (S&H)	
DTIC (S&G)	
DTIC (S&F)	
DTIC (S&E)	
DTIC (S&D)	
DTIC (S&C)	
DTIC (S&B)	
DTIC (S&A)	
DTIC (S&R)	
DTIC (S&Q)	
DTIC (S&P)	
DTIC (S&O)	
DTIC (S&N)	
DTIC (S&M)	
DTIC (S&L)	
DTIC (S&K)	
DTIC (S&J)	
DTIC (S&I)	
DTIC (S&H)	
DTIC (S&G)	
DTIC (S&F)	
DTIC (S&E)	
DTIC (S&D)	
DTIC (S&C)	
DTIC (S&B)	
DTIC (S&A)	
DTIC (S&R)	
DTIC (S&Q)	
DTIC (S&P)	
DTIC (S&O)	
DTIC (S&N)	
DTIC (S&M)	
DTIC (S&L)	
DTIC (S&K)	
DTIC (S&J)	
DTIC (S&I)	
DTIC (S&H)	
DTIC (S&G)	
DTIC (S&F)	
DTIC (S&E)	
DTIC (S&D)	
DTIC (S&C)	
DTIC (S&B)	
DTIC (S&A)	
DTIC (S&R)	
DTIC (S&Q)	
DTIC (S&P)	
DTIC (S&O)	
DTIC (S&N)	
DTIC (S&M)	
DTIC (S&L)	
DTIC (S&K)	
DTIC (S&J)	
DTIC (S&I)	
DTIC (S&H)	
DTIC (S&G)	
DTIC (S&F)	
DTIC (S&E)	
DTIC (S&D)	
DTIC (S&C)	
DTIC (S&B)	
DTIC (S&A)	
DTIC (S&R)	
DTIC (S&Q)	
DTIC (S&P)	
DTIC (S&O)	
DTIC (S&N)	
DTIC (S&M)	
DTIC (S&L)	
DTIC (S&K)	
DTIC (S&J)	
DTIC (S&I)	
DTIC (S&H)	
DTIC (S&G)	
DTIC (S&F)	
DTIC (S&E)	
DTIC (S&D)	
DTIC (S&C)	
DTIC (S&B)	
DTIC (S&A)	
DTIC (S&R)	
DTIC (S&Q)	
DTIC (S&P)	
DTIC (S&O)	
DTIC (S&N)	
DTIC (S&M)	
DTIC (S&L)	
DTIC (S&K)	
DTIC (S&J)	
DTIC (S&I)	
DTIC (S&H)	
DTIC (S&G)	
DTIC (S&F)	
DTIC (S&E)	
DTIC (S&D)	
DTIC (S&C)	
DTIC (S&B)	
DTIC (S&A)	
DTIC (S&R)	
DTIC (S&Q)	
DTIC (S&P)	
DTIC (S&O)	
DTIC (S&N)	
DTIC (S&M)	
DTIC (S&L)	
DTIC (S&K)	
DTIC (S&J)	
DTIC (S&I)	
DTIC (S&H)	
DTIC (S&G)	
DTIC (S&F)	
DTIC (S&E)	
DTIC (S&D)	
DTIC (S&C)	
DTIC (S&B)	
DTIC (S&A)	
DTIC (S&R)	
DTIC (S&Q)	
DTIC (S&P)	
DTIC (S&O)	
DTIC (S&N)	
DTIC (S&M)	
DTIC (S&L)	
DTIC (S&K)	
DTIC (S&J)	
DTIC (S&I)	
DTIC (S&H)	
DTIC (S&G)	
DTIC (S&F)	
DTIC (S&E)	
DTIC (S&D)	
DTIC (S&C)	
DTIC (S&B)	
DTIC (S&A)	
DTIC (S&R)	
DTIC (S&Q)	
DTIC (S&P)	
DTIC (S&O)	
DTIC (S&N)	
DTIC (S&M)	
DTIC (S&L)	
DTIC (S&K)	
DTIC (S&J)	
DTIC (S&I)	
DTIC (S&H)	
DTIC (S&G)	
DTIC (S&F)	
DTIC (S&E)	
DTIC (S&D)	
DTIC (S&C)	
DTIC (S&B)	
DTIC (S&A)	
DTIC (S&R)	
DTIC (S&Q)	
DTIC (S&P)	
DTIC (S&O)	
DTIC (S&N)	
DTIC (S&M)	
DTIC (S&L)	
DTIC (S&K)	
DTIC (S&J)	
DTIC (S&I)	
DTIC (S&H)	
DTIC (S&G)	
DTIC (S&F)	
DTIC (S&E)	
DTIC (S&D)	
DTIC (S&C)	
DTIC (S&B)	
DTIC (S&A)	
DTIC (S&R)	

ACKNOWLEDGEMENTS

I would first like to thank the co-chairmen of my dissertation committee, Professors Egon Tons and Richard D. Woods. Professor Tons served as supervisor and academic counselor throughout my years at the University of Michigan. He also introduced me to and broadened my interest in the subject of highway engineering. For his continued support and encouragement I am grateful. Professor Woods suggested the subject for this dissertation and broadened my interest in geotechnical engineering, especially soil dynamics. For his continued technical support, advice, and encouragement throughout this work I am grateful.

I would also like to thank the remaining members of my dissertation committee:

- Professor Thorne Lay from the University of Michigan Department of Geological Sciences for his interesting and helpful discussions on forward modelling, inverse theory, and seismology in general.
- Professor Soheil Nasarian from the University of Texas at Austin for providing the computer program "INVERT" and for his continued technical support, advice, and friendship.
- Mr. James W. Hall, Jr. of the USAE Waterways Experiment Station, Vicksburg, Mississippi, for his continued support and encouragement throughout this research.

The USAE Waterways Experiment Station, Vicksburg, Mississippi, provided financial support for the author throughout this research. For this support I am grateful. I specifically wish to thank Dr. William F. Marcuson, III, Dr. Albert J. Bush, III, and Mr. Don R. Alexander for their continued interest, advice, and support.

Mr. Starr D. Kohn of Soil and Materials Engineers, Inc., Livonia, Michigan, introduced me to the staff of the USAE Waterways Experiment Station to initiate this research. He

also was instrumental in providing test sites for the research. For these and his continued friendship I am grateful.

I would like to acknowledge the continued enthusiasm and support of Professor Vincent P. Drnevich of the University of Kentucky.

I would like to thank the many fellow civil engineering students that I have had the pleasure to be associated with throughout my years at the University of Michigan, including: F. Balghunaim, D. M. Bergman, D. Y. M. Chang, T. S. Chang, D. W. Godfrey, S. Hassini, C. Hua, B. E. Jacobs, Y. A. Jawad, L. E. Katz, J. Kayser, M. Khuri, M. Maher, X. Qian, M. Razi, J. Sturman, B. Sun, T. G. Thomann, S. Vitton, and C. K. Wu. Thank you for being both my colleagues and my friends.

The University of Michigan Transportation Research Institute provided me with financial support for three semesters during my graduate studies. To this organization I am grateful.

Finally, I would like to acknowledge the Department of Civil Engineering at the University of Michigan for their continued support and encouragement.

TABLE OF CONTENTS

PREFACE	i
ACKNOWLEDGEMENTS	iii
LIST OF FIGURES	vii
LIST OF TABLES	xv
LIST OF APPENDICES	xvii
CHAPTER:	
I . INTRODUCTION	1
1.1 Background/Problem Statement	
1.2 Objectives	
1.3 Organization	
II . BACKGROUND	4
2.1 Introduction	
2.2 Wave Propagation in an Elastic Half-Space	
2.3 Factors Influencing Elastic Moduli	
2.4 Seismic Field Methods for Determining Elastic Moduli	
2.5 Pavement Overlay Design and Nondestructive Evaluation	
2.6 Digital Signal Analysis	
2.7 Excitation Techniques for Frequency Response Testing	
2.8 Summary	
III . THE SPECTRAL-ANALYSIS-OF-SURFACE-WAVES METHOD	45
3.1 Introduction	
3.2 Collection of Data in the Field	
3.3 Determination of the Rayleigh Wave Dispersion Curve	
3.4 Inversion of the Rayleigh Wave Dispersion Curve	
3.5 Summary of Case Studies	
3.6 Disadvantages	
3.7 Summary	
IV . SASW TESTING SYSTEM AND COMPUTER SOFTWARE	63
4.1 Introduction	
4.2 SASW Testing System	
4.3 Computer Software	

4.4	Summary	
V .	EXPERIMENTAL PROGRAM	70
5.1	Introduction	
5.2	Source and Receiver Geometry	
5.3	Source-to-Near-Receiver Distance	
5.4	Source Type	
5.5	Summary	
VI .	INFLUENCE OF SOURCE AND RECEIVER GEOMETRY	84
6.1	Introduction	
6.2	Test Results	
6.3	Discussion and Conclusions	
6.4	Summary	
VII .	INFLUENCE OF SOURCE-TO-NEAR-RECEIVER DISTANCE	99
7.1	Introduction	
7.2	Test Results and Discussion	
7.3	Summary	
VIII .	INFLUENCE OF SOURCE TYPE	141
8.1	Introduction	
8.2	Test Results and Discussion	
8.3	Summary	
IX .	OTHER CASE STUDIES	163
9.1	Introduction	
9.2	Tests at Beal St. Field Site	
9.3	Summary	
X .	CLOSURE	188
10.1	Summary	
10.2	Conclusions	
10.3	Recommendations for Future Research	
	APPENDICES	191
	REFERENCES	298

LIST OF FIGURES

<u>Figure</u>	
2.1 Schematic Representation of Borehole Seismic Methods (from Hoar [1982])	11
2.2 Schematic Representation of Surface Seismic Methods (from Hoar [1982])	13
2.3 Schematic of Dynaflect Device (from Nazarian [1984])	17
2.4 Schematic of Falling Weight Deflectometer (from Nazarian [1984])	18
2.5 Time and Frequency Descriptions of a Sine Wave (from Ramirez [1985])	22
2.6 Summing Frequency Domain Descriptions of Sinusoids (from Ramirez [1985])	24
2.7 Composing a Nonsinusoidal Waveform by Summing Sinusoids (from Ramirez [1985])	25
2.8 Schematic of Idealized and Actual Models of a Linear System (from Nazarian [1984])	30
2.9 Typical Time Signals from a SASW Test at a Pavement Site	31
2.10 Real and Imaginary Components of Linear Spectrum of Channel 1	32
2.11 Magnitude and Phase Components of Linear Spectrum of Channel 1	33
2.12 Auto Power Spectra of Time Signals	34
2.13 Magnitude and Phase of Cross Power Spectrum	36
2.14 Magnitude and Phase of Frequency Response Function	37
2.15 Coherence Function	39
3.1 Schematic of Experimental Arrangement for SASW Tests (after Nazarian [1984])	47
3.2 Typical Cross Power Spectrum and Coherence Function	56
3.3 Dispersion Curve Constructed from SASW Tests on a Flexible Pavement Site (from Nazarian and Stokoe [1986])	58
3.4 Shear Wave Velocity and Young's Modulus Profiles from Flexible Pavement Site (from Nazarian and Stokoe [1986])	61
5.1 Multiple Transducer Configuration Employing Four Transducers and CRMP Geometry	72

5.2	Multiple Transducer Configuration Employing Six Transducers and CRMP Geometry	73
5.3	Multiple Transducer Configuration Employing Eight Transducers and CRMP Geometry	74
5.4	Multiple Transducer Configuration Employing Five Transducers and CS Geometry	75
5.5	Common Source Geometry (from Nazarian [1984])	77
5.6	Common Receivers Midpoint Geometry (from Nazarian [1984])	77
5.7	Dispersion Curve from SASW Tests Performed Using Common Source Geometry (from Nazarian and Stokoe [1983])	78
5.8	Dispersion Curve from SASW Tests Performed Using Common Receivers Midpoint Geometry (from Nazarian and Stokoe [1983])	79
5.9	Schematic of Two-Transducer Tests Employing CRMP Geometry and Various Source-to-Near-Receiver Distances	82
6.1	Location of SEMTA Parking Lot Site	85
6.2	Location of SASW Test Arrays at SEMTA Parking Lot Site	86
6.3	Material Profile of SEMTA Parking Lot Site	87
6.4	CRMP Geometry Used at SEMTA Parking Lot Site	89
6.5	CS Geometry Used at SEMTA Parking Lot Site	89
6.6	Average Experimental Dispersion Curve for SEMTA Parking Lot Site Using CRMP Geometry (all wavelengths)	92
6.7	Average Experimental Dispersion Curve for SEMTA Parking Lot Site Using CRMP Geometry (0 to 5-ft wavelengths)	93
6.8	Average Experimental Dispersion Curve for SEMTA Parking Lot Site Using CS Geometry (all wavelengths)	94
6.9	Average Experimental Dispersion Curve for SEMTA Parking Lot Site Using CS Geometry (0 to 5-ft wavelengths)	95
6.10	Comparison of Dispersion Curves Obtained from CRMP and CS Geometries at SEMTA Parking Lot Site (all wavelengths)	96
6.11	Comparison of Dispersion Curves Obtained from CRMP and CS Geometries at SEMTA Parking Lot Site (0 to 5-ft wavelengths)	97
7.1	Location of G. G. Brown Parking Lot Site	100
7.2	Location of SASW Test Array at G. G. Brown Parking Lot Site	101
7.3	Material Profile of G. G. Brown Parking Lot Site	102
7.4	Cross Power Spectrum and Coherence Function for $X = 0.5$ ft and $S/X = 0.5$ for SEMTA Parking Lot Site	111
7.5	Cross Power Spectrum and Coherence Function for $X = 0.5$ ft and $S/X = 1.0$ for SEMTA Parking Lot Site	112
7.6	Cross Power Spectrum and Coherence Function for $X = 0.5$ ft and $S/X = 1.5$ for SEMTA Parking Lot Site	113
7.7	Cross Power Spectrum and Coherence Function for $X = 0.5$ ft and $S/X = 2.0$ for SEMTA Parking Lot Site	114

7.8	Cross Power Spectrum and Coherence Function for $X = 0.5$ ft and $S/X = 2.5$ for SEMTA Parking Lot Site	115
7.9	Cross Power Spectrum and Coherence Function for $X = 0.5$ ft and $S/X = 3.0$ for SEMTA Parking Lot Site	116
7.10	Magnitude (Absolute) of Cross Power Spectrum for $X = 0.5$ ft for SEMTA Parking Lot Site	118
7.11	Magnitude (Relative) of Cross Power Spectrum for $X = 0.5$ ft for SEMTA Parking Lot Site	119
7.12	Experimental Dispersion Curves for $X/L_R = 0.2$ for G. G. Brown Parking Lot Site	123
7.13	Experimental Dispersion Curves for $X/L_R = 0.25$ for G. G. Brown Parking Lot Site	124
7.14	Experimental Dispersion Curves for $X/L_R = 0.33$ for G. G. Brown Parking Lot Site	125
7.15	Experimental Dispersion Curves for $X/L_R = 0.4$ for G. G. Brown Parking Lot Site	126
7.16	Experimental Dispersion Curves for $X/L_R = 0.5$ for G. G. Brown Parking Lot Site	127
7.17	Experimental Dispersion Curves for $X/L_R = 0.66$ for G. G. Brown Parking Lot Site	128
7.18	Experimental Dispersion Curves for $X/L_R = 1.0$ for G. G. Brown Parking Lot Site	129
7.19	Experimental Dispersion Curves for $X/L_R = 1.33$ for G. G. Brown Parking Lot Site	130
7.20	Experimental Dispersion Curves for $X/L_R = 1.5$ for G. G. Brown Parking Lot Site	131
7.21	Experimental Dispersion Curves for $X/L_R = 1.66$ for G. G. Brown Parking Lot Site	132
7.22	Experimental Dispersion Curves for $X/L_R = 2.0$ for G. G. Brown Parking Lot Site	133
7.23	Average Experimental Dispersion Curves (Unfiltered) for G. G. Brown Parking Lot Site	136
7.24	Average Experimental Dispersion Curves (Filtered) for G. G. Brown Parking Lot Site	137
7.25	Average Experimental Dispersion Curves (Unfiltered) for SEMTA Parking Lot Site	138
7.26	Average Experimental Dispersion Curves (Filtered) for SEMTA Parking Lot Site	139
8.1	Cross Power Spectrum and Coherence Function for $X = 0.5$ ft and 4 oz Hammer for SEMTA Parking Lot Site	148
8.2	Cross Power Spectrum and Coherence Function for $X = 0.5$ ft and 8 oz Hammer for SEMTA Parking Lot Site	149
8.3	Cross Power Spectrum and Coherence Function for $X = 0.5$ ft and 16 oz Hammer for SEMTA Parking Lot Site	150
8.4	Cross Power Spectrum and Coherence Function for $X = 0.5$ ft and 40 oz Hammer for SEMTA Parking Lot Site	151

8.5	Cross Power Spectrum and Coherence Function for $X = 0.5$ ft and 128 oz Hammer for SEMTA Parking Lot Site	152
8.6	Magnitude (Absolute) of Cross Power Spectrum for $X = 0.5$ ft for SEMTA Parking Lot Site	154
8.7	Magnitude (Relative) of Cross Power Spectrum for $X = 0.5$ ft for SEMTA Parking Lot Site	155
8.8	Average Experimental Dispersion Curve for 4 oz and 128 oz Hammers for G. G. Brown Parking Lot Site (all wavelengths)	158
8.9	Average Experimental Dispersion Curve for 4 oz and 128 oz Hammers for G. G. Brown Parking Lot Site (0 to 5-ft wavelengths)	159
8.10	Average Experimental Dispersion Curve for 4 oz and 128 oz Hammers for SEMTA Parking Lot Site (all wavelengths)	160
8.11	Average Experimental Dispersion Curve for 4 oz and 128 oz Hammers for SEMTA Parking Lot Site (0 to 5-ft wavelengths)	161
9.1	Location of Beal St. Field Site	165
9.2	Location of SASW and Crosshole Test Arrays at Beal St. Field Site	166
9.3	Average Experimental Dispersion Curve for Beal St. Field Site	168
9.4	Comparison of Average Experimental and Theoretical Dispersion Curves for Beal St. Field Site (all wavelengths)	169
9.5	Comparison of Average Experimental and Theoretical Dispersion Curves for Beal St. Field Site (4- to 16-ft wavelengths)	170
9.6	Comparison of Average Experimental and Theoretical Dispersion Curves for Beal St. Field Site (10- to 25-ft wavelengths)	171
9.7	Comparison of Average Experimental and Theoretical Dispersion Curves for Beal St. Field Site (20- to 35-ft wavelengths)	172
9.8	Comparison of Average Experimental and Theoretical Dispersion Curves for Beal St. Field Site (30- to 50-ft wavelengths)	173
9.9	Comparison of Shear Wave Velocity Profiles from SASW and Crosshole (Uncorrected) Tests	176
9.10	Comparison of Shear Wave Velocity Profiles from SASW and Crosshole (Corrected) Tests	177
9.11	Comparison of Average Experimental Dispersion Curve and Theoretical Dispersion Curve Obtained from Uncorrected Crosshole Test Results (all wavelengths)	178
9.12	Comparison of Average Experimental Dispersion Curve and Theoretical Dispersion Curve Obtained from Uncorrected Crosshole Test Results (4 to 16-ft wavelengths)	179
9.13	Comparison of Average Experimental Dispersion Curve and Theoretical Dispersion Curve Obtained from Uncorrected Crosshole Test Results (10 to 25-ft wavelengths)	180
9.14	Comparison of Average Experimental Dispersion Curve and Theoretical Dispersion Curve Obtained from Uncorrected Crosshole Test Results (20 to 35-ft wavelengths)	181
9.15	Comparison of Average Experimental Dispersion Curve and Theoretical Dispersion Curve Obtained from Uncorrected Crosshole Test Results (30 to 50-ft wavelengths)	182

9.16	Comparison of Average Experimental Dispersion Curve and Theoretical Dispersion Curve Obtained from Corrected Crosshole Test Results (all wavelengths)	183
9.17	Comparison of Average Experimental Dispersion Curve and Theoretical Dispersion Curve Obtained from Corrected Crosshole Test Results (4 to 16-ft wavelengths)	184
9.18	Comparison of Average Experimental Dispersion Curve and Theoretical Dispersion Curve Obtained from Corrected Crosshole Test Results (10 to 25-ft wavelengths)	185
9.19	Comparison of Average Experimental Dispersion Curve and Theoretical Dispersion Curve Obtained from Corrected Crosshole Test Results (20 to 35-ft wavelengths)	186
9.20	Comparison of Average Experimental Dispersion Curve and Theoretical Dispersion Curve Obtained from Corrected Crosshole Test Results (30 to 50-ft wavelengths)	187
B.1	Magnitude (Absolute) of Cross Power Spectrum for $X = 0.5$ ft for G. G. Brown Parking Lot Site	203
B.2	Magnitude (Relative) of Cross Power Spectrum for $X = 0.5$ ft for G. G. Brown Parking Lot Site	204
B.3	Magnitude (Absolute) of Cross Power Spectrum for $X = 1.0$ ft for G. G. Brown Parking Lot Site	205
B.4	Magnitude (Relative) of Cross Power Spectrum for $X = 1.0$ ft for G. G. Brown Parking Lot Site	206
B.5	Magnitude (Absolute) of Cross Power Spectrum for $X = 2.0$ ft for G. G. Brown Parking Lot Site	207
B.6	Magnitude (Relative) of Cross Power Spectrum for $X = 2.0$ ft for G. G. Brown Parking Lot Site	208
B.7	Magnitude (Absolute) of Cross Power Spectrum for $X = 4.0$ ft for G. G. Brown Parking Lot Site	209
B.8	Magnitude (Relative) of Cross Power Spectrum for $X = 4.0$ ft for G. G. Brown Parking Lot Site	210
B.9	Magnitude (Absolute) of Cross Power Spectrum for $X = 8.0$ ft for G. G. Brown Parking Lot Site	211
B.10	Magnitude (Relative) of Cross Power Spectrum for $X = 8.0$ ft for G. G. Brown Parking Lot Site	212
B.11	Magnitude (Absolute) of Cross Power Spectrum for $X = 1.0$ ft for SEMTA Parking Lot Site	213
B.12	Magnitude (Relative) of Cross Power Spectrum for $X = 1.0$ ft for SEMTA Parking Lot Site	214
B.13	Magnitude (Absolute) of Cross Power Spectrum for $X = 2.0$ ft for SEMTA Parking Lot Site	215
B.14	Magnitude (Relative) of Cross Power Spectrum for $X = 2.0$ ft for SEMTA Parking Lot Site	216
B.15	Magnitude (Absolute) of Cross Power Spectrum for $X = 4.0$ ft for SEMTA Parking Lot Site	217

B.16	Magnitude (Relative) of Cross Power Spectrum for $X = 4.0$ ft for SEMTA Parking Lot Site	218
B.17	Magnitude (Absolute) of Cross Power Spectrum for $X = 8.0$ ft for SEMTA Parking Lot Site	219
B.18	Magnitude (Relative) of Cross Power Spectrum for $X = 8.0$ ft for SEMTA Parking Lot Site	220
C.1	Experimental Dispersion Curves for $X/L_R = 0.2$ for SEMTA Parking Lot Site	222
C.2	Experimental Dispersion Curves for $X/L_R = 0.25$ for SEMTA Parking Lot Site	223
C.3	Experimental Dispersion Curves for $X/L_R = 0.33$ for SEMTA Parking Lot Site	224
C.4	Experimental Dispersion Curves for $X/L_R = 0.4$ for SEMTA Parking Lot Site	225
C.5	Experimental Dispersion Curves for $X/L_R = 0.5$ for SEMTA Parking Lot Site	226
C.6	Experimental Dispersion Curves for $X/L_R = 0.66$ for SEMTA Parking Lot Site	227
C.7	Experimental Dispersion Curves for $X/L_R = 1.0$ for SEMTA Parking Lot Site	228
C.8	Experimental Dispersion Curves for $X/L_R = 1.33$ for SEMTA Parking Lot Site	229
C.9	Experimental Dispersion Curves for $X/L_R = 1.5$ for SEMTA Parking Lot Site	230
C.10	Experimental Dispersion Curves for $X/L_R = 1.66$ for SEMTA Parking Lot Site	231
C.11	Experimental Dispersion Curves for $X/L_R = 2.0$ for SEMTA Parking Lot Site	232
D.1	Average Experimental Dispersion Curve (Unfiltered) for $S/X = 0.5$ for G. G. Brown Parking Lot Site	234
D.2	Average Experimental Dispersion Curve (Unfiltered) for $S/X = 1.0$ for G. G. Brown Parking Lot Site	235
D.3	Average Experimental Dispersion Curve (Unfiltered) for $S/X = 1.5$ for G. G. Brown Parking Lot Site	236
D.4	Average Experimental Dispersion Curve (Unfiltered) for $S/X = 2.0$ for G. G. Brown Parking Lot Site	237
D.5	Average Experimental Dispersion Curve (Unfiltered) for $S/X = 2.5$ for G. G. Brown Parking Lot Site	238
D.6	Average Experimental Dispersion Curve (Unfiltered) for $S/X = 3.0$ for G. G. Brown Parking Lot Site	239
D.7	Average Experimental Dispersion Curve (Filtered) for $S/X = 0.5$ for G. G. Brown Parking Lot Site	240
D.8	Average Experimental Dispersion Curve (Filtered) for $S/X = 1.0$ for G. G. Brown Parking Lot Site	241
D.9	Average Experimental Dispersion Curve (Filtered) for $S/X = 1.5$ for G. G. Brown Parking Lot Site	242

D.10	Average Experimental Dispersion Curve (Filtered) for $S/X = 2.0$ for G. G. Brown Parking Lot Site	243
D.11	Average Experimental Dispersion Curve (Unfiltered) for $S/X = 0.5$ for SEMTA Parking Lot Site	244
D.12	Average Experimental Dispersion Curve (Unfiltered) for $S/X = 1.0$ for SEMTA Parking Lot Site	245
D.13	Average Experimental Dispersion Curve (Unfiltered) for $S/X = 1.5$ for SEMTA Parking Lot Site	246
D.14	Average Experimental Dispersion Curve (Unfiltered) for $S/X = 2.0$ for SEMTA Parking Lot Site	247
D.15	Average Experimental Dispersion Curve (Unfiltered) for $S/X = 2.5$ for SEMTA Parking Lot Site	248
D.16	Average Experimental Dispersion Curve (Unfiltered) for $S/X = 3.0$ for SEMTA Parking Lot Site	249
D.17	Average Experimental Dispersion Curve (Filtered) for $S/X = 0.5$ for SEMTA Parking Lot Site	250
D.18	Average Experimental Dispersion Curve (Filtered) for $S/X = 1.0$ for SEMTA Parking Lot Site	251
D.19	Average Experimental Dispersion Curve (Filtered) for $S/X = 1.5$ for SEMTA Parking Lot Site	252
D.20	Average Experimental Dispersion Curve (Filtered) for $S/X = 2.0$ for SEMTA Parking Lot Site	253
F.1	Magnitude (Absolute) of Cross Power Spectrum for $X = 0.5$ ft for G. G. Brown Parking Lot Site	265
F.2	Magnitude (Relative) of Cross Power Spectrum for $X = 0.5$ ft for G. G. Brown Parking Lot Site	266
F.3	Magnitude (Absolute) of Cross Power Spectrum for $X = 1.0$ ft for G. G. Brown Parking Lot Site	267
F.4	Magnitude (Relative) of Cross Power Spectrum for $X = 1.0$ ft for G. G. Brown Parking Lot Site	268
F.5	Magnitude (Absolute) of Cross Power Spectrum for $X = 2.0$ ft for G. G. Brown Parking Lot Site	269
F.6	Magnitude (Relative) of Cross Power Spectrum for $X = 2.0$ ft for G. G. Brown Parking Lot Site	270
F.7	Magnitude (Absolute) of Cross Power Spectrum for $X = 4.0$ ft for G. G. Brown Parking Lot Site	271
F.8	Magnitude (Relative) of Cross Power Spectrum for $X = 4.0$ ft for G. G. Brown Parking Lot Site	272
F.9	Magnitude (Absolute) of Cross Power Spectrum for $X = 8.0$ ft for G. G. Brown Parking Lot Site	273
F.10	Magnitude (Relative) of Cross Power Spectrum for $X = 8.0$ ft for G. G. Brown Parking Lot Site	274
F.11	Magnitude (Absolute) of Cross Power Spectrum for $X = 1.0$ ft for SEMTA Parking Lot Site	275
F.12	Magnitude (Relative) of Cross Power Spectrum for $X = 1.0$ ft for SEMTA Parking Lot Site	276

F.13	Magnitude (Absolute) of Cross Power Spectrum for $X = 2.0$ ft for SEMTA Parking Lot Site	277
F.14	Magnitude (Relative) of Cross Power Spectrum for $X = 2.0$ ft for SEMTA Parking Lot Site	278
F.15	Magnitude (Absolute) of Cross Power Spectrum for $X = 4.0$ ft for SEMTA Parking Lot Site	279
F.16	Magnitude (Relative) of Cross Power Spectrum for $X = 4.0$ ft for SEMTA Parking Lot Site	280
F.17	Magnitude (Absolute) of Cross Power Spectrum for $X = 8.0$ ft for SEMTA Parking Lot Site	281
F.18	Magnitude (Relative) of Cross Power Spectrum for $X = 8.0$ ft for SEMTA Parking Lot Site	282
G.1	Average Experimental Dispersion Curve for 8 oz Hammer for G. G. Brown Parking Lot Site (all wavelengths)	284
G.2	Average Experimental Dispersion Curve for 8 oz Hammer for G. G. Brown Parking Lot Site (0 to 5-ft wavelengths)	285
G.3	Average Experimental Dispersion Curve for 16 oz Hammer for G. G. Brown Parking Lot Site (all wavelengths)	286
G.4	Average Experimental Dispersion Curve for 16 oz Hammer for G. G. Brown Parking Lot Site (0 to 5-ft wavelengths)	287
G.5	Average Experimental Dispersion Curve for 4 oz Hammer for SEMTA Parking Lot Site (all wavelengths)	288
G.6	Average Experimental Dispersion Curve for 4 oz Hammer for SEMTA Parking Lot Site (0 to 5-ft wavelengths)	289
G.7	Average Experimental Dispersion Curve for 8 oz Hammer for SEMTA Parking Lot Site (all wavelengths)	290
G.8	Average Experimental Dispersion Curve for 8 oz Hammer for SEMTA Parking Lot Site (0 to 5-ft wavelengths)	291
G.9	Average Experimental Dispersion Curve for 16 oz Hammer for SEMTA Parking Lot Site (all wavelengths)	292
G.10	Average Experimental Dispersion Curve for 16 oz Hammer for SEMTA Parking Lot Site (0 to 5-ft wavelengths)	293
G.11	Average Experimental Dispersion Curve for 40 oz Hammer for SEMTA Parking Lot Site (all wavelengths)	294
G.12	Average Experimental Dispersion Curve for 40 oz Hammer for SEMTA Parking Lot Site (0 to 5-ft wavelengths)	295
G.13	Average Experimental Dispersion Curve for 128 oz Hammer for SEMTA Parking Lot Site (all wavelengths)	296
G.14	Average Experimental Dispersion Curve for 128 oz Hammer for SEMTA Parking Lot Site (0 to 5-ft wavelengths)	297

LIST OF TABLES

<u>Table</u>	
6.1 Test Parameters for SEMTA Parking Lot Site and CRMP Geometry	90
6.2 Test Parameters for SEMTA Parking Lot Site and CS Geometry	91
7.1 Test Parameters for G. G. Brown Parking Lot Site, Various Source-to-Near-Receiver Distances, and $X = 0.5, 1, 2$ ft	104
7.2 Test Parameters for G. G. Brown Parking Lot Site, Various Source-to-Near-Receiver Distances, and $X = 4, 8$ ft	105
7.3 Test Parameters for SEMTA Parking Lot Site, Various Source-to-Near-Receiver Distances, and $X = 0.5, 1, 2$ ft	106
7.4 Test Parameters for SEMTA Parking Lot Site, Various Source-to-Near-Receiver Distances, and $X = 4, 8$ ft	107
7.5 Useful Frequency Ranges for 0.5-ft Receiver Spacing (X) for SEMTA Parking Lot Site	110
8.1 Test Parameters for G. G. Brown Parking Lot Site and Various Sources	143
8.2 Test Parameters for SEMTA Parking Lot Site, Various Sources, and $X = 0.5, 1, 2$ ft	144
8.3 Test Parameters for SEMTA Parking Lot Site, Various Sources, and $X = 4, 8$ ft	145
8.4 Useful Frequency Ranges for 0.5-ft Receiver Spacing for SEMTA Parking Lot Site	147
9.1 Test Parameters for SASW Tests at Beal St. Field Site	167
A.1 Useful Frequency Ranges for 0.5-ft Receiver Spacing (X) for G. G. Brown Parking Lot Site	193
A.2 Useful Frequency Ranges for 1-ft Receiver Spacing (X) for G. G. Brown Parking Lot Site	194
A.3 Useful Frequency Ranges for 2-ft Receiver Spacing (X) for G. G. Brown Parking Lot Site	195
A.4 Useful Frequency Ranges for 4-ft Receiver Spacing (X) for G. G. Brown Parking Lot Site	196
A.5 Useful Frequency Ranges for 8-ft Receiver Spacing (X) for G. G. Brown Parking Lot Site	197
A.6 Useful Frequency Ranges for 1-ft Receiver Spacing (X) for SEMTA Parking Lot Site	198

A.7	Useful Frequency Ranges for 2-ft Receiver Spacing (X) for SEMTA Parking Lot Site	199
A.8	Useful Frequency Ranges for 4-ft Receiver Spacing (X) for SEMTA Parking Lot Site	200
A.9	Useful Frequency Ranges for 8-ft Receiver Spacing (X) for SEMTA Parking Lot Site	201
E.1	Useful Frequency Ranges for 0.5-ft Receiver Spacing for G. G. Brown Parking Lot Site	255
E.2	Useful Frequency Ranges for 1-ft Receiver Spacing for G. G. Brown Parking Lot Site	256
E.3	Useful Frequency Ranges for 2-ft Receiver Spacing for G. G. Brown Parking Lot Site	257
E.4	Useful Frequency Ranges for 4-ft Receiver Spacing for G. G. Brown Parking Lot Site	258
E.5	Useful Frequency Ranges for 8-ft Receiver Spacing for G. G. Brown Parking Lot Site	259
E.6	Useful Frequency Ranges for 1-ft Receiver Spacing for SEMTA Parking Lot Site	260
E.7	Useful Frequency Ranges for 2-ft Receiver Spacing for SEMTA Parking Lot Site	261
E.8	Useful Frequency Ranges for 4-ft Receiver Spacing for SEMTA Parking Lot Site	262
E.9	Useful Frequency Ranges for 8-ft Receiver Spacing for SEMTA Parking Lot Site	263

LIST OF APPENDICES

Appendix

A. Tables of Useful Frequency Ranges as a Function of Source-to-Near-Receiver Distance	192
B. Cross Power Spectrum Magnitudes as a Function of Source-to-Near-Receiver Distance	202
C. Combined Dispersion Curves for Constant X/L_R for SEMTA Parking Lot Site	221
D. Combined Dispersion Curves as a Function of Source-to-Near-Receiver Distance	233
E. Tables of Useful Frequency Ranges as a Function of Source Type	254
F. Cross Power Spectrum Magnitudes as a Function of Source Type	264
G. Combined Dispersion Curves as a Function of Source Type	283

CHAPTER I

INTRODUCTION

1.1 Background/Problem Statement

In highway engineering, in situ values of Young's modulus are important parameters in the determination of overlay thicknesses and allowable loads for existing pavement structures and for the assessment of other rehabilitation needs. Young's moduli for pavement systems are typically determined in situ by deflection-based measuring devices such as the Dynaflect and Falling Weight Deflectometer. Modulus values are determined from the deflection measurements through the use of multi-layer elastic analysis. These methods are widely used, but the current data analysis techniques have major drawbacks such as nonuniqueness in determining the stiffness profile from the observed data and representation of a dynamic load with a static load. It is seen, therefore, that a fast, economical, accurate, nondestructive method of determining in situ stiffness profiles of pavement systems is needed.

A new method for measuring in situ elastic moduli, i.e., stiffness, profiles has been under continuous development at the University of Texas at Austin since 1980, and at the Universities of Kentucky and Michigan since 1985. The method is called spectral-analysis-of-surface-waves (SASW). It has been used to date for a number of different applications, including nondestructive pavement evaluation (Heisey, Stokoe, and Meyer [1982]; Nazarian and Stokoe [1983]; Nazarian, Stokoe, and Hudson [1983]; Nazarian and Stokoe [1984]; Drnevich, et al. [1985]; and Nazarian and Stoke [1986]), evaluation of soil liquefaction potential (Stokoe and Nazarian [1985]), evaluation of a concrete dam (Nazarian [1984]), and as a diagnostic tool for determining the effectiveness of soil improvement techniques (Stokoe and Nazarian [1983]). The SASW method is based on the generation and detection of Rayleigh

waves at low strain levels from the surface of the layered system. The method has the following advantages: it is nondestructive, it is performed from the surface of the system, it does not require boreholes, the test setup and procedure is simple, and it has the capability of being fully automated. The main disadvantage at this point is that testing and data reduction are not performed rapidly. It is felt, however, that with continued research and development, the testing and data reduction time can be substantially reduced.

1.2 Objectives

The purpose of this research is to further the development of the SASW method toward a practical technique for in situ investigation of pavement systems. The method has been shown to have tremendous value for future applications. However, the method to date is primarily a research tool. The testing and data reduction currently require a good deal of time. Efforts to decrease the testing time necessary at each location of interest, particularly for nondestructive pavement evaluation, are essential. It is envisioned that eventually an automated testing procedure will be developed to enable one to collect the necessary data on-the-move, analogous to the current deflection measurement procedures currently used in the pavement industry.

The specific objectives of this research are as follows. First, since the SASW method is new and has never been used at the University of Michigan until this research, the development of a SASW testing and data analysis system was necessary. It was felt that a system based upon the use of a microcomputer was particularly attractive, and this has been done as much as possible. It is also felt that the development of a multiple transducer testing procedure, i.e., a procedure employing more than two receivers, is an important step towards the development of an automated testing method. The second objective of this research, then, was to evaluate and produce guidelines for multiple transducer SASW testing. In particular, this research will examine the influence of source and receiver geometry, source-to-near-receiver distance, and source type in the context of a multiple transducer testing procedure.

1.3 Organization

Chapter two provides a review of the background literature related to the SASW method, including wave propagation in an elastic half-space, factors influencing elastic moduli, seismic field methods for determining elastic moduli, pavement overlay design and nondestructive evaluation, digital signal analysis, and excitation techniques for frequency response testing.

Chapter three contains a detailed description of the SASW method as it is currently conducted. Detailed discussion of the three major phases of the testing technique, namely, collection of data in the field, determination of the Rayleigh wave dispersion curve, and inversion of the Rayleigh wave dispersion curve, are included.

A description of the SASW testing system and computer software developed as part of this research is provided in chapter four.

Chapter five outlines the experimental program undertaken to examine the influence of the variables discussed above.

Presentation and discussion of the test results are found in chapters six through nine.

Chapter ten provides a summary, conclusions, and recommendations for further research.

CHAPTER II

BACKGROUND

2.1 Introduction

The following six sections provide a review of: 1) wave propagation in an elastic half-space, 2) factors influencing elastic moduli, 3) seismic field methods for determining elastic moduli, 4) pavement overlay design and nondestructive evaluation, 5) digital signal analysis, and 6) excitation techniques for frequency response testing.

2.2 Wave Propagation in an Elastic Half-Space

This section contains a brief review of wave propagation in an elastic half-space, the concepts of which are essential to understanding the SASW method. A more complete and rigorous discussion can be found in the textbooks by Ewing, Jardetzky, and Press (1957), Grant and West (1965), Richart, Hall, and Woods (1970), and Aki and Richards (1980).

If an elastic half-space is disturbed by a vertical impact on the surface, two kinds of waves will propagate in the medium: body waves and surface waves. Body waves are the waves that propagate within the body of a medium, and they are composed of two different types: compression and shear. Compression and shear waves are differentiated by the direction of particle motion relative to the direction of wave propagation. Particle motions associated with shear waves (S-waves) are perpendicular to the direction of wave propagation, while particle motions associated with compression waves (P-waves) are parallel to the direction of wave propagation. Surface waves resulting from a vertical excitation at the surface are primarily Rayleigh waves (R-waves). Rayleigh waves propagate away from the source along a cylindrical wave front near the surface of the medium, and particle motion

near the surface forms a retrograde ellipse. The amplitude of the wave decays exponentially with depth, so that at a depth of one wavelength, the amplitudes of vertical and horizontal particle motion are only about 30 and 10 percent, respectively, of the amplitudes at the surface. Miller and Pursey (1955) have shown that for a vertical excitation at the surface of an elastic half-space more than 67 percent of the energy propagates as Rayleigh waves.

The velocity of propagation of the different waves are related by Poisson's ratio. Compression waves propagate faster than either shear waves or Rayleigh waves. As Poisson's ratio increases from 0 to 0.5, the ratio of P- to S-wave velocity increases from 1.4 to infinity. The variation of the ratio of R- to S-wave velocity is small, ranging from 0.86 to 0.95 for Poisson's ratios of 0 to 0.5, respectively.

The velocity of propagation is a direct indicator of the stiffness of a material. Young's modulus and shear modulus of a material can be easily determined if the shear wave or compression wave velocity is known. The relationships between velocities and moduli are:

$$G = \rho V_s^2 \quad (2.1)$$

$$E = 2G(1 + \nu) = 2\rho V_s^2(1 + \nu) \quad (2.2)$$

or

$$E = \rho V_p^2 [(1 + \nu)(1 - 2\nu)/(1 - \nu)] \quad (2.3)$$

where: G = shear modulus, E = Young's modulus, ρ = mass density, V_s = shear wave velocity, V_p = compression wave velocity, and ν = Poisson's ratio.

Geophysical measurements of V_s , and hence modulus, normally evaluate these properties at shearing strains below 0.001 percent. Moduli determined in this manner are commonly referred to as low-amplitude moduli and are usually denoted as G_{mas} or E_{mas} . These moduli represent initial tangent moduli used in nonlinear stress-strain relations for static and dynamic analyses. Moduli at higher strain amplitudes are normally determined in the laboratory or are estimated from empirical relationships. Further discussion of the measurement and factors affecting elastic moduli is found in subsequent sections.

An issue of concern in the generation and detection of waves in an elastic medium is the dissipation of wave energy. As wave fronts propagate away from a source, they encounter a greater volume of the medium, which causes the wave energy to dissipate with distance from the source. This phenomenon is referred to as geometrical damping. Body and surface waves differ in the amount of geometrical damping associated with each wave. Near the surface, body waves attenuate proportional to $1/r^2$ (where r is the distance from the source), while Rayleigh waves attenuate more slowly, proportional to $1/\sqrt{r}$. As a result, in a relatively short distance from the source, most of the energy at the surface is Rayleigh wave energy. The SASW method makes use of the lower attenuation and cylindrical wave front characteristics of Rayleigh waves. In addition, the fact that the majority of the energy from a vertical impact goes into Rayleigh wave energy further benefits the method.

A further characteristic of the Rayleigh wave that makes its use desirable for in situ seismic testing is that the Rayleigh wave velocity is constant and independent of frequency in a homogeneous elastic half-space. In this case, the frequency of excitation, f , and Rayleigh wave velocity, V_R , are related by:

$$V_R = f \times L_R \quad (2.4)$$

where L_R is the wavelength of the Rayleigh wave. The components of Rayleigh wave particle motion are not distributed uniformly with depth. As noted previously, at a depth of approximately one wavelength, particle motions are quite small as compared to the surface. It can therefore be assumed that material to a depth of approximately one wavelength is the material predominantly sampled. From eq. 2.4, frequency and wavelength are inversely proportional. Thus, high frequencies are associated with short wavelengths and vice versa. In other words, high frequencies sample material near the surface, while lower frequencies sample deeper materials.

If, on the other hand, the stiffness of the medium varies with depth such as in a pavement system, the Rayleigh wave velocity will become dependent on frequency, and different frequencies will propagate with different velocities. In a simplified fashion, for each frequency an average velocity of the material down to a depth of approximately one wavelength is mea-

sured. This velocity is termed phase velocity or apparent Rayleigh wave velocity. Because the stiffness changes with depth, the phase velocity will vary with frequency (wavelength). This phenomenon is known as the dispersive characteristic of surface waves. This dispersive characteristic is a key element in SASW testing because it allows different materials to be sampled by using different wavelengths (frequencies).

2.3 Factors Influencing Elastic Moduli

This section provides a summary of the principal variables affecting the elastic modulus of the three materials tested during the course of this study, namely, soil, asphaltic concrete, and portland cement concrete.

Soil

Hardin and Black (1968) have indicated the various quantities which influence the shear modulus of soils (including pavement subgrades and unbound subbase and base materials) in the form of the following functional relationship:

$$G = f(\bar{\sigma}_0, e, H, S, \tau_0, C, A, F, T, \theta, K) \quad (2.5)$$

where $\bar{\sigma}_0$ = isotropic component of ambient effective stress (effective octahedral normal stress or effective mean principal stress); e = void ratio; H = ambient stress and vibration history; S = degree of saturation; τ_0 = deviatoric component of ambient stress (octahedral shear stress); C = grain characteristics, grain shape, grain size, grading, and mineralogy; A = amplitude of vibration (strain); F = frequency of vibration; T = secondary effects that are functions of time, and magnitude of load increment; θ = soil structure; and K = temperature, including freezing.

Hardin and Drnevich (1972) have suggested that, among the many parameters that influence the shear modulus of soil, the amplitude of vibration (strain amplitude), effective mean principal stress ($\bar{\sigma}_0$), and void ratio are most important. In general, the shear modulus of soil increases with decreasing strain amplitude and void ratio and increasing effective mean principal stress (confining pressure). Further, numerous studies have shown that

the shear modulus of soil is essentially independent of strain amplitude for amplitudes less than 0.001 percent. Since geophysical methods such as the SASW method are conducted at strains less than 0.001 percent, the modulus determined is the low-amplitude or initial tangent modulus, referred to as G_{max} or E_{max} . Moduli at higher strain amplitudes are normally determined in the laboratory or are estimated from empirical correlations, as mentioned previously.

Asphaltic Concrete

The principal variables affecting the elastic modulus of asphaltic concrete include: temperature of mix, frequency of loading, strain amplitude, number of load applications, age of mix, and the mix properties. The effects of mix temperature and the frequency of loading are typically most significant. The modulus generally increases with decreasing temperature and increasing frequency of loading (Kallas and Riley [1967], Guericke and Weinert [1972], Pell and Brown [1972], Allen and Deen [1980], and Sousa and Monismith [1987]). It is well known that the stiffness of asphaltic concrete generally increases with time due to an aging affect. At the same time, however, the modulus will decrease due to repetitive loads, or fatigue (Kallas and Riley [1967], Guericke and Weinert [1972], and Pell and Brown [1972]). The modulus of asphaltic concrete, like that of soil, is also dependent on the strain (stress) level (Cragg and Pell [1971]). The modulus decreases with increasing strain (stress) amplitude.

In addition to the above environmental factors, the stiffness of asphaltic concrete also depends on the mix variables such as aggregate type and grading, bitumen type and content, degree of mix compaction, and the resulting air void content (Pell and Brown [1972]). Shook and Kallas (1969) presented the following conclusions with respect to the influence of mix variables on the modulus of asphaltic concrete. First, for a constant asphalt content, modulus increases as air voids decrease. Second, for a constant air void content, modulus increases as asphalt content decreases. Third, for constant compactive effort, modulus may increase or decrease as air voids and asphalt content change. Finally, modulus increases as original asphalt viscosity increases.

Portland Cement Concrete

Troxell, Davis, and Kelly (1968) indicate that the factors which influence the strength of concrete generally influence the modulus in similar fashion, although usually to a lesser degree. They suggest that the principal variables influencing the elastic modulus of portland cement concrete include the richness of the mix (cement factor), water-cement ratio, age and curing conditions, kind and gradation of aggregate, and moisture content at time of test.

In general, the elastic modulus increases with increased age, rising rapidly during the first few months and continuing for ages as high as three years. High cement factor and low water-cement ratio also lead to higher elastic moduli. As one might expect, higher values of modulus are obtained for concrete made of stiffer aggregates. The grading of a given type and size of aggregate, as well as the maximum size of a well-graded aggregate, has the same general effect upon the modulus of elasticity as upon strength; if the strength is increased, then the modulus is increased. As long as the mix is not harsh and unworkable, there is a tendency for the modulus to increase with the fineness modulus. Examining the influence of free moisture at time of test upon the modulus of concrete shows that, regardless of mix or age, wet specimens exhibit substantially higher moduli than corresponding dry specimens, although ultimate strengths are higher for the dry concrete than for the wet by about the same ratios. In general, both the modulus and strength are greater for longer mixing times, but the increase in the modulus is considerably less than the increase in strength. A longer curing period likewise benefits both the strength and the modulus.

2.4 Seismic Field Methods for Determining Elastic Moduli

Elastic moduli are often determined from samples using laboratory testing methods, including resonant column, resilient modulus, cyclic triaxial shear, cyclic simple shear, and cyclic torsional shear. Because laboratory samples suffer from mechanical disturbance due to sampling, and because of the general inability of laboratory tests to simulate in situ stress conditions, a more accurate representation of elastic properties in situ can often be obtained from field measurements. In situ measurement of seismic waves yields values of shear and

compression wave velocities and attenuations which can be used to calculate low-amplitude shear and Young's moduli, material damping, and Poisson's ratio.

Methods of measuring seismic wave velocities generally consist of employing a source to generate seismic energy at one point and monitoring wave arrivals at one or more other points to determine the wave travel time. Seismic wave velocities are then calculated by dividing the travel distance by the travel time of the appropriate wave type. A brief discussion of the testing procedure of some of the more popular seismic field methods follows. Similar discussions of the majority of these methods can also be found in Ballard and McLean (1975), Borm (1977), Richart (1977), Woods (1978), Hoar (1982), and Woods (1986).

Borehole Methods

Seismic field methods which utilize boreholes for determining low-strain elastic properties include: 1) crosshole, 2) downhole, 3) uphole, 4) in-hole, and 5) bottom-hole methods. A simplified representation of each of these methods is shown schematically in figure 2.1, and a brief discussion of each method follows.

In the crosshole method (see figure 2.1[a]), the time for body waves to travel horizontally from a source in one borehole to one or more receivers at the same depth as the source in other boreholes is measured (Stokoe and Woods [1972] and Hoar [1982]).

In the downhole method (see figure 2.1[b]), the time for body waves to travel (almost) vertically from a source on the surface to one or more receivers at different depths in a single borehole is measured (Patel [1981]).

With the uphole method (see figure 2.1[c]), the time for body waves to travel (almost) vertically from a source at depth within a borehole to one or more receivers on the ground surface is measured (Ludeling [1977]).

The in-hole, or sonic logging, method utilizes a source and one or more receivers in the same borehole to measure the time for body waves to travel vertically along the borehole wall from the source to the receivers (see figure 2.1[d]) (Hoar [1982]).

In the bottom-hole method, a probe consisting of a source and one or more receivers is pushed into the natural soil beyond the bottom of a predrilled borehole (see figure 2.1[e]),

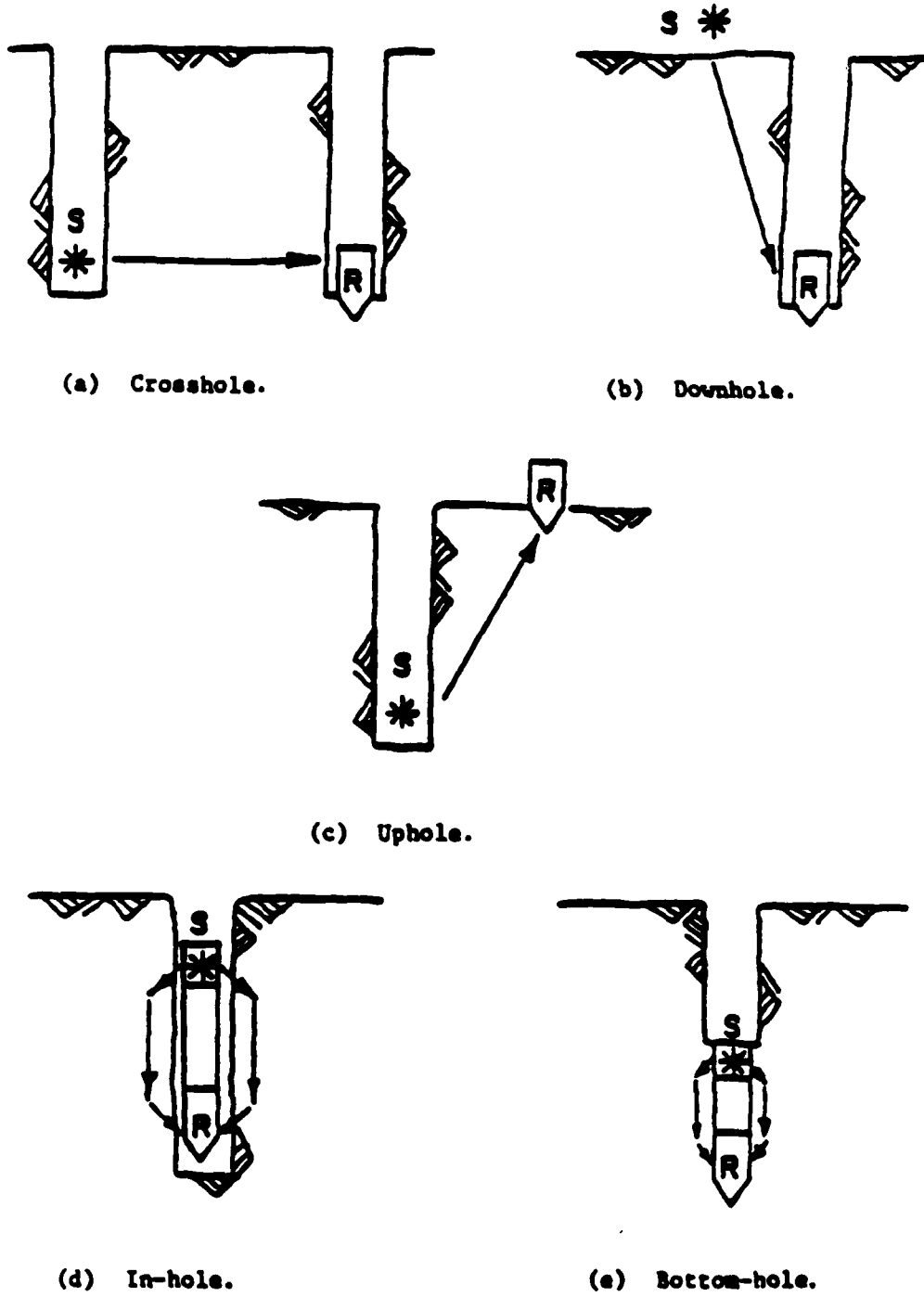


Figure 2.1 — Schematic Representation of Borehole Seismic Methods (from Hoar [1962])

and the time for body waves to travel vertically from the source to the receiver(s) is measured (Hoar [1982]).

The above borehole methods are typically repeated at a number of different depths from the surface to a specified depth in order to adequately define the wave velocity profile. Body wave travel times are measured with the borehole methods, and the velocity of the body waves is calculated using the distance of travel.

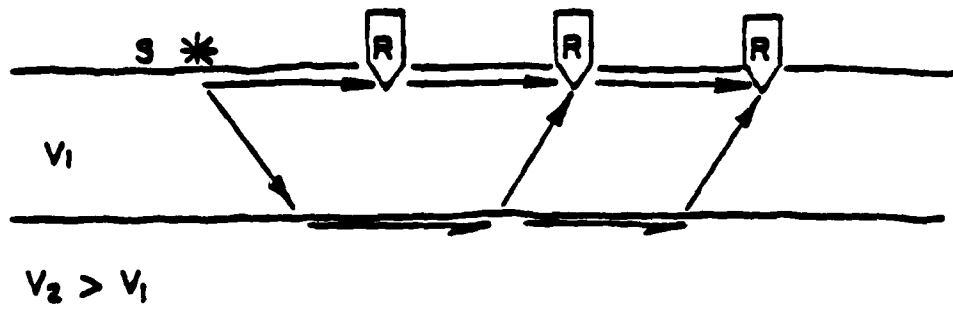
Surface Methods

Surface methods for measurement of seismic waves utilize sources and receivers located at the surface and therefore have an economic advantage over the borehole methods since boreholes are not required. These methods include: 1) surface refraction, 2) surface reflection, 3) steady-state Rayleigh wave, and 4) Rayleigh wave dispersion methods. These methods are shown schematically in figure 2.2.

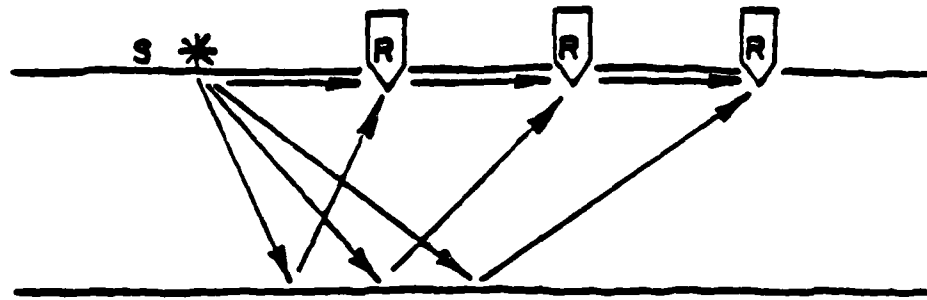
The surface refraction method (Richart, Hall, and Woods [1970]) consists of measuring the travel times of body waves from a surface source to a linear spread of receivers on the surface (see figure 2.2[a]). The fastest paths of the seismic waves depend on the velocity distribution in the substructure, which is inferred from the time of first arrivals at each receiver.

Conceptually, the surface reflection method (Richart, Hall, and Woods [1970]), shown schematically in figure 2.2(b), is similar to the refraction method. A surface source and a linear spread of receivers is used. However, the receiver spread is much closer to the source because this method relies on measurement of first arrivals of direct waves and on later arrivals of waves reflected off the interfaces between layers rather than on measurement of only first arrivals as in the refraction method.

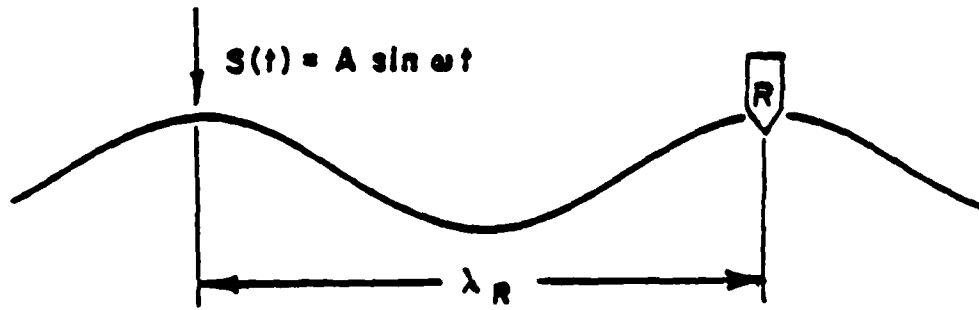
Travel times are not measured in the steady-state Rayleigh wave method (see figure 2.2[c]). Instead, steady-state techniques generally use a vertical, sinusoidally oscillating mass placed on the surface to excite the system with primarily Rayleigh waves (Jones [1958]; Heukelom and Foster [1960]; Jones [1962]; Ballard [1964]; Ballard and Casagrande [1966]; Ballard and Casagrande [1967]; Maxwell and Fry [1967]; and Richart, Hall, and Woods [1970]). Vertical motion transducers are then moved along the surface until the distance



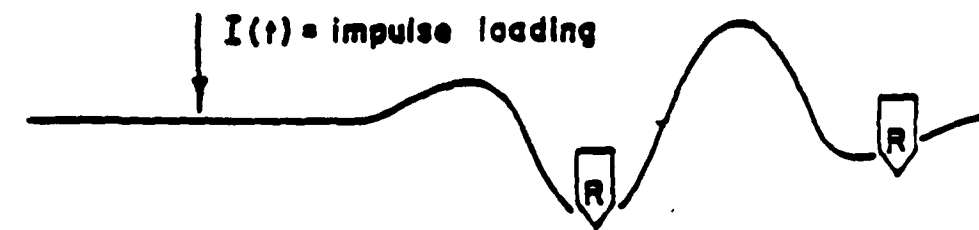
(a) Surface refraction.



(b) Surface reflection.



(c) Steady-state Rayleigh wave.



(d) Rayleigh wave dispersion.

Figure 2.3 — Schematic Representation of Surface Seismic Methods (from Hoar [1982])

between successive troughs or peaks of the wave is established. This distance is the wavelength of the Rayleigh wave, L_R , and, knowing the frequency of vibration of the source, the velocity is readily determined from eq. 2.4. Alternatively, the relative phase difference between two receivers can be measured, from which the travel time and then Rayleigh wave velocity can be determined (see section 3.3).

As discussed in section 2.2, the velocity of the shear wave is approximately equal to the Rayleigh wave velocity, depending on the value of Poisson's ratio of the material. It can therefore be assumed that the shear and Rayleigh wave velocities are equal for many practical applications. (The limitations of this assumption are considered in section 3.4 below.) As also discussed in section 2.2, the majority of the Rayleigh wave travels through a zone of the material about one wavelength deep. It can further be postulated that the average properties within this zone approximate the properties at a depth of one third to one half of a wavelength. (The limitations of this assumption are also discussed in section 3.4 below.) Thus, by decreasing the frequency of vibration from an initial value, the wavelength increases and the Rayleigh wave effectively samples a greater depth. Conversely, by increasing the frequency the wavelength decreases and the sampled depth decreases. For each excitation frequency the transducers must be moved to determine the corresponding wavelength. Because a wide range of frequencies is required to adequately sample a site, this approach can be quite time consuming.

If the steady-state technique is modified to use either an impulsive source to propagate a transient wave pulse through the materials to be tested, or a mechanical shaker excited with a random noise source, a wide range of frequencies can be excited at one time (see figure 2.2(d)). Thus a range of depths can be sampled simultaneously. This is the basis for the Rayleigh wave dispersion technique, i.e., SASW testing. Each frequency can potentially propagate at a different velocity due to the dispersive characteristic of Rayleigh waves in layered media, as discussed in section 2.2. The relative phase difference between the surface waveform measured at two known distances from the source can be determined at each frequency to establish the velocity-frequency or velocity-wavelength relationship. A convenient method of determining the phase difference at each frequency is a fast Fourier transform (FFT)-based cross power spectrum phase analysis. This approach requires that the time

domain waveform be transformed into its frequency spectrum. Instrumentation is required to record, transform, and analyze signals for their frequency and phase relationships. The main advantage of the Rayleigh wave dispersion technique is that it is significantly faster and more efficient than the conventional steady-state technique, since a range of frequencies are excited simultaneously. This technique is the basis for the SASW method and it will be discussed in much more detail in chapter three.

2.5 Pavement Overlay Design and Nondestructive Evaluation

To help justify the need for the SASW method for pavement evaluation, this section contains a brief review of pavement overlay design and nondestructive pavement evaluation.

Monismith and Finn (1984) group existing procedures for the design of overlay structures into three general categories. The first group of procedures is based on the analysis of the structural capabilities of component layers of the existing pavement, the structural capabilities generally having been determined by sampling and subsequent laboratory testing or by testing in situ.

The second group, so called deflection-based methods, depends on deflection measurements at the surface of the existing pavement. Employing empirical correlations between overlay thickness and measured deflection, these methods aim to provide sufficient overlay thickness to reduce the surface deflection to some standard or maximum tolerable value, which is a function of the number of equivalent single axle loads to be carried. Because the methods are based on empirical correlations, they are only valid for the conditions under which the correlations were made.

The third group of procedures are the analytically-based methods, those making use of recently developed mechanistic analyses, such as multi-layer elastic analysis. Monismith and Finn (1984) conclude that it would be worthwhile to move as quickly as possible to the use of these procedures since their use permits effective consideration of a range of materials and treatments, changed traffic conditions, and environmental influences in a "sound" manner.

One of the primary inputs to the analytically-based overlay design procedures is some measure of the stiffness, e.g., elastic modulus, of the various materials comprising the pavement system. There are two possible methods for determining the stiffness characteristics of

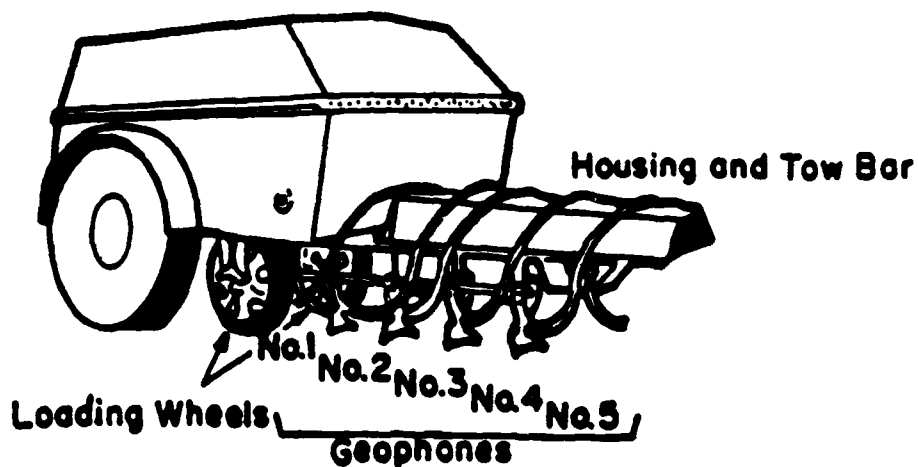
pavement materials. The first method is to conduct laboratory tests on either laboratory-compacted specimens or undisturbed samples taken from the pavement. In situ nondestructive testing comprises the second method. Because of our need for a rapid method of pavement evaluation, minimal laboratory testing is desirable. This leaves us with in situ nondestructive evaluation.

Numerous methods have been developed to determine elastic moduli of pavement systems in the field. Lytton, Moore, and Mahoney (1975), in a state-of-the-art report, discuss four general methods: static deflections, steady-state dynamic deflections, impact load response, and wave propagation methods.

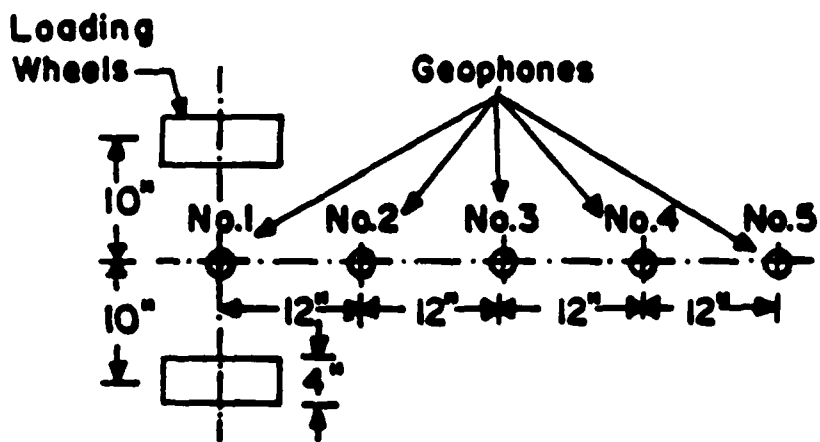
The first three methods measure the deflection of the entire pavement system caused by a static or dynamic load (Moore, Hanson, and Hall [1978], Bush [1980], and Bush and Alexander [1985]). These methods include devices such as the Benkelman beam, the Dynaflect, and the Falling Weight Deflectometer (FWD). The Dynaflect and Falling Weight Deflectometer are perhaps the most widely used devices today. A schematic of the Dynaflect is shown in figure 2.3. A steady-state dynamic force of 1000 lb (4500 N) peak-to-peak is generated by two counter-rotating eccentric masses operating at a constant frequency of 8 Hz. This force is transmitted to the pavement by two, 4-in (10-cm) wide wheels. Five equally-spaced geophones (velocity transducers) are used to measure deflections of the pavement system due to the load.

A schematic of the Falling Weight Deflectometer is shown in figure 2.4. The load is developed by dropping a weight on a plate set on the pavement surface. The energy of the impact can be varied by changing the drop height or the drop weight. The peak force usually varies from 1.5 to 24 kips (6.6 to 1.6 kN). The duration of the impulse is approximately 25 to 30 msec, which is intended to simulate the duration of a load imposed by a vehicle wheel moving at 40 mph (64 km/h). Seven equally-spaced geophones are used to measure deflections of the pavement system due to the applied load.

The popularity of the deflection-based devices is due to their ability to gather large amounts of data in a short time. The devices are fully automated and specialized test personnel are not usually required. The major drawback of these methods is that the overall stiffness of the pavement system is measured, and it is generally difficult to separate

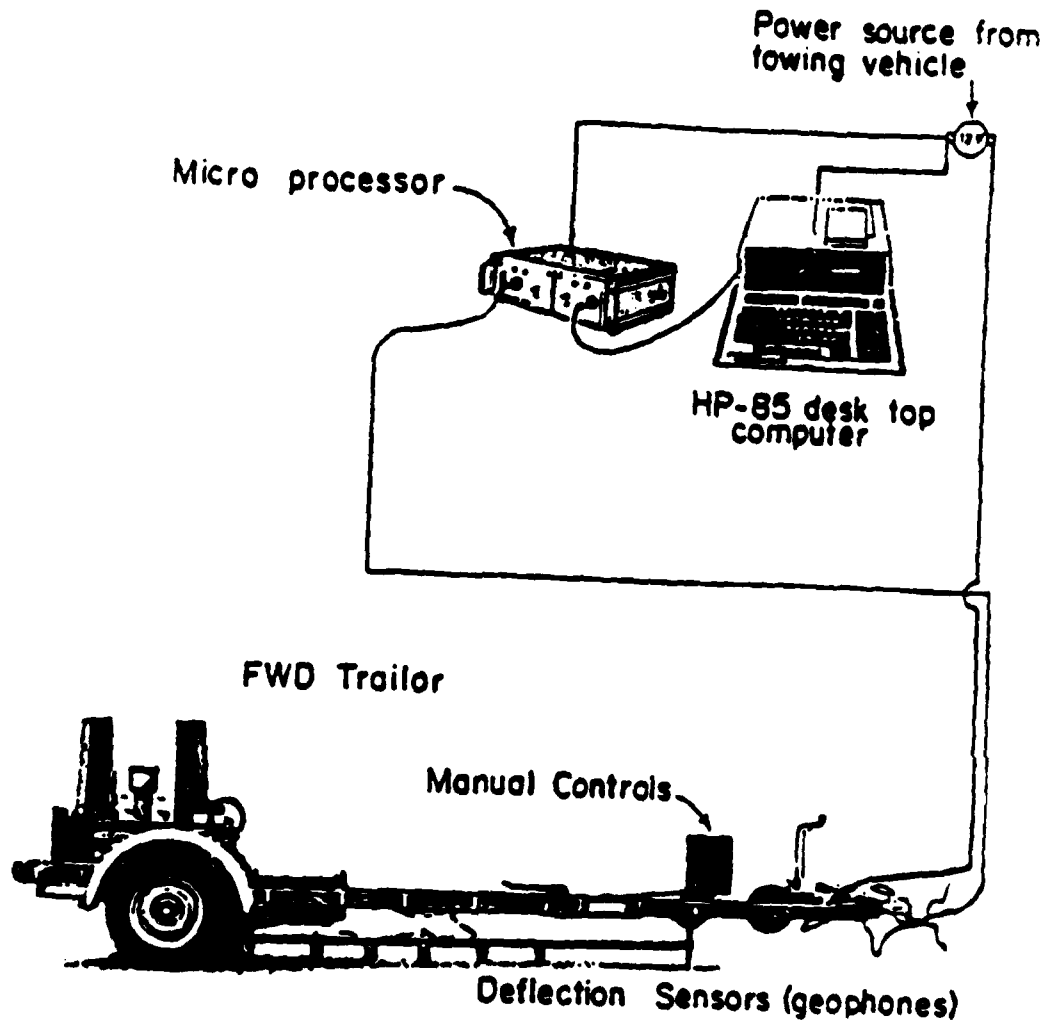


a. The Dynaflect System in Operating Position.

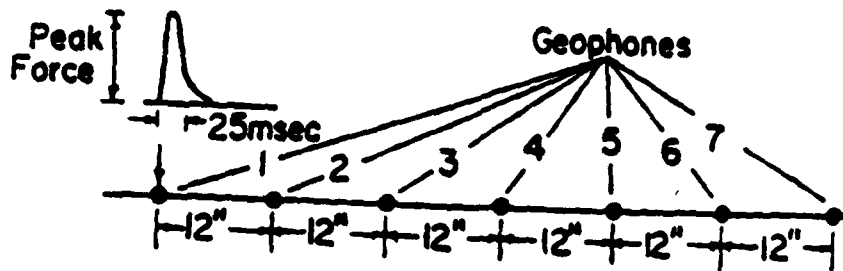


b. Configuration of Load Wheels and Geophones.

Figure 2.3 — Schematic of Dynaflect Device (from Nazarian [1984])



a. FWD in Operating Position



b. Geophones Configuration

Figure 2.4 — Schematic of Falling Weight Deflectometer (from Nazarian [1984])

properties of the individual layers. Attempts have been made to calculate the modulus of each layer based on the measured deflections and the use of multi-layer elastic theory. The procedure is usually trial-and-error: assume a set of modulus values, compute the corresponding static deflections, compare the computed deflections with the measured values, and iterate until the differences are smaller than an acceptable tolerance. Unfortunately, uniqueness of the solution cannot be guaranteed and different sets of elastic moduli can produce results which are within the specified tolerance (Roesset and Shao [1985]). A further drawback is that the methods based on measuring dynamic deflections, while dynamic tests by nature, rely on static analyses to estimate the elastic properties of the pavement system. A number of researchers, including Roesset and Shao (1985), Davies and Mamlouk (1985), and Mamlouk (1985), have shown that this assumption can lead to serious errors. A final shortcoming of the deflection-based methods is that they require the thickness of each layer of the pavement system to be known in order to calculate the elastic modulus of each layer.

Wave propagation methods measure the velocities of elastic waves traveling through the pavement system rather than the deflections caused by the vibratory source. Elastic waves can be generated by steady-state vibrations or by transient impulses, and they can propagate through individual layers or the entire pavement system. Wave propagation methods at low shearing strain amplitudes offer the most direct approach to determining elastic moduli of pavement systems since each layer is uniquely identified by the wave propagation velocity of the material within the layer.

Among wave propagation methods, the steady-state technique is most widely used in nondestructive pavement testing (Heukelom and Foster [1960], Jones [1962], Szendrei and Freeme [1970], and Moore, Hanson, and Hall [1978]). This approach, however, can be quite time consuming, as discussed in section 2.4. As also discussed in section 2.4, a technique based on either a transient impulse or random noise excitation, such as the SASW method, would be able to evaluate each test location much faster. Thus, the SASW method would be a desirable technique for nondestructive pavement evaluation.

In summary, this section has attempted to establish the following: 1) analytically-based pavement overlay design procedures are desirable, 2) analytically-based procedures require a measure of the stiffness of each layer in a pavement system, 3) pavement evaluation

conducted to determine the stiffness of each layer must be done nondestructively because of time constraints, 4) nondestructive evaluation methods based on wave propagation offer the most direct approach to determining elastic moduli of pavement systems, and 5) wave propagation methods based on either impulse loading or random noise excitation, such as the SASW method, are desirable, again because of time constraints.

2.6 Digital Signal Analysis

This section contains a brief review of digital signal analysis. Emphasis is placed on those concepts directly related to SASW testing. A more comprehensive review of the subject can be found in the textbooks by Bendat and Piersol (1971), Bendat and Piersol (1980), and Ramirez (1985), and in the publications by Hewlett Packard Company (1977), Randall (1977), Rockland Systems Corporation (1977), Thornhill and Smith (1980), Bruel & Kjaer Instruments, Inc. (1985), and Hewlett Packard Company (1985).

In the past 10-15 years, the development of microprocessors and the fast Fourier transform (FFT) algorithm has greatly extended the capability to measure and analyze dynamic systems in the frequency domain. Instrumentation now exists that rapidly filters and converts an analog signal to a digitized signal, transforms the signal from its representation in the time domain into its frequency components, and analyzes the data in various formats.

The primary reason for utilizing spectral analysis is that information can be extracted from the data that was not apparent from the time domain representation of the signal. The components of a signal in a time domain record are often indistinguishable, while each frequency component and its relative contribution to the overall waveform are easily observed in the frequency spectrum. Also, the amplitude and phase of each frequency component in the waveform can be determined. In addition, relationships between two signals can be easily identified.

Time versus Frequency Domain

The terms "time domain" and "frequency domain" have been mentioned a number of times thus far. Definition of these terms and the relationship between them is appropriate.

In actuality, the time domain and the frequency domain are merely two different ways of describing the same information. Figure 2.5 depicts a three-dimensional waveform space

with amplitude as one axis and time and frequency as the other two axes. The time and amplitude axes define something that can be called a time plane or time domain. In the same manner, the frequency and amplitude axes define a frequency plane or frequency domain that is normal to the time plane.

The time history of a sinusoid, such as that in figure 2.5, can be treated as a projection on the time plane. In concept, the sinusoid can be thought of as actually existing at some distance from the time plane. This distance is measured along the frequency axis and is equal to the reciprocal of the waveform period.

Similarly, the sinusoid also has a projection onto the frequency plane. This projection takes the form of an impulse with an amplitude equal to the sinusoid's amplitude. Because of symmetry, it is necessary to project only the peak amplitude rather than the full peak-to-peak swing. This is shown in figure 2.5 by the positive amplitude impulse on the magnitude diagram. The position of this impulse on the frequency axis coincides with the frequency of the sinusoid.

The single impulse in the magnitude diagram defines both the amplitude and frequency of the sinusoid. With only this information, the sinusoid can be reconstructed in the time domain. Some additional information is needed, however, to fix the sinusoid's position relative to the zero time reference. This additional information is provided by a phase diagram, which also consists of an impulse located on a frequency axis. The amplitude of this latter impulse indicates the amount of phase associated with the sinusoid.

Phase diagrams for sinusoids can be determined by looking at the positive peak closest to time zero. For the case of figure 2.5, the positive peak occurs after time zero by an amount equal to one-fourth the period. There are 2π radians or 360° in a cycle or period, and the peak is shifted by one-fourth of this, or 90° ($\pi/2$ radians). Since the positive peak occurs after time zero, the sinusoid is said to be delayed or lagged. By convention, delay is denoted by negative phase. If the closest positive peak had been located before time zero, then the sinusoid would have been advanced. An advance or phase lead is denoted by positive phase.

In looking at the phase plot in figure 2.5, it should be pointed out that the total range of phase shift is $-\pi$ to $+\pi$, or 2π . With no reference point fixed to the sinusoid, an

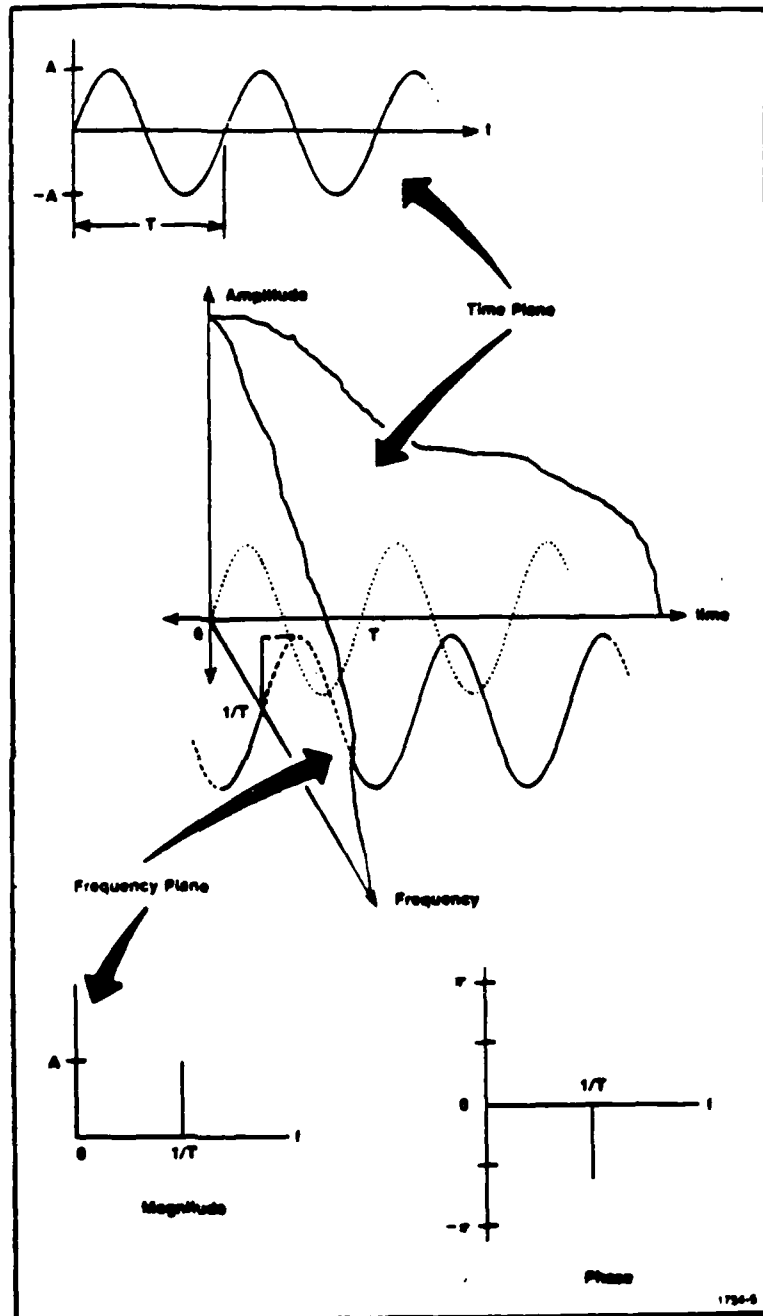


Figure 2.5 — Time and Frequency Descriptions of a Sine Wave (from Ramires [1985])

actual shift out of the 2π range corresponds to a shift within the 2π range. For example, a sinusoid advanced by $2\pi + \pi/2 = 5\pi/2$, or 450° , is not generally distinguishable from the same sinusoid advanced by $\pi/2$, so it can be represented as having a $\pi/2$ or 90° shift. This system of representing phase within a 2π range is referred to as modulo 2π phase. If on the other hand, a reference can be attached to the sinusoid, then shifts beyond the 2π range can be represented as such. This latter approach is referred to as a continuous phase representation and becomes important for SASW data reduction.

Real-life waveforms are usually not single-frequency sinusoids like those in the above discussion. Rather, they often have seemingly complex, nonsensical representations in the time domain. However, these complex waveforms can be thought of as a series of single-frequency sinusoids each potentially having a different frequency, amplitude, and phase all added together. Consider the simple example depicted in figure 2.6. Start with a frequency description of a sinusoid having a frequency of F_0 and a phase of -90° (see figure 2.6[a]). Now, take another sinusoid with a frequency of $2F_0$, half the amplitude of F_0 , and a phase of -45° (see figure 2.6[b]) and add it to the first sinusoid. The frequency description for the sum of the two sinusoids is shown in figure 2.6(c). To complete the picture, recast figure 2.6 in terms of a three-dimensional waveform space. This is shown in figure 2.7, where the concepts of projecting onto a time plane and a frequency plane are used. Additionally, the idea of summing multiple time-plane projections of sinusoids is illustrated. Projections onto the time plane (or into the time domain, if you prefer) are shown by dotted lines, and their sum is indicated by a heavy solid line. Thus, this simple example suggests that any complex waveform can be represented as the sum of an appropriate series of sinusoids. The question that must be answered now is how a complex waveform measured in the time domain can be decomposed into the series of sinusoids representing it. The theory and mathematics of Fourier analysis enables one to do this decomposition, which we turn to next.

Fourier Analysis

If $x(t)$ is a periodic function of time with period T , then it can be represented by a unique infinite trigonometric series, called a Fourier series, of the form:

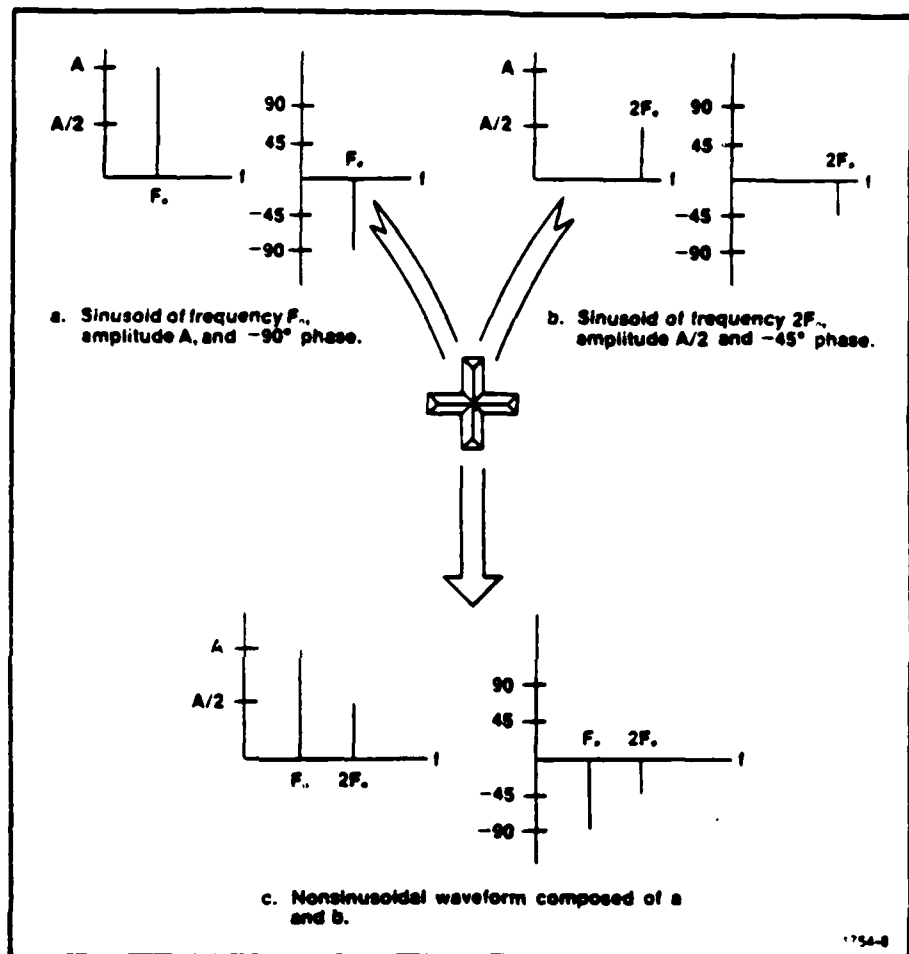
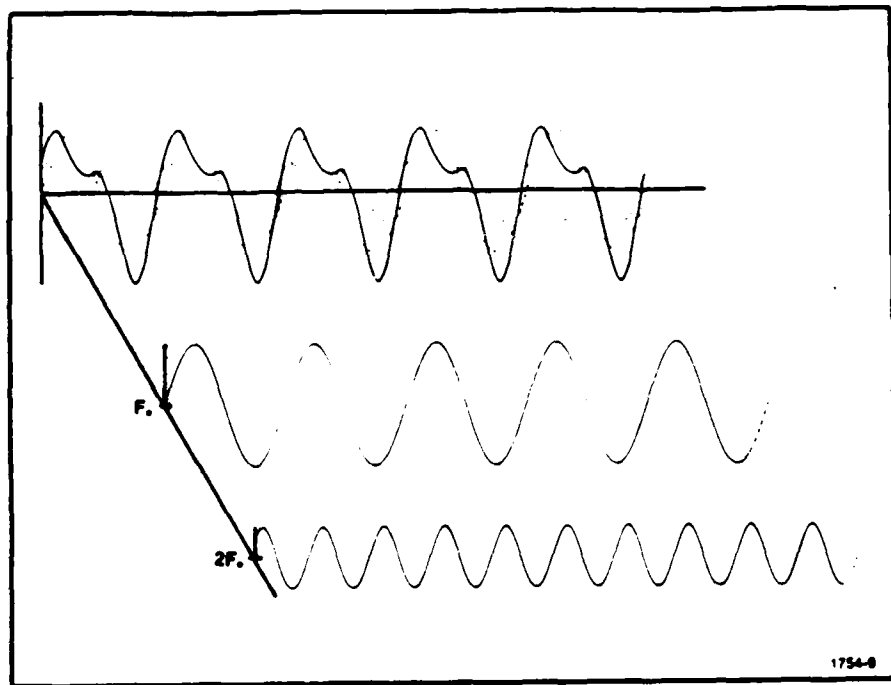


Figure 2.6 — Summing Frequency Domain Descriptions of Sinusoids (from Ramires [1985])



**Figure 2.7 — Composing a Nonsinusoidal Waveform by Summing Sinusoids
(from Ramirez [1985])**

$$x(t) = a_0 - \sum_{n=1}^{\infty} (a_n \cos 2\pi n f_0 t + b_n \sin 2\pi n f_0 t) \quad (2.6)$$

where $f_0 = 1/T$ (fundamental frequency) and the a_n 's and b_n 's are called Fourier coefficients, and are defined as:

$$a_n = \frac{2}{T} \int_{-T/2}^{T/2} x(t) \cos \frac{2\pi n t}{T} dt \quad (2.7)$$

$$b_n = \frac{2}{T} \int_{-T/2}^{T/2} x(t) \sin \frac{2\pi n t}{T} dt \quad (2.8)$$

for $n = 0, 1, 2, \dots$ (except that b_0 is undefined). Alternatively, the Fourier series and coefficients can be expressed in complex exponential form:

$$x(t) = \sum_{n=-\infty}^{\infty} c_n \exp(i2\pi n f_0 t) \quad (2.9)$$

$$c_n = \frac{1}{T} \int_{-T/2}^{T/2} x(t) \exp(-i2\pi n f_0 t) dt \quad (2.10)$$

where \exp is the base of the natural logarithm, and $i = \sqrt{-1}$.

In the case where the period of the waveform approaches infinity, i.e., the waveform has no apparent periodicity, the Fourier series above becomes, in the limit, a Fourier integral defined by:

$$x(t) = \int_{-\infty}^{\infty} X(f) \exp(i2\pi f t) df \quad (2.11)$$

The Fourier coefficients are now continuous values of frequency rather than discrete, as with the Fourier series, and they are given by:

$$X(f) = \int_{-\infty}^{\infty} x(t) \exp(-i2\pi f t) dt \quad (2.12)$$

The above two integrals are referred to as the Fourier transform pair. The former, eq. 2.11, is generally referred to as the inverse Fourier transform, and the later, eq. 2.12, as the direct Fourier transform, or simply the Fourier transform. The Fourier transform pair perform the transformations between the time and frequency domains. The problem faced now, however, is that in order to use the above Fourier transform pair it is necessary to have a continuous functional description of either the time or frequency domain waveform, depending on the direction of the transformation. This is impossible to obtain for random processes, and, in the case of digital signal processing, only values of the waveform at discrete points are known. Thus, some form of numerical integration must be applied to evaluate the Fourier integrals. In addition, because the Fourier integrals extend from minus to plus infinity, any numerical integration technique must truncate the integration since it is not possible to sample the waveform over all time or frequency.

With the above considerations in mind, an approximation to the Fourier transform integral, called the discrete Fourier transform (DFT), is defined as follows:

$$X_d(k\Delta f) = \Delta t \sum_{n=0}^{N-1} x(n\Delta t) \exp(-i2\pi k\Delta f n\Delta t) \quad (2.13)$$

This expression will transform a time series of samples into a series of frequency-domain samples. Similarly, the inverse DFT is defined as:

$$x(n\Delta t) = \Delta f \sum_{k=0}^{N-1} X_d(k\Delta f) \exp(i2\pi k\Delta f n\Delta t) \quad (2.14)$$

The inverse DFT will transform a series of frequency-domain samples back to a series of time-domain samples.

In both of the above discrete expressions, the variables have the following definitions:

N = number of samples being considered.

Δt = the time between samples, referred to as the sampling interval. From this, $N\Delta t$ gives the window length, often referred to as the time record length.

Δf = the sample interval in the frequency domain and is equal to $1/N\Delta t$.

n = the time sample index. Its values are $n = 0, 1, 2, \dots, N - 1$.

k = the index for the computed set of discrete frequency components. Its values are $k = 0, 1, 2, \dots, N - 1$.

$x(n\Delta t)$ = the discrete set of time samples that defines the waveform to be sampled.

$X(k\Delta f)$ = the set of Fourier coefficients obtained by the DFT of $x(n\Delta t)$.

exp = the base of the natural logarithm.

$i = \sqrt{-1}$.

The above discrete transformations, then, enable one to transform discrete sampled values of a waveform between the time and frequency domains. However, for large samples (large N) the number of computations required to compute the DFT and inverse DFT is extremely large. Therefore, a means to decrease the number of required computations would be appropriate. This leads us to the so-called fast Fourier transform (FFT) and inverse FFT. The FFT is nothing more than an efficient means of calculating the DFT. It recognizes repetition in the calculation of the DFT to reduce the number of computations, particularly multiplications.

In summary, the time and frequency domains are merely two different ways of presenting the same information. However, each domain allows certain characteristics of a waveform to be discerned more clearly than in the opposing domain. The Fourier series will transform periodic time functions into the frequency domain, while a Fourier integral transform is required to transform a nonperiodic time function. The discrete Fourier transform (DFT) and inverse DFT are numerical approximations to the Fourier integrals. Finally, the fast Fourier transform (FFT) and inverse FFT are efficient algorithms for computing the discrete transform approximations. We now turn our attention to some of the techniques for analyzing signals once they have been transformed into the frequency domain.

Spectral Analysis

Many different measurements can be made once the signals are transformed into the frequency domain, so-called spectral analyses. Measurements are typically made on two channels of data. The first channel is labeled the "input" while the second channel is

labeled the "output." Spectral analyses are basically statistical operations performed on the frequency domain data. Typically it involves either the correlation of the input or output with itself, or the correlation of the input with the output, assuming that the device or object under test is a linear system.

The idealized and actual models used in spectral analyses are shown schematically in figure 2.8. In the idealized model (figure 2.8[a]), the output, $y(t)$, is the response of the linear system to the input, $x(t)$. In an actual system (figure 2.8[b]), however, the measured input, $u(t)$, is composed of the input signal, $x(t)$, contaminated with background noise, $n(t)$. The measured output, $v(t)$, is composed of the response of the linear system to the input, $y(t)$, the output due to the noise at the input, $n'(t)$, plus background noise, $m(t)$.

Several of the frequency domain functions of interest are discussed below. The definition of and the equation for calculating each function is given. The equations are given as continuous functions of frequency, while in practice digital signal processing techniques are used and the continuous functions are replaced by their discrete approximations. The results of calculating each function for the time signals shown in figure 2.9 are shown as well. Typical uses of each function are also briefly described.

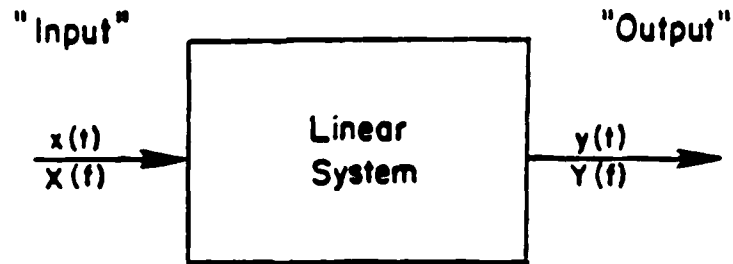
Linear Spectrum

The linear spectrum, $S_x(f)$, of a signal is the Fourier transform of the signal recorded in the time domain. The linear spectrum is a complex function and consists of either real and imaginary components (figure 2.10) or magnitude and phase (figure 2.11). The linear spectrum is used to identify the predominant frequencies and their absolute amplitudes and phases in a record. It is also used in the calculation of many of the frequency domain functions, as seen below.

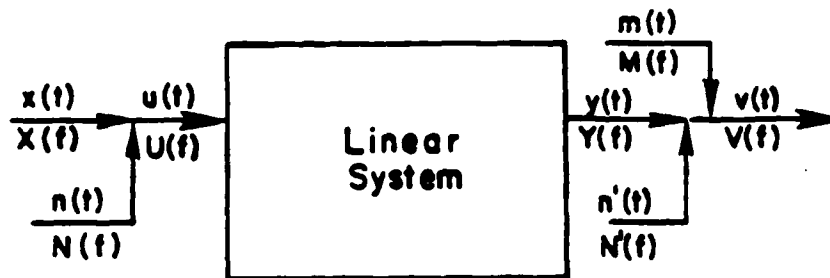
Auto Power Spectrum

The auto power spectrum, $G_{xx}(f)$, is the product of the linear spectrum, $S_x(f)$, and its complex conjugate, $S_x^*(f)$ (see figure 2.12). The magnitude of the auto power spectrum is equal to the magnitude of the linear spectrum squared, and it can be expressed as:

$$G_{xx}(f) = S_x(f) \times S_x^*(f) \quad (2.15)$$



a. Idealized System



b. Actual System

Note:

- $x(t)$ = Input due to Experiment.
- $y(t)$ = Output due to Experiment.
- $n(t)$ = Noise Source at Input.
- $n'(t)$ = Output due to Noise at Input.
- $m(t)$ = Noise Source at Output.
- $u(t) = x(t) + n(t)$ = Actual Input.
- $v(t) = y(t) + n'(t) + m(t)$ = Actual Output.

Capital letters denote the Fourier Transform of the functions described.

Figure 2.8 — Schematic of Idealized and Actual Models of a Linear System
(from Nasarian [1984])

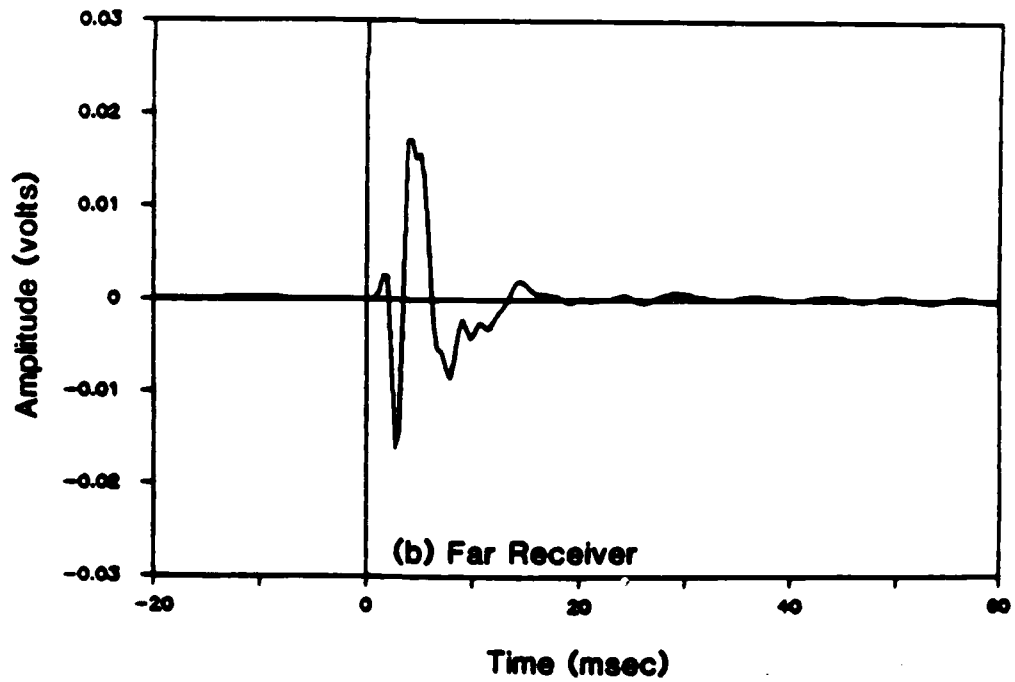
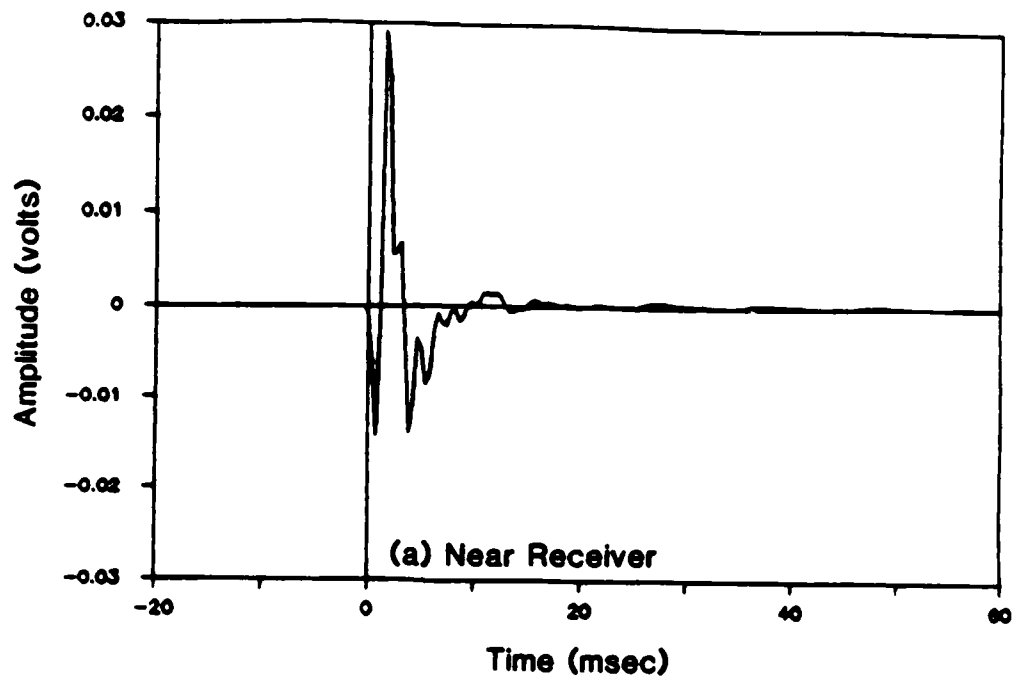


Figure 2.9 — Typical Time Signals from a SASW Test at a Pavement Site

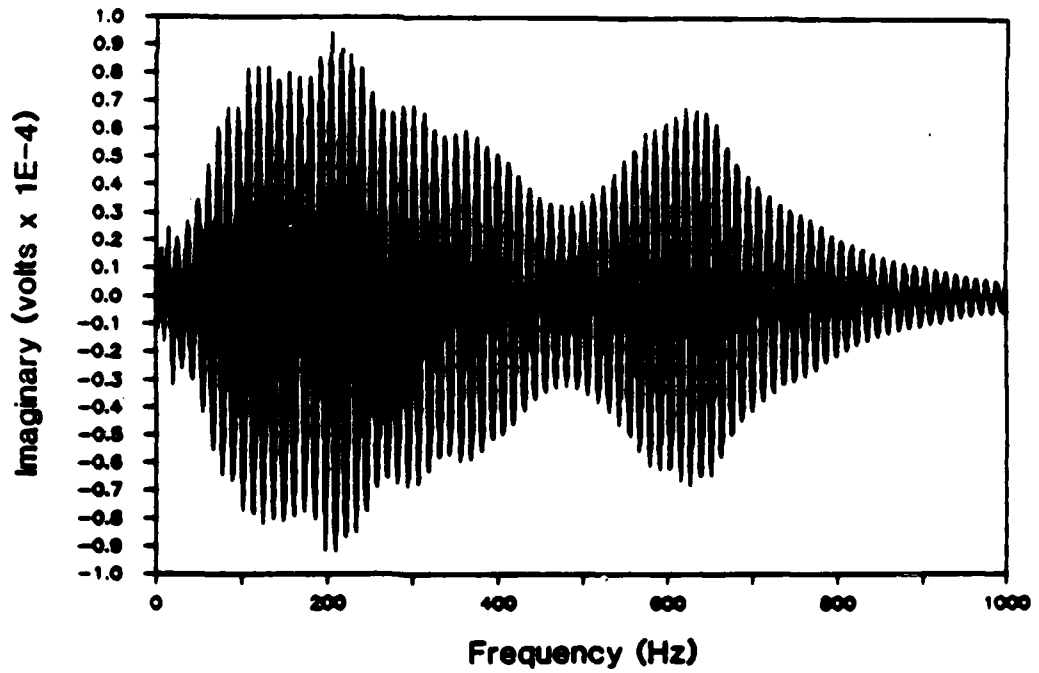
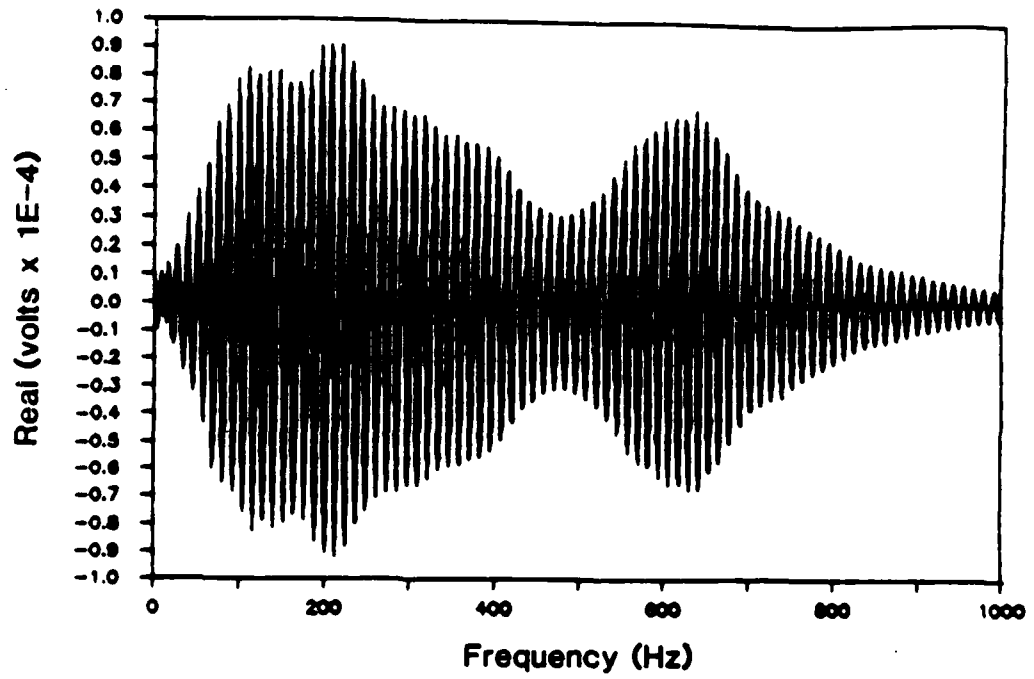


Figure 2.10 — Real and Imaginary Components of Linear Spectrum of Channel 1

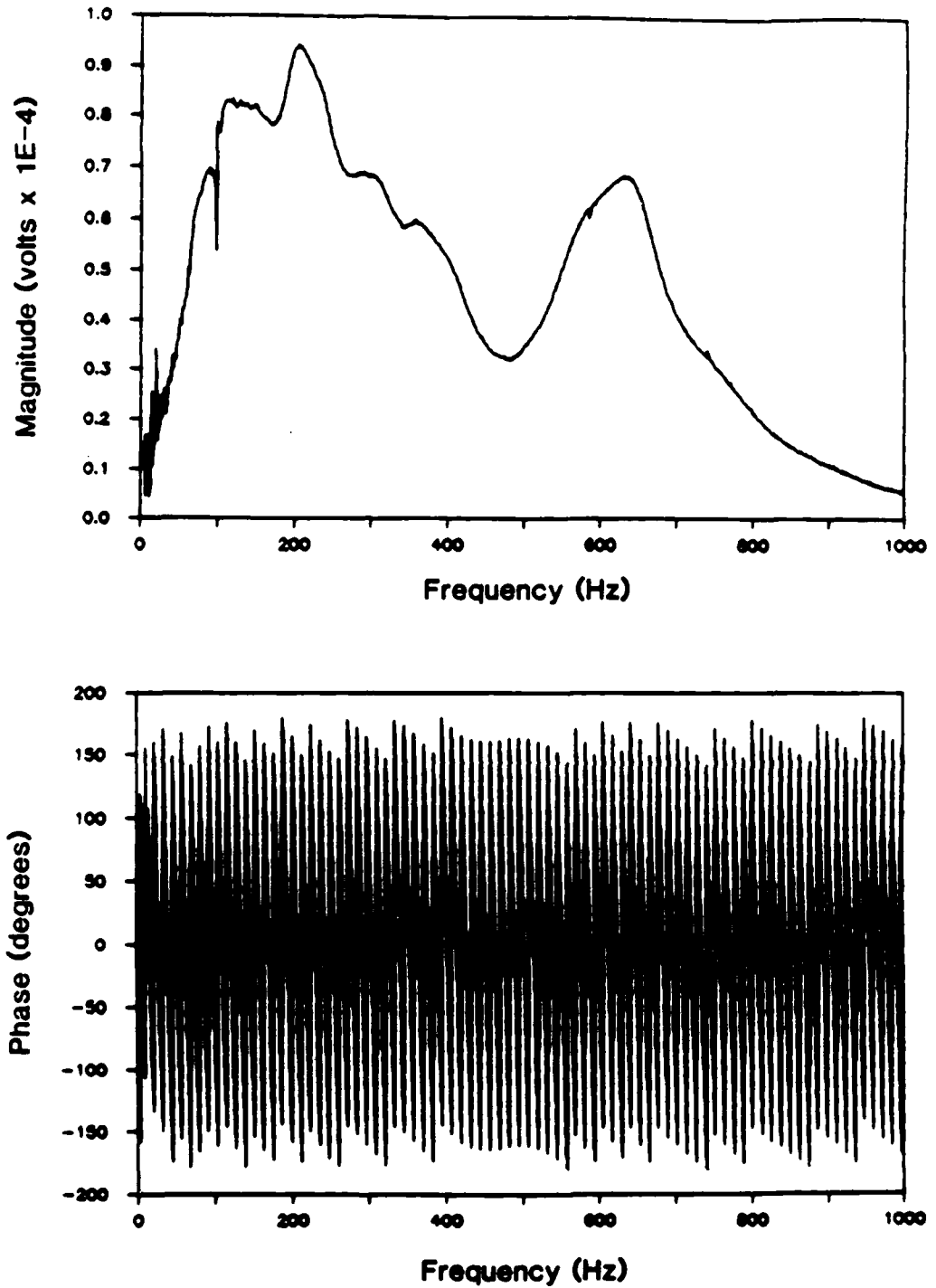


Figure 2.11 — Magnitude and Phase Components of Linear Spectrum of Channel 1

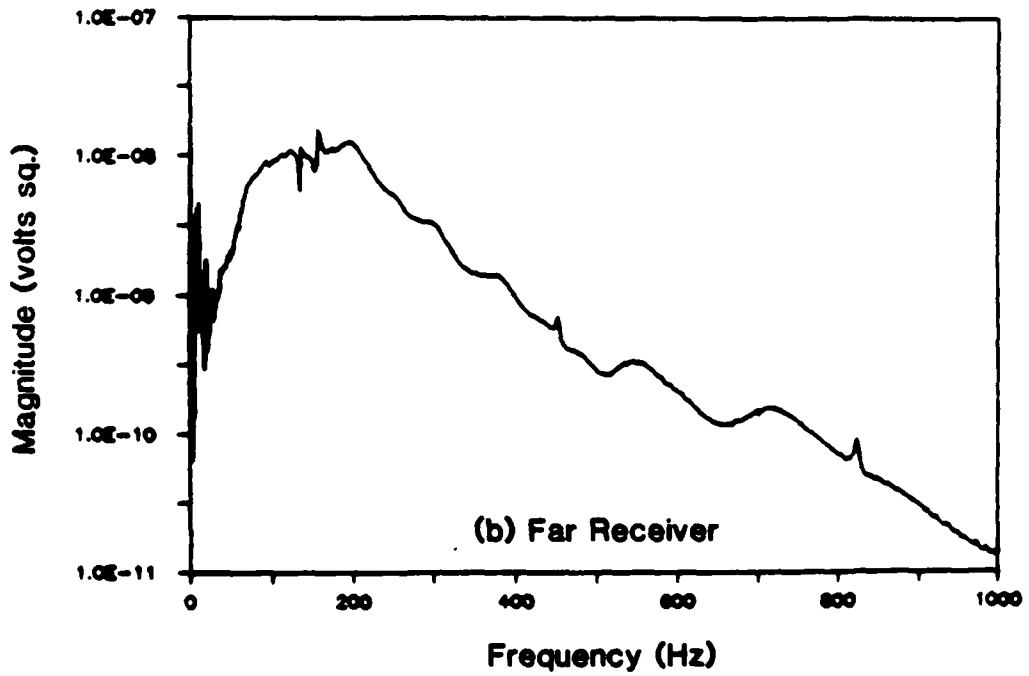
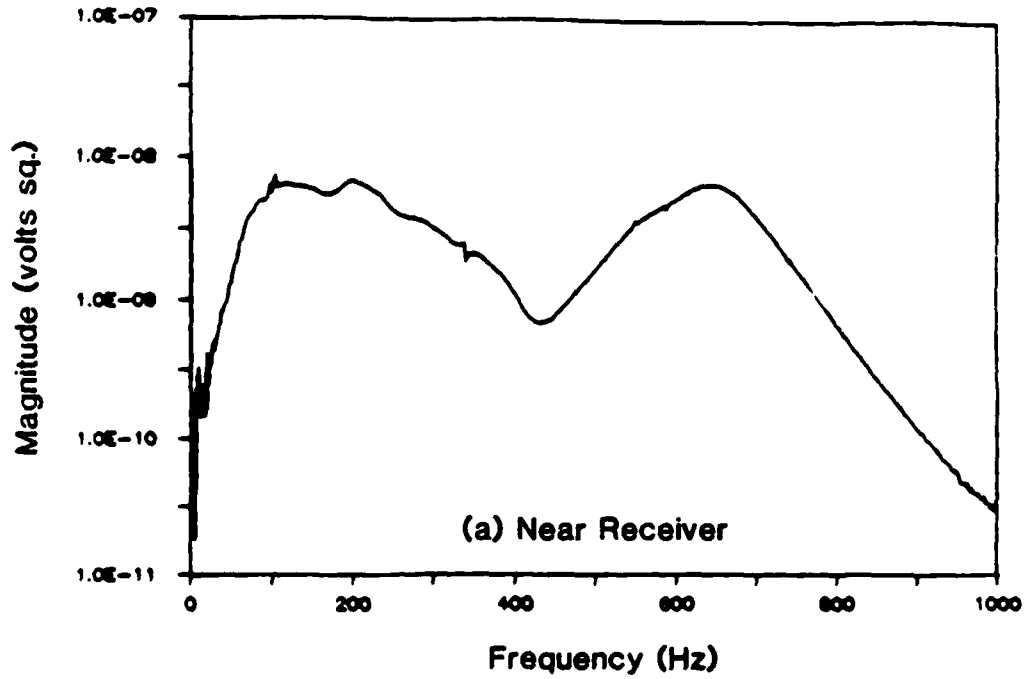


Figure 2.12 — Auto Power Spectra of Time Signals

This magnitude can be thought of as the power (or energy of a transient signal) at each frequency in the measurement bandwidth. $G_{xx}(f)$ is a real-valued function and thus does not contain any phase information. The auto power spectrum can be used to find predominant periods from a time record. The auto power spectrum is the Fourier transform of the auto correlation function in the time domain.

Cross Power Spectrum

If a system can be modeled as a linear system, signals from two records obtained simultaneously can be compared utilizing the cross power spectrum. The cross power spectrum (see figure 2.13), $G_{xy}(f)$, can be defined by the following equation:

$$G_{xy}(f) = S_x^*(f) \times S_y(f) \quad (2.16)$$

where $S_x^*(f)$ is the complex conjugate of the linear spectrum of the input, and $S_y(f)$ is the linear spectrum of the output. $G_{xy}(f)$ is a complex function. The magnitude of $G_{xy}(f)$ is a measure of the mutual power between the two signals. The phase of $G_{xy}(f)$ is the relative phase between the signals at each frequency in the measurement bandwidth. The cross power spectrum is the Fourier transform of the cross correlation function in the time domain. The cross power spectrum is a useful tool in determining the relative phase difference between two signals that may be caused by time delays, propagation delays, or varying wave paths between receivers. The cross power spectrum is the key measurement in SASW testing, since it is precisely the relative phase difference between two signals that we wish to determine.

Frequency Response Function

The frequency response function (figure 2.14), $H(f)$, is the ratio of the linear spectrum of the output signal to the linear spectrum of the input signal:

$$H(f) = \frac{S_y(f)}{S_x(f)} \quad (2.17)$$

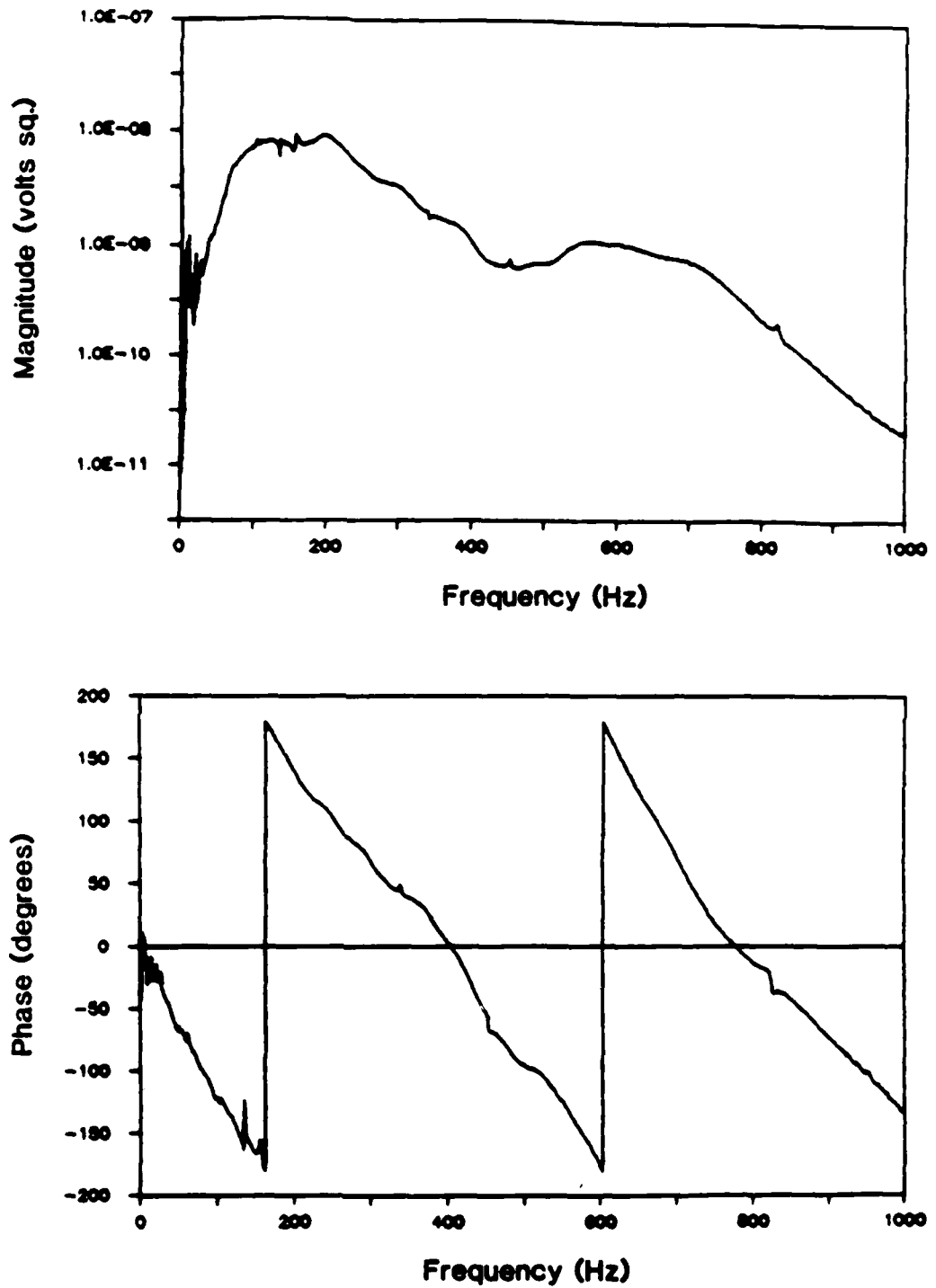


Figure 2.13 — Magnitude and Phase of Cross Power Spectrum

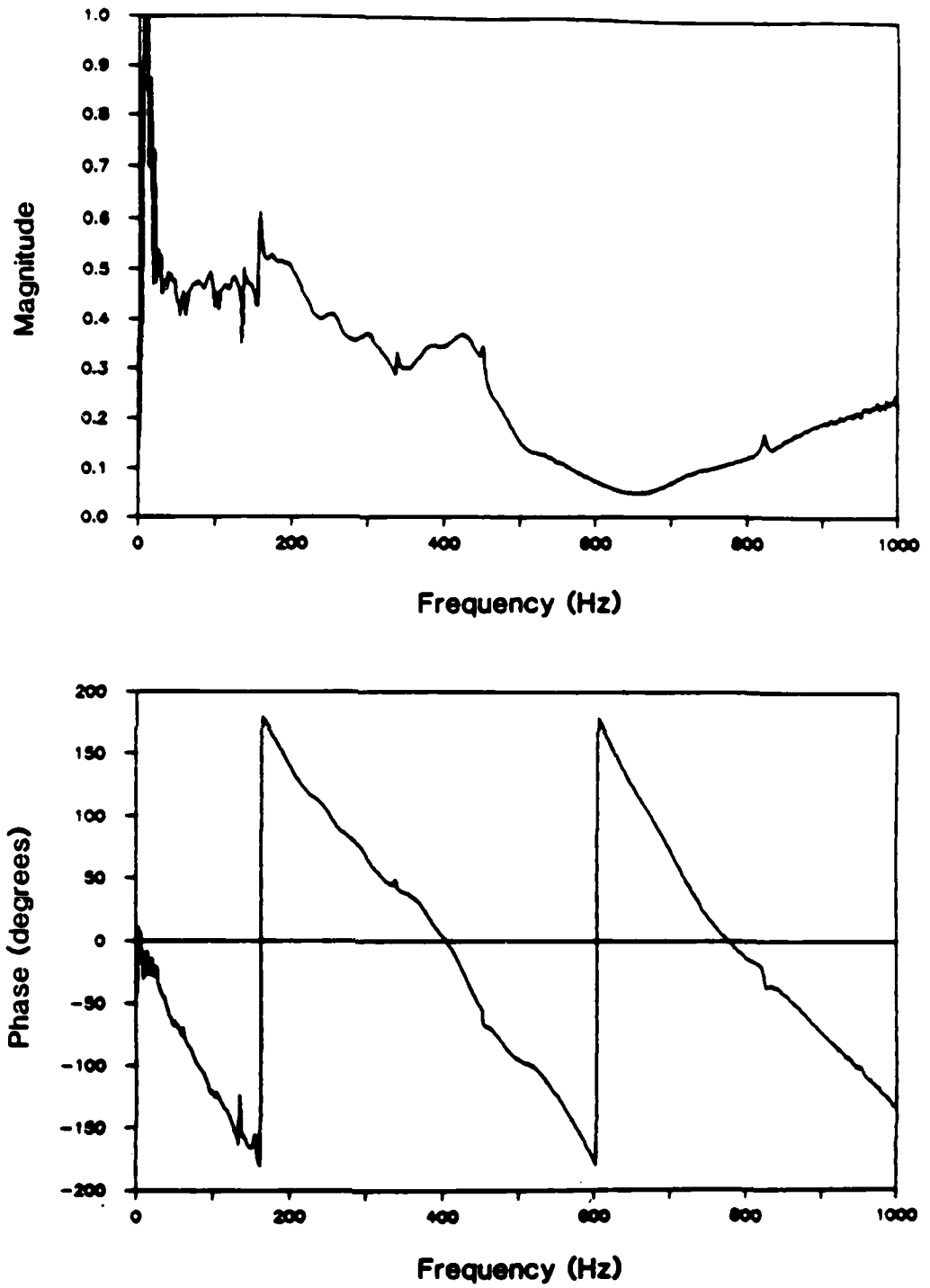


Figure 2.14 — Magnitude and Phase of Frequency Response Function

The frequency response function is equal to the Laplace domain transfer function evaluated along the frequency axis of the complex Laplace plane. The frequency response function is a complex function. The magnitude is a measure of the magnification of the input by the linear system at each frequency. The phase is identical to that of the cross power spectrum. The frequency response function is the Fourier transform of the impulse response function in the time domain. The frequency response function is used to identify the modal parameters of a linear system, i.e., the natural frequencies, damping parameters, and mode shapes. An alternative representation of the frequency response function is found by multiplying the numerator and denominator of eq. 2.17 by the complex conjugate of the linear spectrum of the input signal, $S_x^*(f)$. The result is:

$$H(f) = \frac{G_{xy}(f)}{G_{xx}(f)} \quad (2.18)$$

Thus the frequency response function is also the ratio of the cross power spectrum to the auto power spectrum of the input signal. $H(f)$ is usually calculated using eq. 2.18 rather than eq. 2.17 because it provides a better statistical estimate of the true frequency response function when the input and output signals are contaminated with background noise (the situation depicted in figure 2.8[b]).

Coherence Function

The last function applicable to SASW testing is coherence. The coherence function (figure 2.15), $\gamma^2(f)$, is analogous to a signal-to-noise ratio. Coherence is defined as:

$$\gamma^2(f) = \frac{\overline{G_{xy}(f)} \times \overline{G_{xy}^*(f)}}{\overline{G_{xx}(f)} \times \overline{G_{yy}(f)}} \quad (2.19)$$

where the barred quantities are the previously defined auto and cross power spectra arithmetically averaged in the frequency domain over multiple input records. The coherence is a real-valued function with a value between zero and one corresponding to the ratio of the response (output) power caused by the measured input to the total measured response power.

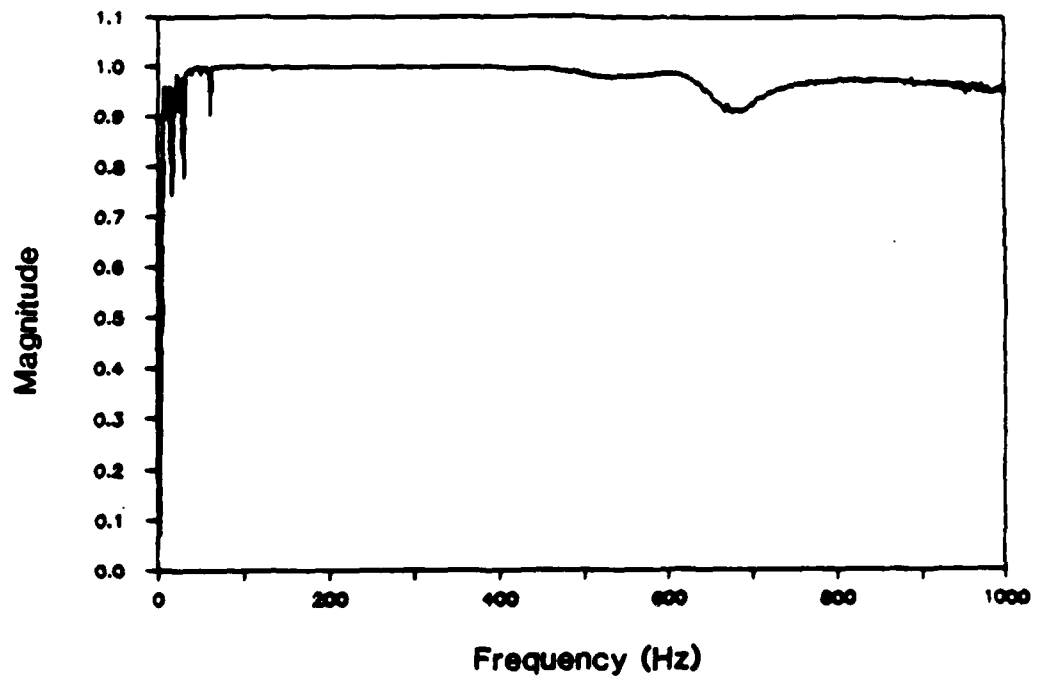


Figure 2.15 — Coherence Function

A value of coherence equal to unity at a certain frequency corresponds to perfect correlation between the two signals. Averaged values of the auto and cross power spectra are required to obtain a meaningful coherence function since the function will take a value of unity at all frequencies if only one signal pair is used in the computation regardless of whether there is perfect correlation between the two signals or not. Bendat and Piersol (1980) suggest the following reasons for why the coherence function may not equal unity:

- 1) Extraneous noise is present in the measurements (figure 2.8[b])
- 2) Resolution bias errors are present in the spectral estimates (Δf in eq. 2.13 too large)
- 3) The frequency response function of the system is not linear
- 4) The output is due to other inputs besides the one under consideration
- 5) Waves in the frequency range of poor coherence are not adequately excited

The coherence function is used to check the data obtained during SASW testing to establish the range of frequencies providing accurate cross power spectrum phase values.

2.7 Excitation Techniques for Frequency Response Testing

This section briefly reviews the excitation techniques available for frequency response testing. The three principal types are sinusoidal, random, and impact. Discussion of each of these methods follows. A more comprehensive review of the techniques can be found in the publications by Ramsey (1976), Brown, Carbon, and Ramsey (1977), and Halvorsen and Brown (1977).

Sinusoidal

The sinusoidal excitation technique was briefly discussed in conjunction with the steady-state Rayleigh wave method in section 2.4. This technique has been in use since the 1950's and hence is probably the most popular and best understood of the excitation techniques. The procedure used is a simple one. A controlled sinusoidal force is input to the structure by means of an electro-mechanical or hydraulic shaker and the response of the system is measured with a suitable transducer.

The principle advantage of swept sine testing is that the input force can be precisely controlled. This is particularly useful in the study of nonlinear systems. Another advantage

is that large amounts of energy can be input to the structure at each frequency. This results in high signal-to-noise ratios as compared to the other excitation techniques.

The major disadvantage of swept sine testing is that it is slow. Since only one frequency is studied at a time, it takes a long time to obtain the complete frequency response characteristics of a system. Another disadvantage of swept sine testing is that it gives a very poor linear approximation of a nonlinear system.

Random

In this section three types of broadband random excitation are discussed. The three types are pure random, pseudo random, and periodic random. All random excitation techniques are alike in that the input is applied by a shaker driven by a signal containing equal energy over the entire frequency range of interest, i.e., a signal with a flat auto power spectrum. Typically, the random signal is passed through a bandpass filter to concentrate energy in the frequency range of interest. The signal spectrum will thus be flat over the range of interest except for filter roll-off. The three methods differ in the characteristics of the random signal.

Pure Random

Pure random excitation is characterized by the fact that it is in no way periodic. With a pure random signal each sampled record of data is different from the preceding and following records. This gives rise to the most important advantage of using a pure random signal. Successive records of frequency domain data can be arithmetically averaged together to remove nonlinear effects, noise, and distortion from the measurement. As more and more averages are taken, all of these undesirable components will average toward an expected value of zero in the frequency domain data. Thus, a better measure of the linear estimate of the response of the structure can be obtained.

The most serious drawback of pure random excitation is that the measured input and response signals are not periodic in the measurement time window of the frequency domain analyzer. A key assumption of digital Fourier analysis is that the time waveforms be exactly periodic in the observation window. If this condition is not met, the corresponding frequency spectrum will contain so-called "leakage" due to the nature of the discrete Fourier

transform. That is, energy from the non-periodic parts of the signal will "leak" into the periodic parts of the spectrum, thus giving a less accurate result.

Pseudo Random

In order to avoid the leakage effects of using a pure random signal, a waveform known as pseudo random can be used. This type of signal is usually generated with a digital frequency domain analyzer and its digital-to-analog converter (DAC). It typically has a flat auto power spectrum and random phase. The signal is generated in the analyzer and repeatedly output to a shaker through the DAC every T seconds (the measurement time window of the analyzer). Since the length of the pseudo random signal is exactly the same as the analyzer's measurement record length, it is periodic in the measurement window and leakage problems are eliminated.

The major disadvantage of this type of signal is that because it repeats with every measurement, nonlinearities, distortion, and periodicities due to loose components on the structure cannot be removed by averaging, since they are excited equally every time the pseudo random record is output.

Periodic Random

Periodic waveforms combine the best features of pure random and pseudo random while at the same time eliminating the disadvantages. Periodic random signals satisfy the conditions for a periodic signal, yet change with time to excite the structure in a truly random manner.

The process begins by producing a pseudo random signal from the DAC to the exciter. After the transient part of the excitation has died out and the structure is vibrating in its steady-state condition, a measurement is taken. Then, instead of continuing to produce the same signal again, a different uncorrelated pseudo random signal is produced. This new signal excites the structure in a new steady-state manner and another measurement is made.

When the measured responses are averaged together, nonlinearities and distortion components are removed. Thus, the ability to use a periodic random signal eliminates leakage problems and averaging is now useful for removing distortion.

The only drawback to this approach is that it is not as fast as pseudo random or pure random, since the transient part of the structure's response must be allowed to die out before a new average can be made.

Impact

The last excitation technique to be discussed is impact testing. The test procedure is very simple. Strike the structure under test with a hammer or other object and record the response.

In general, impact testing has important advantages over other methods. First, no electro-mechanical or other type of shaker is required. Second, the method is faster than any of the other excitation techniques.

The method does have its drawbacks, however. The most serious is that the auto power spectrum of the input force is not as easily controlled as with a mechanical shaker. This causes nonlinearities to be excited and can result in some variability between successive measurements. The impact force can be somewhat controlled by changing the impactor. The characteristics of the impactor determine the magnitude and duration of the force pulse, which, in turn, determine the magnitude and content of the pulse in the frequency domain. The two impactor characteristics of most importance are its weight and tip hardness. The frequency content of the force is inversely proportional to the weight of the impactor and directly proportional to the hardness of the tip. A further problem is that since the total energy supplied by an impulse is distributed over a broad frequency range, the actual excitation energy density is often quite small. This can result in poor signal-to-noise ratios in the measurements.

Another major problem is that of frequency resolution. Adequate frequency resolution is essential in making good frequency response measurements. The fundamental nature of a transient response signal places a practical limitation on the resolution obtainable. In order to obtain good frequency resolution a large number of digital data points must be used to represent the signal, and thus the time record becomes longer. As the response signal decays to zero, its signal-to-noise ratio becomes smaller and smaller. If it has decayed to a small value before a data record is completely filled, the Fourier transform will be operating mostly

on noise, causing added uncertainty in the measurements. The problem becomes more important as higher frequency resolutions are needed and with heavily damped structures.

2.8 Summary

This chapter discussed the background information necessary for a complete understanding of the SASW method. The discussion covered six major topics: 1) wave propagation in an elastic half-space, 2) factors influencing elastic moduli, 3) seismic field methods for determining elastic moduli, 4) pavement overlay design and nondestructive evaluation, 5) digital signal analysis, and 6) excitation techniques for frequency response testing. The reader is directed to the references cited for a more thorough discussion of the topics covered.

CHAPTER III

THE SPECTRAL-ANALYSIS-OF-SURFACE-WAVES METHOD

3.1 Introduction

A new method for measuring shear wave velocity and elastic moduli, i.e., stiffness, profiles in situ, called the spectral-analysis-of-surface-waves (SASW) method, has been under continuous development since 1980. The method has been used to date for a number of applications, including nondestructive pavement evaluation, evaluation of soil liquefaction potential, evaluation of a concrete dam, and as a diagnostic tool for determining the effectiveness of soil improvement techniques. The SASW method is based on the generation and detection of Rayleigh waves at low strain levels from the surface of the layered system. The method has the following advantages: it is nondestructive, it is performed from the surface of the system, it does not require boreholes, the test setup and procedure is simple, and it has the capability of being fully automated.

It was stated above that the SASW method is new and that its development began about 1980. This requires some qualification. The historical development of the use of surface wave techniques has been reviewed by Nazarian (1984). From this review it is evident that the concepts upon which the SASW method is based are not new. Seismologists have been using surface wave techniques to determine earth structure for many years. Civil engineers have used surface waves for some time as well. However, previous use of surface waves for civil engineering applications have had at least one of the following two deficiencies: 1) use of steady-state excitation, which we have seen greatly increases the required testing time, and 2) use of some approximate procedure to determine the shear wave velocity profile

from the collected data. The use, starting about 1980, of modern frequency spectrum analyzers that enable one to analyze many frequencies simultaneously, and the application of theoretically-based methods of determining the shear wave velocity profile from the collected data (Nazarian 1984), have led to a "new" surface wave technique for civil engineering applications, i.e., the SASW method.

Investigation of a site using the SASW method consists of the following three phases: 1) collection of data in the field, 2) determination of the Rayleigh wave dispersion curve, and 3) inversion of the Rayleigh wave dispersion curve. Each phase is individually discussed in the following sections.

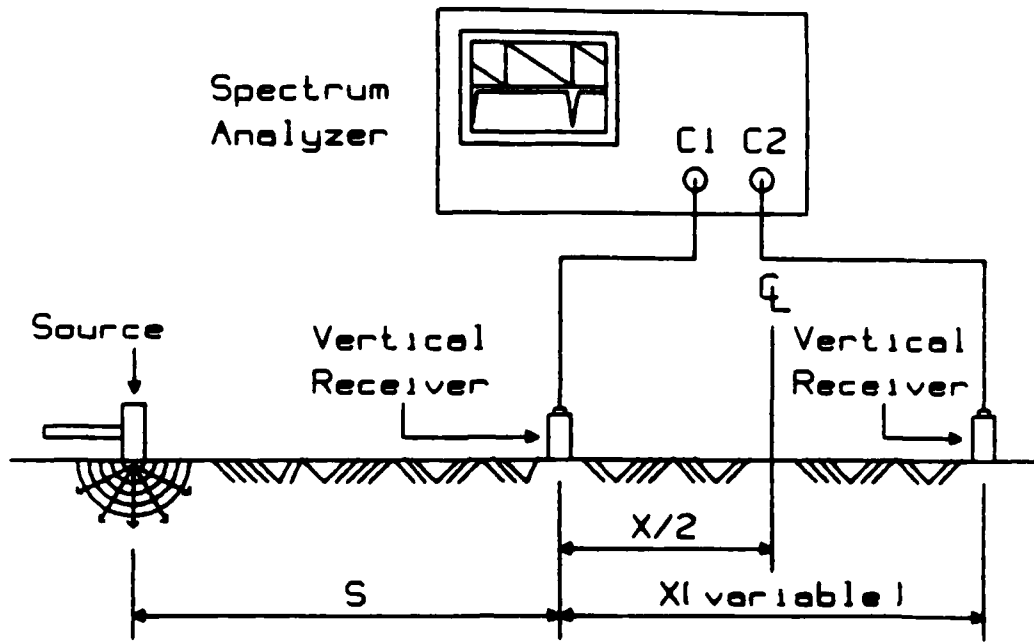
3.2 Collection of Data in the Field

A schematic of the current test procedure is shown in figure 3.1. The procedure is quite simple. Two vertical receivers are located on the surface at the site. A surface wave is generated by an appropriate source. The generated wave front is detected by the receivers as it propagates past them and is recorded on the appropriate device. A more thorough discussion of the equipment required and of how the measurements are made follows.

Source

The source should be able to generate Rayleigh waves over a wide range of frequencies with adequate amplitude so that they can be detected by the receivers. Simultaneously, the source should generate minimal P- and S-wave energy. Heisey et al. (1982) identified two important factors in source selection. First, the magnitude of the input energy does not seem to be a critical factor as long as it exceeds the background noise level. Rather, source selection should be based on the range of frequencies that can be sufficiently excited to adequately sample the site. Further, the energy of excitation should not be focused on a few frequencies but should be distributed over all frequencies in the measurement bandwidth.

The actual frequency values required for testing a site are dependent upon the stiffness of the materials to be tested and on the desired depth of investigation. Nazarian (1984) has indicated that the highest frequency required for testing soil sites is typically 200-800 Hz. The more important value for testing soil sites, however, is usually the lowest frequency to



(a) General Configuration of SASW Tests

							Distance, ft
12	8	4	0	4	8	12	Spacing, ft
↓ Receiver			↓	↓ Source			0.5
			↓	↓			1
		↓	↓	↓	↓		2
	↓	↓	↓	↓	↓		4
↓	↓	↓	↓	↓	↓		8

(b) Common Receivers Midpoint Geometry

Figure 3.1 — Schematic of Experimental Arrangement for SASW Tests (after Nazarian (1984))

be excited. This is because it is usually desirable to measure the shear wave velocity profile as deep as possible and it is the low frequency (long wavelength) surface waves that sample the deep materials. Nazarian (1984) indicated that one of the most important additions to the SASW method would be a source capable of generating frequencies below 5 Hz so that deeper deposits can be sampled. The author has sometimes found it difficult to obtain acceptable data below 25 Hz at sites where strong background noise is present. A source capable of generating adequate energy at these low frequencies would indeed be a very important addition to the SASW method.

For testing pavement sites, on the other hand, it is the high frequencies that are typically most important and more difficult to generate and resolve. Since it is normally not required to determine the stiffness profile below about 10 feet from the surface, the lowest frequency to be generated is usually on the order of 30 Hz, which is usually not difficult to produce. However, for sampling the thin, stiff layers near the surface of pavement systems, it is necessary to generate very high frequencies, occasionally as high as 100 kHz. For impact testing methods this requires a source capable of producing a very short impulse, as discussed in chapter two.

A second important factor identified is the coupling of the source with the test surface, which influences the transfer of energy. Heisey et al. (1982) found that the use of a plate between the hammer and impact surface should be avoided if the generation of low frequencies (long wavelengths) is desired.

Two excitation techniques have been employed to date, namely, impact and random vibration. The salient characteristics of each method have been reviewed in chapter two. Impact techniques are more popular at the present time, although Drnevich, et al. (1985) have used random noise excitation with some success. Based upon the discussion in chapter two and the discussion of required frequency ranges above, it comes as no surprise to find that for testing the stiff layers near the surface of pavements using an impact source, a light hammer producing a short impulse is much better than a large weight which produces a relatively cushioned impulse. The opposite is true for testing soil sites.

Examples of sources used to date include: claw hammer, range of sizes of ball peen and sledge hammers, drop hammer (compaction hammer), hammer and chisel, Standard Pene-

tration Test (SPT) hammer, and various size shakers excited with a random signal. Again, the light-weight sources capable of generating high frequencies are used for investigations where the properties of shallow layers are of primary concern. The size and weight of the source (for impact testing) is increased, and thus the upper frequency bound decreased, as the required depth of investigation increases. An SPT hammer has been successfully employed in one case study by the author to sample materials as deep as approximately 50 feet. The case studies presented in later chapters should give more of an indication of the frequencies capable of being generated by many of the above sources.

Receivers

Vertically oriented transducers (velocity or acceleration, depending on required frequency range) are used as receivers in the field. Based on tests performed on pavements, Heisey et al. (1982) found that vertical transducers provide a more accurate velocity profile than do horizontal. They found that velocities obtained from measurements using horizontal transducers were generally too high, and suggested that this was probably due to the greater sensitivity of horizontal transducers to higher-velocity P-waves that contaminate the measured signal to some degree.

The range of frequencies over which the receivers should function depends on the site being tested. To sample deep materials (50 to 100 ft), velocity transducers with a low natural frequency, typically within the range of 1 to 2 Hz, are appropriate. In contrast, for sampling the shallow layers more common to pavement sites, the receivers should be able to respond to frequencies in the kHz range, i.e., the use of accelerometers is more appropriate. Velocity transducers are typically useful in the range 1-1,000 Hz, while accelerometers can have a useful range from 1 to 20,000 Hz. However, accelerometers will generally produce less output at lower frequencies than velocity transducers. It is recommended, therefore, that velocity transducers be used if the frequencies to be measured are less than 1000 Hz. The result of this recommendation is that velocity transducers are used almost exclusively for investigating soil sites. For investigating pavement systems, on the other hand, a combination of velocity transducers and accelerometers are used. The accelerometers in this study (100 mV/g sensitivity, see chapter four for other characteristics) were typically used

for receiver spacings below 4 feet, while velocity transducers were used for spacings of 4 feet and above. Accelerometers with higher sensitivity (1 V/g) could be used for larger spacings and their purchase is recommended.

An issue of some concern when employing velocity transducers in the SASW method is that of phase-angle distortion. It is usually desirable to use velocity transducers that display a horizontal response curve over the widest range of frequencies possible. This is achieved by adding a certain amount of damping to the velocity transducer. However, damped velocity transducers always introduce distortion of complex or superimposed waveforms. This is due to a phase shift or time delay between the mechanical input and the electrical output signal of the instrumentation system (Eller and Conrad [1976]). Therefore, velocity transducers that are intended for use in measuring either transient disturbances or vibrations containing several frequency components simultaneously, such as in the SASW method, should be calibrated to determine that the phase-angle distortion is acceptably small. Alternatively, because it is the relative phase difference between two velocity transducer signals that is desired in the SASW method, some phase-angle distortion can be tolerated as long as the distortion caused by each transducer is approximately the same. Phase-angle distortion is also possible with accelerometers. It is highly recommended that a matched pair of receivers be used at all times and that periodic checks be made of transducer pairs to ascertain the range of frequencies where the phase-angle distortion is below a tolerable level. The transducers should be used only within this frequency range or the measured results will be questionable.

Another important aspect related to receivers is that of attaching them to the test surface. Positive coupling between the receivers and the test surface is essential. Velocity transducers used at soil sites are typically coupled through detachable spikes. For sites with loose materials near the surface, partially burying the velocity transducers often provides more positive coupling. Both velocity transducers and accelerometers have been successfully mounted on pavement surfaces with materials such as bees-wax (Nazarian [1984]), potter's clay, epoxy, and Super Glue. This technique, however, would not be practical for an automated testing procedure. More research is required to develop an efficient means to positively couple receivers to a pavement surface.

Location of Source and Receivers

The factors that affect appropriate spacing of the receivers have been studied by Heisey et al. (1982). These factors include: 1) velocity of the material to be tested, 2) desired depth of investigation, 3) range of frequencies, 4) attenuation properties of the medium, and 5) sensitivity of the instrumentation.

On the basis of studies conducted at several soil sites, Heisey et al. (1982) found that a spacing arrangement in which the first receiver (receiver nearest the source) is located at an increasing distance from the source is more favorable than an arrangement in which the first receiver is fixed at a reference location close to the source. In addition, Heisey et al. (1982) found that much of the scatter in the velocity profile can be reduced by filtering out data for wavelengths which are inappropriate for the spacing of the receivers. Wavelengths which are too short for a given spacing may attenuate excessively, whereas wavelengths which are too long may not have traveled a sufficient distance to sample adequately the depth proportional to the wavelength. Furthermore, since frequency analyzers possess a potential relative error, i.e., percentage error, in measuring phase relationships, it is desirable to set a lower limit on the measured phase angles one is willing to accept in order to keep the absolute error below a specified level. This transforms in the present case to setting an upper limit on the wavelengths one is willing to accept at each receiver spacing. Based on these considerations, an appropriate range of wavelengths (L_R) for a given receiver spacing (x) was found to be:

$$x/2 \leq L_R \leq 3x \quad (3.1)$$

Eq. 3.1 is used at each receiver spacing to eliminate those data points not satisfying the wavelength criterion.

Theoretically, one test at one receiver spacing is sufficient to determine the properties of the medium. However, due to the factors discussed above, several tests with different receiver spacings are typically required to obtain data over the complete range of frequencies desired. In each test the distance between the receivers is generally doubled. A typical

setup is shown in figure 3.1(b). The receivers are always placed symmetrically about the selected, imaginary centerline. This pattern of testing is called the common receivers midpoint (CRMP) geometry. Nazarian and Stokoe (1983) have shown that use of this setup reduces scatter in the data due to the fact that the distances covered in the previous tests are always included in the next tests. Small receiver spacings are used to obtain short wavelengths (high frequencies) and thus shallow depths, while large spacings are used to obtain long wavelengths (low frequencies) and thus large depths. Typical receiver spacings range from 0.5 to 8 feet for pavement sites and from 2 to 64 feet for soil sites. These values may change depending on the range of depths to be sampled at a particular site.

In addition, at each receiver spacing, two series of experiments are performed. First, the test is carried out from one direction (forward profile). Then, without relocating the receivers, the same test is performed with the source on the opposite side of the receivers and the receiver cables switched on the recording device (reverse profile). By running forward and reverse profiles and by averaging the results of these two tests, the effect of any internal phase shift between receivers is minimized, and the effect of dipping layers along the distance between the receivers is averaged.

Recording Device

The records of wave arrivals at different receivers can be easily recorded on an oscilloscope or other data acquisition hardware and then stored on magnetic tape or disk. These measurements are thus made in the time domain. By means of the fast Fourier transform algorithm, the results can then be converted to the frequency domain, and the data can be reduced to develop the Rayleigh wave dispersion curve.

A more convenient device is a Fourier spectrum analyzer. A Fourier spectrum analyzer is a digital oscilloscope that has the ability to operate in either the time or frequency domain. The analyzer can directly calculate all of the time and frequency domain functions previously discussed in section 2.6. Thus, the data can be easily checked in the field to determine its suitability for future analysis. In addition, the type and number of averages, frequency span, trigger conditions, input voltage ranges, and the type of measurement window function can all be specified by the operator. The analyzer can also be easily interfaced with a

magnetic tape recorder or disk drive for permanent storage and recall of data. The major drawbacks of Fourier spectrum analyzers, however, are that they are relatively expensive (approximately \$25,000), and they commonly can only record and analyze two channels of data simultaneously.

Measurement Parameters

The measurement parameters of concern here are the setup parameters for the recording equipment. The discussion is primarily directed towards the use of a Fourier spectrum analyzer as the recording device. The pertinent parameters are the type and number of signal averages, frequency span, input ranges, triggering, and measurement window function.

As discussed above, SASW testing is conducted at each site for a series of receiver spacings. In addition, to help decrease the effect of background noise, more than one record is obtained at each receiver spacing and source location and the records are ensemble averaged in the frequency domain. As discussed in section 2.6, averaging of signal pairs in the frequency domain is also necessary to provide a meaningful coherence function. Heisey et al. (1982) have found that results obtained with five averages will provide reliable data. They have shown that additional averages are not warranted because they do not significantly improve the end results.

The second setup parameter of concern is the frequency span, i.e., the maximum frequency to be included in the measurements (assuming baseband or zero start frequency measurements). The primary objective in choosing the frequency span is to obtain the best resolution in the frequency domain (and thus in the dispersion curve) as possible while at the same time obtaining the complete range of frequencies for the particular test setup. A trade off must be made because a spectrum analyzer digitizes a fixed number of points independent of any of the setup parameters. Thus, as the frequency span increases the frequency resolution decreases.

The choice of frequency span depends upon two factors: the receiver spacing and the stiffness of the material under test. For small receiver spacings, large frequency spans are required because it is the high frequencies that are of interest, and vice versa for large receiver spacings. For a given receiver spacing, as the stiffness of the material under test increases, the required frequency span must increase to fully describe the dispersion curve.

The phase of the cross power spectrum and the coherence function are used as guides for selecting the appropriate frequency span for a given receiver spacing and material profile. Nazarian (1984) suggests a rule of thumb for selecting the frequency span: the optimum bandwidth is obtained when more than $3/4$ of the frequency range contains data of high quality, identified by coherence values greater than 0.9. Use of eq. 3.1 can also be made in selecting the appropriate frequency span. Eq. 3.1 suggests that the data should be filtered for wavelengths smaller than $1/2$ the receiver spacing and larger than 3 times the receiver spacing. This transforms into accepting continuous or unwrapped phase values from the cross power spectrum between 120 and 720 degrees. Thus, frequencies with phase values larger than 720 degrees should not be recorded in the field since they will subsequently be filtered out of the data. The optimum frequency span, then, is obtained as the lesser of the two frequencies from the above rules.

The third input parameter to be chosen are the voltage ranges for the recording channels. The voltage ranges should be set as low as possible without overloading to obtain the best resolution in the analog to digital conversion. The value for the channel connected to the receiver nearer the source (usually channel 1) will typically be higher than the value for the farther receiver; this does not create any problems and is preferred to obtain the best resolution. Also, the ranges will likely need adjustment for each receiver spacing.

The fourth consideration is triggering of the instrument to begin recording data. The primary objective is to obtain the complete signal for all channels and not to introduce any internal phase difference between the channels. For the impact testing technique the recorder is typically triggered off the signal from the near receiver about half way up (down) the first major pulse. A pre-trigger delay is then set to ensure that the initial portion of the signal is obtained. It is imperative that the pre-trigger delay be an equal amount for all recording channels, otherwise an internal phase difference will be introduced. Nazarian (1984) suggests that a pre-trigger delay of 10 percent of the total time record is sufficient.

The final measurement parameter to select is the measurement window function. The measurement window function is the function applied to the time domain records to ensure that the signals have zero value at each end of the record, and thus be periodic with respect to the measurement window. This is necessary to prevent leakage, as discussed in

section 2.7. For impact testing the signal usually decays to zero before the end of the record and a rectangular or uniform window function is used. This, in effect, does nothing to the measured time signal. For testing techniques where leakage may be a problem, e.g., pure random, an appropriate window should be applied, a Hanning window for example.

3.3 Determination of the Rayleigh Wave Dispersion Curve

The in-house data reduction associated with the SASW method consists of construction of the dispersion curve and then inversion of the dispersion curve. It was noted earlier that the variation of wave velocity with frequency (or wavelength) is known as dispersion. A plot of velocity versus wavelength is called a dispersion curve. The dispersion curve is constructed from the spectral analysis functions discussed in section 2.6. The information of major interest is obtained from the coherence function and from the phase of the cross power spectrum. A typical coherence function and phase of the cross power spectrum are shown in figure 3.2. From the coherence function, the range of frequencies that should be considered in each record is selected. Nazarian and Stokoe (1986) have found that frequencies with a coherence value greater than 0.90 provide useful data. The phase information of the cross power spectrum provides the relative phase between two signals at each frequency in the range of frequencies excited in the SASW test. Phase information should only be accepted for those frequencies satisfying the coherence criterion above. As seen in figure 3.2, regions with low coherence exist, and phase data in these regions would be deleted in constructing the dispersion curve. In the end, however, it is the phase angle of the cross power spectrum that is used in the calculation of the dispersion curve. Using the coherence function as the sole criterion can lead to questionable results if correlated "noise" is measured at each receiver. The coherence function will indicate "good" data in this instance, yet the phase angle may yield incorrect dispersion data. The experienced user will consider both the phase angle of the cross power spectrum and the coherence function to determine the ranges of good data.

For a travel time equal to the period of the wave, the phase difference is 360 degrees. Thus, for each frequency the travel time between receivers can be calculated by:

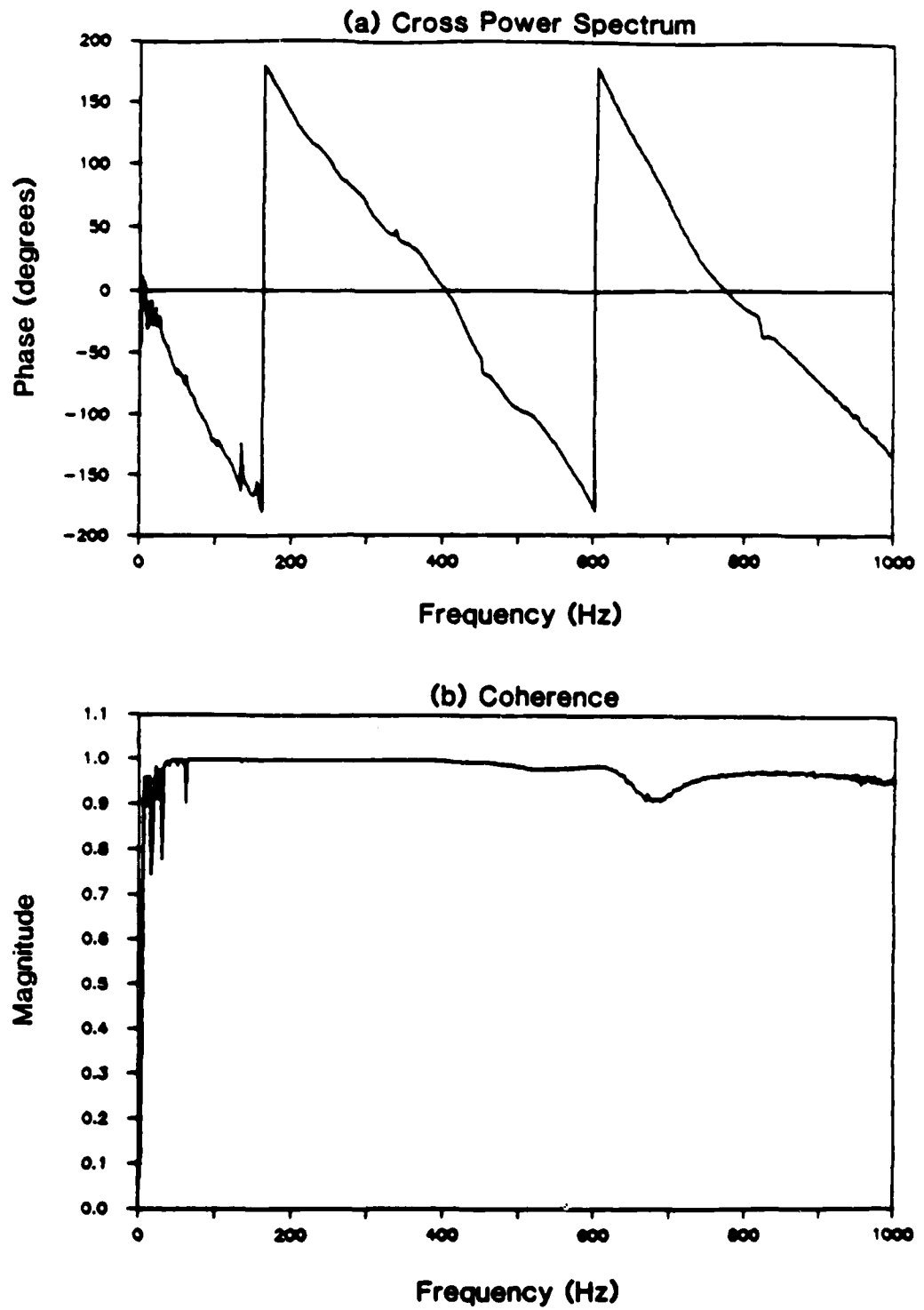


Figure 3.2 — Typical Cross Power Spectrum and Coherence Function

$$t = T \frac{\phi}{360} \quad (3.2)$$

where: t = travel time associated with the given frequency, ϕ = phase shift (continuous or unwrapped) for that frequency, $T = 1/f$ = period of the wave for the given frequency, and f = the given frequency. The distance between the receivers, x , is known. Therefore, the phase velocity, V_{ph} , at the given frequency is calculated by:

$$V_{ph} = \frac{x}{t} \quad (3.3)$$

and the corresponding wavelength is equal to:

$$L_R = \frac{V_{ph}}{f} \quad (3.4)$$

By repeating this procedure for each frequency in the acceptable range of frequencies, a dispersion curve for the given receiver spacing and source location (forward or reverse) is obtained. The procedure is repeated for the data from all receiver spacings and source locations. Each dispersion curve is then filtered for wavelengths not meeting the requirements of eq. 3.1. Typically, the dispersion data from one receiver spacing will cover a different range of wavelengths than the other spacings. However, some overlap in the data will occur between spacings so that the complete range in wavelengths is covered. The filtered dispersion curve data from all receiver spacings and source locations are then statistically combined to provide an average curve to represent the site. A typical dispersion curve for a pavement site is shown in figure 3.3.

3.4 Inversion of the Rayleigh Wave Dispersion Curve

The velocities from the dispersion curve are not actual Rayleigh wave velocities but are apparent or phase velocities. The existence of a layer with a higher or lower velocity at the surface of the medium affects the measurements of the velocities for the underlying

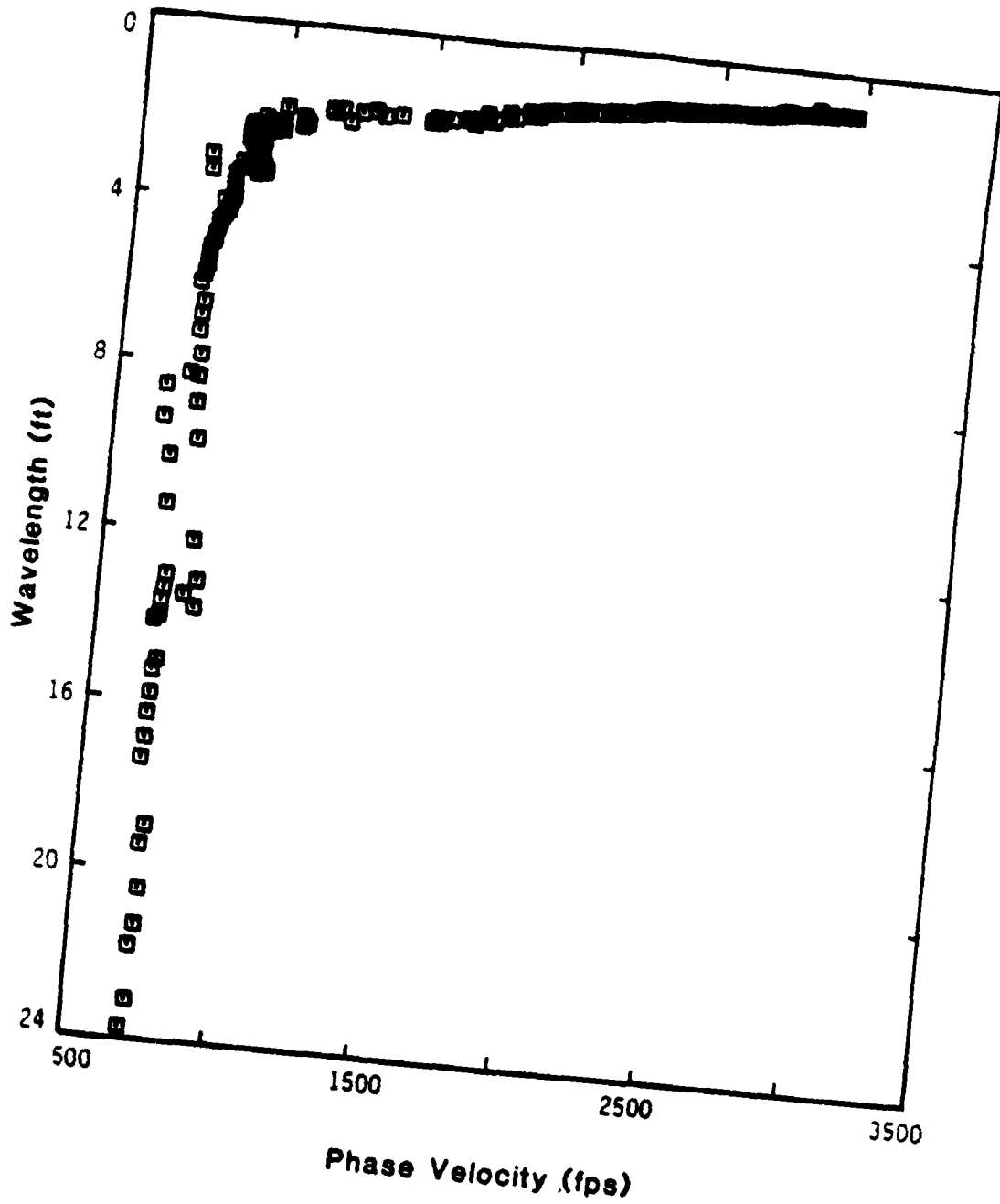


Figure 3.3 — Dispersion Curve Constructed from SASW Tests on a Flexible Pavement Site (from Nasarian and Stokoe [1988])

layers. Thus, a method of determining actual wave velocities from the apparent velocities is necessary.

Inversion of the Rayleigh wave dispersion curve consists of determining the shear wave velocity profile from the phase velocity versus wavelength data. Stokoe and Nazarian (1985) suggest that the simplest method of inversion is to assume that the shear wave velocity is approximately equal to 110 percent of the phase velocity, and that the effective sampling depth (the depth to material having the calculated shear wave velocity) for each wavelength is equal to $1/3$ to $1/2$ of that wavelength.

Use of this simple inversion method inevitably results in some error due to the assumptions made. As noted above, existence of a layer with a relatively high or low velocity near the surface causes a shift in the measured velocities of the underlying layers towards higher or lower velocities. If the contrast in velocities is small, then the simple inversion method may work reasonably well. However, Nazarian and Stokoe (1983) have found that use of the simple method normally results in shear wave velocity profiles which are doubtful. Therefore, a refined inversion process has been developed by Nazarian (1984).

The refined inversion process used is to obtain a theoretical dispersion curve that matches reasonably well with the experimental dispersion curve. The theoretical dispersion curve is constructed using a modified version of the Thomson (1950)-Haskell (1953) matrix formulation for multi-layered elastic media, as developed by Thrower (1965). The mathematics have been thoroughly described by Nazarian (1984) and will not be repeated here.

To begin the process, the medium is divided into a number of layers and a shear wave velocity, Poisson's ratio (or compression wave velocity), and mass density is assigned to each layer. The theoretical dispersion curve for this assumed profile is then calculated and compared with the experimental dispersion curve. If the theoretical and experimental curves match, the desired profile is obtained. However, if the two curves do not match, the shear wave velocity profile is modified and another theoretical curve is constructed. This trial-and-error procedure is continued until the two curves match to within a reasonable tolerance. The final velocity profile obtained, then, is the postulated variation of shear wave velocity with depth. The shear or Young's modulus profile can then be constructed

using eq. 2.1 or 2.2, respectively. The shear wave velocity and Young's modulus profiles constructed from the dispersion curve in figure 3.3 are shown in figure 3.4.

It should be noted that the inversion process also requires that the mass density and Poisson's ratio of each layer in the profile be known. However, reasonably assumed values for these parameters can usually be used, since it has been shown by Nazarian (1984) that the effect of these parameters on the final outcome is small, especially for civil engineering materials in which Poisson's ratio and mass density fall into fairly narrow ranges.

At the same time, care should be exercised in choosing the value of Poisson's ratio. Nazarian and Stokoe (1983) indicate that several studies to evaluate Poisson's ratio of different materials show that the values are quite small in the low-strain range. This should be considered for dynamic tests such as the wave propagation methods.

3.5 Summary of Case Studies

Nazarian (1984) reported that as of 1984, the SASW method had been employed at over 60 sites nationwide. The author has used the method to date at 29 sites. Together, the sites have included both flexible and rigid pavements, soil sites, and a concrete dam. In a number of cases the results have been compared with crosshole seismic tests, a well established method for measuring shear wave velocity in situ. The procedure for performing crosshole tests has been reviewed in section 2.4 and it is discussed in detail in a number of articles, including Stokoe and Woods (1972), Stokoe and Hoar (1978), and Hoar (1982), and is not repeated here. In general, the moduli obtained from the two methods compare favorably with one another.

One comparison between the two methods for a flexible pavement site is shown in figure 3.4. The profile consists of 5 in of asphaltic concrete, 8 in of lime rock base, and subgrade. The shear wave velocity profile determined from SASW tests, along with the results from crosshole tests, are shown in figure 3.4(a). It is observed that the results from the two methods compare well. Young's modulus profiles calculated from the shear wave velocity profiles are shown in figure 3.4(b). These results also agree well with one another, which is not surprising, since the two shear wave velocity profiles are nearly alike.

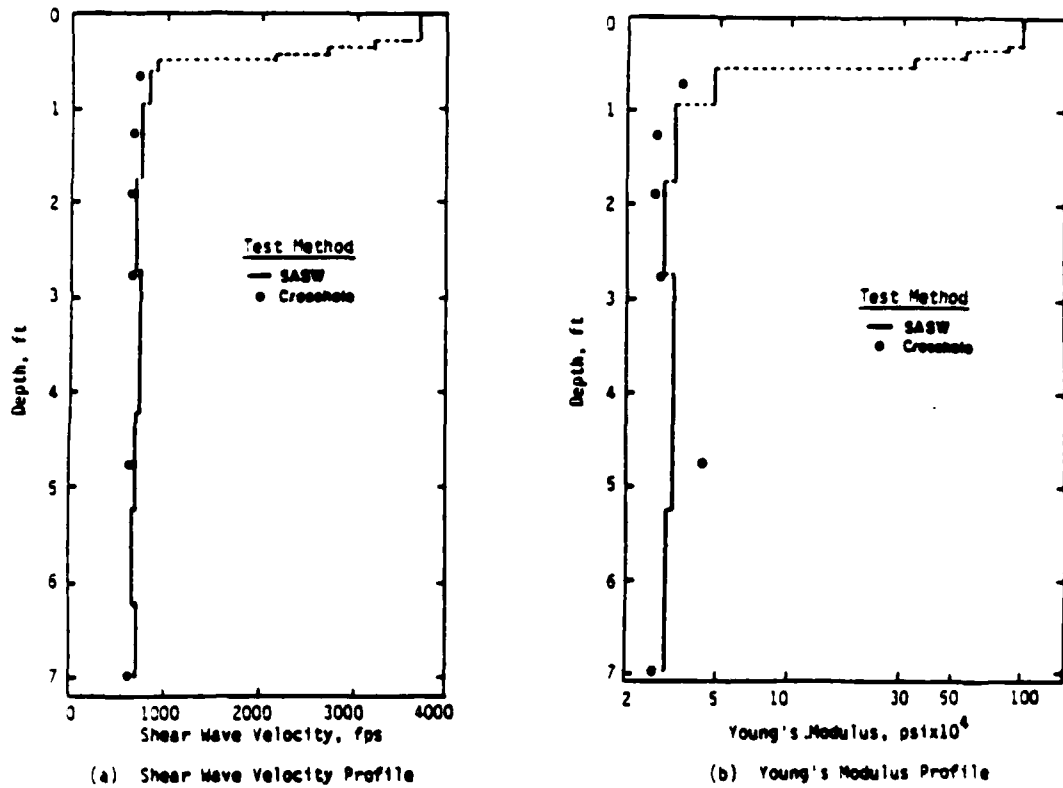


Figure 3.4 — Shear Wave Velocity and Young's Modulus Profiles from Flexible Pavement Site (from Nazarian and Stokoe [1986])

3.6 Disadvantages

The primary disadvantage of the SASW method at this time is that the testing and data reduction are not performed rapidly. The SASW method currently requires that several impact tests be performed at each location of interest. For each impact test, two transducers are placed on the surface of the ground or pavement at a known distance apart. To fully characterize the layered system, the series of tests at each location requires increasing the distance between the two transducers and generating impacts with different frequency contents to correspond to the transducer spacings. This technique must currently be performed in a stationary mode, and it requires a good deal of time at each location. However, with some development, it seems possible to convert this technique to a rapid, on-the-move test.

A further limitation of the SASW method for pavement evaluation and other applications may be the fact that the moduli obtained are for low strain levels, i.e., in the range of strains where the moduli are not strain dependent. The loadings encountered in real pavements are often large enough to cause the pavement materials to exhibit strain-dependent behavior with respect to modulus. However, the SASW method does give a starting point from which strain-dependent moduli can be determined from correlations with laboratory results, such as resonant column or cyclic shear tests. This technique is used regularly in earthquake engineering applications.

3.7 Summary

This chapter has described the SASW test method in detail. The three phases of SASW testing, namely, collection of data in the field, determination of the Rayleigh wave dispersion curve, and inversion of the Rayleigh wave dispersion curve, were individually described. Many case studies have shown that the results obtained from SASW tests compare well with the results from crosshole tests, a well established testing technique. The major limitations of the SASW method at this time are that the testing and data reduction are time consuming and the modulus measured with the SASW test is for small strains.

CHAPTER IV

SASW TESTING SYSTEM AND COMPUTER SOFTWARE

4.1 Introduction

This chapter reviews the SASW testing system and computer software developed as part of this research.

To help describe each part of the SASW testing system and computer software package, a review of the steps required in SASW testing will be useful. They include:

- 1) Create surface wave with appropriate source
- 2) Measure waveform at known locations with appropriate transducers
- 3) Apply a low-pass filter to transducer signals to prevent aliasing of high frequency components
- 4) Convert analog transducer signals to digital form and store for further processing
- 5) Apply a window function to digital data to prevent leakage (usually a uniform window)
- 6) Compute the FFT of each signal
- 7) Compute the auto and cross power spectrums from the FFTs of selected transducer pairs
- 8) Repeat steps 1-7 a number of times (usually 5) and average the signal pairs in the frequency domain, i.e., average the auto and cross power spectrums of the selected signal pairs
- 9) Compute the coherence function from the average auto and cross power spectrums
- 10) Convert the phase of the average cross power spectrum from modulo 2π format to continuous format, i.e., unwrap the phase diagram

- 11) From the phase of the average cross power spectrum and the known distance between the transducer pair, compute the phase velocity and wavelength for each frequency exhibiting good coherence, e.g., greater than 0.9
- 12) Filter the phase velocity-wavelength data based on eq. 3.1
- 13) Repeat steps 1-12 for all receiver spacings and source locations
- 14) Construct the dispersion curve from the filtered phase velocity-wavelength data from all spacings and source locations
- 15) Invert the dispersion curve to determine the shear wave velocity versus depth relationship
- 16) Compute Young's and/or shear modulus profile from shear wave velocity profile
- 17) Plot results at all desired stages of analysis

4.2 SASW Testing System

The major components of the SASW testing system described here are: sources for generating the waveforms, receivers for measuring the waveforms, and recording devices for monitoring, recording, and performing calculations on the waveforms.

Sources

Two types of excitation (step 1 from above) were used in this research: impact and random. Impact excitation was used primarily, although the use of random excitation was investigated at one site.

The impact sources used were hammers of various types and sizes. They included: ball peen hammers (4 oz and 8 oz), claw hammer (16 oz), sledge hammers (40 oz, 8 lb, and 20 lb), and Standard Penetration Test hammers (140 lb, both donut and safety types).

The random source investigated was a shaker excited with band-selected pure random noise. The shaker used was a Model 113 Electro-Seis manufactured by Acoustic Power Systems, Inc. The shaker was equipped with a Model 124 Dual-Mode Power Amplifier, also manufactured by APS. The random noise was supplied by the spectrum analyzer described below.

Receivers

The receivers (step 2) used in this research were of two primary types: velocity transducers (geophones) and accelerometers. All receivers were vertically oriented and were used as matched pairs.

Velocity Transducers

Three pairs of velocity transducers were used in this research. Velocity transducers were used exclusively at all soil sites. They were also employed at pavement sites for the larger spacings (2 or 4 ft and above). The velocity transducers used, along with their significant characteristics, are:

- 1) Electro-Tech Model EVS-4: Natural frequency approximately 10 Hz, 1.3 and 0.5 V/ips sensitivity
- 2) Geosource Model PC-3
- 3) Mark Products, Inc. Model L-4: Natural frequency 1 Hz, 7 V/ips sensitivity

Accelerometers

Two pairs of accelerometers were used for testing at pavement sites. Their manufacturers and significant characteristics are:

- 1) PCB Piezotronics, Inc. Model 303A11: Natural frequency 70 kHz, useful frequency range 1-20,000 Hz, sensitivity 100 mV/g
- 2) Dytran Instruments, Inc. Model 3100A14: Useful frequency range 1-10,000 Hz, sensitivity 100 mV/g

Recording Devices

Two recording devices were used during the course of this research. The first device was a DATA 6000 Universal Waveform Analyzer manufactured by Analogic Corporation, Data Precision Division. The device is basically a 4-channel digital oscilloscope capable of digitizing and recording the time signals generated by the transducers during SASW testing (step 4). The unit is equipped with dual disk drives for storing the recorded data. The disk drives are compatible with IBM PC format, and, by means of a software interface, the data is transferred to the signal analysis program described below for further processing.

A much more useful device for SASW testing is the spectrum analyzer used throughout most of this research. The device used was a Hewlett Packard Model 3562A Dynamic Signal Analyzer equipped with a HP Model 9153A disk drive. The analyzer is a 2-channel device capable of performing steps 3-9 above. The major advantage of this device is the ability to view the frequency domain functions immediately during field testing. By means of a hardware interface with a personal computer (National Instruments GPIB-PC board and Compaq Portable 286) the data is transferred to the SASW data analysis software described below for further processing.

4.3 Computer Software

A number of computer programs have been developed for the SASW data analysis, including: a signal analysis program, a program for generating dispersion curves from the raw cross power spectrum phase and coherence data obtained during testing, a utilities program for performing various side tasks pertinent to the testing and data analysis, a program for performing the inversion process, and routines for plotting the data at all stages of the analysis. All of the programs are written in BASIC for an IBM PC or compatible, except for the inversion program which is written in FORTRAN 77. A brief discussion of some of the features of each of these programs follows.

Signal Analysis Program

The signal analysis program essentially performs three major functions. First, the program contains a spectral analysis subroutine that performs all of the calculations for SASW testing as a spectrum analyzer (steps 5-9). The inputs for the subroutine are digitized time signals collected in the field. The subroutine calculates and provides as output the auto and cross power spectrums and the coherence function, i.e., the functions required for generating an SASW dispersion curve. The subroutine will also calculate a system frequency response function and a cross correlation function. The subroutine is generic in that it can process time signals collected with any recording device as long as the data is in digitized form. The subroutine is able to process any number of time signals making its use attractive for data collected with a multiple channel recording device.

The second major feature of the signal analysis program is that both forward and inverse fast Fourier transforms (FFT) can be computed. The FFT subroutine is used in the above spectral analysis subroutine, but it also can be called separately to perform both forward and inverse FFTs.

The third feature of the signal analysis program is a digital filter subroutine. The digital filter subroutine is based upon a program developed by Carpenter (1985), formerly with Soil and Materials Engineers, Inc., Ann Arbor, Michigan, and contains a lowpass, highpass, and a bandpass filter. This subroutine has a number of uses including the ability to remove undesirable noise from recorded time signals.

SASW Data Analysis Program

The SASW data analysis program performs four primary functions. First, the program converts the raw cross power spectrum phase and coherence function data obtained during field testing into a usable form. The program first removes the phase data for frequencies exhibiting poor phase and/or coherence values. The program then converts the remaining phase data from the standard $\pm 180^\circ$ display format (modulo 2π) to continuous values of phase as a function of frequency (step 10).

The second function of the program is to generate dispersion curve data, i.e., phase velocity versus wavelength and frequency, from the continuous phase values determined in the previous part of the program (step 11).

The third function of the SASW data analysis program is to filter the dispersion curve data based upon an empirically-determined wavelength/receiver spacing filter, i.e., eq. 3.1 (step 12). The filter has been found to reduce the scatter in the dispersion curve data.

The fourth function of the program is to generate an average dispersion curve (step 14). The program is based upon a subroutine developed by Drnevich (1986). The program will average any specified number of dispersion curves on either a frequency or wavelength basis. Typically one average dispersion curve is determined for each test site from the dispersion curves obtained at various transducer spacings and source locations (forward and reverse). The program generates the average dispersion curve data by first interpolating at equal frequency or wavelength intervals the data from each individual dispersion curve and then averages the results.

Utilities

The utilities consist of two primary subroutines. The first subroutine transfers and converts data obtained with a Hewlett Packard 3562A Dynamic Signal Analyzer during field testing to a Compaq Portable 286 personal computer via a National Instruments GPIB-PC interface board. The second subroutine converts binary data files recorded with a DATA 6000 Universal Waveform Analyzer to ASCII format.

Inversion Program

The inversion program (step 15) currently in use is the program "INVERT" developed by Dr. Soheil Nazarian of the University of Texas at Austin and as described in Nazarian (1984). Minor modifications have been made for implementation on computers available at the University of Michigan, e.g., IBM 3090 mainframe, Apollo, and IBM PC (and compatibles). The program calculates a theoretical dispersion curve based upon an assumed material profile. The assumed profile is systematically adjusted until the theoretical and experimental dispersion curves agree within a reasonable tolerance as judged by the user.

Plot Routines

Routines have been developed for plotting the data at all stages of the data analysis (step 17). Included in the plot routines at the present time are plots of the following type:

- 1) Phase of cross power spectrum and coherence function versus frequency
- 2) Phase velocity versus wavelength or frequency
- 3) Shear wave velocity, shear modulus, or Young's modulus versus depth

Special features of the plot routines include the ability to save a plot in a disk plot file, produce a hard copy of a plot on a graphics printer, and generate a plot queue to produce and print a string of plots automatically.

4.4 Summary

This chapter has described the SASW testing system and computer software developed as part of this research. The primary components of the testing system are: sources for generating the waveforms, receivers for measuring the waveforms, and recording devices for

monitoring, recording, and performing calculations on the waveforms. The major functions of the computer software developed are: computing spectral analysis functions, determining the dispersion curve, inversion of the dispersion curve, and plotting the results at all desired stages of the analysis.

CHAPTER V

EXPERIMENTAL PROGRAM

5.1 Introduction

The ultimate objective in the development of the SASW method is a totally automated, moveable test rig for conducting the investigation. An important step toward this objective is the development of a multiple transducer testing procedure in which all the data for a given site can be obtained with the least number of source excitations on the test surface as possible.

Currently, the SASW method is conducted using only two transducers, primarily because a two-channel spectrum analyzer is a convenient means of collecting and observing the data in the field. This means of data collection requires a good deal of time, since several different receiver spacings are usually required to fully investigate a site. The extension of this procedure to more than two transducers, i.e., a multiple transducer testing procedure, thus seems appropriate.

Previous research has shown that the receiver spacings suggested in chapter three are usually sufficient to fully investigate a site and that the common receivers midpoint (CRMP) geometry provides data with the least amount of scatter. Therefore, the development of a multiple transducer testing procedure should begin by using these suggested spacings and the CRMP geometry. Another source and receiver geometry possibly appropriate to a multiple transducer testing procedure is the common source (CS) geometry investigated by Heisey, et al. (1982) and Nazarian and Stokoe (1983). The CS geometry employs a fixed source location and places the receivers at appropriate distances away from the source to achieve the desired receiver spacings.

Several multiple transducer configurations that follow the above suggestions are shown schematically in figures 5.1-5.4. In figures 5.1-5.3 the transducers are arranged following the CRMP geometry and the spacing between transducer pairs doubles as one moves out from the imaginary centerline. The numerical values for the receiver spacings are not shown since it is anticipated that these values will be somewhat site dependent. For pavement sites the receiver spacings are typically between 0.5 and 8 ft. In addition, the distance from the source to the first receiver is designated as S , since the optimum location for the source in a multiple transducer array is not known at this time. Figure 5.4 suggests a multiple transducer array designed around the CS geometry. The distance between successive transducers is doubled to achieve the desired spacings. The distance from the source to the receivers is such that the distance between the source to the near receiver for a transducer pair is equal to the distance between the transducer pair. This is typically how the source and receivers have been arranged with the CRMP geometry. The difference between the two geometries is that the receiver pairs are not placed about a fixed imaginary centerline in the CS geometry.

The immediate questions one needs to answer in order to implement a multiple transducer array are: 1) which source and receiver geometry, 2) where should the source be located, and 3) what source type(s) should be used. These are the questions that this research has attempted to answer and each is discussed in more detail in the following sections.

5.2 Source and Receiver Geometry

The factors that affect the source and receiver geometry have been studied by Heisey, et al. (1982) and were discussed in chapter three. On the basis of studies conducted at several soil sites, Heisey, et al. (1982) found that, in general, an equally-spaced receiver arrangement, where both the near receiver and the far receiver (from the source) are located at increasing distances from the source, is more desirable than a "reference" arrangement, where the near receiver is fixed at a location close to the source and only the far receiver is located at increasing distances from the source.

Nazarian and Stokoe (1983) compared results from two source and receiver geometries, both of which followed the above recommendation of Heisey, et al. (1982). The first geometry was designated the common source/receiver (CSR) geometry. In the CSR geometry,

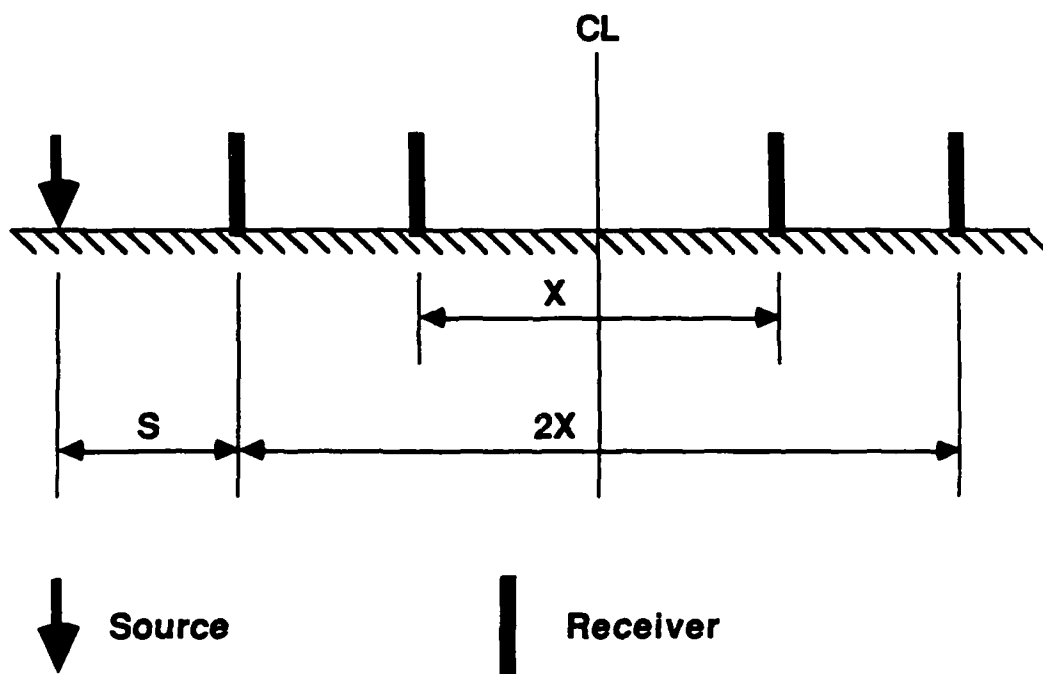


Figure 5.1 — Multiple Transducer Configuration Employing Four Transducers and CRMP Geometry

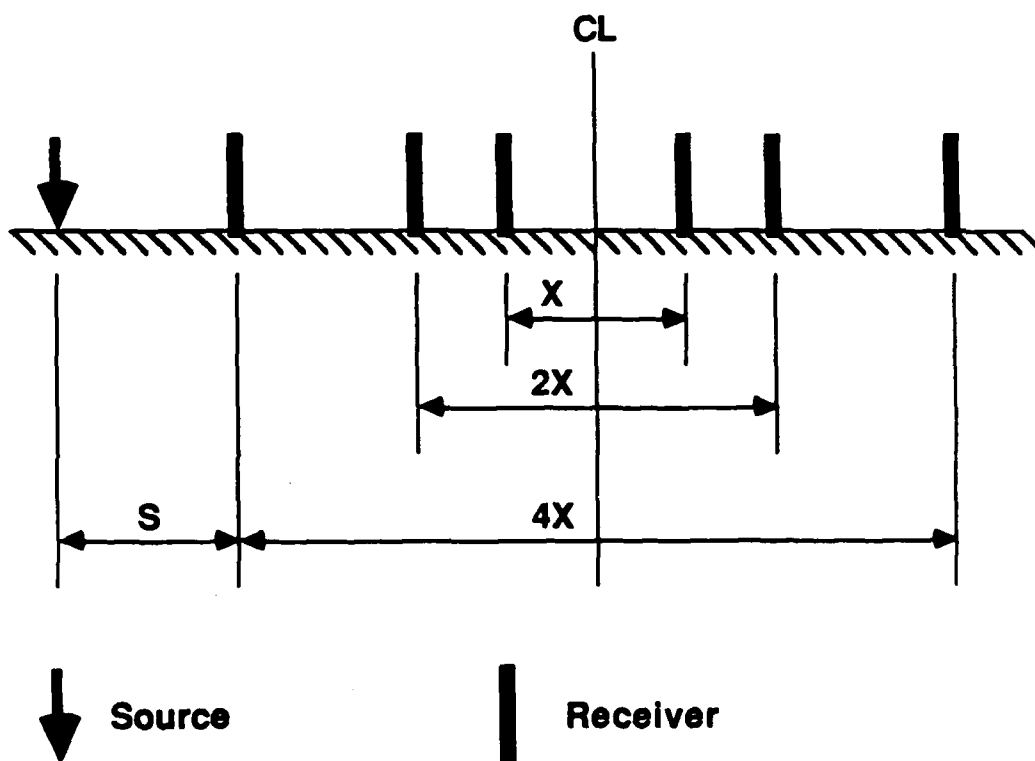


Figure 5.2 — Multiple Transducer Configuration Employing Six Transducers
and CRMP Geometry

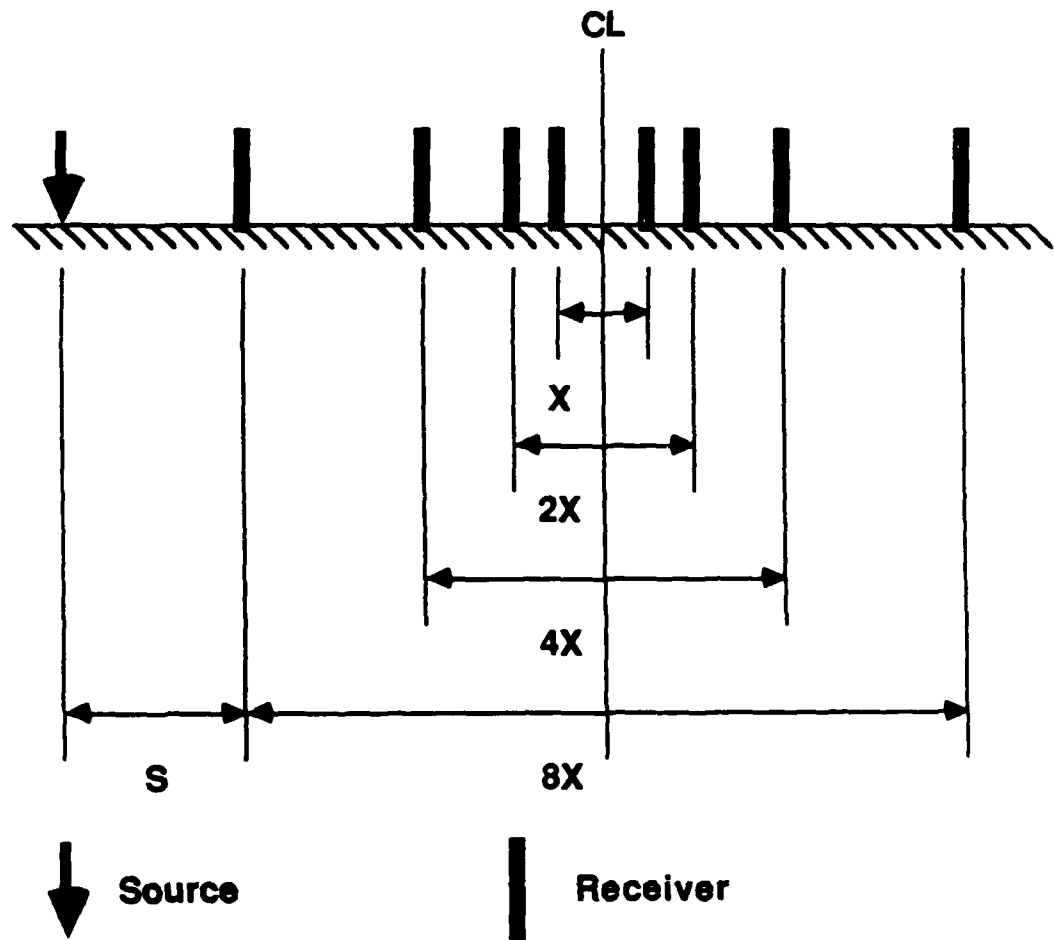


Figure 5.3 — Multiple Transducer Configuration Employing Eight Transducers and CRMP Geometry

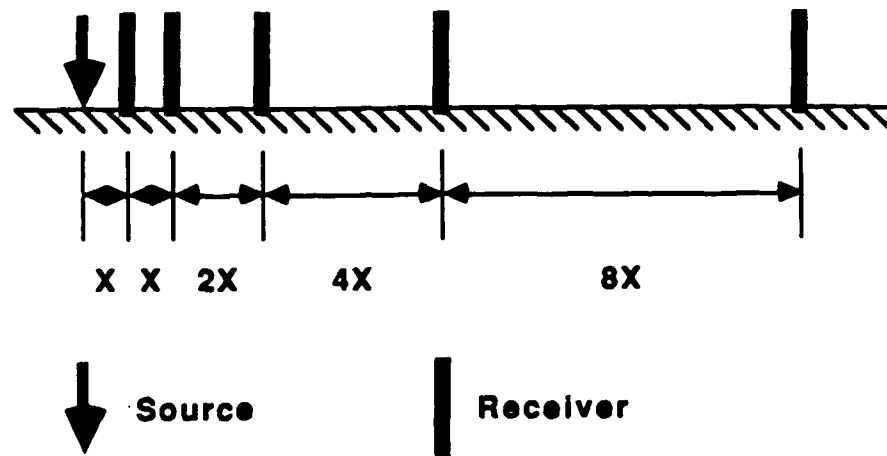


Figure 5.4 — Multiple Transducer Configuration Employing Five Transducers and CS Geometry

either the source or receivers are fixed at one location and the other is moved during testing. In the case studied the source was fixed, thus the geometry was designated as common source (CS) (see figure 5.5).

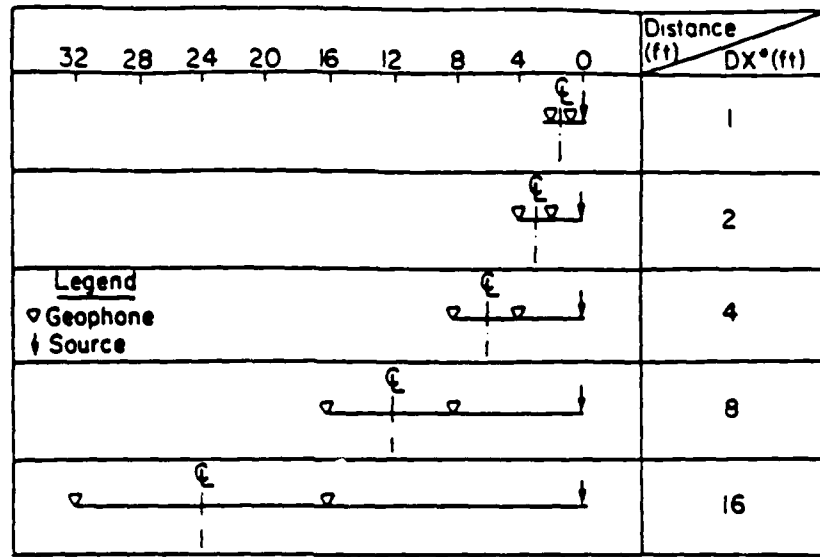
The second geometry studied was termed the common receivers midpoint (CRMP) geometry (see figure 5.6). In the CRMP geometry, an imaginary centerline is selected between the receivers. The two receivers are moved away from the imaginary centerline at an equal pace, and the source is moved such that the distance between the source and near receiver is equal to the distance between the two receivers.

Nazarian and Stokoe (1983) performed a series of tests at a soil site using the above two geometries. The dispersion curves obtained from the two geometries are shown in figures 5.7 and 5.8. Also shown on each figure is the range in data from the other figure. It is observed that the scatter in the curve obtained using the CRMP geometry is much less than from the CS geometry. It was thus concluded that the CRMP geometry is preferred and it has been used exclusively since.

However, no such comparison has been reported for a pavement site. The larger scatter from the CS geometry was attributed to lateral nonhomogeneity in the material tested. Because the materials in pavements are usually placed under more controlled conditions than natural soil, and because the lateral extent of the test array is less when testing pavements because smaller receiver spacings are used, it might be reasonable to expect that the affect of the source and receiver geometry is less for pavement testing. Because some doubt existed, and because features of the CS geometry are more suited for a multiple transducer array (fixed source location and source-to-near-receiver distance equal to the receiver spacing), a series of tests were conducted at an asphaltic concrete pavement site to assess the influence of source and receiver geometry. More details of these tests and the results obtained are found in chapter six.

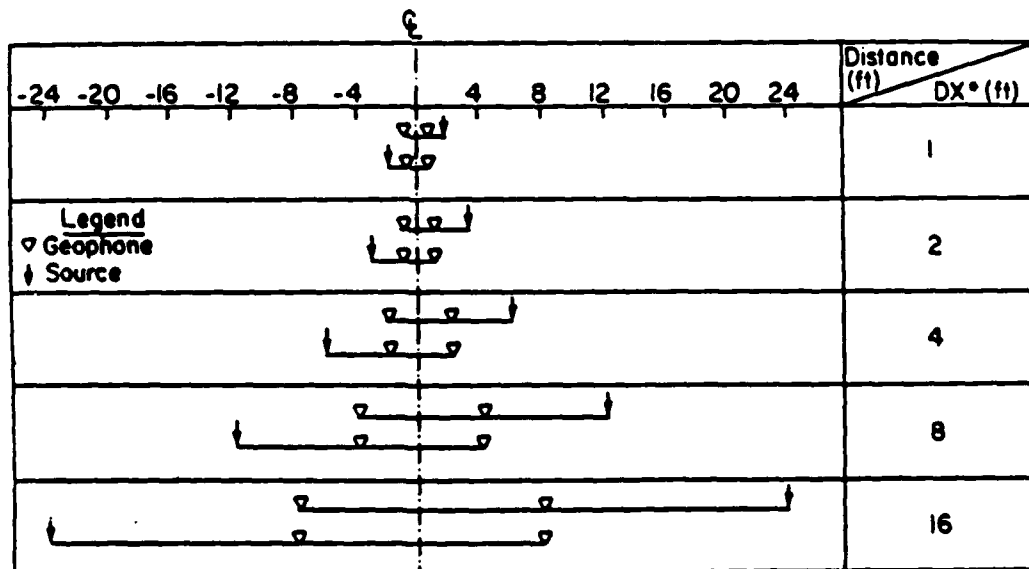
5.3 Source-to-Near-Receiver Distance

Nazarian (1984) discussed the factors that limit the range in possible source-to-near-receiver distances. On the one hand, the source should be far enough away from the near receiver so that a significant amount of the body wave energy dies out before arriving at



*DX = Receiver Spacing

Figure 5.5 — Common Source Geometry (from Nasarian [1984])



*DX = Receiver Spacing

Figure 5.6 — Common Receivers Midpoint Geometry (from Nasarian [1984])

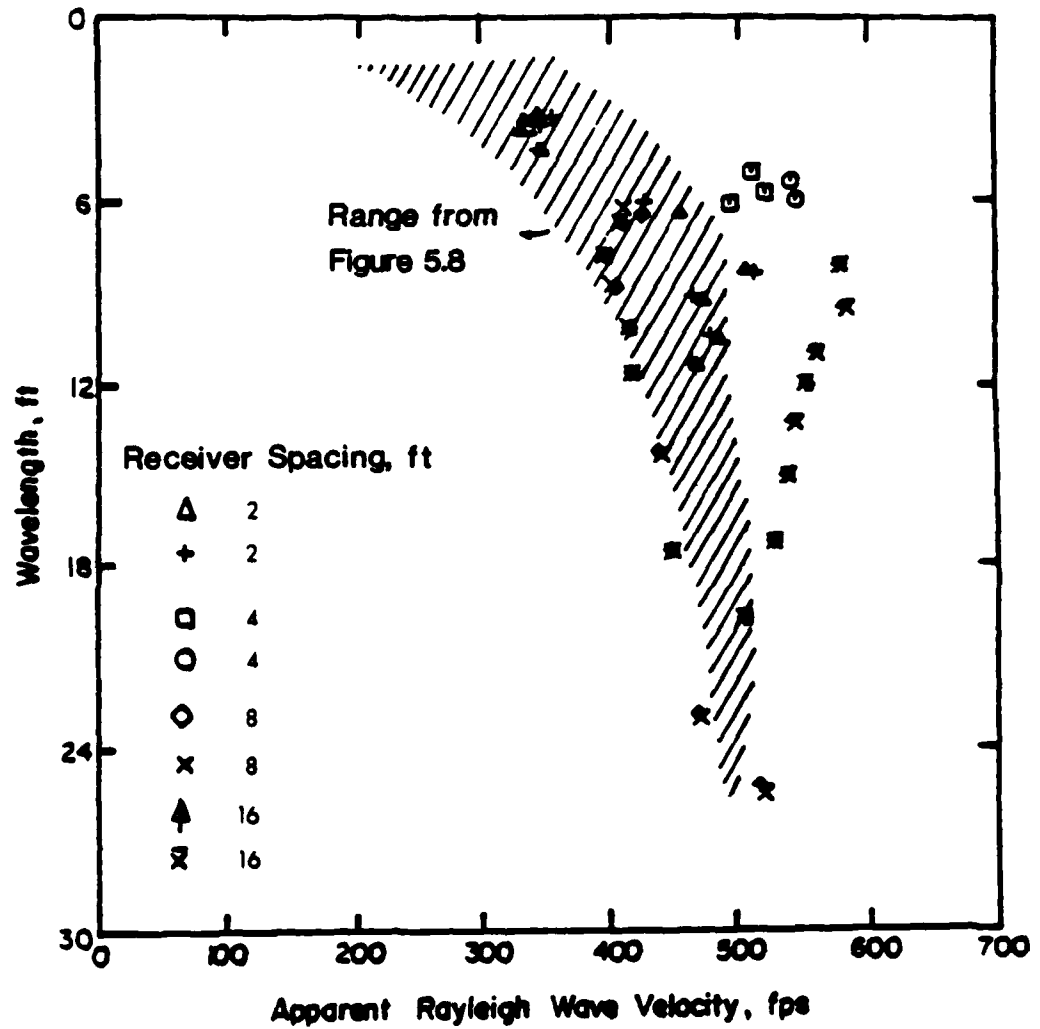


Figure 5.7 — Dispersion Curve from SASW Tests Performed Using Common Source Geometry (from Nasarian and Stokoe [1983])

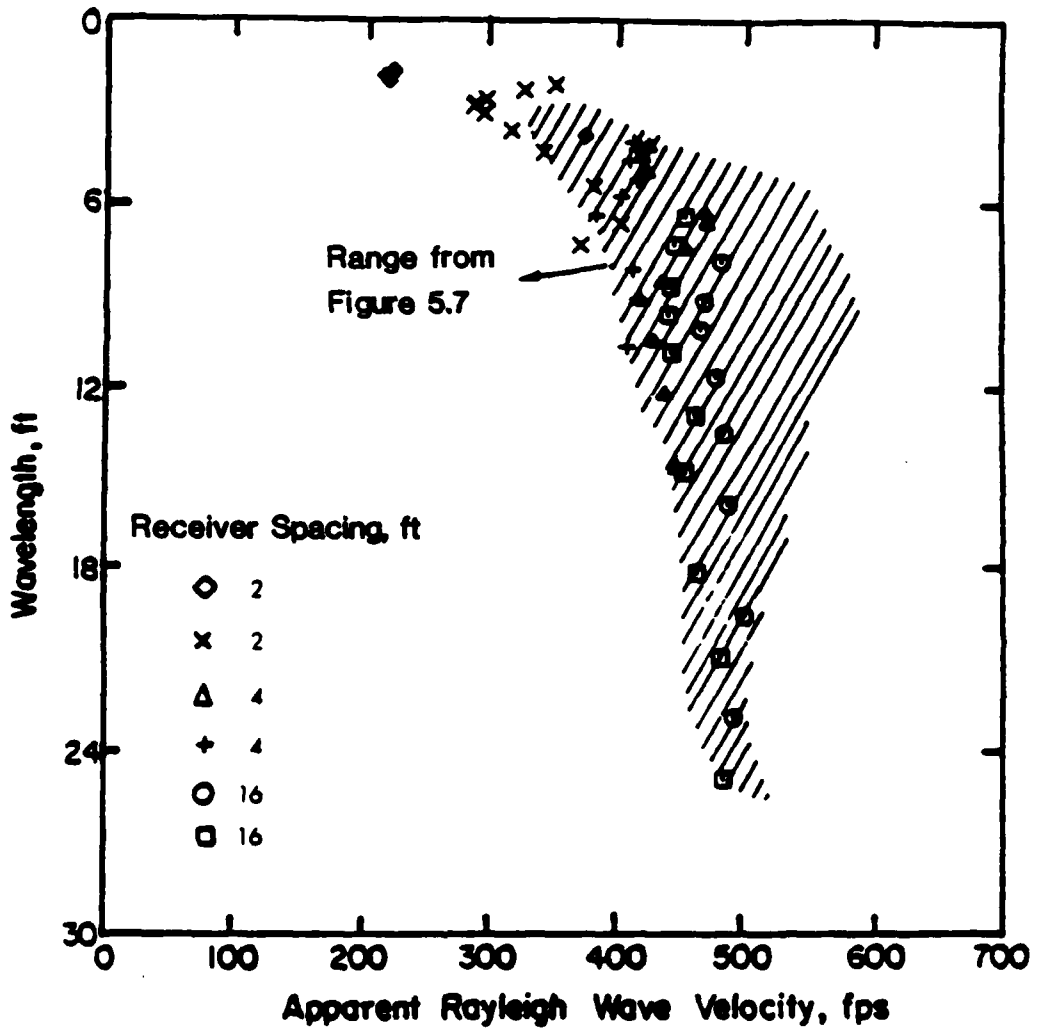


Figure 5.8 — Dispersion Curve from SASW Tests Performed Using Common Receivers Midpoint Geometry (from Nazarian and Stokoe [1983])

the near receiver. On the other hand, if the source is too far away from the receivers, the Rayleigh wave energy associated with the frequencies of interest may not be sufficient to be detected by the receivers, and background noise will dominate the record.

Theoretical studies conducted by Lysmer (1966) suggest that it takes 2.5 wavelengths from the source for a surface wave field to fully develop.

Heisey, et al. (1982), based upon experimental studies, suggested that a distance from the source to the near receiver equal to the receiver spacing is adequate, provided the wavelength/receiver spacing filter criteria given in eq. 3.1 is used.

Nazarian (1984) reported results from one series of tests where the distance from the source to the near receiver varied from one to three times the distance between the receivers. The difference between the experimental dispersion curves from each source location was small. Nazarian (1984) recommends that the effect of the distance between the source and near receiver be more thoroughly investigated in order to define the optimum distance.

Nazarian and Stokoe (1986) suggest that the distance from the source to the near receiver be one to two times the receiver spacing. No data was presented, however, to support this recommendation.

Theoretical studies conducted by Sanchez-Salinerro, et al. (1987) indicate a drastically different criteria than the experimental results of Heisey, et al. (1982). They suggest that for CRMP geometry and for a setup in which the distance from the source to the first receiver is equal to the distance between the receivers, and if the theoretical model being used assumes plane Rayleigh waves (which the current inversion program does), the field data be filtered for wavelengths greater than one-half the receiver spacing (compare with eq. 3.1). A value of one times the receiver spacing could be used if more data is required in the low frequency range.

The disparity between theoretical and experimental results is evident in the above discussion. More importantly, however, it is evident that little work has been done to systematically study the influence of the source-to-near-receiver distance by examining the effect of changing it over a range of values. Yet the results of such a study are vital to the development of a multiple transducer array employing a fixed source location and the CRMP geometry (see figures 5.1-5.3). Therefore, tests were conducted to examine this

question.

A series of two-transducer tests were conducted at two asphaltic concrete pavement sites to examine the influence of the source-to-near-receiver distance. The transducer placement for these tests followed the common receivers midpoint (CRMP) geometry (see figure 5.9). Receiver spacings of 0.5, 1, 2, 4, and 8 ft were used. A range of source locations was used at each receiver spacing such that the ratio of source-to-near-receiver distance (S) to receiver spacing (X), i.e., S/X , was varied over values between 0.5 and 3. The goal was to examine the influence of S/X in order to determine the optimum value and to provide guidance in developing a multiple transducer array. The results of these tests are found in chapter seven.

5.4 Source Type

Nearly all previous work reported about the SASW method has somehow addressed the issue of source selection, particularly sources for impact testing. It has been clearly demonstrated that the choice of source is dependent on the frequency range of interest. Small, lightweight sources produce high frequencies necessary for sampling shallow depths while larger, heavier sources produce low frequencies for sampling greater depths. The intent here was not to reaffirm these findings. Rather, the question that arises when confronted with implementing a multiple transducer array is how many sources are required and of what size.

Past work has shown that it is often necessary to use a different source for each receiver spacing when conducting SASW tests using two receivers. However, this often results in overlap in the dispersion curve data for different receiver spacings. This is good in that it provides some insurance that the data obtained is reliable, but it may be possible to adequately sample a site with fewer sources if one is willing to give up some of the overlap in data between different receiver spacings. Thus, two series of tests were conducted to examine the influence of source type in order to determine the minimum number of sources necessary for adequately defining the dispersion curve for a site. The first test series was performed in conjunction with the tests described above concerning the influence of the source-to-near-receiver distance. At each receiver spacing and source location (see figure 5.9 and section 5.3) tests were conducted with three sources of varying size, ranging from a

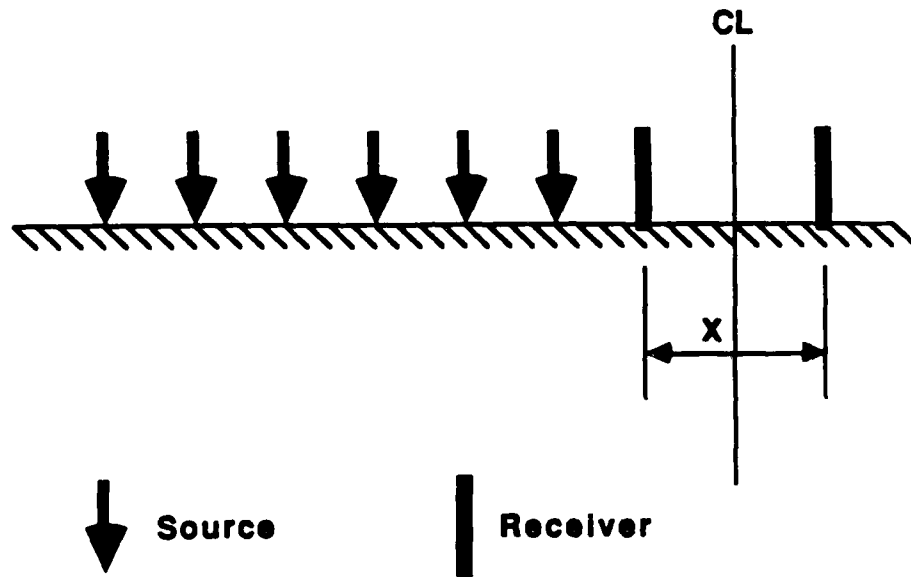


**Figure 5.9 — Schematic of Two-Transducer Tests Employing CRMP
Geometry and Various Source-to-Near-Receiver Distances**

4 oz ball peen hammer to an 8 lb sledge hammer. The second test series was performed in conjunction with the tests described above concerning the influence of source and receiver geometry. For the tests employing the CS geometry (see figure 5.5) five sources of varying size, ranging from a 4 oz ball peen hammer to an 8 lb sledge hammer, were used to examine the influence of source type. The results of these tests are found in chapter eight.

5.5 Summary

The intent of this chapter was to outline the experimental work conducted as part of this research and to review previous work concerning the issues in question. The ultimate objective in the development of the SASW method is a totally automated test rig for conducting the tests. An important step toward this objective is the development of a multiple transducer testing array to significantly decrease the testing time required. Three primary questions arise when one is faced with implementing such an array: 1) which source and receiver geometry, 2) where should the source be located, and 3) which source type(s) should be used. In order to provide answers to these questions, the work of previous investigators was reviewed and a series of field tests have been conducted to examine the influence of source and receiver geometry, source-to-near-receiver distance, and source type in the context of a multiple transducer testing procedure.

CHAPTER VI

INFLUENCE OF SOURCE AND RECEIVER GEOMETRY

6.1 Introduction

The factors affecting the selection of the source and receiver geometry and a review of previous investigations have been presented in chapters three and five. It was suggested that further studies be conducted at pavement sites to examine the influence of source and receiver geometry since this is an important issue with respect to a multiple transducer testing procedure. In particular, a comparison of the results obtained from the common receivers midpoint (CRMP) geometry and the common source (CS) geometry at a pavement site was felt to be important. Thus, such a study was conducted.

A series of tests were conducted at a parking lot in Livonia, Michigan in June of 1987 (hereafter referred to as the SEMTA Parking Lot site). The general location of the site is shown in figure 6.1. The specific location as well as the location of the SASW test arrays are shown in figure 6.2. The material profile as determined from construction records (constructed in 1987) consisted of approximately (see figure 6.3) 2.5 in of asphaltic concrete surface course, 8 in of 21AA dense-graded aggregate base course (state of Michigan specification), fine to medium sand to a depth of approximately 8 ft, and followed by natural gravel to an undetermined depth. SASW tests were conducted employing both the CRMP and CS geometries. The testing parameters and geometries as well as the test results are presented in the following section.

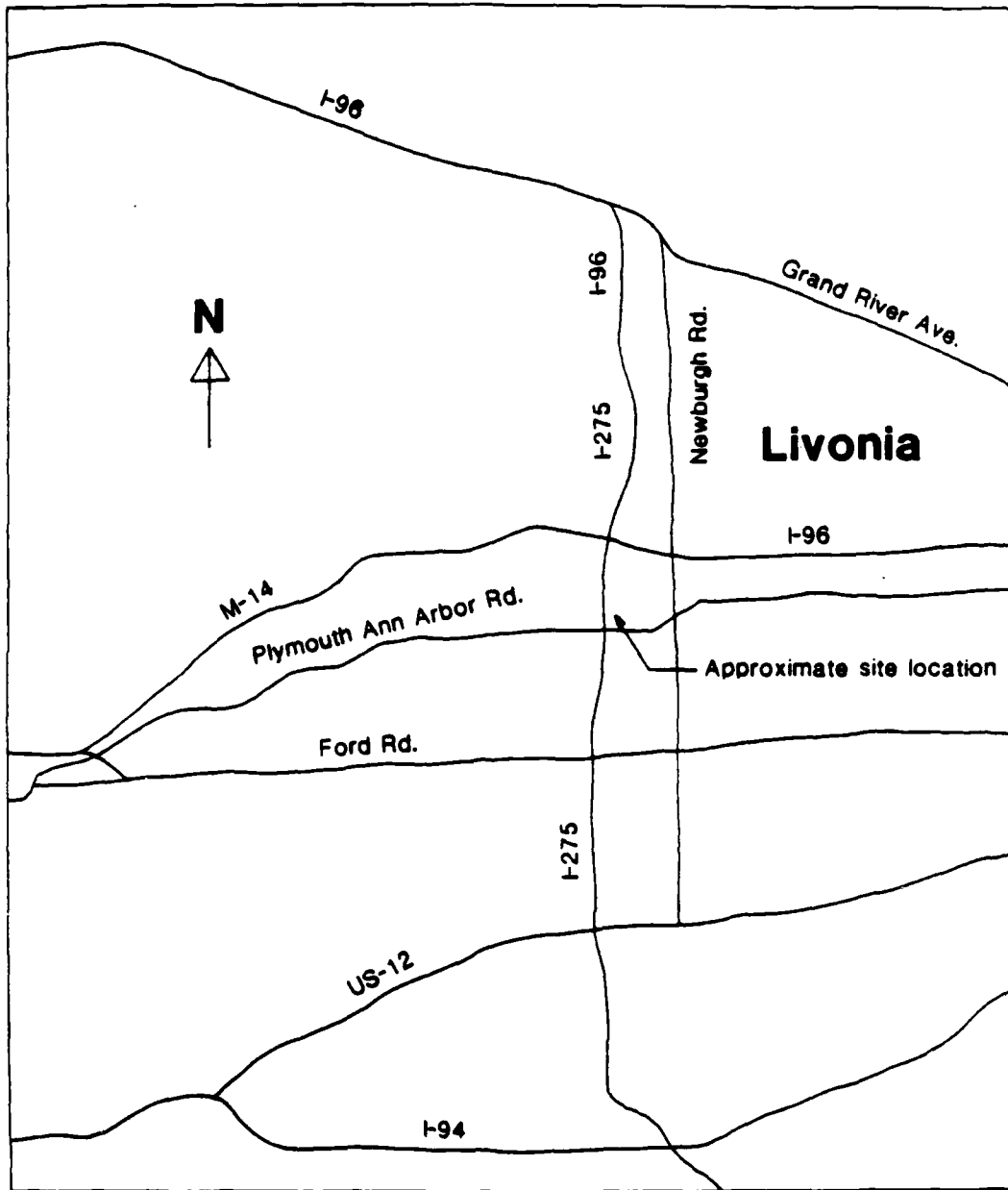


Figure 6.1 — Location of SEMTA Parking Lot Site

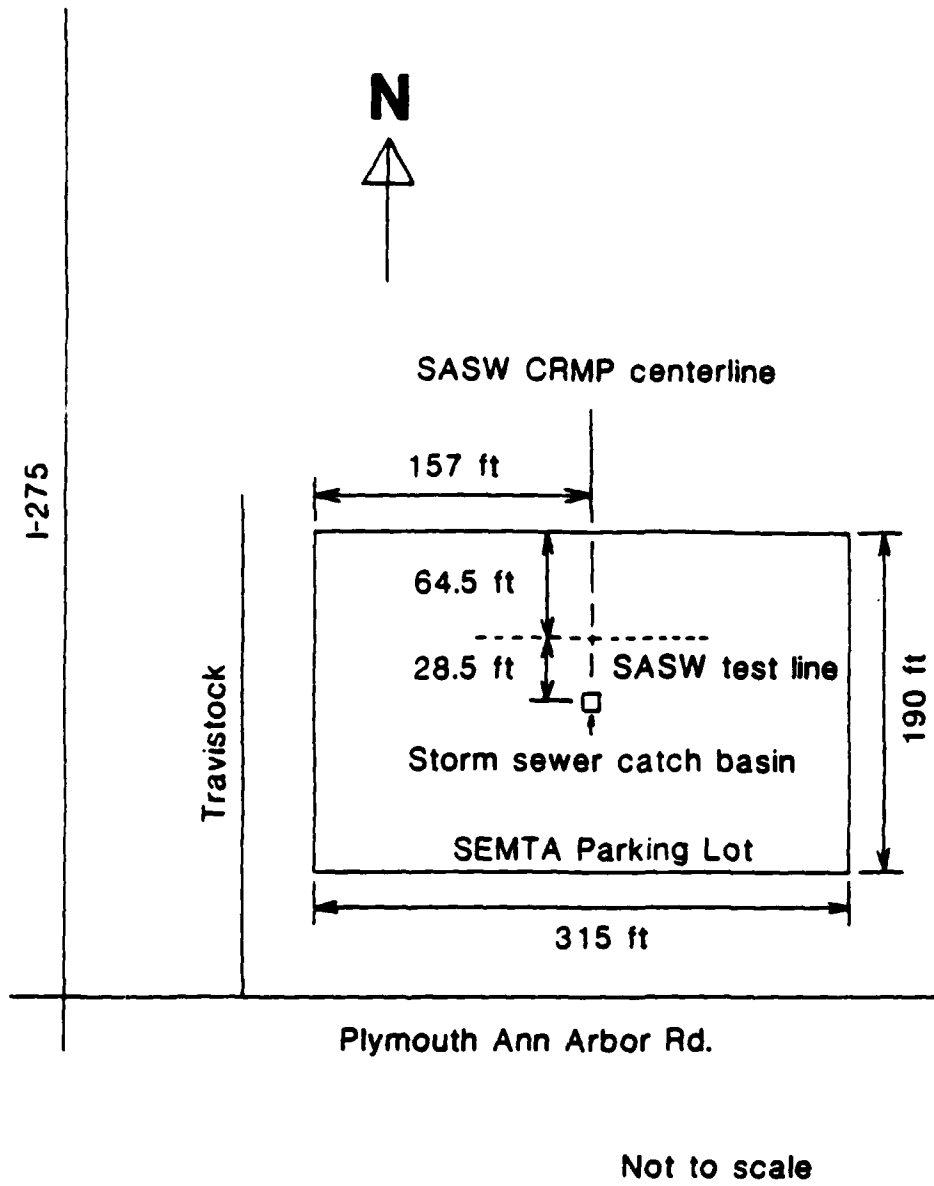


Figure 6.2 -- Location of SASW Test Arrays at SEMTA Parking Lot Site

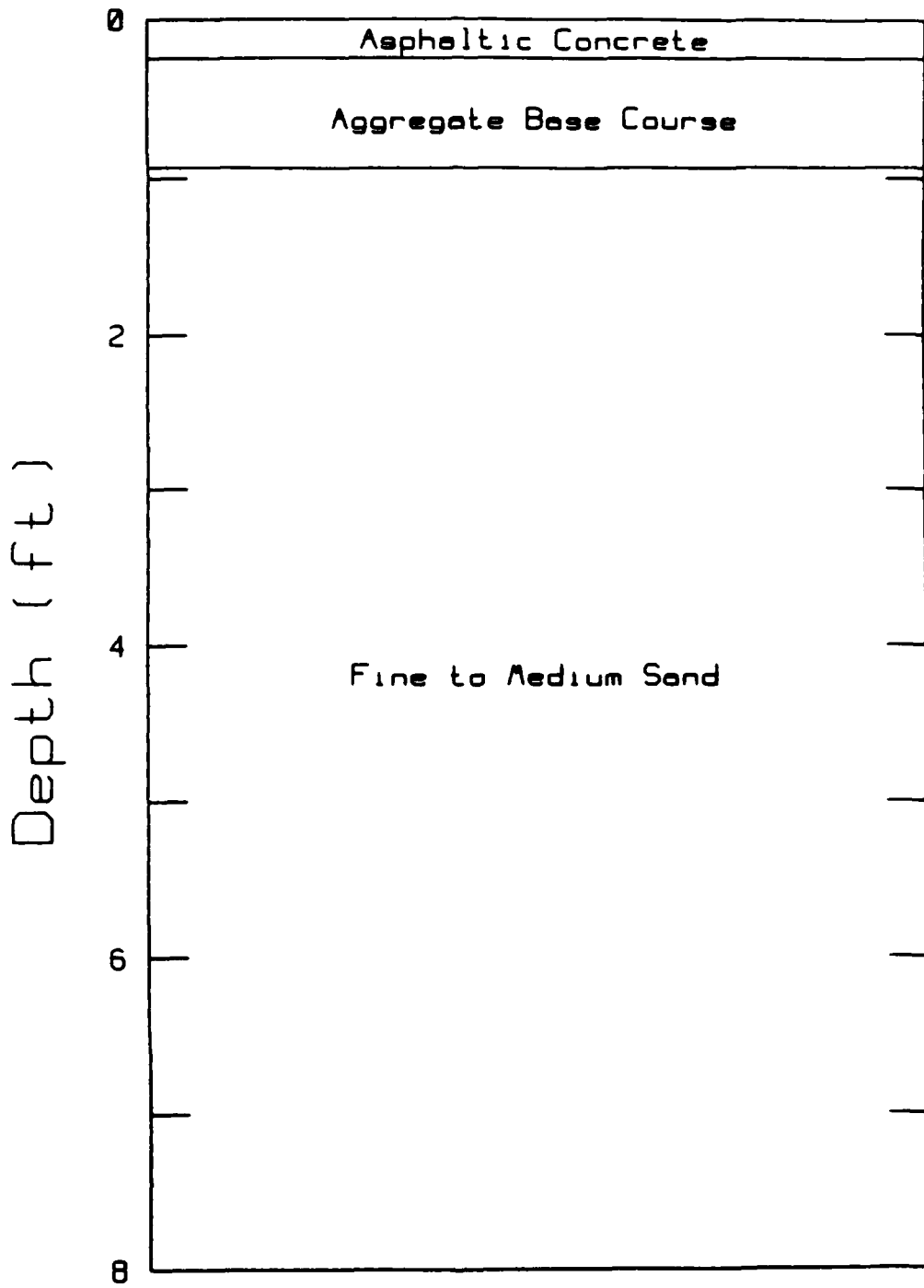


Figure 6.3 — Material Profile of SEMTA Parking Lot Site

6.2 Test Results

Tests were first conducted employing the CRMP geometry as depicted in figure 6.4. Table 6.1 summarizes the test parameters. SASW tests were then conducted using the CS geometry as shown in figure 6.5. Also shown in figure 6.5 is the location of the centerline from the CRMP geometry tests. Further, for the CS geometry tests, five source types were used at each receiver spacing to examine the influence of source type. The influence of the source type will be discussed in chapter eight. The results for the "optimum" source for each receiver spacing will be discussed here. Table 6.2 summarizes the test parameters used during the CS tests. It should be noted that exactly the same tests parameters were used in the CRMP tests and in the CS tests except for the geometry.

The test results presented and compared will be the experimental dispersion curves obtained using each geometry. It should be noted that Heisey's criterion ($x/2 \leq L_R \leq 3x$, eq. 3.1) was used to filter the dispersion data obtained from both geometries. The results obtained using the CRMP geometry are shown in figures 6.6 and 6.7. Figure 6.6 shows the average experimental dispersion curve for all wavelengths measured at the site, while figure 6.7 shows only the data for wavelengths from 0 to 5 ft. The dispersion curve shown is the result of using the averaging program discussed in chapter four to combine the data obtained for each receiver spacing and source location as discussed in chapter three. Superimposed on each figure is the range of all the data from which the average dispersion curve was obtained. The test results obtained employing the CS geometry are similarly shown in figures 6.8 and 6.9. A comparison of the average dispersion curves obtained with each geometry are shown in figures 6.10 and 6.11.

6.3 Discussion and Conclusions

It is immediately observed upon reviewing the data presented above that the results obtained from the SASW tests at the SEMTA Parking Lot site are not significantly dependent on either of the two geometries investigated. The average experimental dispersion curves are nearly identical. There are, however, two notable differences between the average dispersion curves. First, the maximum wavelength generated using the CRMP geometry is larger than that from the CS geometry. Both geometries provide data well into the subgrade

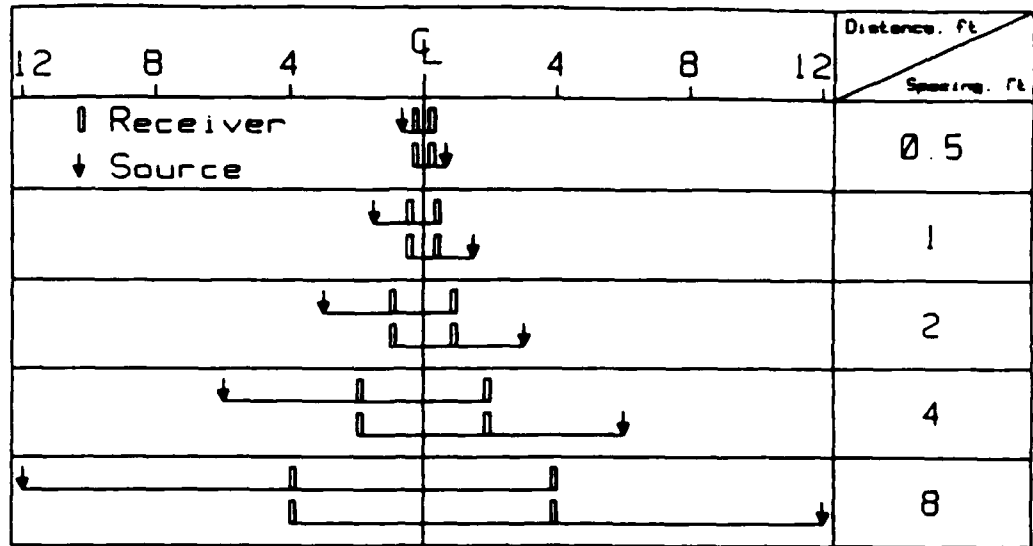


Figure 6.4 — CRMP Geometry Used at SEMTA Parking Lot Site

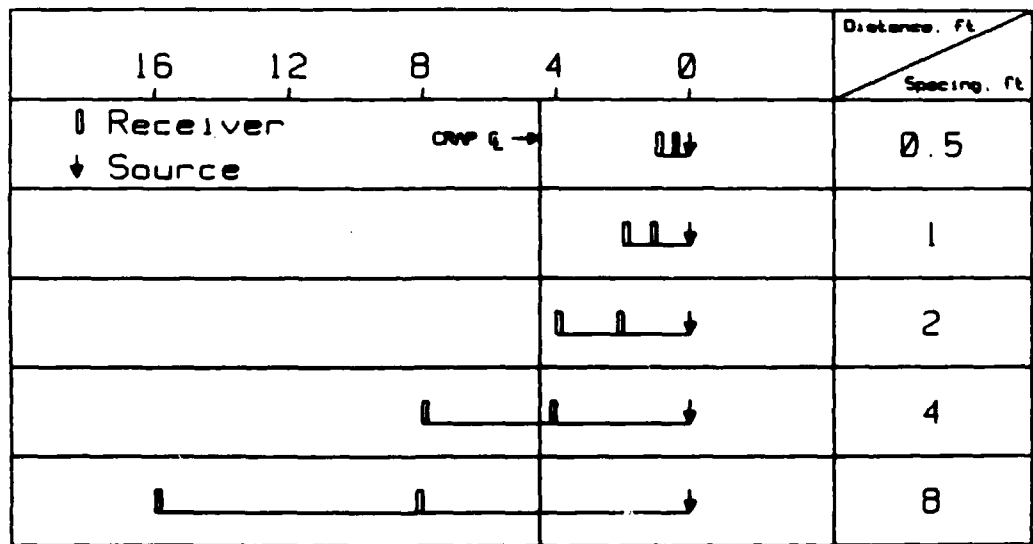


Figure 6.5 — CS Geometry Used at SEMTA Parking Lot Site

Table 6.1 — Test Parameters for SEMTA Parking Lot Site and CRMP
Geometry

Receiver Spacing (ft)	Receiver Type	Source Type	Frequency Span (Hz)	Profile (F = Forward, R = Reverse)	Site File No.
0.5	Dytran Accel.	4 oz	10000	F	801
0.5	Dytran Accel.	4 oz	10000	R	802
1	Dytran Accel.	4 oz	6250	F	808
1	Dytran Accel.	4 oz	6250	R	809
2	Geosource Veloc.	16 oz	1000	F	815
2	Geosource Veloc.	16 oz	1000	R	816
4	Geosource Veloc.	40 oz	800	F	822
4	Geosource Veloc.	40 oz	800	R	823
8	Geosource Veloc.	128 oz	250	F	829
8	Geosource Veloc.	128 oz	250	R	830

Table 6.2 — Test Parameters for SEMTA Parking Lot Site and CS Geometry

Receiver Spacing (ft)	Receiver Type	Source Type	Frequency Span (Hz)	Site File No.
0.5	Dytran Accel.	4 oz	10000	835
1	Dytran Accel.	4 oz	6250	840
2	Geosource Veloc.	16 oz	1000	847
4	Geosource Veloc.	40 oz	800	853
8	Geosource Veloc.	128 oz	250	859

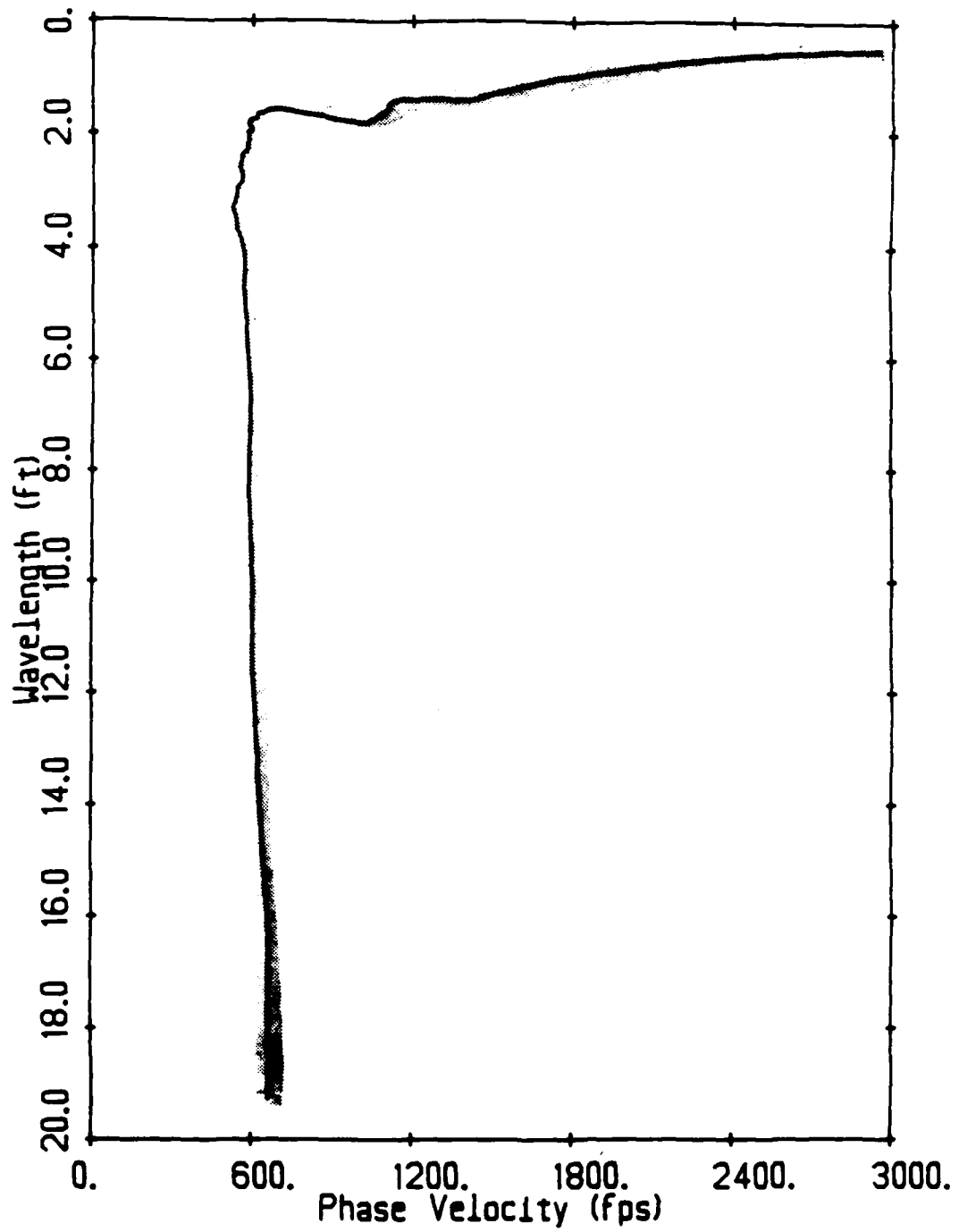


Figure 6.6 — Average Experimental Dispersion Curve for SEMTA Parking Lot Site Using CRMP Geometry (all wavelengths)

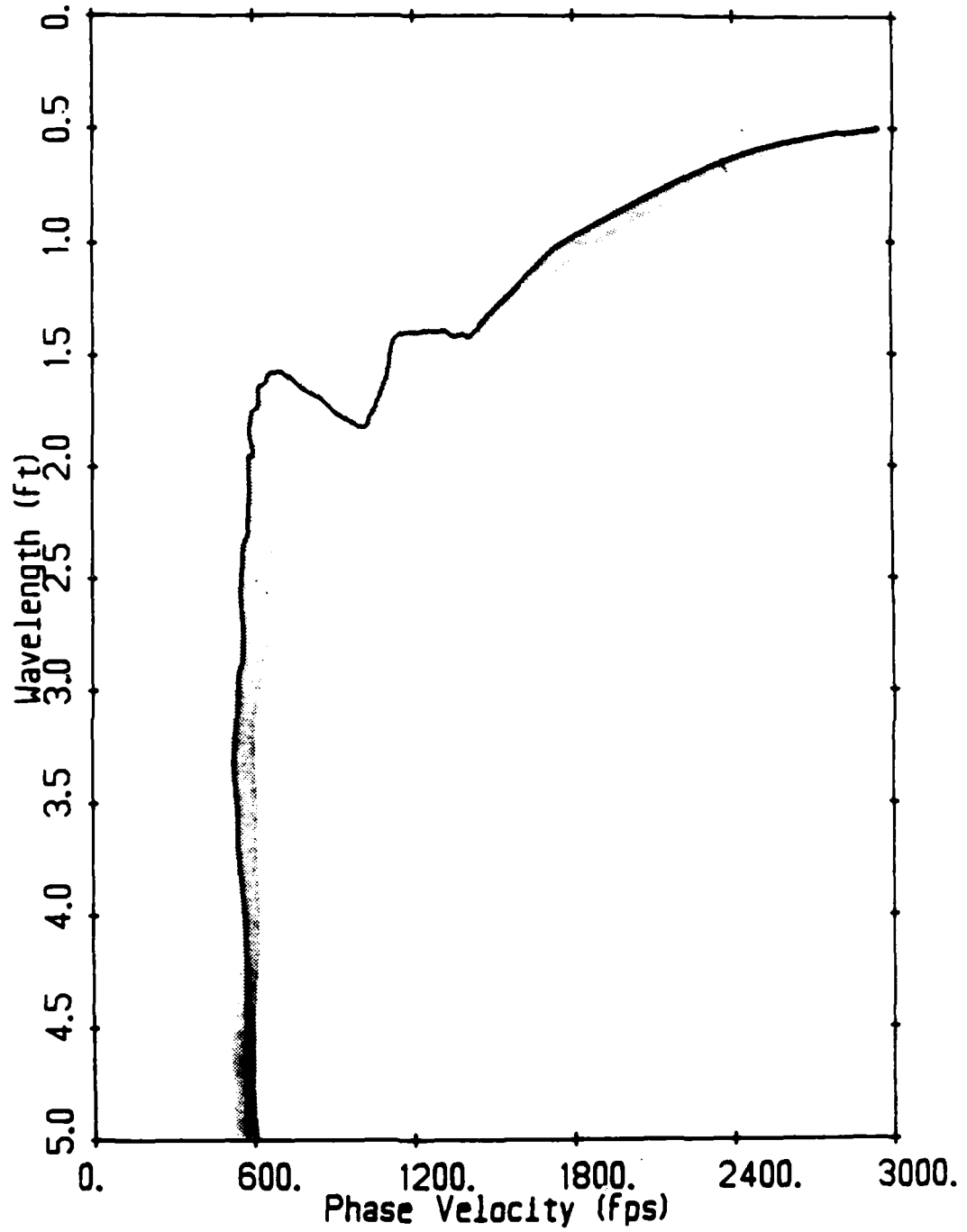


Figure 6.7 — Average Experimental Dispersion Curve for SEMTA Parking Lot Site Using CRMP Geometry (0 to 5-ft wavelengths)

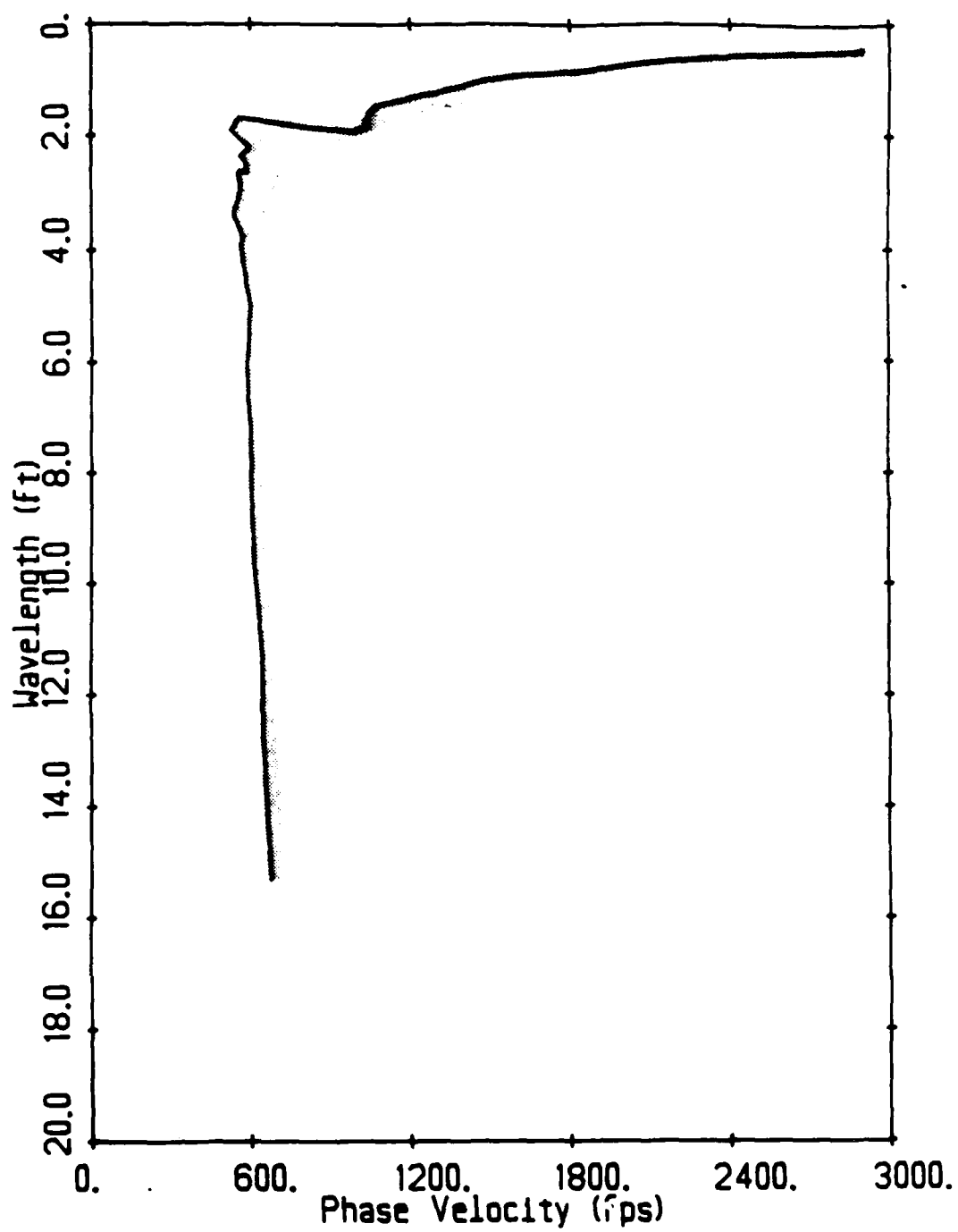


Figure 6.8 — Average Experimental Dispersion Curve for SEMTA Parking Lot Site Using CS Geometry (all wavelengths)

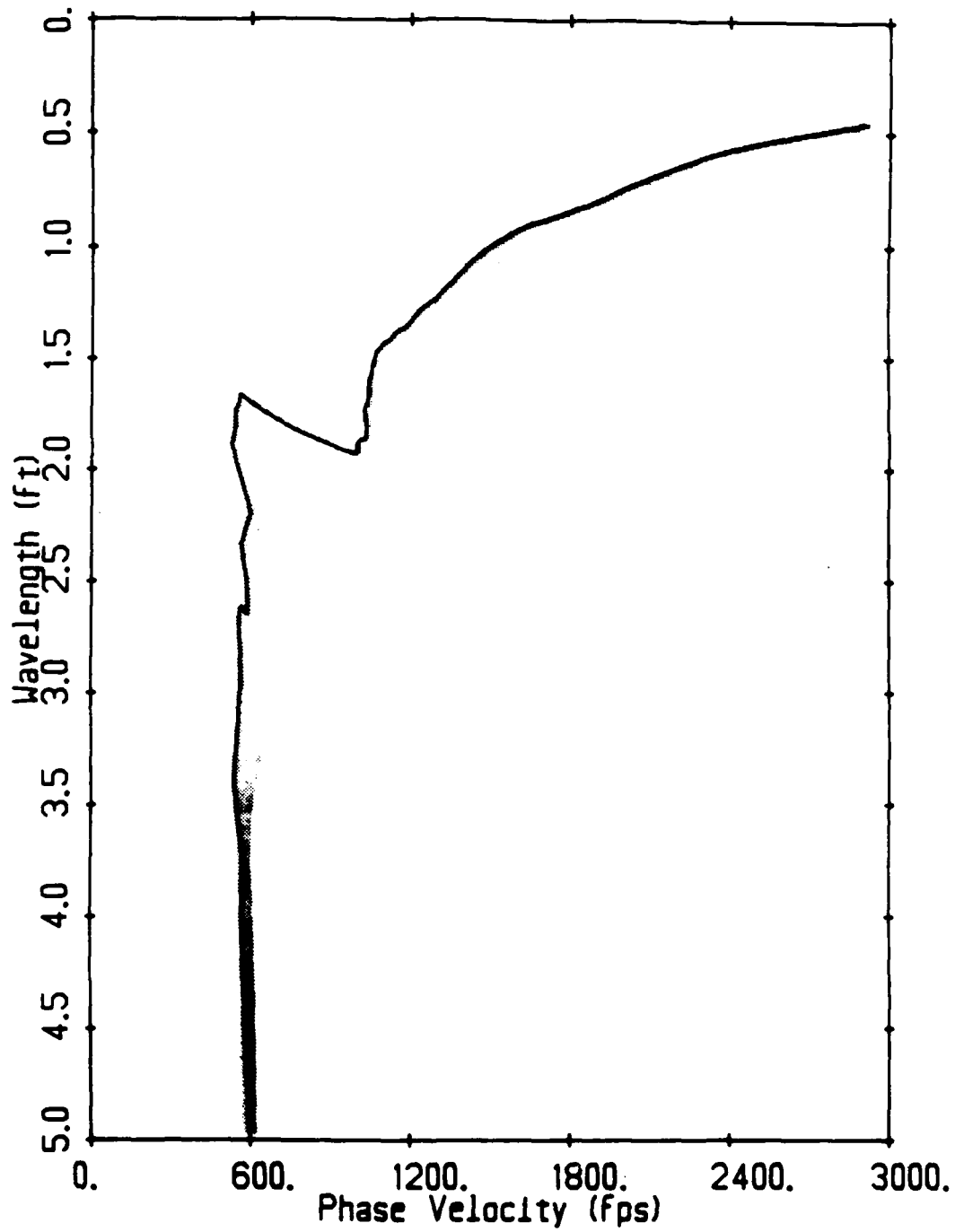


Figure 6.9 — Average Experimental Dispersion Curve for SEMTA Parking Lot Site Using CS Geometry (0 to 5-ft wavelengths)

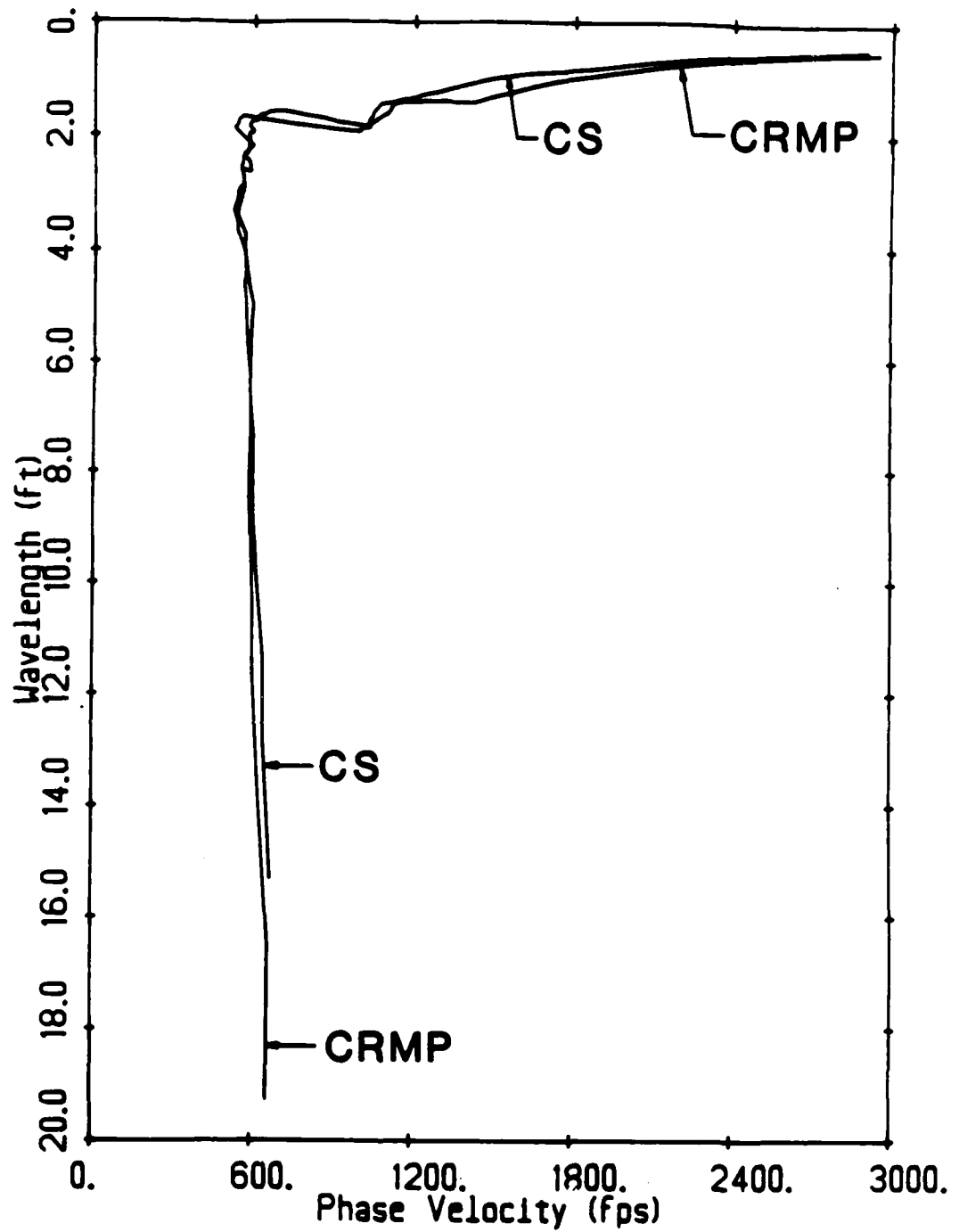


Figure 6.10 — Comparison of Dispersion Curves Obtained from CRMP and CS Geometries at SEMTA Parking Lot Site (all wavelengths)

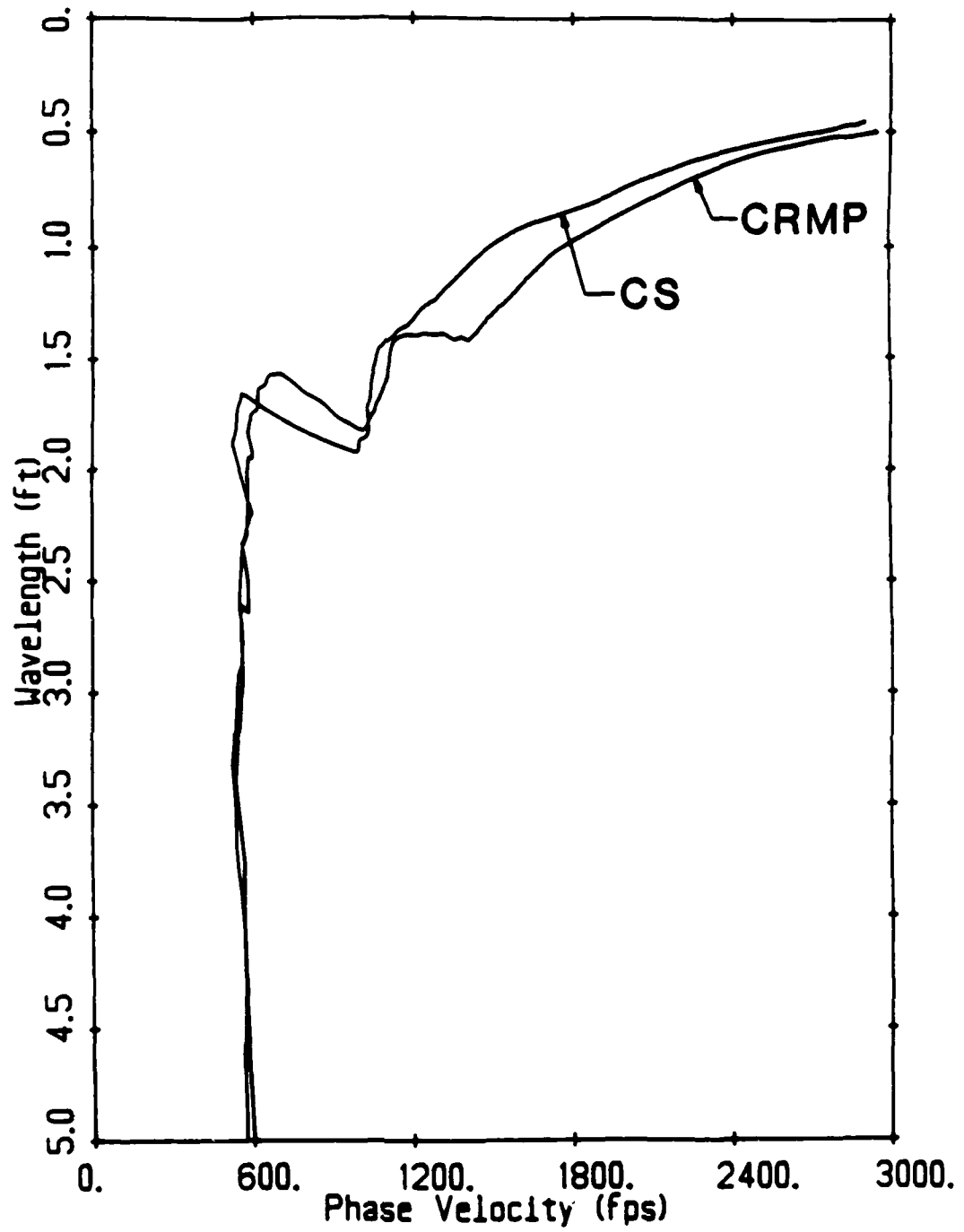


Figure 8.11 — Comparison of Dispersion Curves Obtained from CRMP and CS Geometries at SEMTA Parking Lot Site (0 to 5-ft wavelengths)

material of the pavement and thus this difference is minor. The second difference noted is that the phase velocities are slightly lower in the 0 to 1.5 ft wavelength range for the CS geometry curve. This is likely explained by the fact that the ambient temperatures were higher during the CS tests. The temperature ranged from 71 to 72°F during the CRMP tests, while the range was 71 to 78°F during the CS tests. The higher temperature would cause the asphaltic concrete near the surface to be softer and thus the measured velocities to be lower.

The results also show little difference in the amount of scatter in the data from which the average curves were derived. It was discussed in chapter five that the scatter was greater with the CS geometry for the soil site investigated by Nazarian and Stokoe (1983). They suggested that this was due to lateral nonhomogeneity in the material tested. For the pavement site investigated in this work, little difference is observed between the results obtained with the two geometries. This is probably due to less lateral variations in the materials tested and because the test array extended over a smaller area than in the tests conducted by Nazarian and Stokoe (1983). This should be typical for pavement sites. The materials are usually placed under more controlled conditions than are natural soils, and the maximum receiver spacing is usually only 8 ft. Therefore, a multiple transducer array could be designed using either geometry type.

6.4 Summary

A series of SASW tests were conducted at an asphaltic concrete pavement site to study the influence of source and receiver geometry. Two geometries were investigated: the common receivers midpoint (CRMP) geometry and the common source (CS) geometry. The dispersion curves obtained from each geometry were compared. It was found that the numerical values were nearly identical and that the scatter within all the collected data was similar for each geometry. It thus was concluded that a multiple transducer testing array could be designed using either geometry.

CHAPTER VII

INFLUENCE OF SOURCE-TO-NEAR-RECEIVER DISTANCE

7.1 Introduction

The factors affecting the choice of source-to-near-receiver distance have been discussed in chapter five. It was indicated that little work has been reported on this aspect of the SASW test, yet understanding the influence of this parameter is crucial to the development of a multiple transducer array. Thus, tests have been conducted to systematically study the influence of the source-to-near receiver distance.

Tests were conducted at two sites to study the influence of the source-to-near-receiver distance. The first series of tests was conducted at a parking lot on the University of Michigan campus near the Civil Engineering Department in August of 1986. The site is hereafter referred to as the G. G. Brown Parking Lot site. The general location of the site is shown in figure 7.1. The specific location as well as the location of the SASW test array are shown in figure 7.2. The approximate material profile as determined from construction records (constructed in 1985) is as follows (see figure 7.3): 1.5 in of No. 12 WM asphaltic concrete wearing course (state of Michigan specification), 2 in of No. 1100 20AA asphaltic concrete leveling course, 6 in of 21AA limestone base course, and a fine sand to an undetermined depth.

The second series of tests was conducted at the SEMTA Parking Lot site previously described in chapter six. The location of the site and the material profile are found in figures 6.1 to 6.3. The testing parameters and geometries as well as the test results for both sites are presented in the following section.

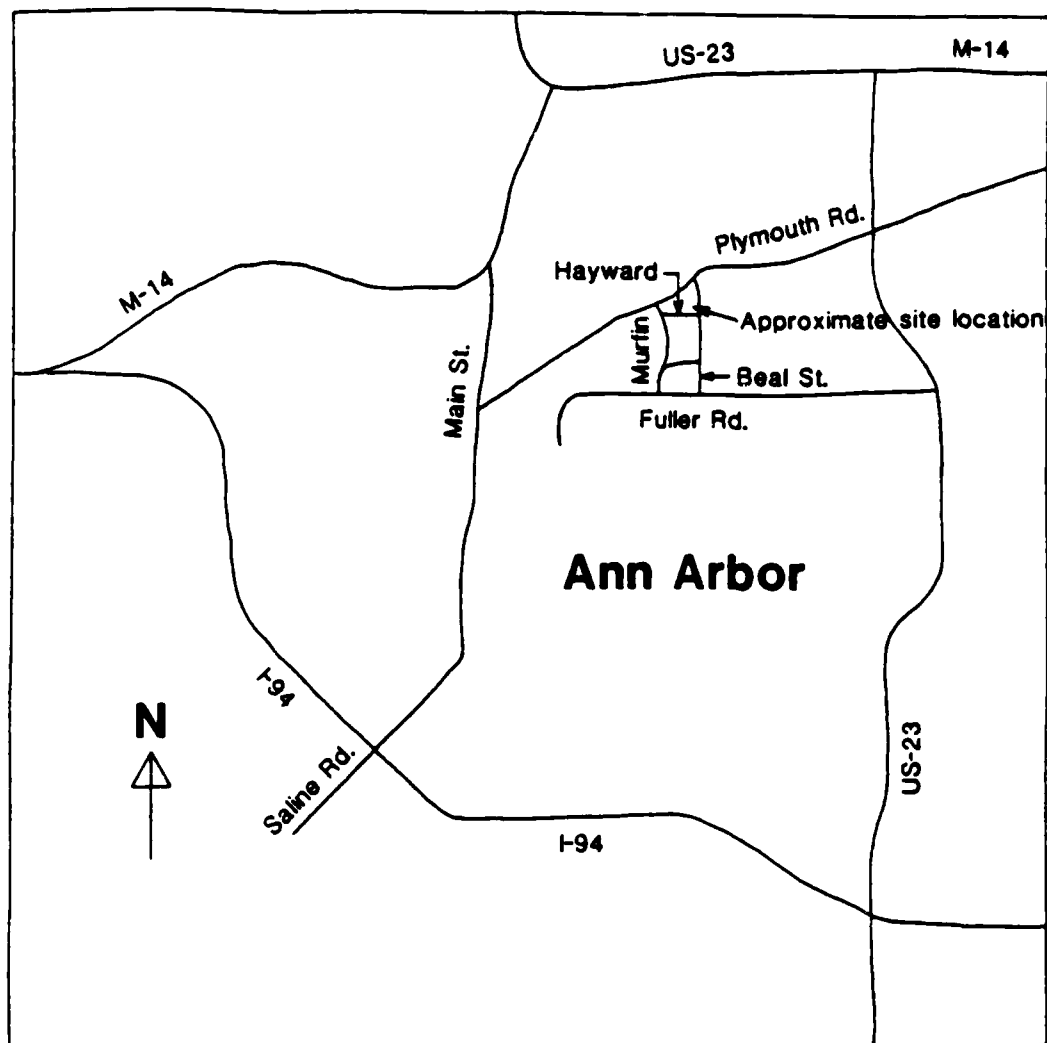


Figure 7.1 — Location of G. G. Brown Parking Lot Site

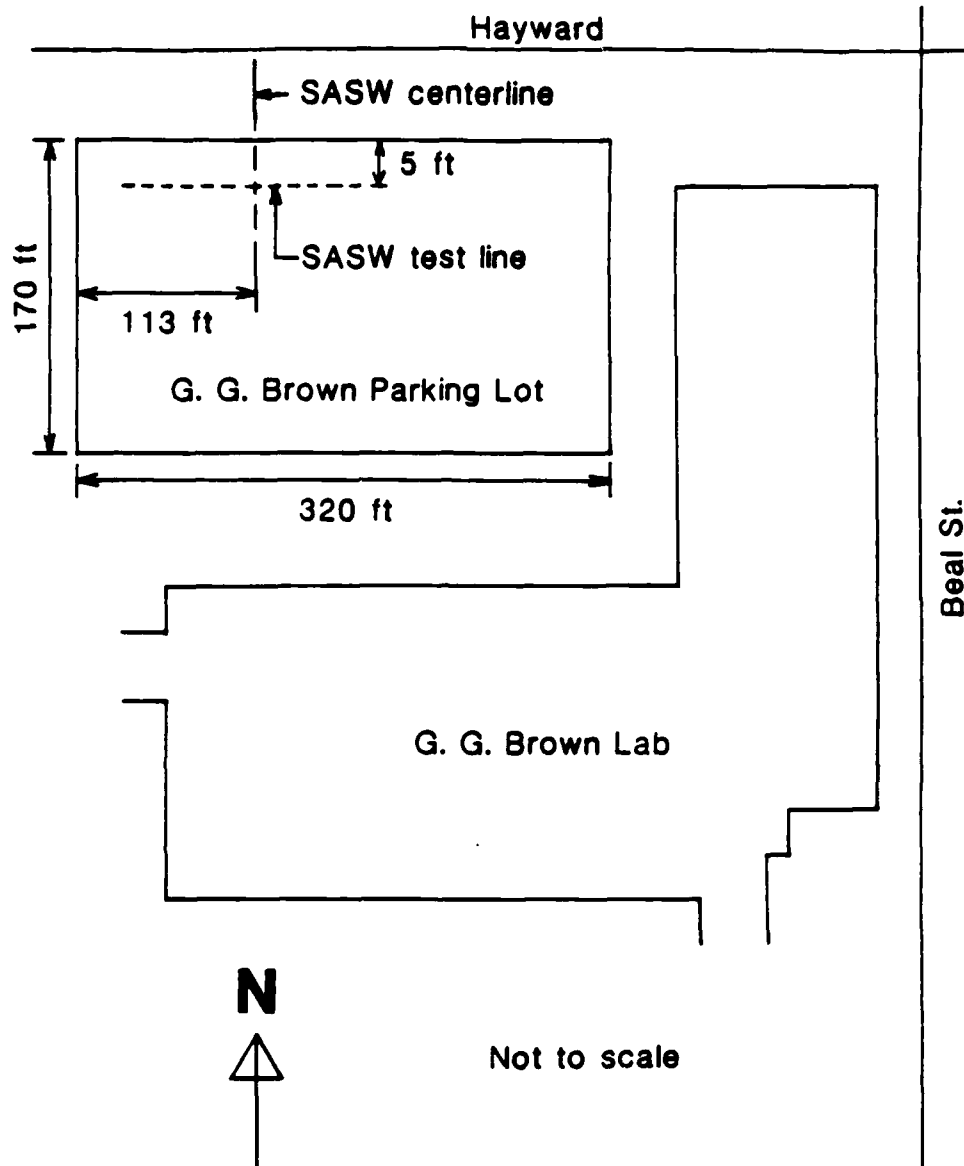


Figure 7.2 — Location of SASW Test Array at G. G. Brown Parking Lot Site

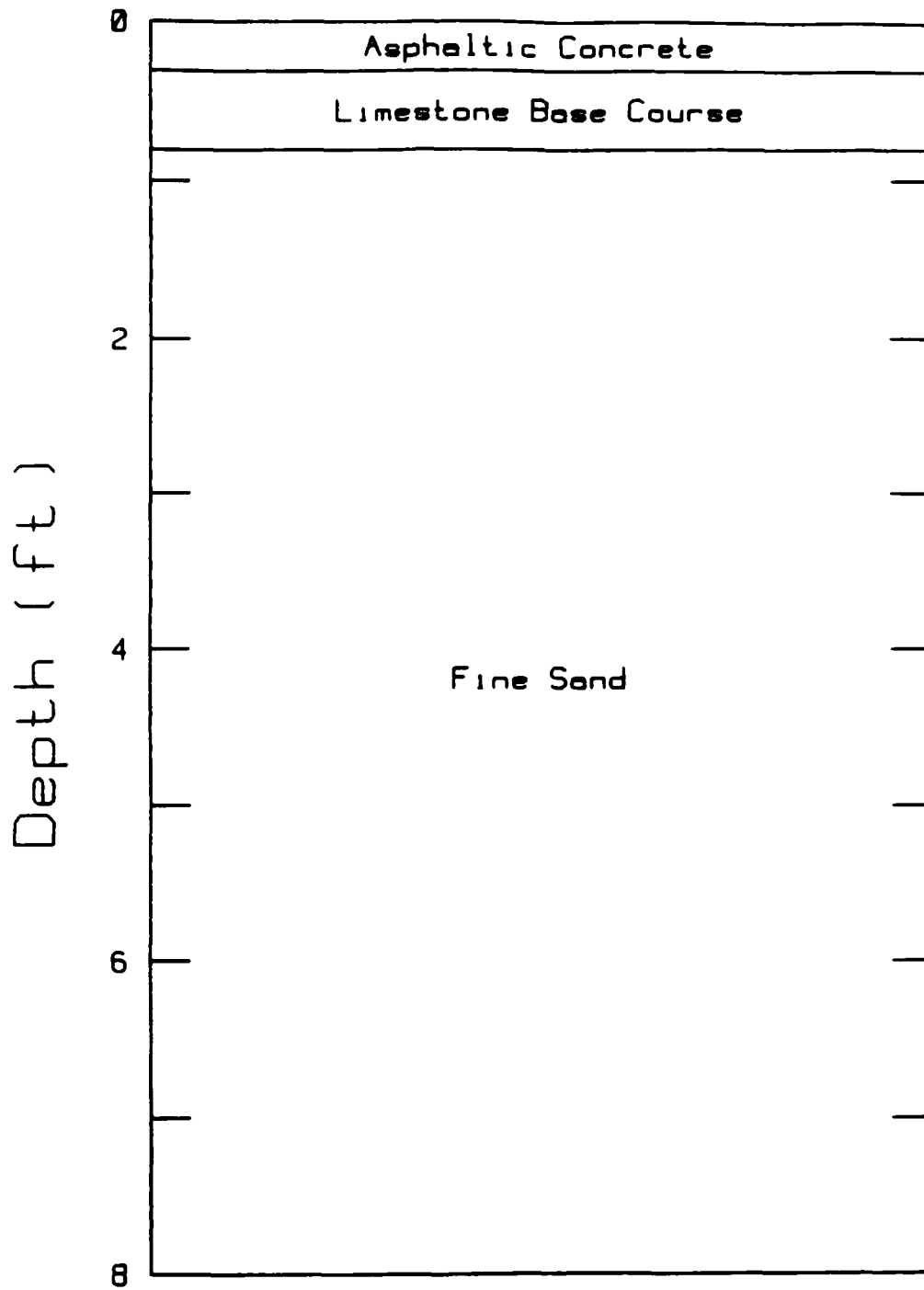


Figure 7.3 — Material Profile of G. G. Brown Parking Lot Site

7.2 Test Results and Discussion

A schematic of the tests conducted at the G. G. Brown Parking Lot site and at the SEMTA Parking Lot site is shown in figure 5.9. The same geometry and test setup was used at each site. A series of two-transducer tests were conducted to examine the influence of source-to-near-receiver distance. The transducer placement followed the common receivers midpoint (CRMP) geometry in that each transducer pair was placed about the same imaginary centerline. Transducer spacings of 0.5, 1, 2, 4, and 8 ft were examined. A range of source locations was used at each receiver spacing such that the ratio of source-to-near-receiver distance (S) to receiver spacing (X), i.e., S/X , was varied over values between 0.5 and 3. The intent was to examine the influence of S/X in order to determine the optimum value and to provide guidance in developing a multiple transducer array. Further, at the G. G. Brown Parking Lot site, three source types were used at each receiver spacing and source location to examine the influence of source type. The influence of source type will be discussed in the following chapter. The results for the "optimum" source for each receiver spacing will be discussed here. Tables 7.1-7.4 summarize the test parameters for each site.

In chapter six the combined dispersion curves obtained from all receiver spacings and source locations for each test geometry were sufficient to examine the influence of source and receiver geometry. A more detailed look at the test data would not have provided any new insights. Since the experimental dispersion curves were nearly identical, the data from which they were obtained were alike as well. This is not the case with respect to the influence of the source-to-near-receiver distance. A much more detailed examination of the data is necessary to understand the problem. Presentation of only the combined experimental dispersion curves would provide the correct conclusions, but little would be understood as to why things turned out as such. Thus, the test results will be presented in a number of formats, including: tables of useful frequency range, from cross power spectrum and coherence function data as a function of source-to-near-receiver distance for each receiver spacing, plots of cross power spectrum magnitudes for each receiver spacing as a function of source-to-near-receiver distance, combined dispersion curves for constant values of receiver spacing to wavelength ratios as a function of source-to-near-receiver distance, and combined dispersion curves (both unfiltered and filtered) as a function of source-to-near-receiver dis-

Table 7.1 — Test Parameters for G. G. Brown Parking Lot Site, Various Source-to-Near-Receiver Distances, and $X = 0.5, 1, 2$ ft

Receiver Spacing (X) (ft)	Receiver Type	Source Type	Frequency Span (Hz)	Source-to-Near-Receiver Distance (S) (ft)	S/X	Site File No.
0.5	PCB Accel.	4 oz	20000	0.25	0.5	13
0.5	PCB Accel.	4 oz	20000	0.50	1.0	14
0.5	PCB Accel.	4 oz	20000	0.75	1.5	15
0.5	PCB Accel.	4 oz	20000	1.00	2.0	16
0.5	PCB Accel.	4 oz	20000	1.50	3.0	25
1	PCB Accel.	4 oz	10000	0.5	0.5	28
1	PCB Accel.	4 oz	10000	1.0	1.0	29
1	PCB Accel.	4 oz	10000	1.5	1.5	30
1	PCB Accel.	4 oz	10000	2.0	2.0	31
1	PCB Accel.	4 oz	10000	2.5	2.5	32
1	PCB Accel.	4 oz	10000	3.0	3.0	33
2	Electro-Tech Veloc.	8 oz	1000	1.0	0.5	64
2	Electro-Tech Veloc.	8 oz	1000	2.0	1.0	65
2	Electro-Tech Veloc.	8 oz	1000	3.0	1.5	66
2	Electro-Tech Veloc.	8 oz	1000	4.0	2.0	67
2	Electro-Tech Veloc.	8 oz	1000	5.0	2.5	68
2	Electro-Tech Veloc.	8 oz	1000	6.0	3.0	69

Table 7.2 — Test Parameters for G. G. Brown Parking Lot Site, Various Source-to-Near-Receiver Distances, and $X = 4, 8$ ft

Receiver Spacing (X) (ft)	Receiver Type	Source Type	Frequency Span (Hz)	Source-to-Near-Receiver Distance (S) (ft)	S/X	Site File No.
4	Electro-Tech Veloc.	128 oz	312.5	2.0	0.5	116
4	Electro-Tech Veloc.	128 oz	312.5	4.0	1.0	117
4	Electro-Tech Veloc.	128 oz	312.5	6.0	1.5	118
4	Electro-Tech Veloc.	128 oz	312.5	8.0	2.0	119
4	Electro-Tech Veloc.	128 oz	312.5	10.0	2.5	120
4	Electro-Tech Veloc.	128 oz	312.5	12.0	3.0	121
8	Electro-Tech Veloc.	128 oz	200	4.0	0.5	124
8	Electro-Tech Veloc.	128 oz	200	8.0	1.0	125
8	Electro-Tech Veloc.	128 oz	200	12.0	1.5	126
8	Electro-Tech Veloc.	128 oz	200	16.0	2.0	127
8	Electro-Tech Veloc.	128 oz	200	20.0	2.5	128
8	Electro-Tech Veloc.	128 oz	200	24.0	3.0	129

Table 7.3 — Test Parameters for SEMTA Parking Lot Site, Various Source-to-Near-Receiver Distances, and $X = 0.5, 1, 2$ ft

Receiver Spacing (X) (ft)	Receiver Type	Source Type	Frequency Span (Hz)	Source-to-Near-Receiver Distance (S) (ft)	S/X	Site File No.
0.5	Dytran Accel.	4 oz	10000	0.25	0.5	800
0.5	Dytran Accel.	4 oz	10000	0.50	1.0	801
0.5	Dytran Accel.	4 oz	10000	0.75	1.5	803
0.5	Dytran Accel.	4 oz	10000	1.00	2.0	804
0.5	Dytran Accel.	4 oz	10000	1.25	2.5	805
0.5	Dytran Accel.	4 oz	10000	1.50	3.0	806
1	Dytran Accel.	4 oz	10000	0.5	0.5	807
1	Dytran Accel.	4 oz	6250	1.0	1.0	808
1	Dytran Accel.	4 oz	6250	1.5	1.5	810
1	Dytran Accel.	4 oz	6250	2.0	2.0	811
1	Dytran Accel.	4 oz	6250	2.5	2.5	812
1	Dytran Accel.	4 oz	6250	3.0	3.0	813
2	Geosource Veloc.	16 oz	1000	1.0	0.5	814
2	Geosource Veloc.	16 oz	1000	2.0	1.0	815
2	Geosource Veloc.	16 oz	1000	3.0	1.5	817
2	Geosource Veloc.	16 oz	1000	4.0	2.0	818
2	Geosource Veloc.	16 oz	1000	5.0	2.5	819
2	Geosource Veloc.	16 oz	1000	6.0	3.0	820

**Table 7.4 — Test Parameters for SEMTA Parking Lot Site, Various
Source-to-Near-Receiver Distances, and $X = 4, 8$ ft**

Receiver Spacing (X) (ft)	Receiver Type	Source Type	Frequency Span (Hz)	Source-to-Near-Receiver Distance (S) (ft)	S/X	Site File No.
4	Geosource Veloc.	40 oz	800	2.0	0.5	821
4	Geosource Veloc.	40 oz	800	4.0	1.0	822
4	Geosource Veloc.	40 oz	800	6.0	1.5	824
4	Geosource Veloc.	40 oz	800	8.0	2.0	825
4	Geosource Veloc.	40 oz	800	10.0	2.5	826
4	Geosource Veloc.	40 oz	800	12.0	3.0	827
8	Geosource Veloc.	128 oz	250	4.0	0.5	828
8	Geosource Veloc.	128 oz	250	8.0	1.0	829
8	Geosource Veloc.	128 oz	250	12.0	1.5	831
8	Geosource Veloc.	128 oz	250	16.0	2.0	832
8	Geosource Veloc.	128 oz	250	20.0	2.5	833
8	Geosource Veloc.	128 oz	250	24.0	3.0	834

tance.

Useful Frequency Ranges

The first test results to be presented are tables of useful frequency ranges from cross power spectrum and coherence function data as a function of source-to-near-receiver distance for each receiver spacing. In section 3.3 it was described how the cross power spectrum and coherence function data collected in the field are used to determine the Rayleigh wave dispersion curve. Part of this process involves determining the frequency ranges where useful data exists. The coherence function is used as an indicator of good data as described. Frequencies where the value of the coherence function is less than 0.9 are typically eliminated. In the end, however, it is the phase angle of the cross power spectrum that is used in the calculation of the dispersion curve. Using the coherence function as the sole criterion can lead to questionable results if correlated "noise" is measured at each receiver. The coherence function will indicate "good" data in this instance, yet the phase angle may yield incorrect dispersion data. The experienced user will consider both the phase angle of the cross power spectrum and the coherence function to determine the ranges of good data. This process must be completed for every cross power spectrum and coherence function pair collected.

The influence of the source-to-near-receiver distance on the range of useful frequencies is important since this ultimately determines how well the dispersion curve is defined. For a given test setup, as more frequencies are eliminated due to poor phase and/or coherence the less defined the dispersion curve becomes. Because of the large amount of data collected, tables of the useful frequency ranges determined from each cross power spectrum and coherence function pair will be presented to summarize the data. The minimum and maximum frequency cutoffs for each pair will be shown as a function of source-to-near-receiver distance. Plots of cross power spectrum and coherence function pairs will be presented for one receiver spacing to demonstrate how the tables were generated. The influence of source-to-near-receiver distance is found to be significant.

The ranges of useful frequencies for the 0.5-ft receiver spacing at the SEMTA Parking Lot site are shown in table 7.5. Tables A.1-A.5 in appendix A contain the data for the

G. G. Brown Parking Lot site. The remaining data for the SEMTA Parking Lot site is found in tables A.6-A.9 in appendix A. The cross power spectrum and coherence function pairs for the 0.5-ft receiver spacing at the SEMTA Parking Lot site are presented in figures 7.4-7.9. The figures are for source-to-near-receiver distances of 0.25, 0.5, 0.75, 1.0, 1.25, and 1.5 ft, i.e., S/X ratios of 0.5, 1.0, 1.5, 2.0, 2.5, and 3.0. The cross-hatched regions on these figures illustrate the frequency ranges eliminated from the data and the cutoff frequencies shown are those found in table 7.5.

The key observation that should be made upon reviewing the test results presented above is the decrease of the upper cutoff frequency with increasing S/X for all receiver spacings. The decline is particularly dramatic for values of S/X greater than two. Although there is some variation of the lower cutoff frequency with S/X , it is in many cases relatively constant. The decline of the upper cutoff frequency is especially important for the testing of pavements because high frequencies are required to define the dispersion curve of the shallow portions of the pavement system. Inadequate definition of the high frequency portion of the dispersion curve for pavement systems will result in an inaccurate modulus profile for all layers in the system. Thus, it can be concluded that S/X should not be greater than two for SASW testing of pavements. The next sections will examine the reasons for the decline in the upper cutoff frequency and the resulting influence on the dispersion curve.

Cross Power Spectrum Magnitudes

The previous section documented the marked influence that the source-to-near-receiver distance has on the range of useful frequencies for a given receiver spacing. It was shown in particular that the upper cutoff frequency significantly decreased for S/X ratios greater than two. This section will attempt to establish why this occurred.

The magnitude of the cross power spectrum was defined in section 2.6 to be a measure of the mutual power between two signals. It is the product of the magnitudes of the two signals and is thus useful for isolating signals that are common to both. For SASW testing it establishes the energy distribution as a function of frequency common to both signals. Where the energy is high as compared to the background noise one would expect good coherence and thus good data. Conversely, where the energy is low poor coherence and

**Table 7.5 — Useful Frequency Ranges for 0.5-ft Receiver Spacing (*X*) for
SEMTA Parking Lot Site**

Source-to-Near-Receiver Distance (<i>S</i>) (ft)	<i>S/X</i>	Lower Cutoff Frequency (Hz)	Upper Cutoff Frequency (Hz)
0.25	0.5	112	5800
0.50	1.0	125	5875
0.75	1.5	887	5900
1.00	2.0	1000	5950
1.25	2.5	1000	5000
1.50	3.0	1050	4100

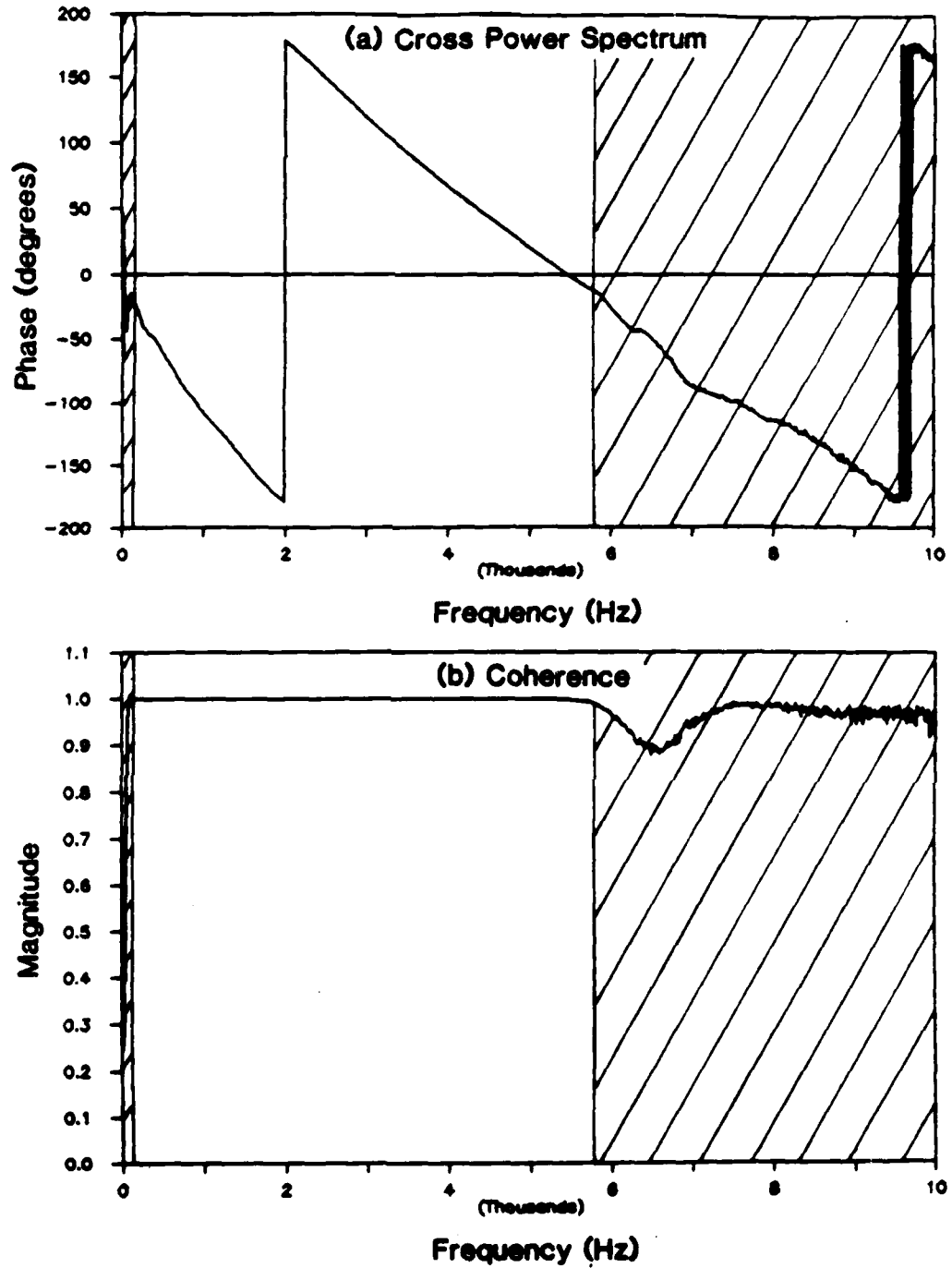


Figure 7.4 — Cross Power Spectrum and Coherence Function for $X = 0.5$ ft
and $S/X = 0.5$ for SEMTA Parking Lot Site

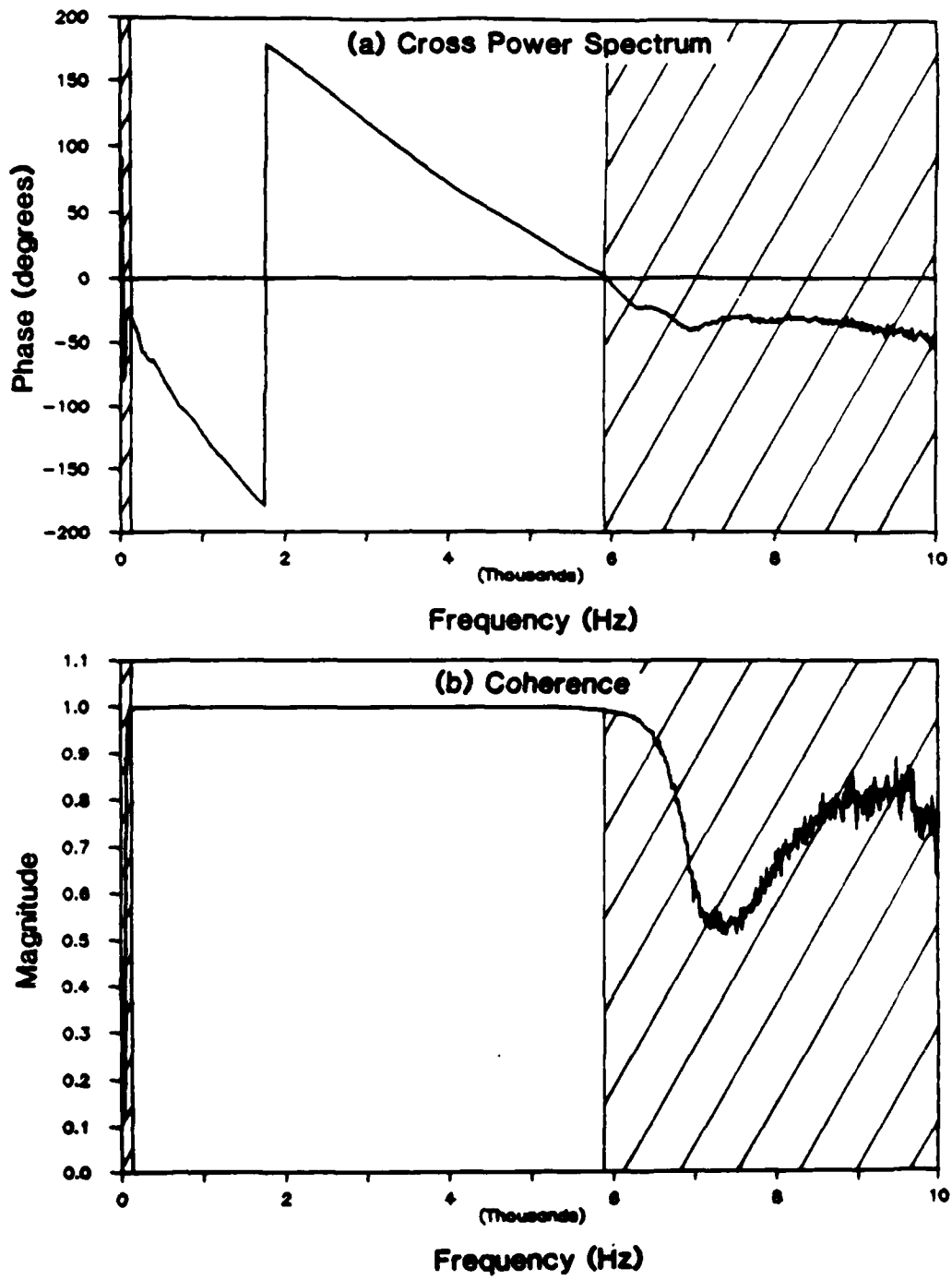


Figure 7.5 — Cross Power Spectrum and Coherence Function for $X = 0.5$ ft
and $S/X = 1.0$ for SEMTA Parking Lot Site

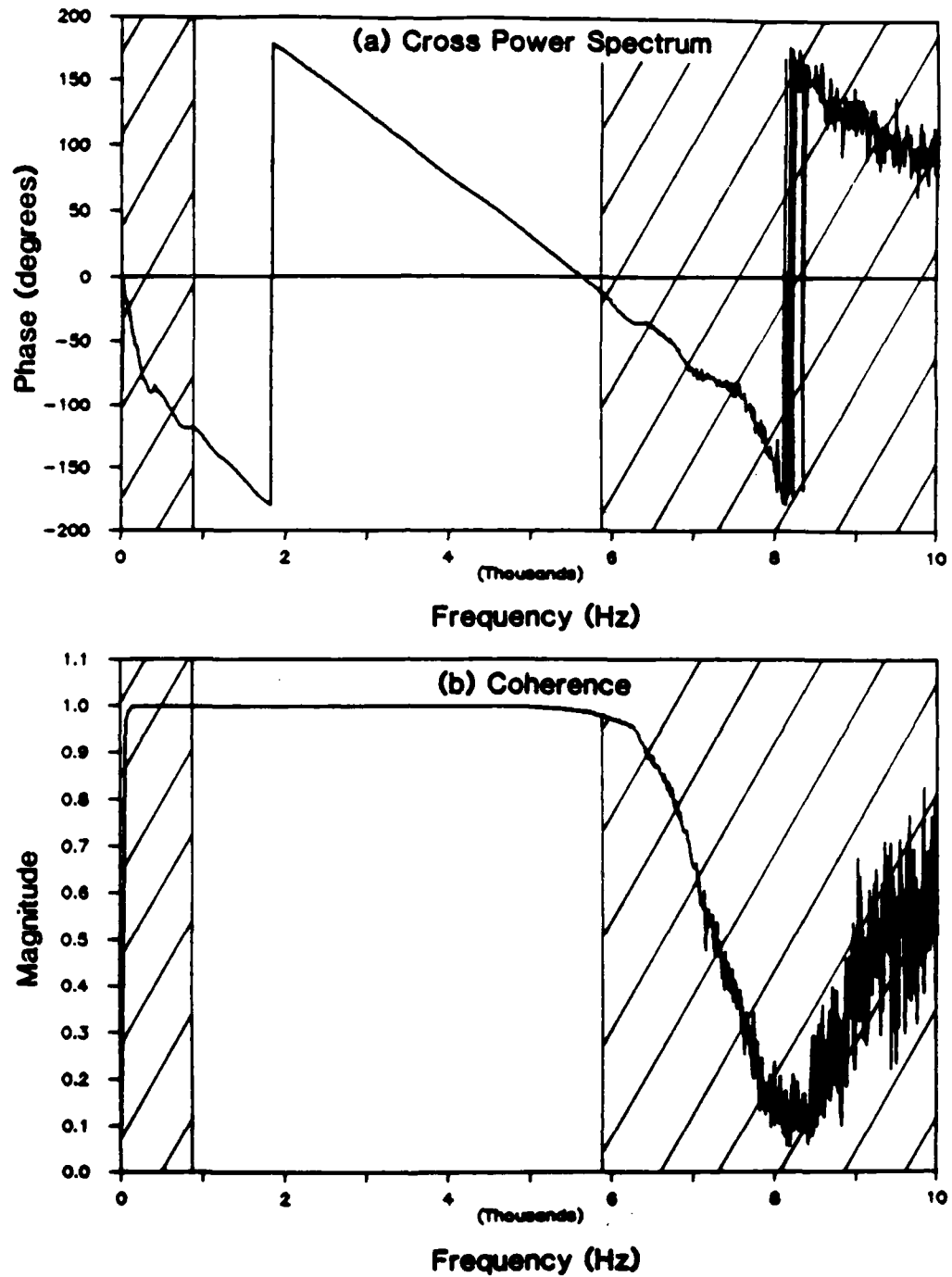


Figure 7.6 — Cross Power Spectrum and Coherence Function for $X = 0.5$ ft
and $S/X = 1.5$ for SEMTA Parking Lot Site

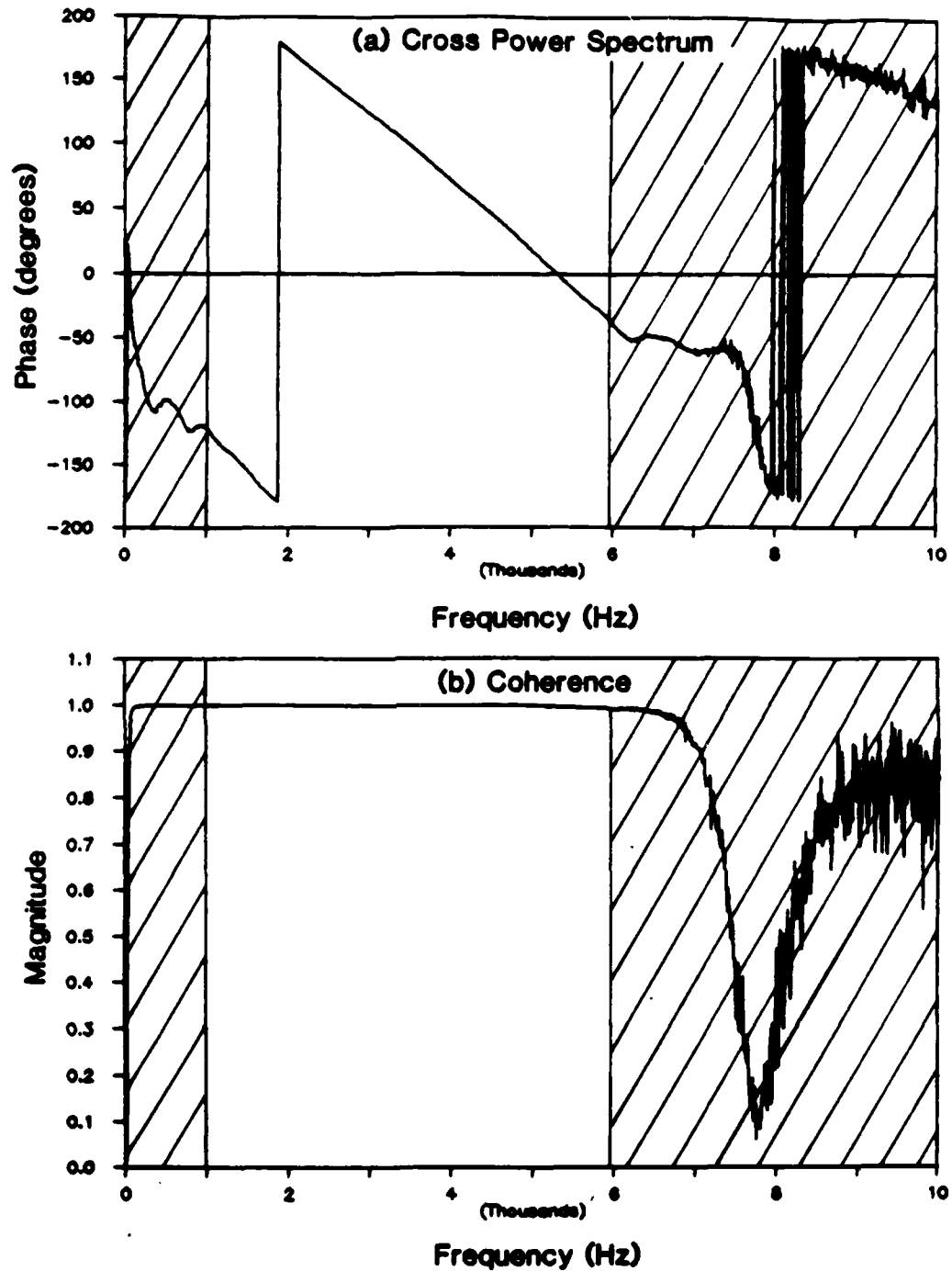


Figure 7.7 — Cross Power Spectrum and Coherence Function for $X = 0.5$ ft
and $S/X = 2.0$ for SEMTA Parking Lot Site

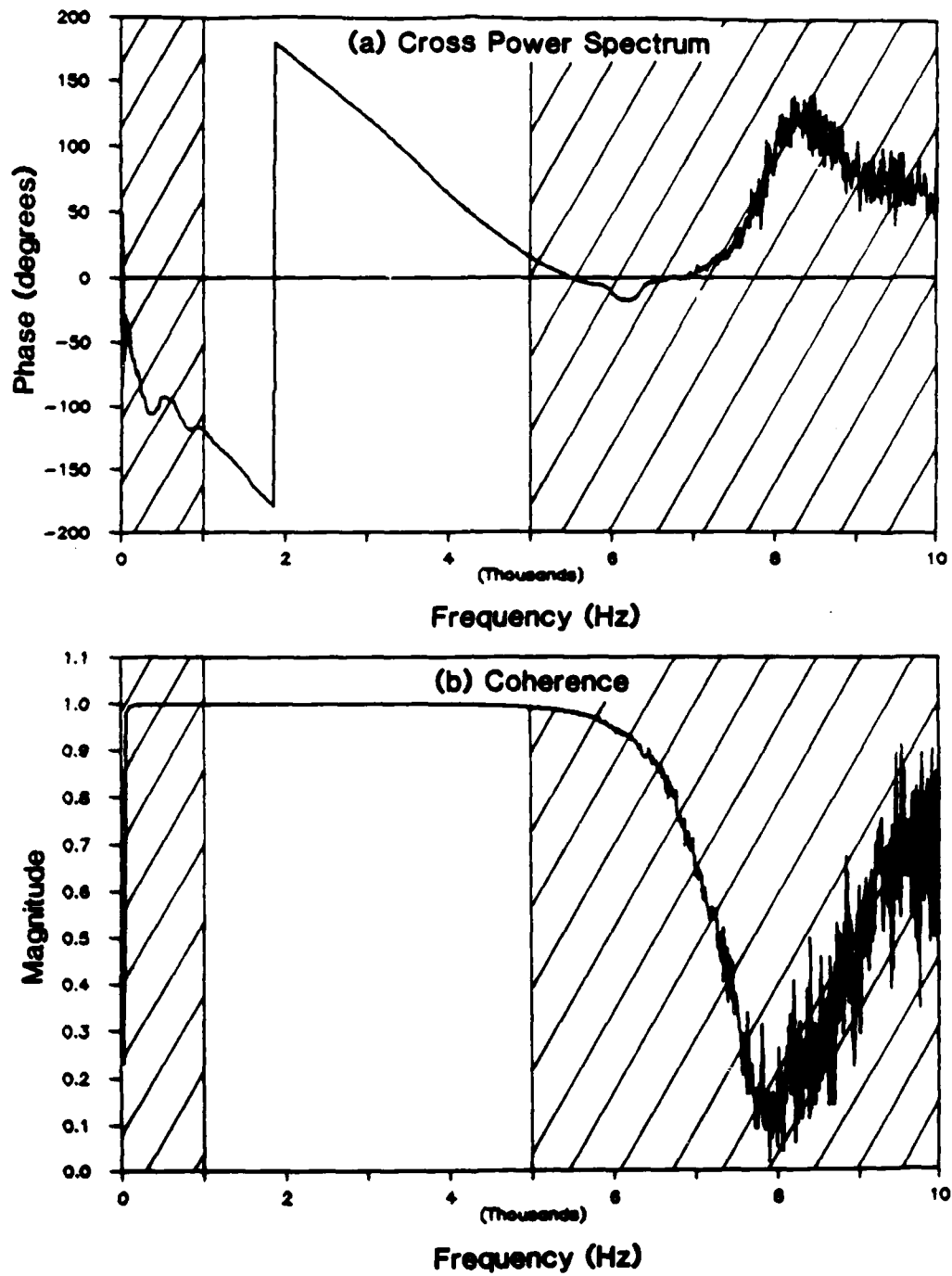


Figure 7.8 — Cross Power Spectrum and Coherence Function for $X = 0.5$ ft
and $S/X = 2.5$ for SEMTA Parking Lot Site

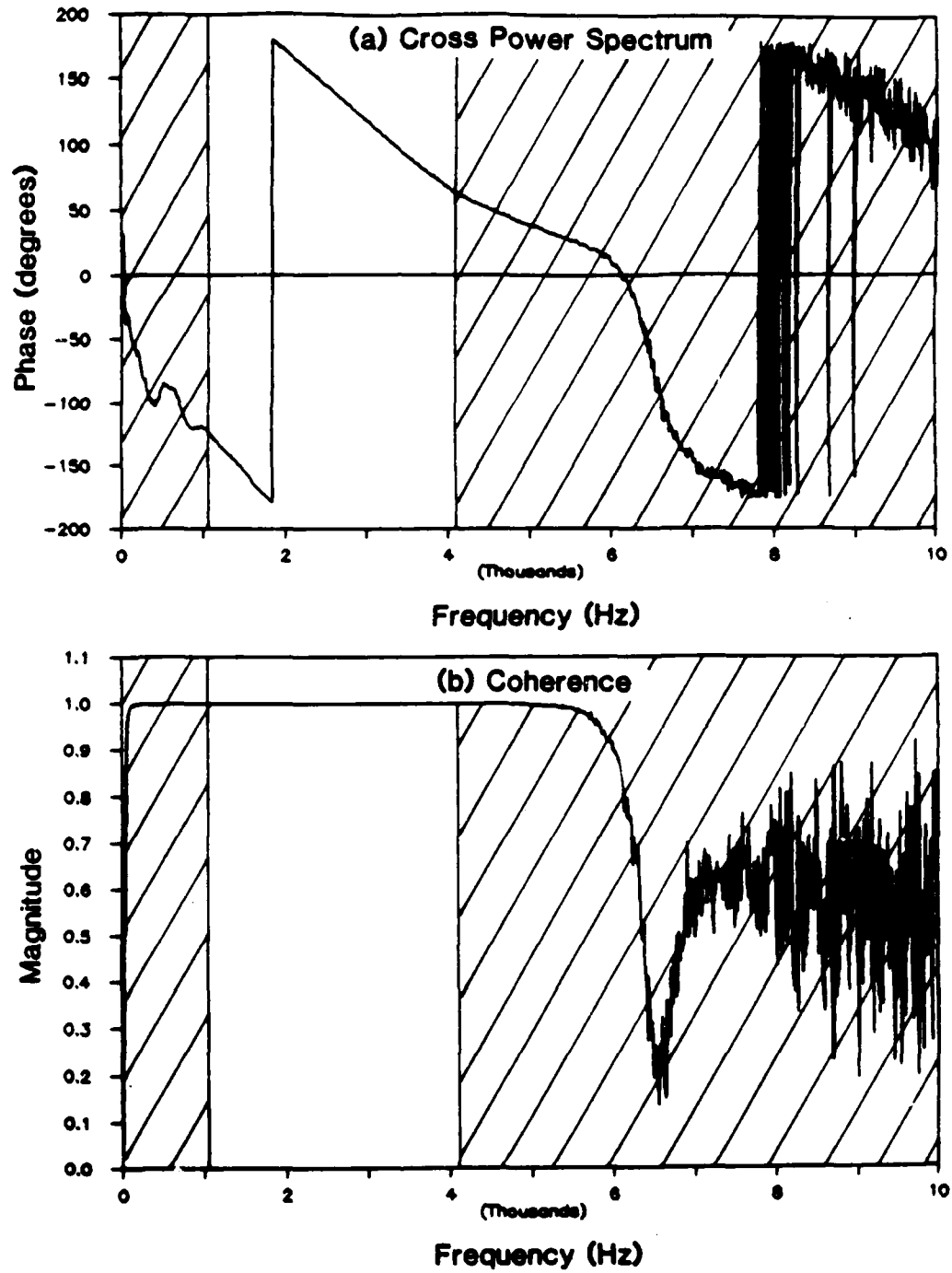


Figure 7.9 — Cross Power Spectrum and Coherence Function for $X = 0.5$ ft
and $S/X = 3.0$ for SEMTA Parking Lot Site

thus bad data can be expected. The magnitude of the cross power spectrum is a useful tool for explaining the influence of the source-to-near-receiver distance discovered in the previous section.

The magnitude of the cross power spectrum for each test will be presented. The spectrums for the 0.5-ft receiver spacing at the SEMTA Parking Lot site are shown in figures 7.10-7.11. The spectrums for the G. G. Brown Parking Lot site are found in figures B.1-B.10 in appendix B. The remaining spectrums for the SEMTA Parking Lot site are found in figures B.11-B.18 in appendix B. Each plot contains the spectrums for S/X ratios of 0.5, 1.0, 1.5, 2.0, 2.5, and 3.0 for a given receiver spacing. The spectrums on each plot are difficult to separate, but it is not intended that they be individually distinguished. The trend is more important. Further, each spectrum is presented in two formats. First, the actual or absolute magnitudes as recorded in the field are shown. The second plot presents normalized or relative magnitudes. The relative magnitude is defined as the absolute magnitude normalized by the peak magnitude for each spectrum. The intent of the absolute magnitude plot is to illustrate how the actual energy levels change with source-to-near-receiver distance. The relative magnitude plot illustrates how the energy distribution with frequency (or shape) changes as the source-to-near-receiver distance is varied.

The first observation that should be made is that the absolute magnitude of the cross power spectrum decreases with increasing S/X . This is partially due to geometric damping of the signals and should come as no surprise. Further, it does not in itself account for the decrease in upper cutoff frequency as S/X increases. It is much more revealing to examine the shape or relative magnitude as a function of S/X . For a perfectly elastic system the shape of the cross power spectrum should be independent of source-to-near-receiver distance. This is because the only damping present in the system is geometric, which is not dependent on the frequency of the waveform. In a real system, e.g., pavement, however, material damping of the waveform will occur as well. Material damping is frequency dependent. Higher frequency waves attenuate more over equivalent propagation distances since they undergo more cycles of motion. The plots of relative magnitude of the cross power spectrum illustrate this point quite clearly. The spectrums as a function of S/X for a given receiver spacing do not lie on top of one another as they would if the system under test was

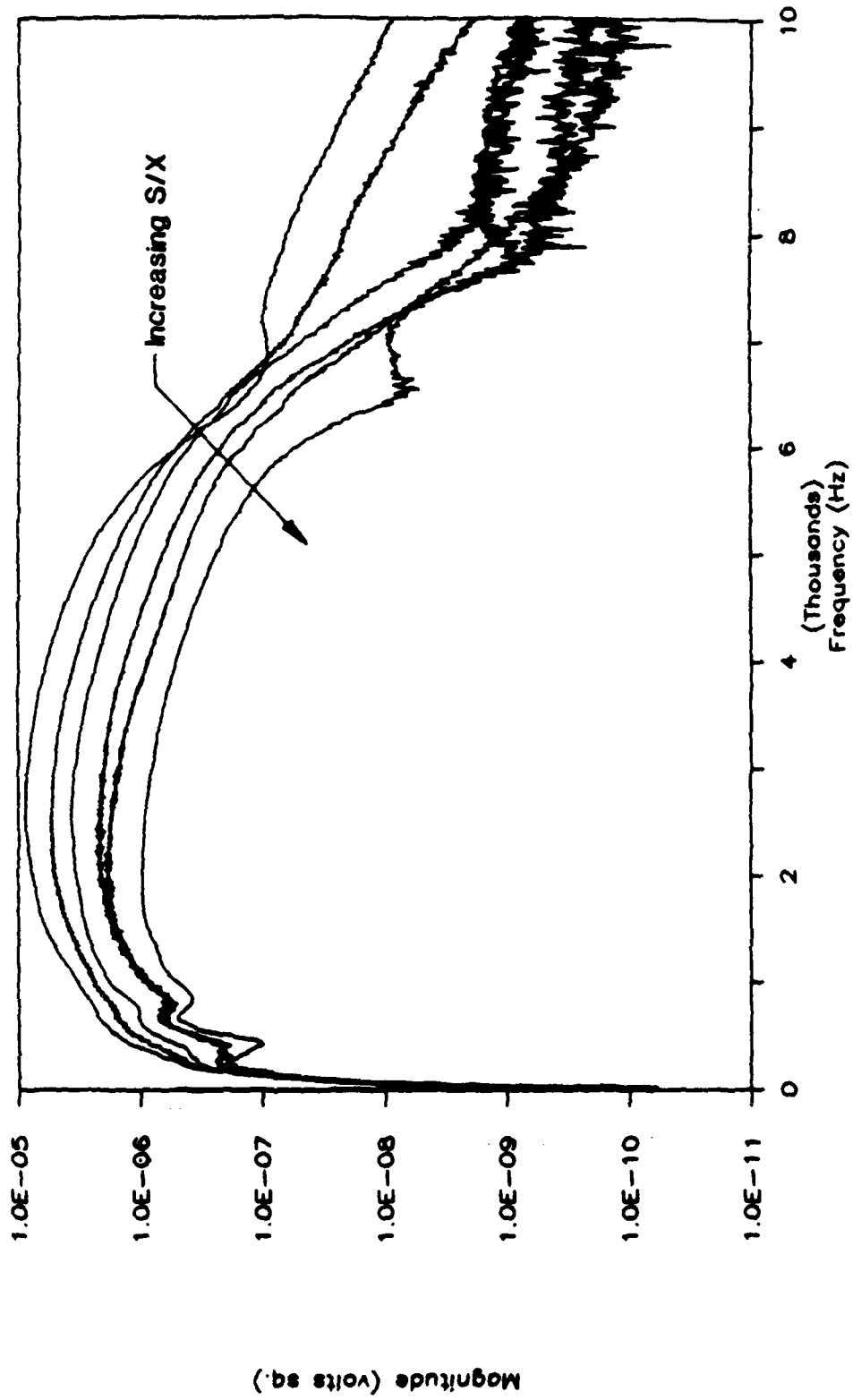


Figure 7.10 - Magnitude (Absolute) of Cross Power Spectrum for X = 0.5 ft for SEMTA Parking Lot Site

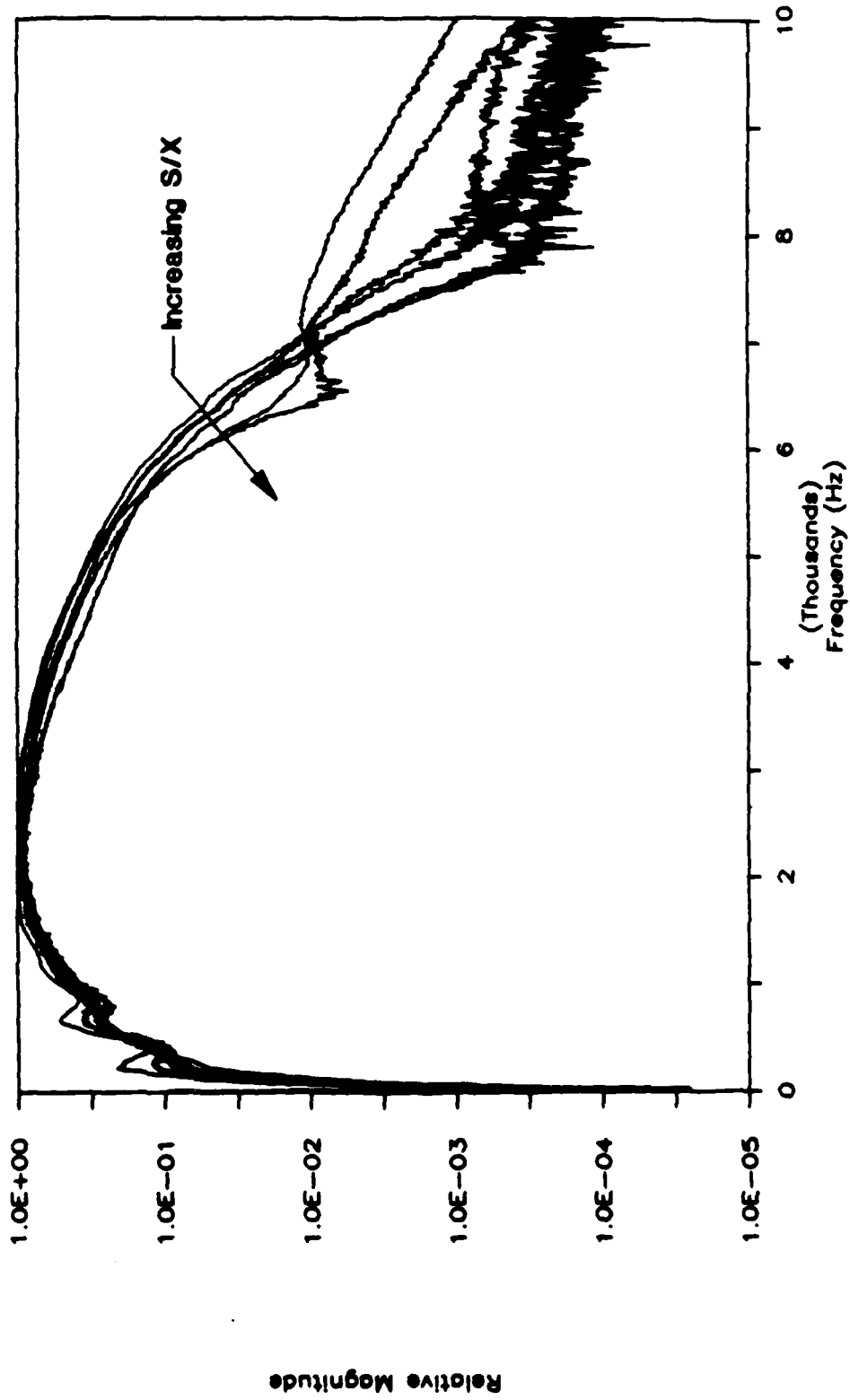


Figure 7.11 - Magnitude (Relative) of Cross Power Spectrum for $X = 0.5$ ft for SEMTA Parking Lot Site

perfectly elastic. On the contrary, there is a dramatic decrease in the magnitude of the high frequency components as S/X increases (the reader is strongly encouraged to review the plots in appendix B). This is due to material damping. The decline in the upper frequency cutoff as S/X increases is due to material damping. For S/X values larger than two the high frequency components of the waveforms attenuate excessively and become buried in background noise. Poor phase and/or coherence data result.

Combined Dispersion Curves for Constant X/L_R

The influence of the source-to-near-receiver distance on the range of useful data collected in the field has been discussed. The discussion will now focus on the affect the source-to-near-receiver distance has on the resulting dispersion curve and thus the interpreted stiffness profile.

In section 3.2 a criterion for filtering out data for wavelengths which are inappropriate for the spacing of the receivers was given for a test setup such that S/X always equals one (see eq. 3.1). This filter was found to eliminate much of the scatter in the dispersion curve (Heisey et al. [1982]). Wavelengths smaller than one-half the receiver spacing and greater than three times the receiver spacing are eliminated according to the criterion. In other words, for a given receiver spacing waves which have traveled fewer than one-third of a cycle and greater than two cycles are filtered out. Heisey et al. (1982) explained that waves traveling less than one-third of a cycle might not be accurately measured in the field because the possible error in measuring phase angle becomes significant as compared to the phase difference between the two receivers. On the other hand, waves traveling more than two cycles will likely attenuate greatly and thus become buried in background noise. The two-cycle limit was determined from examining a number of cross power spectrum and coherence function pairs collected in the field. The upper cutoff frequency was consistently found to occur near a phase angle of 720 degrees or two cycles.

Sanchez-Salinerio et al. (1987) studied the wavelength/receiver spacing filter criterion from a theoretical point of view. In the SASW method it is assumed that since about two-thirds of the energy generated by the source is transmitted by Rayleigh waves and because these waves attenuate less (see section 2.2), the wavetrain passing by the receivers is composed primarily of Rayleigh waves. It is further assumed that the Rayleigh waves are plane

waves, i.e., generated by a source at infinity. This leads one to the question of how many cycles must the wave travel before these assumptions are valid. To examine this question a series of analytical studies that simulate the testing procedure were performed. Theoretical dispersion curves were generated by two methods, one that assumes plane Rayleigh waves only and one that includes the Rayleigh and body waves generated by a point source located at a finite distance from the receivers. The studies were performed for test setups such that S/X always equalled one. Further, dispersion curves generated by the method that includes the body waves were for constant values of X/L_R , the ratio of the receiver spacing to the wavelength of the Rayleigh wave. In other words, the curves were generated for constant values of the number of cycles the waves traveled. By comparing the dispersion curves for different values of the X/L_R ratio with the curve generated by assuming only plane Rayleigh waves, one could establish the number of cycles necessary for the wave to travel before the plane-Rayleigh-wave-only assumption is valid. Sanchez-Salinero et al. (1987) found that for a test setup in which the distance from the source to the first receiver is equal to the distance between the receivers, the field data should be filtered for wavelengths greater than one-half the receiver spacing. Thus, the assumption that only plane Rayleigh waves exist is best when the wave has traveled two or more cycles.

The disparity between the experimental and theoretical criterion should be observed. Heisey et al. (1982) suggest that waves traveling more than two cycles will attenuate excessively and thus should be eliminated from the collected data, while Sanchez-Salinero et al. (1987) suggest that the waves must travel at least two cycles to prevent contamination by body waves. Which criterion should be used for analyzing field data from SASW tests? If the entire wavetrain attenuates excessively after two cycles, as the experimental results indicate, after how many cycles do the body waves attenuate to an insignificant level? Some insight into these questions can be gained by examining the data collected as part of this research. If the experimental dispersion curves for constant values of X/L_R are compared as a function of S/X , some indication of the body wave attenuation can be obtained. For a given value of X/L_R , as the source (S/X) is moved farther from the receivers the wavetrain at the receivers should contain a higher percentage of Rayleigh wave energy. When the body wave energy attenuates to an insignificant level, i.e., the value of X/L_R becomes large

enough, the dispersion curves for all values of S/X should be the same since the only energy of significance is from the Rayleigh wave. This section will thus compare the experimental dispersion curves for constant values of X/L_R as a function of S/X for the data collected at the G. G. Brown and SEMTA Parking Lot sites to gain possible insights on the issues in question.

Experimental dispersion curves for constant values of X/L_R as a function of S/X for the G. G. Brown Parking Lot site are shown in figures 7.12-7.22. The corresponding curves for the SEMTA Parking Lot site are found in figures C.1-C.11 in appendix C. The figures have been prepared for values of X/L_R between 0.2 and 2. Little data existed on either side of these limits after eliminating the frequencies displaying poor phase and/or coherence. In fact, one observes that only in the middle of these limits does data exist for all values of S/X . This is due to the narrowing of the useful frequency range as S/X increases, as documented in the previous sections. The dispersion curves differ from any previously presented in that fewer points are used to describe the curve. This is because only one value from the dispersion data for a given spacing will satisfy the constraint that X/L_R be constant. Since five receiver spacings were investigated at each test site, a maximum of five points is available to describe the dispersion curve for a given X/L_R and S/X .

The first observation to be made is that the measured phase velocities are practically independent of S/X for wavelengths larger than 5 ft for all values of X/L_R . The data for all values of S/X are nearly the same. This suggests that wavelengths larger than approximately 5 ft are not contaminated with body wave energy. Thus, body wave energy is only significant in the upper layers of the pavement system.

The second observation to be made is that the measured phase velocities are significantly dependent on S/X for small values of X/L_R for wavelengths smaller than 5 ft. In particular, the measured phase velocities generally increase with decreasing S/X for a given X/L_R . This suggests that body wave energy is present in the signals. The velocities of both compression and shear waves are larger than the velocity of the Rayleigh wave. As the source is moved closer to the first receiver the amount of body wave energy in the signals will increase, as discussed previously. The result should be an increase in the measured velocity, which is exactly what has been measured.

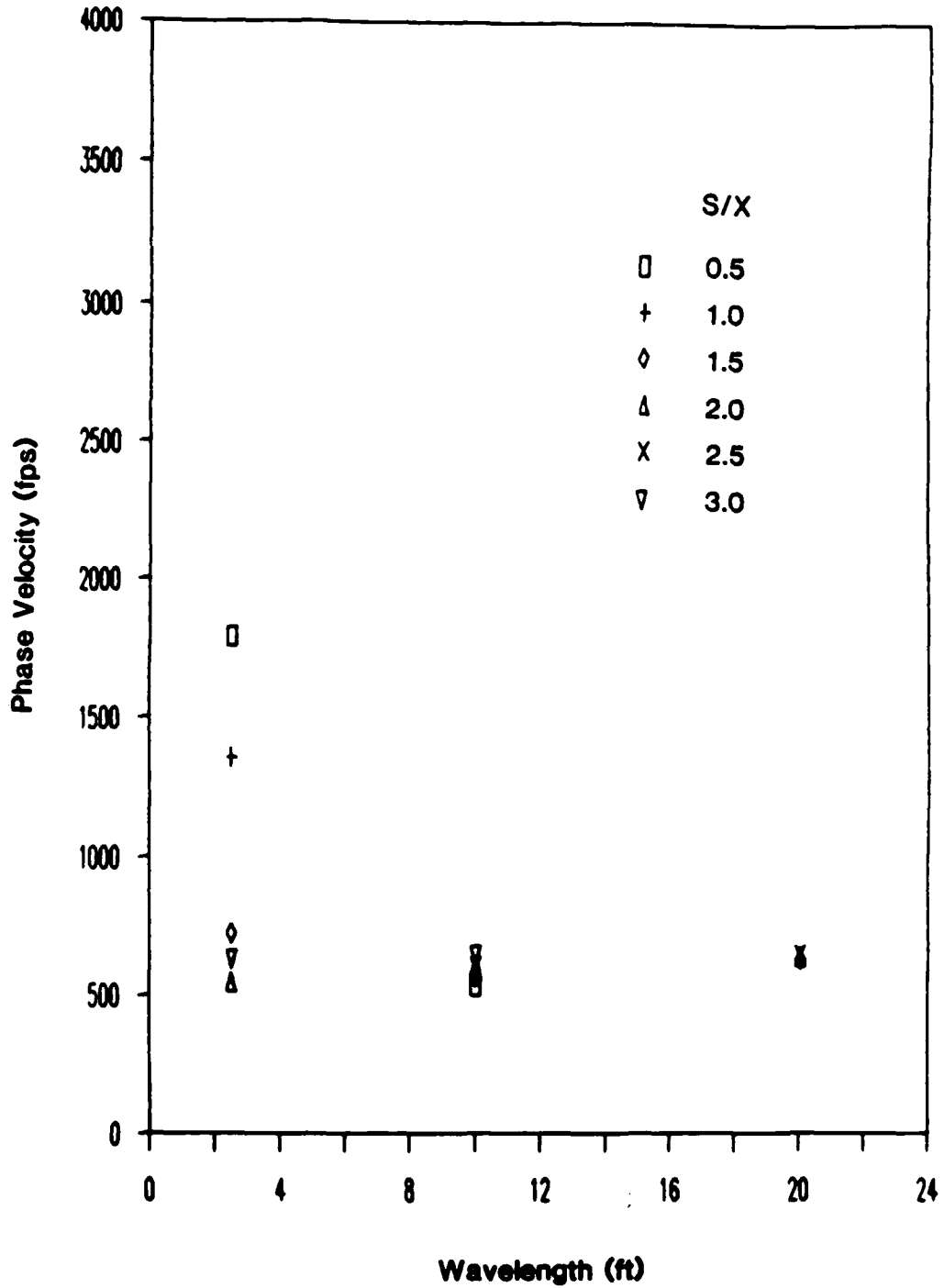


Figure 7.12 — Experimental Dispersion Curves for $X/L_R = 0.2$ for
G. G. Brown Parking Lot Site

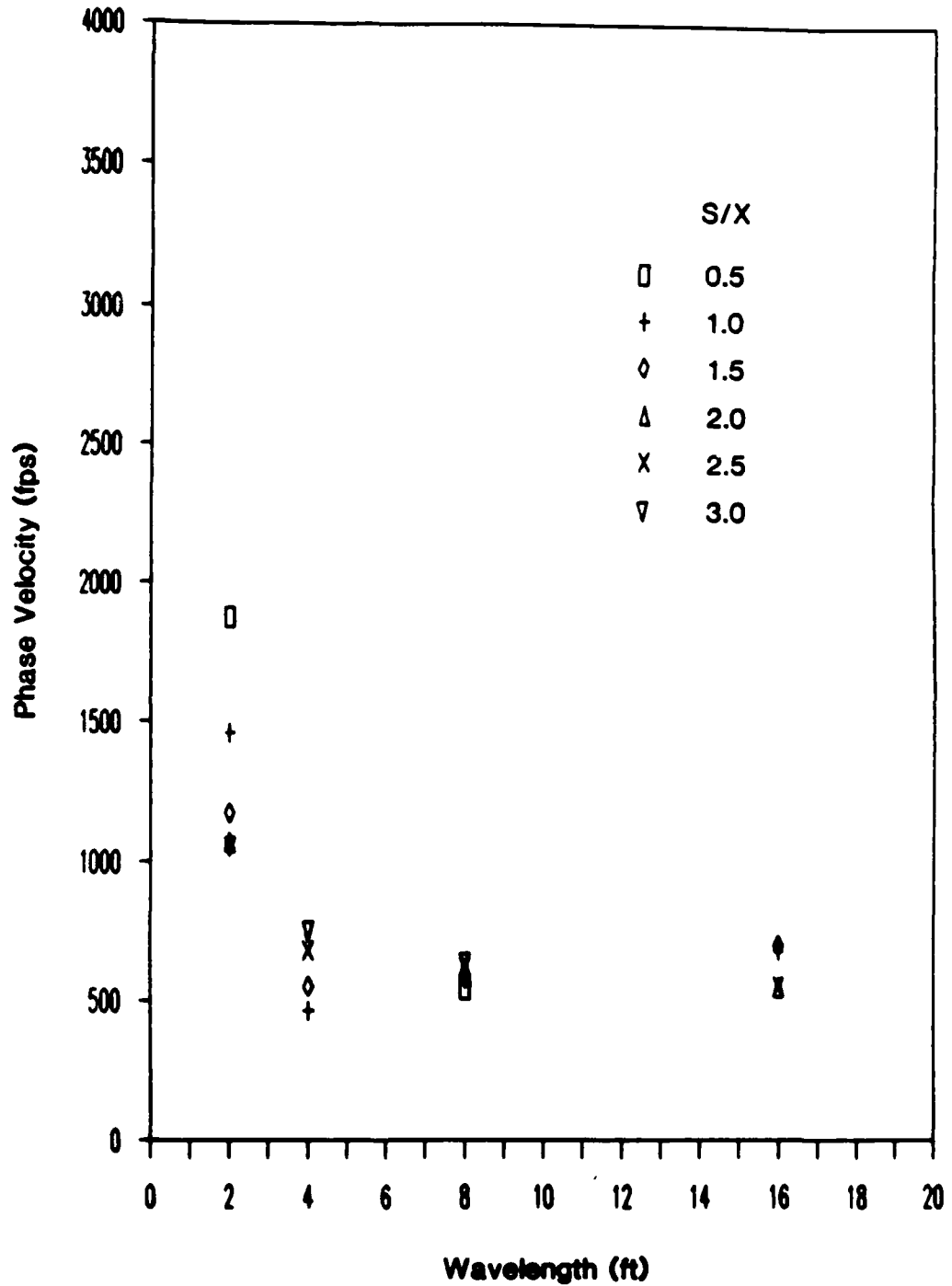


Figure 7.13 — Experimental Dispersion Curves for $X/L_R = 0.25$ for
G. G. Brown Parking Lot Site

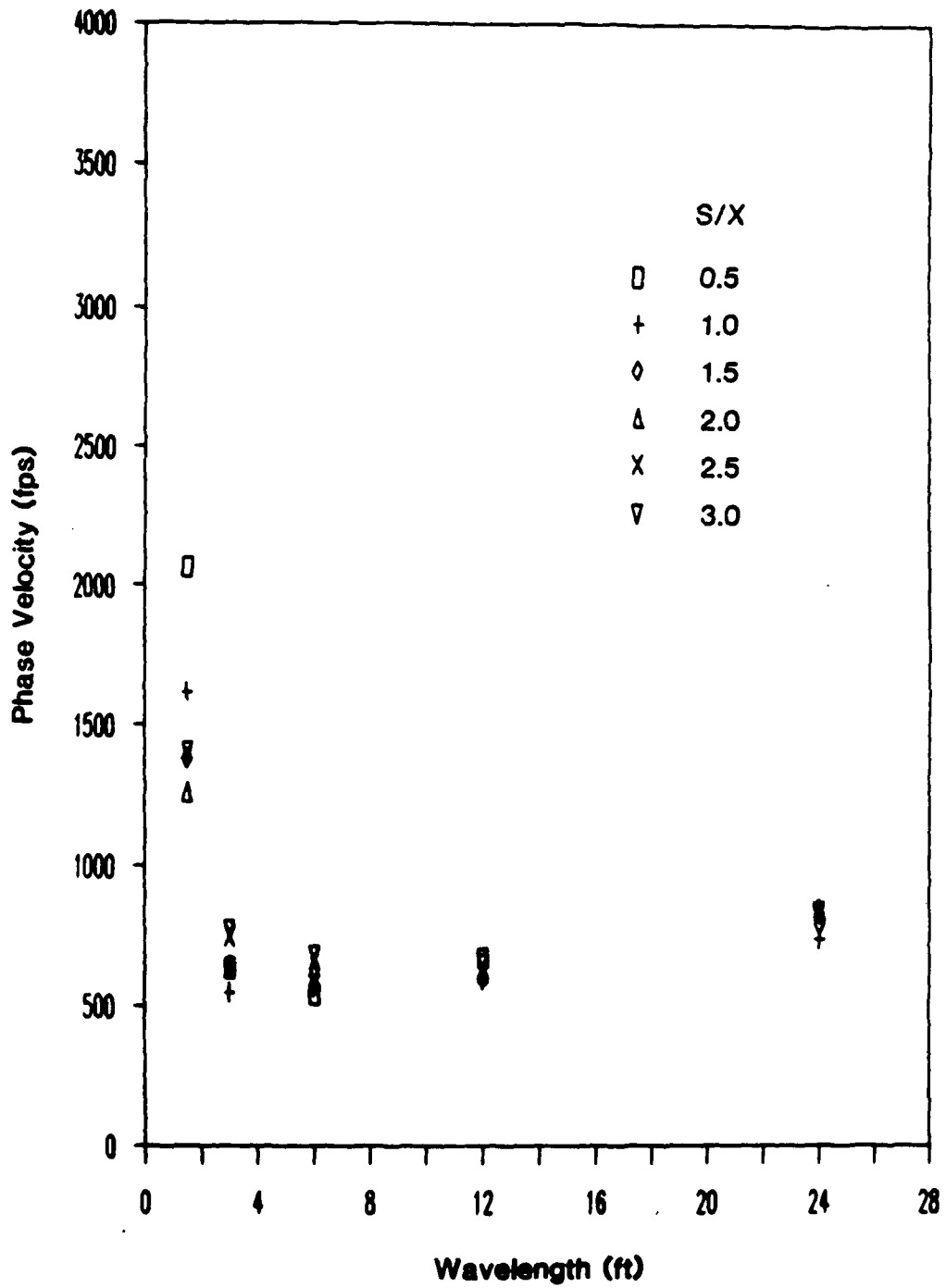


Figure 7.14 — Experimental Dispersion Curves for $X/L_R = 0.33$ for
G. G. Brown Parking Lot Site

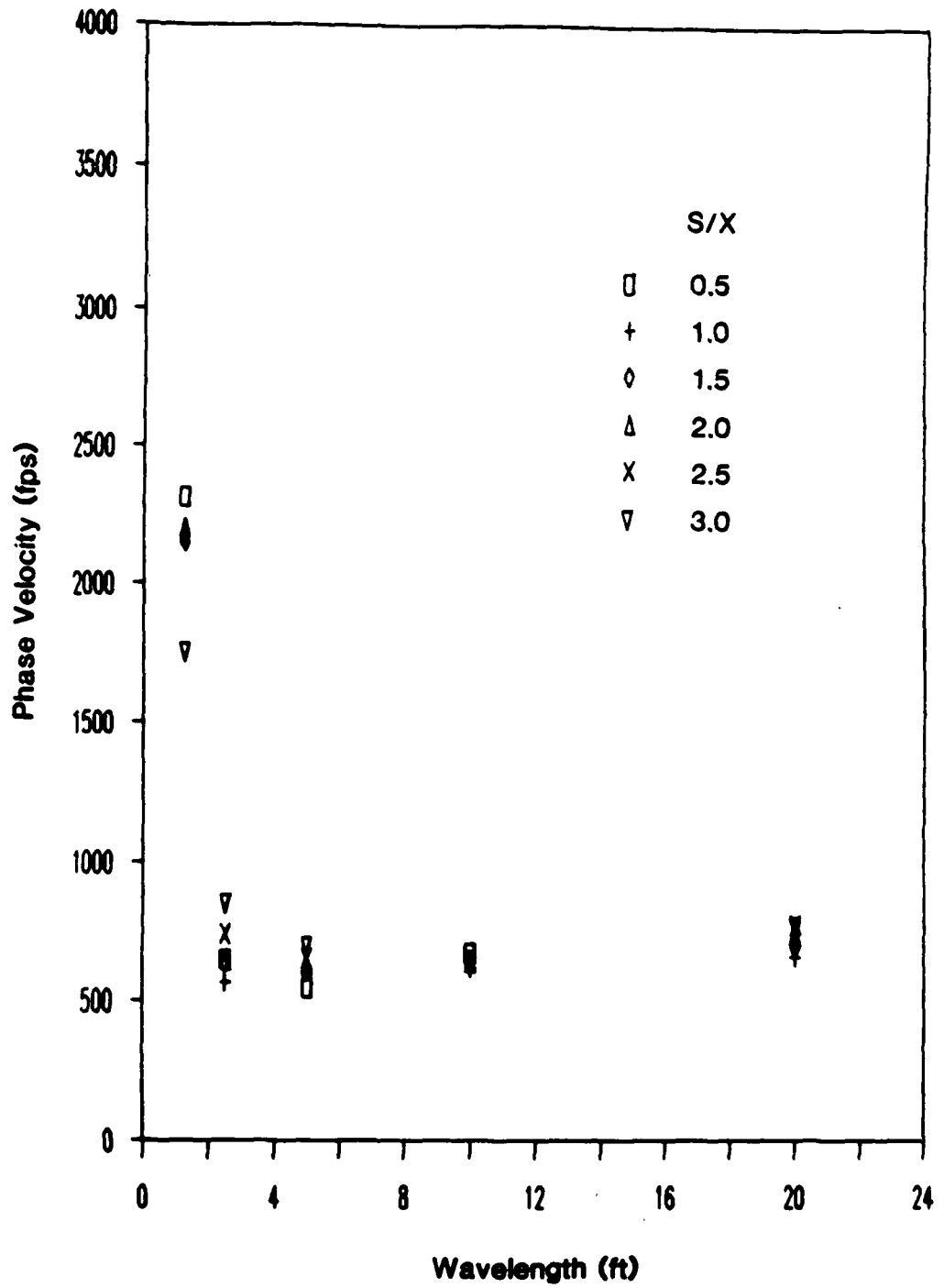


Figure 7.15 — Experimental Dispersion Curves for $X/L_R = 0.4$ for
G. G. Brown Parking Lot Site

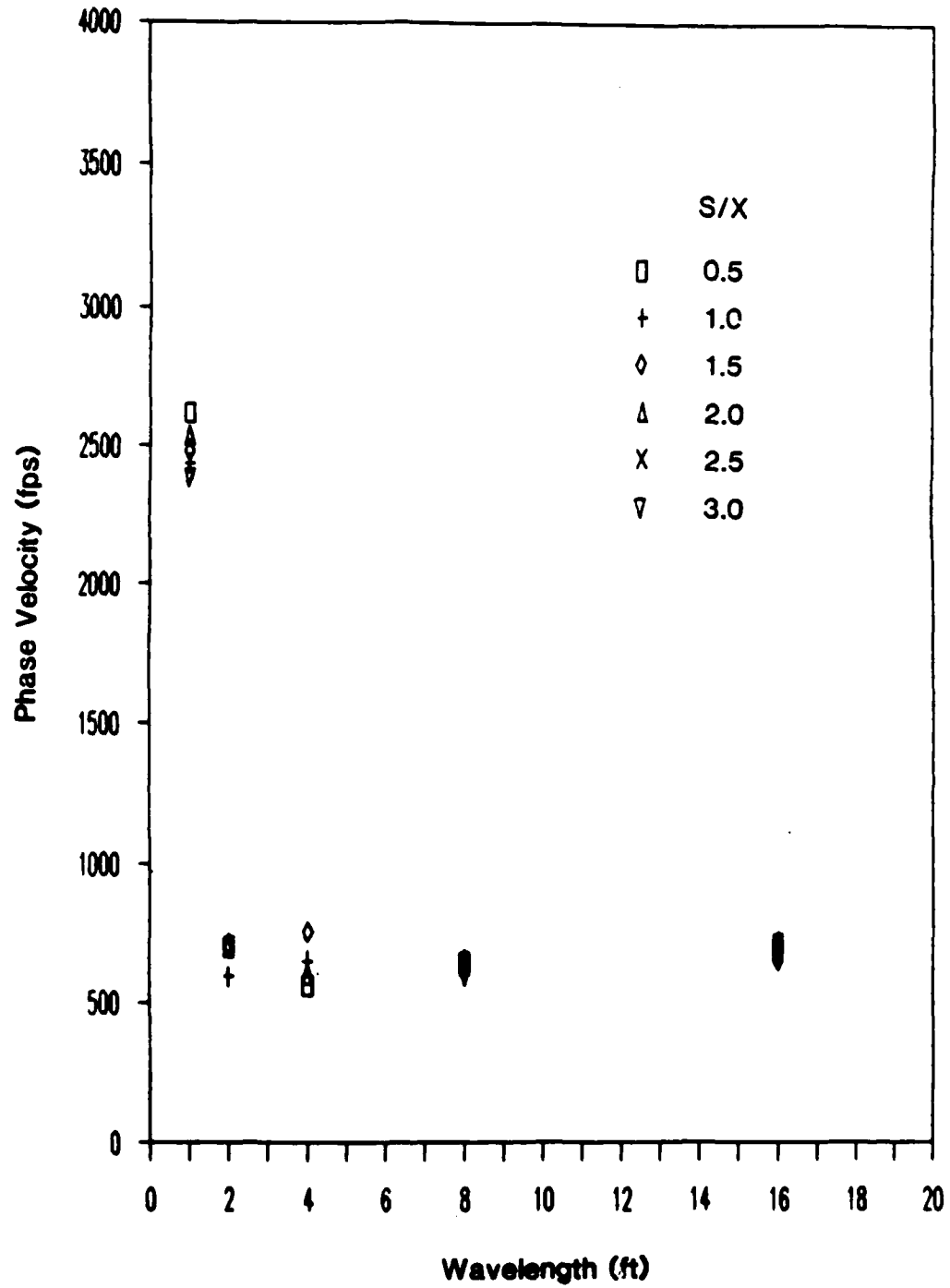


Figure 7.16 — Experimental Dispersion Curves for $X/L_R = 0.5$ for
G. G. Brown Parking Lot Site

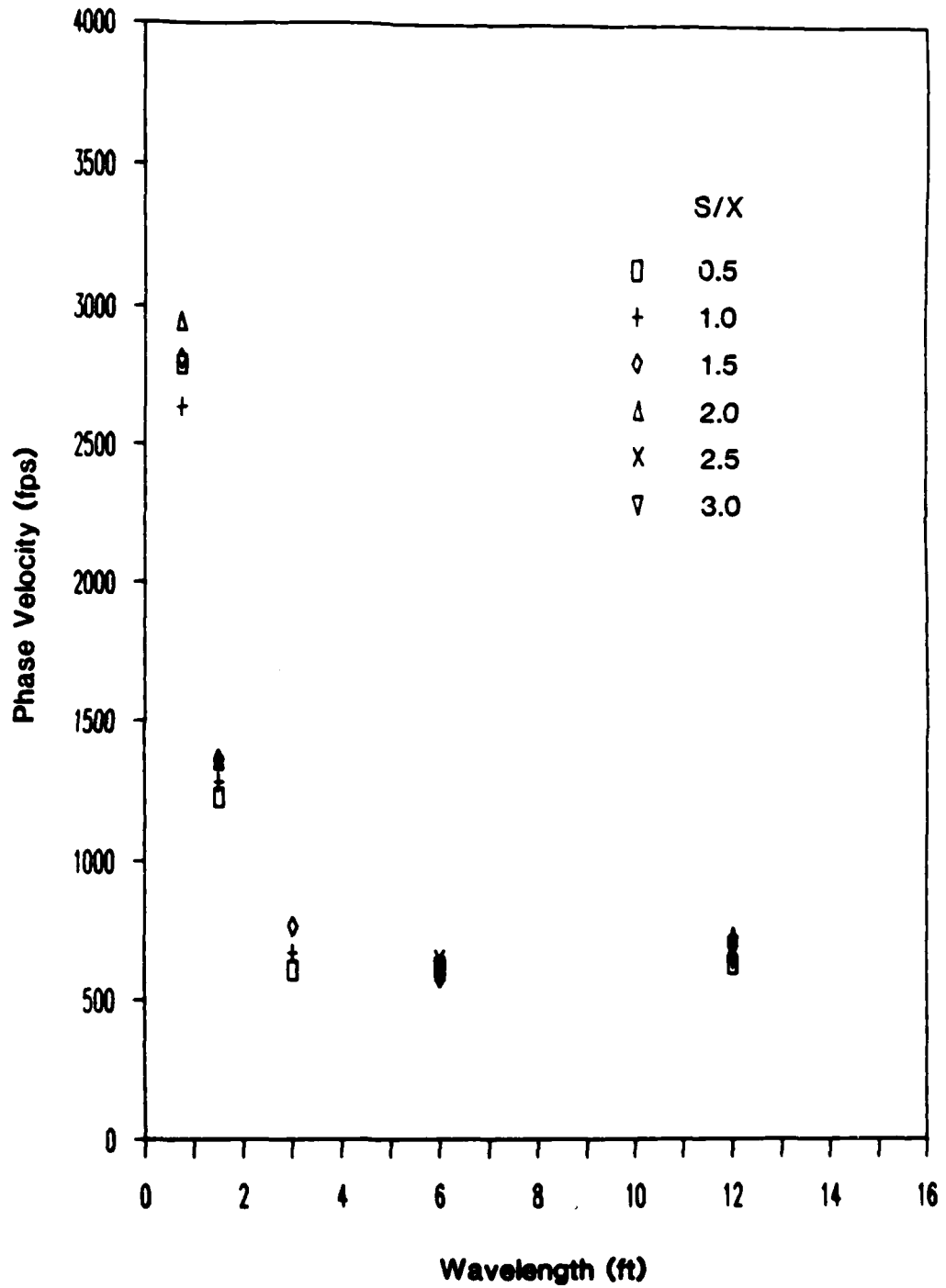


Figure 7.17 — Experimental Dispersion Curves for $X/L_R = 0.66$ for
G. G. Brown Parking Lot Site

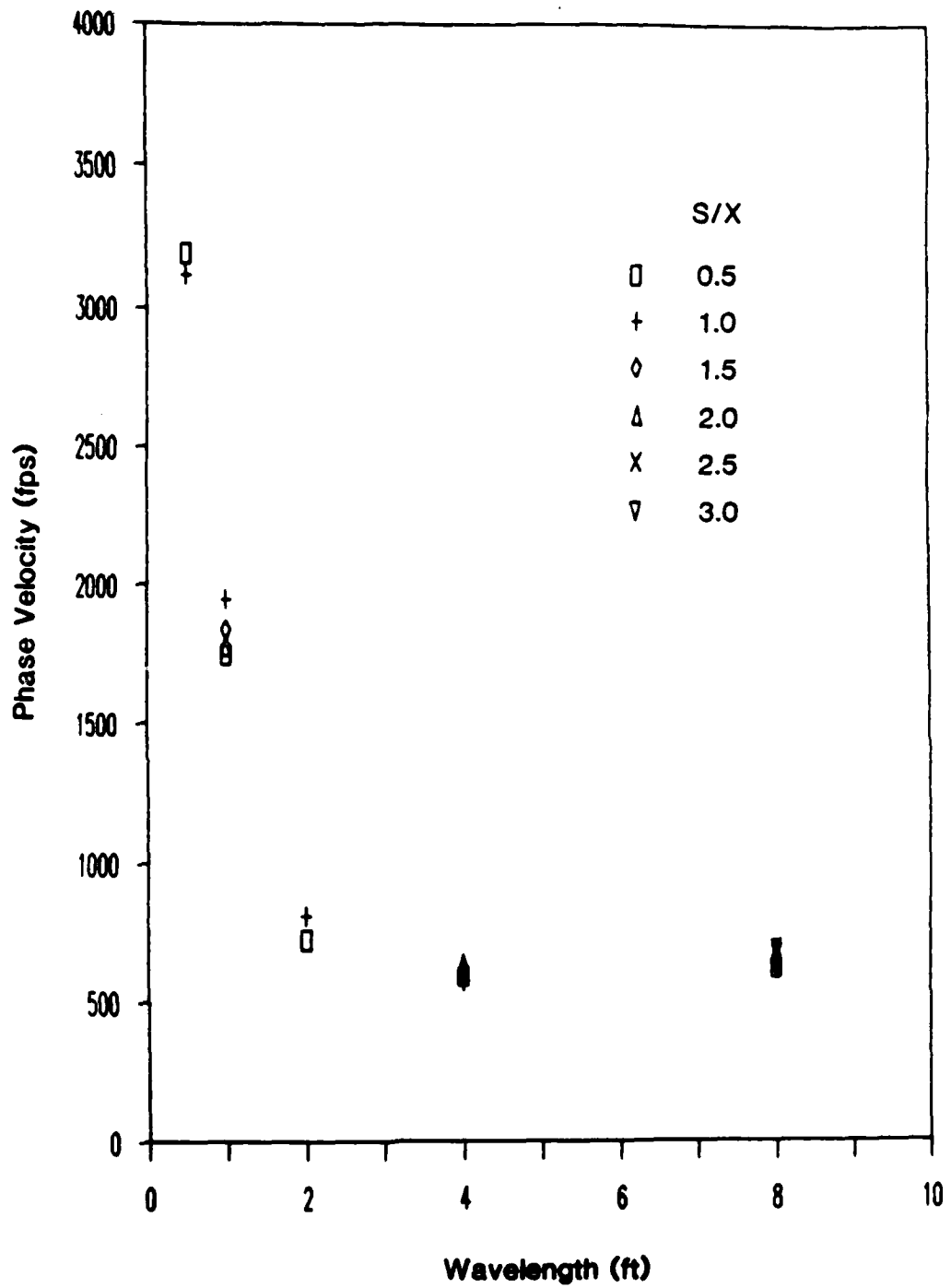


Figure 7.18 — Experimental Dispersion Curves for $X/L_R = 1.0$ for
G. G. Brown Parking Lot Site

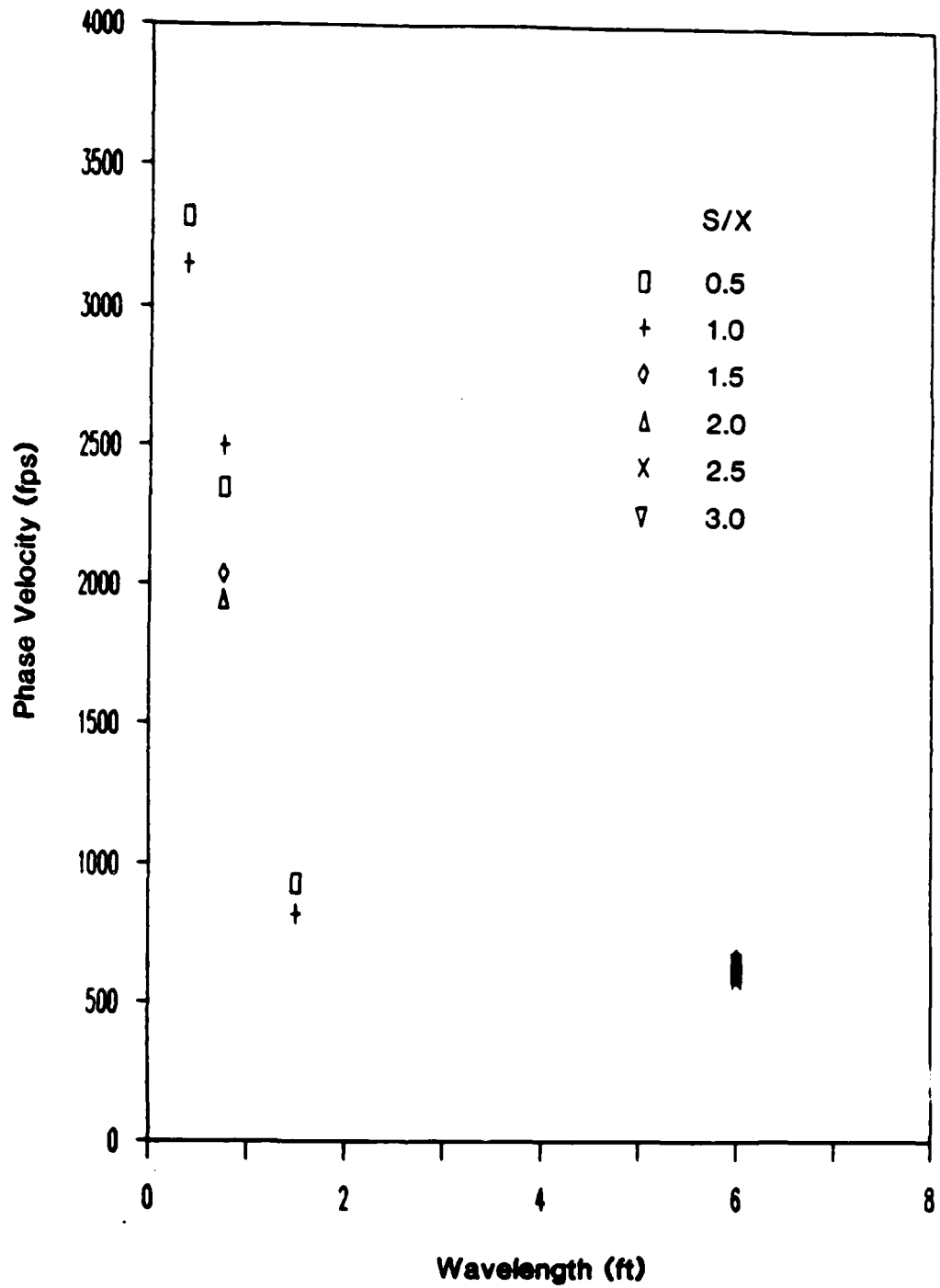


Figure 7.19 — Experimental Dispersion Curves for $X/L_R = 1.33$ for
G. G. Brown Parking Lot Site

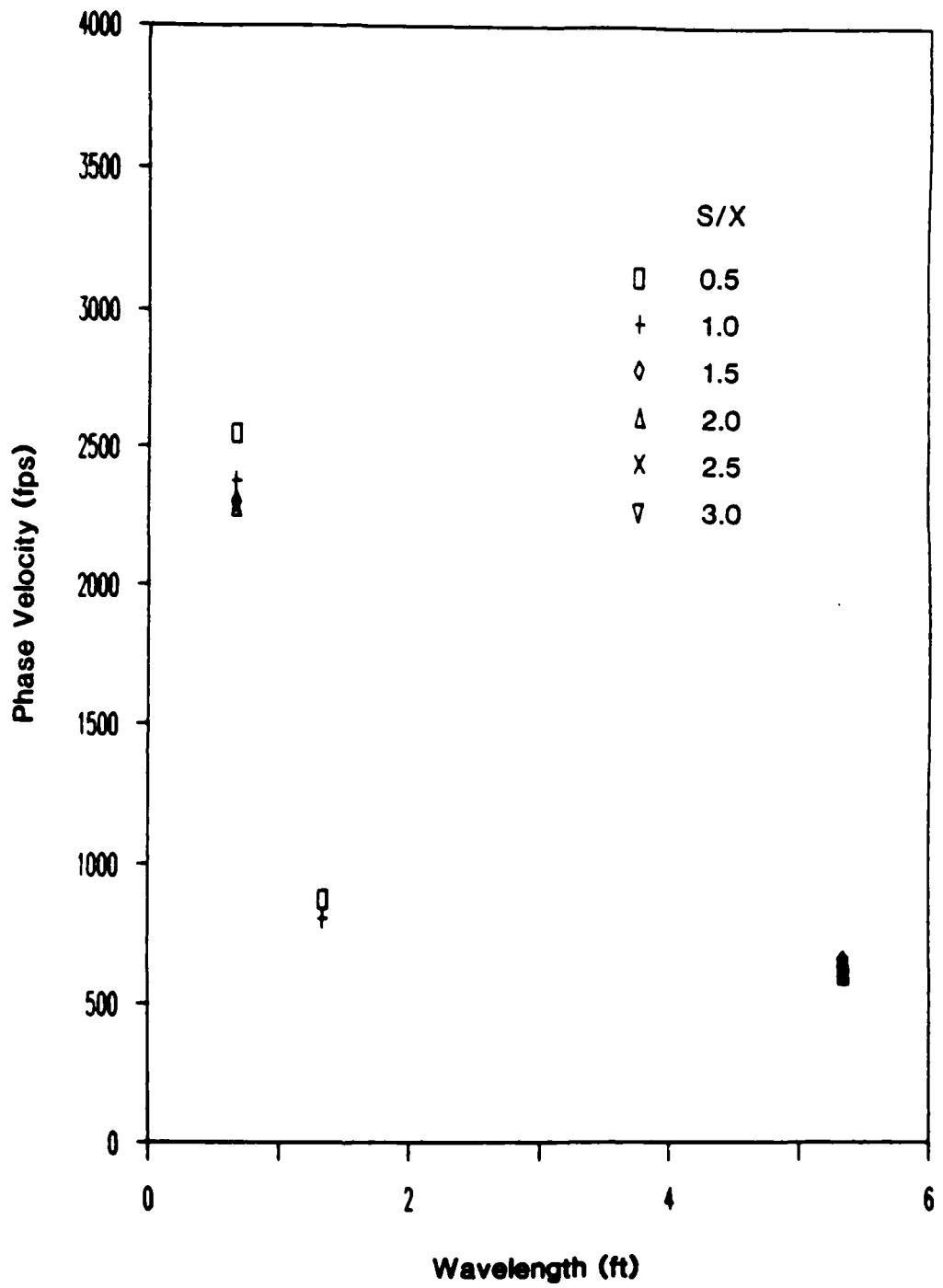


Figure 7.20 — Experimental Dispersion Curves for $X/L_R = 1.5$ for
G. G. Brown Parking Lot Site

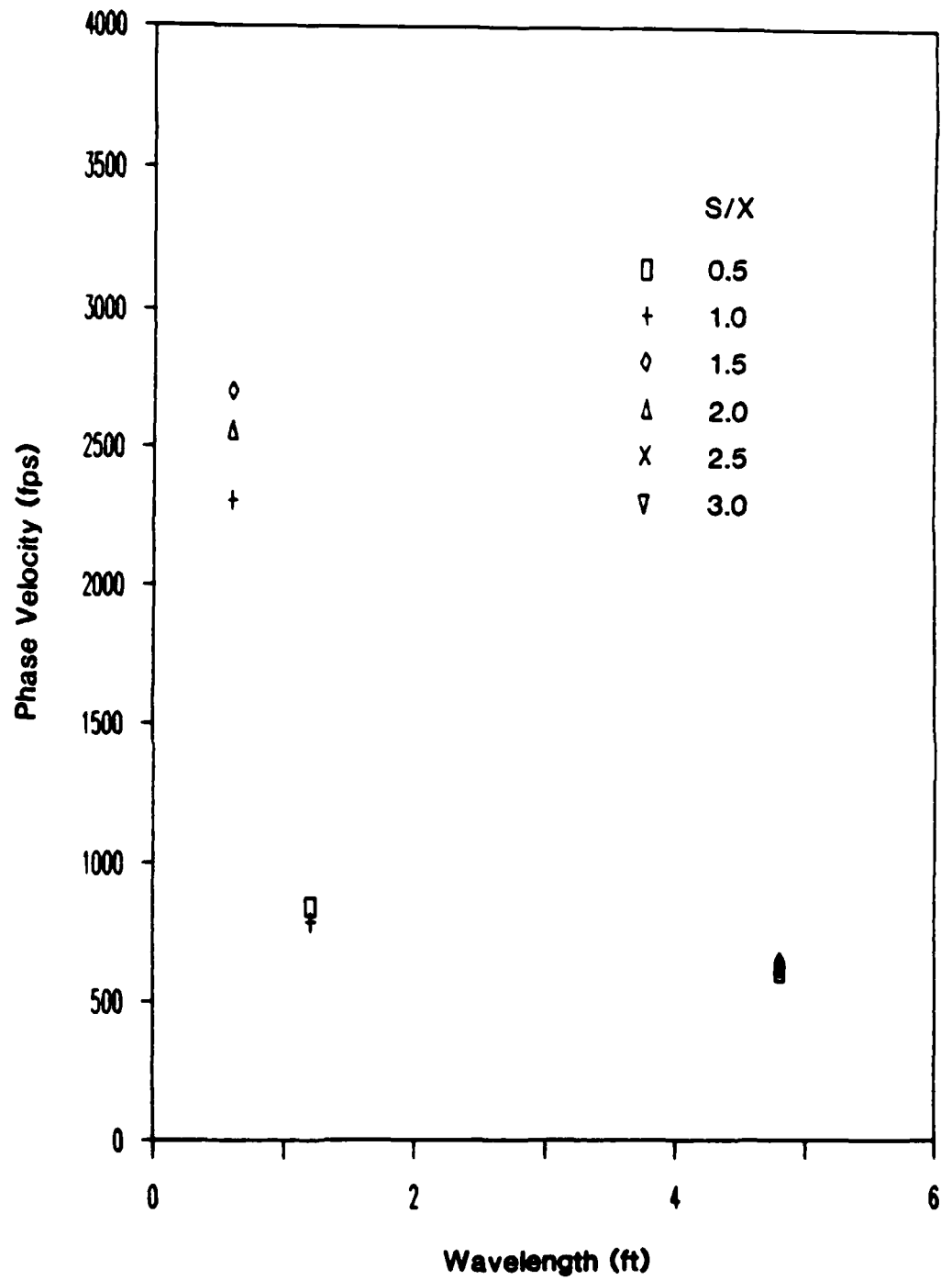


Figure 7.21 — Experimental Dispersion Curves for $X/L_R = 1.66$ for
G. G. Brown Parking Lot Site

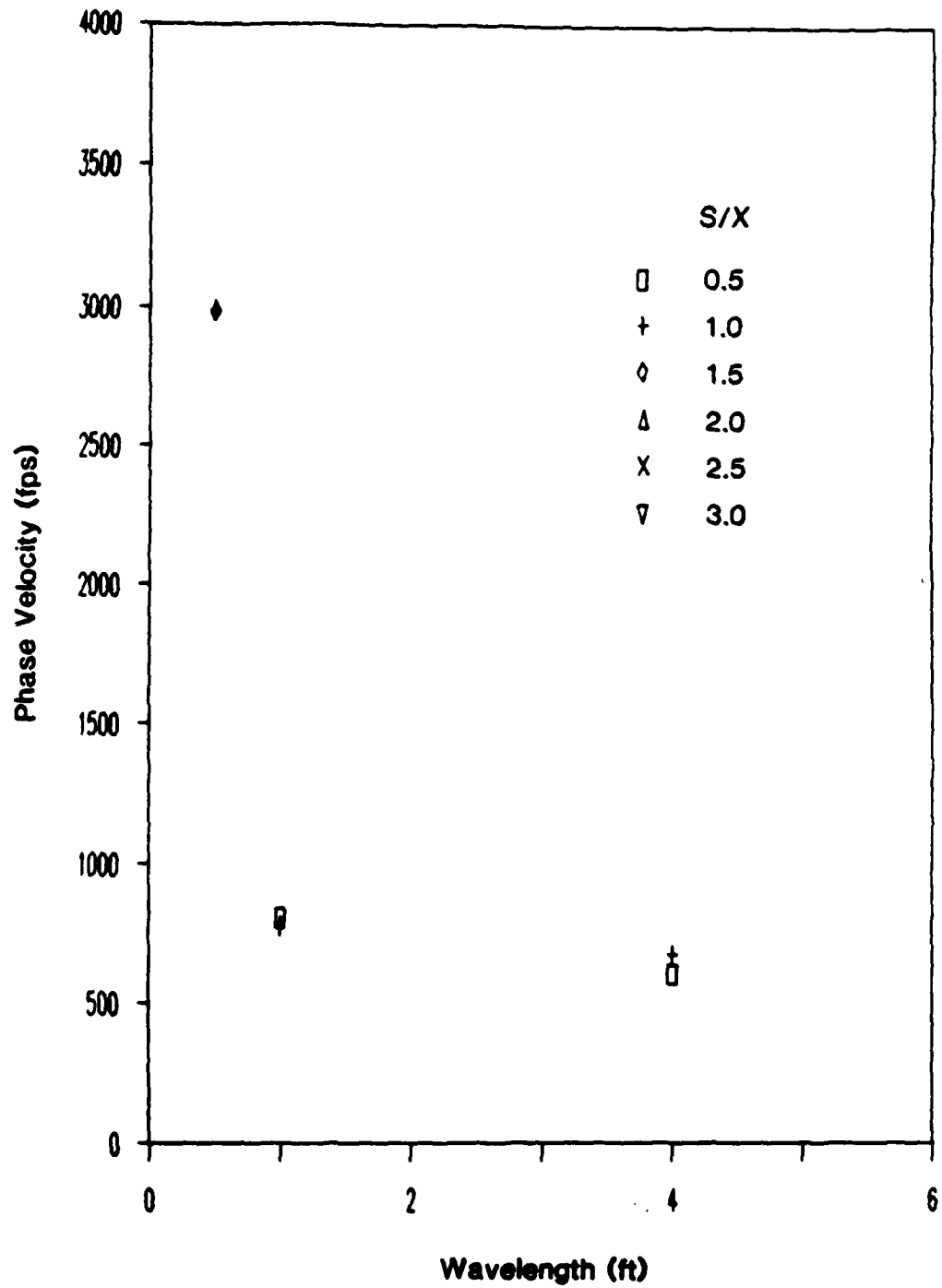


Figure 7.22 — Experimental Dispersion Curves for $X/L_R = 2.0$ for
G. G. Brown Parking Lot Site

The third observation to be made is that the measured phase velocities are practically independent of S/X for values of X/L_R of 0.5 or greater for all wavelengths. This suggests that body wave energy is insignificant if the wave has traveled at least one-half cycle between the two receivers. Thus, the assumption of plane Rayleigh waves can be made if wavelengths larger than twice the receiver spacing are eliminated from the data. Note that the present data suggests that this filtering only has to be made for wavelengths smaller than approximately 5 ft.

Combined Dispersion Curves

This section will examine the influence of the source-to-near-receiver distance on the combined experimental dispersion curves generated from the test data. These dispersion curves are the result of using the averaging program discussed in chapter four to combine the data obtained for each receiver spacing. They are also the dispersion curves that would be used in the inversion process to determine a stiffness profile. Two curves will be shown for each receiver spacing and source-to-near-receiver distance. The first will be designated as unfiltered, meaning that it contains data for all frequencies not eliminated from the field data due to poor phase and/or coherence. The second curve will be designated as filtered, meaning that the wavelength/receiver spacing filter criterion suggested in the previous section has been applied to the data. All wavelengths greater than two times the receiver spacing have been eliminated from each individual dispersion curve before processing with the averaging program. A lower bound on wavelengths for a given receiver spacing was not applied to the data. Recall that Heisey et al. (1982) recommended that wavelengths smaller than one-half the receiver spacing be eliminated because they will likely attenuate greatly and become buried in background noise. These wavelengths (frequencies) will likely result in bad phase and/or coherence data. However, this has already been taken into account when determining the ranges of poor data previously. Thus, this filtering has already been done. In addition, it is the author's belief that a single criterion based upon the receiver spacing will not adequately remove poor high-frequency data in all cases. The data must be scrutinized by the process described previously.

The combined dispersion curves for the G. G. Brown Parking Lot site are shown collec-

tively in figures 7.23-7.24. Figures D.1-D.6 in appendix D contain the individual unfiltered dispersion curves for S/X values of 0.5, 1.0, 1.5, 2.0, 2.5, and 3.0. Figures D.7-D.10 in appendix D contain the corresponding filtered dispersion curves for S/X values of 0.5, 1.0, 1.5, and 2.0. The curves for S/X values of 2.5 and 3.0 are not shown because very little data existed after filtering due to the large amount of data removed due to poor quality phase and/or coherence as discussed above. This is further verification of the conclusion reached previously that the value of S/X should be less than or equal to two for SASW testing of pavements. In addition, only wavelengths from 0 to 5 ft are shown since the data are essentially identical for wavelengths larger than 5 ft, as discussed previously.

The combined dispersion curves for the SEMTA Parking Lot site are similarly shown in figures 7.25-7.26 and figures D.11-D.20 in appendix D.

The primary observation to be made upon comparing the unfiltered with the filtered dispersion curves for both sites is that the recommended filter criterion substantially eliminates the dependence of the results on the source-to-near-receiver distance. The filtered curves are nearly the same after wavelengths larger than twice the receiver spacing are removed. This suggests, as discussed above, that body wave energy in the signals is negligible if the waves have traveled a minimum of one-half cycle between the receivers. Thus, the present data suggests that a new wavelength/receiver spacing filter should be implemented for SASW data analysis of pavement sites: remove wavelengths larger than twice the receiver spacing.

7.3 Summary

SASW tests were conducted at two asphaltic concrete pavement sites to study the influence of source-to-near-receiver distance. A series of two-transducer tests were conducted. The transducer placement followed the common receivers midpoint (CRMP) geometry in that each transducer pair was placed about the same imaginary centerline. Transducer spacings of 0.5, 1, 2, 4, and 8 ft were examined. A range of source locations was used at each receiver spacing such that the ratio of source-to-near-receiver distance (S) to receiver spacing (X), i.e., S/X , was varied over values between 0.5 and 3. The intent was to examine the influence of S/X in order to determine the optimum value and to provide guidance in developing a multiple transducer array.

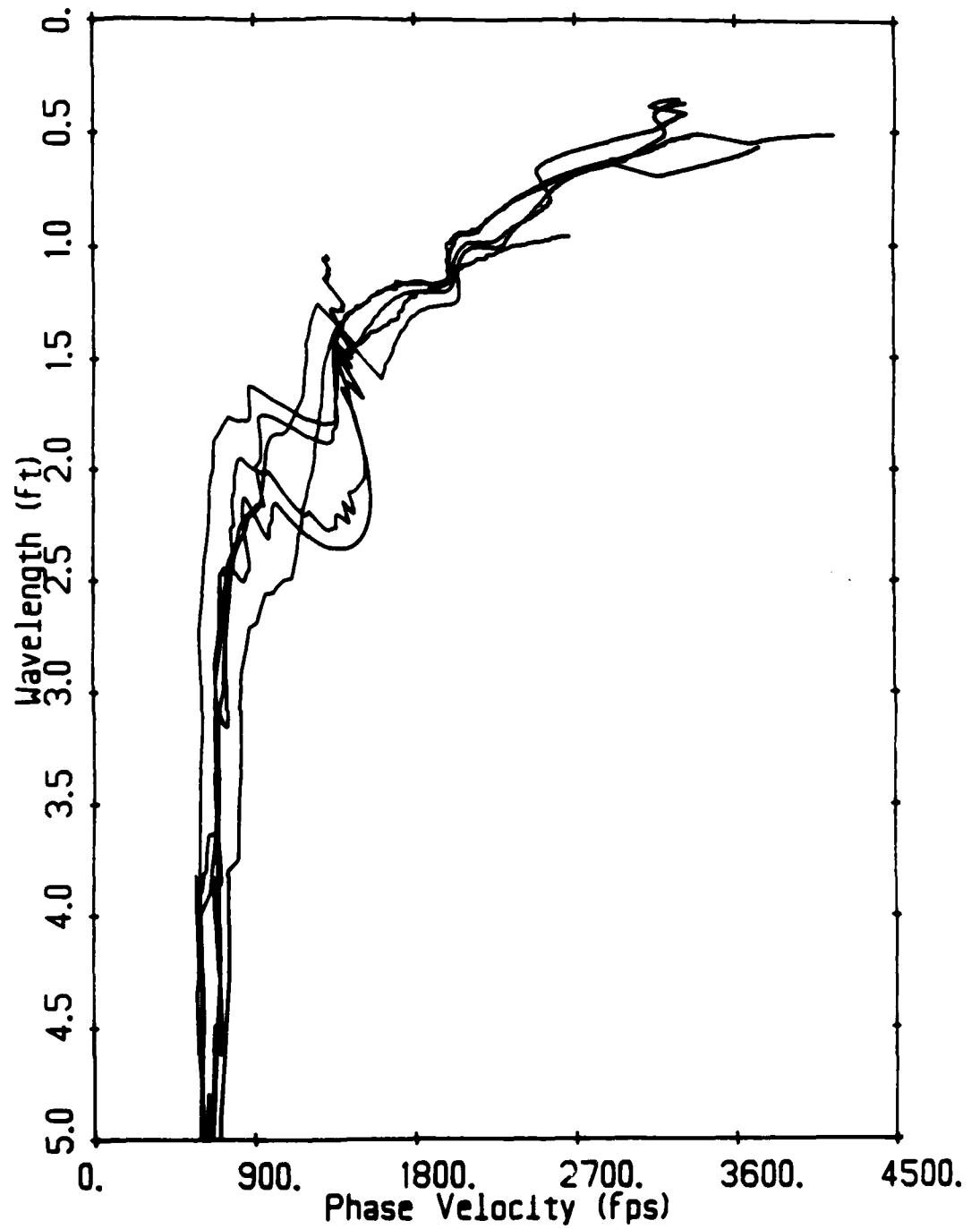


Figure 7.23 — Average Experimental Dispersion Curves (Unfiltered) for
G. G. Brown Parking Lot Site

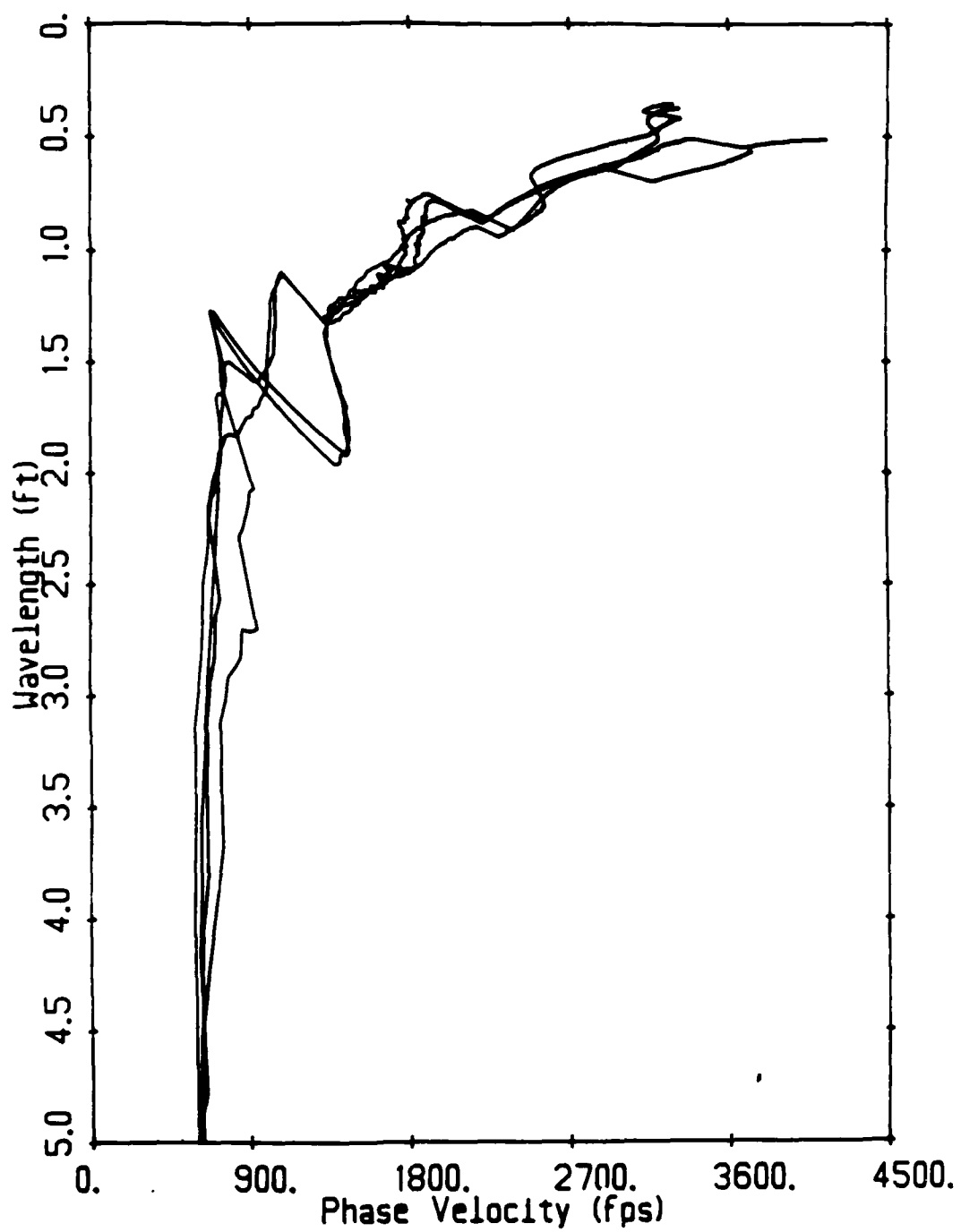


Figure 7.24 — Average Experimental Dispersion Curves (Filtered) for G. G. Brown Parking Lot Site

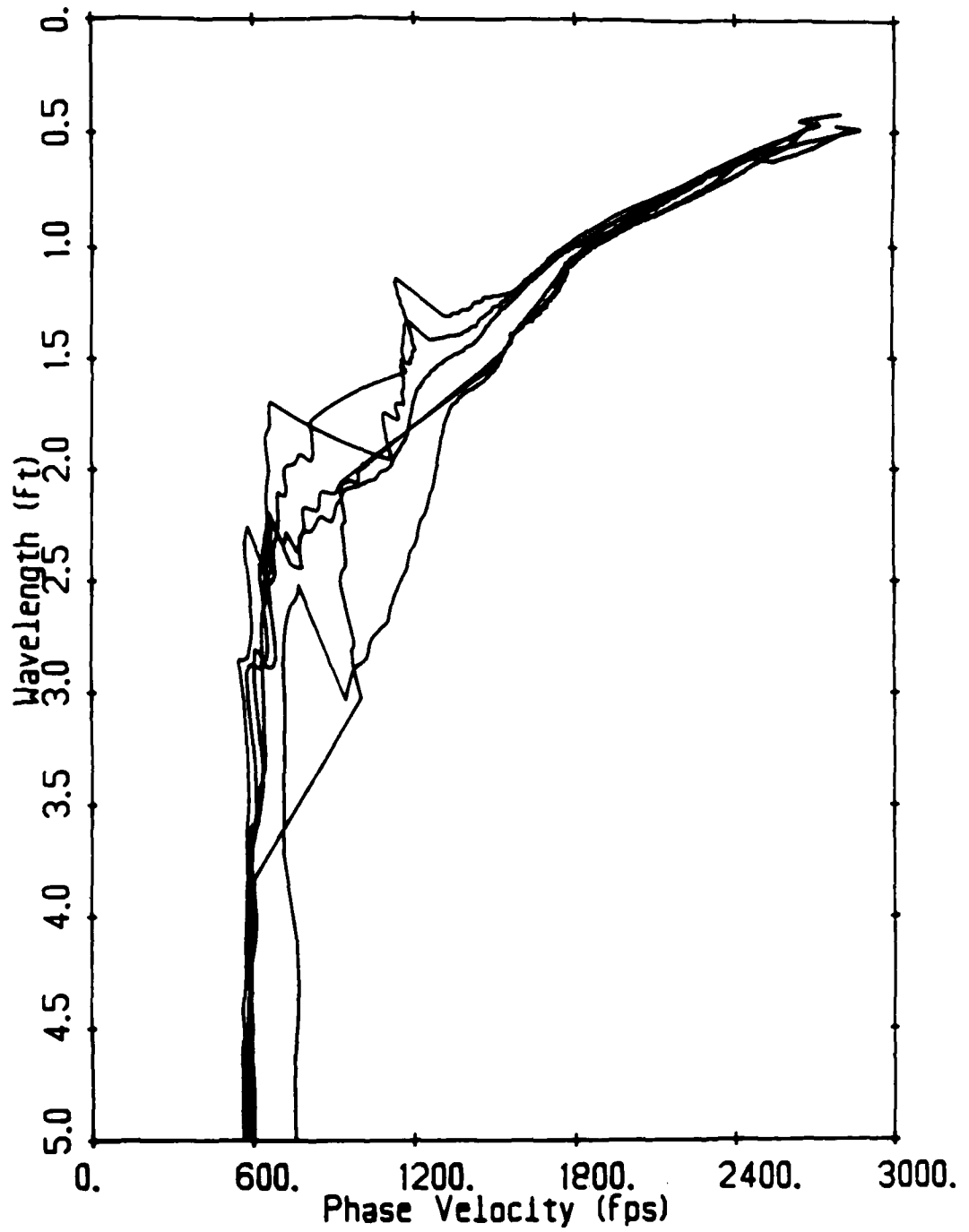


Figure 7.25 — Average Experimental Dispersion Curves (Unfiltered) for
SEMTA Parking Lot Site

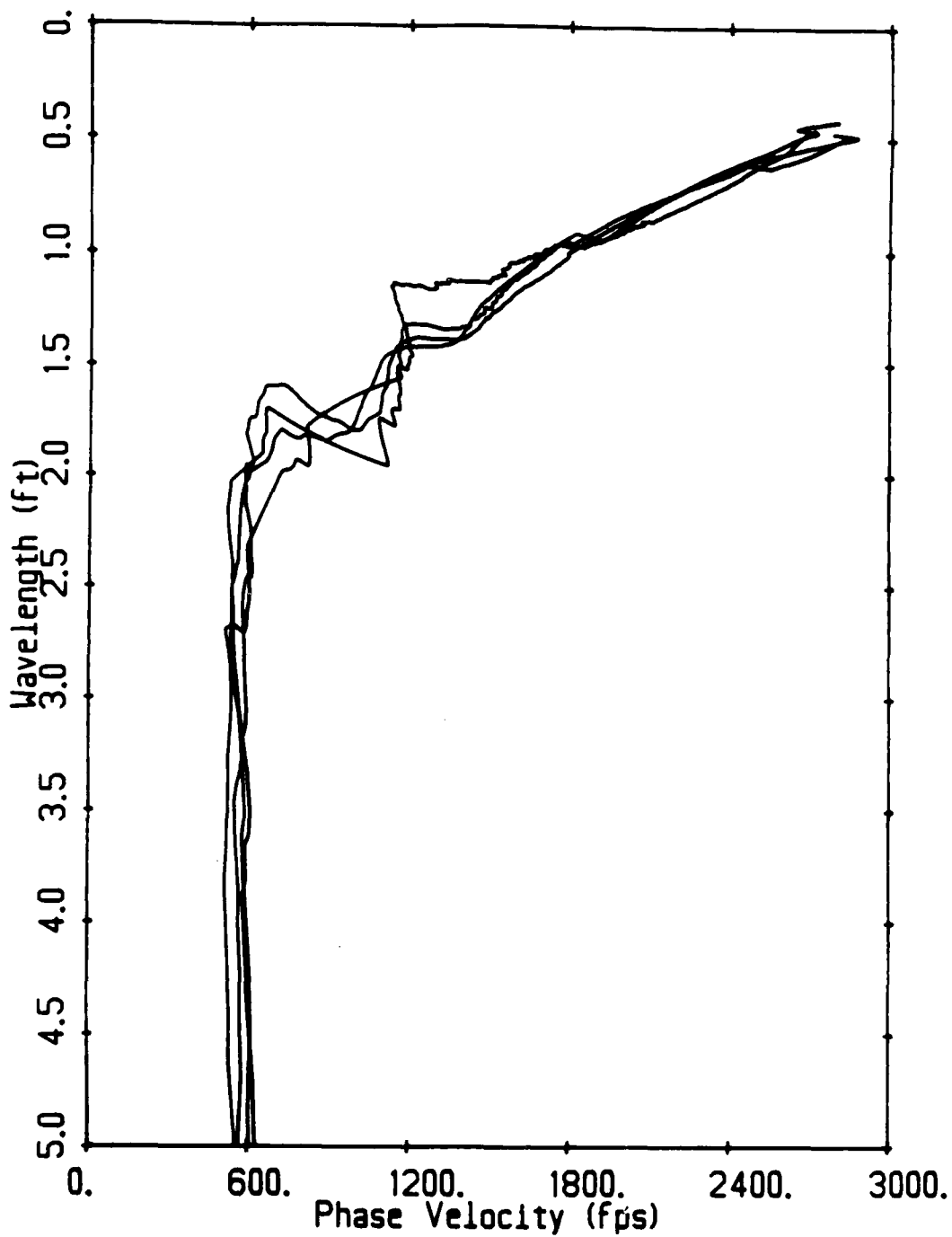


Figure 7.26 — Average Experimental Dispersion Curves (Filtered) for SEMTA Parking Lot Site

Upon comparing the ranges of useful frequencies obtained as a function of source-to-near-receiver distance, it was concluded that the value of S/X should not be larger than two. For larger values of S/X the signals measured at the receivers contain substantial proportions of background noise due to excessive attenuation of the generated impulse. The attenuation is attributed to frequency-dependent material damping by the pavement materials.

By combining the phase velocity-wavelength (dispersion) data as a function of source-to-near-receiver distance for constant values of the ratio X/L_R it was concluded that the results are independent of source-to-near-receiver distance if wavelengths larger than twice the receiver spacing are eliminated. This suggests that the influence of body wave energy is eliminated if this filtering process is carried out. The usefulness of this process was illustrated for the data from two sites. The unfiltered and filtered dispersion curves for constant values of S/X were compared and it was found that the filtering process substantially eliminated the differences noted between the unfiltered data.

The implications of the results obtained is that the common receivers midpoint (CRMP) geometry is not appropriate for a multiple transducer testing procedure with a fixed source location. It would not be possible to design such an array to meet the criterion that the value of S/X be less than or equal to two. On the other hand, an array based upon a common source (CS) geometry can easily be constructed to meet this criterion.

CHAPTER VIII

INFLUENCE OF SOURCE TYPE

8.1 Introduction

The choice of source(s) in SASW testing has been discussed in chapter five. It was indicated that more than one source is usually necessary for conducting SASW tests. A different source is sometimes required for each receiver spacing to obtain "optimum" results. For implementation of a multiple transducer testing array, however, it would be beneficial to be able to limit the number of required sources to some minimum value. The intent of the tests described in this chapter was to determine this minimum value and to ascertain the characteristics of the sources required. It should be noted that the sources under investigation were all of the impact type and conclusions made are for this type of excitation.

Tests were conducted at two sites to study the influence of source type. The first series of tests was conducted at the G. G. Brown Parking Lot site previously discussed in chapter seven. The location of the site and the material profile are found in figures 7.1 to 7.3. The second series of tests was conducted at the SEMTA Parking Lot site previously described in chapter six. The location of the site and the material profile are found in figures 6.1 to 6.3. The testing parameters and geometries as well as the test results are presented in the following section.

8.2 Test Results and Discussion

As discussed in chapter seven, the influence of source type was studied in conjunction with the tests conducted to examine the influence of source-to-near-receiver distance at the G. G. Brown Parking Lot site. A schematic of these tests is shown in figure 5.9. At each

receiver spacing and source location data was obtained using three sources. The sources ranged in size from a 4 oz ball peen hammer to an 8 lb (128 oz) sledge hammer. The influence of source-to-near-receiver distance was examined in the previous chapter using the data for the "optimum" source for each receiver spacing. The data for all sources will be examined in this chapter, but only for source-to-near-receiver distances equal to the receiver spacing, i.e., for S/X ratios of one. It was shown in the previous chapter that $S/X = 1$ is in the "optimum" range, and it is evident from examining all of the data that the influence of source type is independent of source-to-near-receiver distance. Table 8.1, then, summarizes the data to be presented from the tests at the G. G. Brown Parking Lot site.

At the SEMTA Parking Lot site, the influence of source type was studied in conjunction with the tests conducted to examine the influence of source and receiver geometry, as discussed in chapter six. During the CS geometry tests (see figure 6.5), data was collected using five sources at each receiver spacing to examine the influence of source type. The sources again ranged in size from a 4 oz ball peen hammer to an 8 lb (128 oz) sledge hammer. The influence of source and receiver geometry was studied in chapter six using data for the "optimum" source for each receiver spacing. The data for all sources will be examined in this chapter. Tables 8.2 and 8.3 summarize the data to be presented from the tests at the SEMTA Parking Lot site.

As in chapter seven the test results obtained will be presented in a number of different formats, including: tables of useful frequency ranges from cross power spectrum and coherence function pairs as a function of source type for each receiver spacing, plots of cross power spectrum magnitudes for each receiver spacing as a function of source type, and combined dispersion curves for constant source type.

Useful Frequency Ranges

The first test results to be presented are tables of useful frequency ranges from cross power spectrum and coherence function data as a function of source type. This is similar to the results presented in chapter seven, only there the results were presented as a function of source-to-near-receiver distance. The discussion in chapter seven concerning the relevancy

Table 8.1 — Test Parameters for G. G. Brown Parking Lot Site and Various Sources

Receiver Spacing (ft)	Receiver Type	Frequency Span (Hz)	Source Type	Site File No.
0.5	PCB Accel.	20000	4 oz *	14
0.5	PCB Accel.	20000	8 oz	18
0.5	PCB Accel.	20000	16 oz	22
1	PCB Accel.	10000	4 oz *	29
1	PCB Accel.	10000	8 oz	35
1	PCB Accel.	10000	16 oz	41
2	Electro-Tech Veloc.	1000	8 oz *	65
2	Electro-Tech Veloc.	1000	16 oz	71
2	Electro-Tech Veloc.	1000	128 oz	77
4	Electro-Tech Veloc.	312.5	8 oz	109
4	Electro-Tech Veloc.	312.5	16 oz	144
4	Electro-Tech Veloc.	312.5	128 oz *	101
8	Electro-Tech Veloc.	200	8 oz	166
8	Electro-Tech Veloc.	200	16 oz	160
8	Electro-Tech Veloc.	200	128 oz *	125

* "optimum" source for given receiver spacing

**Table 8.2 — Test Parameters for SEMTA Parking Lot Site, Various Sources,
and $X = 0.5, 1, 2$ ft**

Receiver Spacing (X) (ft)	Receiver Type	Frequency Span (Hz)	Source Type	Site File No.
0.5	Dytran Accel.	10000	4 oz *	835
0.5	Dytran Accel.	10000	8 oz	836
0.5	Dytran Accel.	10000	16 oz	837
0.5	Dytran Accel.	10000	40 oz	838
0.5	Dytran Accel.	10000	128 oz	839
1	Dytran Accel.	6250	4 oz *	840
1	Dytran Accel.	6250	8 oz	841
1	Dytran Accel.	6250	16 oz	842
1	Dytran Accel.	6250	40 oz	843
1	Dytran Accel.	6250	128 oz	844
2	Geosource Veloc.	1000	4 oz	845
2	Geosource Veloc.	1000	8 oz	846
2	Geosource Veloc.	1000	16 oz *	847
2	Geosource Veloc.	1000	40 oz	848
2	Geosource Veloc.	1000	128 oz	849

* "optimum" source for given receiver spacing

Table 8.3 — Test Parameters for SEMTA Parking Lot Site, Various Sources,
and $X = 4, 8 \text{ ft}$

Receiver Spacing (X) (ft)	Receiver Type	Frequency Span (Hz)	Source Type	Site File No.
4	Geosource Veloc.	800	4 oz	850
4	Geosource Veloc.	800	8 oz	851
4	Geosource Veloc.	800	16 oz	852
4	Geosource Veloc.	800	40 oz *	853
4	Geosource Veloc.	800	128 oz	854
8	Geosource Veloc.	250	4 oz	855
8	Geosource Veloc.	250	8 oz	856
8	Geosource Veloc.	250	16 oz	857
8	Geosource Veloc.	250	40 oz	858
8	Geosource Veloc.	250	128 oz *	859

* "optimum" source for given receiver spacing

of these data are equally valid here. The influence of the source type on the range of useful frequencies ultimately determines how well the dispersion curve is defined. As before, plots of cross power spectrum and coherence function pairs will be presented for one receiver spacing to demonstrate how the tables were generated.

The ranges of useful frequencies for the 0.5-ft receiver spacing at the SEMTA Parking Lot site are shown in table 8.4. Tables E.1-E.5 in appendix E contain the data for the G. G. Brown Parking Lot site. The remaining data for the SEMTA Parking Lot site is found in tables E.6-E.9 in appendix E. The cross power spectrum and coherence function pairs for the 0.5-ft receiver spacing at the SEMTA Parking Lot site are presented in figures 8.1-8.5. The figures are for source types ranging in size from a 4 oz ball peen hammer to an 8 lb (128 oz) sledge hammer. The cross-hatched regions on these figures illustrate the frequency ranges eliminated from the data and the cutoff frequencies shown are those found in table 8.4.

It is obvious from observing the tables of useful frequency ranges that the size of the source has a dramatic influence on the results obtained. In general, both the upper and lower cutoff frequency decrease as the size of the source is increased. This effect has been noted previously and is thus not surprising. The following sections will discuss the reasons for the decrease in cutoff frequencies and the resulting influence on the dispersion curve.

Cross Power Spectrum Magnitudes

As was the case in chapter seven, the magnitude of the cross power spectrum is a useful tool for explaining the influence of source type on the useful frequency ranges presented in the previous section. The magnitude of the cross power spectrum will be presented for each test. The spectrums for the 0.5-ft receiver spacing at the SEMTA Parking Lot site are shown in figures 8.6-8.7. The spectrums for the G. G. Brown Parking Lot site are found in figures F.1-F.10 in appendix F. The remaining spectrums for the SEMTA Parking Lot site are found in figures F.11-F.18 in appendix F. Each plot contains the spectrums for each source type studied at a given receiver spacing. Further, each spectrum is presented in two formats, as in chapter seven. First, the actual or absolute magnitudes as recorded in the field are shown. The second plot presents normalized or relative magnitudes. Again, the

**Table 8.4 — Useful Frequency Ranges for 0.5-ft Receiver Spacing for SEMTA
Parking Lot Site**

Source Type	Lower Cutoff Frequency (Hz)	Upper Cutoff Frequency (Hz)
4 oz	100	6375
8 oz	100	6012
16 oz	87	5950
40 oz	75	5300
128 oz	62	5250

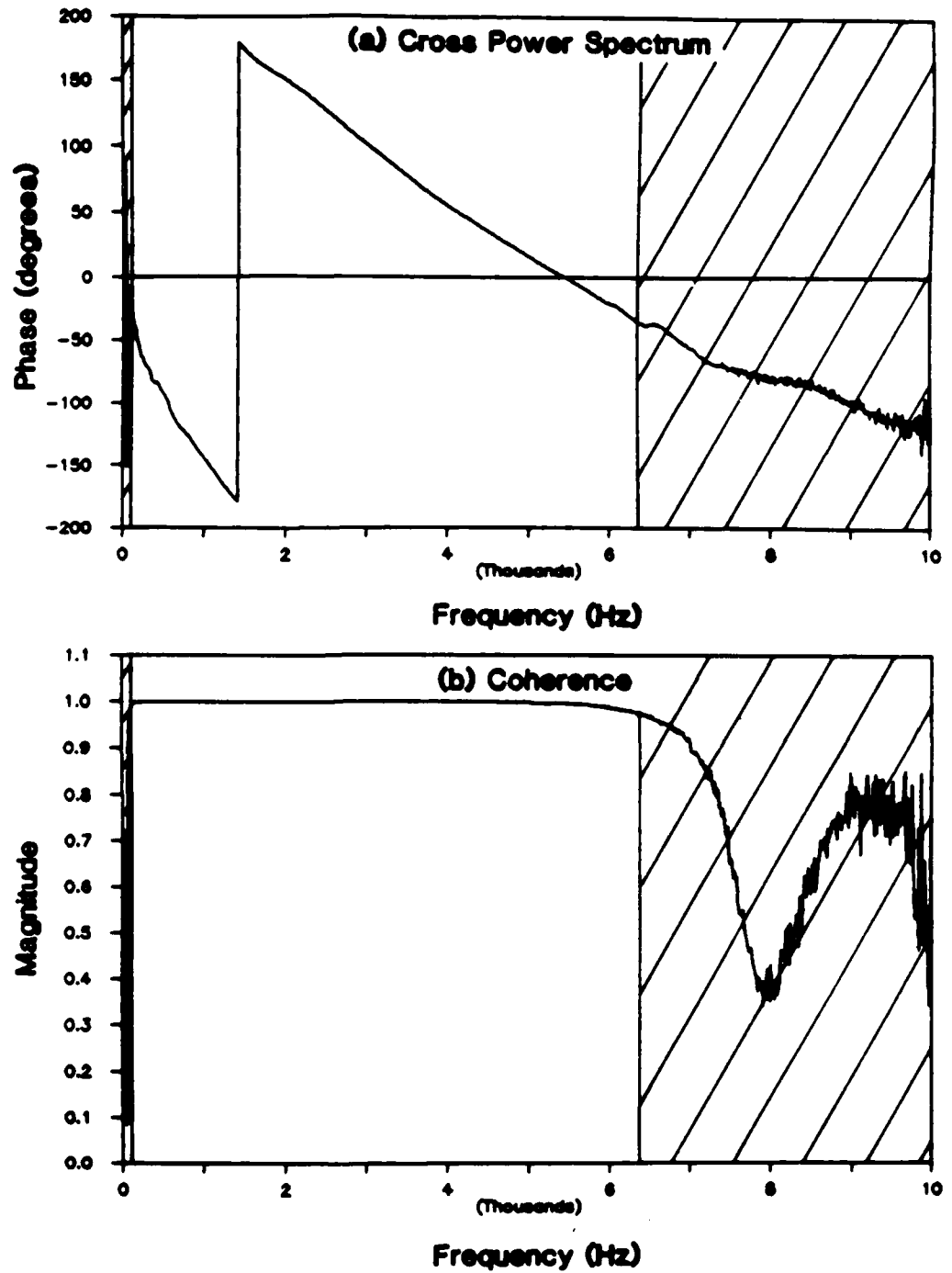


Figure 8.1 — Cross Power Spectrum and Coherence Function for $X = 0.5$ ft and 4 os Hammer for SEMTA Parking Lot Site

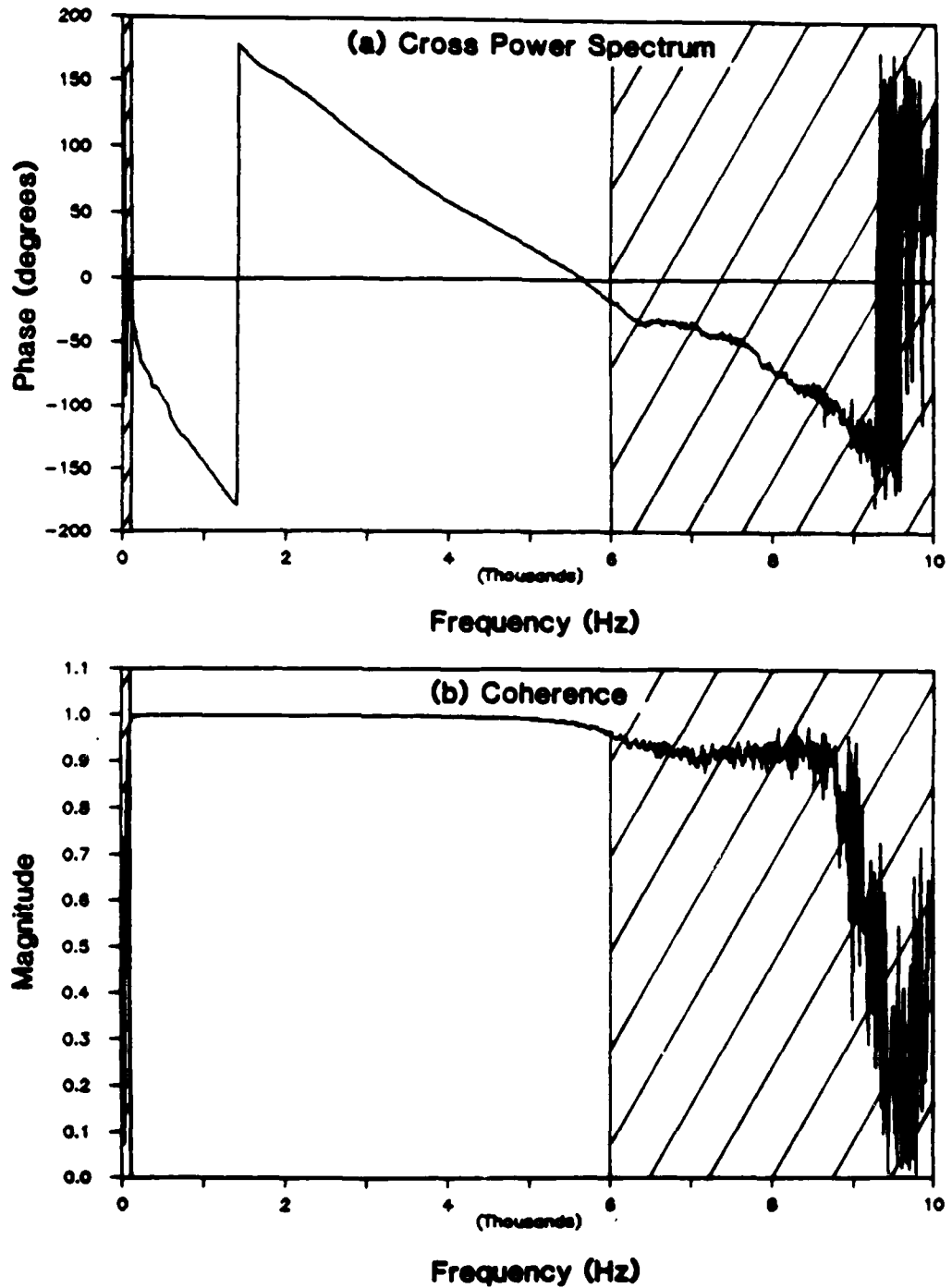


Figure 8.2 — Cross Power Spectrum and Coherence Function for $X = 0.5$ ft and 8 oz Hammer for SEMTA Parking Lot Site

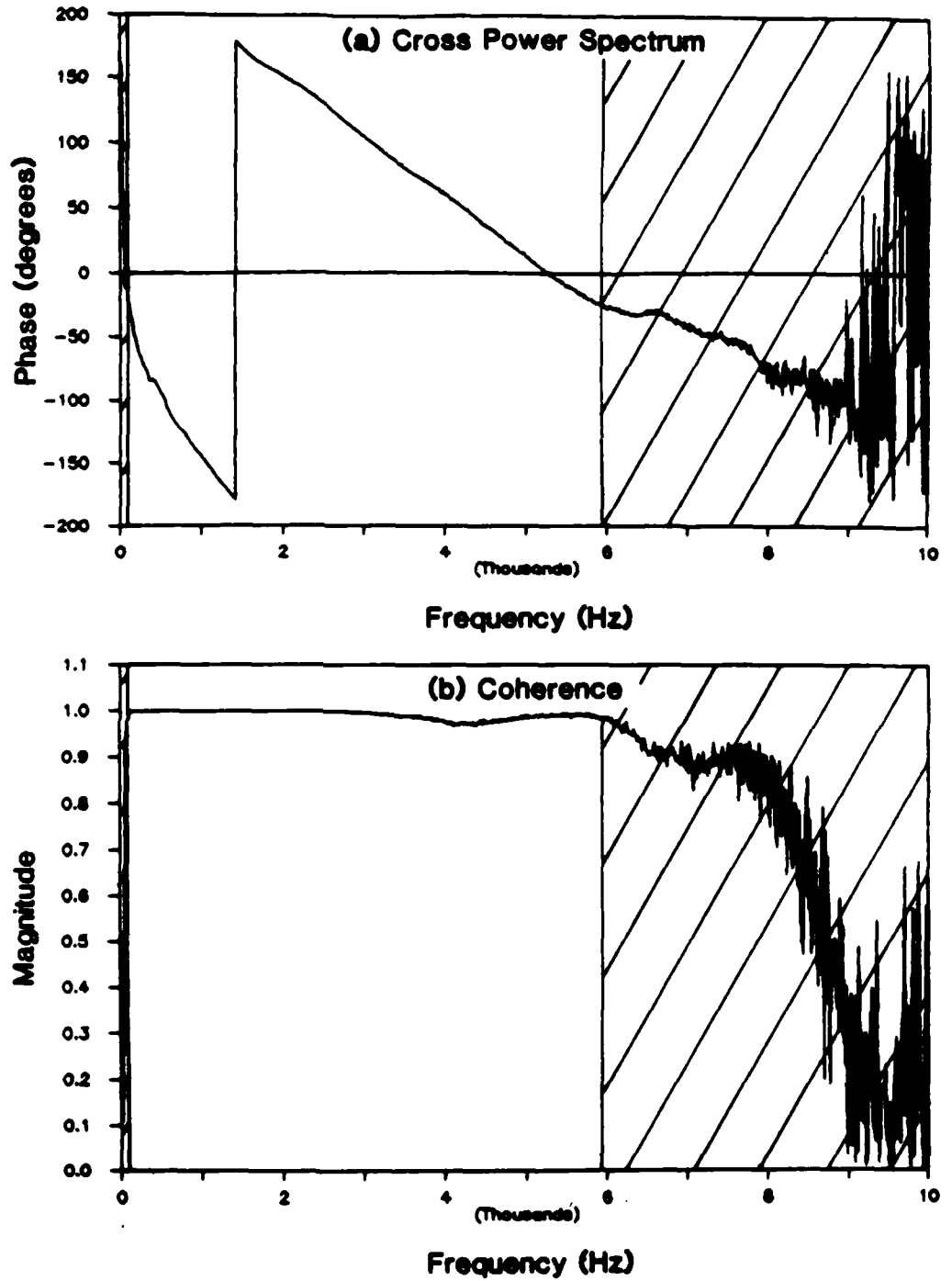


Figure 8.3 — Cross Power Spectrum and Coherence Function for $X = 0.5$ ft and 16 oz Hammer for SEMTA Parking Lot Site

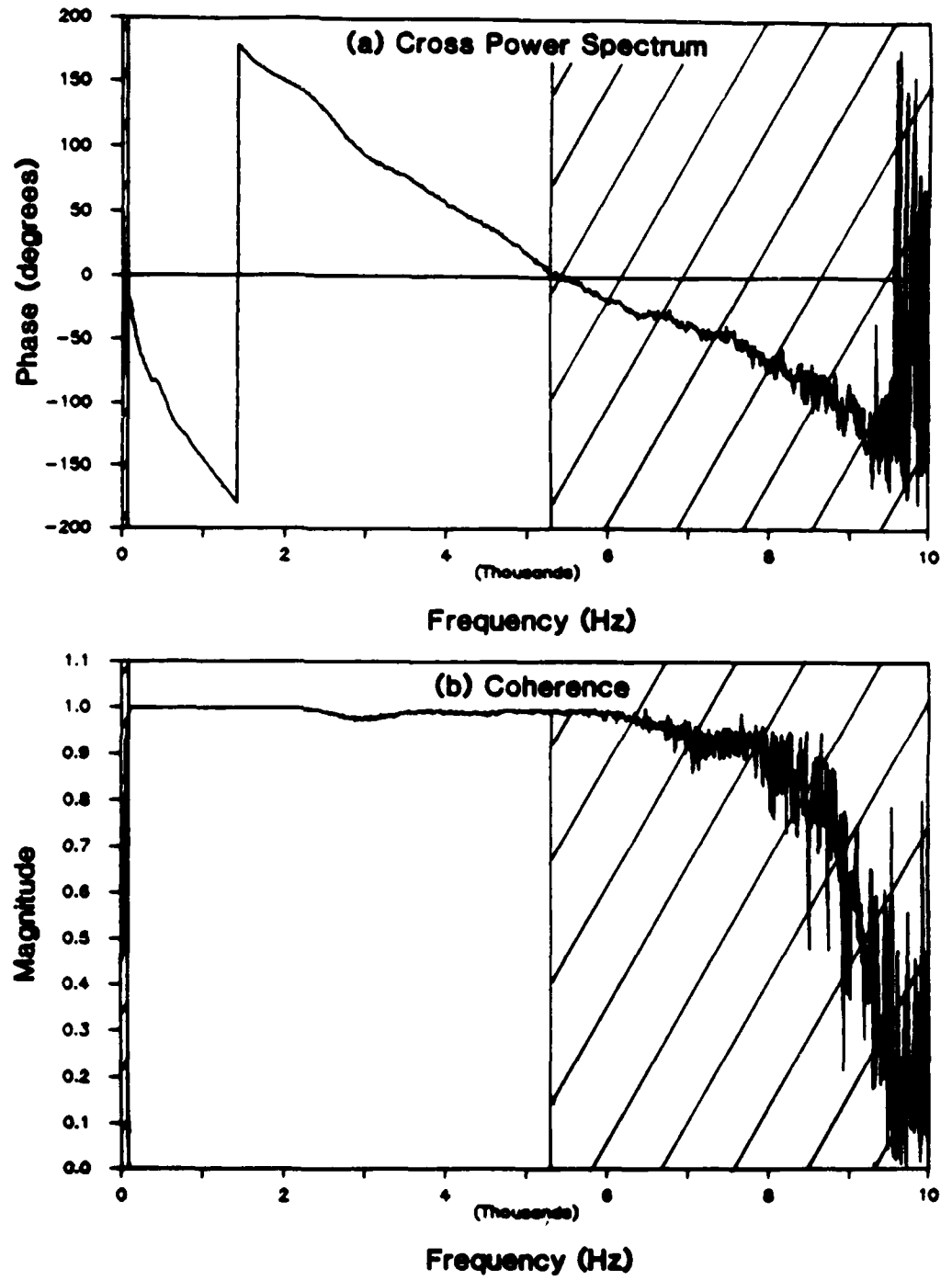


Figure 8.4 — Cross Power Spectrum and Coherence Function for $X = 0.5$ ft and 40 oz Hammer for SEMTA Parking Lot Site

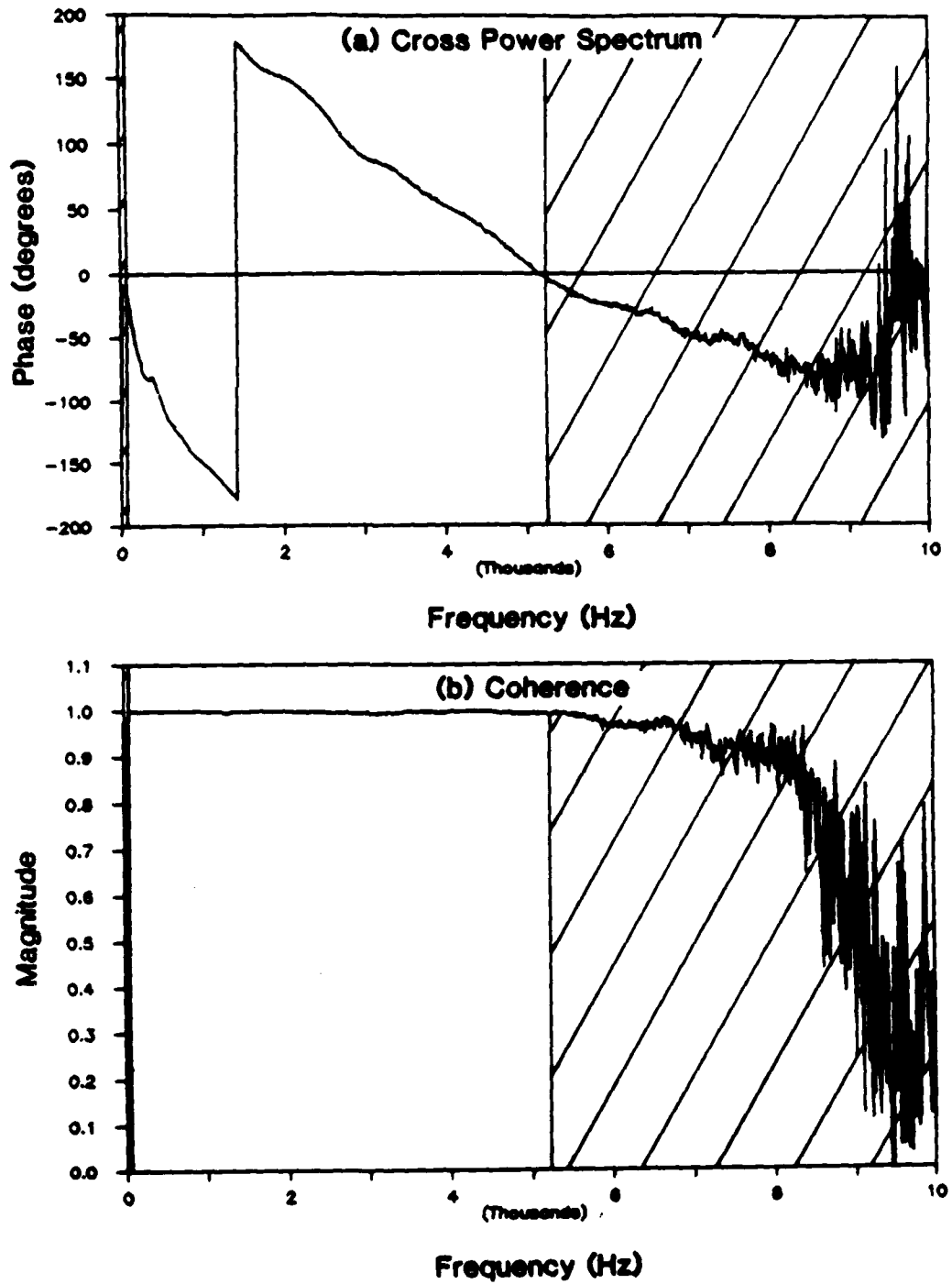


Figure 8.5 — Cross Power Spectrum and Coherence Function for $X = 0.5$ ft and 128 oz Hammer for SEMTA Parking Lot Site

relative magnitude is defined as the absolute magnitude normalized by the peak magnitude for each spectrum. The intent of the absolute magnitude plot is to illustrate how the actual energy levels change with source type. The relative magnitude plot illustrates how the energy distribution with frequency (or shape) changes as the source type is varied.

Upon observing the cross power spectrum magnitude plots one is reminded of similar plots from chapter seven. The influence of source type on the magnitude of the cross power spectrum is similar to that of the source-to-near-receiver distance. However, the underlying reasons for the observed trends are different in each case. Material damping explained the influence of the source-to-near-receiver distance. The mechanics of the source impulse are behind the influence of source type.

The time signal of the force created by each hammer is an impulse, i.e., the duration of the force is very small in comparison to the total record length. The energy distribution of an impulse signal in the frequency domain is inversely proportional to the time duration of the impulse. A short duration impulse dilutes the energy over a wide frequency band, while a longer duration impulse concentrates the energy at low frequencies. The impulse duration for a specific source is determined by the elasticity of the materials of the structure and source which are in contact during impact and on the mass of the source. In our case the "structure" (pavement) is the same for all sources. In addition, all of the sources used were steel hammers. Thus, the remaining factor is the mass of the source. The duration of the impulse is directly proportional to the mass of the source. Thus, lightweight hammers produce a short impulse and distribute the energy over a wide frequency band, while heavier hammers produce a longer impulse and concentrate the energy at low frequencies. This is exactly the behavior observed in the plots of the cross power spectrum magnitudes. In the low frequency range of the absolute magnitude plots the energy levels are largest for the heavier hammers. The relative magnitude plots, however, reveal that the light hammers distribute the energy over a much wider frequency band.

The upper and lower cutoff frequencies are the result of poor phase and/or coherence data. The poor data occurs in areas where the signals contain a large proportion of background noise. Thus, the lower cutoff frequency decreases with increasing hammer size because the heavier hammers concentrate more energy at low frequencies. Similarly, the

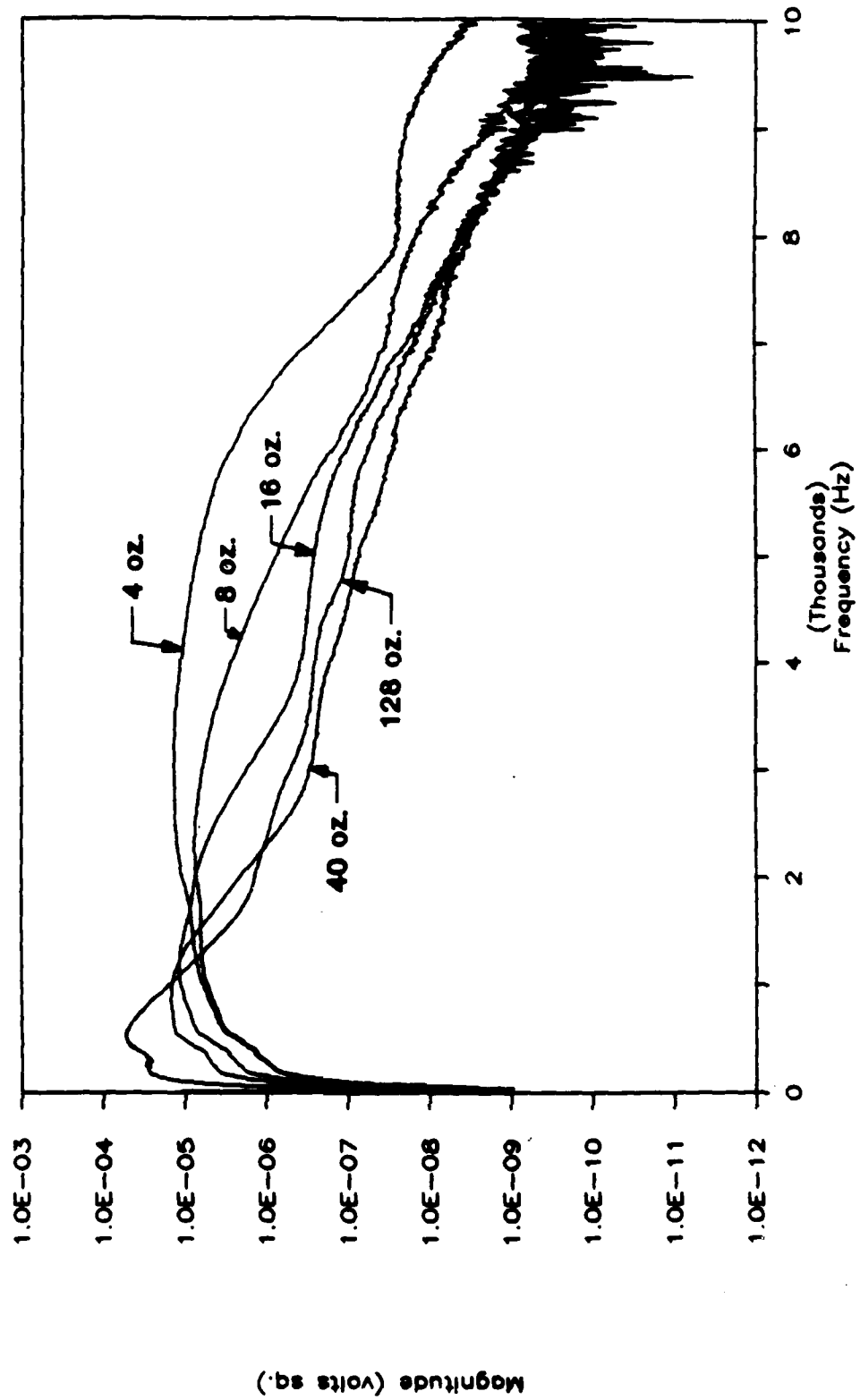


Figure 8.6 - Magnitude (Absolute) of Cross Power Spectrum for X = 0.5 ft for SEMTA Parking Lot Site

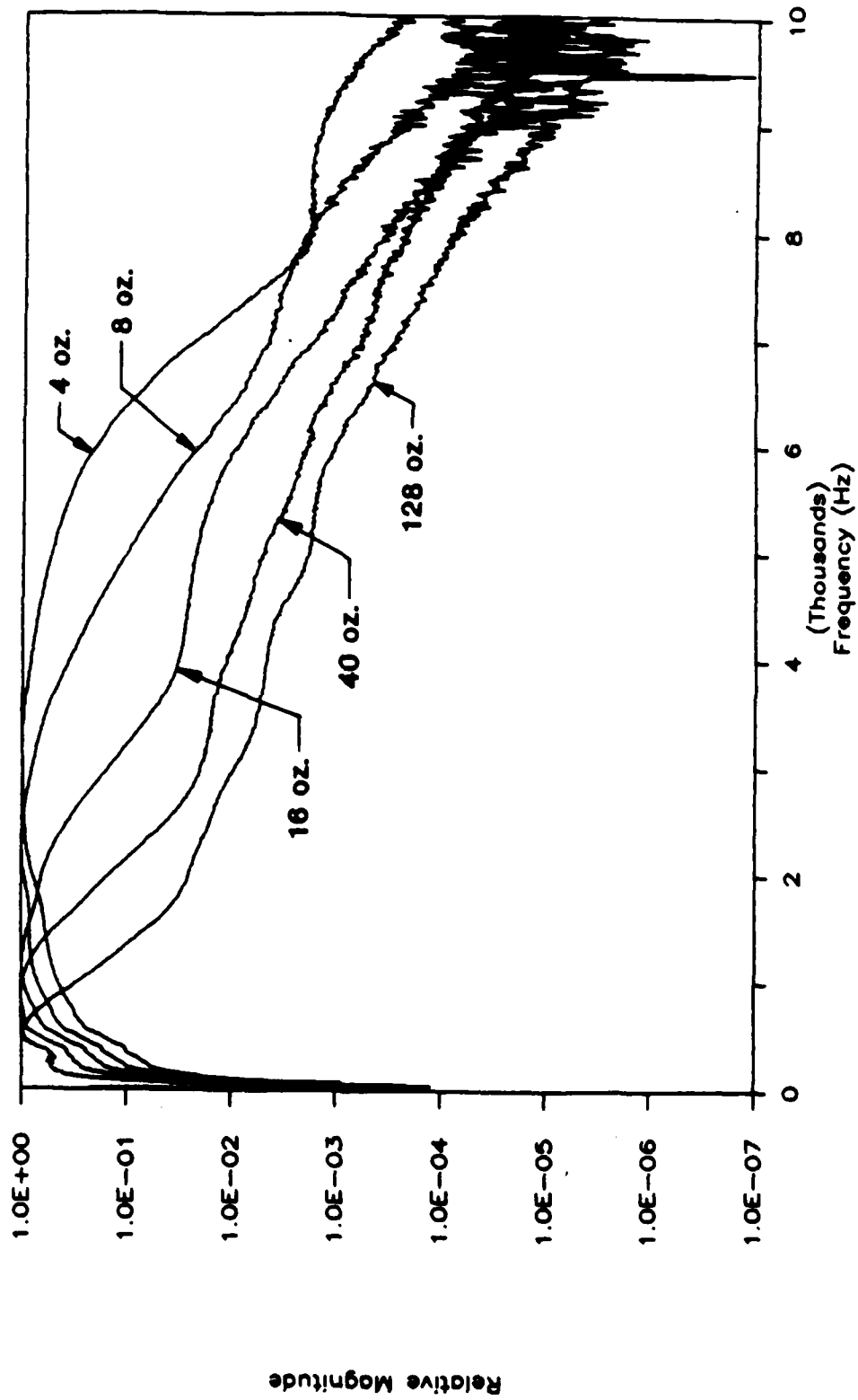


Figure 8.7 - Magnitude (Relative) of Cross Power Spectrum for $X = 0.5$ ft for SEMTA Parking Lot Site

upper cutoff frequency increases with decreasing hammer size because the lighter hammers distribute the energy over a wider frequency band.

Filtered Dispersion Curves

This section will examine the influence of source type on the combined experimental dispersion curves generated from the test data. These dispersion curves are the result of using the averaging program discussed in chapter four to combine the data obtained for each receiver spacing. All of the dispersion data used to generate the combined curves was filtered using the wavelength/receiver spacing filter criterion recommended in chapter seven, i.e., all wavelengths larger than twice the receiver spacing were eliminated. Two dispersion curves are presented on each plot to illustrate the influence of source type. First, for all of the plots for a given test site (G. G. Brown or SEMTA) the combined dispersion curve obtained using the "optimum" hammers (identified with an asterisk in tables 8.1, 8.2, and 8.3) is shown. The "optimum" hammer for a given receiver spacing is the hammer providing data over the largest frequency range. The dispersion curve thus determined should be the "best" curve for the given site and provides a means to illustrate the influence of source type. The second curve displayed on each plot is the combined dispersion curve for a constant source type, i.e., the result of combining the data obtained from all receiver spacings using the same source. Remember our stated goal: to determine the minimum number of sources required to adequately define the dispersion curve for a given site. By comparing the two curves as described above, one is able to ascertain which source(s) are able to duplicate the "optimum" results.

The combined dispersion curves for the G. G. Brown Parking Lot site are found in figures 8.8-8.9 and in figures G.1-G.4 in appendix G. Two plots are presented for each source type. The first plot compares the data from the "optimum" curve with the data from the constant source for all wavelengths. The second plot makes the same comparison for wavelengths from 0 to 5 ft. Figures G.1-G.2 in appendix G compare the "optimum" results with the results from the 8 oz ball peen hammer. Figures G.3-G.4 are for the 16 oz ball peen hammer. Figures 8.8-8.9 compare the "optimum" results with the data from the 4 oz and 128 oz (8 lb) hammers combined. The 4 oz and 128 oz hammers are not

individually compared with the "optimum" results because data was not collected at all receiver spacings with either hammer (see table 8.1).

The combined dispersion curves for the SEMTA Parking Lot site are found in figures 8.10-8.11 and in figures G.5-G.14 in appendix G. As with the G. G. Brown Parking Lot site discussed above, two plots are presented for each constant source type, the first showing all wavelengths collected, the second showing wavelengths from 0 to 5 ft. Five sources were used at the SEMTA Parking Lot site and data was collected with each source at all receiver spacings (see tables 8.2 and 8.3). Thus, a more extensive comparison of the constant source type results with the "optimum" results can be made. Figures G.5-G.14 in appendix G compare the "optimum" results with the results from the 4, 8, 16, 40, and 128 oz hammers, respectively. Figures 8.10-8.11 compare the "optimum" results with the data from the 4 oz and 128 oz hammers combined.

The plots in appendix G compare the "optimum" results with the dispersion data generated from one source type. It can be observed from these plots that no single source can consistently duplicate the "optimum" results over all wavelengths. The light hammers cannot generate low enough frequencies, while the heavy hammers cannot generate high enough frequencies. This probably comes as no surprise after the discussion in the previous sections. What is encouraging, however, is that the results are independent of source type. In the wavelength ranges where data exists from the constant source type, the phase velocities are nearly identical to the "optimum" results.

Since one source type is not able to consistently duplicate the "optimum" results the obvious question of how many are required arises. Figures 8.8-8.11 compare the "optimum" results with the results obtained from combining the data for the 4 oz and 128 oz hammers. These are the lightest and heaviest hammers tested, respectively, and thus should be able to match the "optimum" results at the high and low frequencies. The overlap of the frequency ranges generated by each was thus in question. It is observed from the figures that the results are indistinguishable from the "optimum." Thus, only two sources are required to fully characterize the dispersion curve.

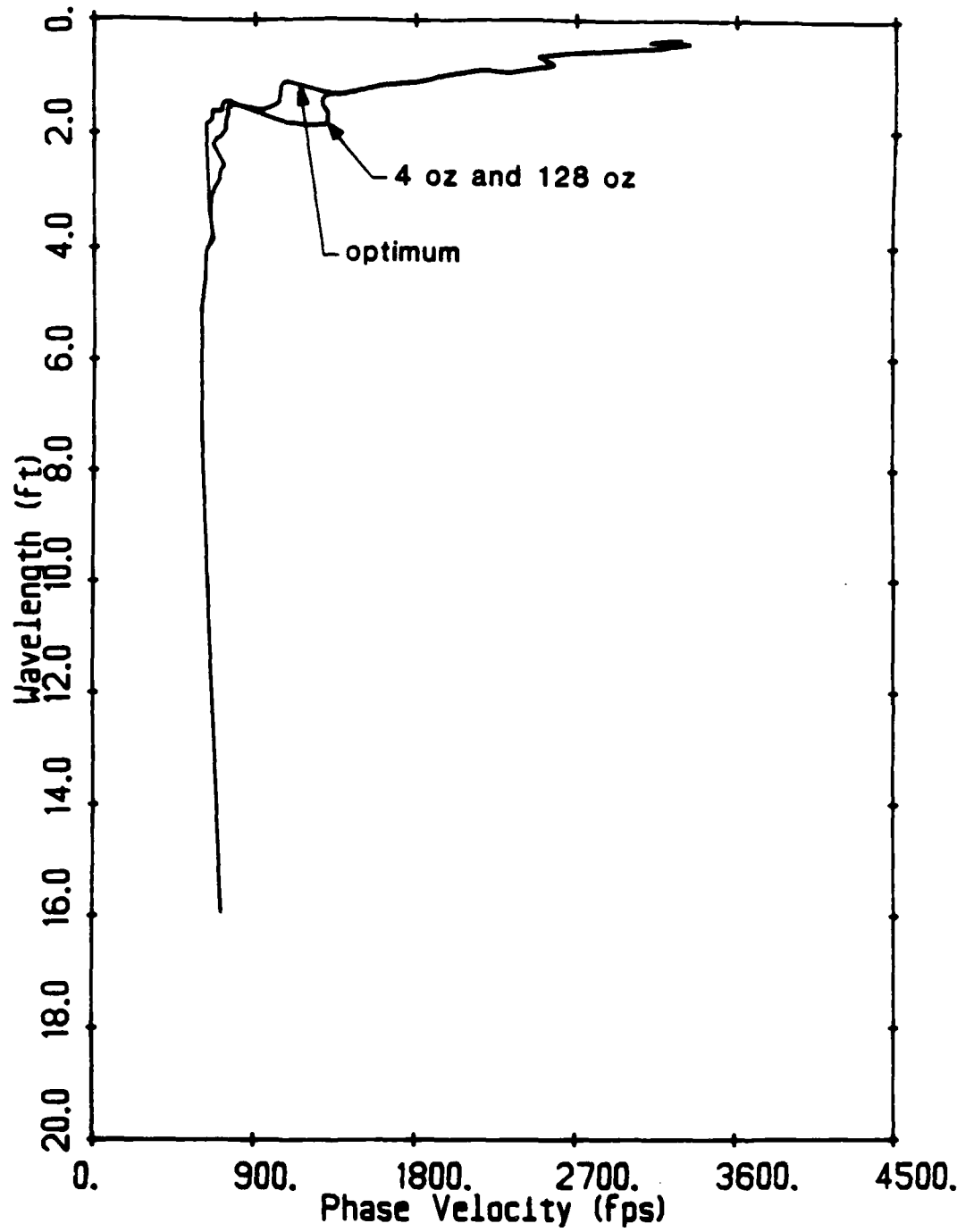


Figure 8.8 — Average Experimental Dispersion Curve for 4 oz and 128 oz Hammers for G. G. Brown Parking Lot Site (all wavelengths)

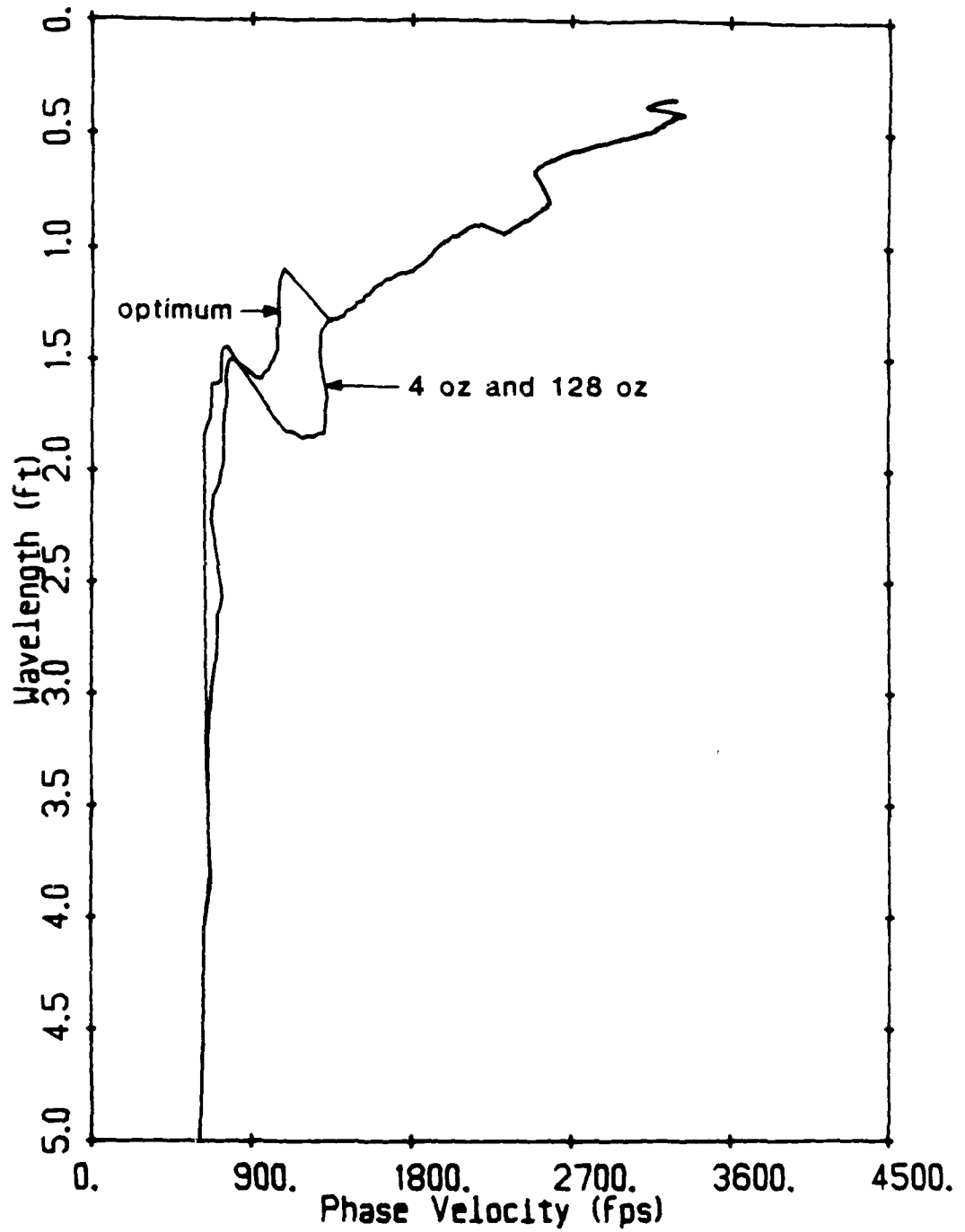


Figure 8.9 — Average Experimental Dispersion Curve for 4 oz and 128 oz Hammers for G. G. Brown Parking Lot Site (0 to 5-ft wavelengths)

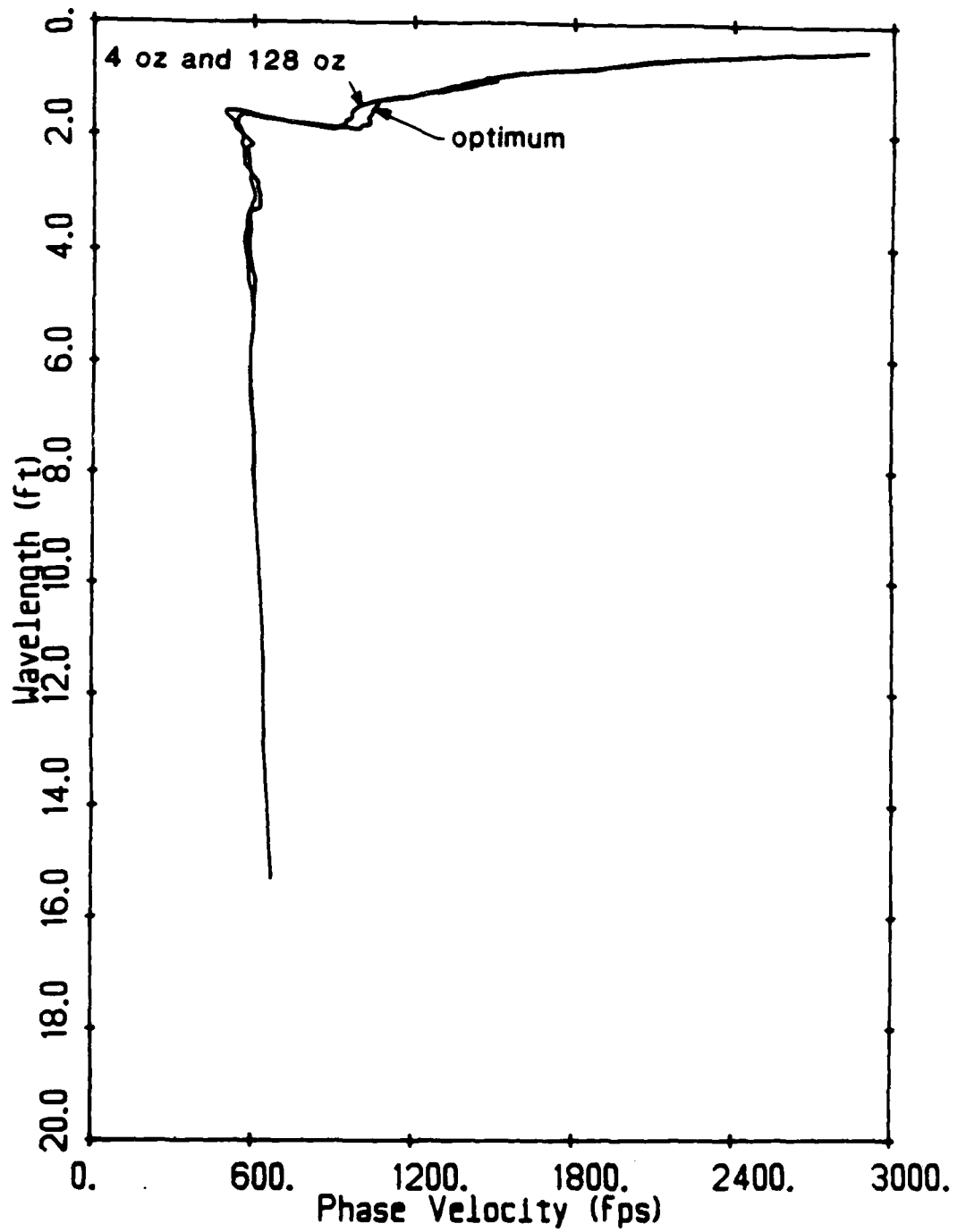


Figure 8.10 — Average Experimental Dispersion Curve for 4 oz and 128 oz Hammers for SEMTA Parking Lot Site (all wavelengths)

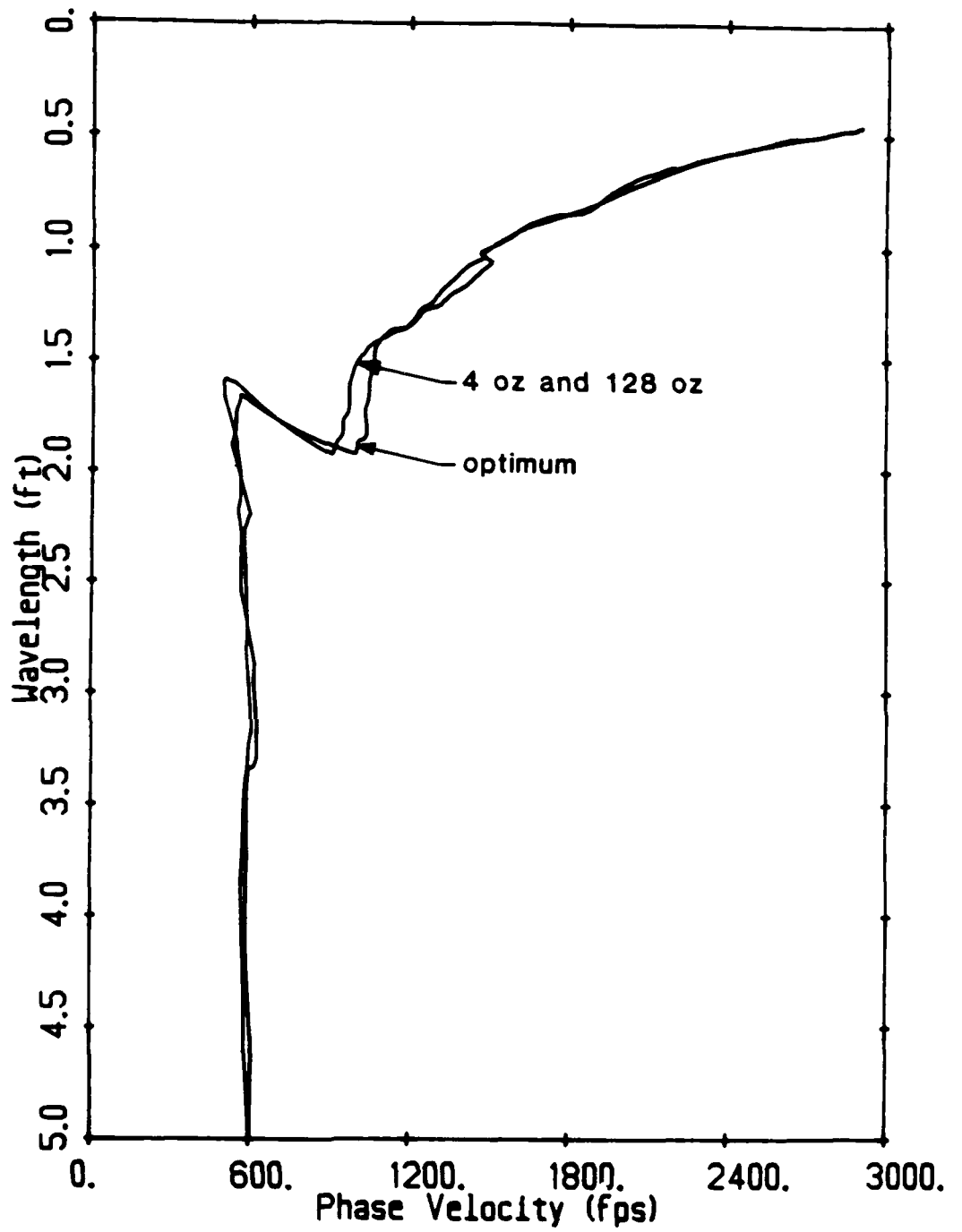


Figure 8.11 — Average Experimental Dispersion Curve for 4 oz and 128 oz Hammers for SEMTA Parking Lot Site (0 to 5-ft wavelengths)

8.3 Summary

For implementation of a multiple transducer testing array it would be beneficial to be able to limit the number of required sources to some minimum value. The intent of the tests described in this chapter was to determine this minimum value and to ascertain the characteristics of the sources required.

Tests were conducted at two sites to study the influence of source type. The tests were conducted in conjunction with the tests described in chapters six and seven. The sources studied were of the impact type and their sizes ranged from a 4 oz ball peen hammer to an 8 lb sledge hammer.

The influence of source type on the ranges of useful frequencies for a given receiver spacing was found to be dramatic. In general both the lower and upper cutoff frequencies decreased as the size of the hammer increased. The magnitude of the cross power spectrums revealed that the influence of source type on the range of useful frequencies was directly related to the energy distribution with frequency generated by each source. Lightweight hammers generate short impulses which result in energy being distributed over a wide frequency band. Heavier hammers produce a longer duration impulse which concentrates energy at low frequencies.

By comparing the dispersion curves generated with the data using a constant source type with "optimum" results it was found that one source type could not consistently duplicate the "optimum" results for all frequencies. In general the light (heavy) hammers could not define the dispersion curve on the low (high) frequency end. Over the frequencies ranges where data did exist, however, the results were in excellent agreement.

Dispersion curves generated by combining the data from a 4 oz ball peen hammer and an 8 lb sledge hammer were found to duplicate the "optimum" results over all wavelengths. Thus, the present data suggests that the dispersion curve for pavement sites can be fully defined with a minimum of two sources.

CHAPTER IX

OTHER CASE STUDIES

9.1 Introduction

A number of sites in addition to the G. G. Brown and SEMTA Parking Lot sites have been investigated during the course of this research (total of 29 sites). The other investigations were part of the author's process of learning the SASW method since it is relatively new. The sites have included both flexible and rigid pavements as well as soil sites. The author has recently participated in a project with the U. S. Army Engineer Waterways Experiment Station to evaluate the characteristics of currently available equipment for the nondestructive testing of pavements. SASW tests were conducted at all sites concurrent with the other testing devices. The results from this research will be reported in future publications.

One of the case studies conducted will be reported here because it serves to validate both the testing and data analysis procedures used throughout this research. The testing was conducted at a soil site on the University of Michigan campus and will be discussed in the following section.

9.2 Tests at Beal St. Field Site

SASW tests were conducted at a soil site on the University of Michigan campus hereafter referred to as the Beal St. Field Site. The general location of the site is shown in figure 9.1. The specific location of the site as well as the location of the SASW test array is shown in figure 9.2. The site has been used for many years for both research and teaching purposes and the soil profile is relatively well known. The soil is a glacially-overconsolidated silty

sand to a depth of at least 8 m. In addition to the SASW tests performed as part of this case study, crosshole tests were performed as well. The location of the crosshole array is shown in figure 9.2. The crosshole test is a well established method for determining shear wave velocity profiles as discussed previously, and thus will serve to validate (or invalidate) both the SASW test and data analysis procedures followed throughout this research.

The SASW tests were conducted following the CRMP geometry. The test parameters used are shown in table 9.1. The crosshole tests were performed using a 3-borehole array (see figure 6[b] in Woods [1986]). The average dispersion curve from the SASW test obtained by combining the dispersion curves from each receiver spacing and source location by the averaging program described in chapter four is shown in figure 9.3. The program "INVERT", described in chapter four, was then used to obtain the shear wave velocity profile from the experimental dispersion curve by the process described in chapter three. The soil profile was divided into 2-ft layers of constant shear wave velocity, Poisson's ratio, and unit weight to a depth of 16 feet (equal to one-third the maximum wavelength measured). A homogeneous half-space was assumed below a depth of 16 feet. Constant values of Poisson's ratio (0.33) and unit weight (110 pcf) were assumed for the entire profile as Nazarian (1984) has shown that the effect of these parameters is very small in comparison to the shear wave velocity. Further, it is only the ratio of unit weights of the individual layers that enter into the calculations, and thus the actual value chosen is not significant. Of course, the actual unit weight of the soil is required to calculate the shear modulus from the shear wave velocity. A shear wave velocity was then assigned to each of the layers and the theoretical dispersion curve was calculated and compared with the experimental. The assumed shear wave velocity profile was then systematically adjusted until the theoretical and experimental dispersion curves matched to within a reasonable tolerance. The resulting match between the two dispersion curves is shown in figures 9.4-9.8. Figure 9.4 demonstrates the two curves for all wavelengths, while figures 9.4-9.8 show selected portions at a larger scale to further demonstrate the match. It is seen that the agreement between the theoretical and experimental curves is excellent for all wavelengths.

The assumed shear wave velocity profile that results in the desired match between the theoretical and experimental dispersion curves is taken as the shear wave velocity profile

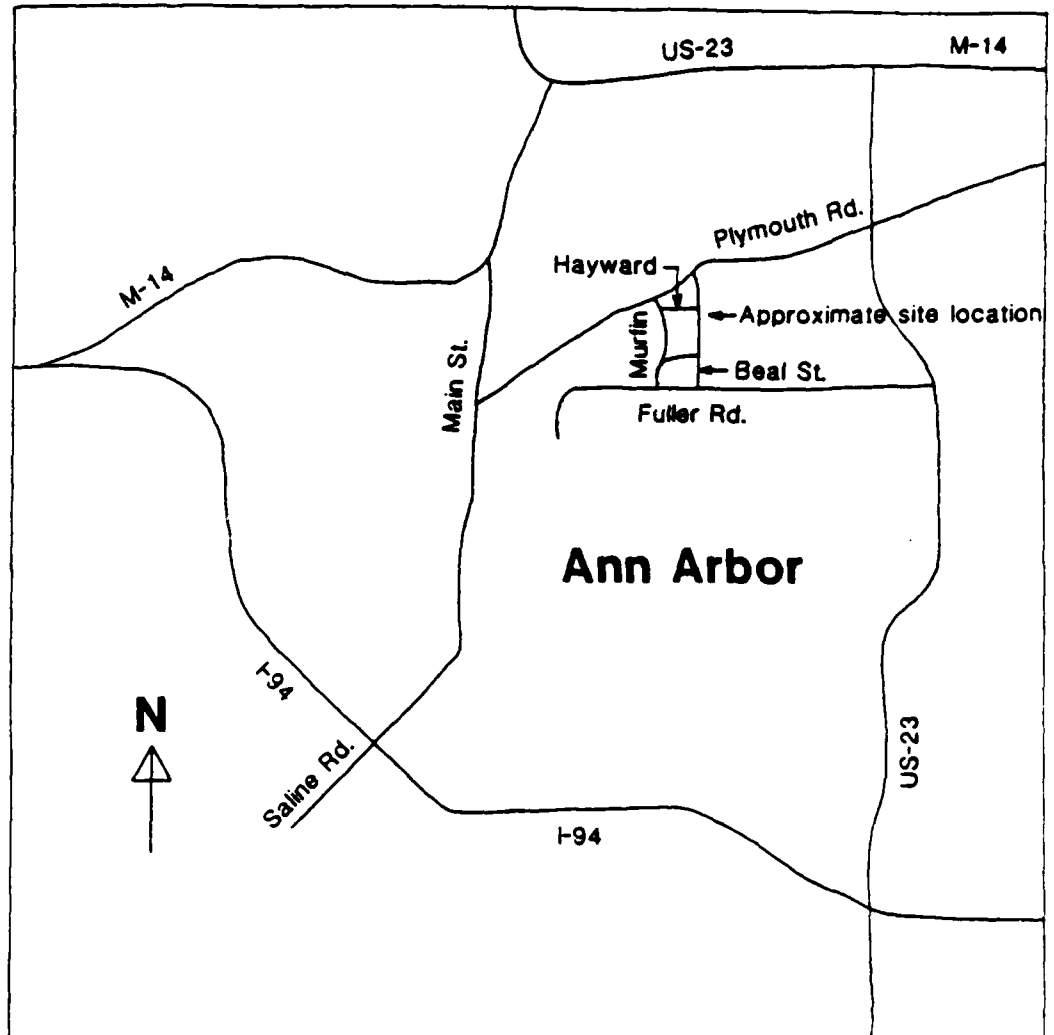


Figure 9.1 — Location of Beal St. Field Site

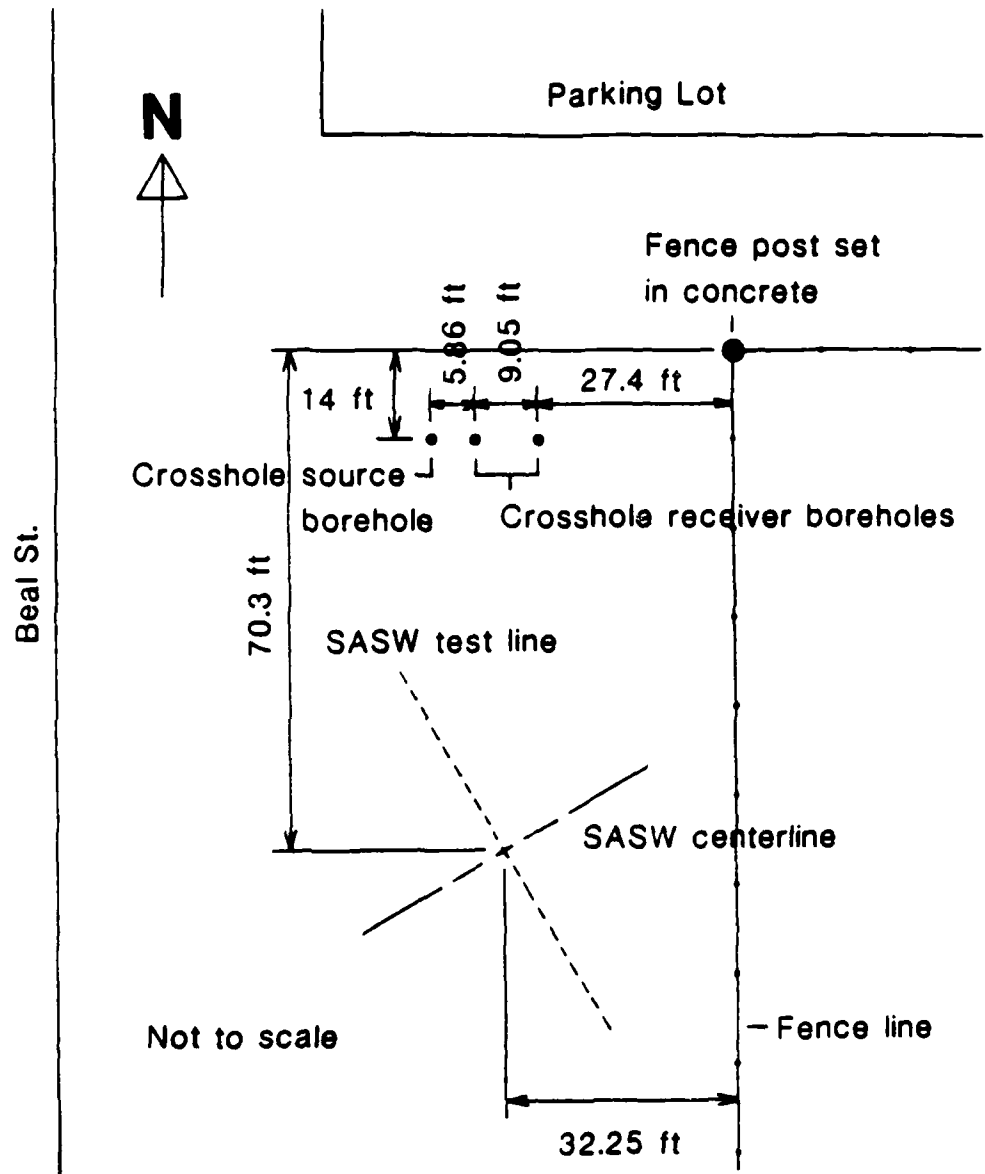


Figure 9.2 — Location of SASW and Crosshole Test Arrays at Beal St. Field Site

Table 9.1 — Test Parameters for SASW Tests at Beal St. Field Site

Receiver Spacing (ft)	Receiver Type	Source Type	Frequency Span (Hz)	Profile (F = Forward, R = Reverse)	Site File No.
4	Mark Products Veloc.	8 lb	125	F	600
4	Mark Products Veloc.	8 lb	125	R	601
8	Mark Products Veloc.	8 lb	98.65625	F	602
8	Mark Products Veloc.	8 lb	98.65625	R	603
16	Mark Products Veloc.	140 lb	50	F	606
16	Mark Products Veloc.	140 lb	62.5	R	607

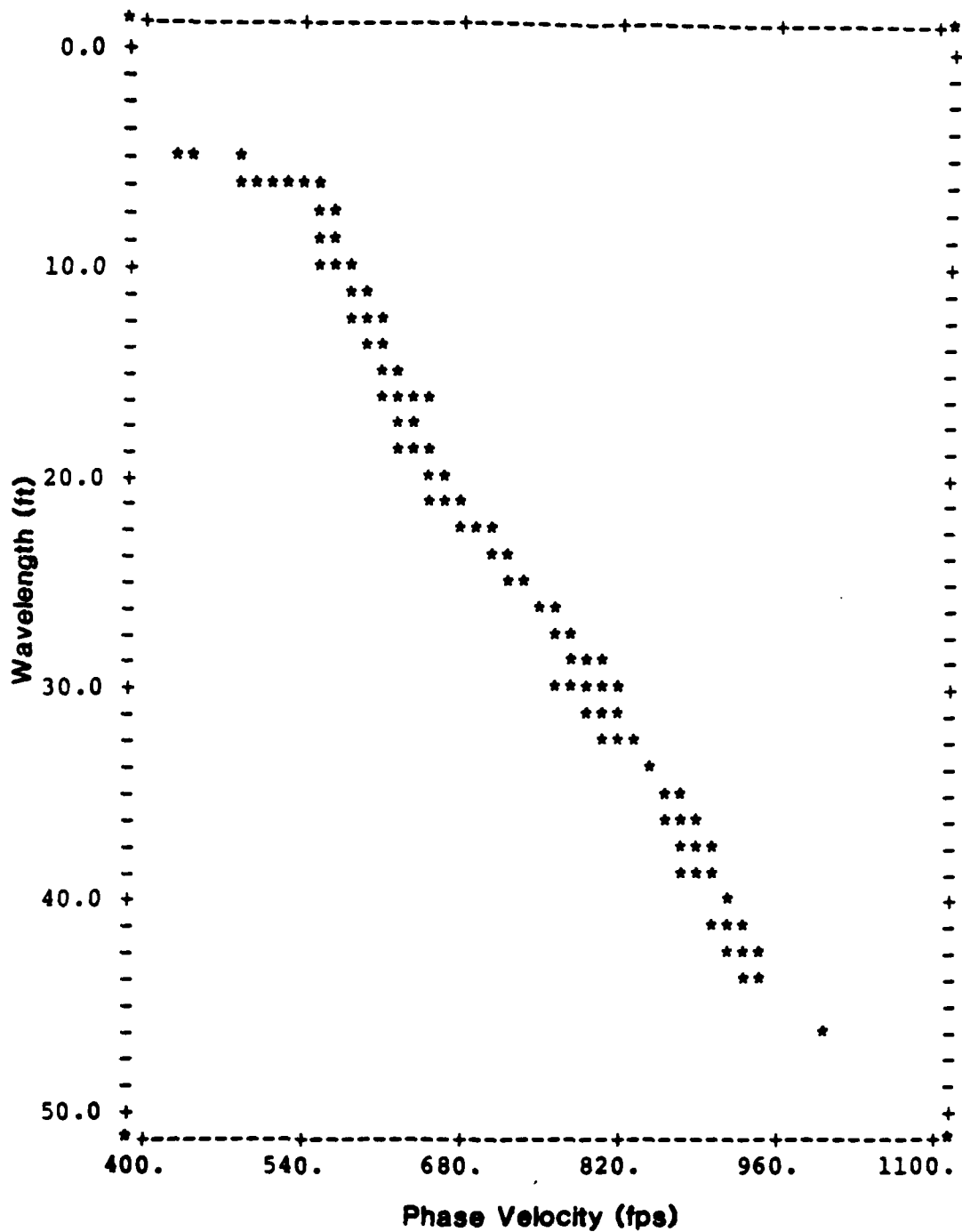


Figure 9.3 — Average Experimental Dispersion Curve for Beal St. Field Site

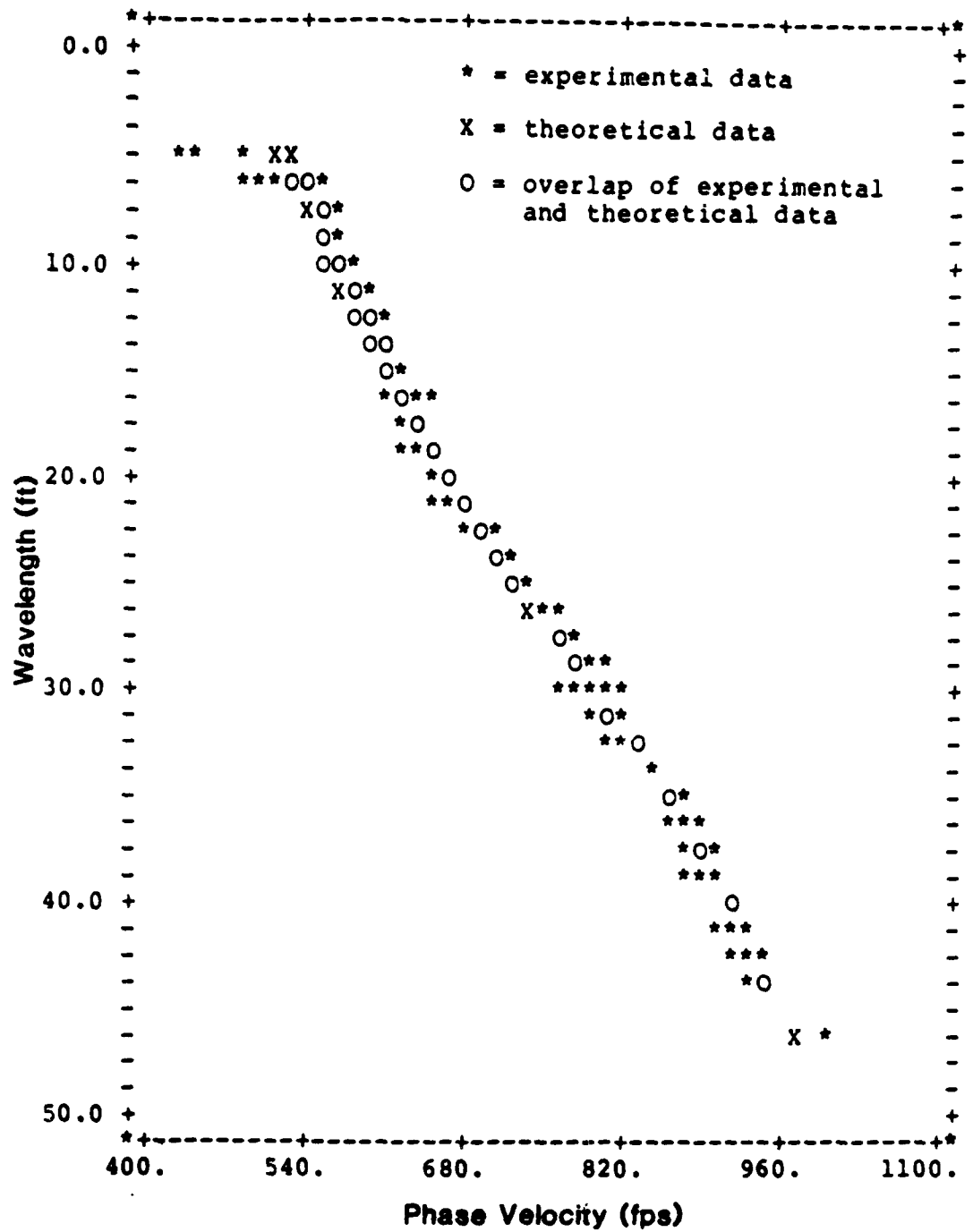


Figure 9.4 — Comparison of Average Experimental and Theoretical Dispersion Curves for Beal St. Field Site (all wavelengths)

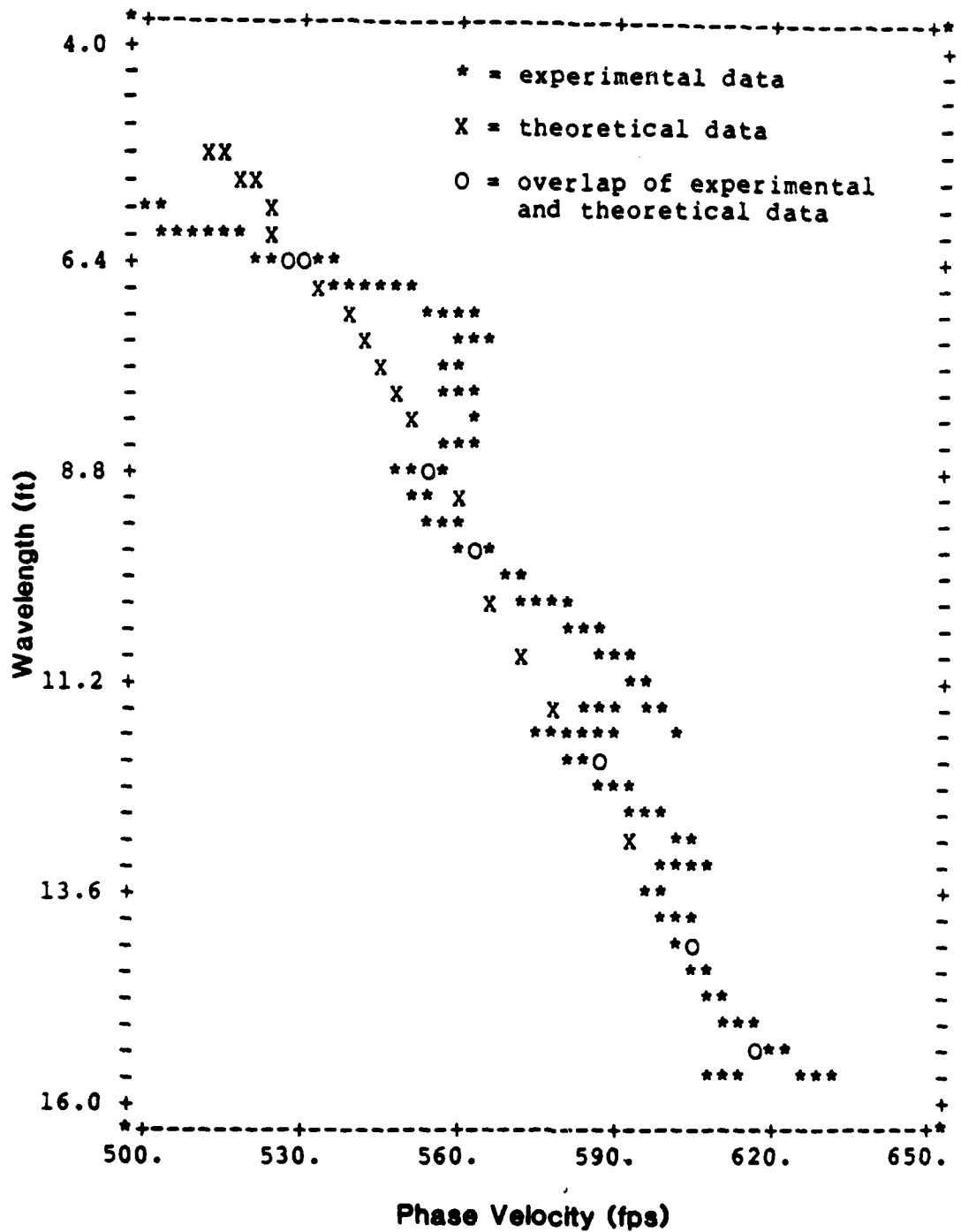


Figure 9.5 — Comparison of Average Experimental and Theoretical Dispersion Curves for Beal St. Field Site (4- to 16-ft wavelengths)

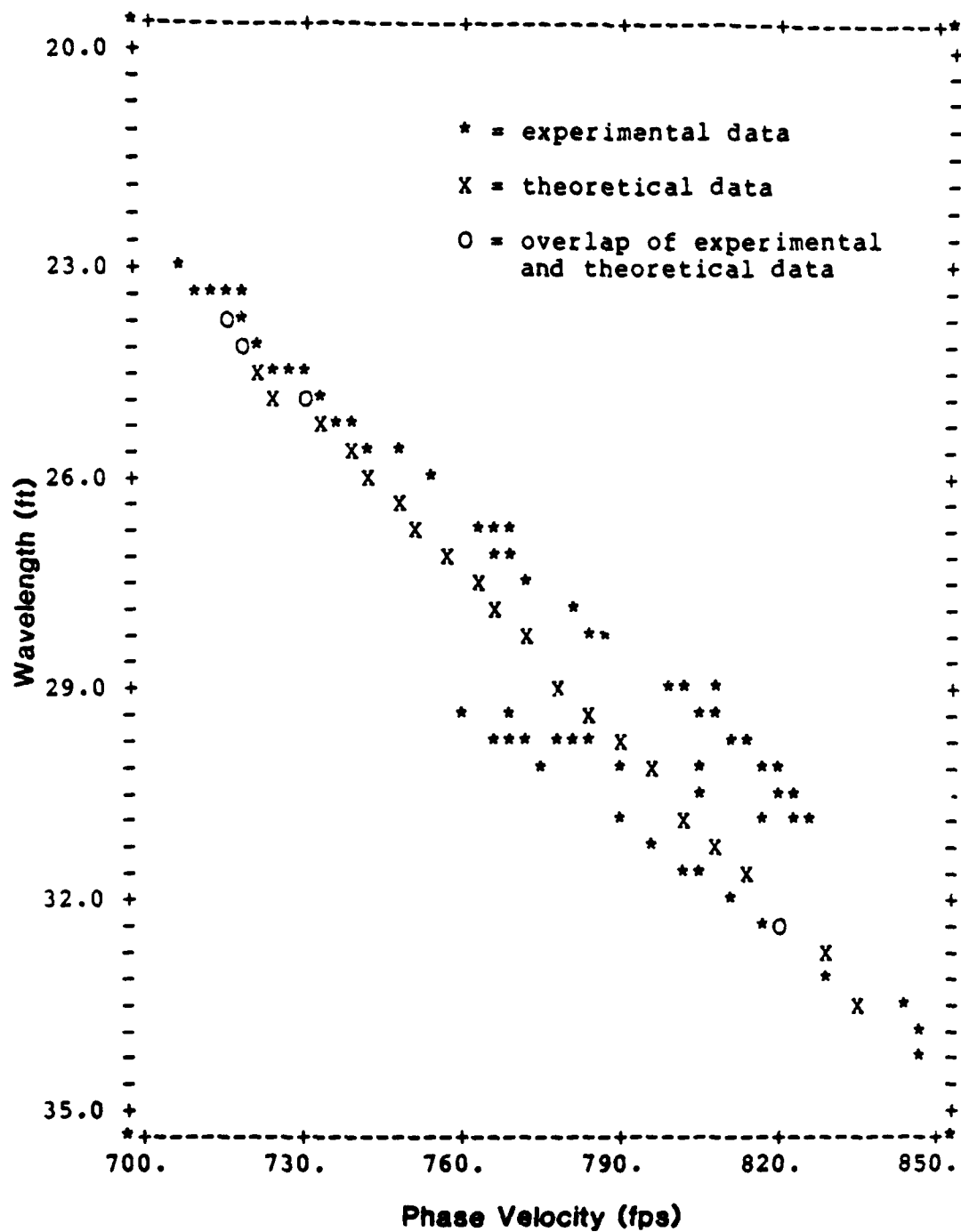


Figure 9.7 — Comparison of Average Experimental and Theoretical Dispersion Curves for Beal St. Field Site (20- to 35-ft wavelengths)

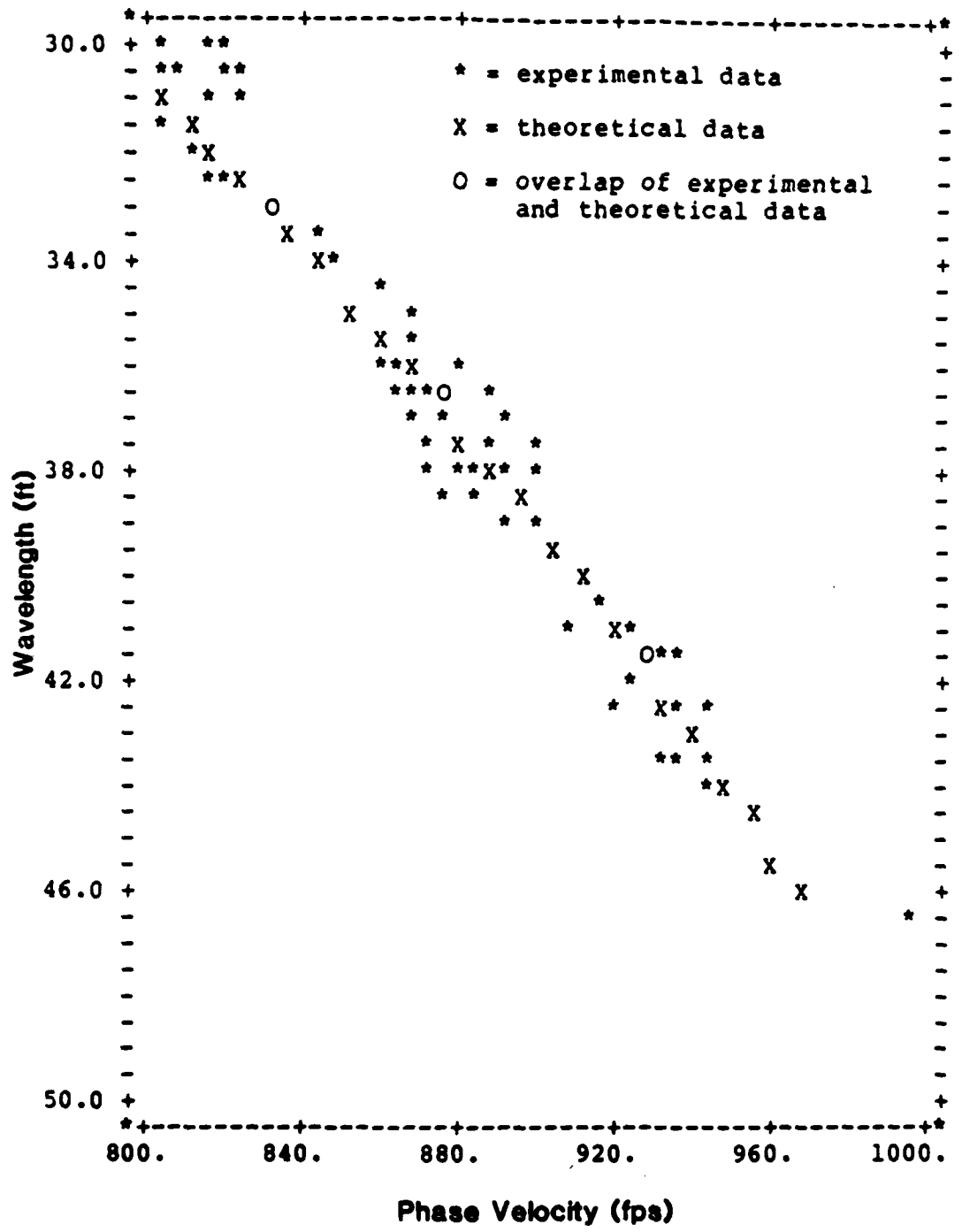


Figure 9.8 — Comparison of Average Experimental and Theoretical Dispersion Curves for Beal St. Field Site (30- to 50-ft wavelengths)

representing the site. The shear wave velocity profile used to produce the theoretical dispersion curve shown in figures 9.4-9.8 is shown in figure 9.9. Also shown in figure 9.9 is the shear wave velocity profile obtained from the crosshole test. The crosshole test results shown in this figure have been designated as "uncorrected". They were obtained by dividing the horizontal distance between the boreholes by the travel time measured in the field. The travel path is thus assumed to be a horizontal straight line. No correction for possible refraction or wave path curvature effects was made. It is observed that the shear wave velocity profiles from the two methods compare very favorably. In all but one case the results differ by less than 10 percent. The difference between the results at a depth of approximately 6.5 ft is about 15 percent. It is also observed that all but one of the crosshole velocities are larger than the SASW results. Both of these observations follow very closely the results from previous investigations. Nazarian (1984) conducted numerous case studies to compare SASW results with the results from both crosshole and downhole tests. He found that the results from SASW tests were usually within 20 percent of those from crosshole and downhole. He also found that the shear wave velocities obtained from SASW tests were usually less than those from the crosshole test. No explanation for this observation was provided. One possible explanation is that wave path curvature in the crosshole test may yield shear wave velocities which are too high. The wave path followed by seismic waves in a medium that varies in stiffness with depth is curved and not a straight line. It is common practice in the crosshole test with small borehole spacings to ignore the effects of wave path curvature. This assumption was checked in the present case study.

Figure 9.10 compares the same SASW results as in figure 9.9 with "corrected" crosshole results. The crosshole results were corrected for possible wave path curvature by an approximate method described in Hoar (1982). The correction procedure assumes that the shear wave velocity varies linearly with depth, which is a reasonable assumption for the profile under study. The correction was found to be small, as all correction factors were between 0.97 and 1, and thus suggests that wave path curvature did not significantly influence the crosshole test results in this case study. The crosshole test results were reduced, but they are still larger than the velocities from the SASW test. The differences are, however, well within the range found in previous investigations as stated earlier, and are also within the

expected accuracy of either the SASW or crosshole testing techniques.

A second means was employed to compare the results from the SASW and crosshole tests. The crosshole test results (uncorrected and corrected) were used as the assumed shear wave velocity profile for calculation of the theoretical dispersion curve for comparison with the dispersion curve obtained in the field using the SASW test. This comparison is shown in figures 9.11-9.15 for the uncorrected crosshole results, and similarly in figures 9.16-9.20 for the corrected. As should be expected from the close agreement between the SASW and crosshole shear wave velocity profiles, the dispersion curves calculated using the crosshole shear wave velocity profiles compare reasonably well with the experimental dispersion curve from the SASW test.

9.3 Summary

The case study conducted at the Beal St. Field Site and discussed in this chapter was provided to validate (or invalidate) the SASW testing and data analysis techniques employed throughout the course of this research. The results from crosshole tests, an established method for determining the shear wave velocity profile of soil systems, were compared with the results from SASW tests conducted at the same site. The results were found to compare very favorably. In addition, the results followed closely the trends observed in previous investigations. Thus it can be concluded that the SASW testing and data analysis techniques used in this research are valid.

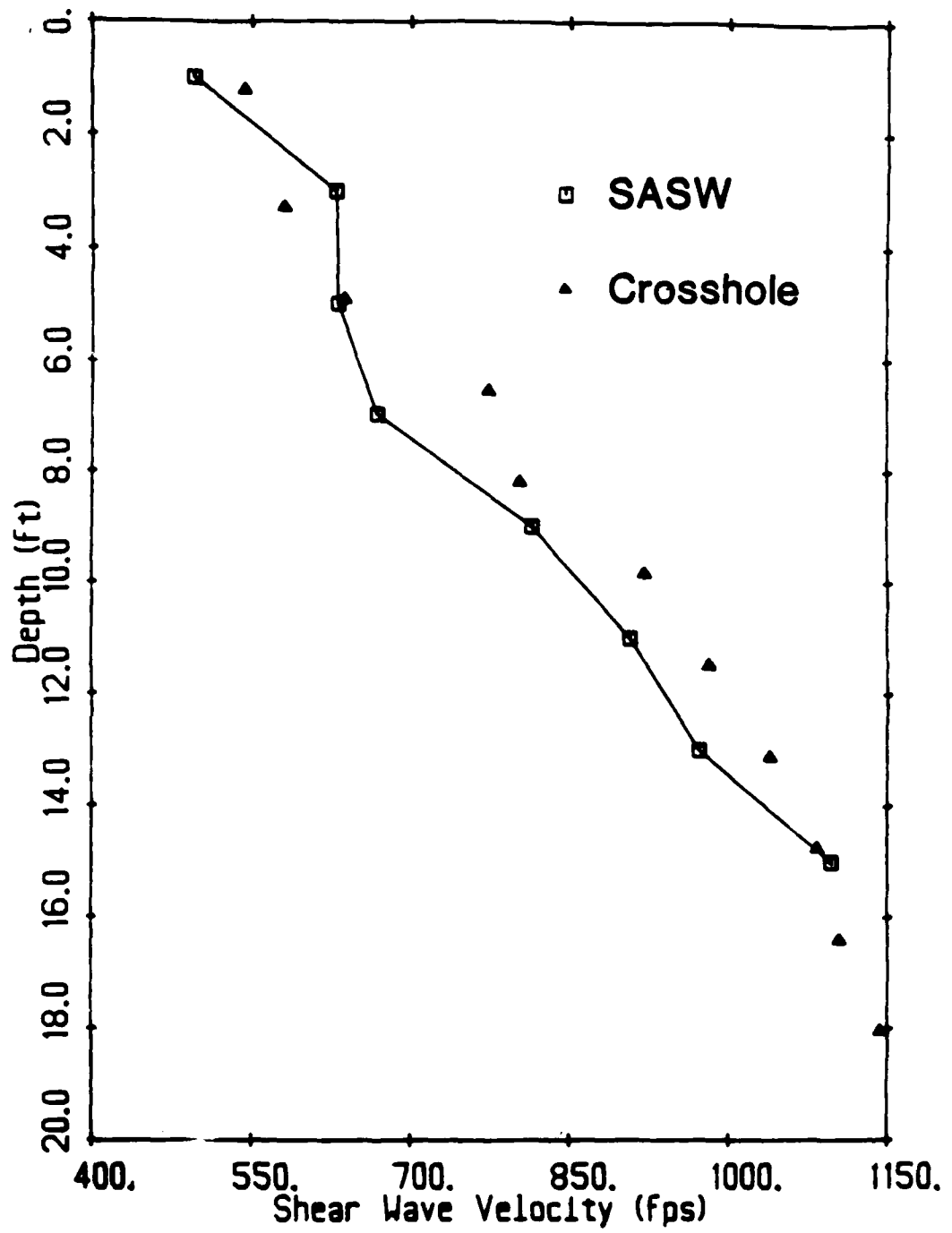


Figure 9.9 — Comparison of Shear Wave Velocity Profiles from SASW and Crosshole (Uncorrected) Tests

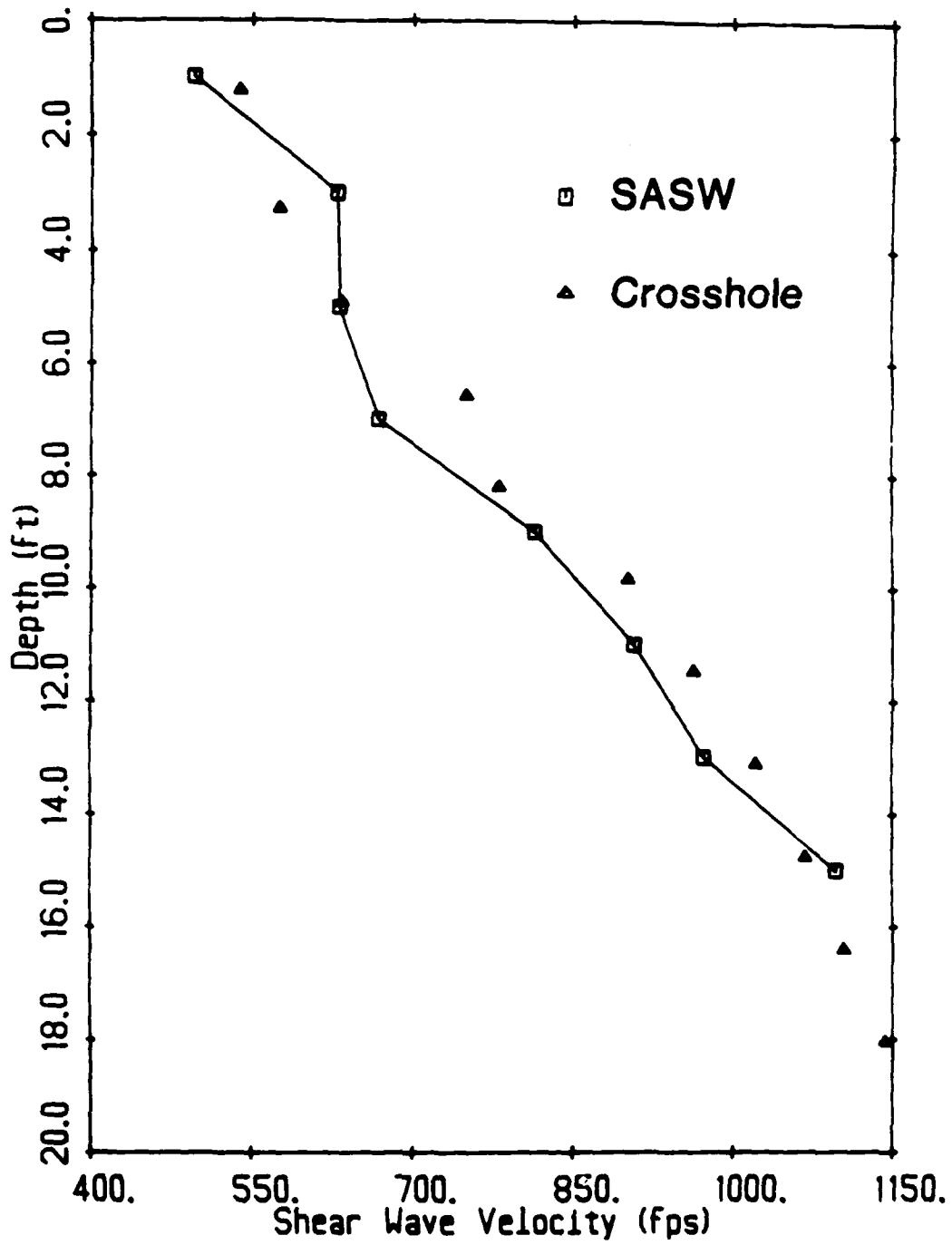


Figure 9.10 — Comparison of Shear Wave Velocity Profiles from SASW and Crosshole (Corrected) Tests

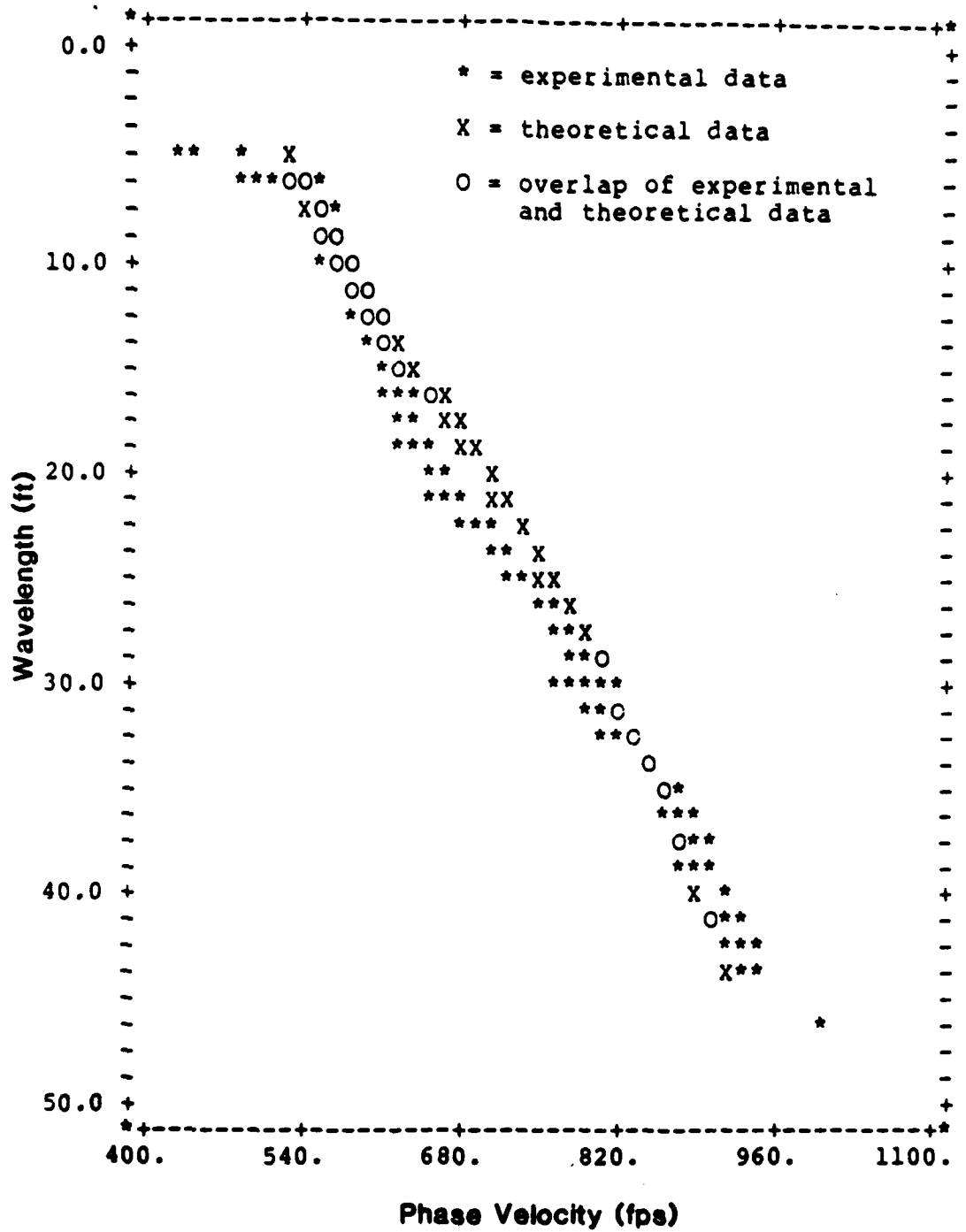


Figure 9.11 — Comparison of Average Experimental Dispersion Curve and Theoretical Dispersion Curve Obtained from Uncorrected Crosshole Test Results (all wavelengths)

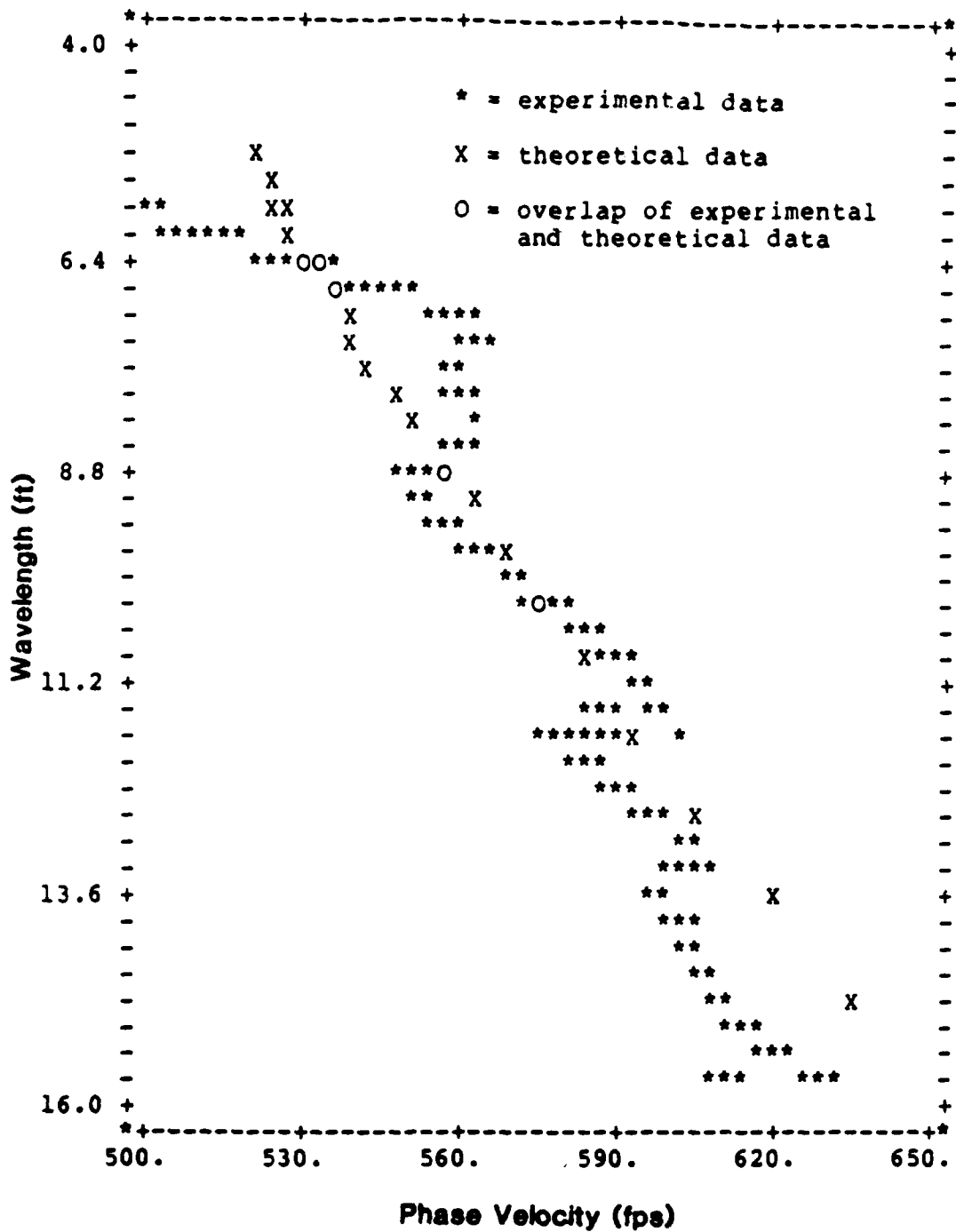


Figure 9.12 — Comparison of Average Experimental Dispersion Curve and Theoretical Dispersion Curve Obtained from Uncorrected Crosshole Test Results (4 to 16-ft wavelengths)

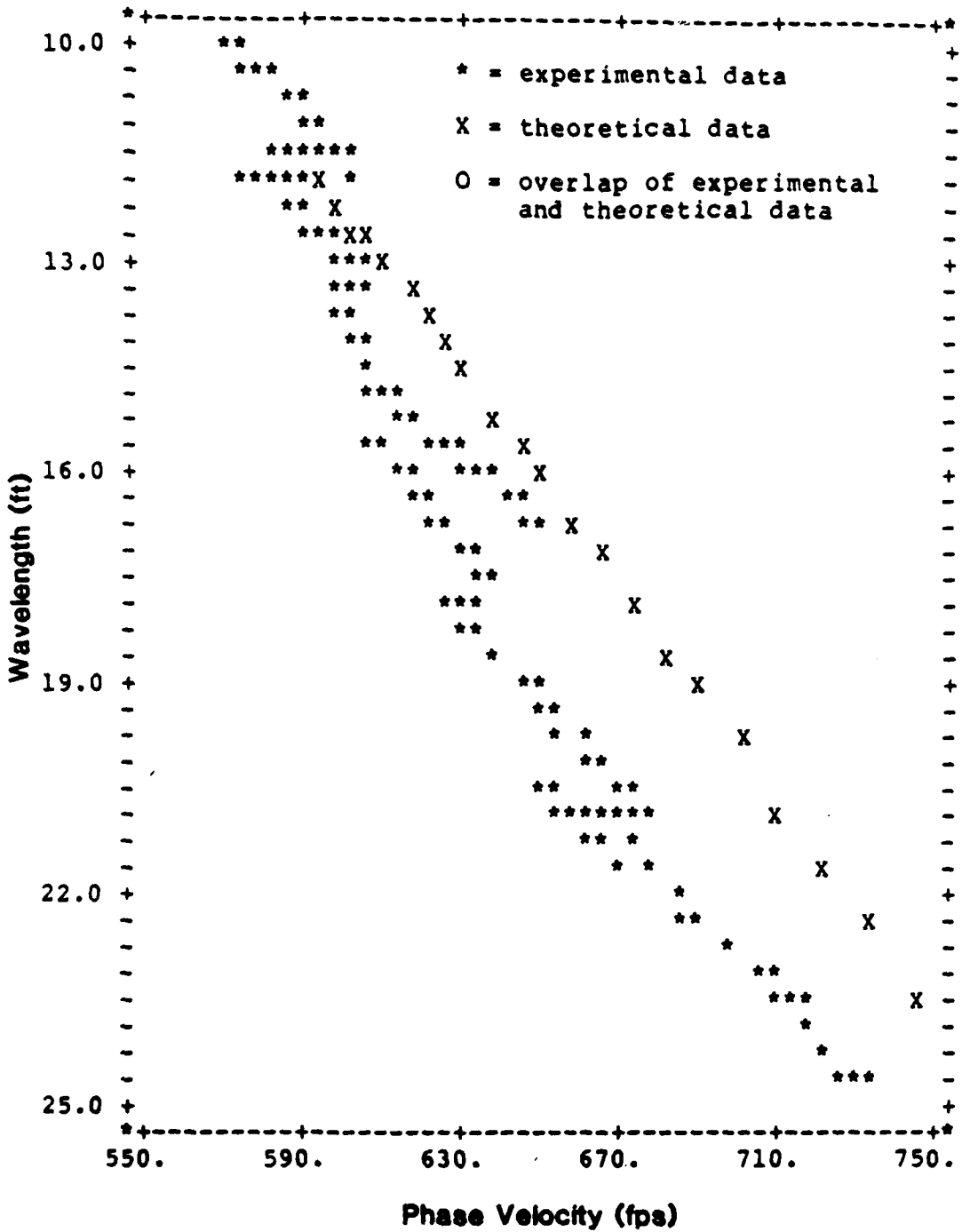


Figure 9.13 — Comparison of Average Experimental Dispersion Curve and Theoretical Dispersion Curve Obtained from Uncorrected Crosshole Test Results (10 to 25-ft wavelengths)

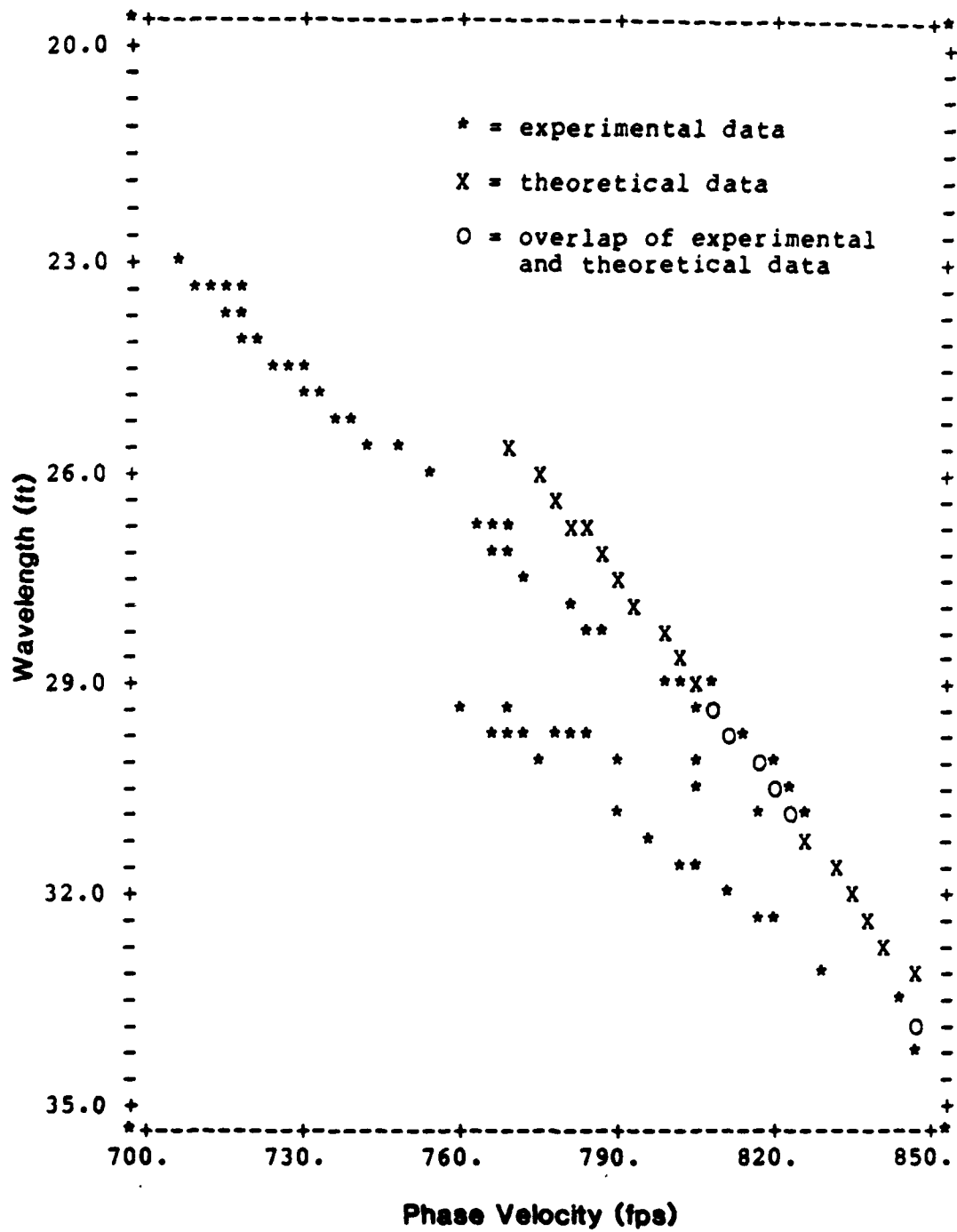


Figure 9.14 — Comparison of Average Experimental Dispersion Curve and Theoretical Dispersion Curve Obtained from Uncorrected Crosshole Test Results (20 to 35-ft wavelengths)

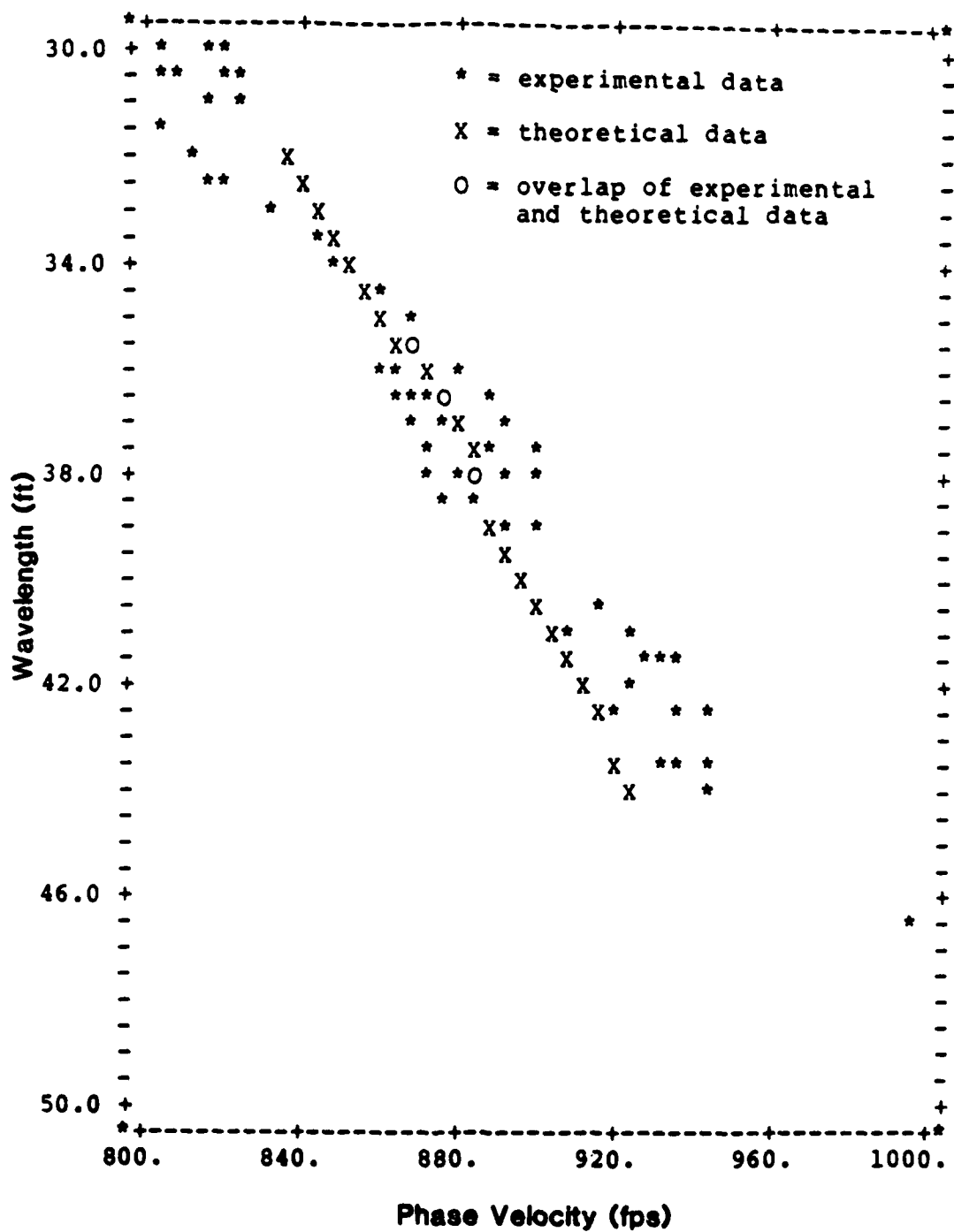


Figure 9.15 — Comparison of Average Experimental Dispersion Curve and Theoretical Dispersion Curve Obtained from Uncorrected Crosshole Test Results (30 to 50-ft wavelengths)

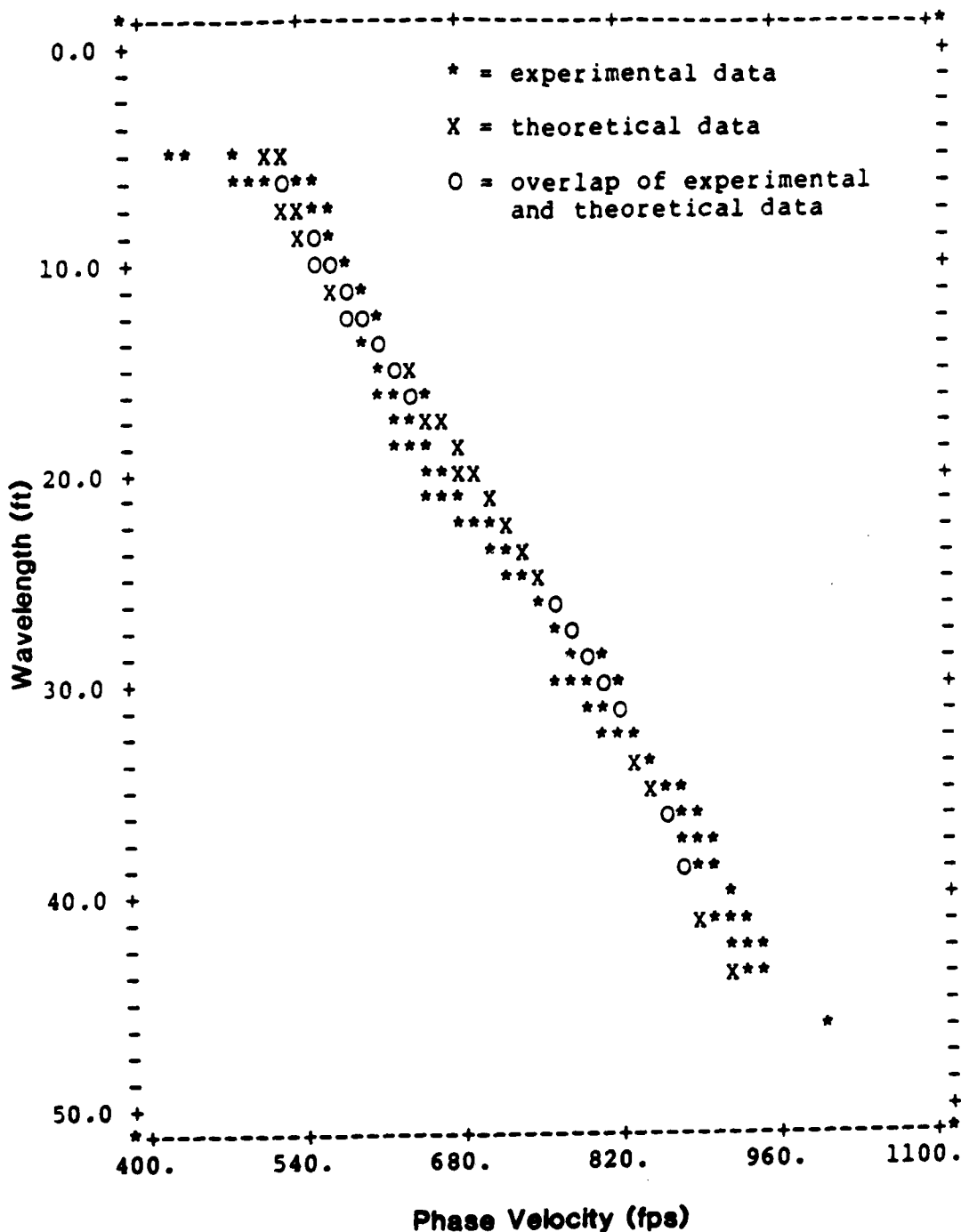


Figure 9.16 — Comparison of Average Experimental Dispersion Curve and Theoretical Dispersion Curve Obtained from Corrected Crosshole Test Results (all wavelengths)

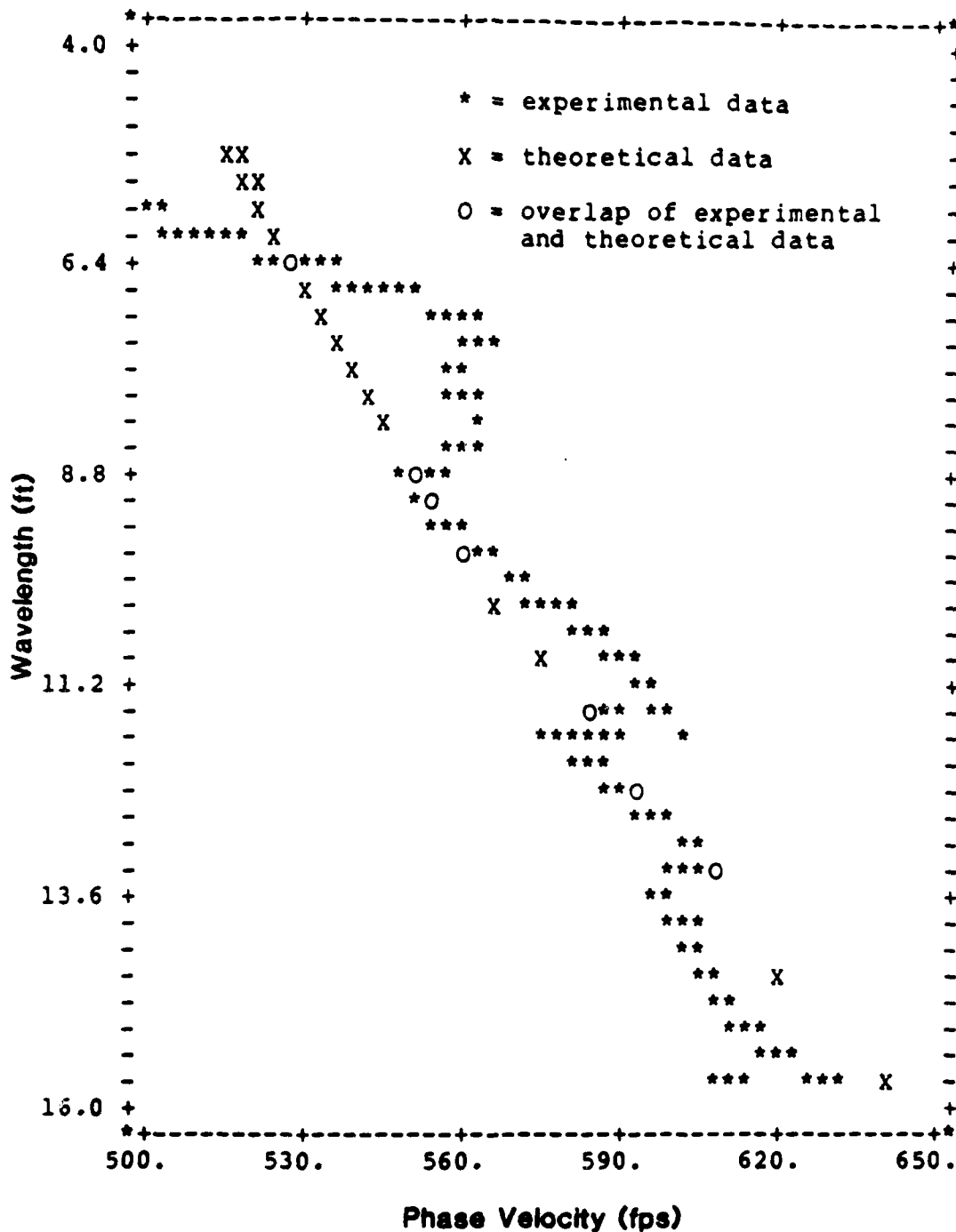


Figure 9.17 — Comparison of Average Experimental Dispersion Curve and Theoretical Dispersion Curve Obtained from Corrected Crosshole Test Results (4 to 16-ft wavelengths)

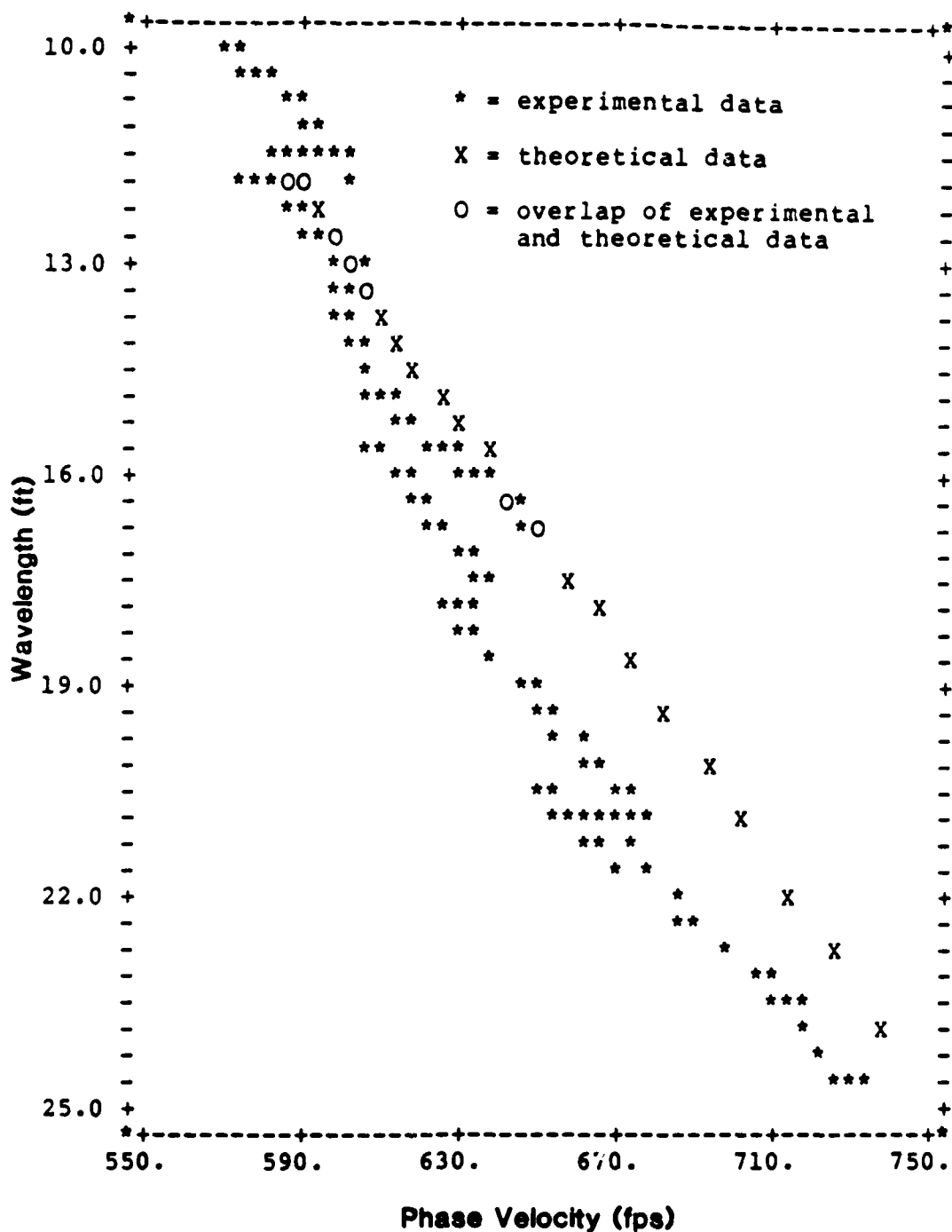


Figure 9.18 — Comparison of Average Experimental Dispersion Curve and Theoretical Dispersion Curve Obtained from Corrected Crosshole Test Results (10 to 25-ft wavelengths)

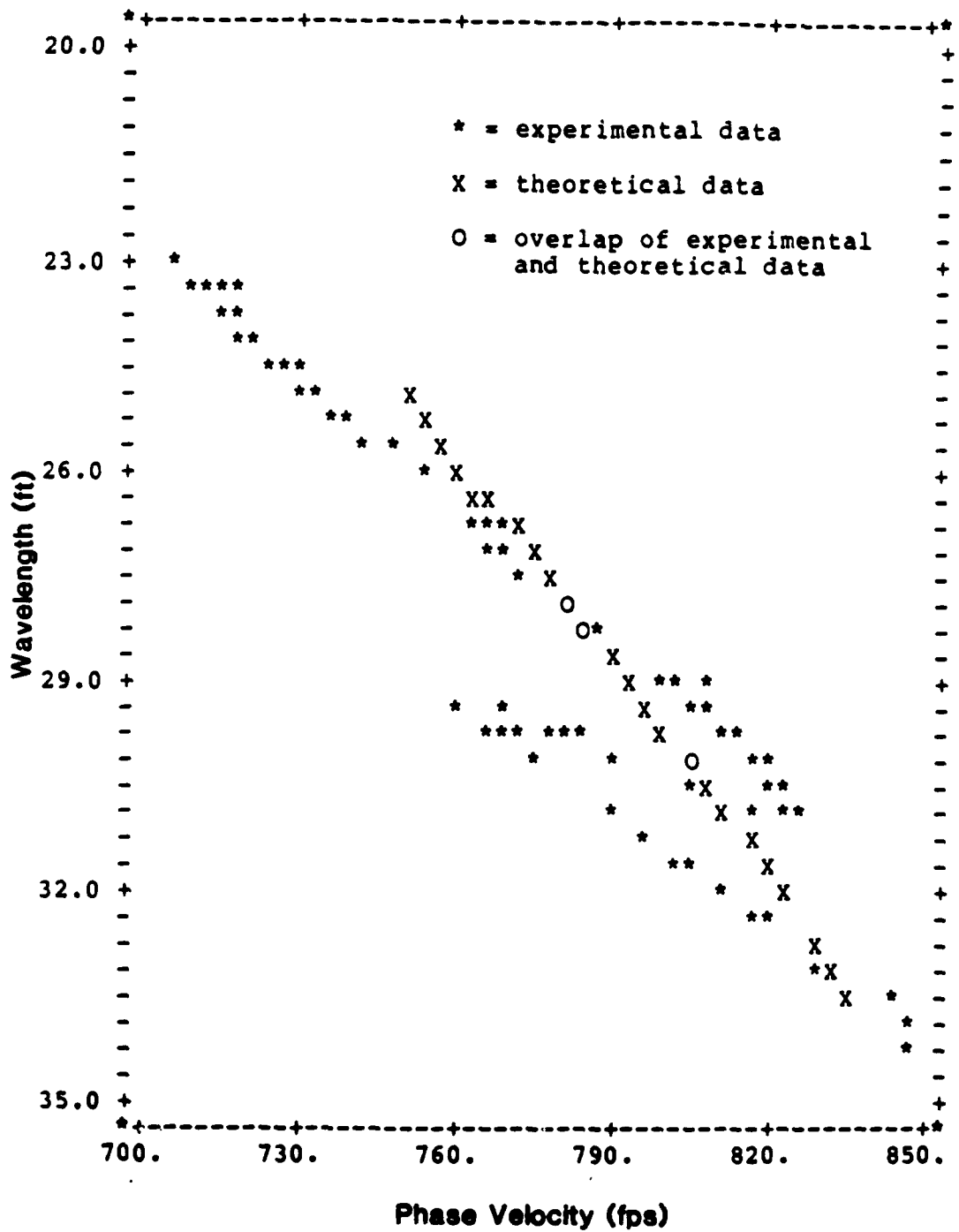


Figure 9.19 — Comparison of Average Experimental Dispersion Curve and Theoretical Dispersion Curve Obtained from Corrected Crosshole Test Results (20 to 35-ft wavelengths)

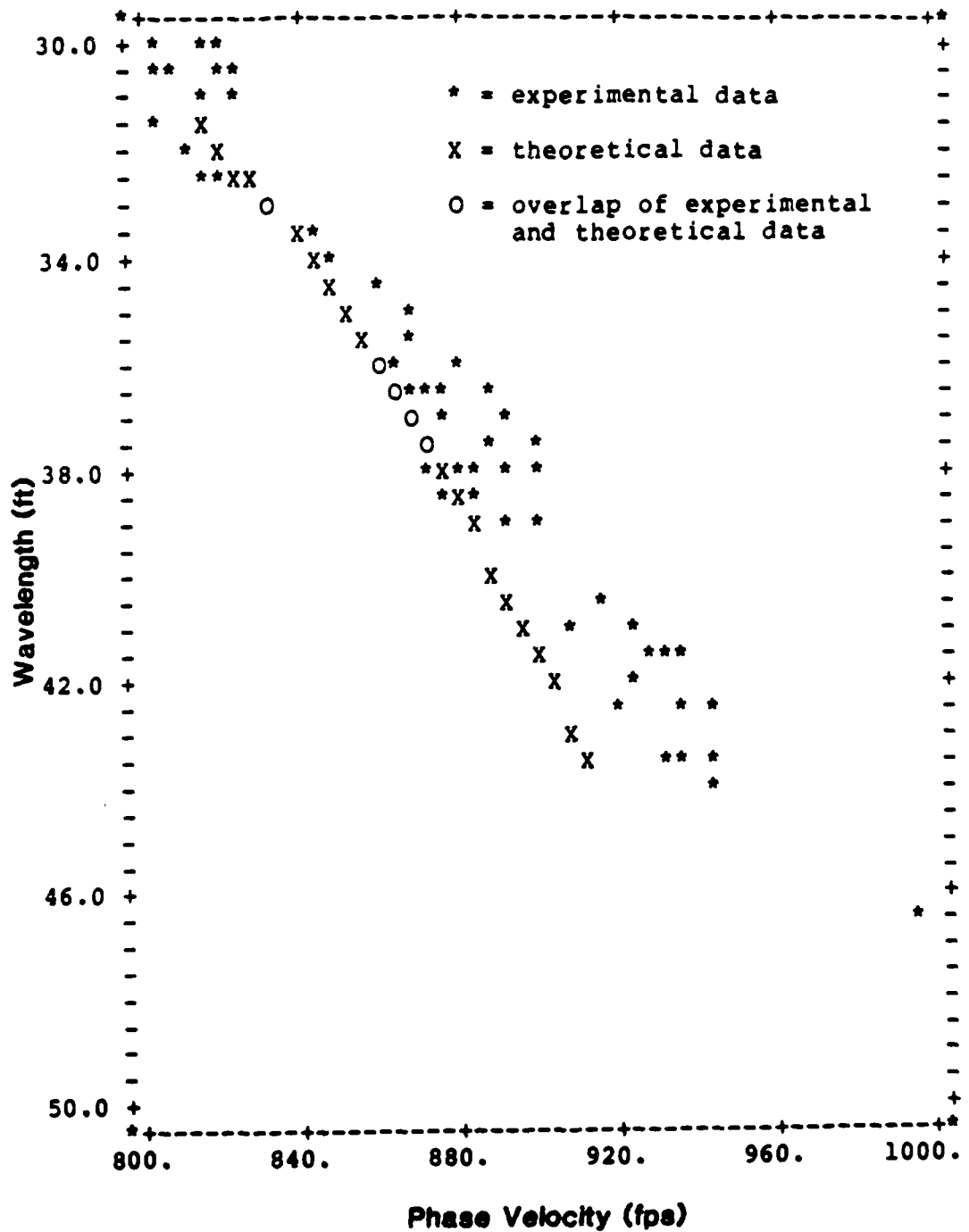


Figure 9.20 — Comparison of Average Experimental Dispersion Curve and Theoretical Dispersion Curve Obtained from Corrected Crosshole Test Results (30 to 50-ft wavelengths)

CHAPTER X

CLOSURE

10.1 Summary

The purpose of this research was to further the development of the SASW method toward a practical technique for in situ investigation of pavement systems. It is envisioned that eventually an automated testing procedure will be developed to enable one to collect the necessary data on-the-move, analogous to the current deflection measurement procedures currently used in the pavement industry. It was felt that the development of a multiple transducer testing procedure, i.e., a procedure employing more than two transducers, is an important step towards this goal. Three questions immediately arose when implementation of a multiple transducer array was considered: 1) which source and receiver geometry, 2) where should the source be located, and 3) what source type(s) should be used. This research has attempted to answer these questions by conducting a systematic experimental investigation at two asphaltic concrete pavement sites of the influence of source and receiver geometry, source-to-near-receiver distance, and source type in the context of a multiple transducer testing procedure. It was found that the results are independent of source and receiver geometry. The common source (CS) geometry is recommended since it employs a fixed source location. The influence of the source-to-near-receiver distance was found to be extremely important. It was found that the ratio of the source-to-near-receiver distance to the receiver spacing should be less than or equal to two. In addition, phase velocity measurements are independent of source-to-near-receiver distance if wavelengths larger than twice the receiver spacing are filtered from the data. The influence of source type was

confirmed to be extremely important. Two sources, one comparable to a 4 oz ball peen hammer, the other similar to an 8 lb sledge hammer, were found sufficient for defining the dispersion curve.

10.2 Conclusions

The major conclusions which result from this research, based upon tests conducted at two asphaltic concrete pavement sites, are as follows:

- 1) The dispersion curves obtained from the common receivers midpoint (CRMP) geometry and the common source (CS) geometry are nearly identical and the scatter within all the data collected with each geometry is similar.
- 2) The value of the ratio of the source-to-near-receiver distance to the receiver spacing (S/X) should be less than or equal to two.
- 3) Dispersion data are independent of source-to-near-receiver distance if wavelengths larger than twice the receiver spacing are eliminated from the data.
- 4) One source type is not consistently capable of defining the dispersion curve.
- 5) The dispersion curve at these two sites can be completely defined with a minimum of two sources, one comparable to a 4 oz ball peen hammer, the other similar to an 8 lb sledge hammer.
- 6) The implications of these findings for a multiple transducer testing procedure are as follows:
 - a) The common receivers midpoint (CRMP) geometry is not appropriate for a multiple transducer testing procedure with a fixed source location. It would not be possible to design such an array to meet the criterion that S/X be less than or equal to two.
 - b) The common source (CS) geometry with $S/X = 1$ is recommended for a multiple transducer array.
 - c) One means of collecting the data in a multiple transducer testing procedure is to employ two impact sources.

10.3 Recommendations for Future Research

The SASW method has been shown to have tremendous value for future applications. However, the method to date is primarily a research tool. Efforts to decrease the testing and data reduction time are essential, particularly for nondestructive pavement evaluation. Some suggested topics for moving the SASW method toward the ultimate goal of a totally automated testing and data analysis procedure are:

- 1) More extensive investigation of the variables investigated in this research. In particular, tests should be conducted for a broader range of pavement types and environmental conditions to ascertain the generality of the conclusions presented above.
- 2) Implementation and testing of a multiple transducer array based upon the guidelines produced from this and further research.
- 3) Development of a rapid means of coupling transducers to pavements for implementation in an automated testing procedure.
- 4) Addition of formalized inverse theory to the current method of determining the shear wave velocity profile from the dispersion curve.
- 5) Development of nonlinear stress-strain models for pavement materials to extrapolate the small-strain moduli determined by the SASW method to conditions under actual pavement loads.

APPENDICES

APPENDIX A

TABLES OF USEFUL FREQUENCY RANGES AS A FUNCTION OF
SOURCE-TO-NEAR-RECEIVER DISTANCE

**Table A.1 — Useful Frequency Ranges for 0.5-ft Receiver Spacing (X) for
G. G. Brown Parking Lot Site**

Source-to-Near-Receiver Distance (S) (ft)	S/X	Lower Cutoff Frequency (Hz)	Upper Cutoff Frequency (Hz)
0.25	0.5	100	8900
0.50	1.0	125	9250
0.75	1.5	100	8125
1.00	2.0	100	6650
1.50	3.0	125	2800

**Table A.2 — Useful Frequency Ranges for 1-ft Receiver Spacing (X) for
G. G. Brown Parking Lot Site**

Source-to-Near-Receiver Distance (S) (ft)	S/X	Lower Cutoff Frequency (Hz)	Upper Cutoff Frequency (Hz)
0.5	0.5	175	4700
1.0	1.0	112	7975
1.5	1.5	137	6725
2.0	2.0	137	4562
2.5	2.5	125	1263
3.0	3.0	150	675

**Table A.3 — Useful Frequency Ranges for 2-ft Receiver Spacing (X) for
G. G. Brown Parking Lot Site**

Source-to-Near-Receiver Distance (S) (ft)	S/X	Lower Cutoff Frequency (Hz)	Upper Cutoff Frequency (Hz)
1.0	0.5	41.2	1000
2.0	1.0	31.2	1000
3.0	1.5	20	451.2
4.0	2.0	26.2	148.7
5.0	2.5	21.2	153.7
6.0	3.0	21.2	155

**Table A.4 — Useful Frequency Ranges for 4-ft Receiver Spacing (X) for
G. G. Brown Parking Lot Site**

Source-to-Near-Receiver Distance (S) (ft)	S/X	Lower Cutoff Frequency (Hz)	Upper Cutoff Frequency (Hz)
2.0	0.5	46.48	173.05
4.0	1.0	21.09	168.36
6.0	1.5	21.09	153.91
8.0	2.0	17.58	187.5
10.0	2.5	23.05	152.73
12.0	3.0	44.92	126.17

**Table A.5 — Useful Frequency Ranges for 8-ft Receiver Spacing (X) for
G. G. Brown Parking Lot Site**

Source-to-Near- Receiver Distance (S) (ft)	S/X	Lower Cutoff Frequency (Hz)	Upper Cutoff Frequency (Hz)
4.0	0.5	38.25	200
8.0	1.0	30.25	200
12.0	1.5	30.25	135.5
16.0	2.0	31.5	135
20.0	2.5	30.25	134.25
24.0	3.0	30.25	118

**Table A.6 — Useful Frequency Ranges for 1-ft Receiver Spacing (X) for
SEMTA Parking Lot Site**

Source-to-Near- Receiver Distance (S) (ft)	S/X	Lower Cutoff Frequency (Hz)	Upper Cutoff Frequency (Hz)
0.5	0.5	187	6675
1.0	1.0	125	5914.1
1.5	1.5	125	4046.9
2.0	2.0	101.6	2429.7
2.5	2.5	109.4	460.9
3.0	3.0	328.1	492.2

**Table A.7 — Useful Frequency Ranges for 2-ft Receiver Spacing (X) for
SEMTA Parking Lot Site**

Source-to-Near-Receiver Distance (S) (ft)	S/X	Lower Cutoff Frequency (Hz)	Upper Cutoff Frequency (Hz)
1.0	0.5	70	306.2
2.0	1.0	41.2	301.2
3.0	1.5	35	263.7
4.0	2.0	32.5	257.5
5.0	2.5	32.5	306.2
6.0	3.0	66.2	161.2

**Table A.8 — Useful Frequency Ranges for 4-ft Receiver Spacing (X) for
SEMTA Parking Lot Site**

Source-to-Near-Receiver Distance (S) (ft)	S/X	Lower Cutoff Frequency (Hz)	Upper Cutoff Frequency (Hz)
2.0	0.5	34	306
4.0	1.0	38	317
6.0	1.5	38	189
8.0	2.0	34	184
10.0	2.5	67	200
12.0	3.0	63	160

Table A.9 — Useful Frequency Ranges for 8-ft Receiver Spacing (X) for SEMTA Parking Lot Site

Source-to-Near-Receiver Distance (S) (ft)	S/X	Lower Cutoff Frequency (Hz)	Upper Cutoff Frequency (Hz)
4.0	0.5	32.5	127.5
8.0	1.0	34.37	101.25
12.0	1.5	33.44	90
16.0	2.0	33.44	85
20.0	2.5	34.06	55
24.0	3.0	34.69	44.37

APPENDIX B

CROSS POWER SPECTRUM MAGNITUDES AS A FUNCTION OF
SOURCE-TO-NEAR-RECEIVER DISTANCE

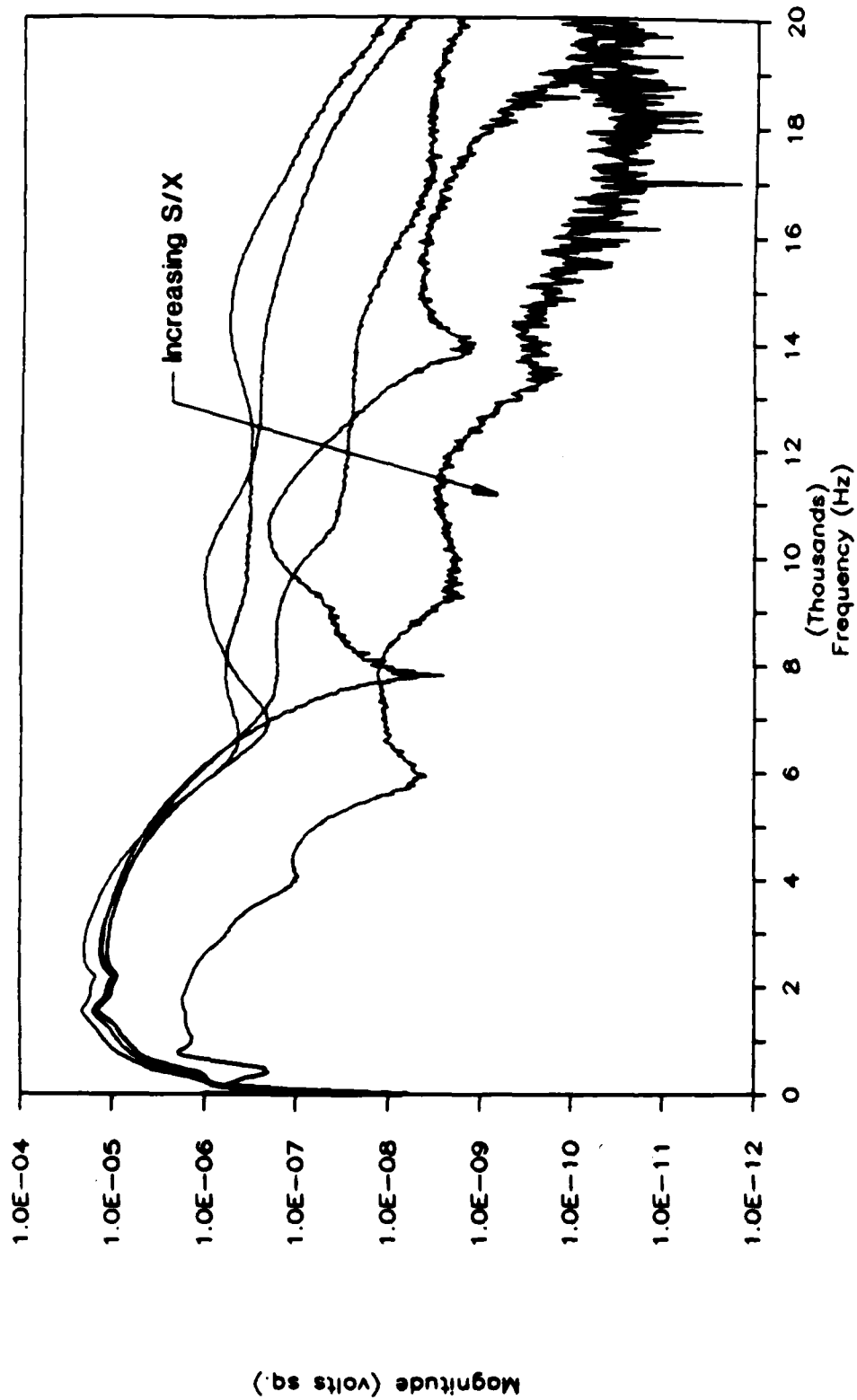


Figure B.1 - Magnitude (Absolute) of Cross Power Spectrum for X = 0.5 ft for G. G. Brown Parking Lot Site

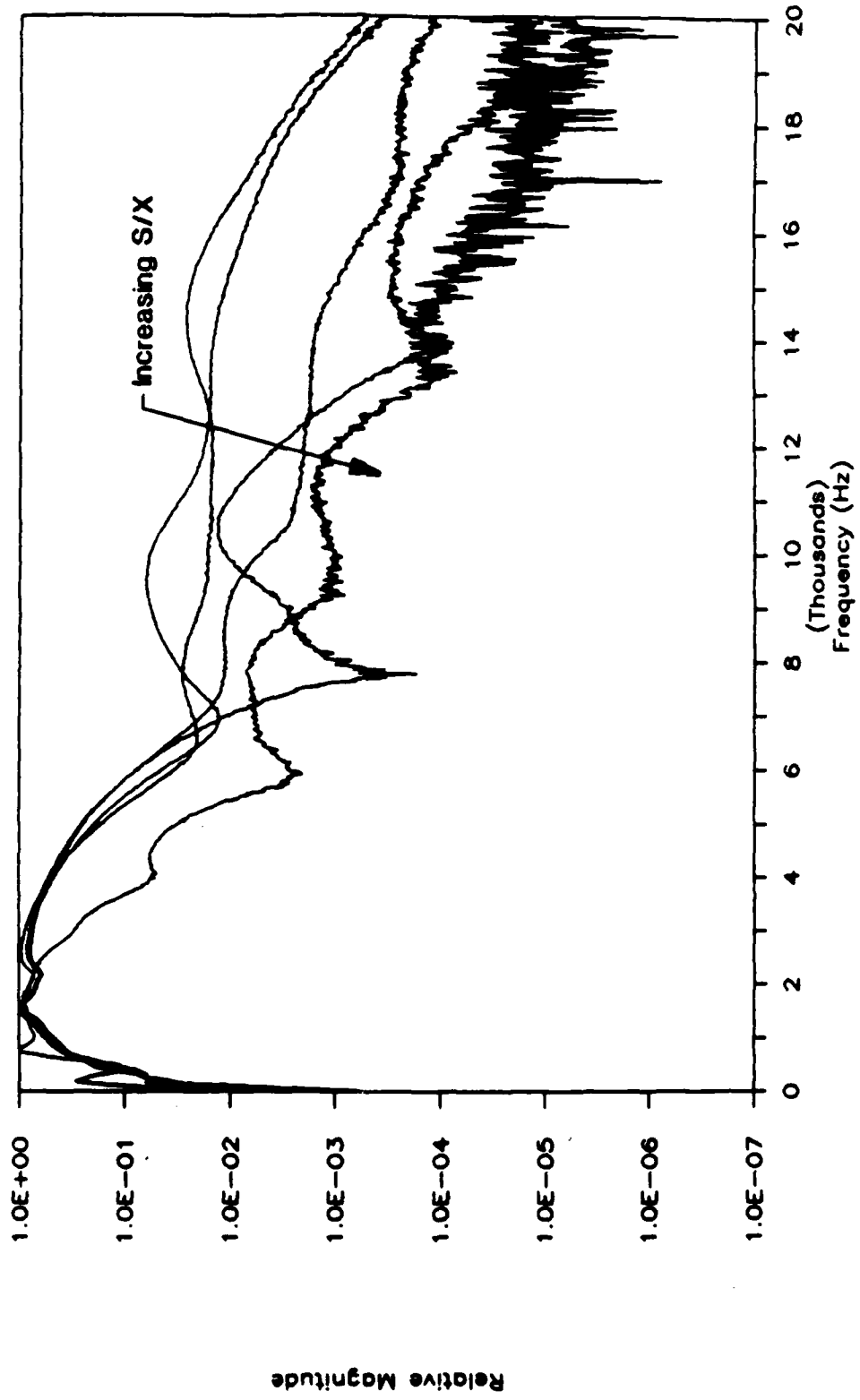


Figure B.2 - Magnitude (Relative) of Cross Power Spectrum for X = 0.5 ft for G. G. Brown Parking Lot Site

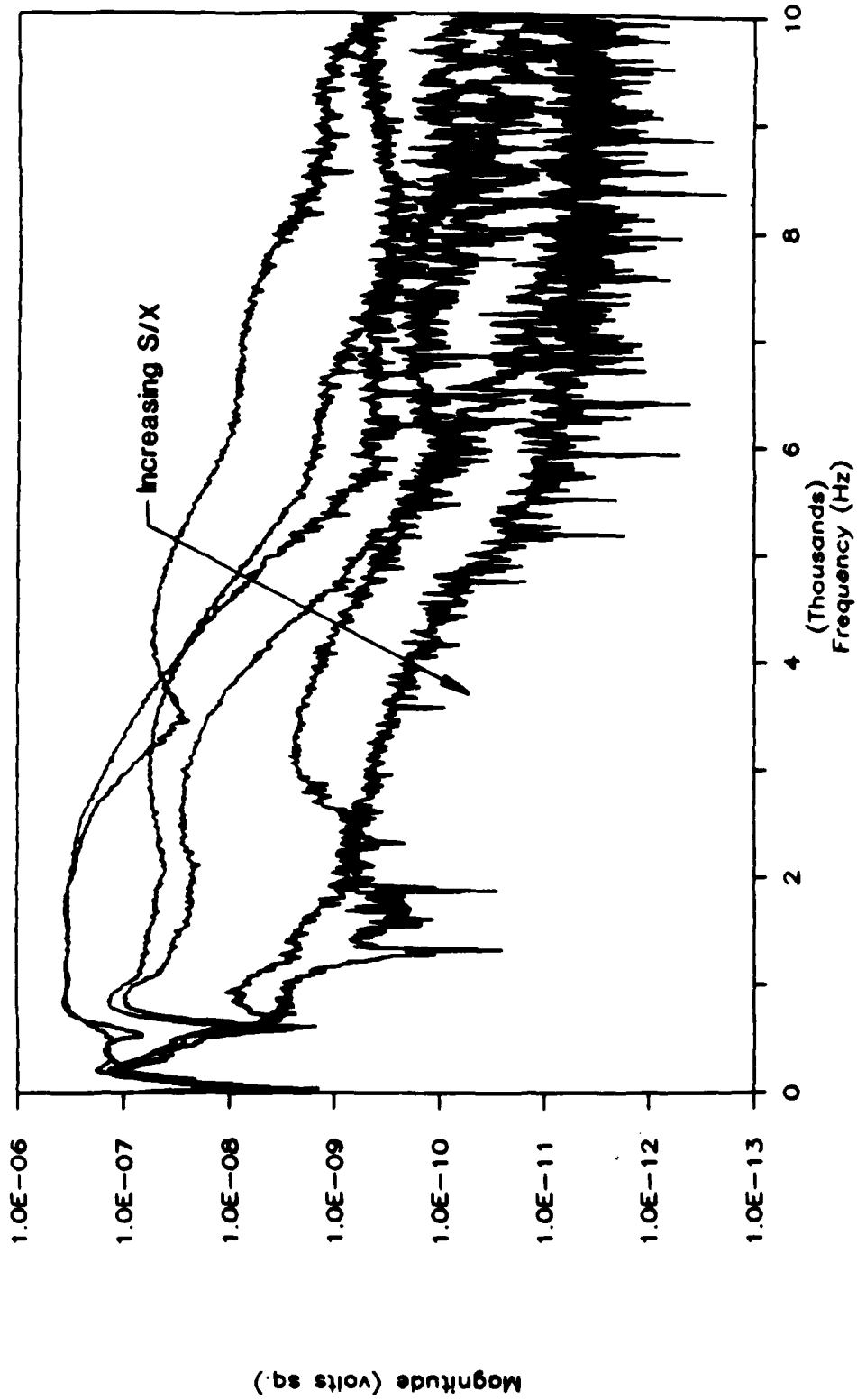


Figure B.3 - Magnitude (Absolute) of Cross Power Spectrum for X = 1.0 ft for G. G. Brown Parking Lot Site

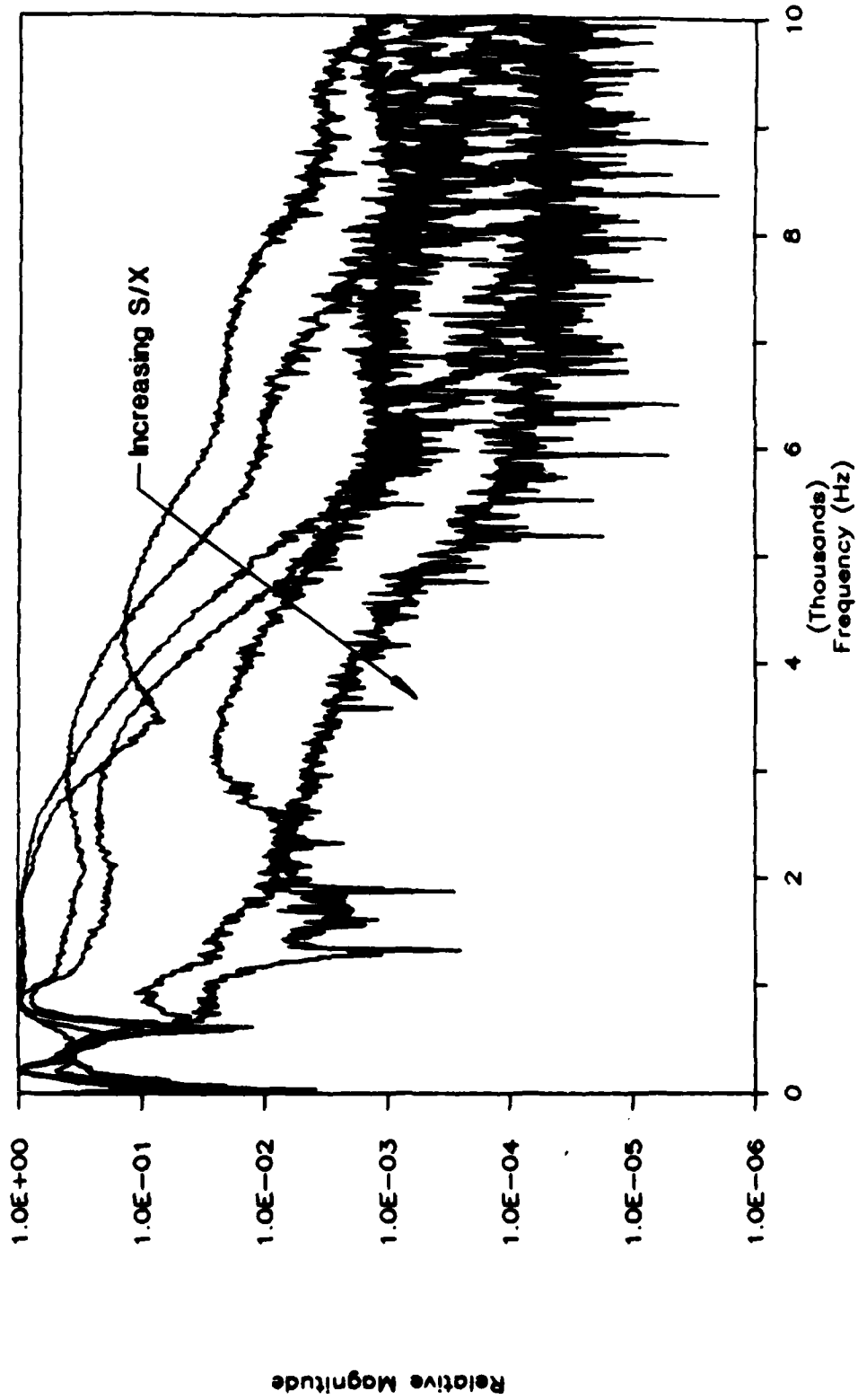


Figure B.4 - Magnitude (Relative) of Cross Power Spectrum for X = 1.0 ft for G. G. Brown Parking Lot Site

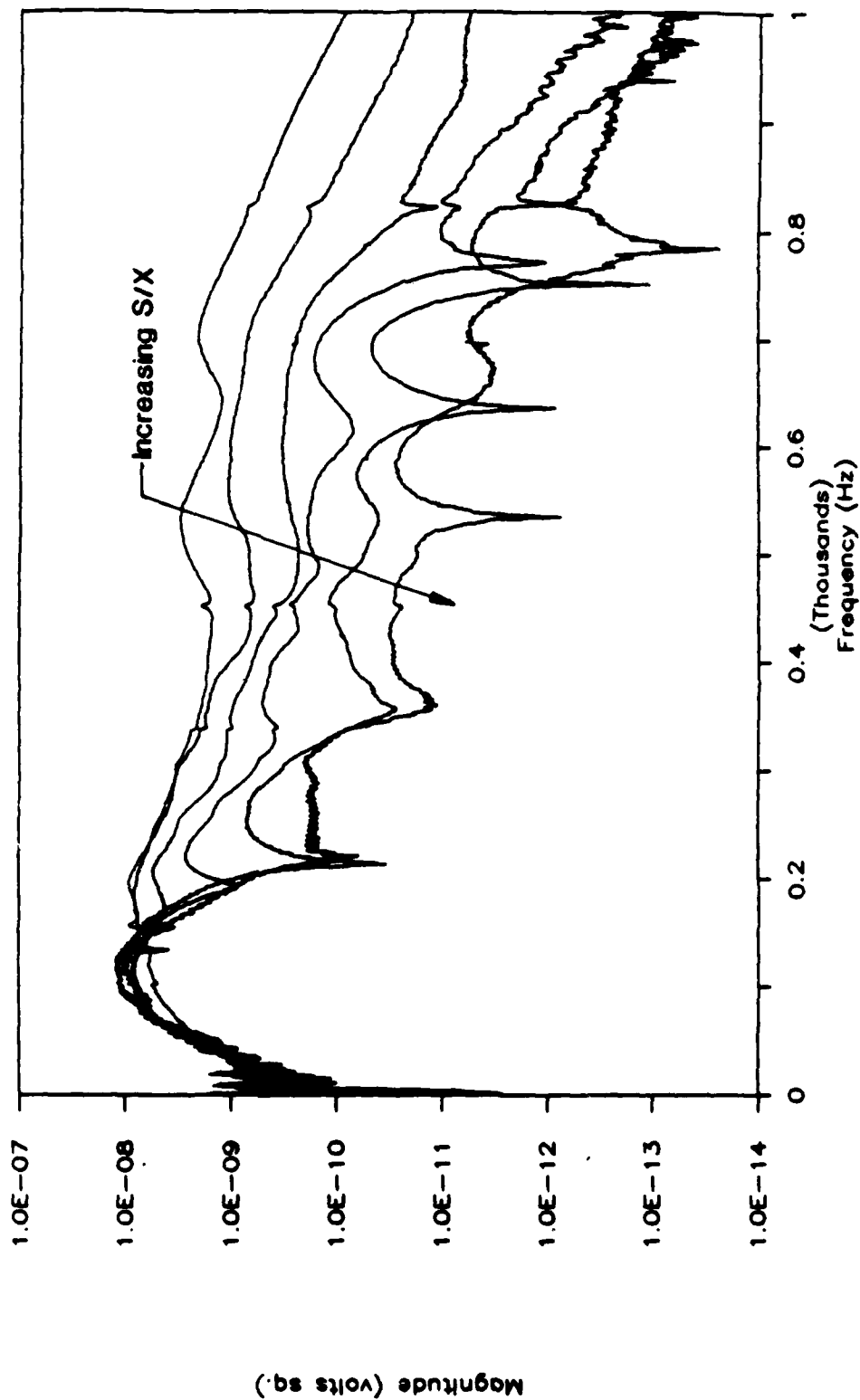


Figure B.5 - Magnitude (Absolute) of Cross Power Spectrum for X = 2.0 ft for G. G. Brown Parking Lot Site

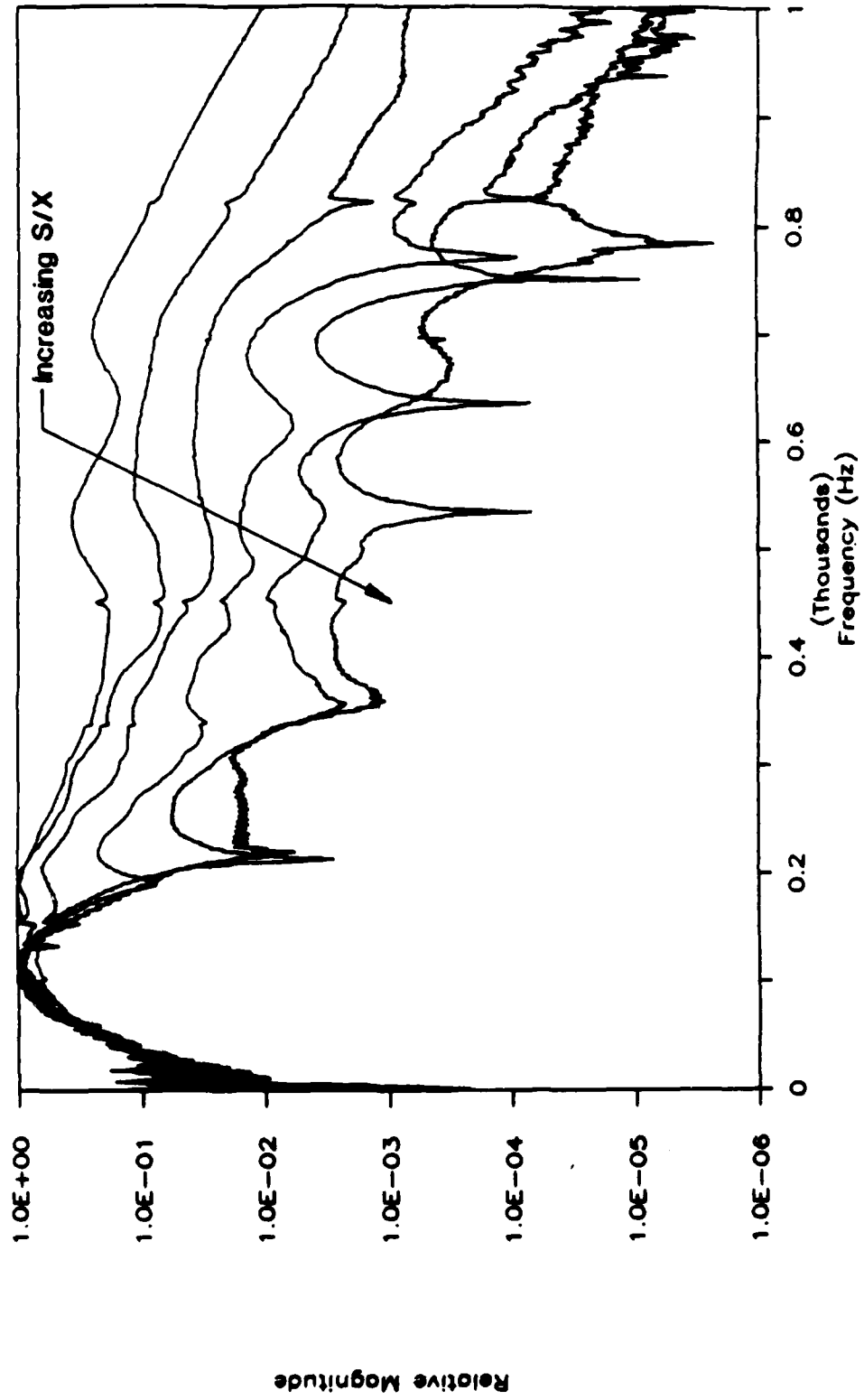


Figure B.6 - Magnitude (Relative) of Cross Power Spectrum for X = 2.0 ft for G. G. Brown Parking Lot Site

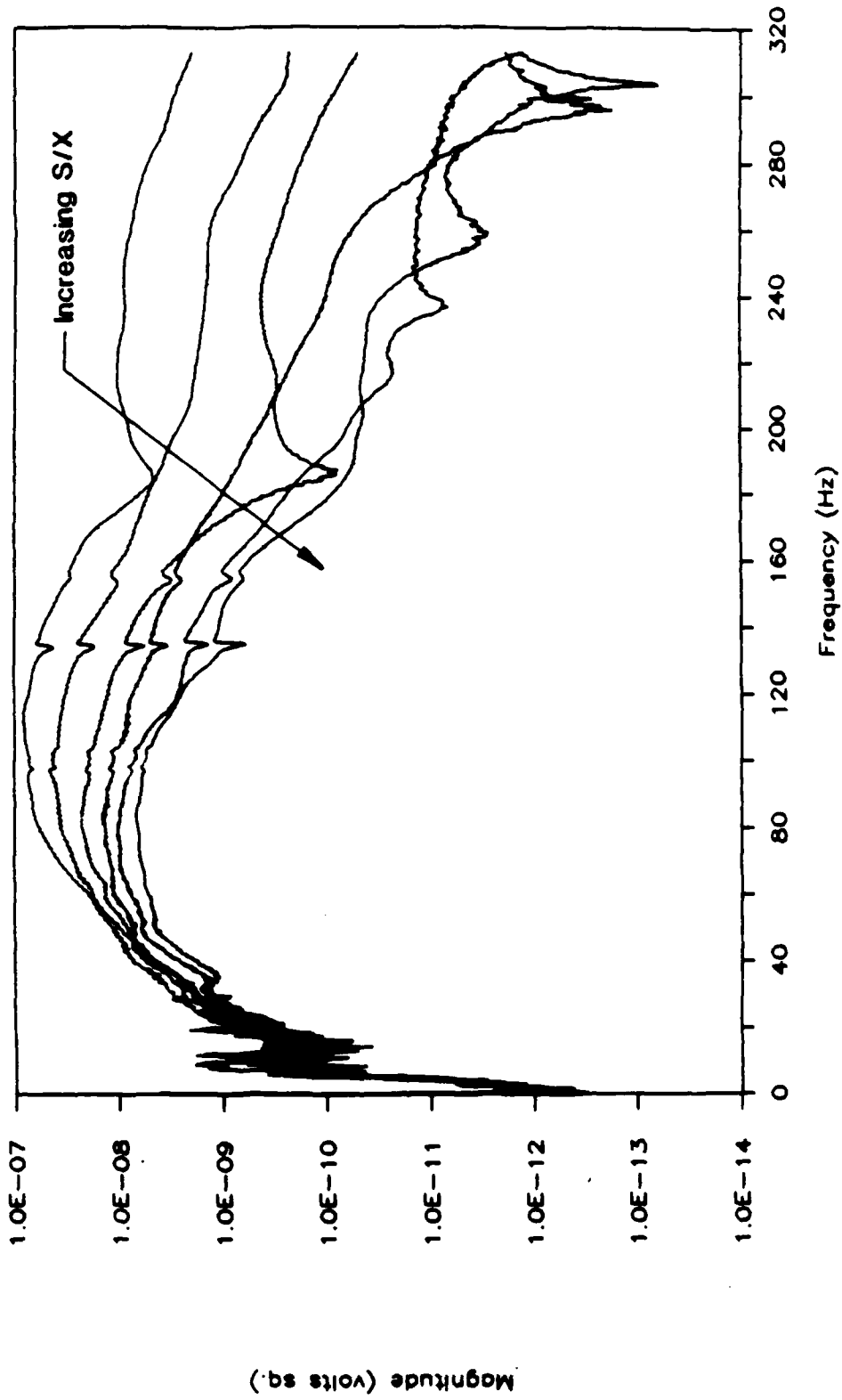


Figure B.7 - Magnitude (Absolute) of Cross Power Spectrum for $X = 4.0$ ft for G. G. Brown Parking Lot Site

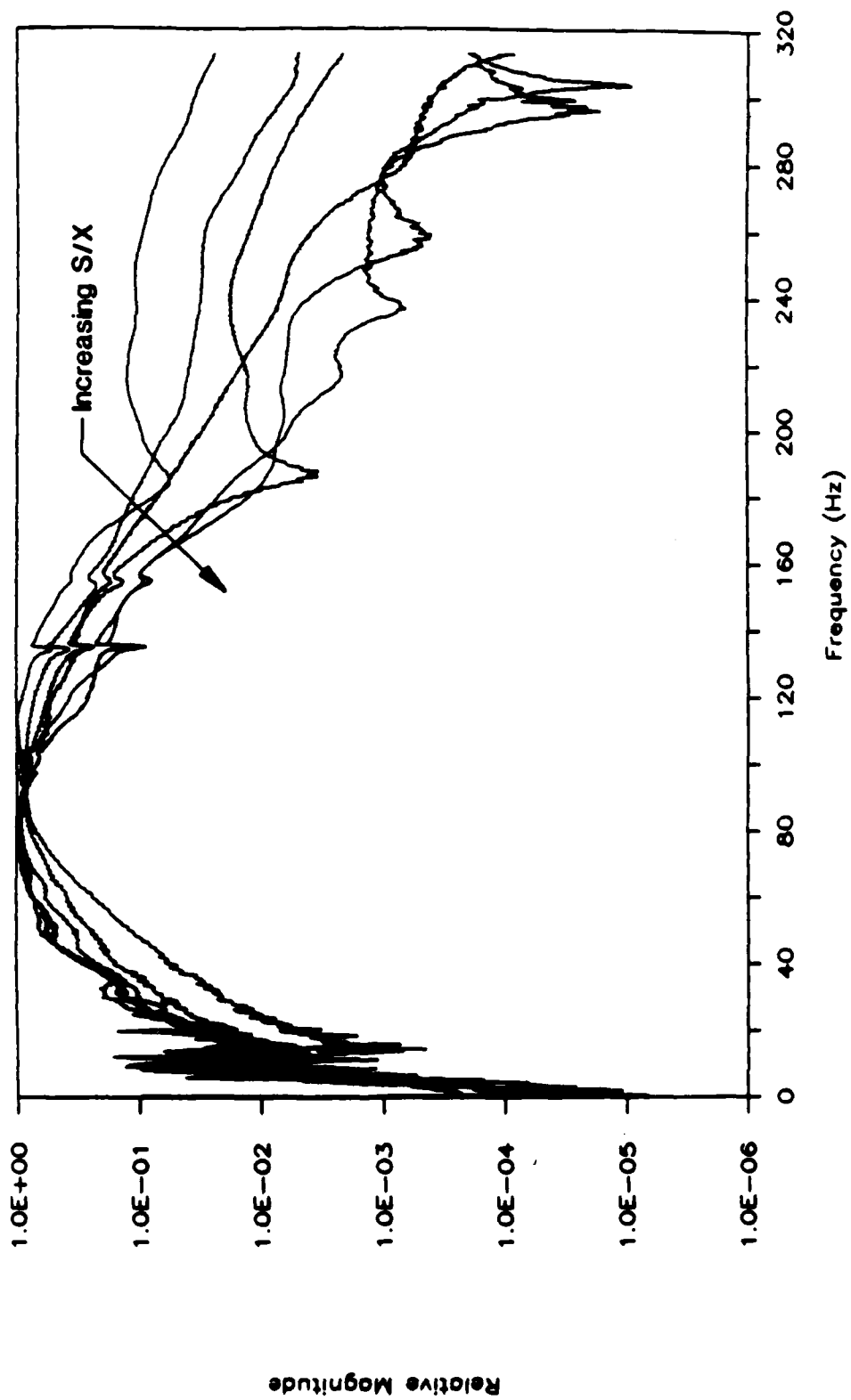


Figure B.8 - Magnitude (Relative) of Cross Power Spectrum for $X = 4.0$ ft for G. G. Brown Parking Lot Site

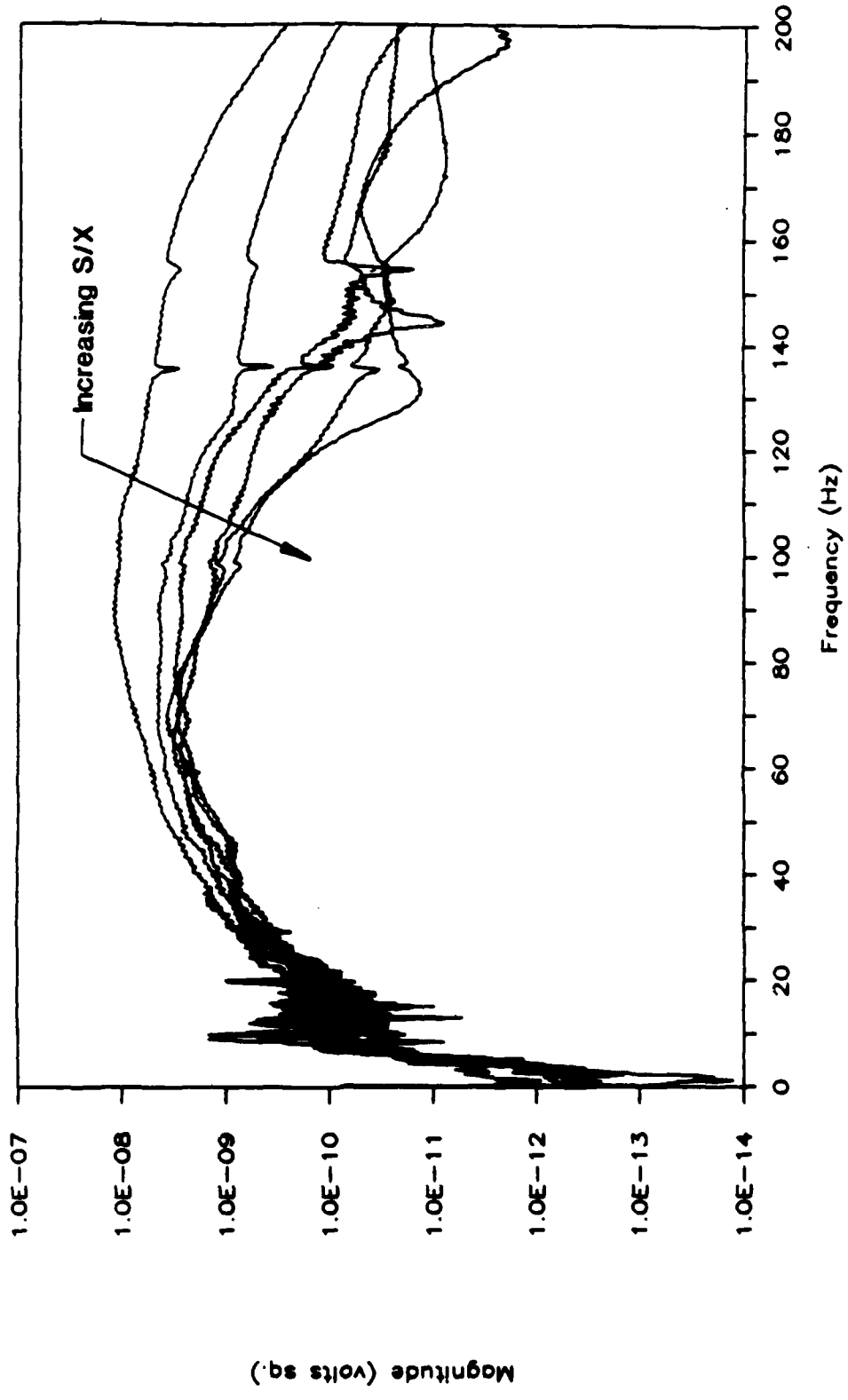


Figure B.9 - Magnitude (Absolute) of Cross Power Spectrum for X = 8.0 ft for G. G. Brown Parking Lot Site

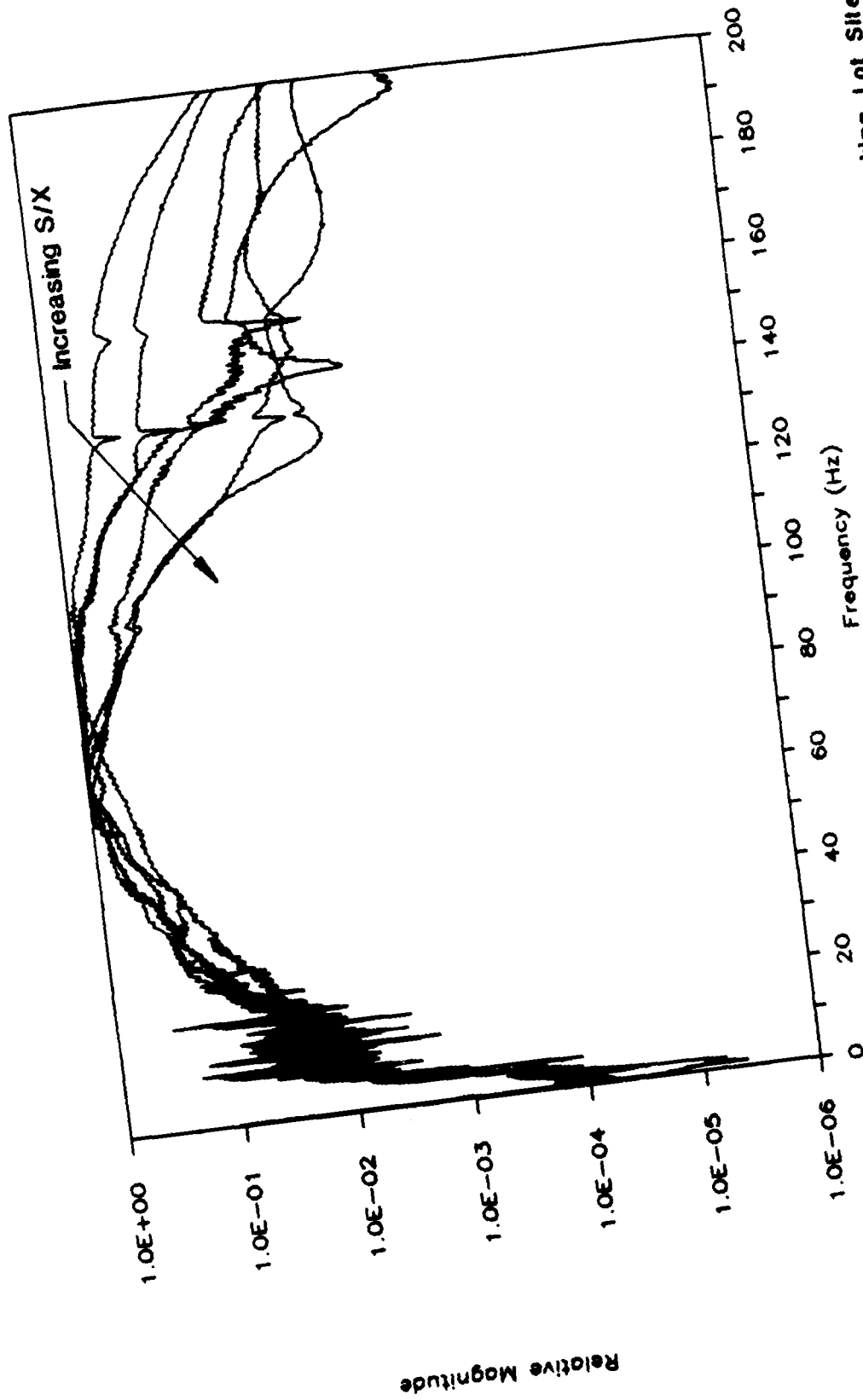


Figure B.10 - Magnitude (Relative) of Cross Power Spectrum for X = 8.0 ft for G. G. Brown Parking Lot Site

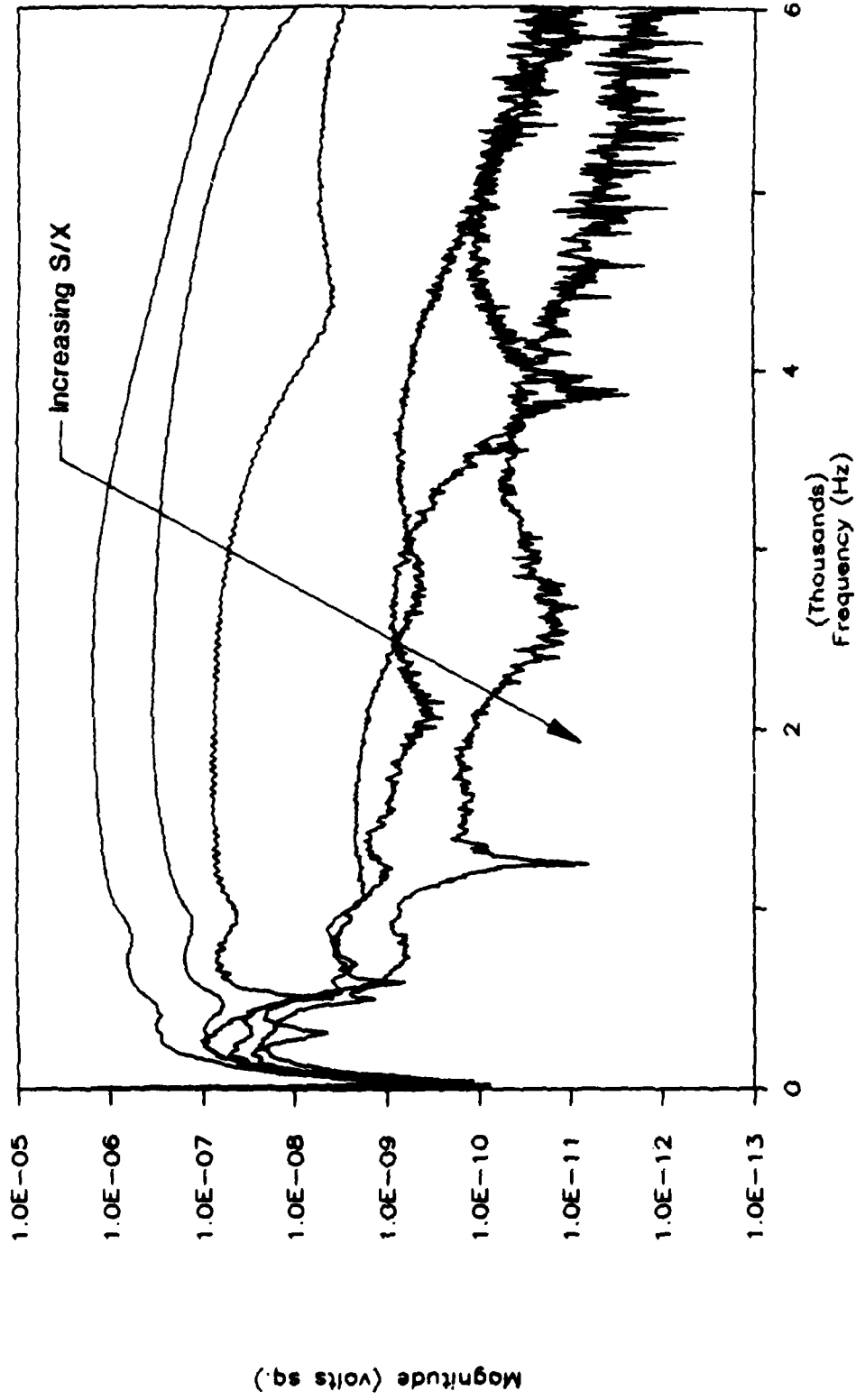


Figure B.11 - Magnitude (Absolute) of Cross Power Spectrum for X = 1.0 ft for SENTA Parking Lot Site

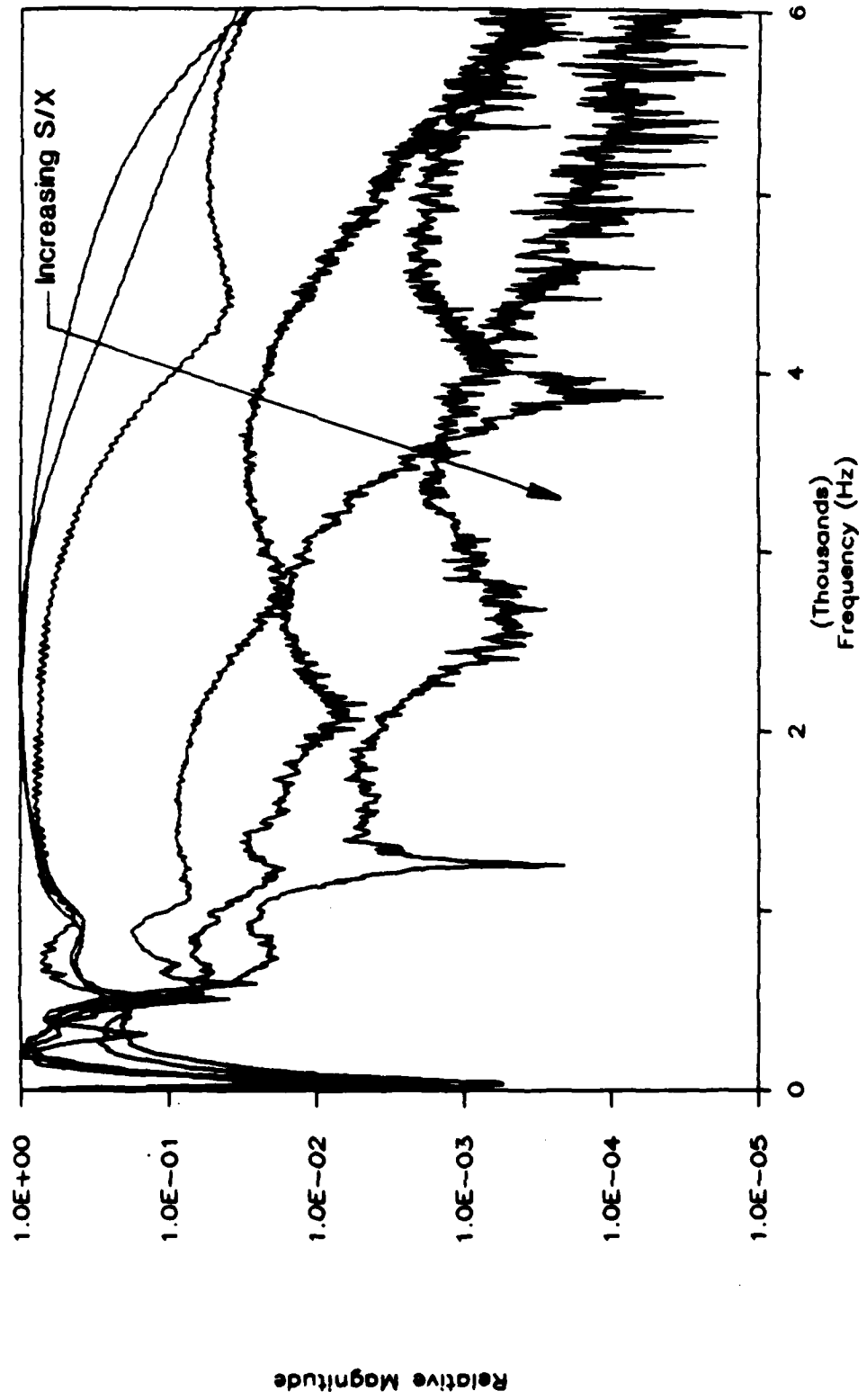


Figure B.12 - Magnitude (Relative) of Cross Power Spectrum for X = 1.0 ft for SEMTA Parking Lot Site

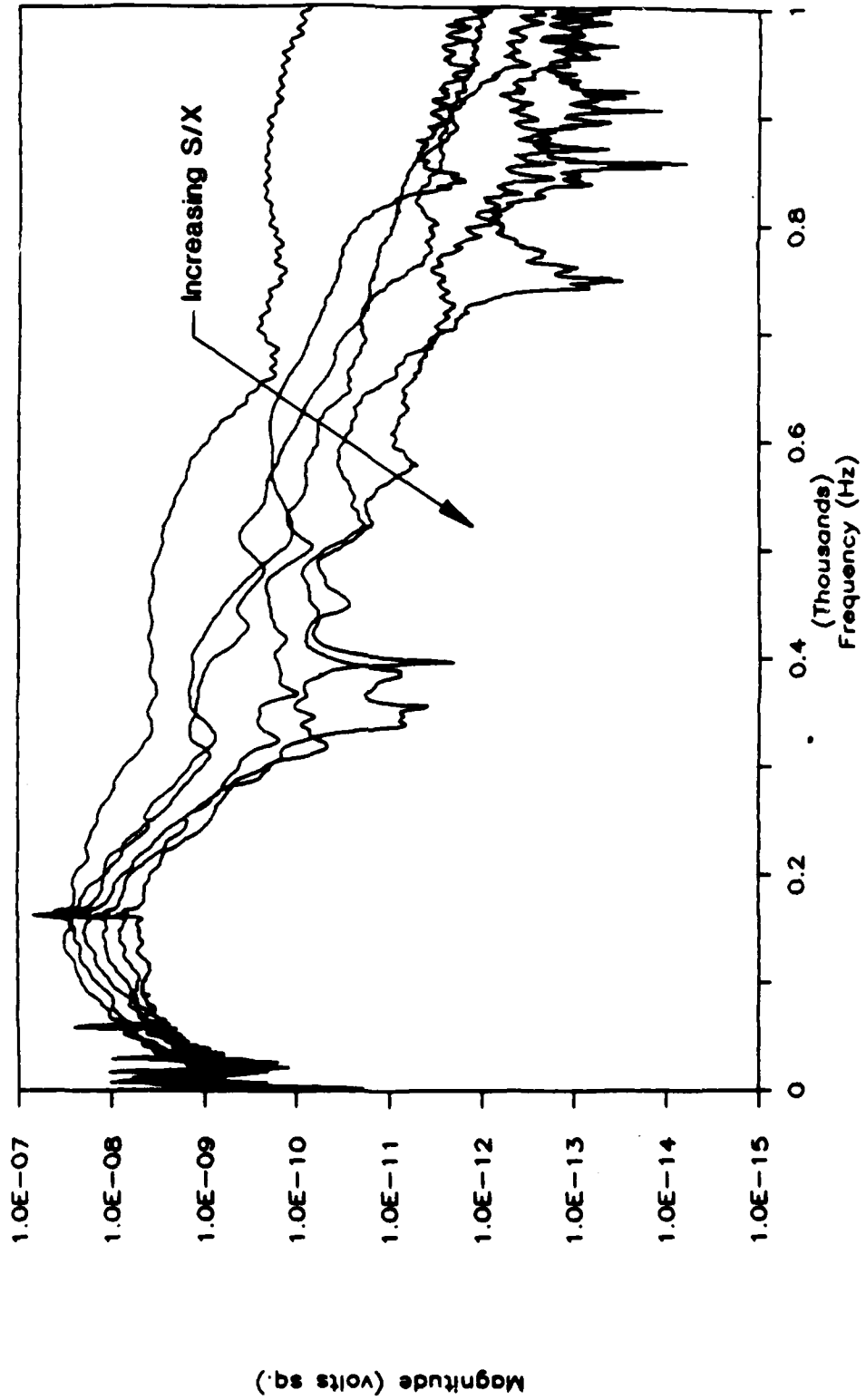


Figure B.13 - Magnitude (Absolute) of Cross Power Spectrum for X = 2.0 ft for SEMTA Parking Lot Site

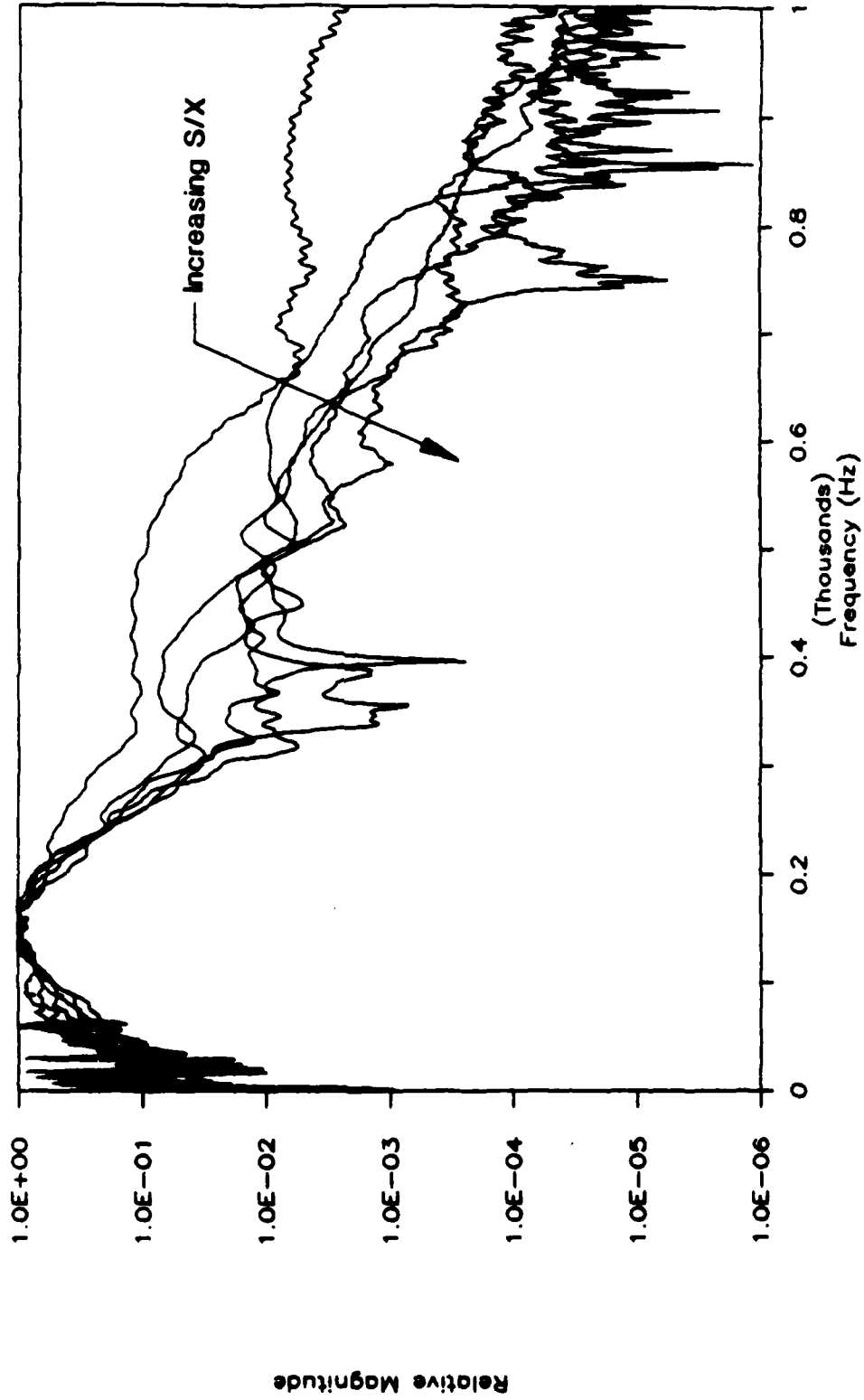


Figure B.14 - Magnitude (Relative) of Cross Power Spectrum for X = 2.0 ft for SEMTA Parking Lot Site

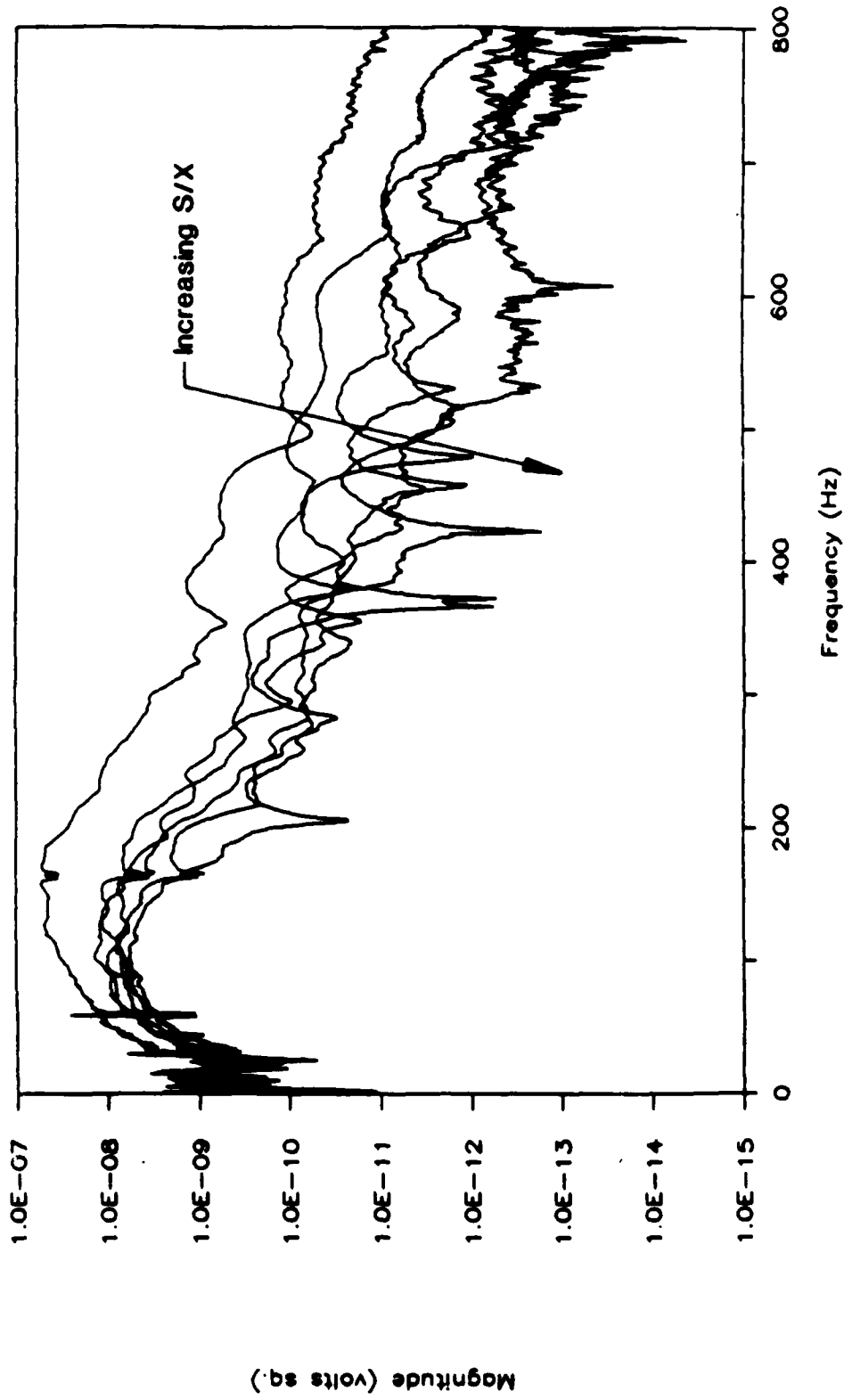


Figure B.15 - Magnitude (Absolute) of Cross Power Spectrum for X = 4.0 ft for SEMTA Parking Lot Site

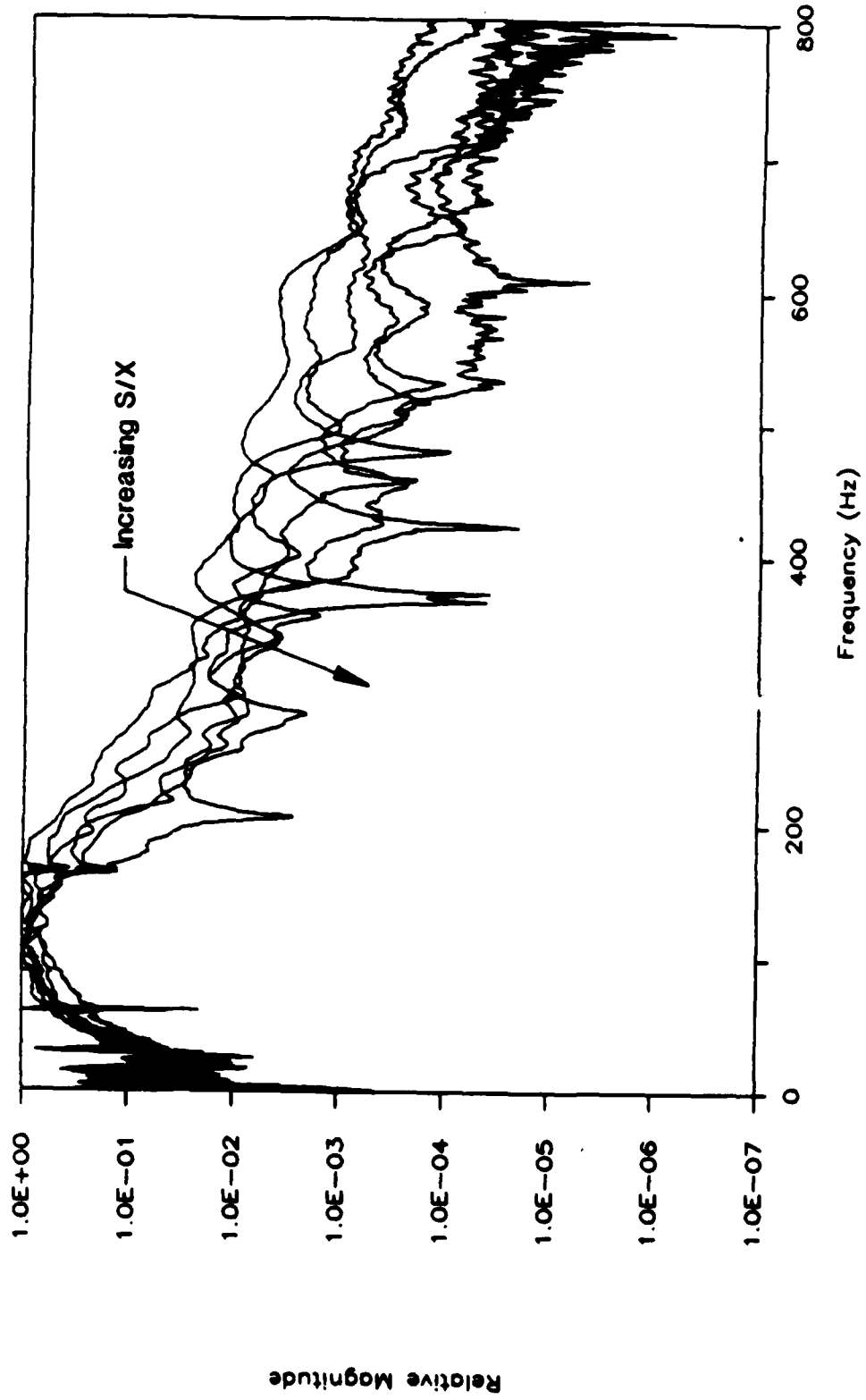


Figure B.16 - Magnitude (Relative) of Cross Power Spectrum for X = 4.0 ft for SEMTA Parking Lot Site

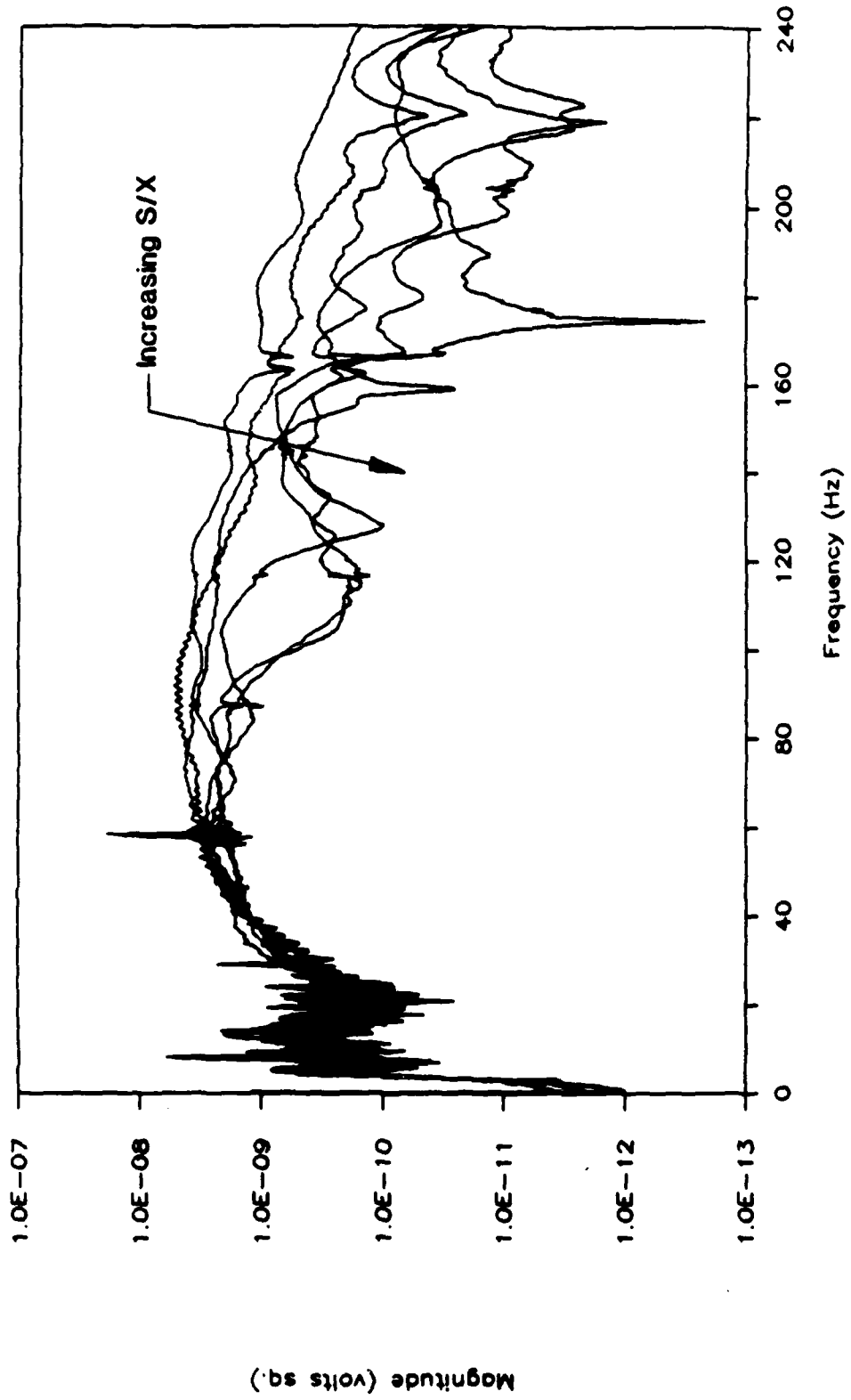


Figure B.17 - Magnitude (Absolute) of Cross Power Spectrum for X = 8.0 ft for SEMTA Parking Lot Site

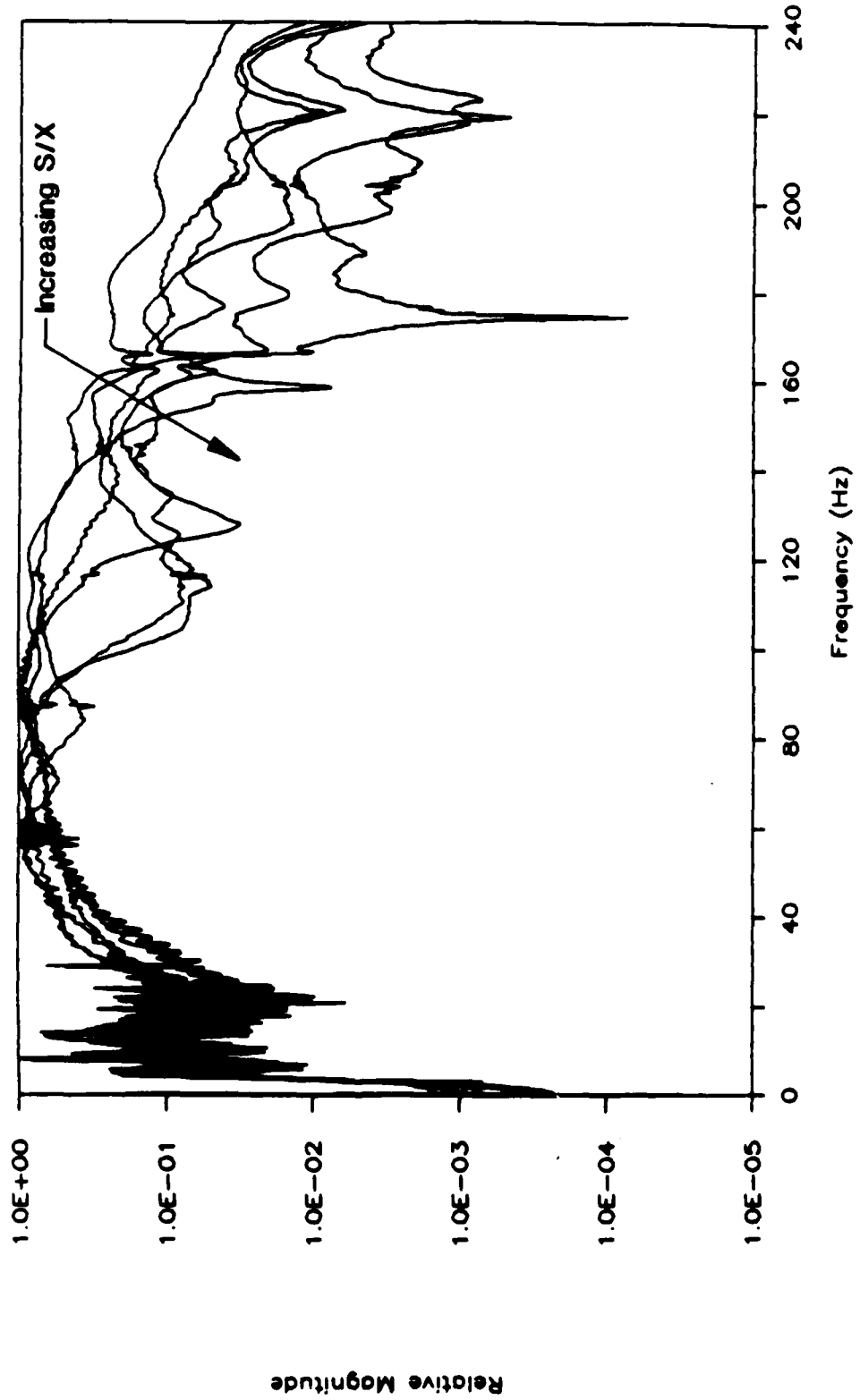


Figure B.10 - Magnitude (Relative) of Cross Power Spectrum for X = 8.0 ft for SEMTA Parking Lot Site

APPENDIX C

COMBINED DISPERSION CURVES FOR CONSTANT X/L_R FOR SEMTA
PARKING LOT SITE

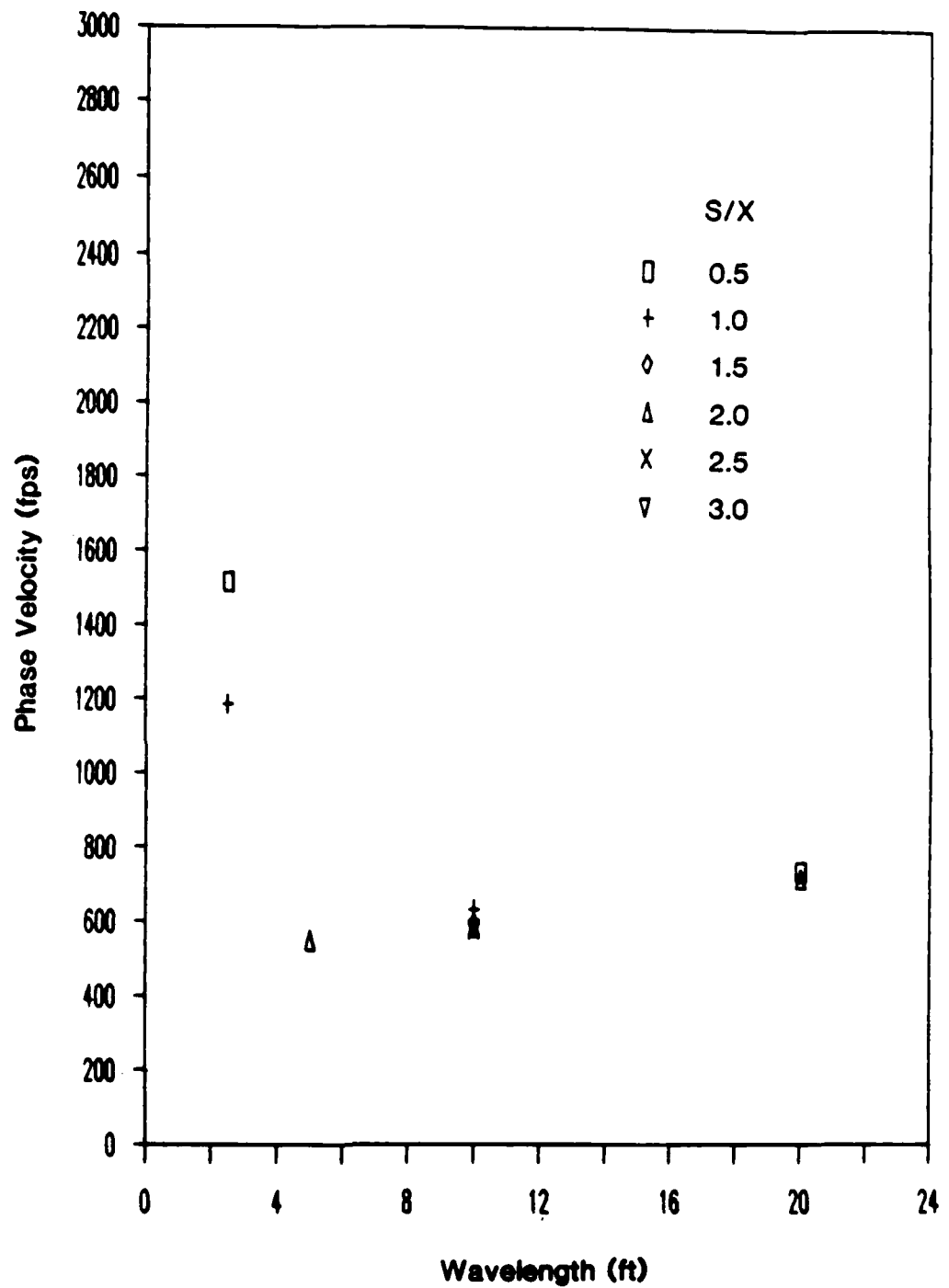


Figure C.1— Experimental Dispersion Curves for $X/L_R = 0.2$ for SEMTA Parking Lot Site

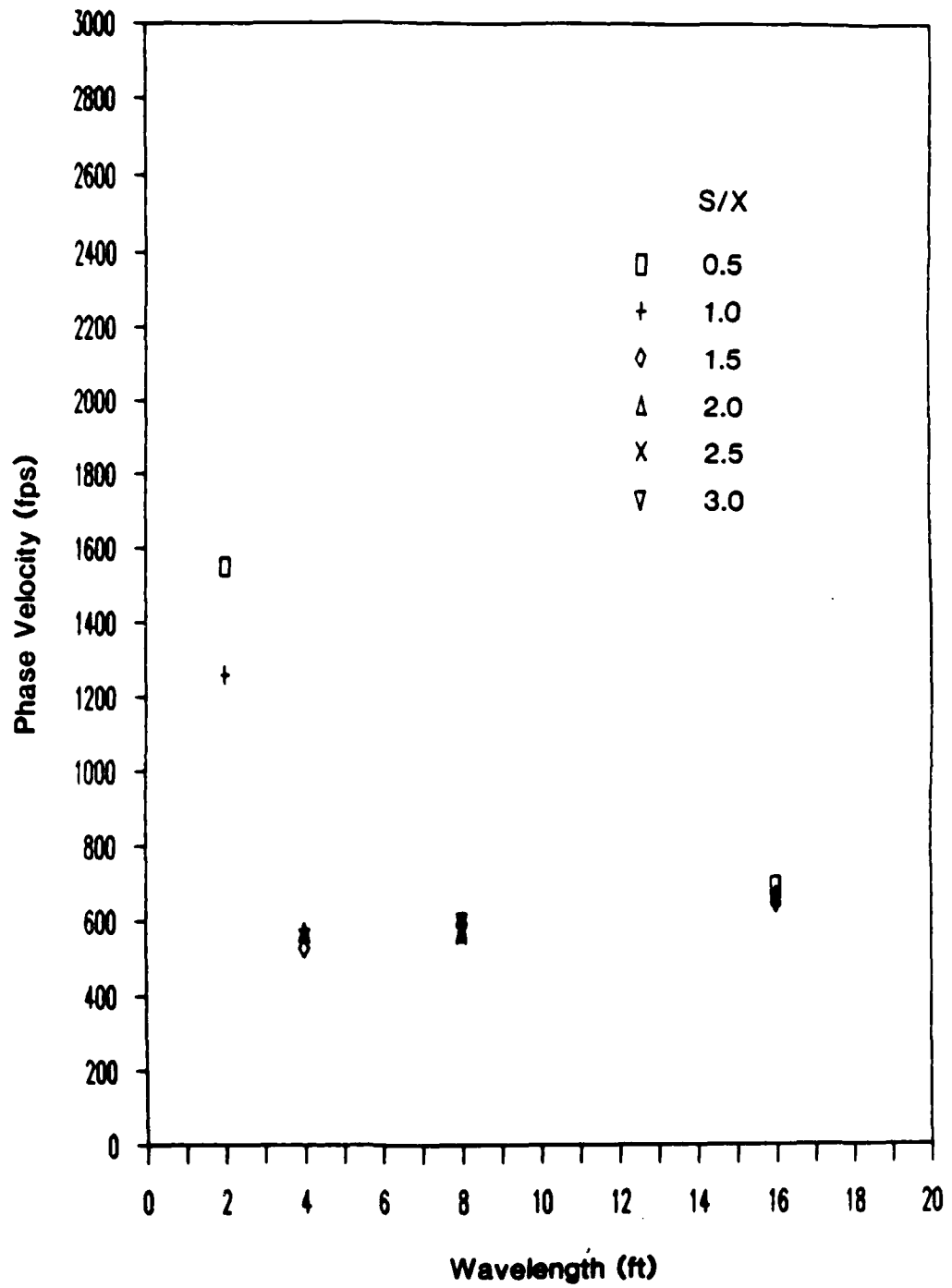


Figure C.2— Experimental Dispersion Curves for $X/L_R = 0.25$ for SEMTA Parking Lot Site

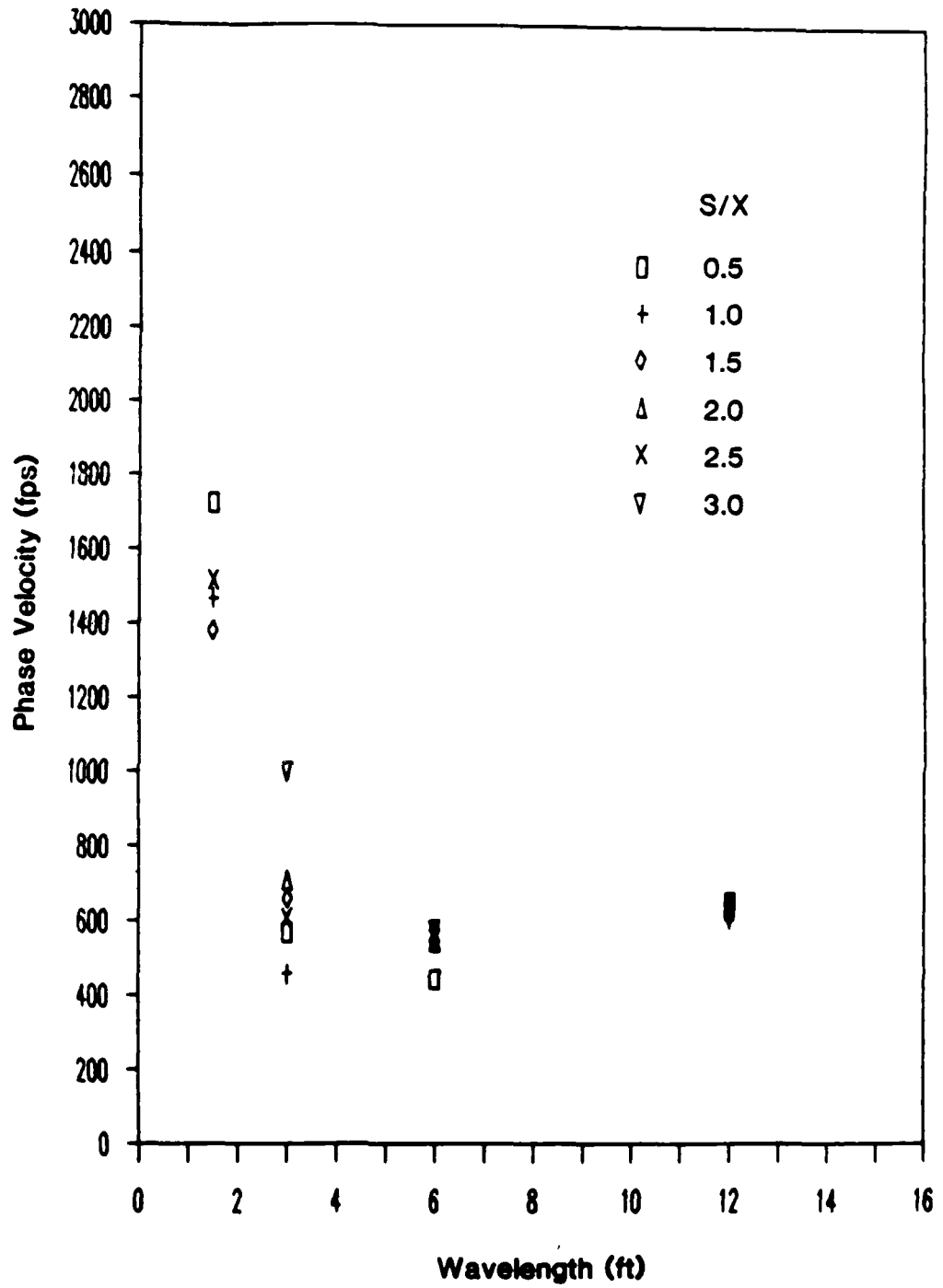


Figure C.3— Experimental Dispersion Curves for $X/L_R = 0.33$ for SEMTA Parking Lot Site

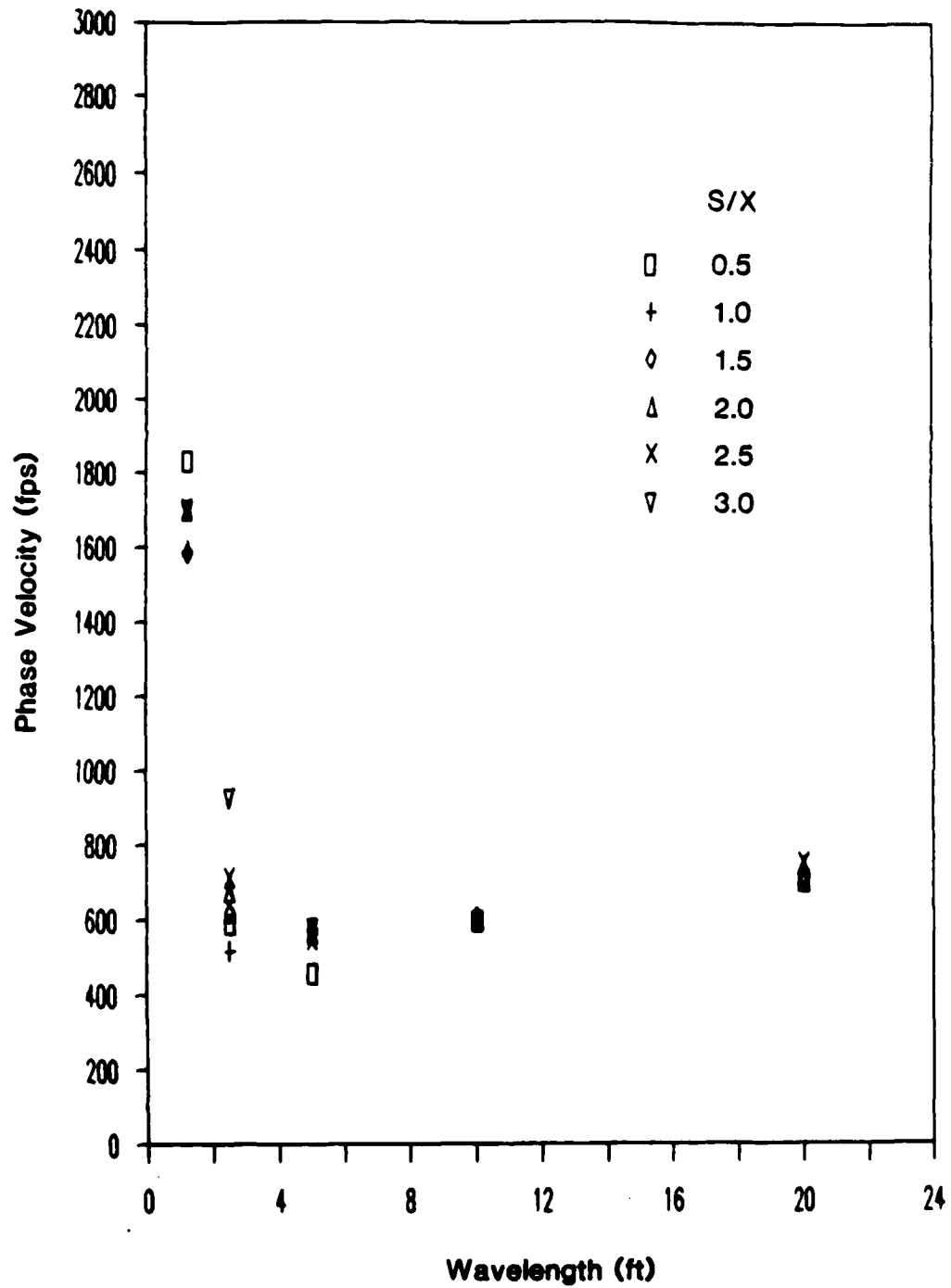


Figure C.4— Experimental Dispersion Curves for $X/L_R = 0.4$ for SEMTA Parking Lot Site

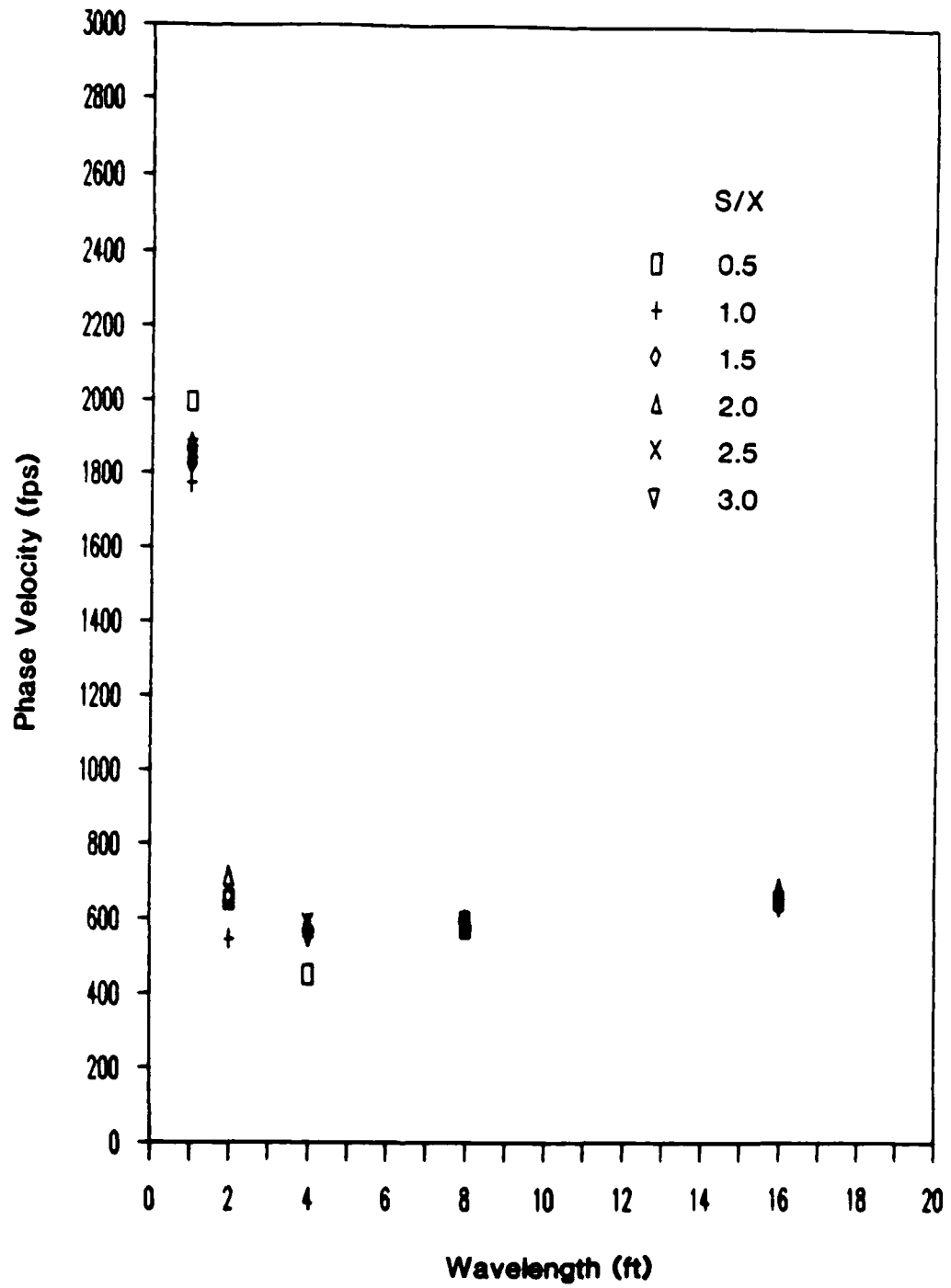


Figure C.5— Experimental Dispersion Curves for $X/L_R = 0.5$ for SEMTA Parking Lot Site

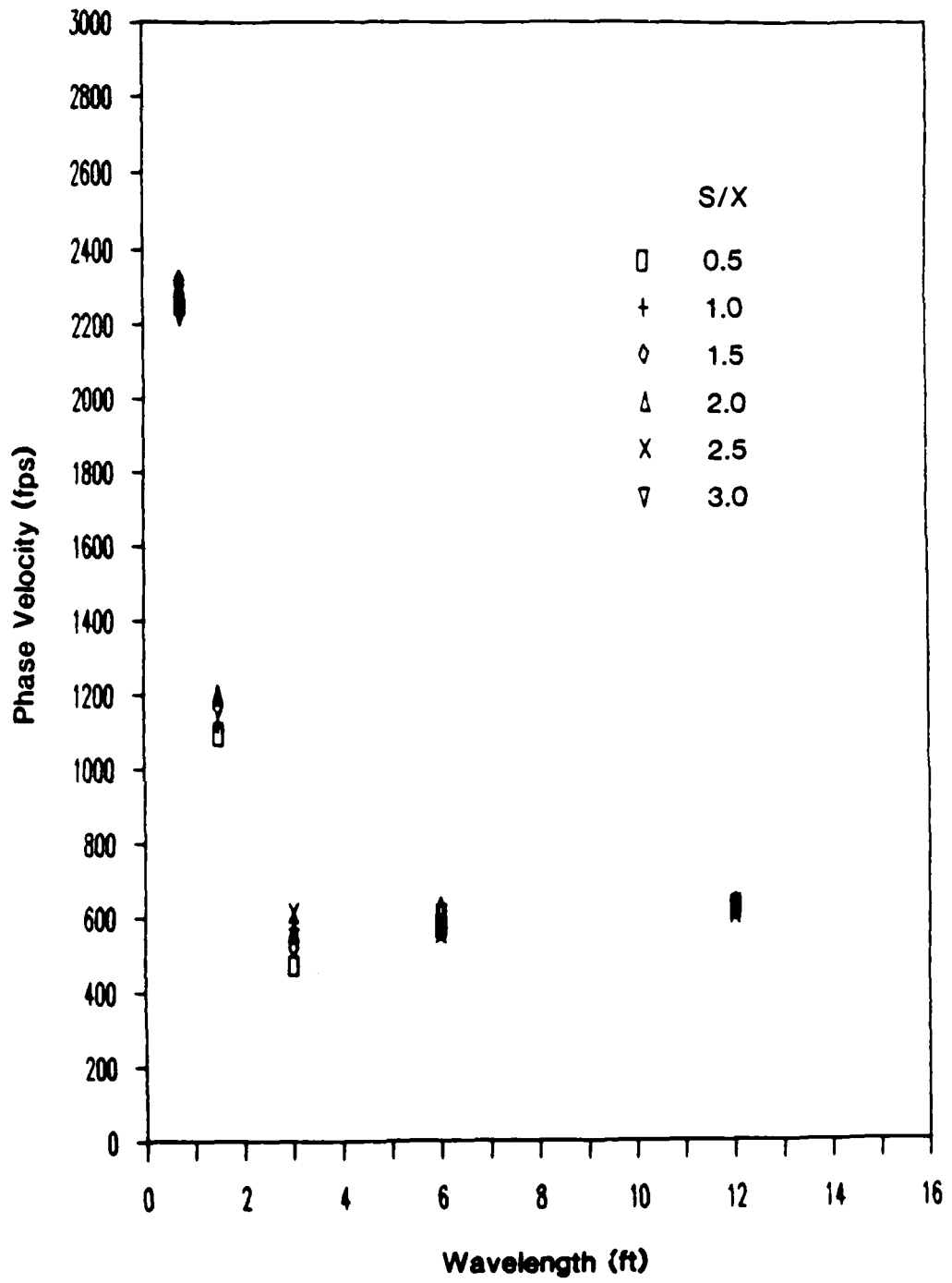


Figure C.6— Experimental Dispersion Curves for $X/L_R = 0.66$ for SEMTA Parking Lot Site

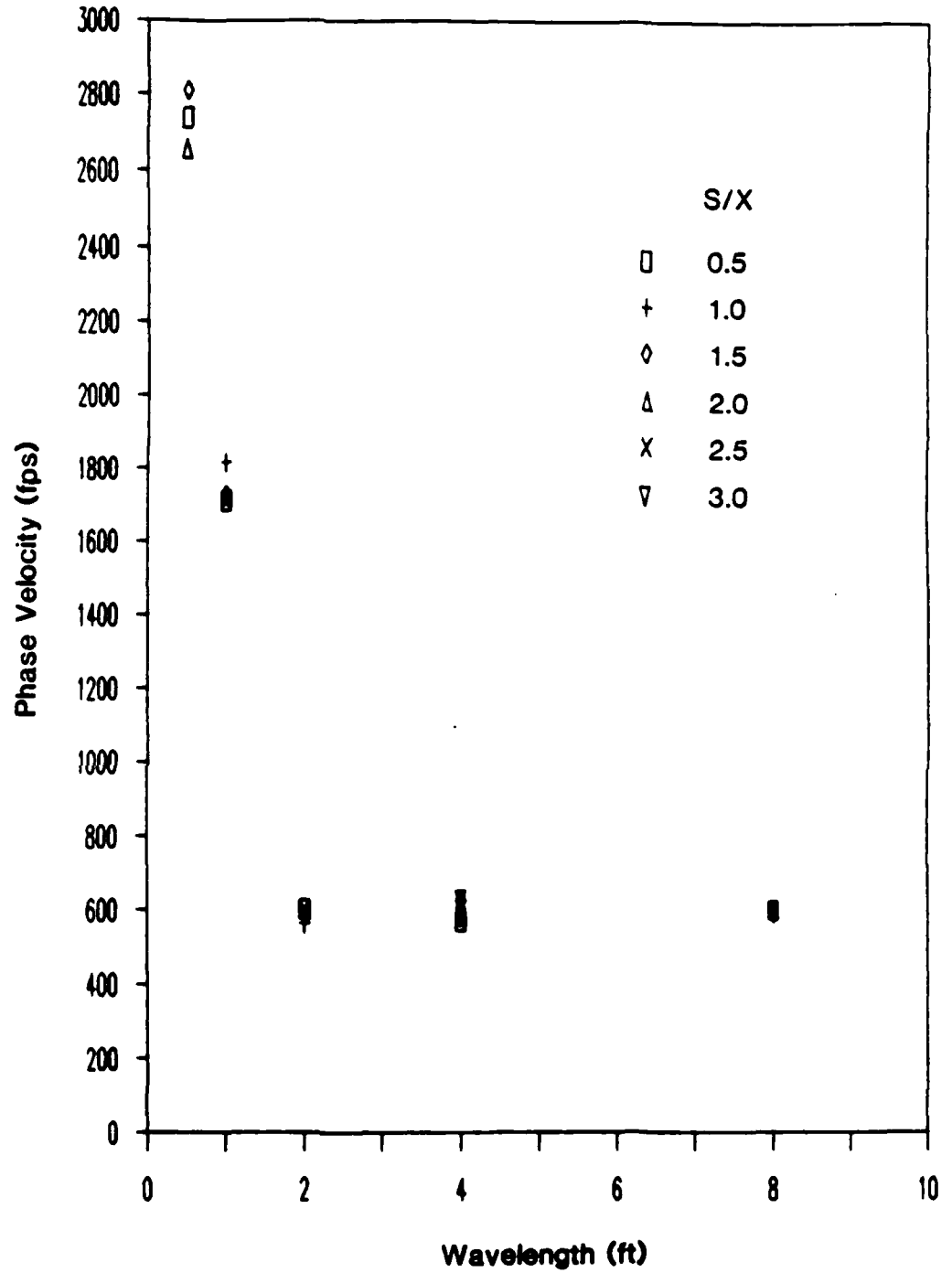


Figure C.7— Experimental Dispersion Curves for $X/L_R = 1.0$ for SEMTA
Parking Lot Site

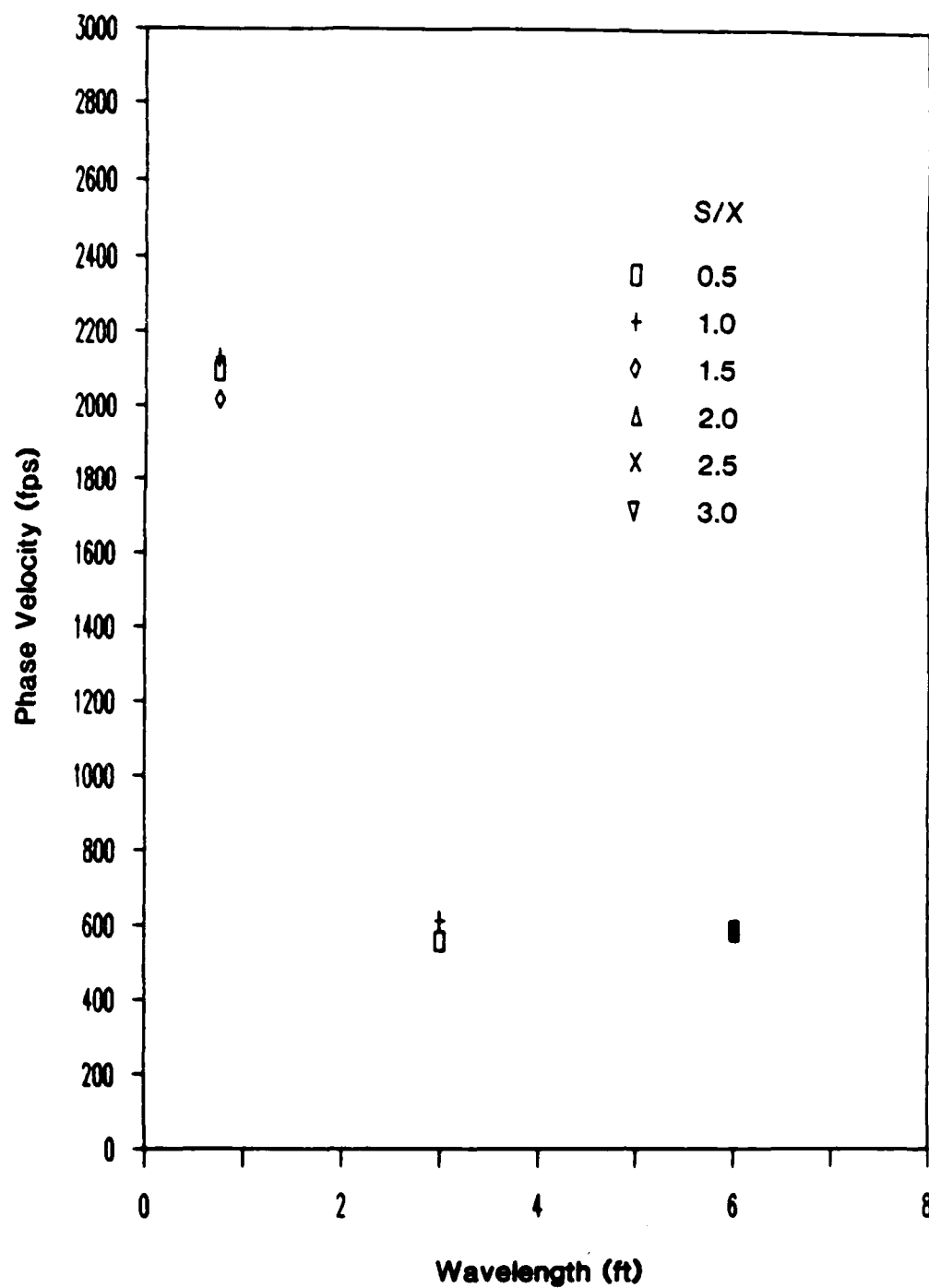


Figure C.8— Experimental Dispersion Curves for $X/L_R = 1.33$ for SEMTA Parking Lot Site

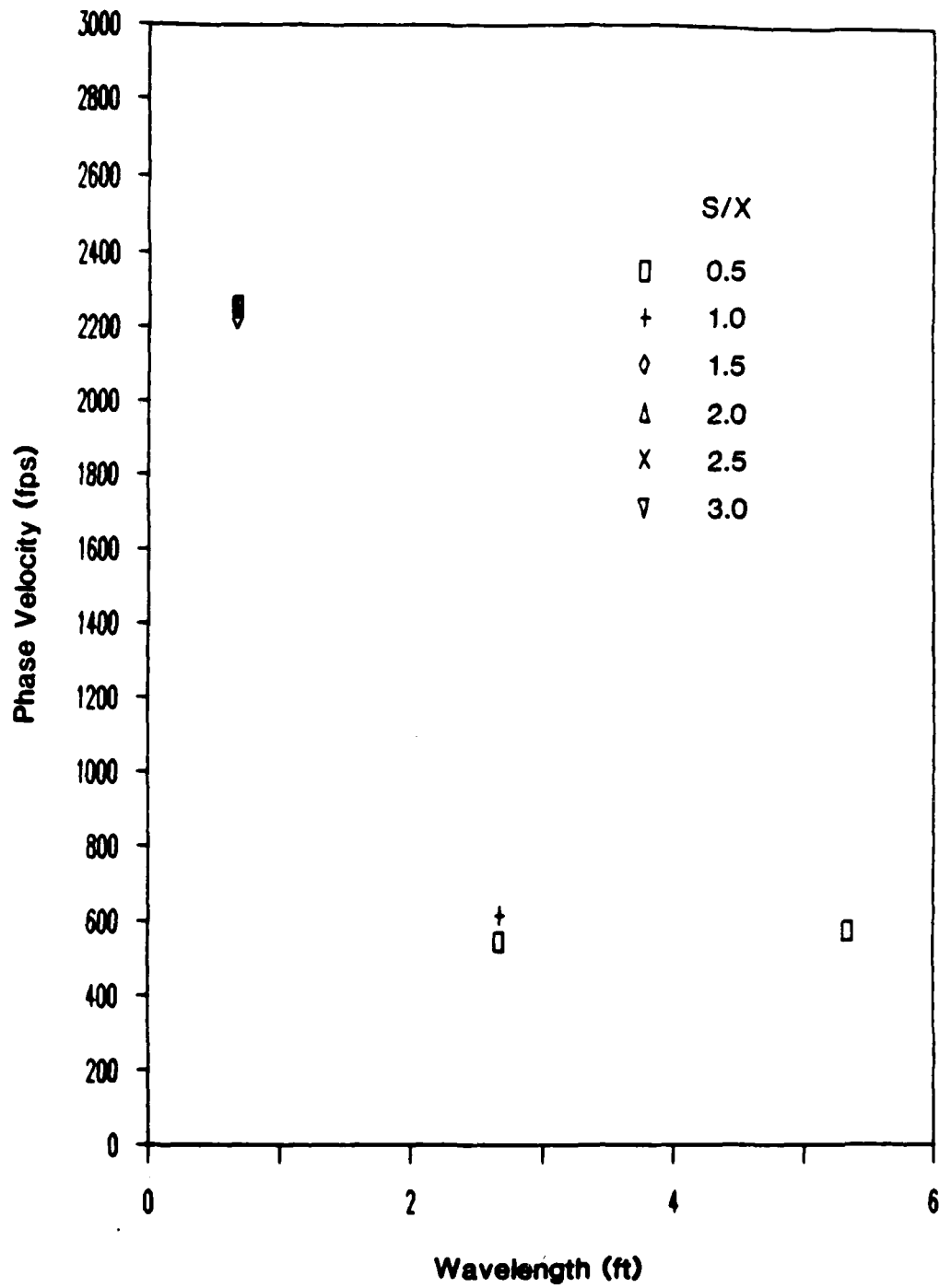


Figure C.9— Experimental Dispersion Curves for $X/L_R = 1.5$ for SEMTA Parking Lot Site

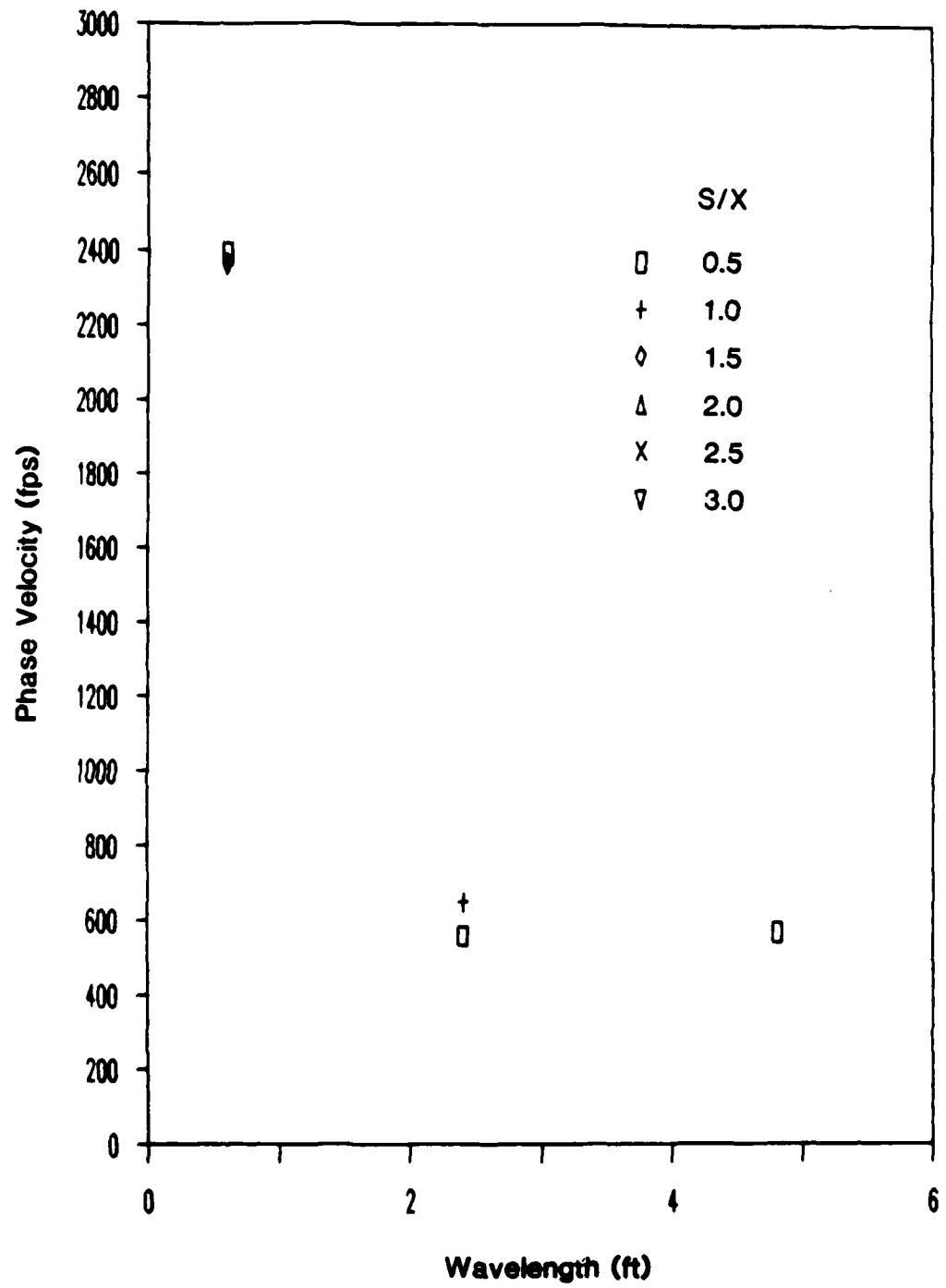


Figure C.10— Experimental Dispersion Curves for $X/L_R = 1.66$ for SEMTA Parking Lot Site

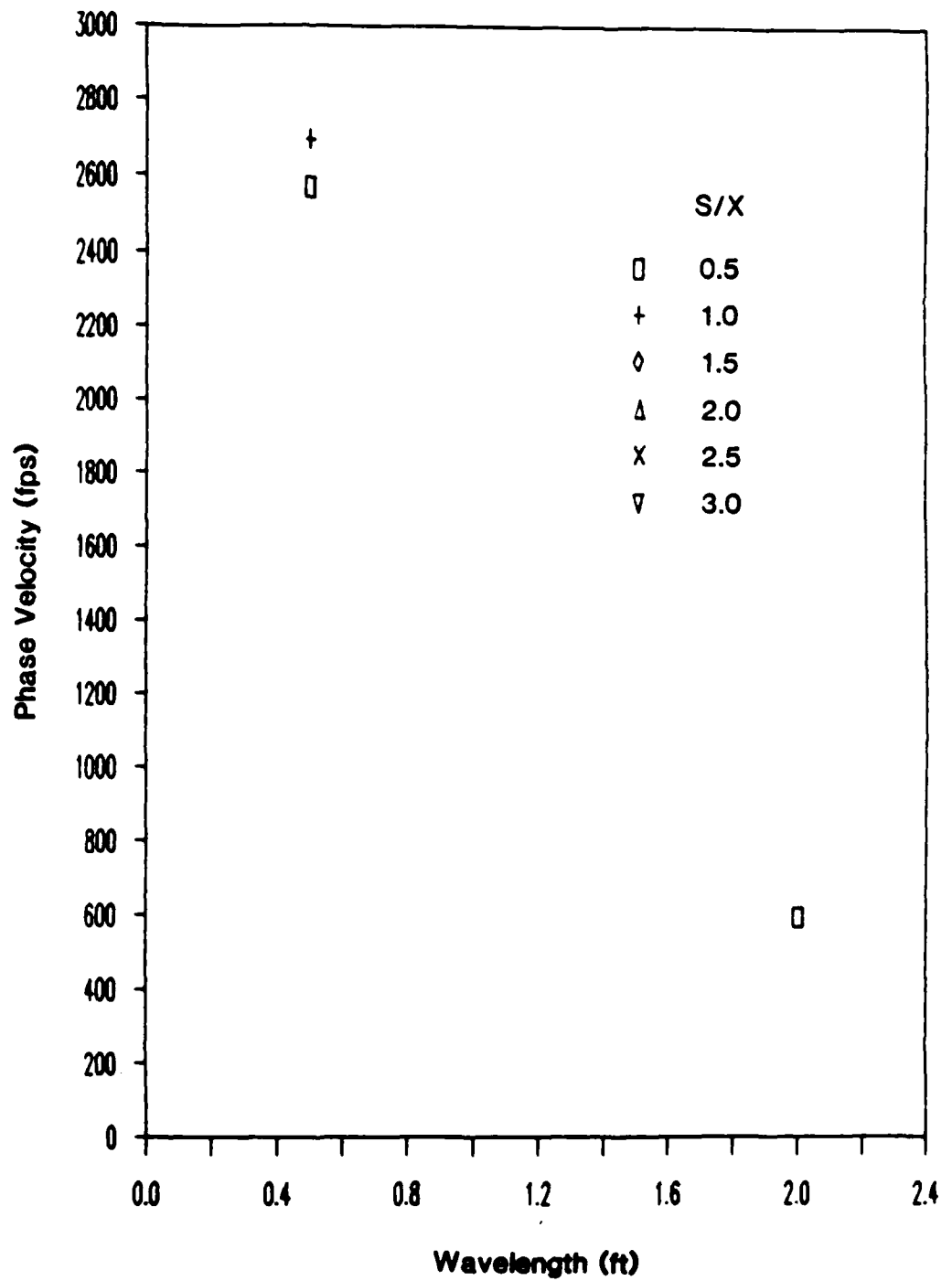


Figure C.11— Experimental Dispersion Curves for $X/L_R = 2.0$ for SEMTA
Parking Lot Site

APPENDIX D

COMBINED DISPERSION CURVES AS A FUNCTION OF
SOURCE-TO-NEAR-RECEIVER DISTANCE

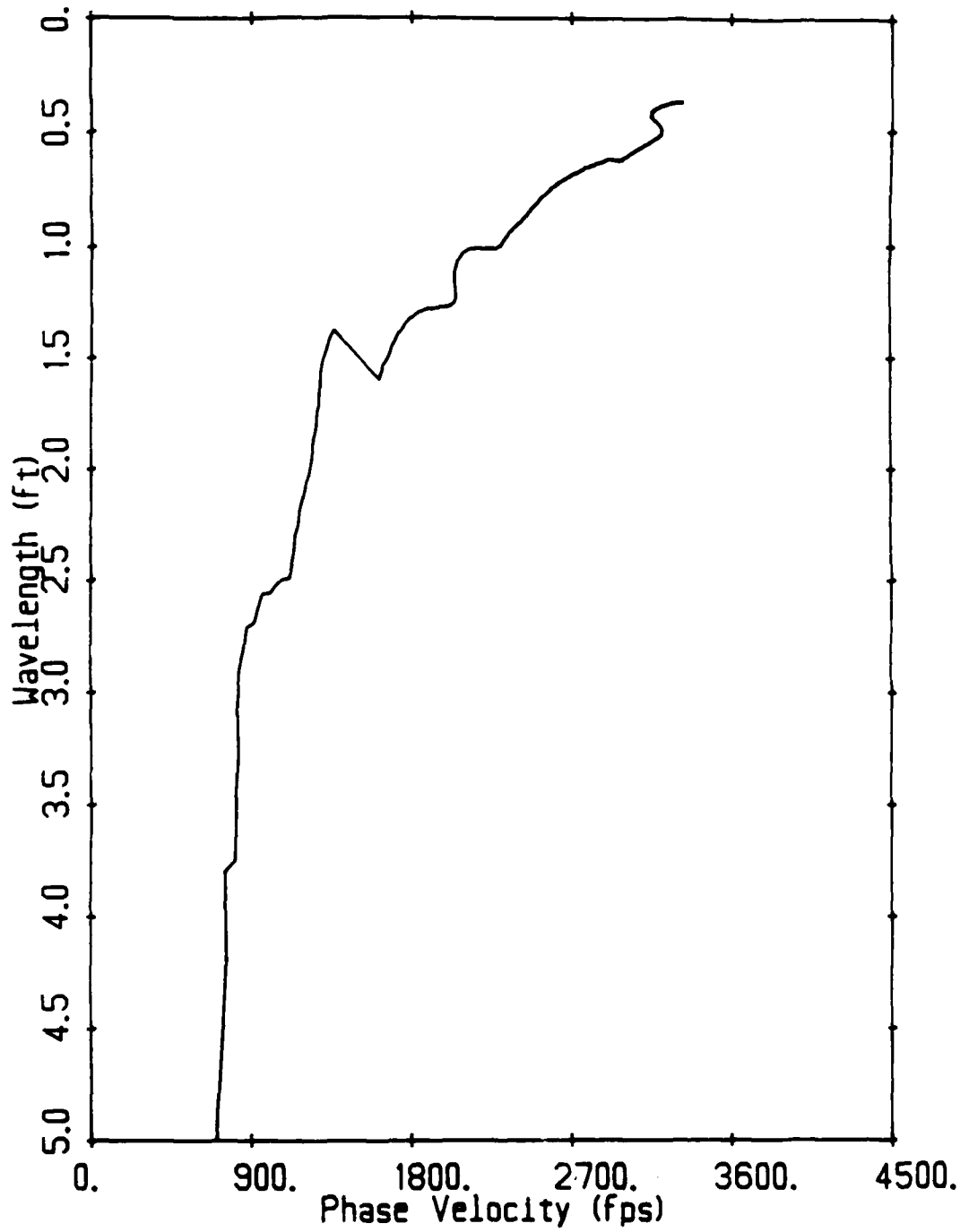


Figure D.1— Average Experimental Dispersion Curve (Unfiltered) for
 $S/X = 0.5$ for G. G. Brown Parking Lot Site

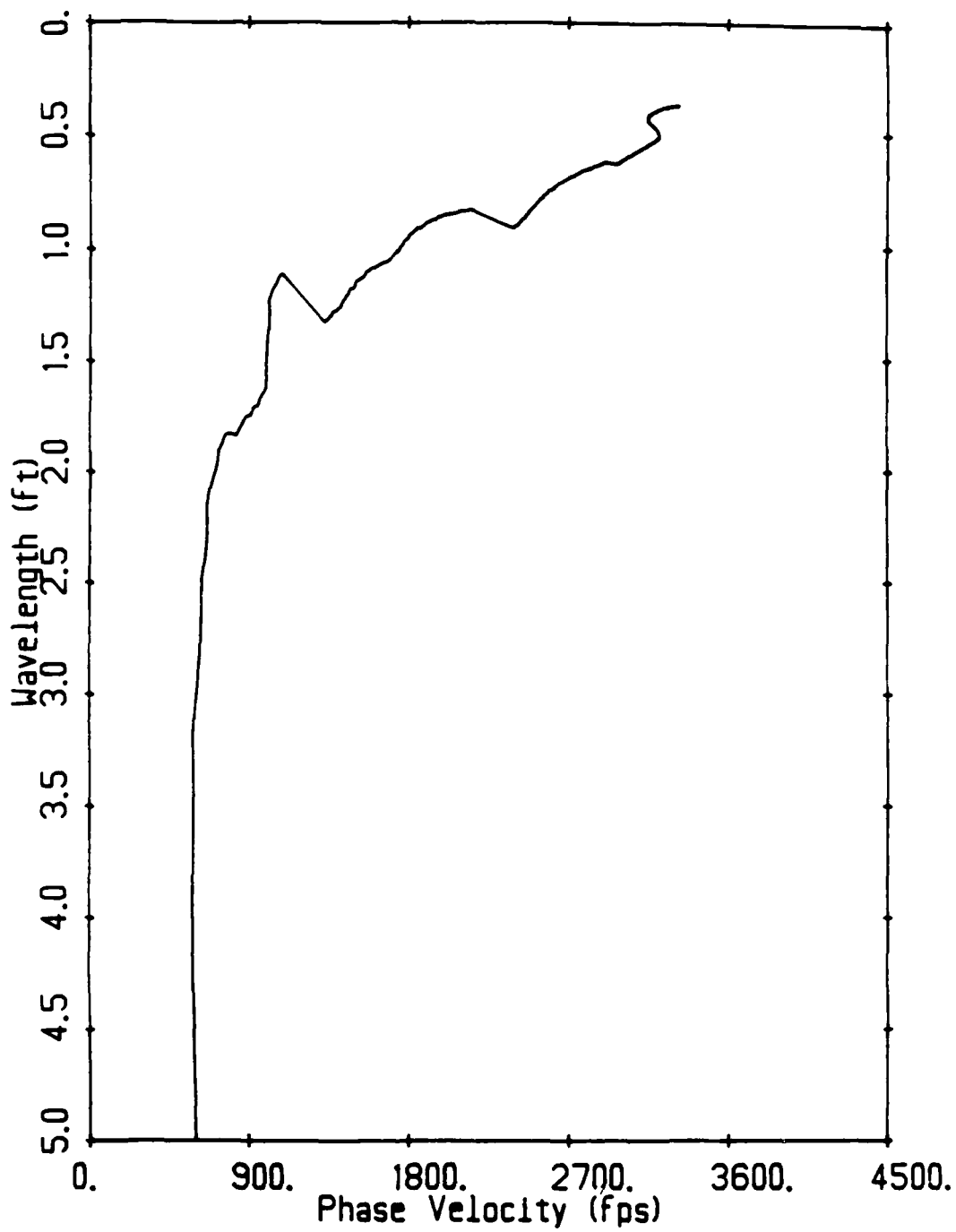


Figure D.2— Average Experimental Dispersion Curve (Unfiltered) for
 $S/X = 1.0$ for G. G. Brown Parking Lot Site

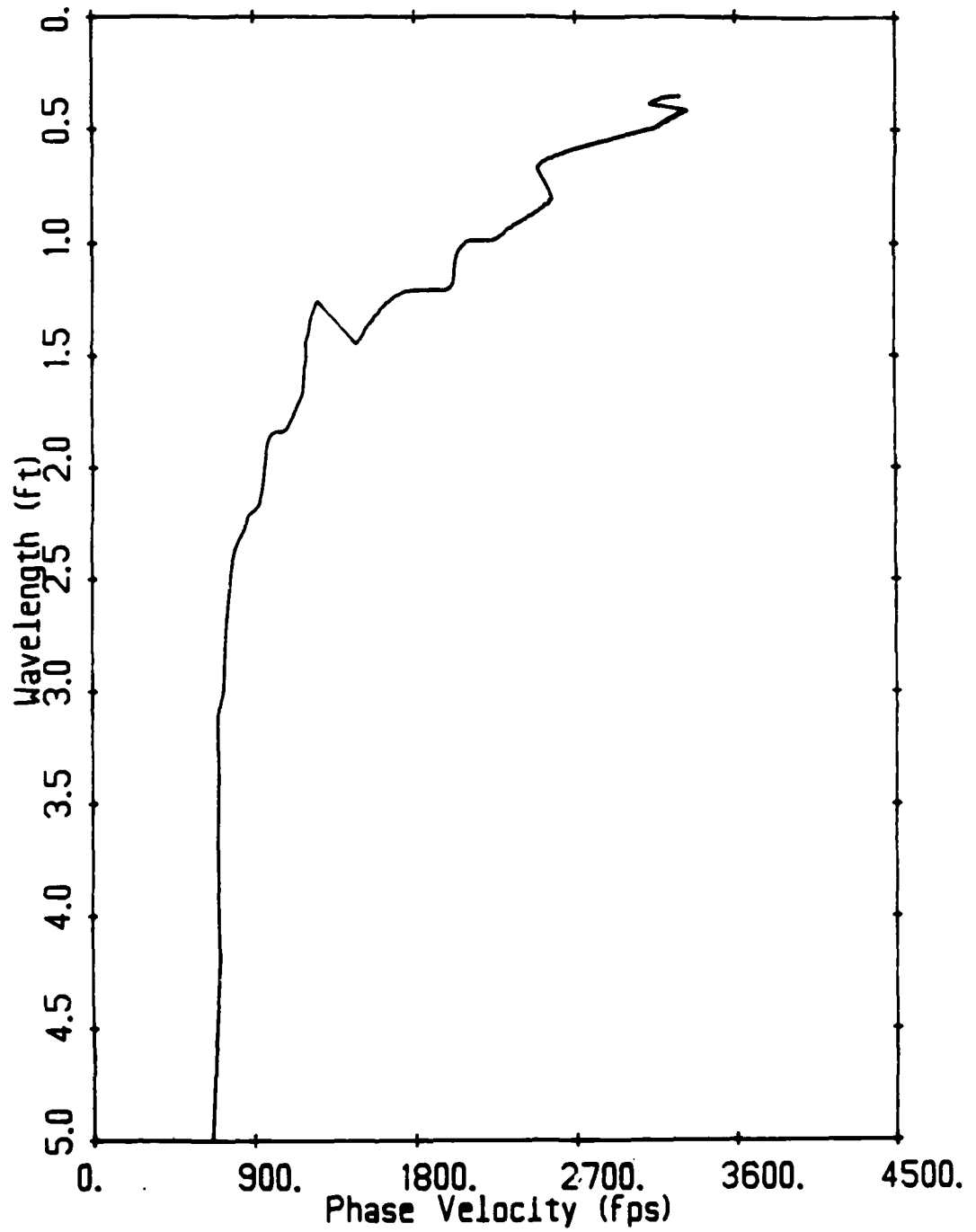


Figure D.3— Average Experimental Dispersion Curve (Unfiltered) for
 $S/X = 1.5$ for G. G. Brown Parking Lot Site

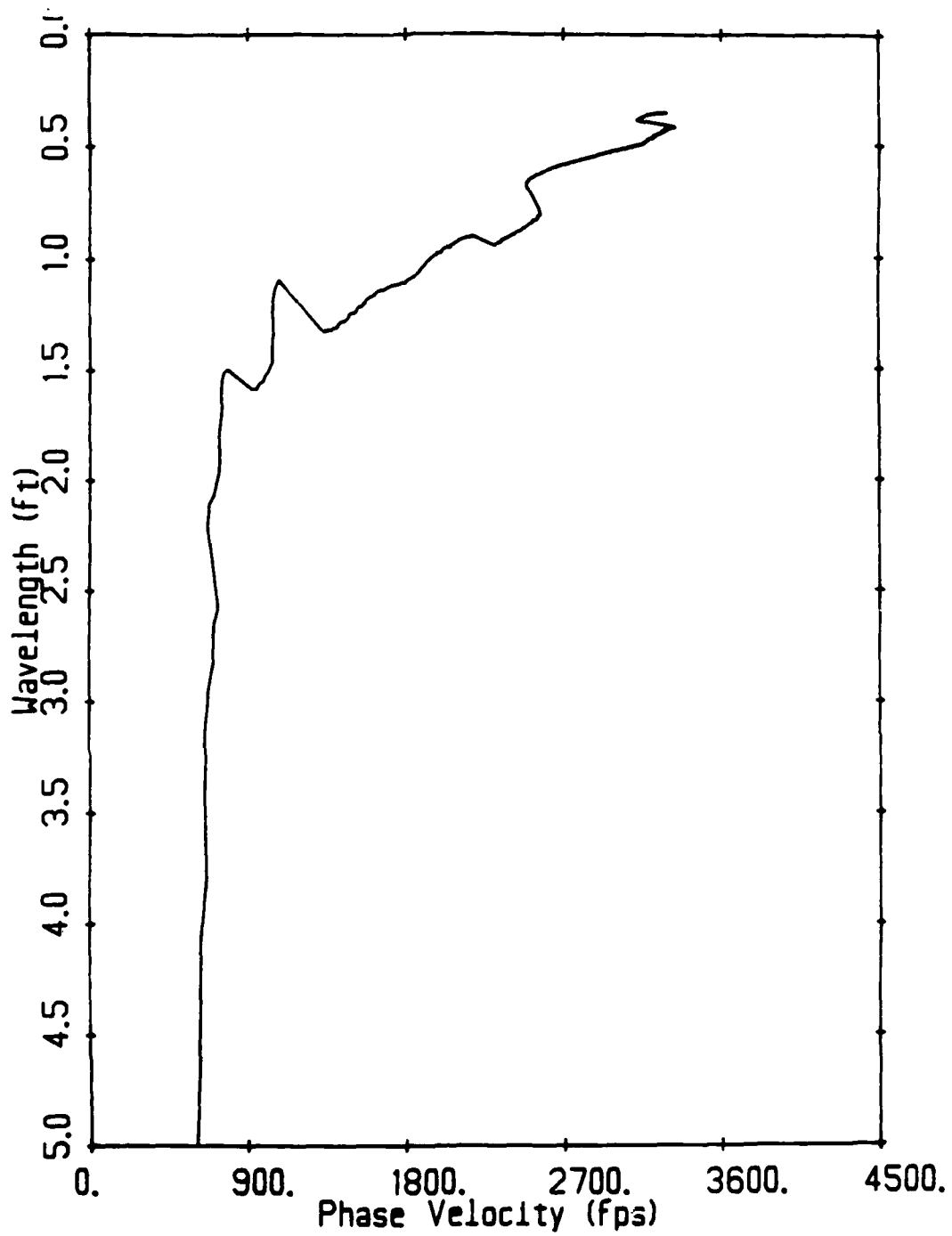


Figure D.4— Average Experimental Dispersion Curve (Unfiltered) for
 $S/X = 2.0$ for G. G. Brown Parking Lot Site

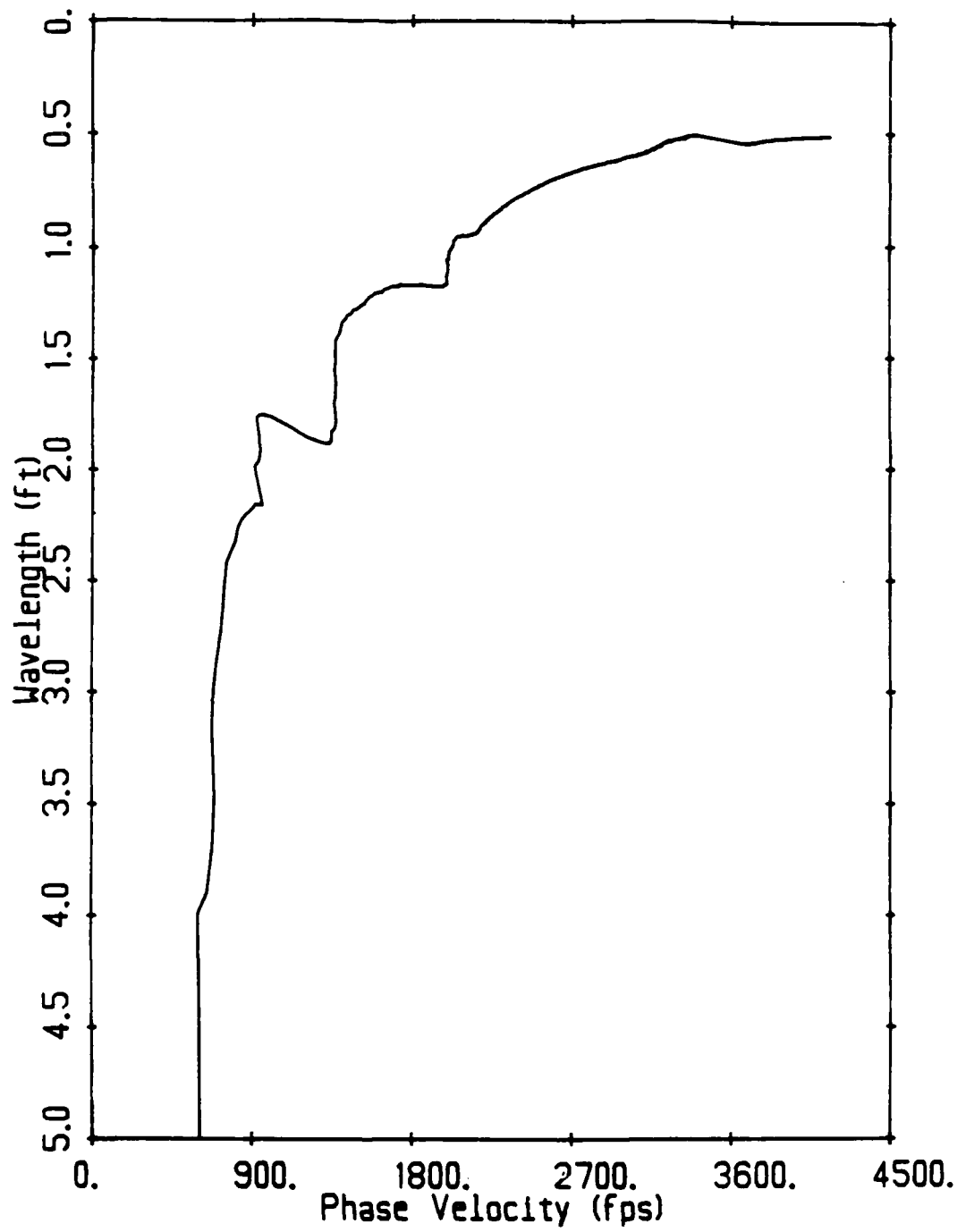
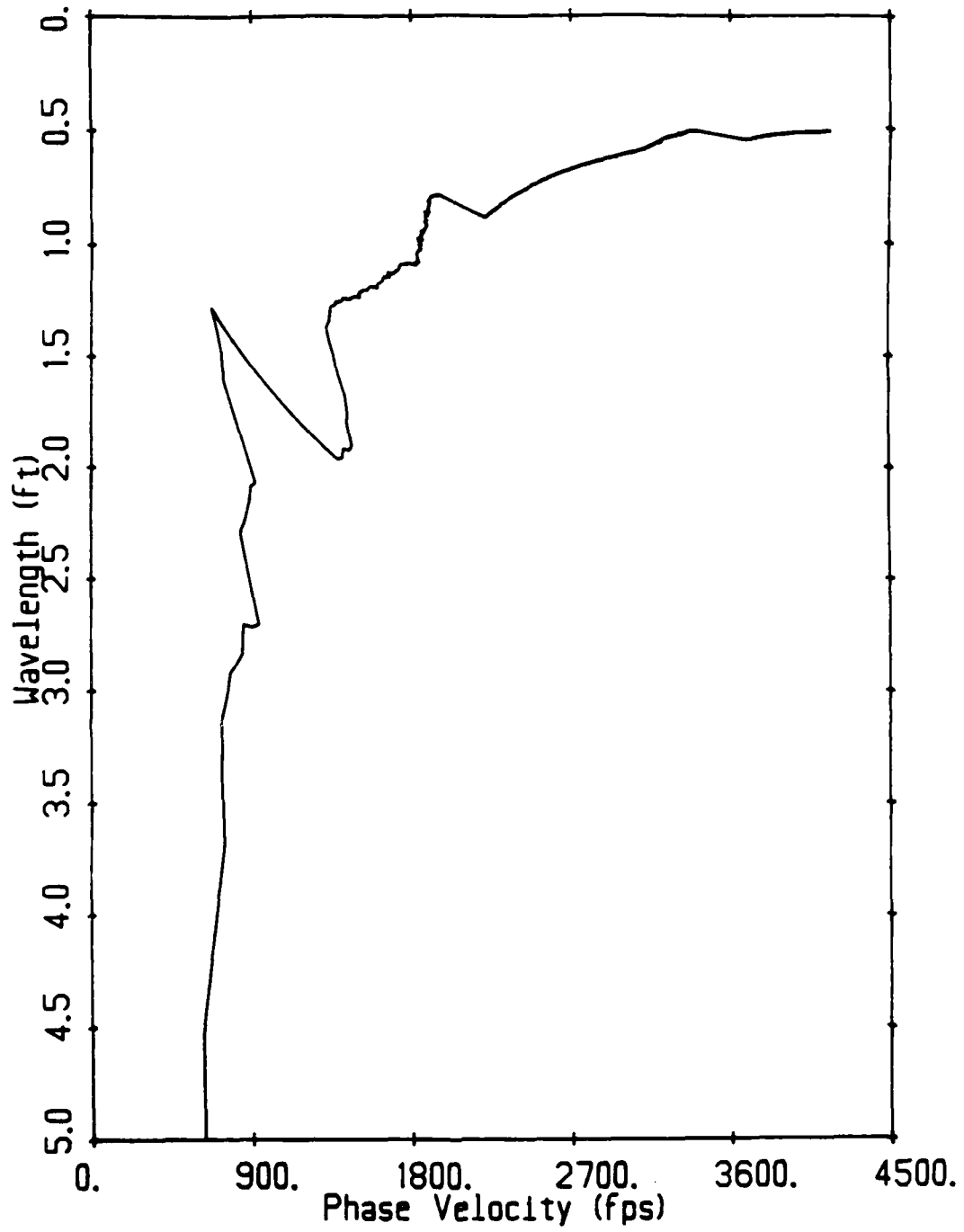


Figure D.5— Average Experimental Dispersion Curve (Unfiltered) for
 $S/X = 2.5$ for G. G. Brown Parking Lot Site



**Figure D.6— Average Experimental Dispersion Curve (Unfiltered) for
 $S/X = 3.0$ for G. G. Brown Parking Lot Site**

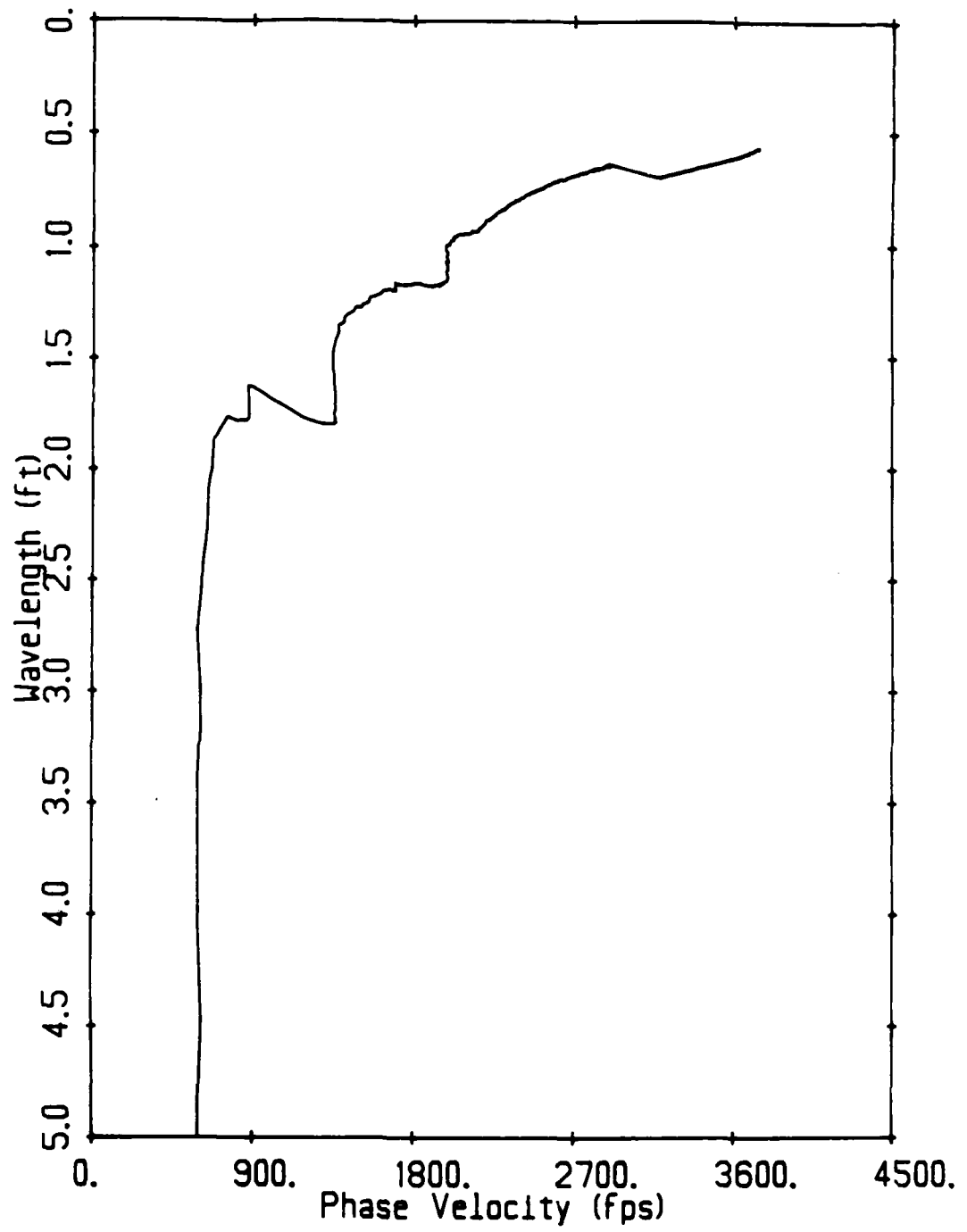


Figure D.7— Average Experimental Dispersion Curve (Filtered) for $S/X = 0.5$
for G. G. Brown Parking Lot Site

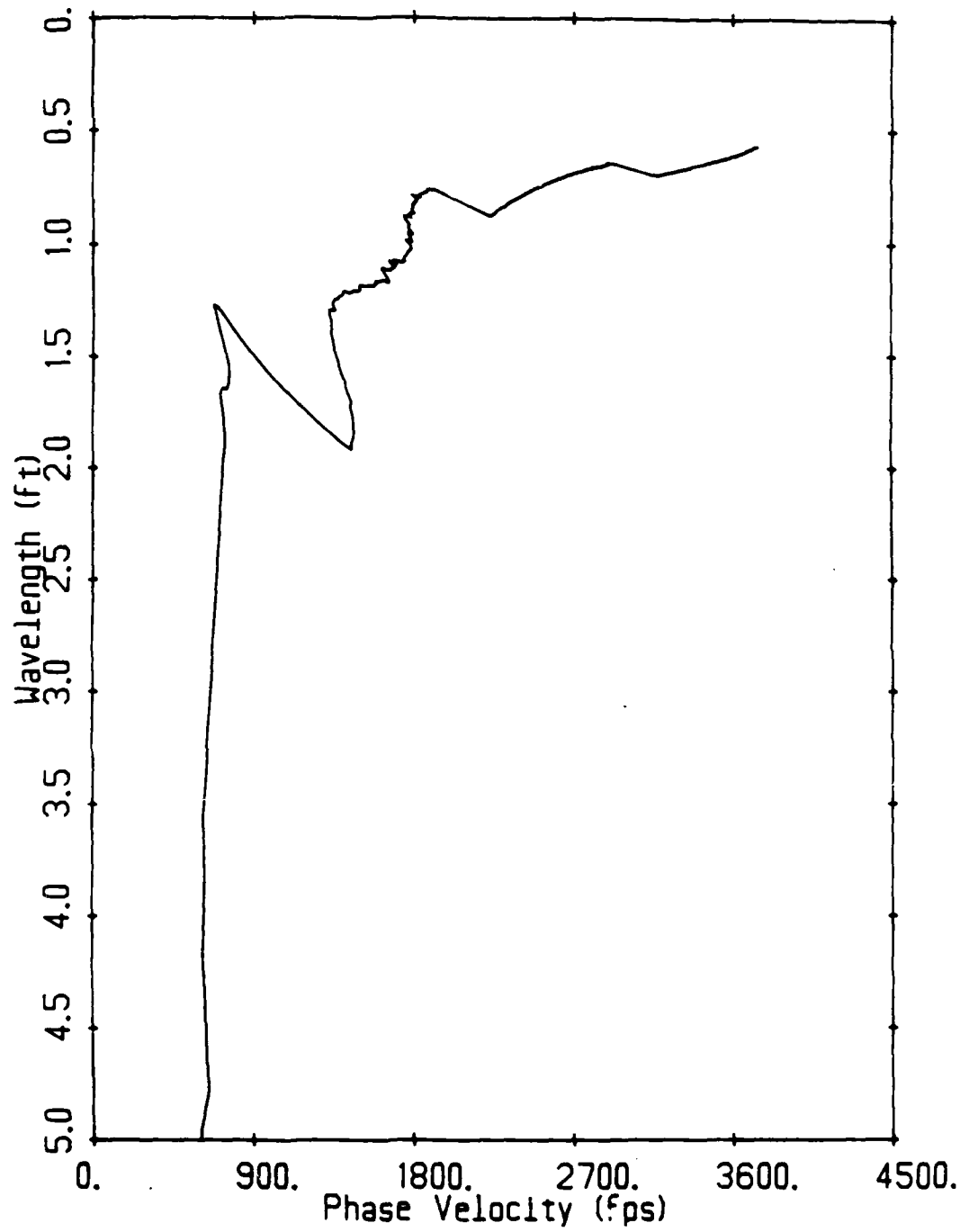


Figure D.8— Average Experimental Dispersion Curve (Filtered) for $S/X = 1.0$
for G. G. Brown Parking Lot Site

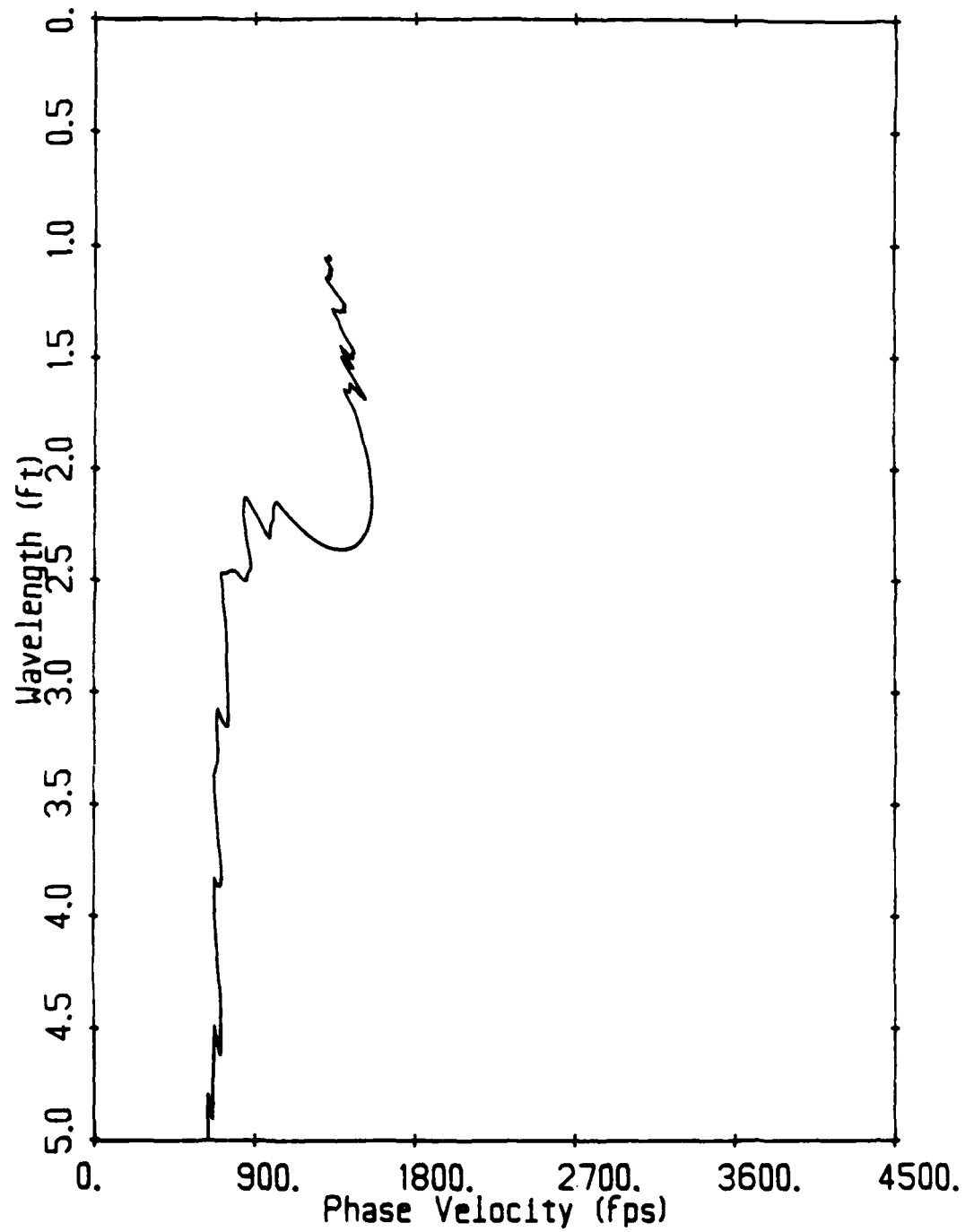


Figure D.9— Average Experimental Dispersion Curve (Filtered) for $S/X = 1.5$
for G. G. Brown Parking Lot Site

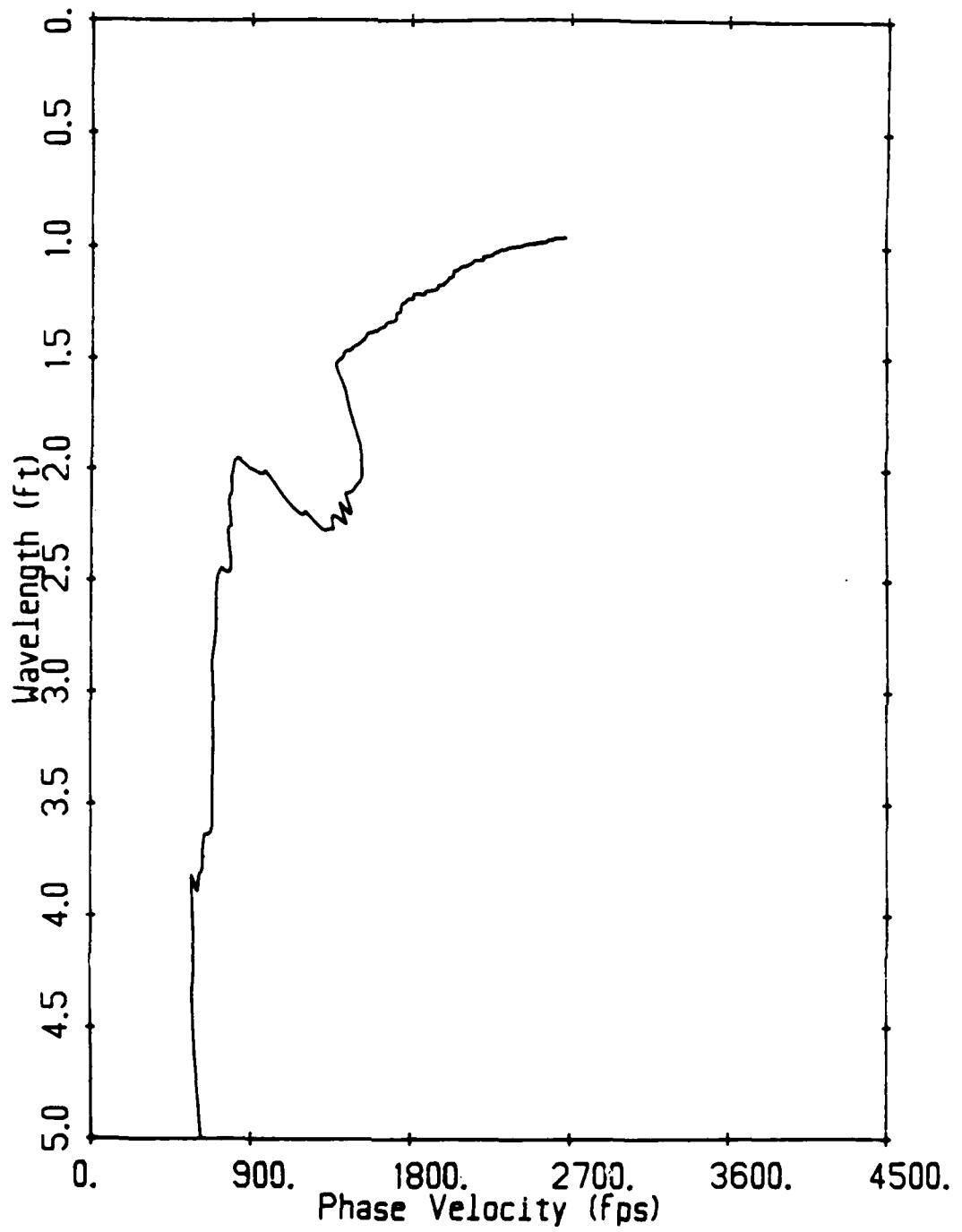


Figure D.10— Average Experimental Dispersion Curve (Filtered) for
 $S/X = 2.0$ for G. G. Brown Parking Lot Site

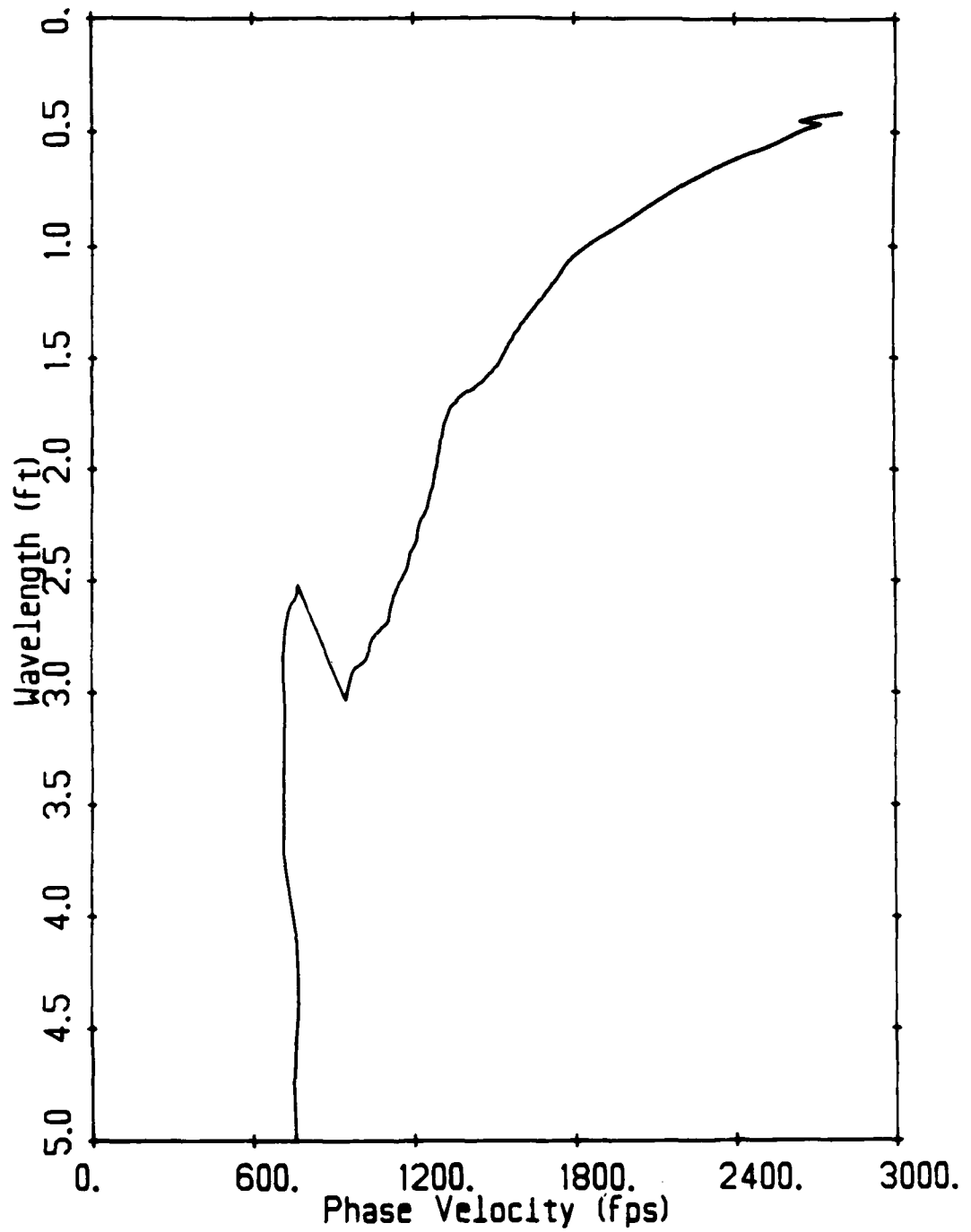


Figure D.11— Average Experimental Dispersion Curve (Unfiltered) for
 $S/X = 0.5$ for SEMTA Parking Lot Site

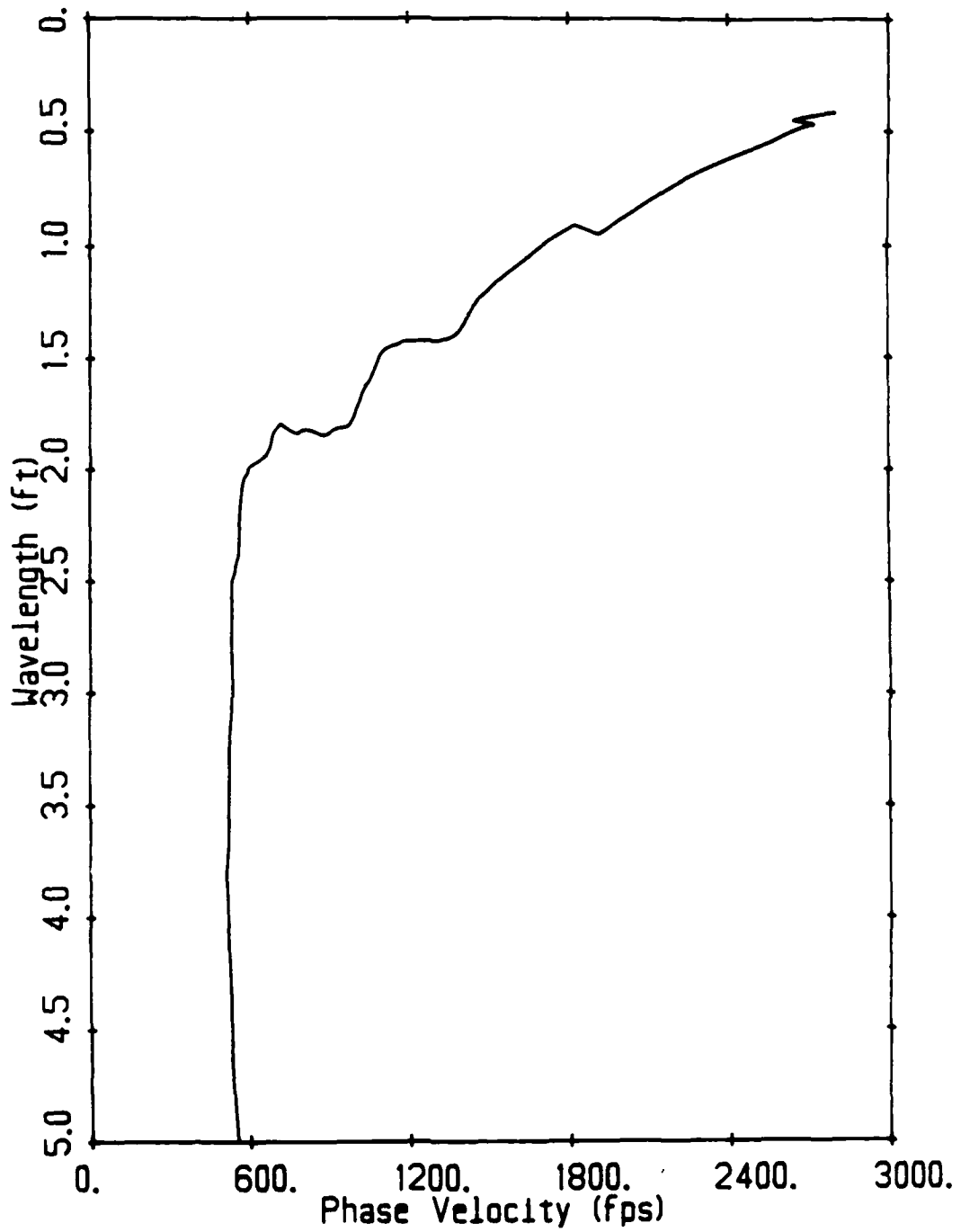


Figure D.12— Average Experimental Dispersion Curve (Unfiltered) for
 $S/X = 1.0$ for SEMTA Parking Lot Site

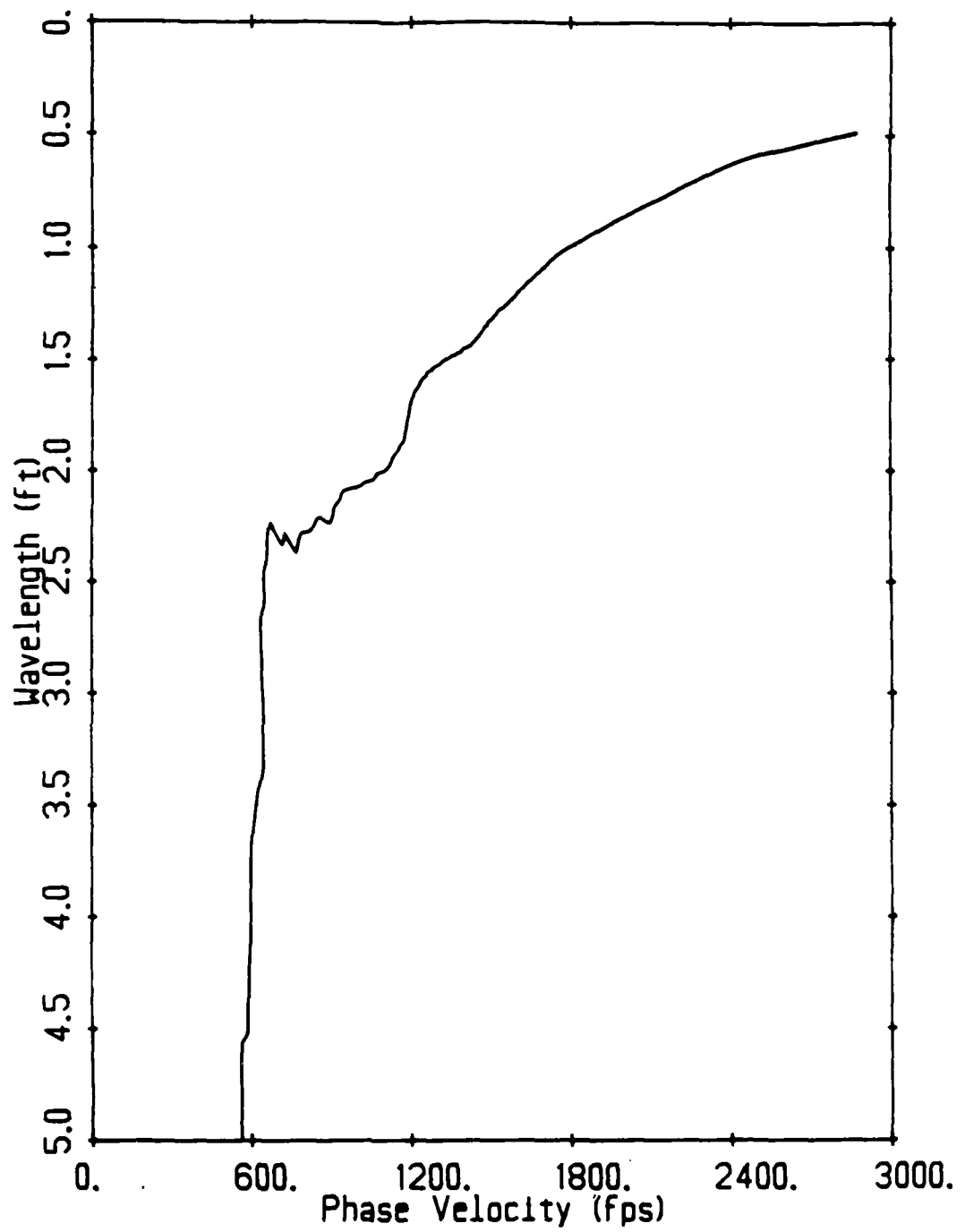


Figure D.13— Average Experimental Dispersion Curve (Unfiltered) for
 $S/X = 1.5$ for SEMTA Parking Lot Site

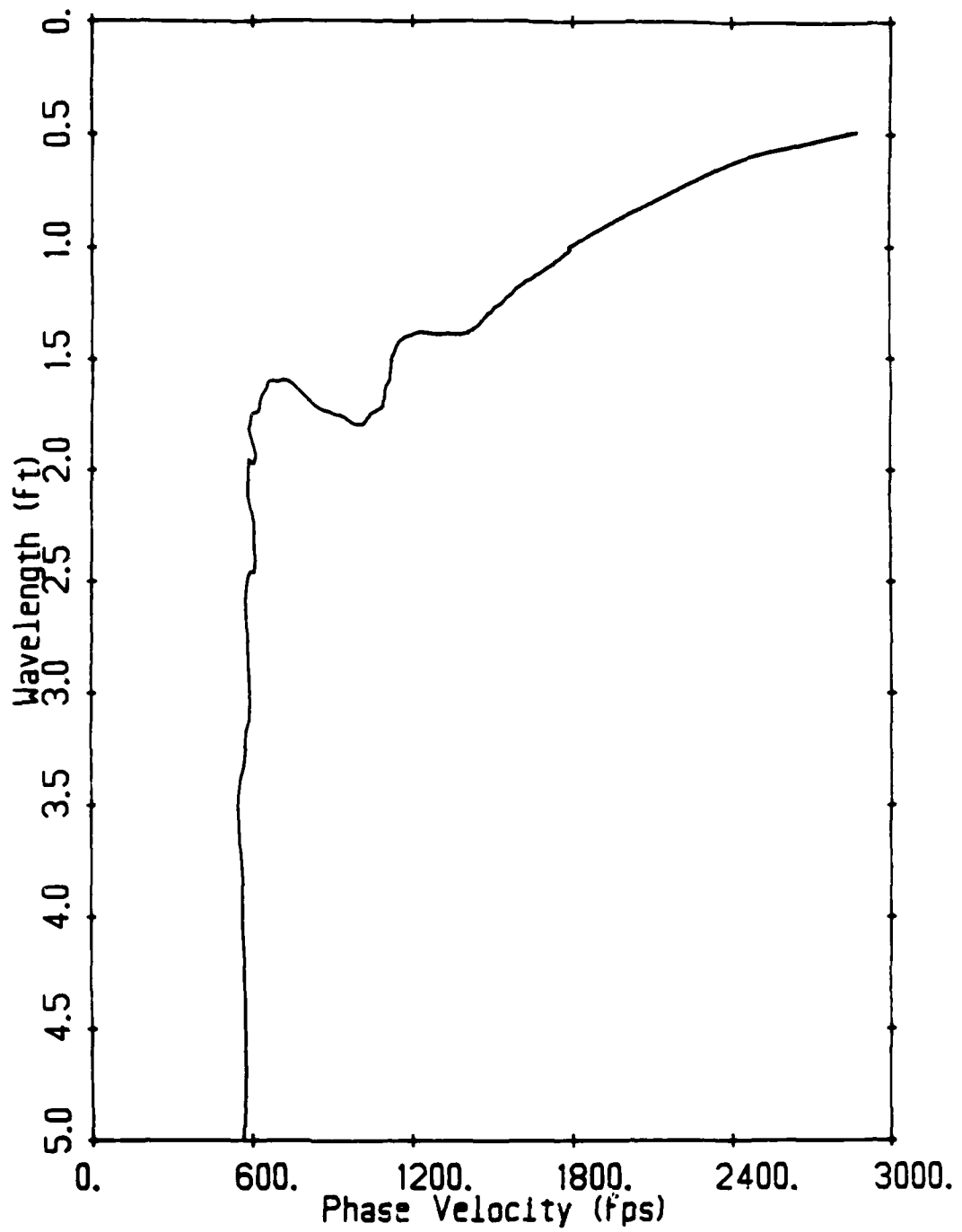


Figure D.14— Average Experimental Dispersion Curve (Unfiltered) for
 $S/X = 2.0$ for SEMTA Parking Lot Site

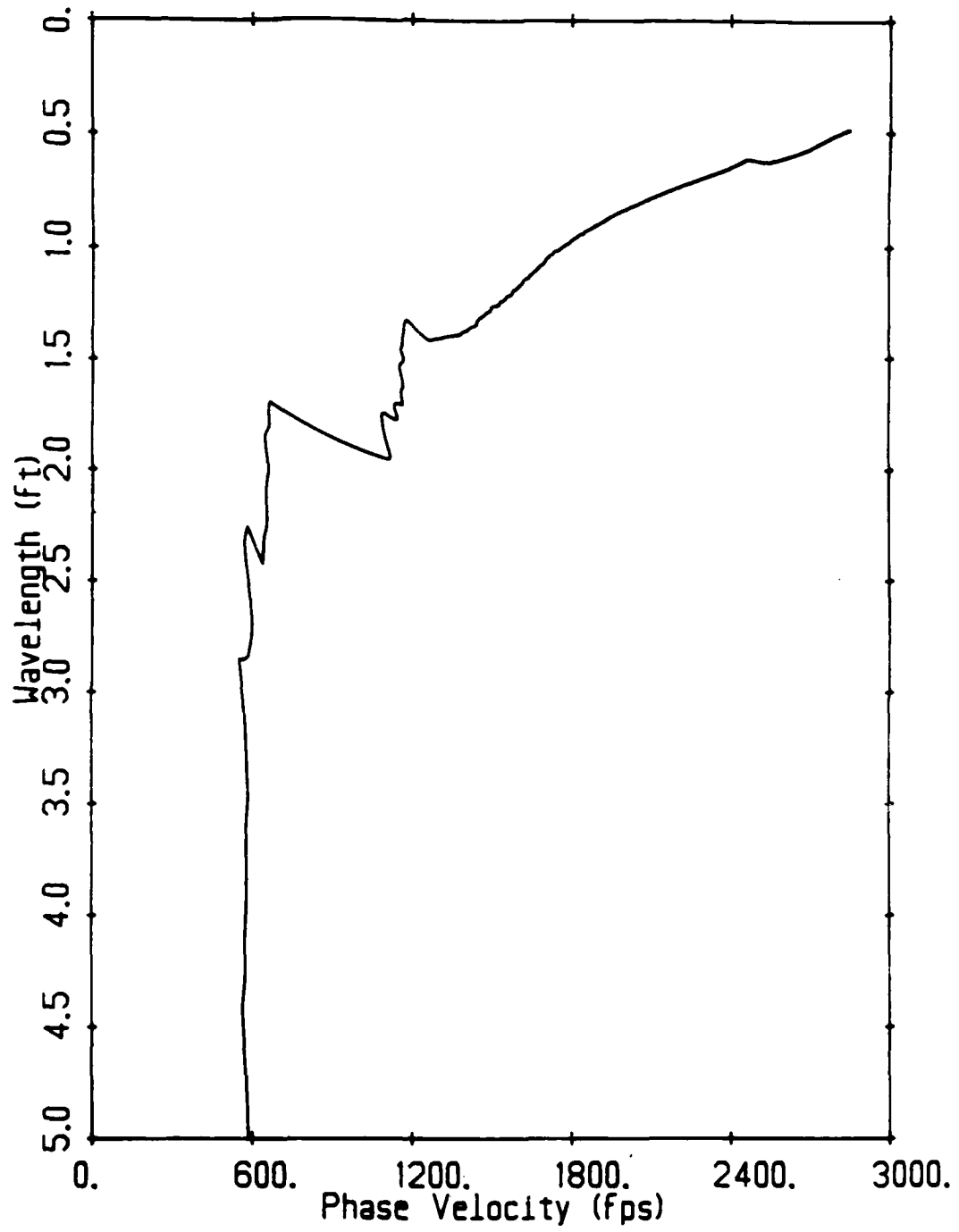


Figure D.15— Average Experimental Dispersion Curve (Unfiltered) for
 $S/X = 2.5$ for SEMTA Parking Lot Site

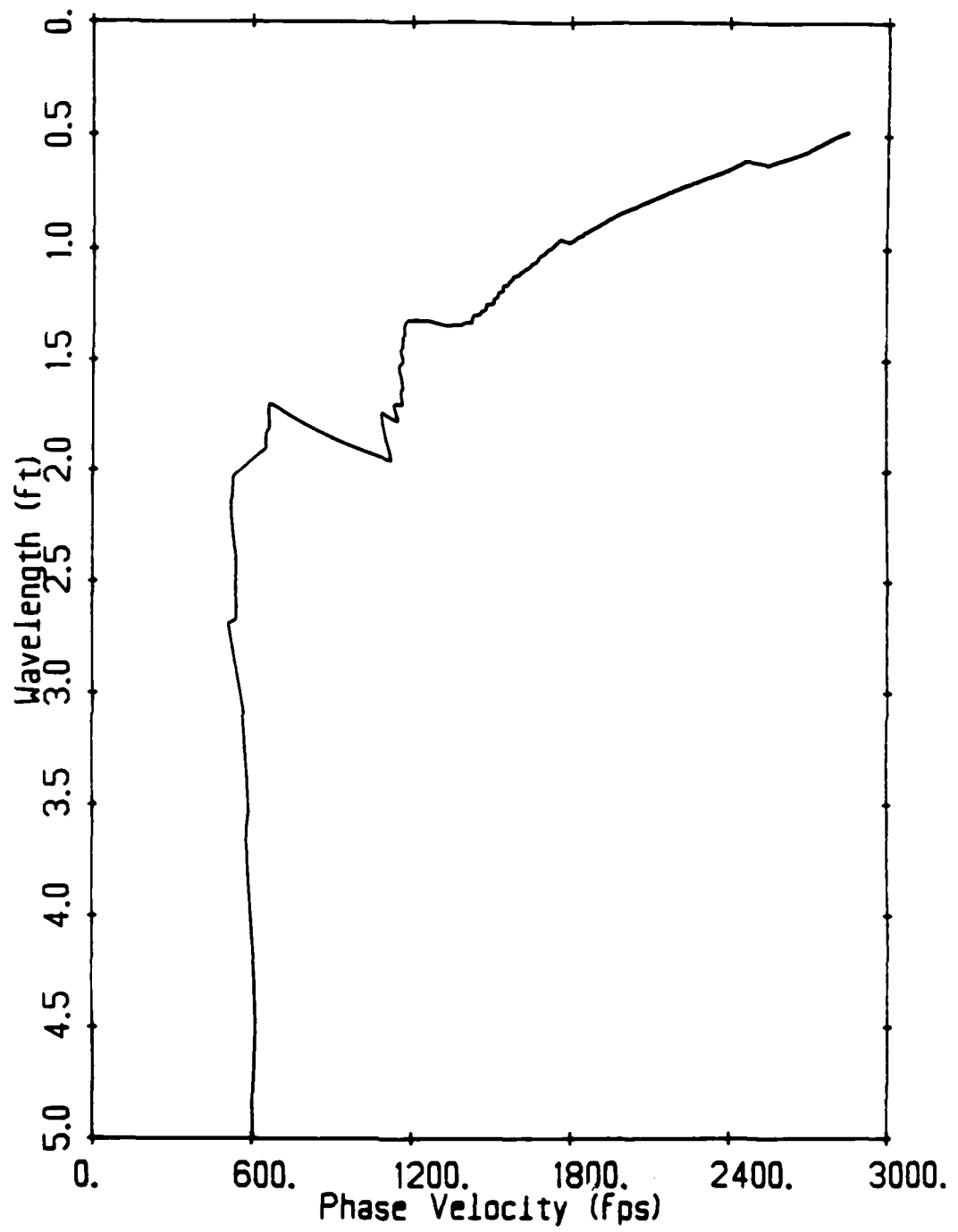


Figure D.16— Average Experimental Dispersion Curve (Unfiltered) for
 $S/X = 3.0$ for SEMTA Parking Lot Site

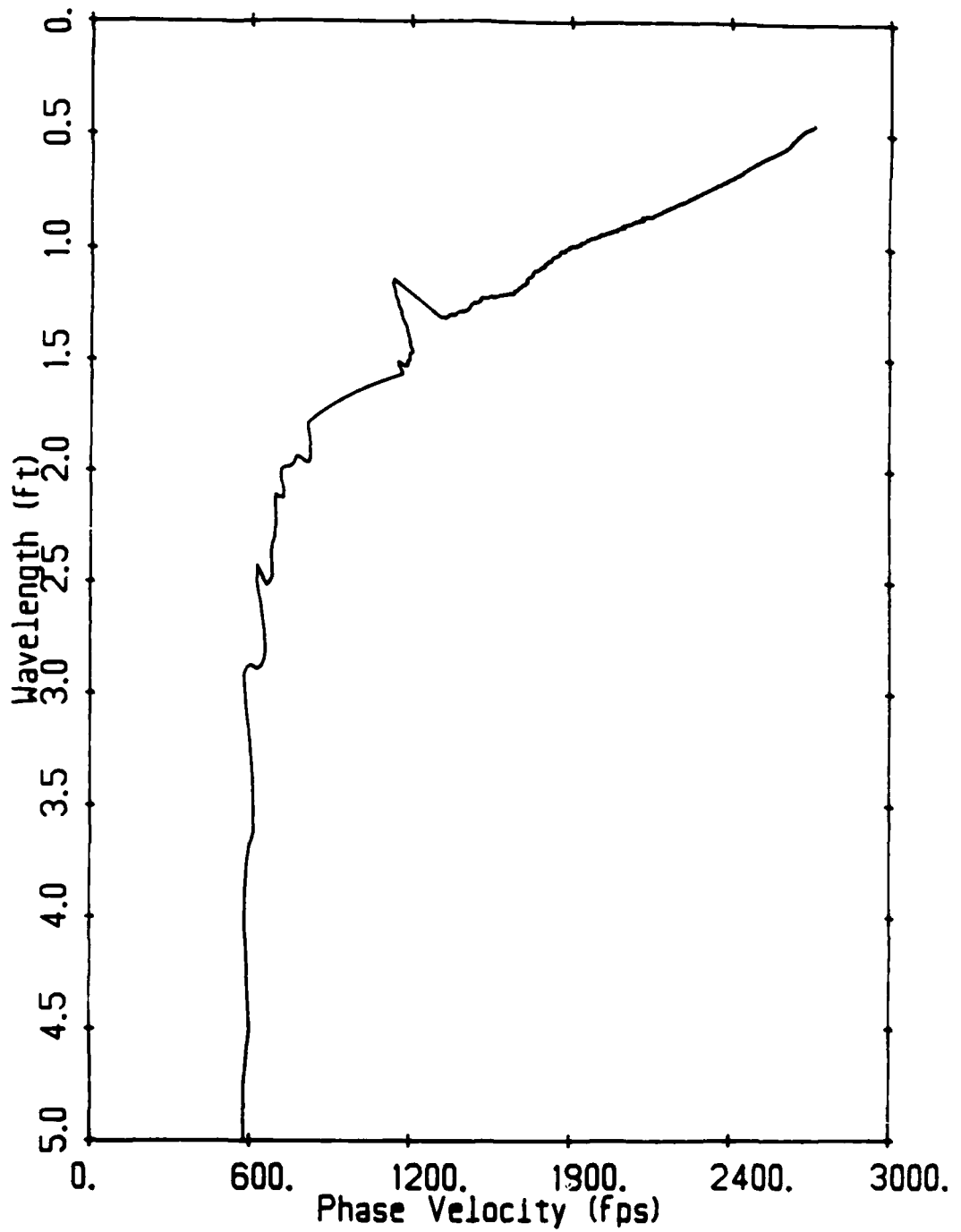


Figure D.17— Average Experimental Dispersion Curve (Filtered) for
 $S/X = 0.5$ for SEMTA Parking Lot Site

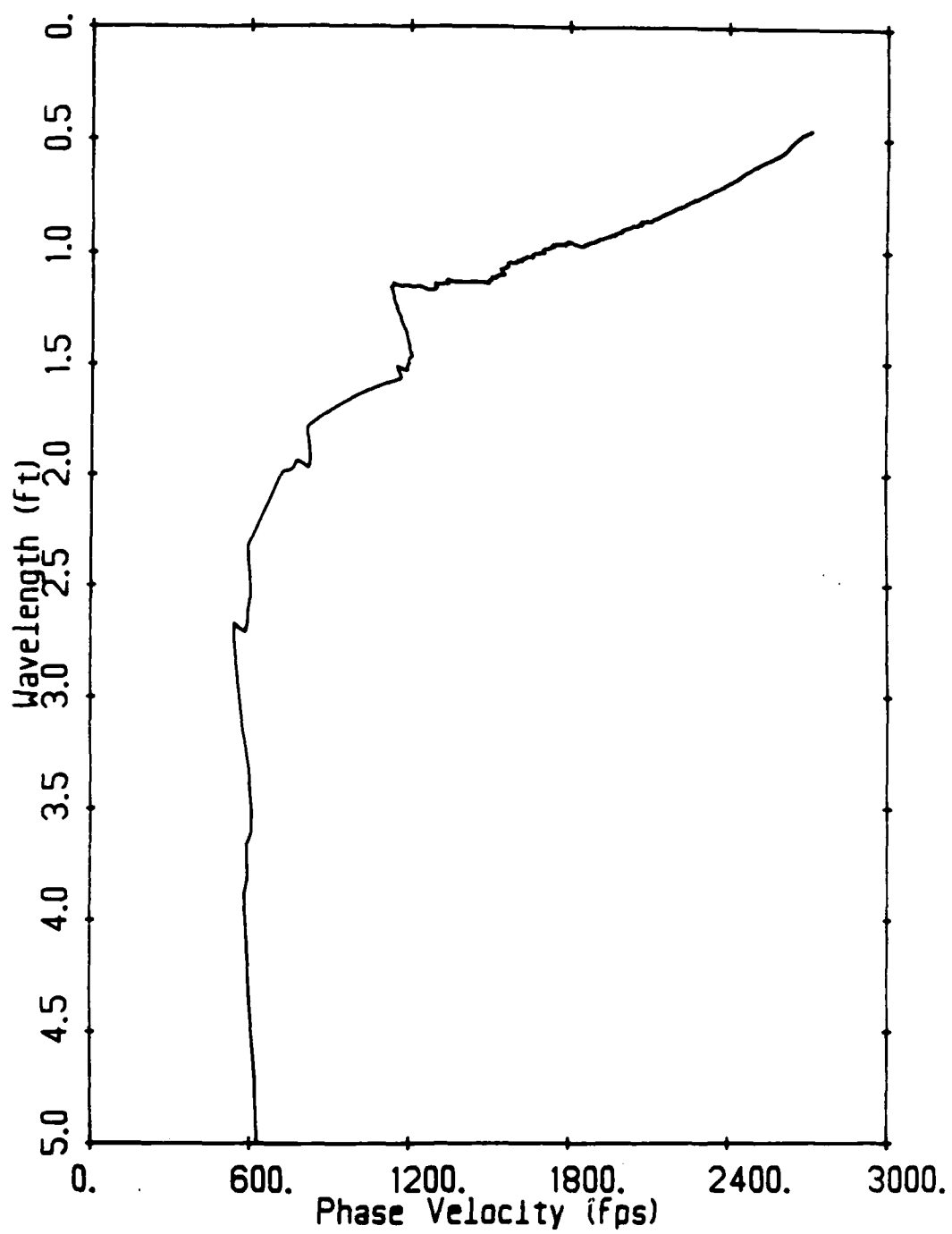


Figure D.18— Average Experimental Dispersion Curve (Filtered) for
 $S/X = 1.0$ for SEMTA Parking Lot Site

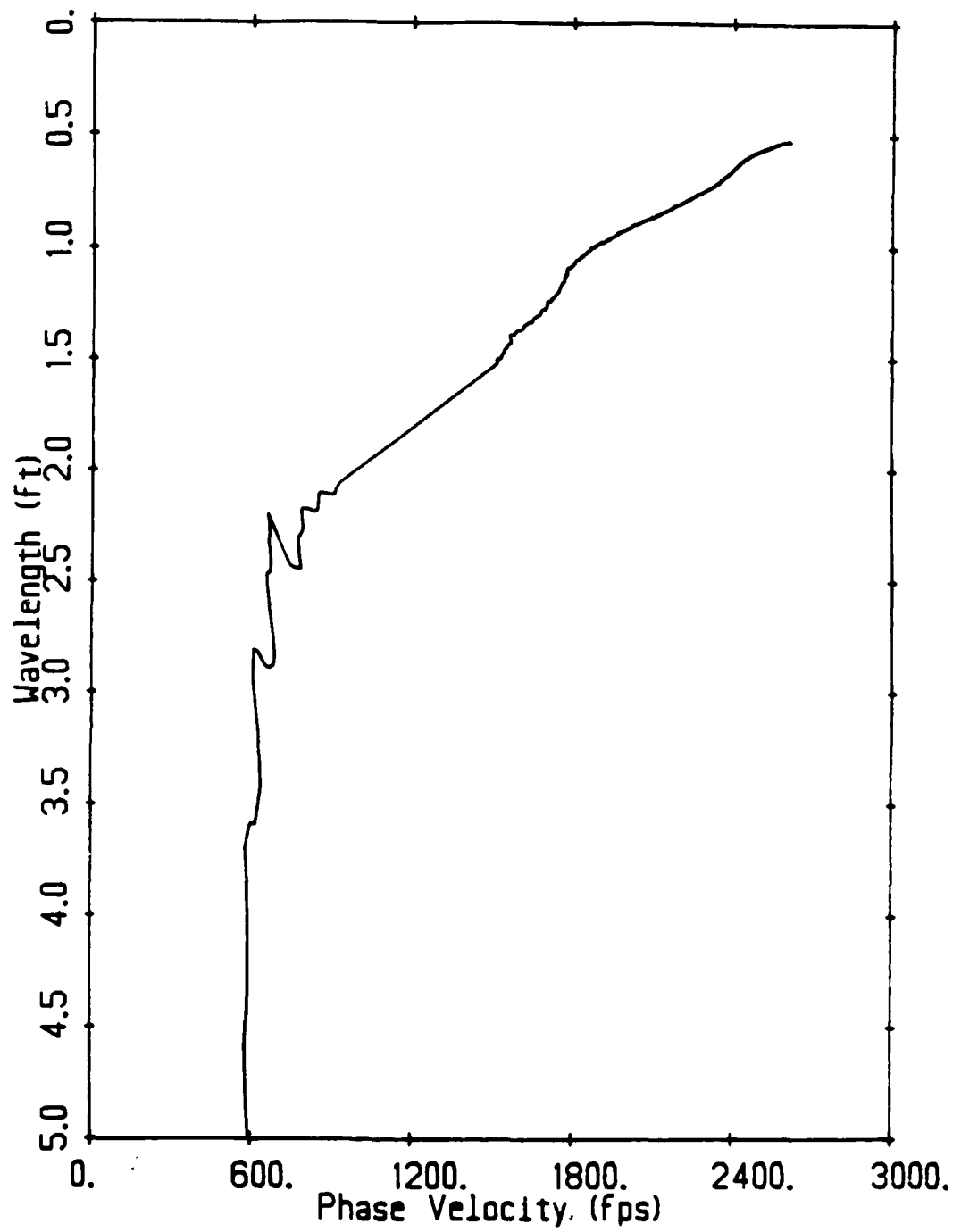


Figure D.10— Average Experimental Dispersion Curve (Filtered) for
 $S/X = 1.5$ for SEMTA Parking Lot Site

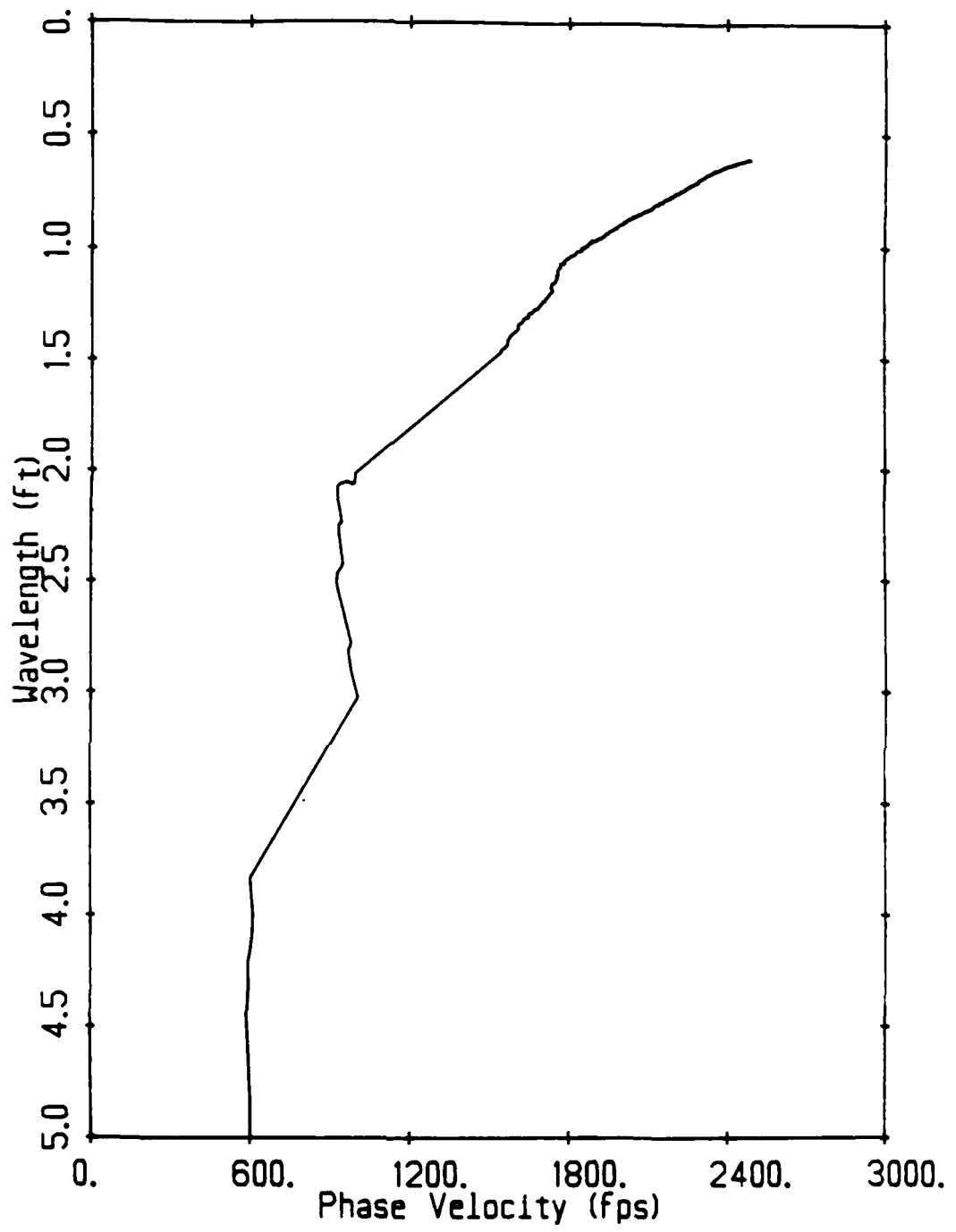


Figure D.20— Average Experimental Dispersion Curve (Filtered) for
 $S/X = 2.0$ for SEMTA Parking Lot Site

APPENDIX E

**TABLES OF USEFUL FREQUENCY RANGES AS A FUNCTION OF
SOURCE TYPE**

Table E.1 — Useful Frequency Ranges for 0.5-ft Receiver Spacing for G. G.
Brown Parking Lot Site

Source Type	Lower Cutoff Frequency (Hz)	Upper Cutoff Frequency (Hz)
4 oz	125	9250
8 oz	100	9400
16 oz	75	9650

Table E.2 — Useful Frequency Ranges for 1-ft Receiver Spacing for
G. G. Brown Parking Lot Site

Source Type	Lower Cutoff Frequency (Hz)	Upper Cutoff Frequency (Hz)
4 oz	112	7975
8 oz	87	6337
16 oz	75	6225

**Table E.3 — Useful Frequency Ranges for 2-ft Receiver Spacing for
G. G. Brown Parking Lot Site**

Source Type	Lower Cutoff Frequency (Hz)	Upper Cutoff Frequency (Hz)
8 oz	31.2	1000
16 oz	20	982.5
128 oz	46.2	337.5

Table E.4 — Useful Frequency Ranges for 4-ft Receiver Spacing for
G. G. Brown Parking Lot Site

Source Type	Lower Cutoff Frequency (Hz)	Upper Cutoff Frequency (Hz)
8 oz	33.2	208.98
16 oz	30.86	148.44
128 oz	21.09	168.36

**Table E.5 — Useful Frequency Ranges for 8-ft Receiver Spacing for
G. G. Brown Parking Lot Site**

Source Type	Lower Cutoff Frequency (Hz)	Upper Cutoff Frequency (Hz)
8 oz	41.75	200
16 oz	40.5	200
128 oz	30.25	200

Table E.6 — Useful Frequency Ranges for 1-ft Receiver Spacing for SEMTA
Parking Lot Site

Source Type	Lower Cutoff Frequency (Hz)	Upper Cutoff Frequency (Hz)
4 oz	109.4	5320.3
8 oz	70.3	4843.7
16 oz	78.1	4875
40 oz	46.9	3273.4
128 oz	31.2	3437.5

Table E.7 — Useful Frequency Ranges for 2-ft Receiver Spacing for SEMTA
Parking Lot Site

Source Type	Lower Cutoff Frequency (Hz)	Upper Cutoff Frequency (Hz)
4 oz	38.7	292.5
8 oz	37.5	275
16 oz	32.5	275
40 oz	32.5	215
128 oz	30	183.7

Table E.8 — Useful Frequency Ranges for 4-ft Receiver Spacing for SEMTA
Parking Lot Site

Source Type	Lower Cutoff Frequency (Hz)	Upper Cutoff Frequency (Hz)
4 oz	65	279
8 oz	40	280
16 oz	35	275
40 oz	31	236
128 oz	30	185

Table E.9 — Useful Frequency Ranges for 8-ft Receiver Spacing for SEMTA
Parking Lot Site

Source Type	Lower Cutoff Frequency (Hz)	Upper Cutoff Frequency (Hz)
4 oz	73.75	207.19
8 oz	71.25	210.62
16 oz	65.94	130
40 oz	44.06	132.19
128 oz	44.06	122.5

APPENDIX F

CROSS POWER SPECTRUM MAGNITUDES AS A FUNCTION OF
SOURCE TYPE

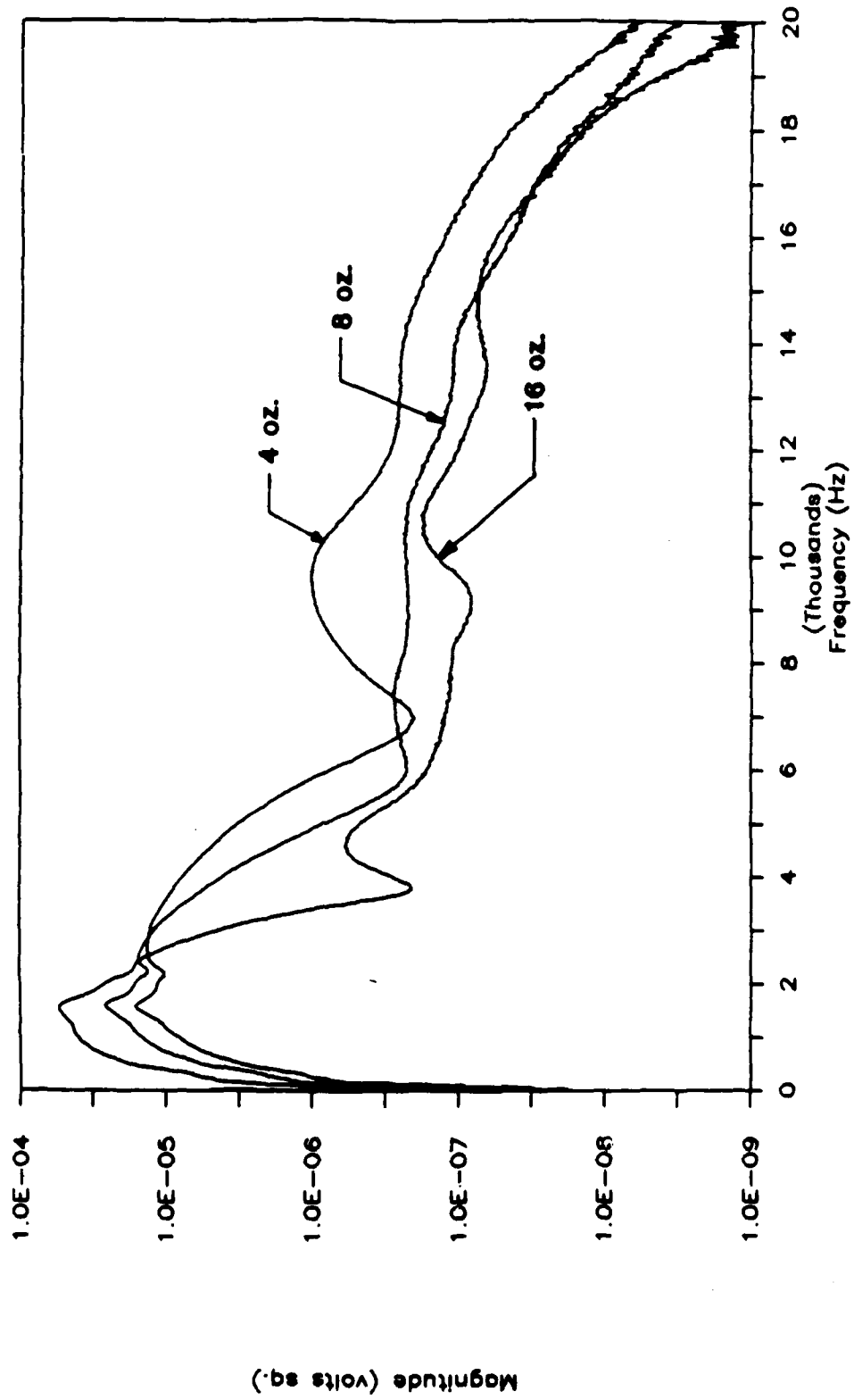


Figure F.1 - Magnitude (Absolute) of Cross Power Spectrum for X = 0.5 ft for G. G. Brown Parking Lot Site

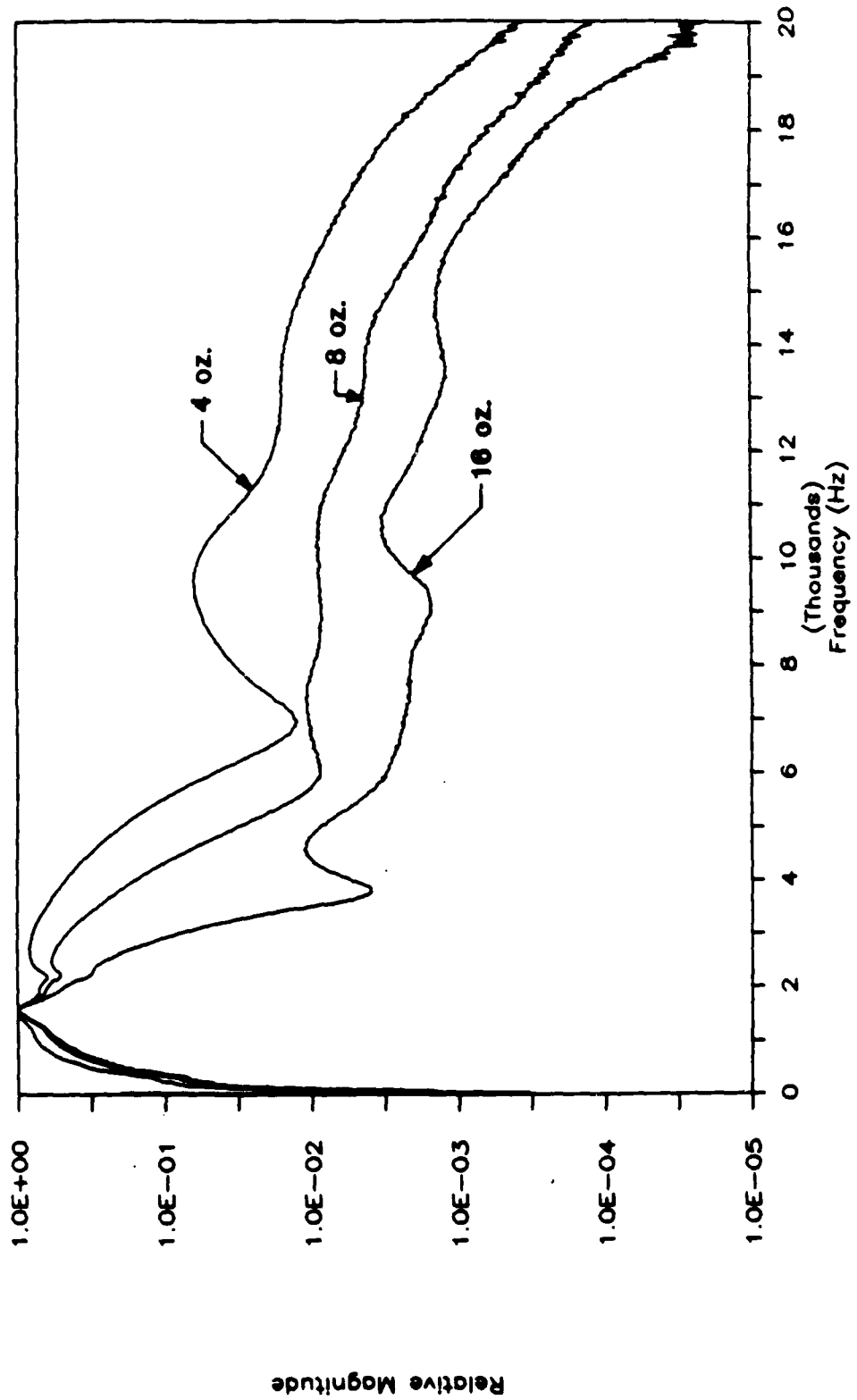


Figure F.2 - Magnitude (Relative) of Cross Power Spectrum for X = 0.5 ft for G. G. Brown Parking Lot Site

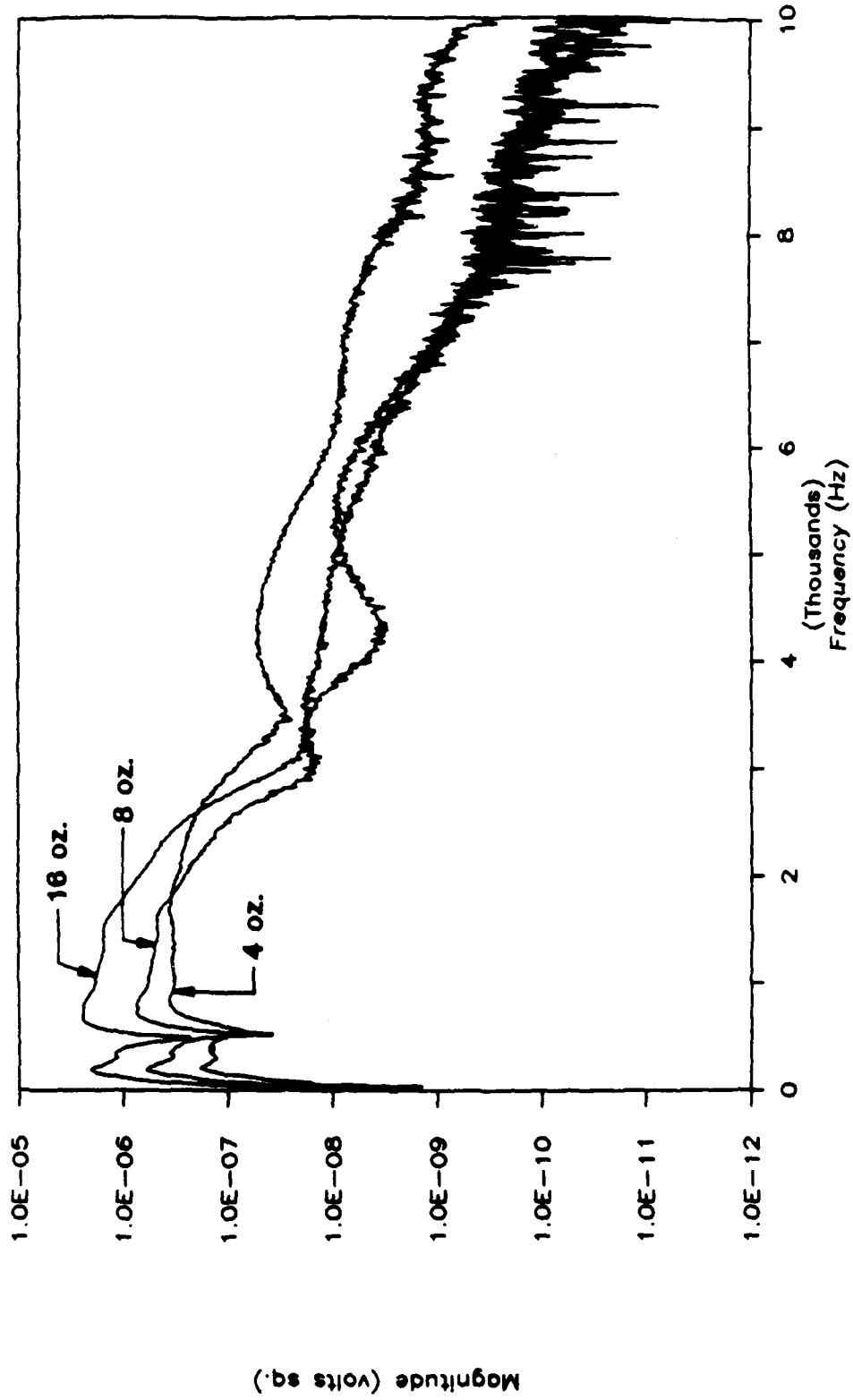


Figure F.3 - Magnitude (Absolute) of Cross Power Spectrum for X = 1.0 ft for G. G. Brown Parking Lot Site

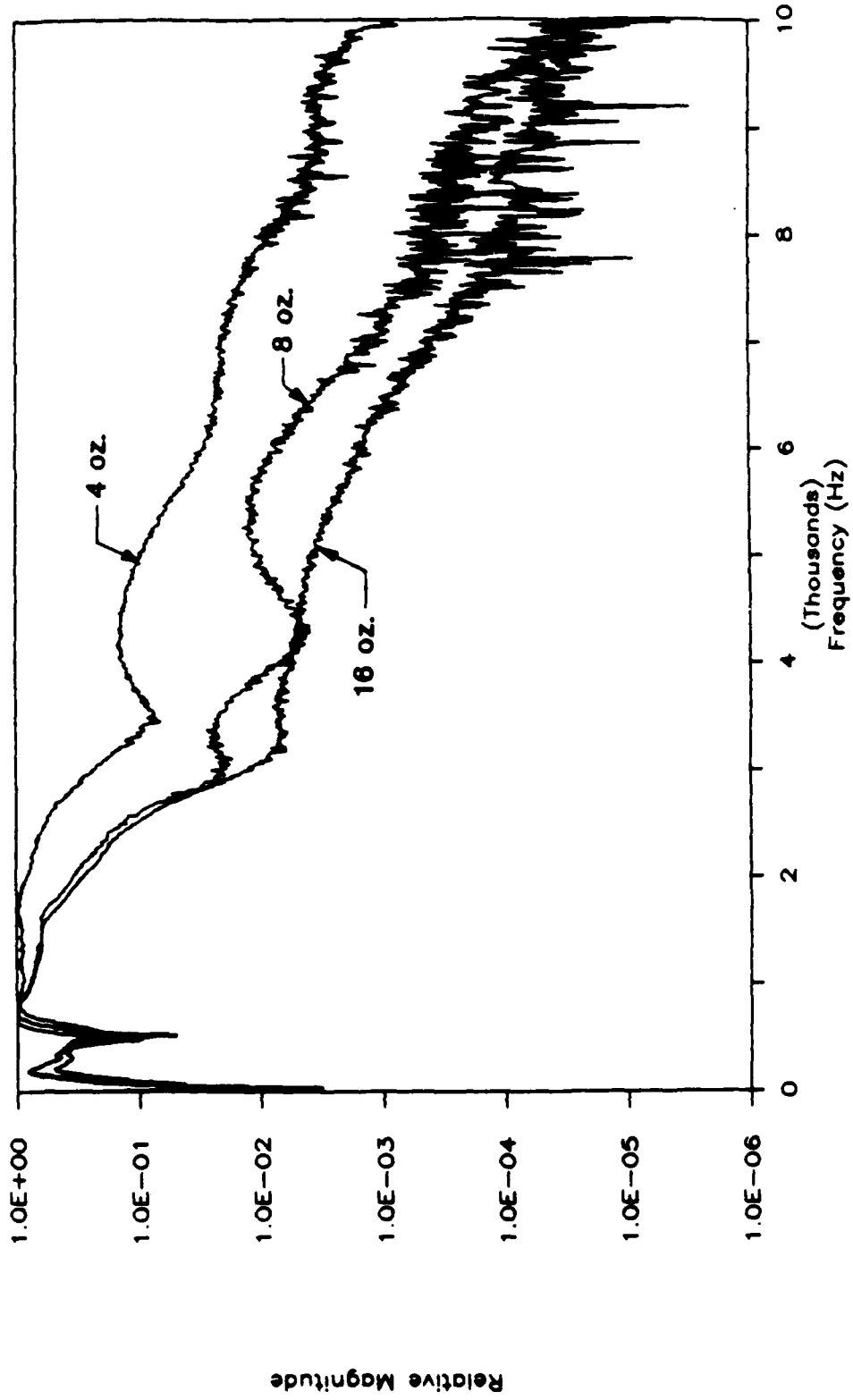


Figure F.4 - Magnitude (Relative) of Cross Power Spectrum for X = 1.0 ft for G. G. Brown Parking Lot Site

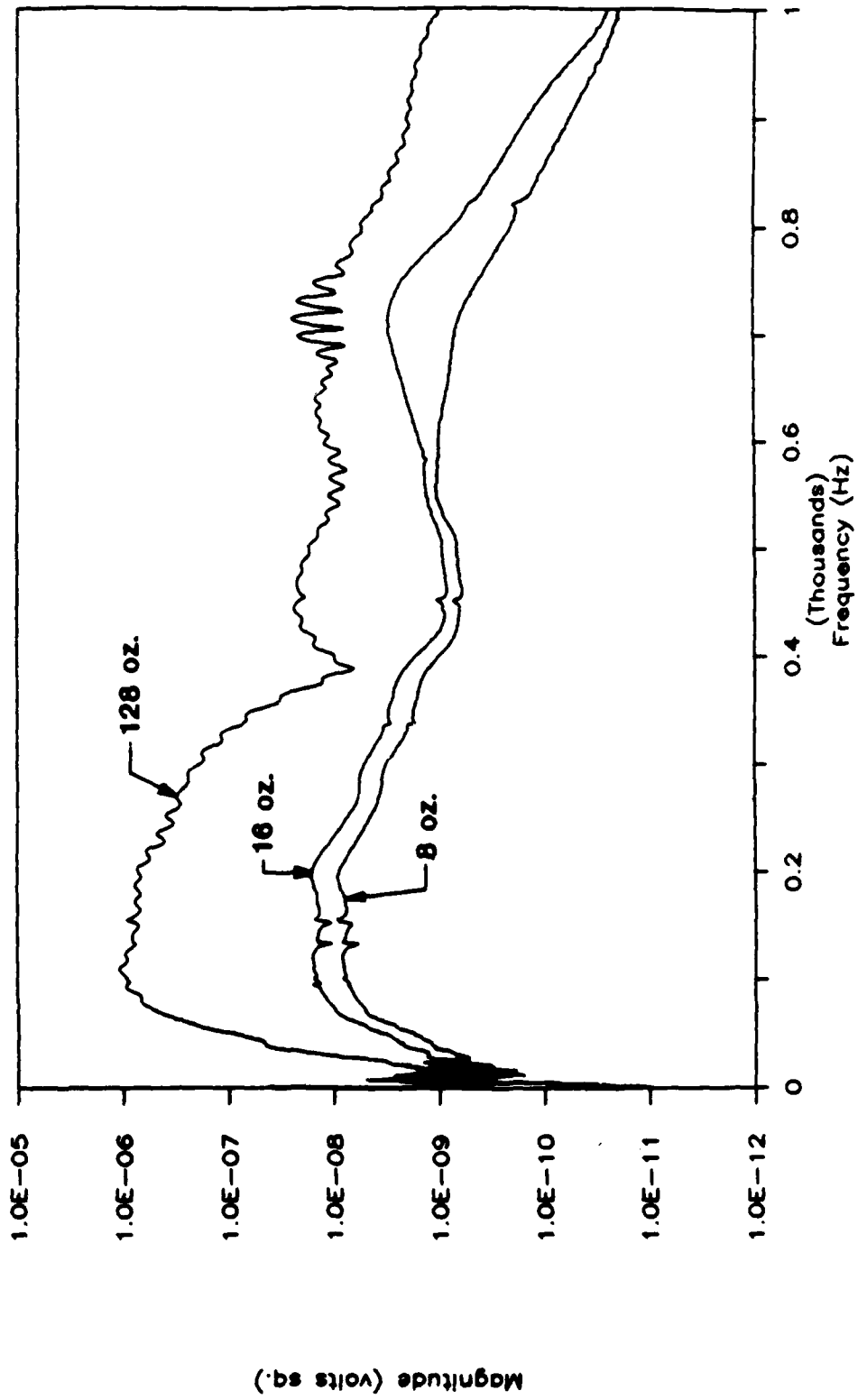


Figure F.5 - Magnitude (Absolute) of Cross Power Spectrum for X = 2.0 ft for G. G. Brown Parking Lot Site

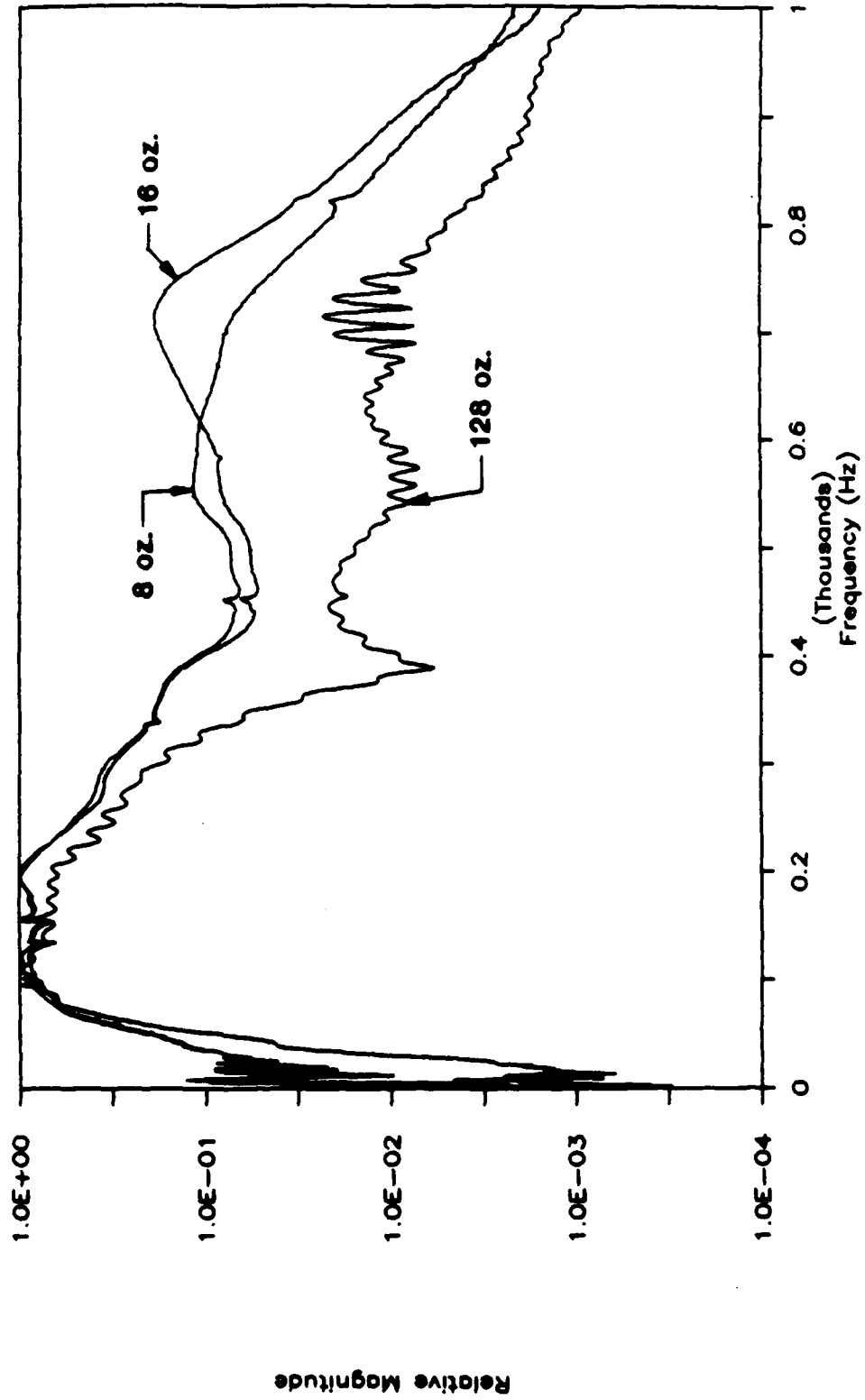


Figure F.6 - Magnitude (Relative) of Cross Power Spectrum for X = 2.0 ft for G. G. Brown Parking Lot Site

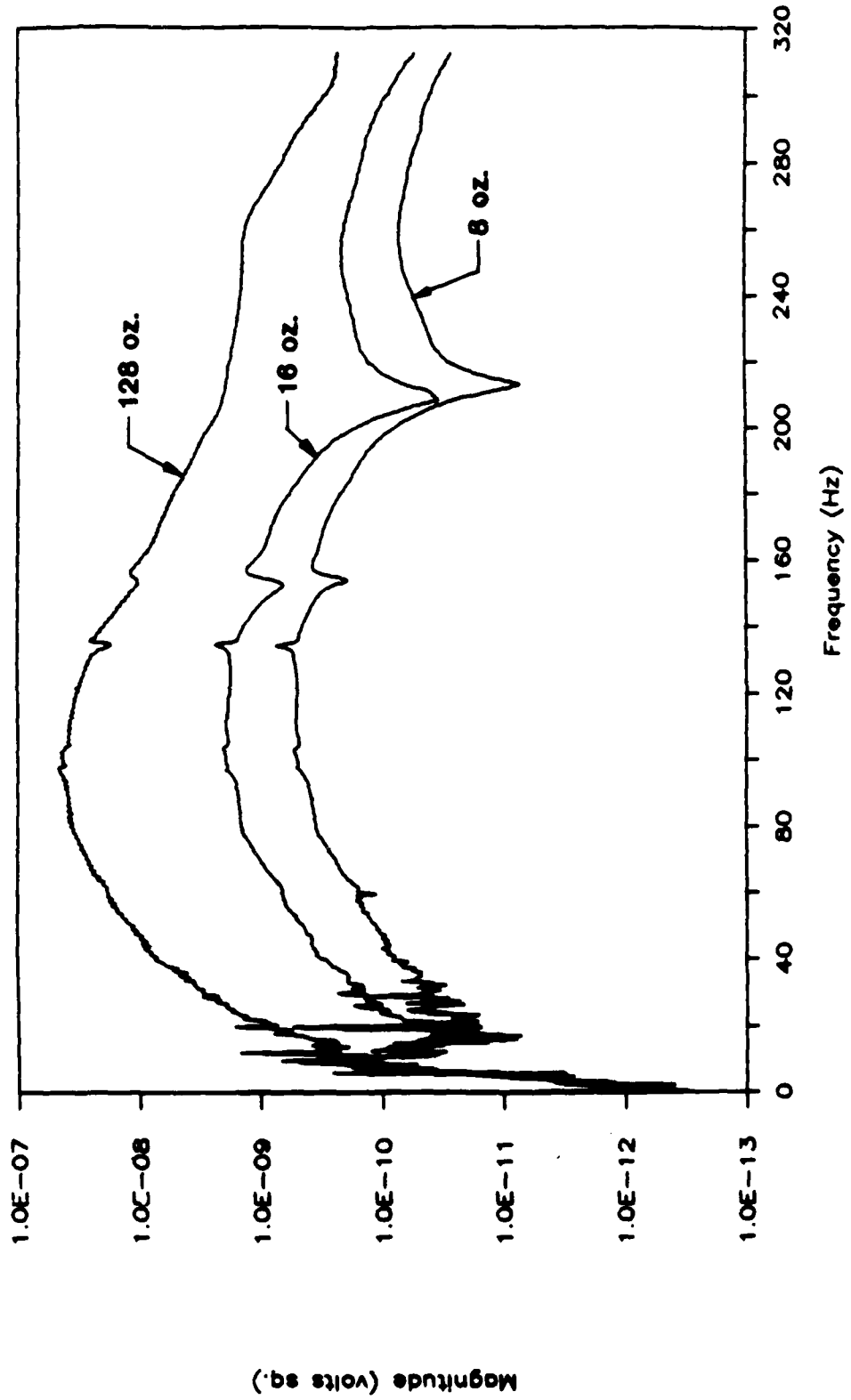


Figure F.7 - Magnitude (Absolute) of Cross Power Spectrum for X = 4.0 ft for G. G. Brown Parking Lot Site

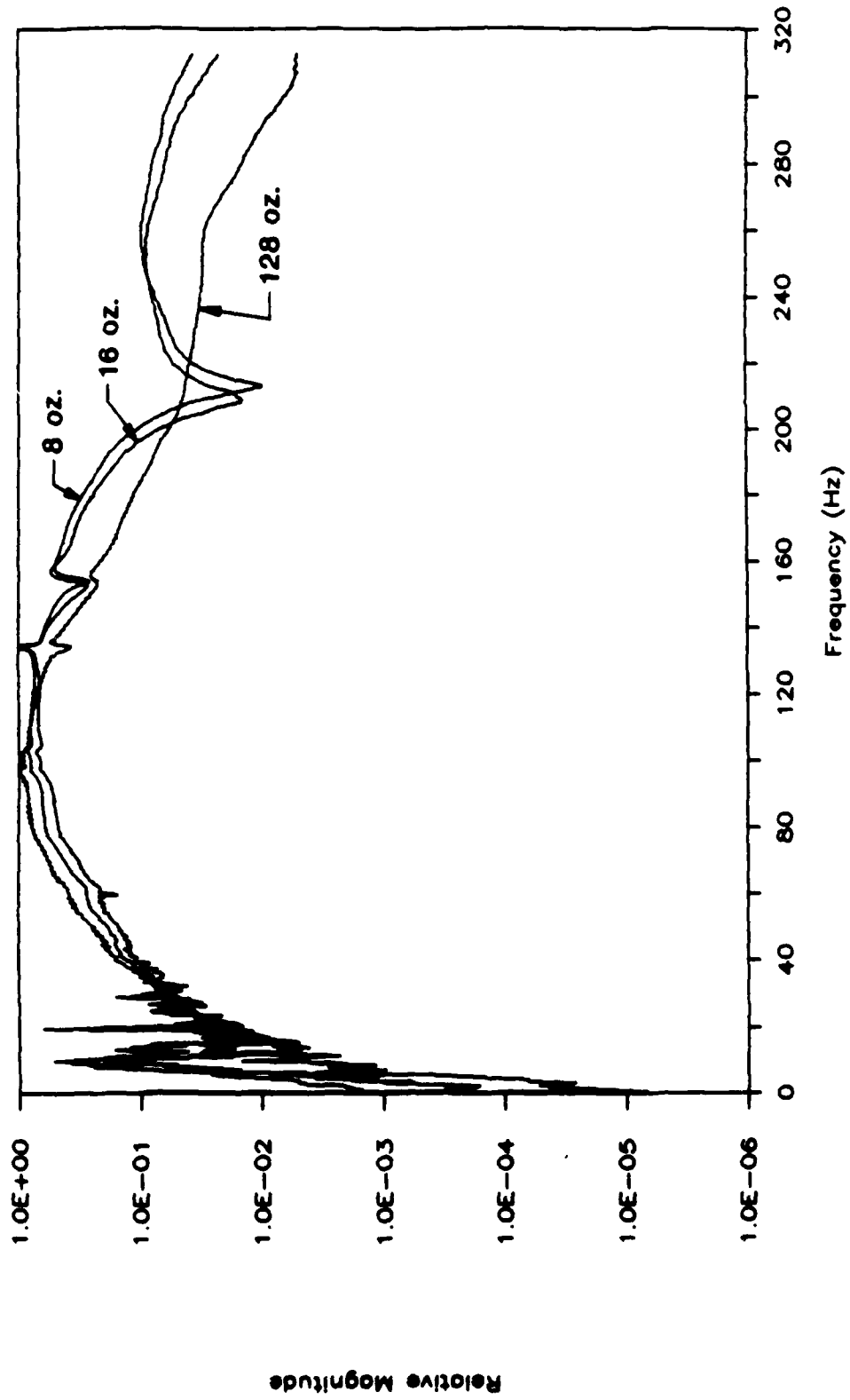


Figure F.9 - Magnitude (Relative) of Cross Power Spectrum for X = 4.0 ft for G. G. Brown Parking Lot Site

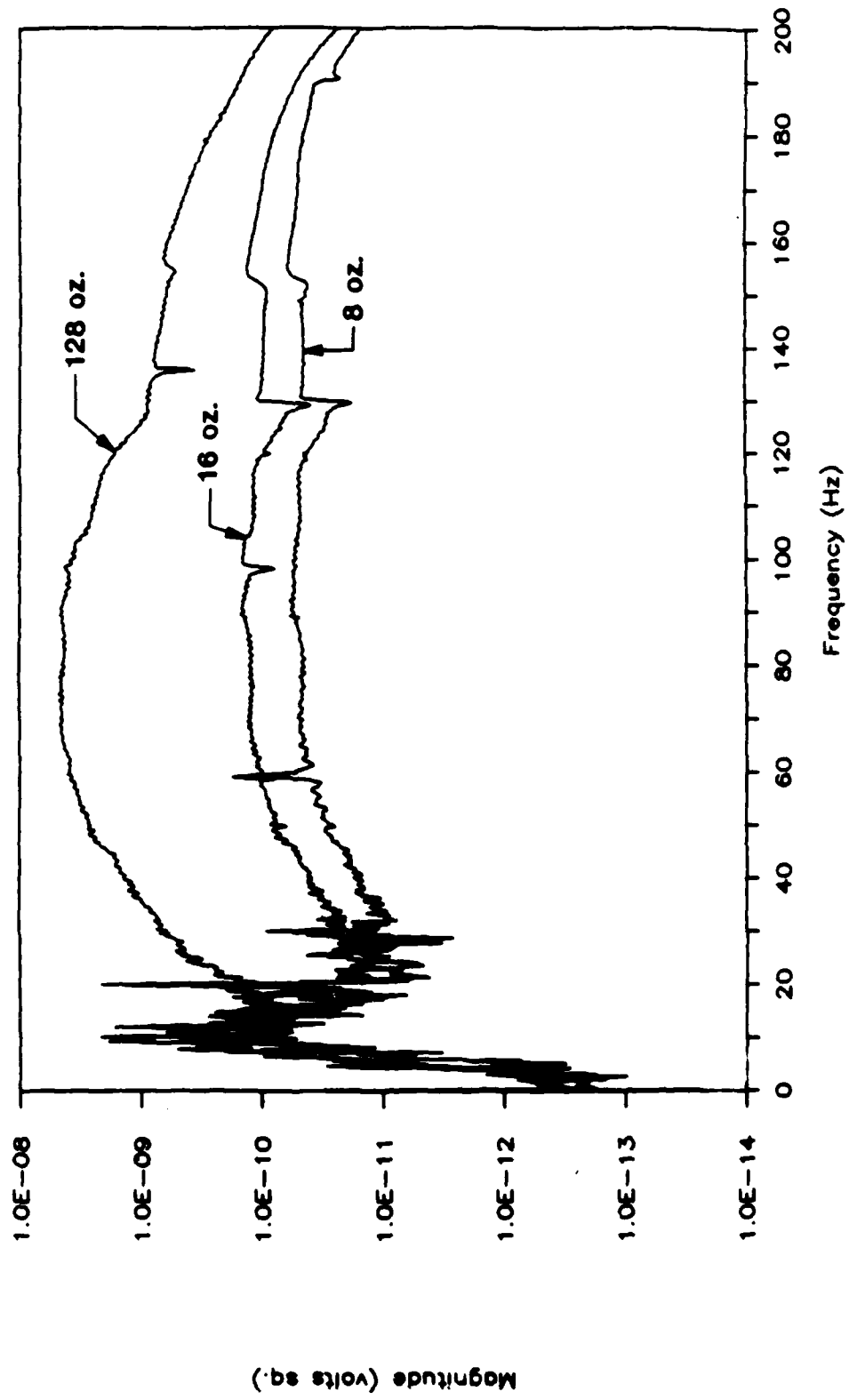


Figure F.9 - Magnitude (Absolute) of Cross Power Spectrum for X = 8.0 ft for G. G. Brown Parking Lot Site

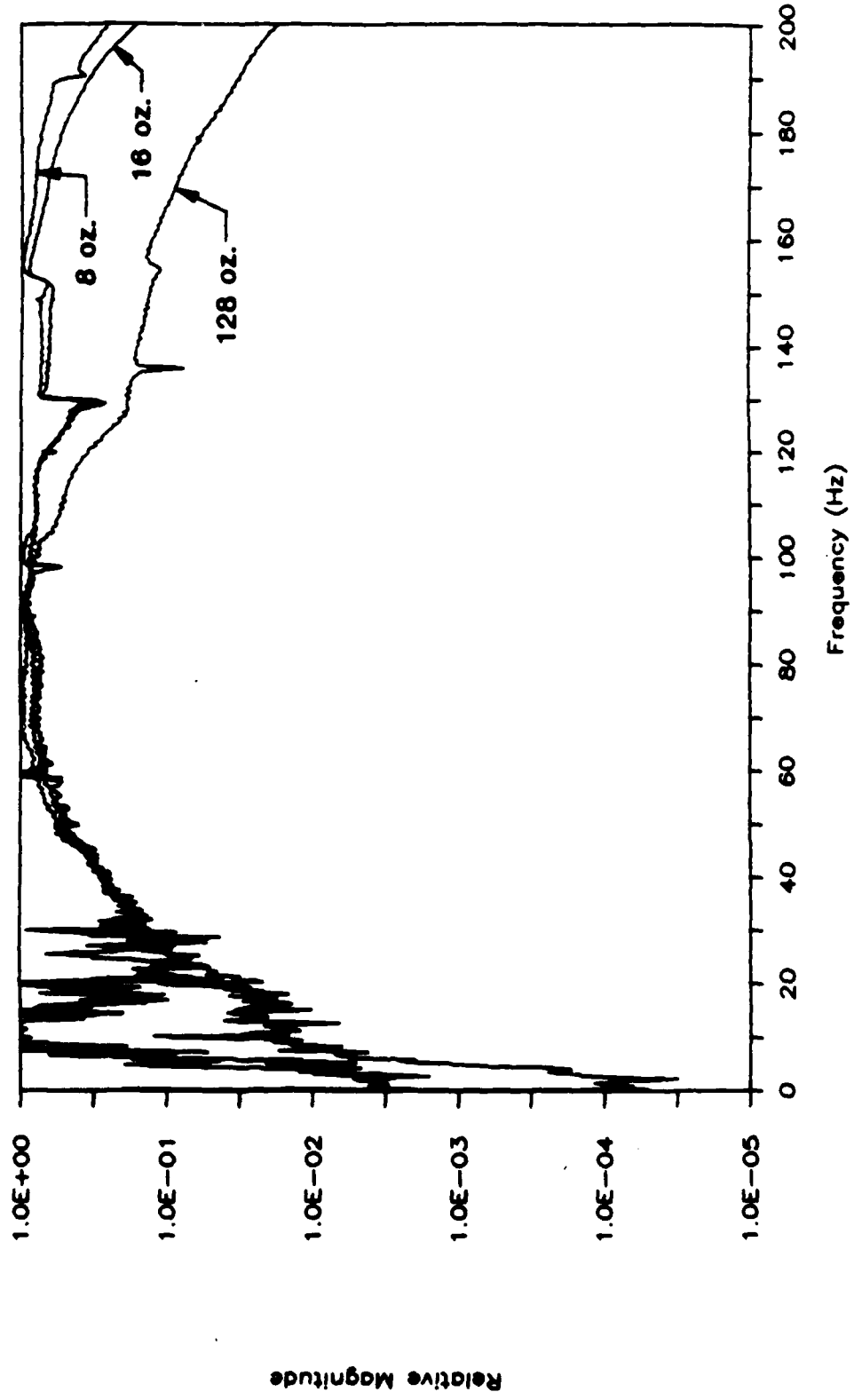


Figure F.10 - Magnitude (Relative) of Cross Power Spectrum for X = 8.0 ft for G. G. Brown Parking Lot Site

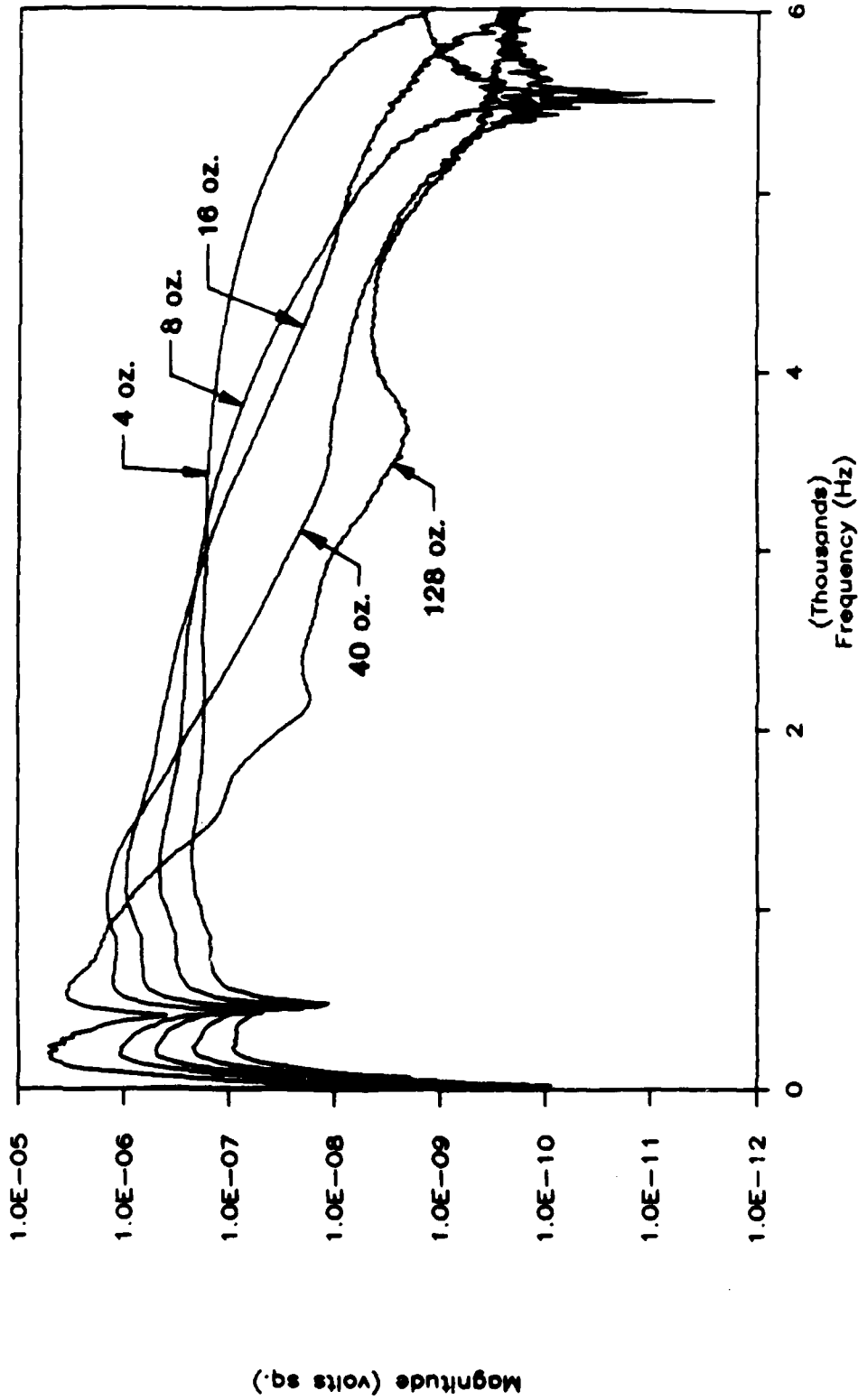


Figure F.11 - Magnitude (Absolute) of Cross Power Spectrum for X = 1.0 ft for SEMTA Parking Lot Site

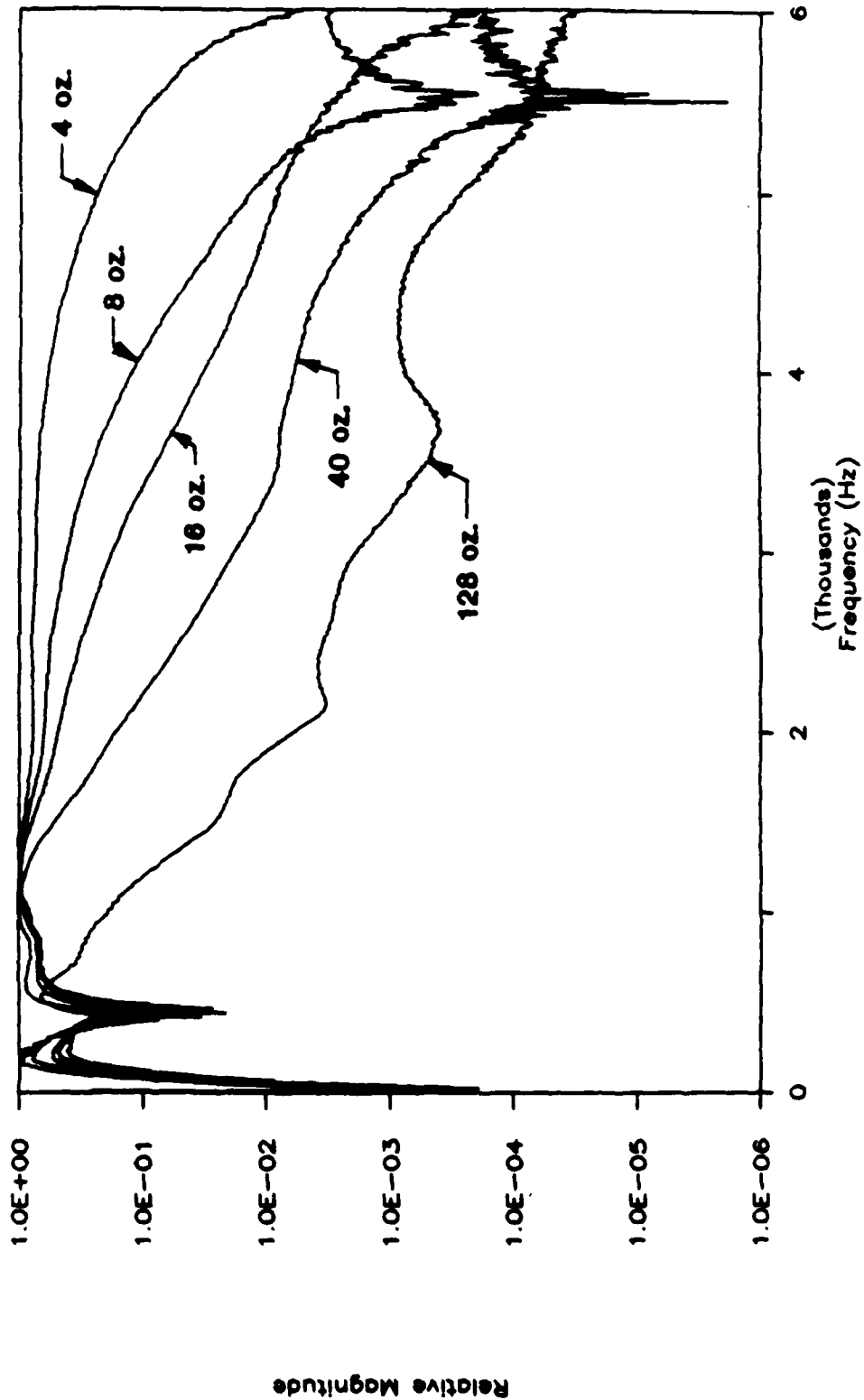


Figure F.12 - Magnitude (Relative) of Cross Power Spectrum for X = 1.0 ft for SEMTA Parking Lot Site

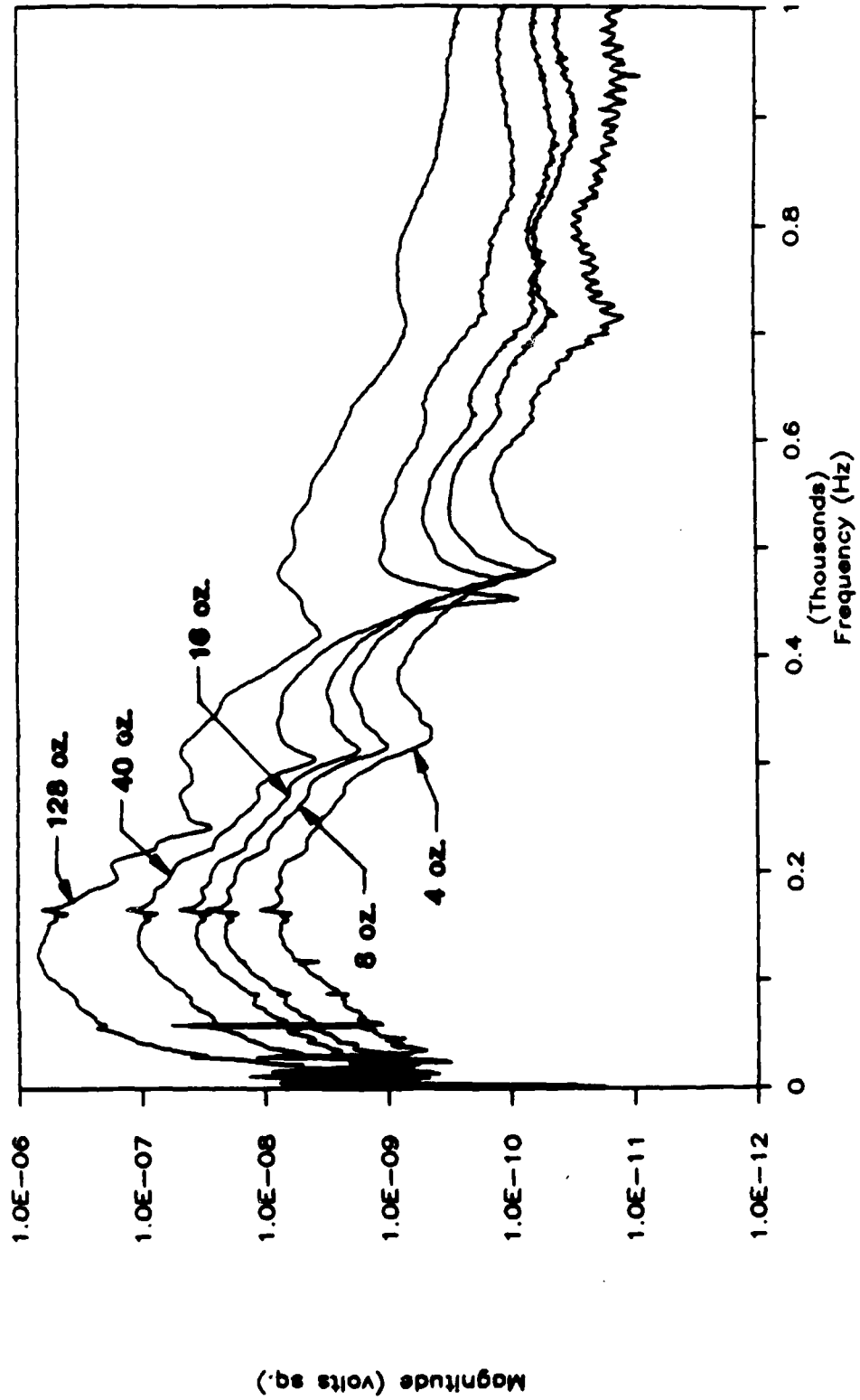


Figure F.13 - Magnitude (Absolute) of Cross Power Spectrum for X = 2.0 ft for SEMTA Parking Lot Site

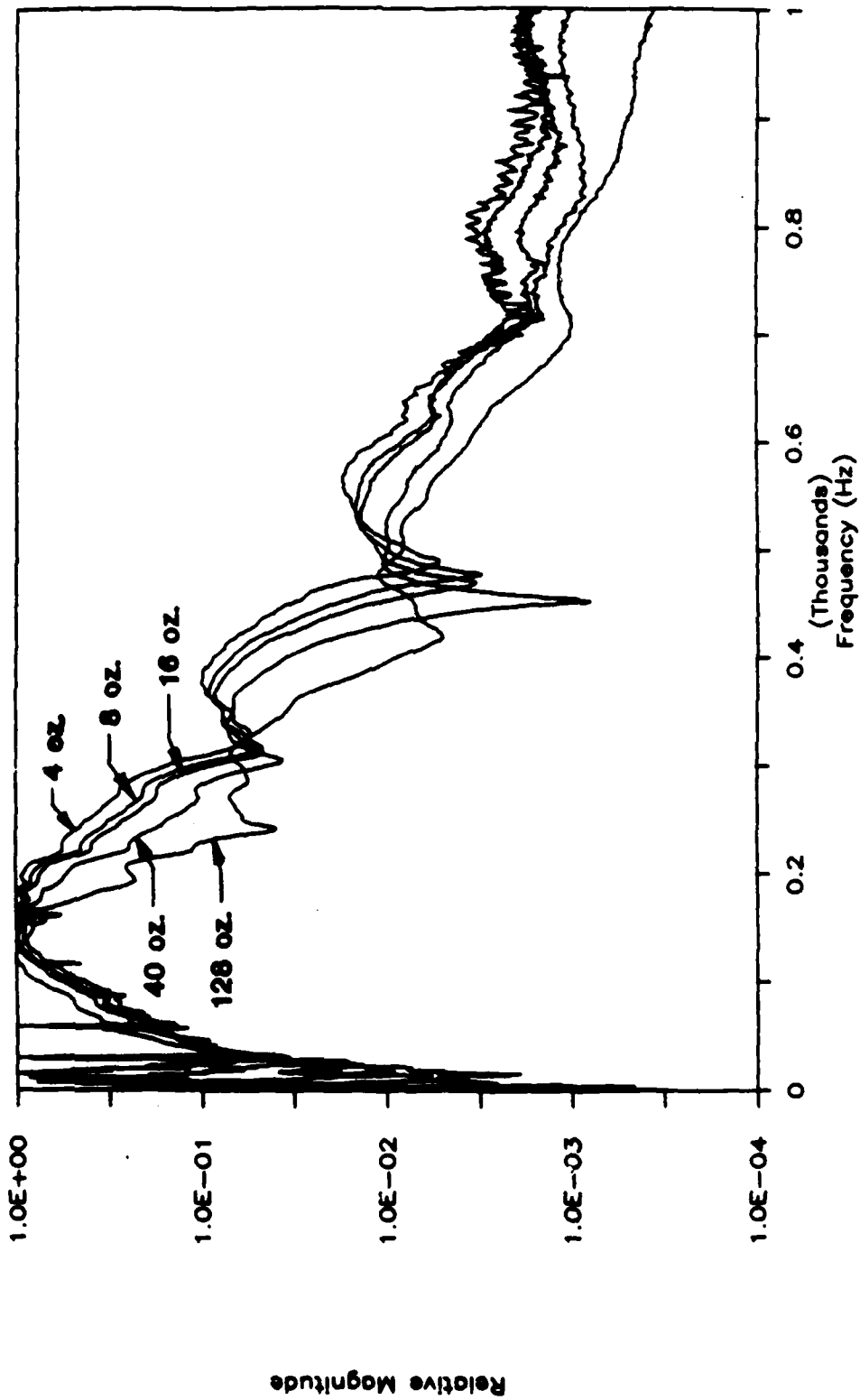


Figure F.14 - Magnitude (Relative) of Cross Power Spectrum for X = 2.0 ft for SEMTA Parking Lot Site

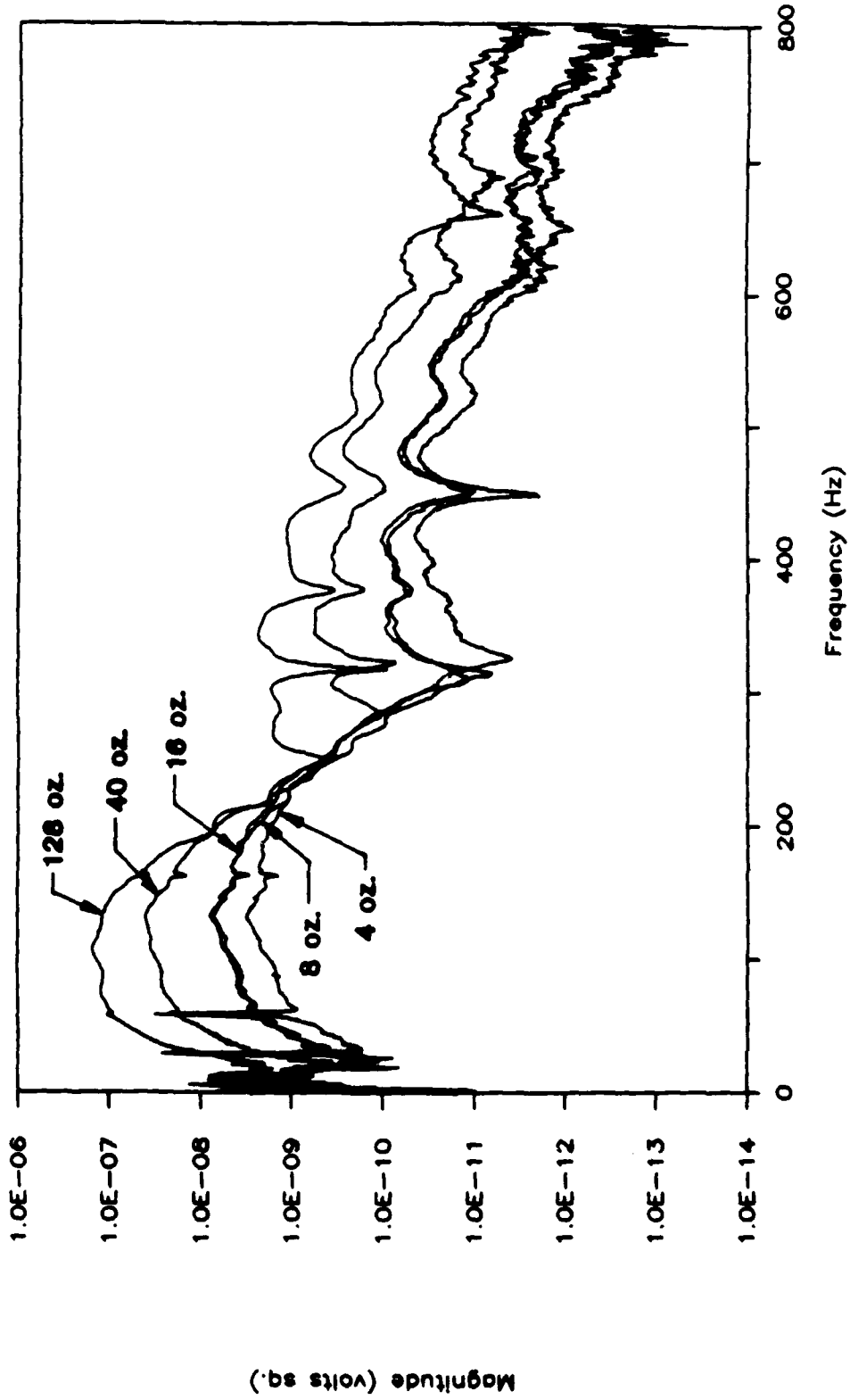


Figure F.15 - Magnitude (Absolute) of Cross Power Spectrum for X = 4.0 ft for SEMTA Parking Lot Site

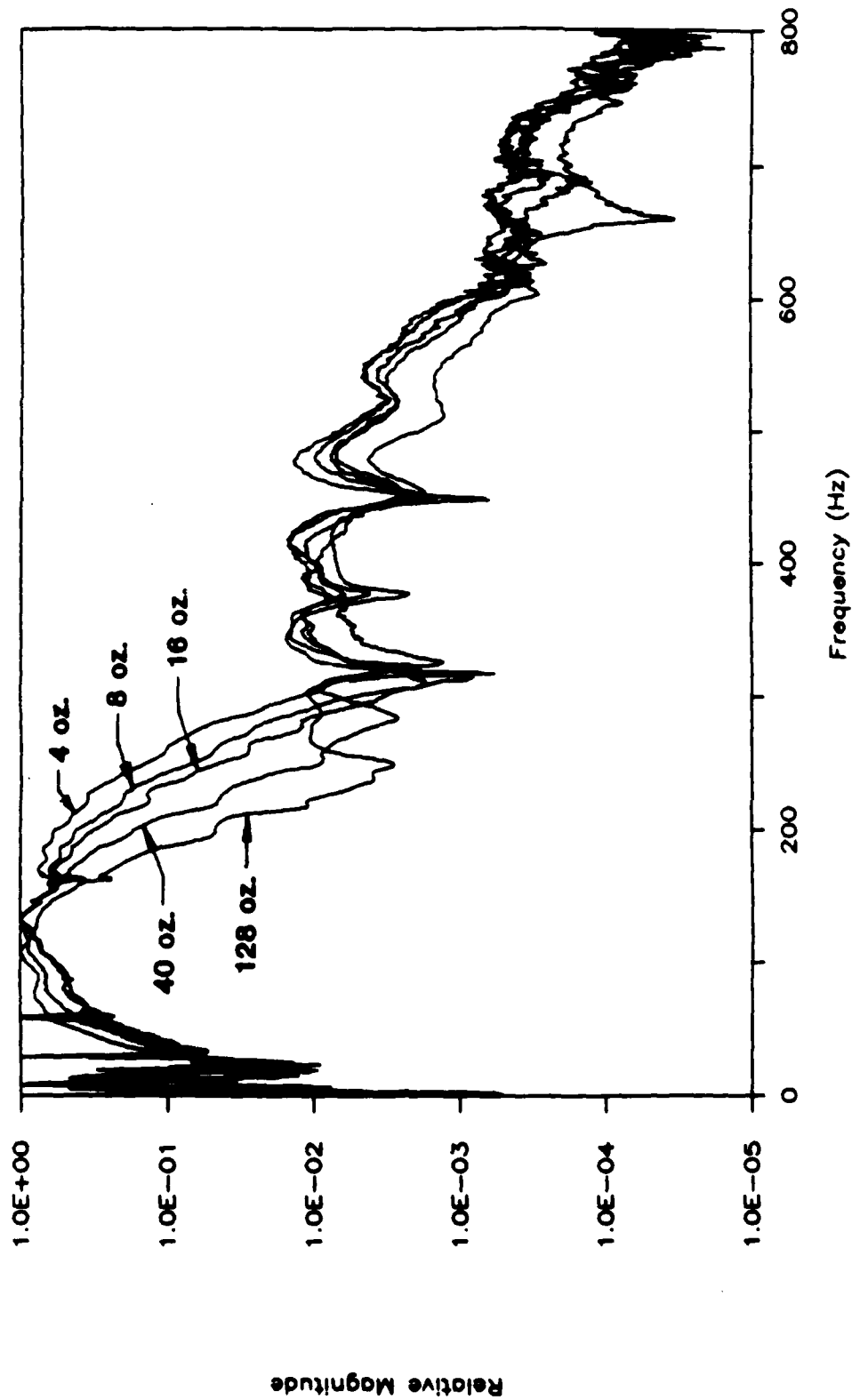


Figure F.16 - Magnitude (Relative) of Cross Power Spectrum for X = 4.0 ft for SEMTA Parking Lot Site

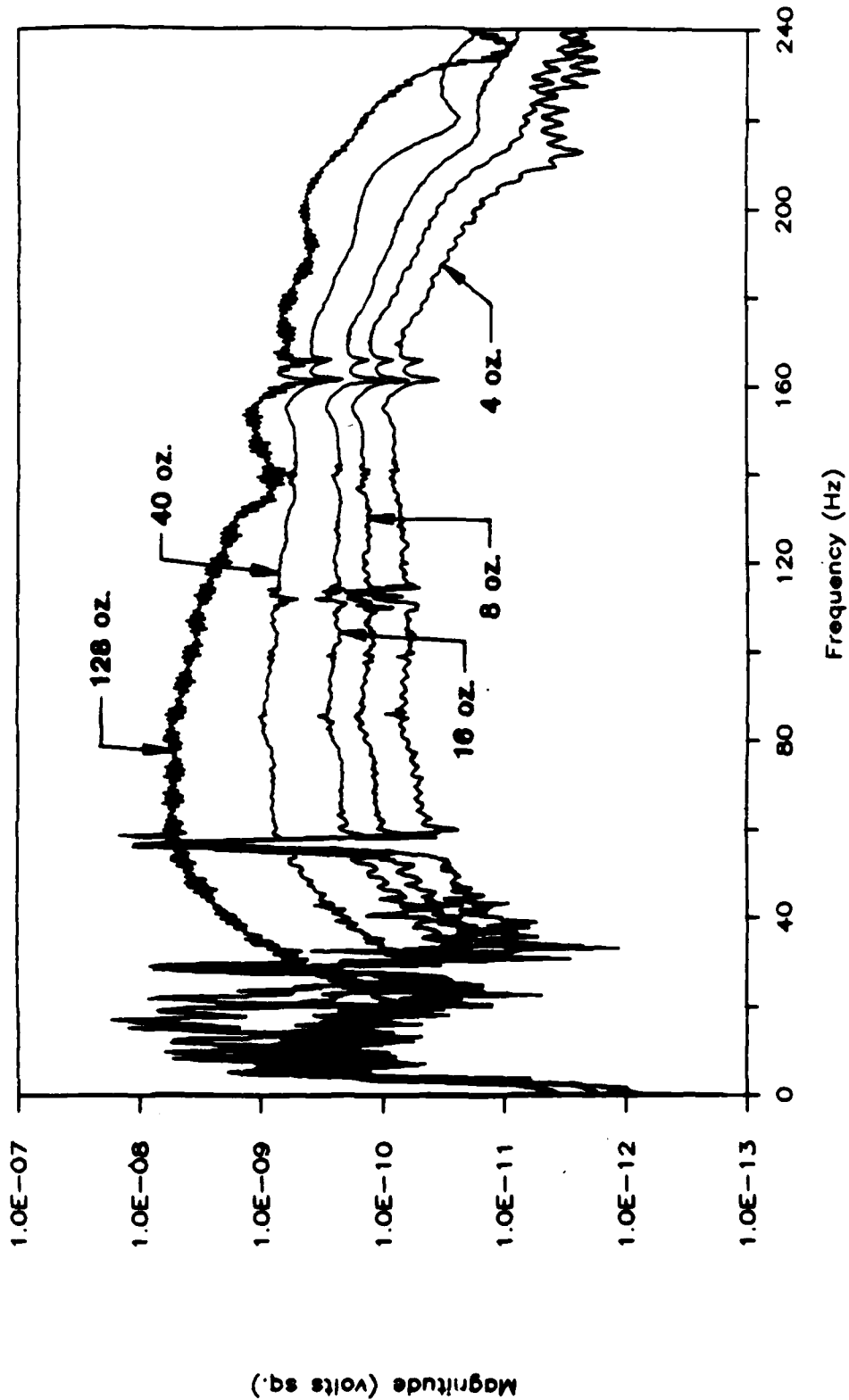


Figure F.17 - Magnitude (Absolute) of Cross Power Spectrum for X = 8.0 ft for SEMTA Parking Lot Site

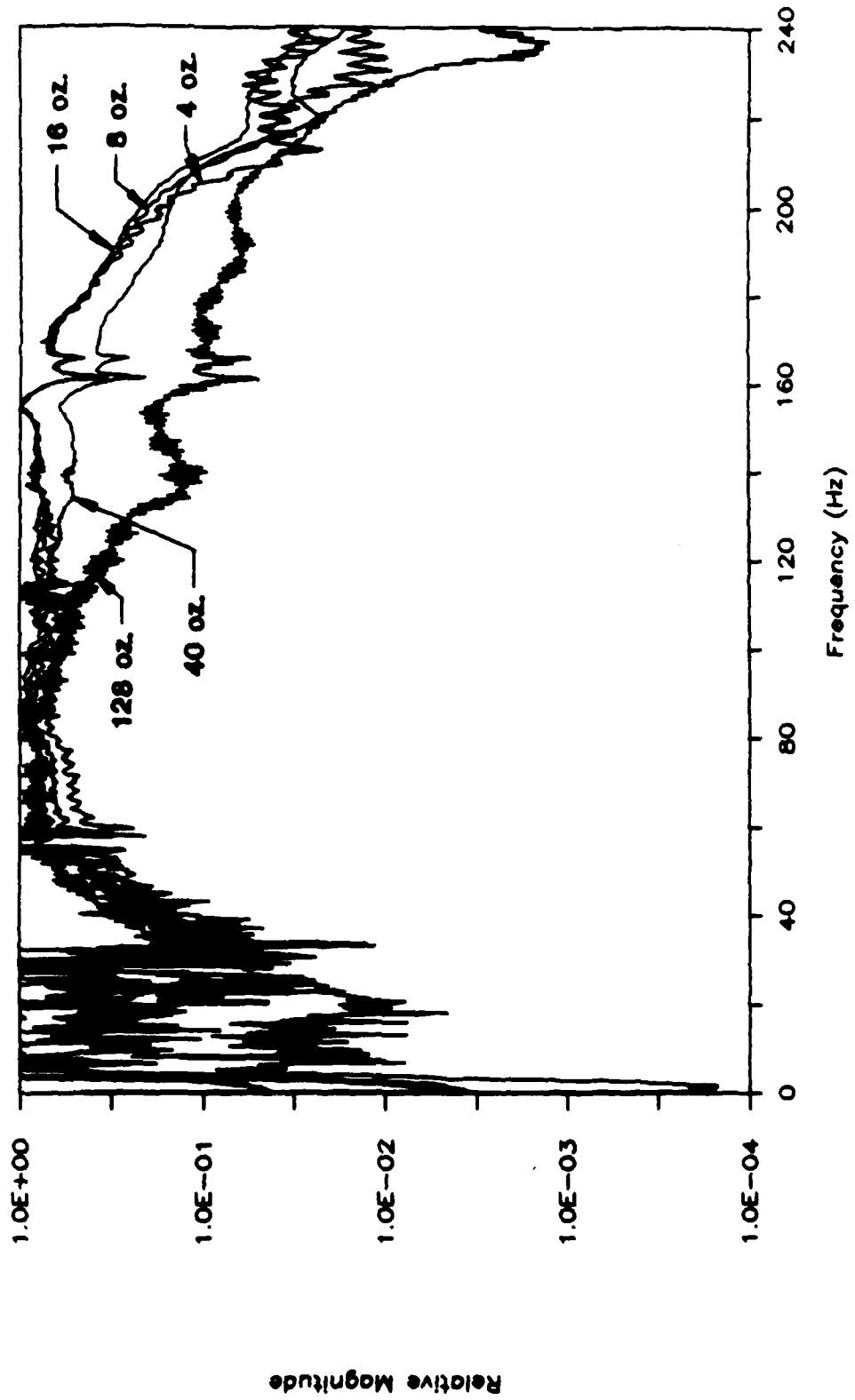


Figure F.18 - Magnitude (Relative) of Cross Power Spectrum for X = 8.0 ft for SEMTA Parking Lot Site

APPENDIX G

COMBINED DISPERSION CURVES AS A FUNCTION OF SOURCE TYPE

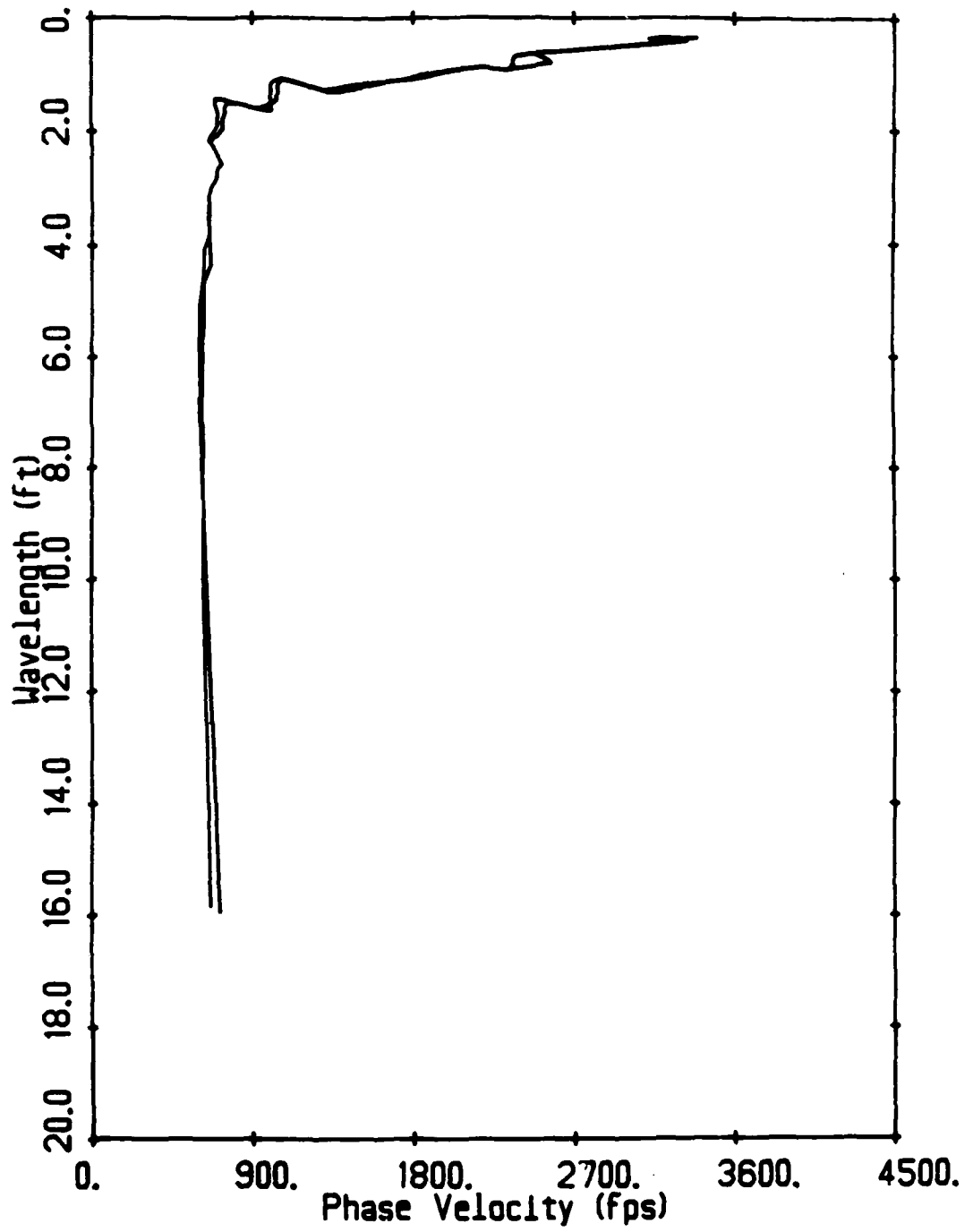


Figure G.1— Average Experimental Dispersion Curve for 8 oz Hammer for G. G. Brown Parking Lot Site (all wavelengths)

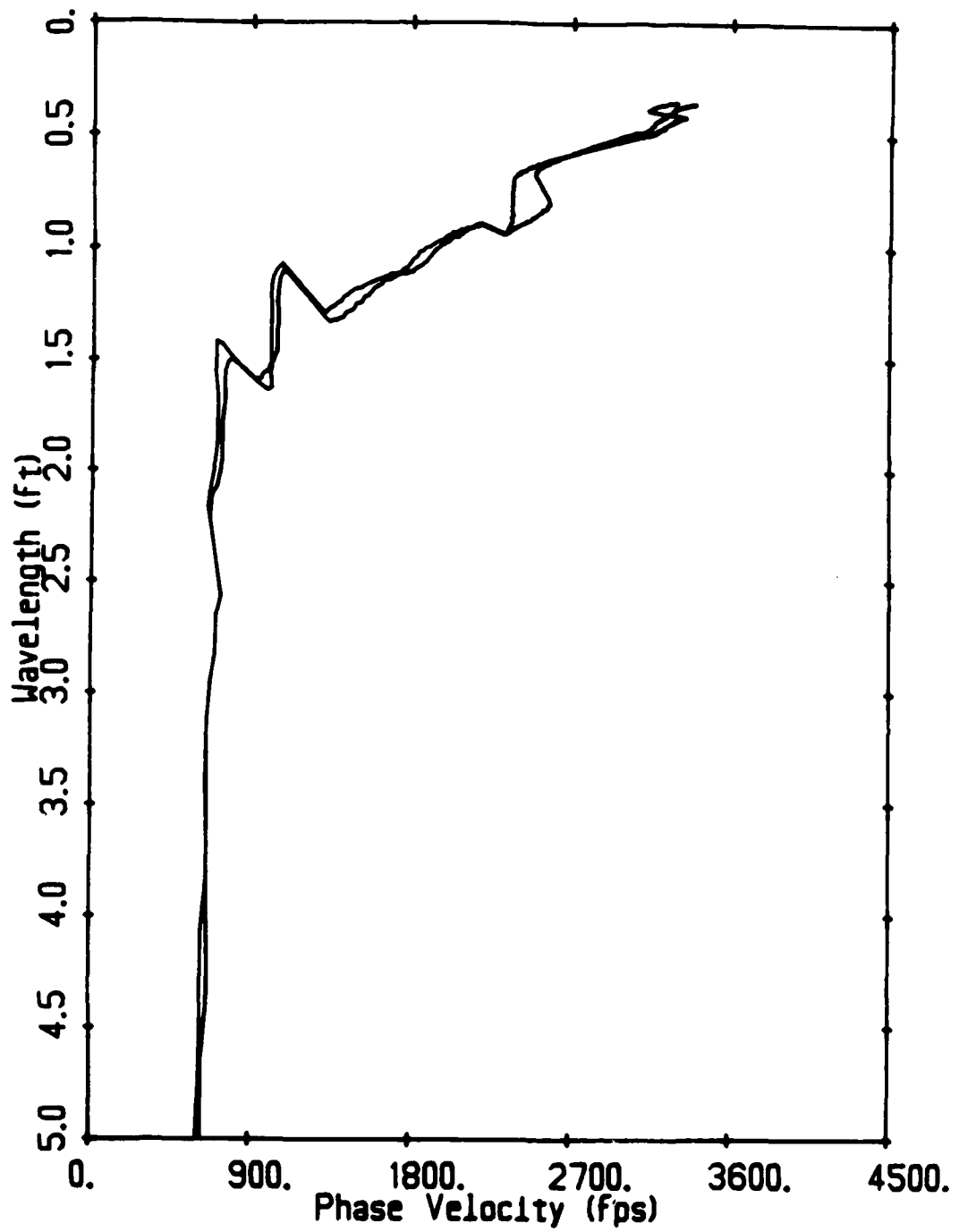


Figure G.2— Average Experimental Dispersion Curve for 8 os Hammer for
G. G. Brown Parking Lot Site (0 to 5-ft wavelengths)

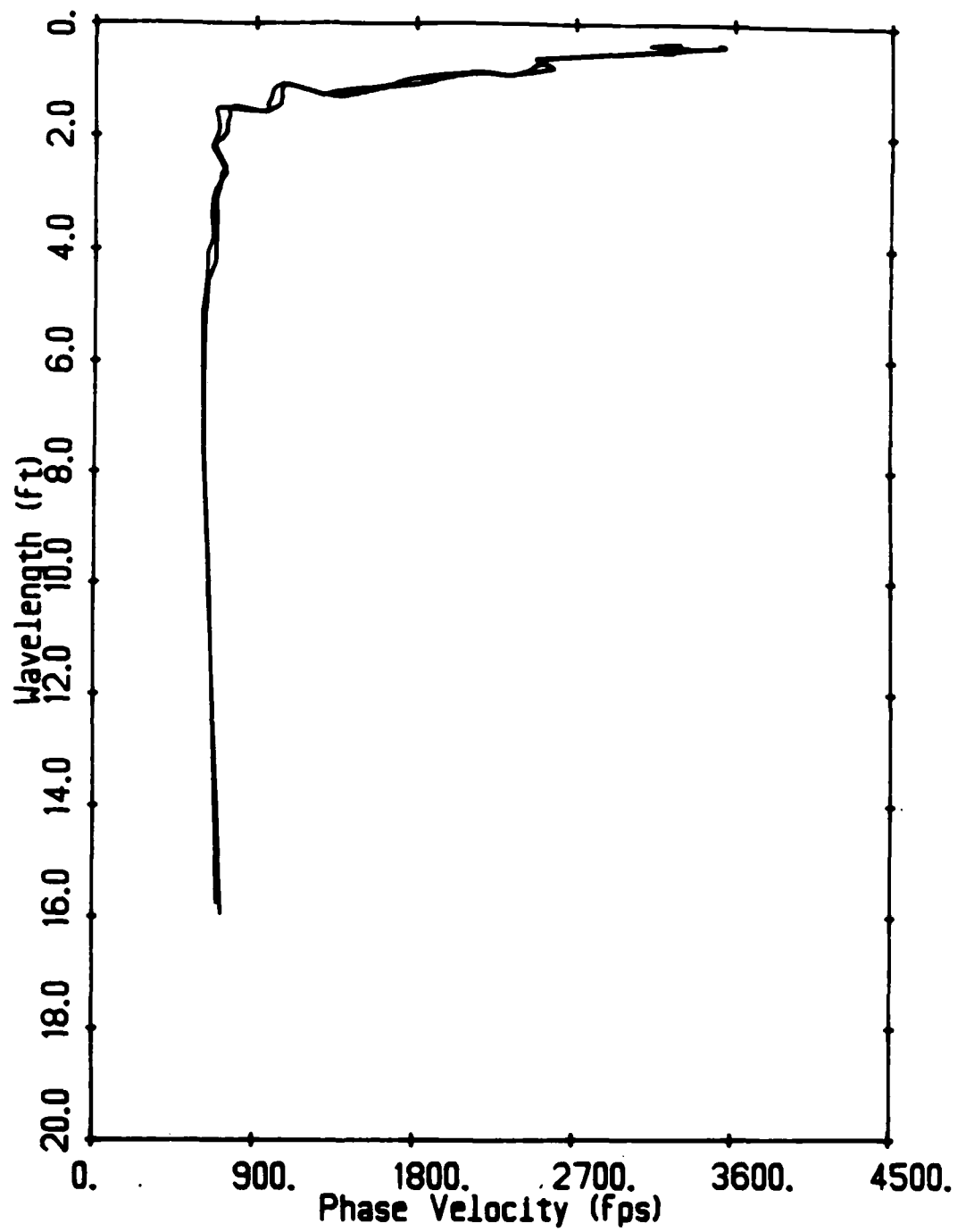


Figure G.3— Average Experimental Dispersion Curve for 16 oz Hammer for
G. G. Brown Parking Lot Site (all wavelengths)

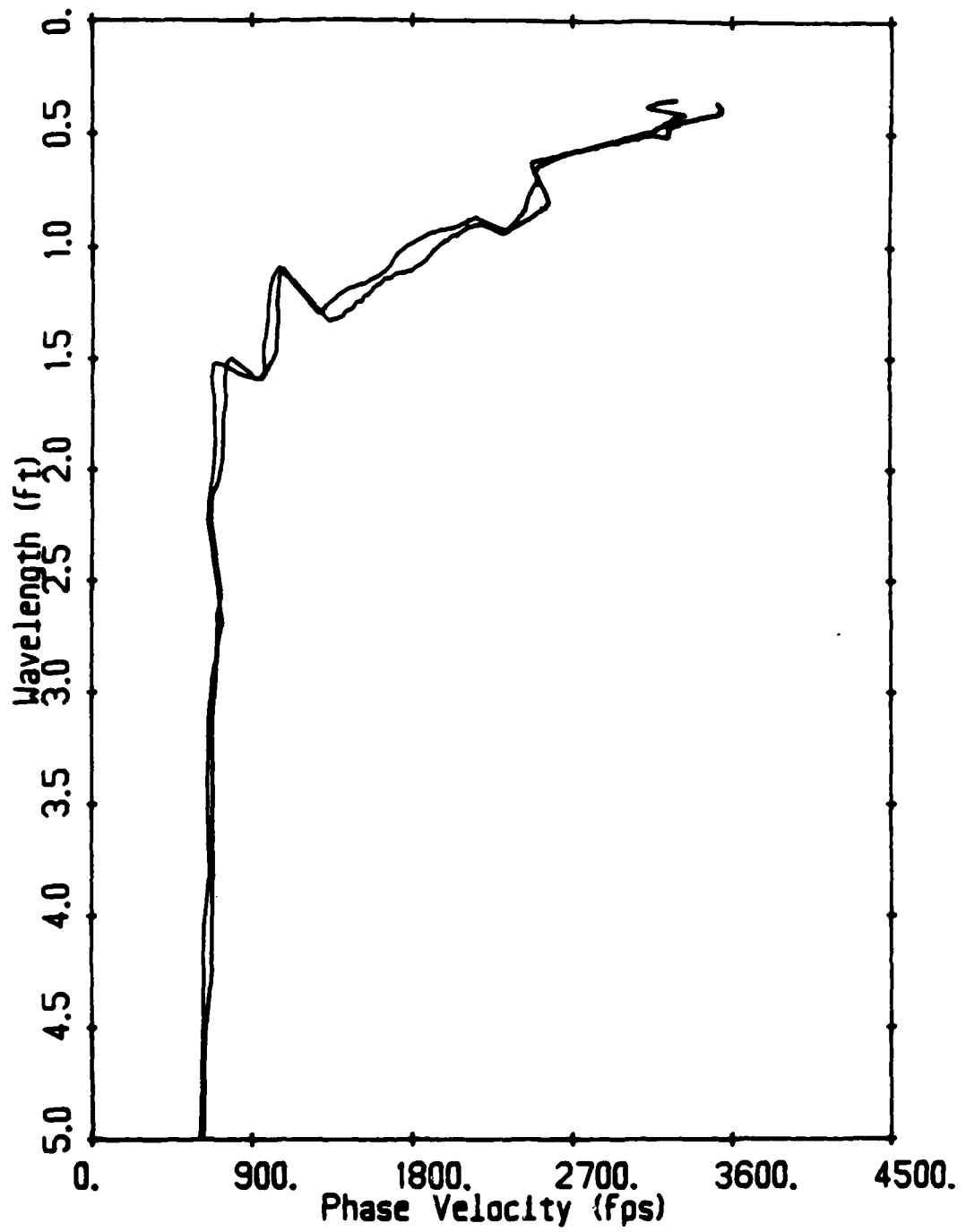


Figure G.4— Average Experimental Dispersion Curve for 16 oz Hammer for G. G. Brown Parking Lot Site (0 to 5-ft wavelengths)

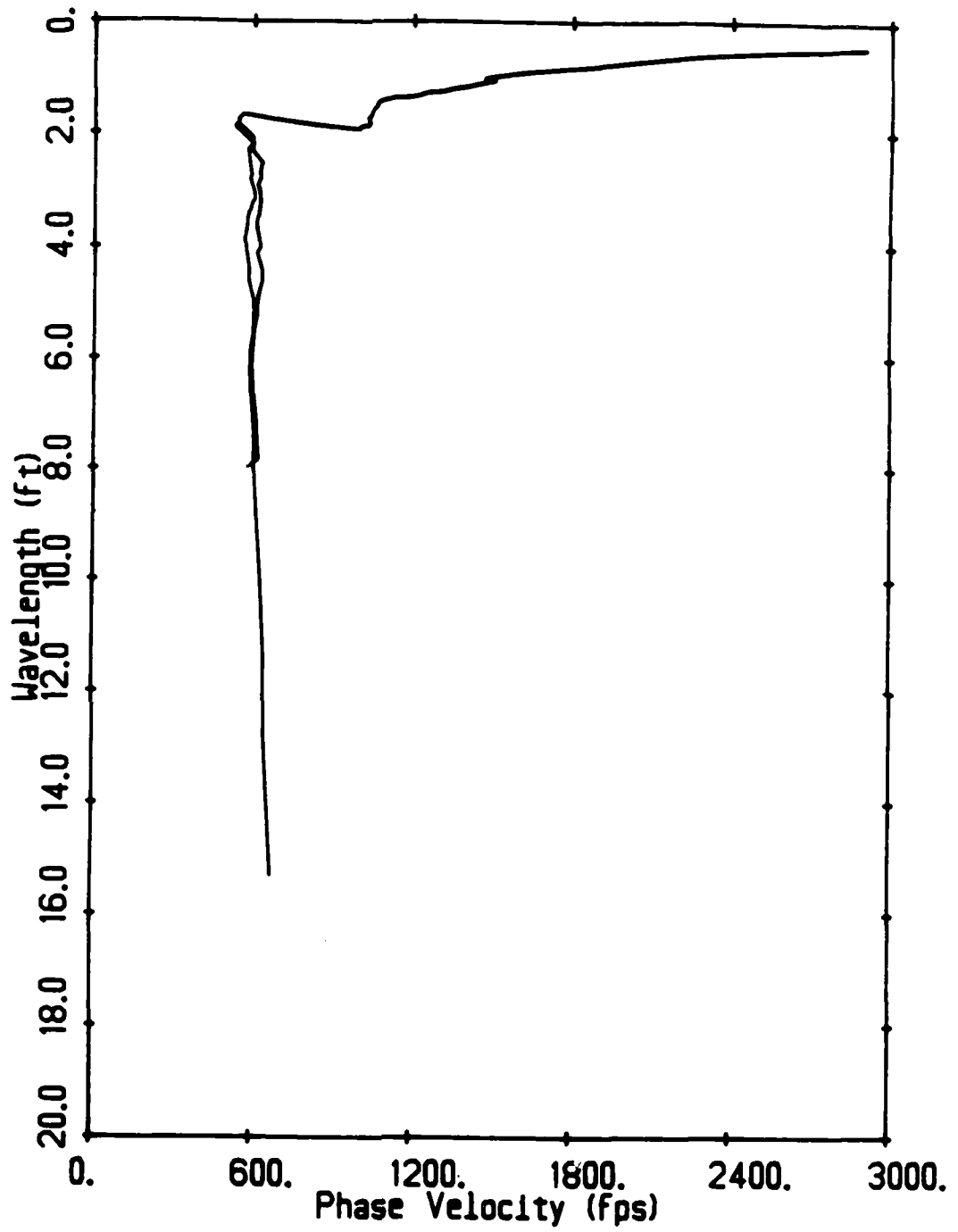


Figure G.5— Average Experimental Dispersion Curve for 4 oz Hammer for SEMTA Parking Lot Site (all wavelengths)

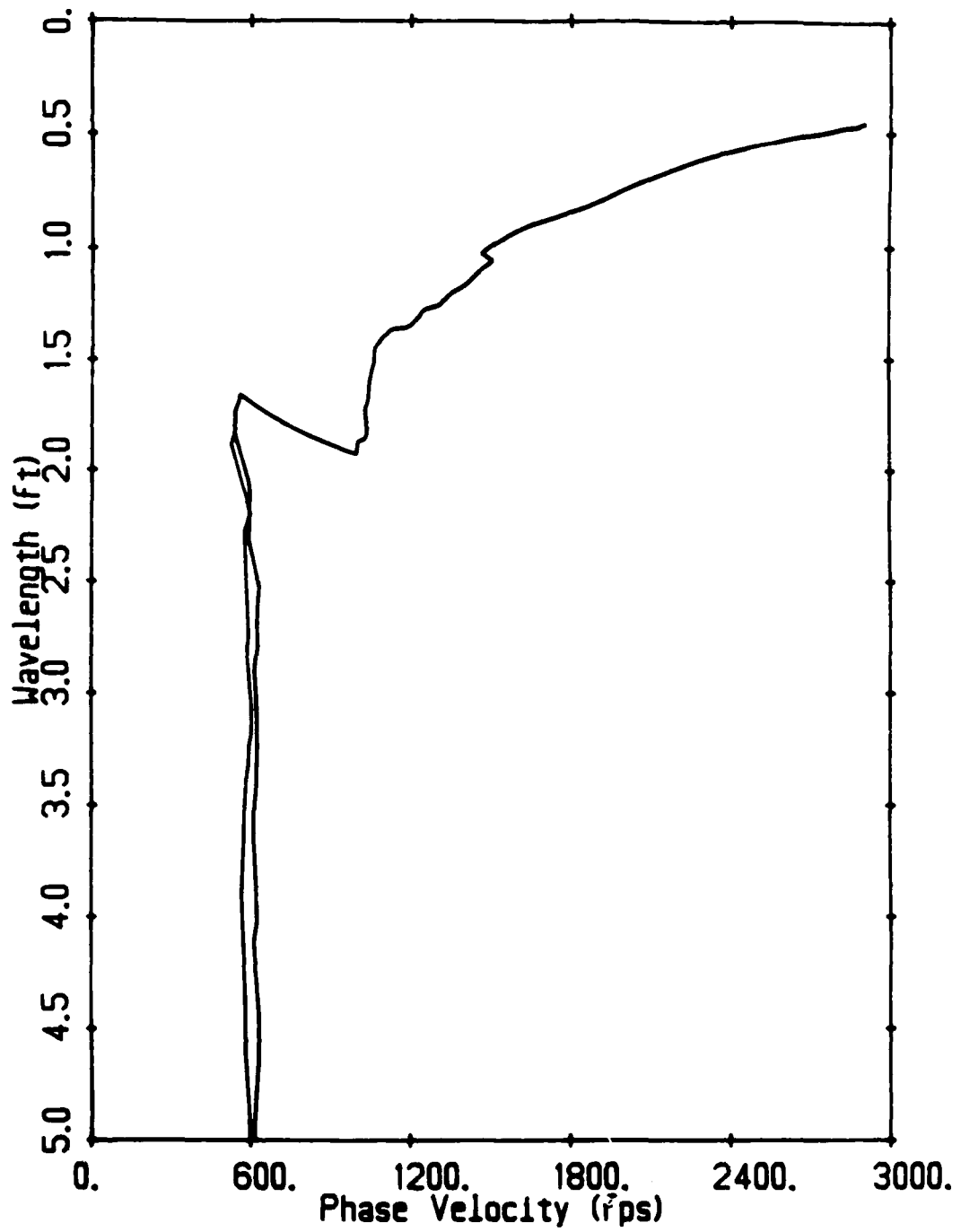


Figure G.6— Average Experimental Dispersion Curve for 4 os Hammer for SEMTA Parking Lot Site (0 to 5-ft wavelengths)

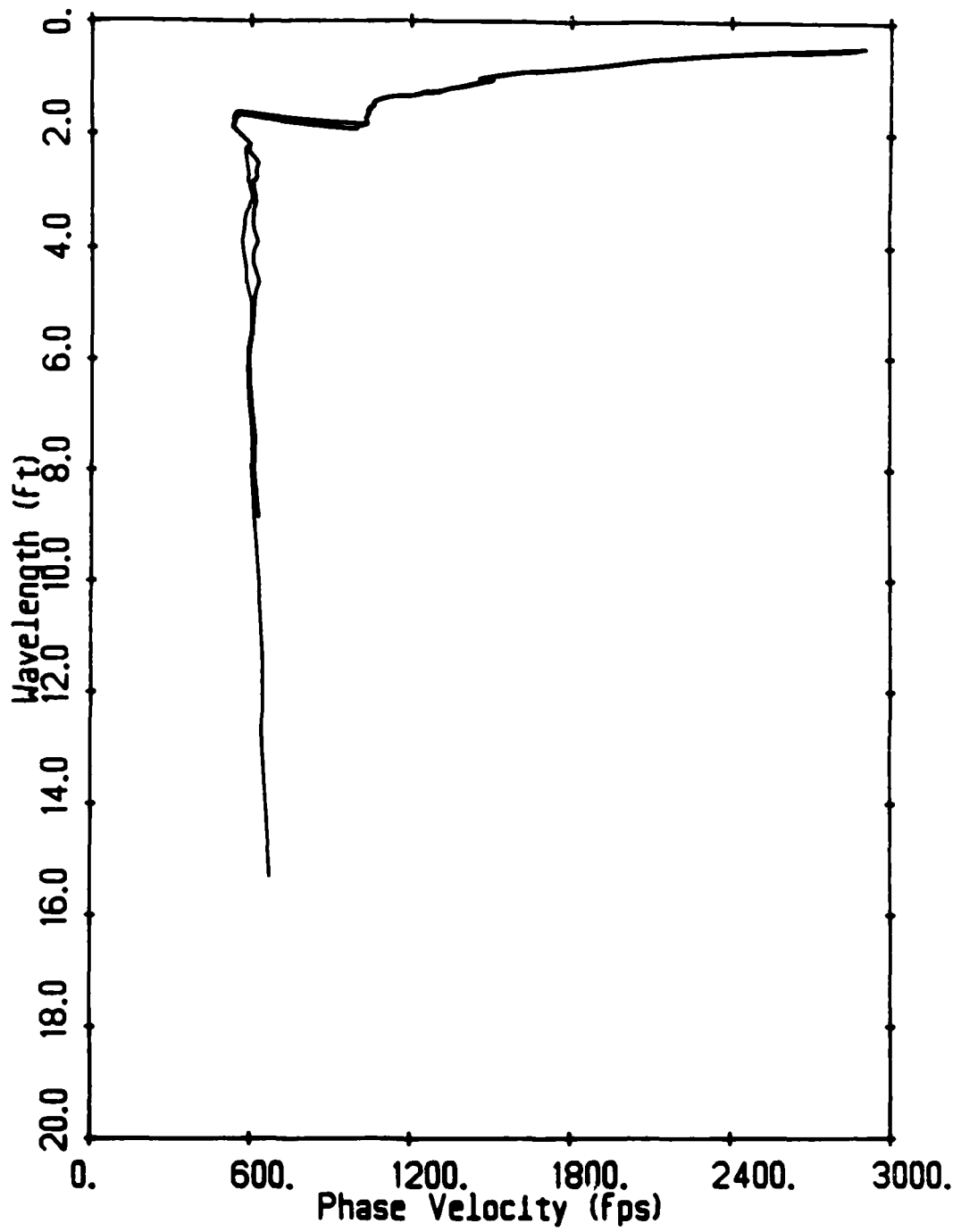


Figure G.7— Average Experimental Dispersion Curve for 8 oz Hammer for SEMTA Parking Lot Site (all wavelengths)

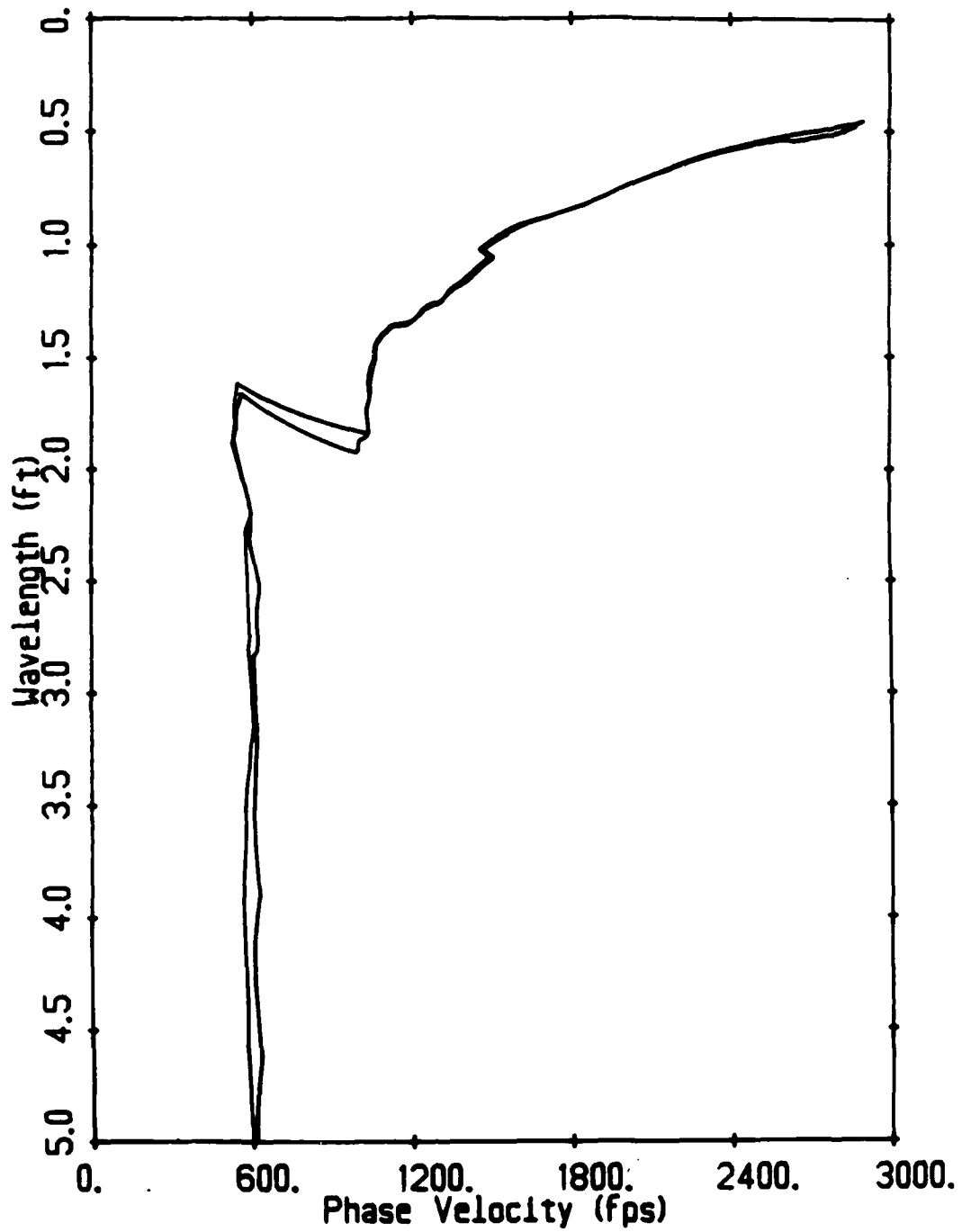


Figure G.8— Average Experimental Dispersion Curve for 8 oz Hammer for SEMTA Parking Lot Site (0 to 5-ft wavelengths)

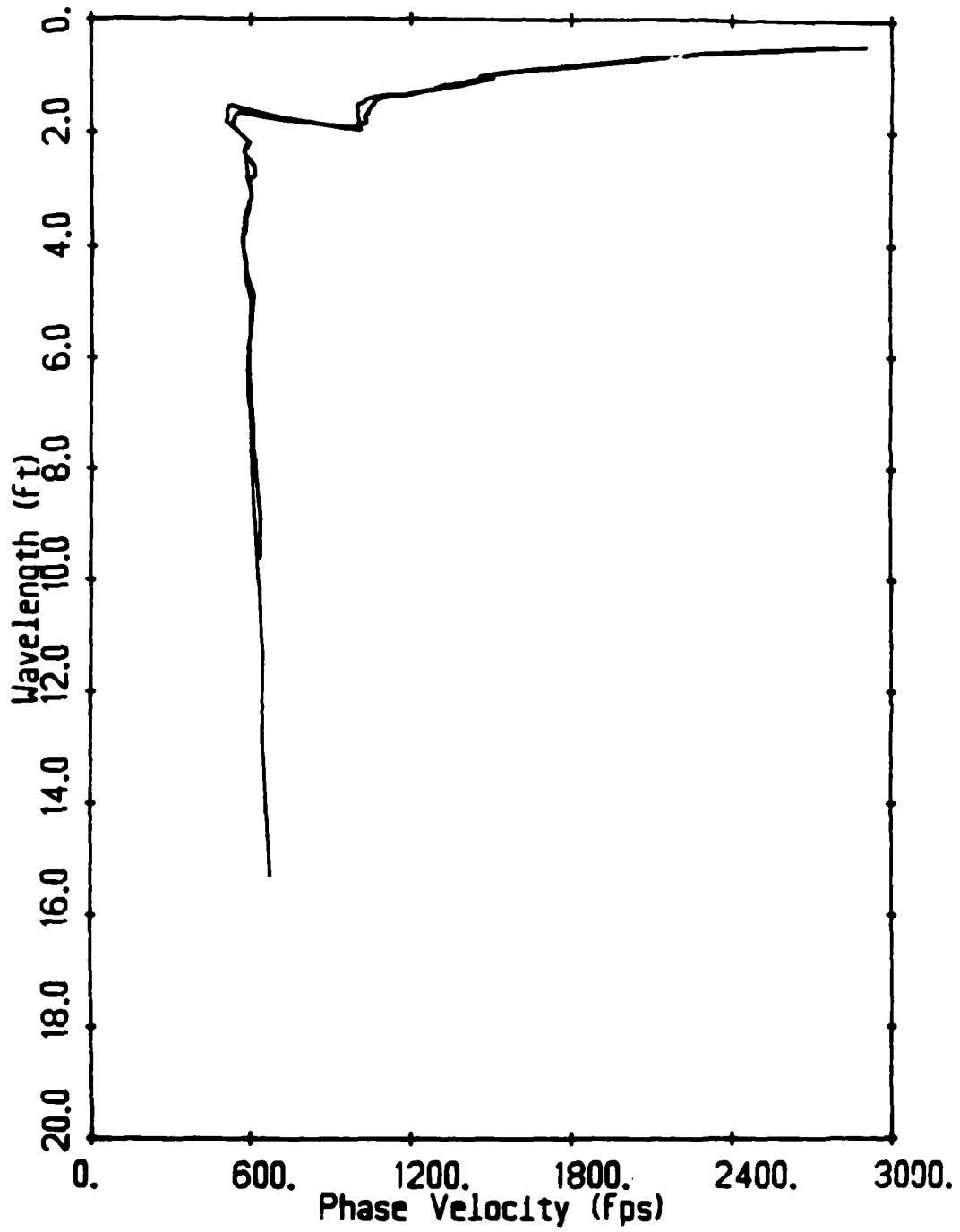


Figure G.9— Average Experimental Dispersion Curve for 16 oz Hammer for SEMTA Parking Lot Site (all wavelengths)

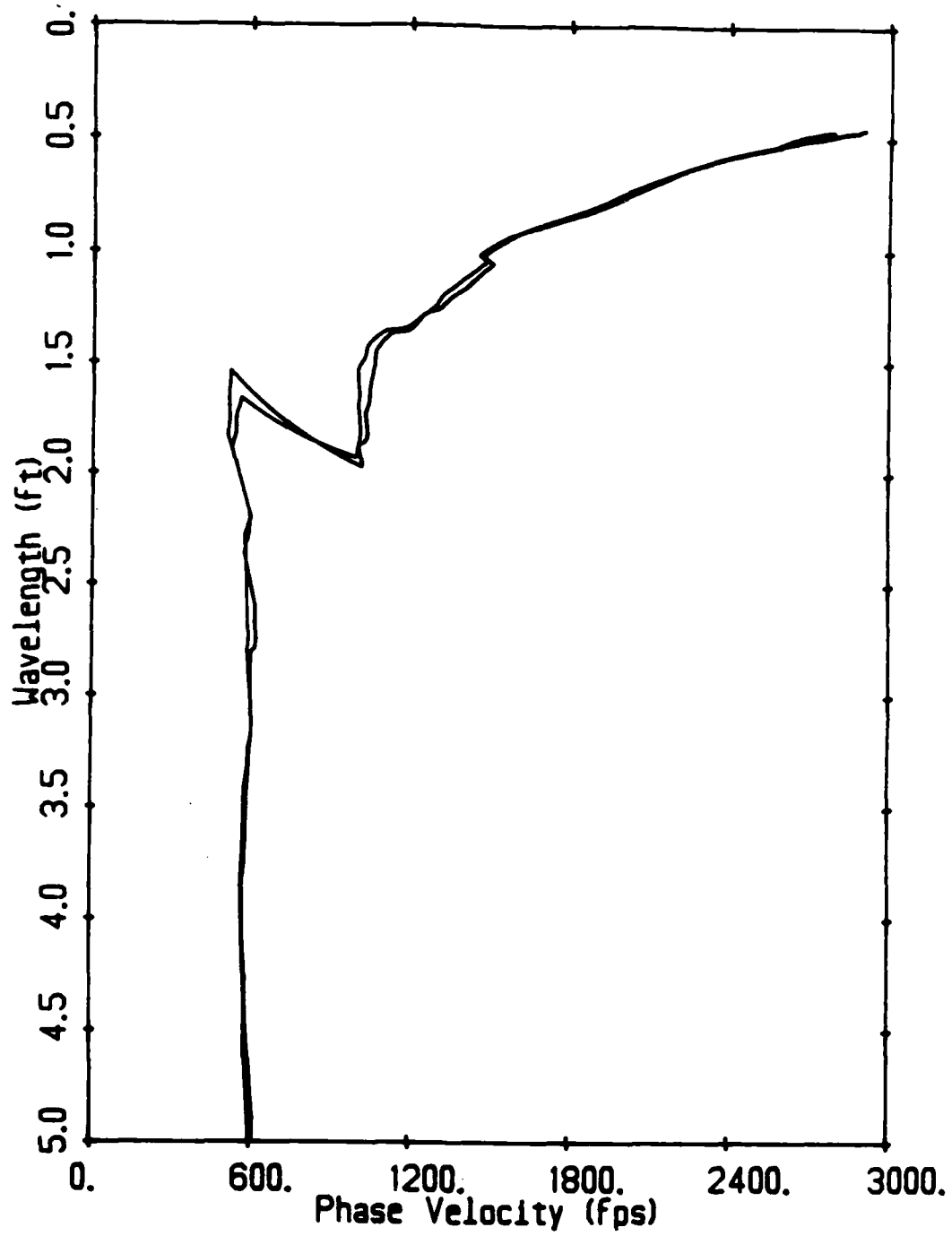


Figure G.10— Average Experimental Dispersion Curve for 16 oz Hammer for SEMTA Parking Lot Site (0 to 5-ft wavelengths)

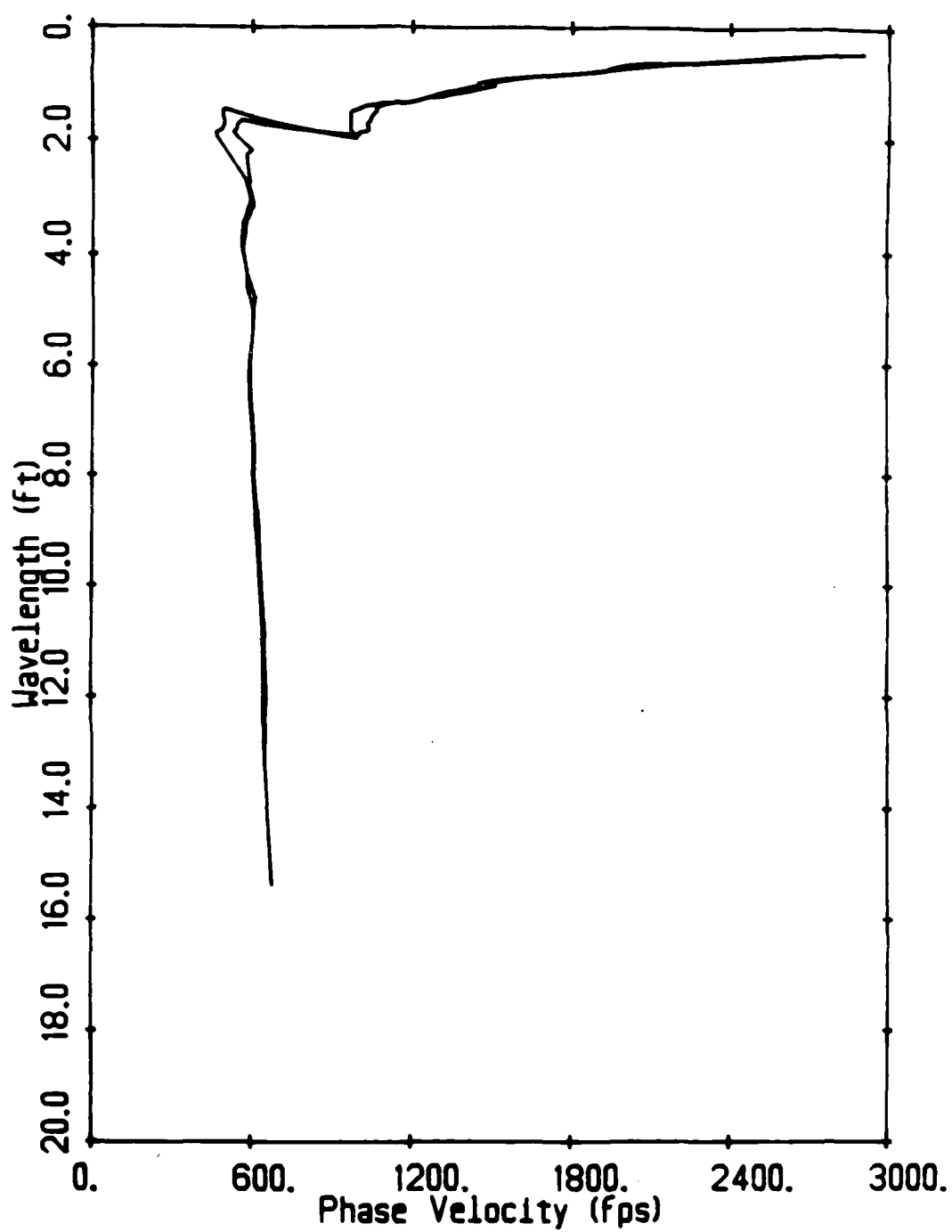


Figure G.11— Average Experimental Dispersion Curve for 40 os Hammer for SEMTA Parking Lot Site (all wavelengths)

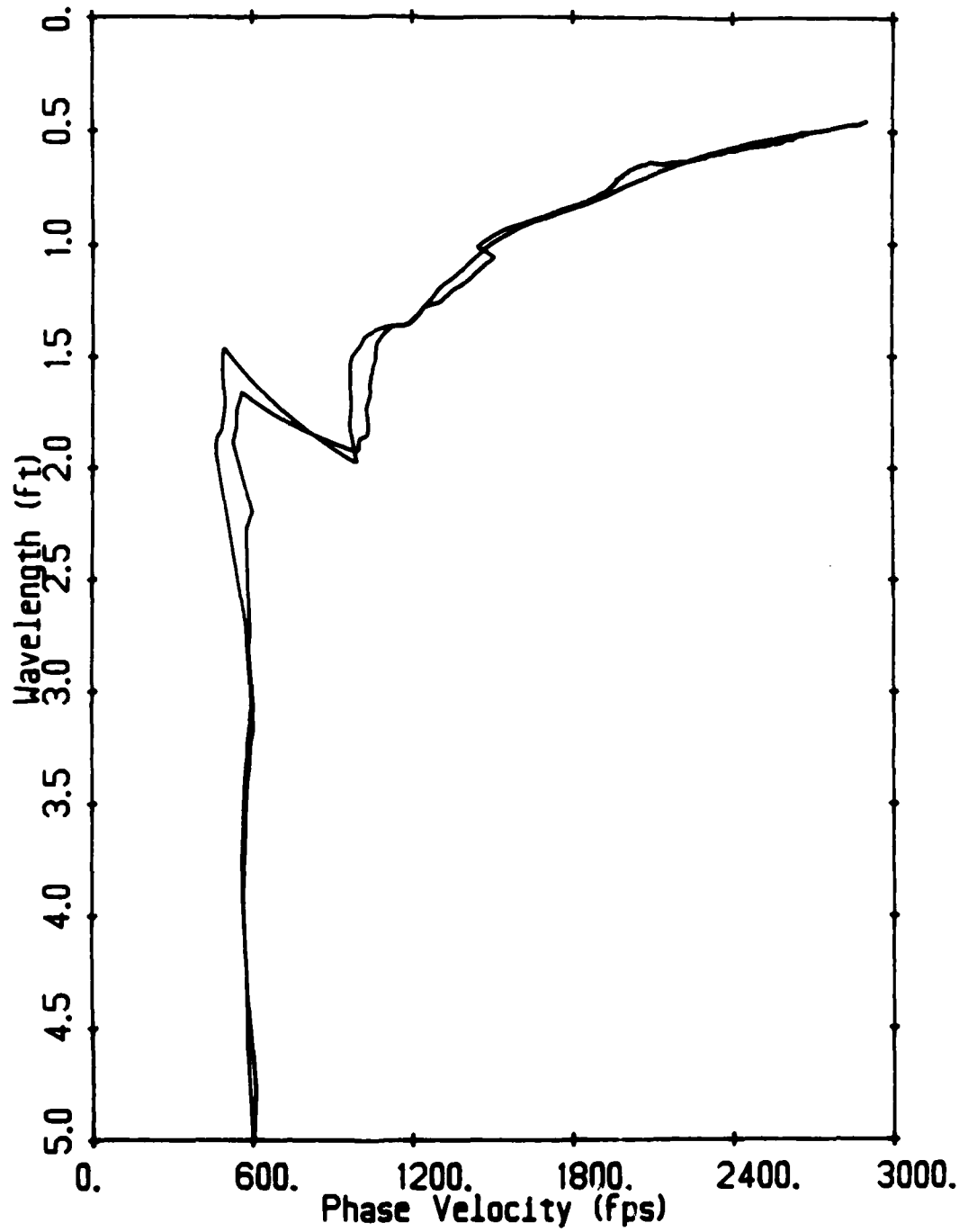


Figure G.12— Average Experimental Dispersion Curve for 40 oz Hammer for SEMTA Parking Lot Site (0 to 5-ft wavelengths)

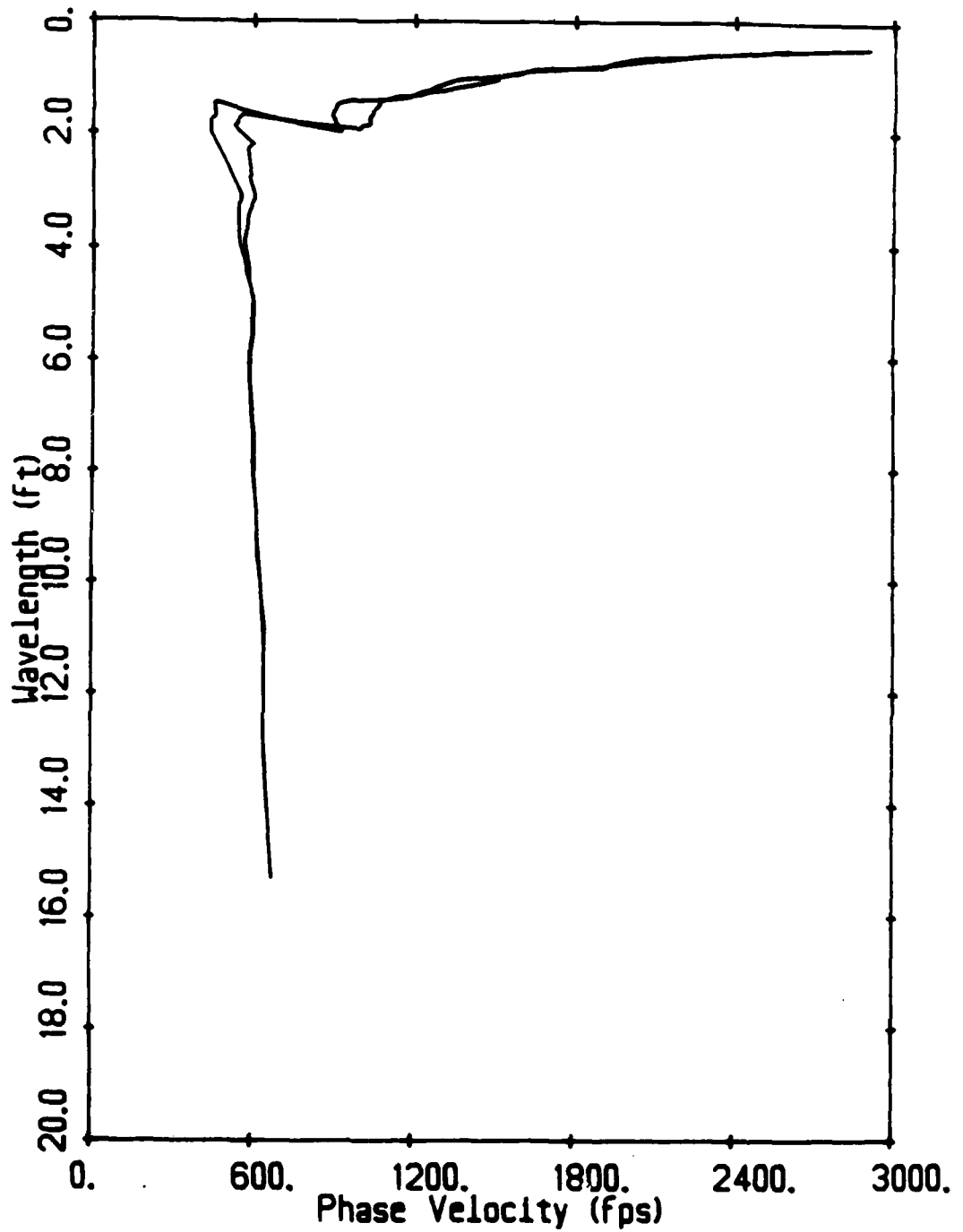


Figure G.13— Average Experimental Dispersion Curve for 128 os Hammer for SEMTA Parking Lot Site (all wavelengths)

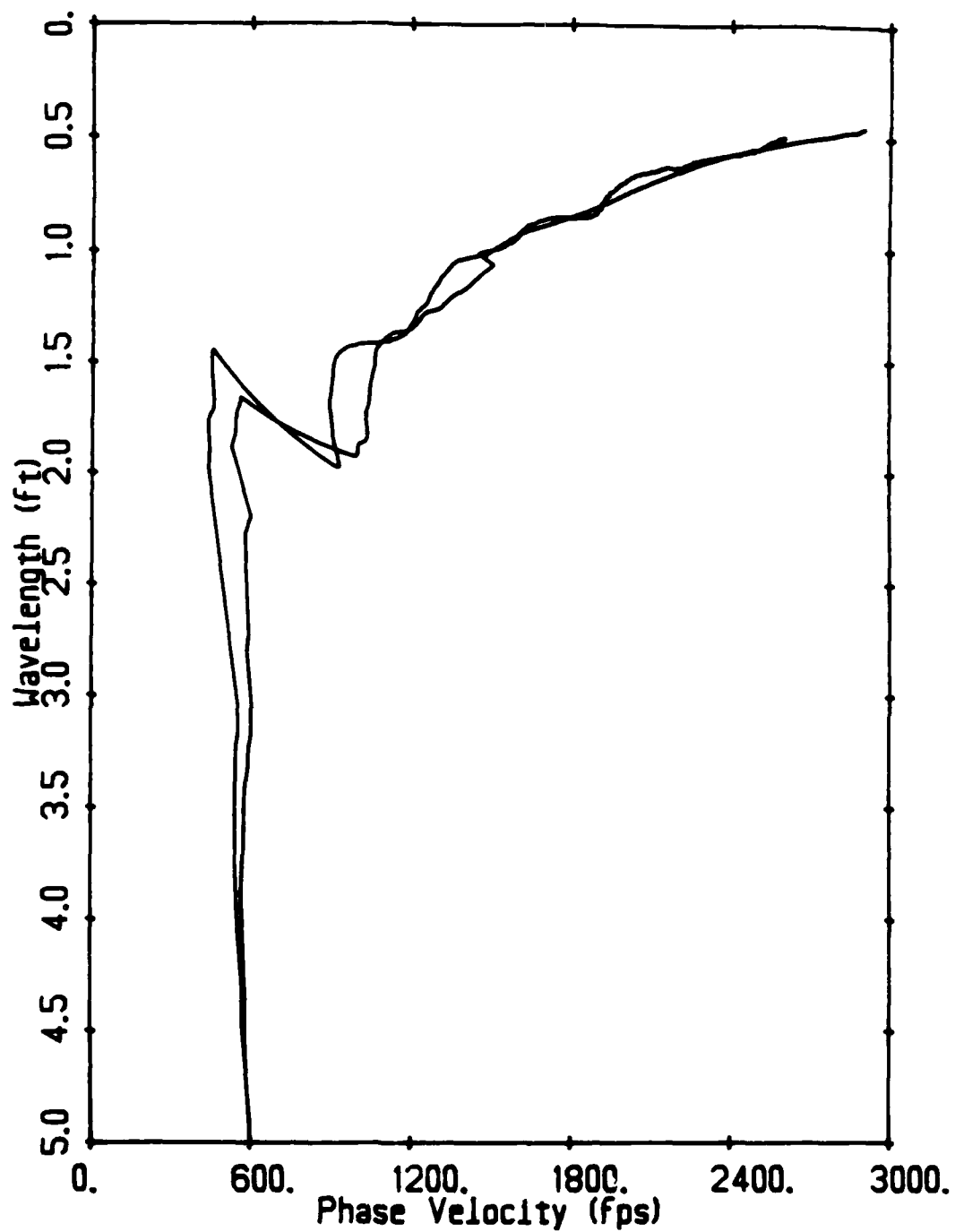


Figure G.14— Average Experimental Dispersion Curve for 128 oz Hammer for SEMTA Parking Lot Site (0 to 5-ft wavelengths)

REFERENCES

REFERENCES

- Aki, K. and Richards, P. G. (1980), *Quantitative Seismology: Theory and Methods*, W. H. Freeman and Company, San Francisco, California, Vol. I and II, 932 pp.
- Allen, D. L. and Deen, R. C. (1980), "Modulus and Damping of Asphaltic Concrete Using the Resonant Column," *Geotechnical Testing Journal*, ASTM, Vol. 3, No. 4, December, pp. 167-171.
- Ballard, R. F., Jr. (1964), "Determination of Soil Shear Moduli at Depths by In-Situ Vibratory Techniques," *Miscellaneous Paper No. 4-691*, U.S. Army Engineer Waterways Experiment Station, Vicksburg, Mississippi, December.
- Ballard, R. F., Jr. and Casagrande, D. R. (1966), "Dynamic Foundation Investigation, Roi-Namur, Kwajalein Atoll, Marshall Islands," *Miscellaneous Paper No. 4-858*, U.S. Army Engineer Waterways Experiment Station, Vicksburg, Mississippi, November.
- Ballard, R. F., Jr. and Casagrande, D. R. (1967), "Dynamic Foundation Investigations, TAA-2R Radar Site, Cape Kennedy, Florida," *Miscellaneous Paper No. 4-878*, U.S. Army Engineer Waterways Experiment Station, Vicksburg, Mississippi, February.
- Ballard, R. F., Jr. and McLean, F. G. (1975), "Seismic Field Methods for In Situ Moduli," *Proc. of the Conf. on In Situ Measurement of Soil Properties*, ASCE, Raleigh, North Carolina, Vol. 1, June 1-4, pp. 121-150.
- Bendat, J. S. and Piersol, A. G. (1971), *Random Data: Analysis and Measurement Procedures*, John Wiley & Sons, Inc., New York, 407 pp.
- Bendat, J. S. and Piersol, A. G. (1980), *Engineering Applications of Correlation and Spectral Analysis*, John Wiley & Sons, Inc., New York, 302 pp.
- Borm, G. W. (1977), "Methods from Exploration Seismology: Reflection, Refraction and Borehole Prospecting," *Proceedings of Dynamical Methods in Soil and Rock Mechanics*, Institute of Soil and Rock Mechanics, Karlsruhe, Germany, Vol. 3, September 5-16, pp. 87-114.
- Brown, D., Carbon, G., and Ramsey, K., (1977), "Survey of Excitation Techniques Applicable to the Testing of Automotive Structures," *Publication No. 770029*, Society of Automotive Engineers, Warrendale, Pennsylvania, 15 pp.
- Bruel & Kjaer Instruments, Inc. (1985), *Digital Signal Analysis Using Digital Filters and FFT Techniques*, January, 321 pp.
- Bush, A. J. III (1980), "Nondestructive Testing for Light Aircraft Pavements: Phase II, Development of the Nondestructive Evaluation," *Report No. FAA-RD-80-9-II*, Federal Aviation Administration, Washington, D. C., November.
- Bush, A. J. III and Alexander, D. R. (1985), "Pavement Evaluation Using Deflection Basin Measurements and Layered Theory," *Research Record No. 1022*, Transportation Research Board, Washington, D. C., pp. 16-25.

- Carpenter, T. (1985), Personal communication.
- Cragg, R. and Pell, P. S. (1971), "The Dynamic Stiffness of Bituminous Road Materials," *Proceedings of the Association of Asphalt Paving Technologists*, Vol. 40, pp. 126-147.
- Davies, T. G. and Mamlouk, M. S. (1985), "Theoretical Response of Multilayer Pavement Systems to Dynamic Non-Destructive Testing," *Research Record No. 1022, Transportation Research Board, Washington, D. C.*, pp. 1-7.
- Drnevich, V. P. (1986), Personal communication.
- Drnevich, V. P., Kim, S.-I., Alexander, D. R., and Kohn, S. (1985), "Spectral Analysis of Surface Waves in Pavement Systems with Random Noise Excitation," *Expanded Abstracts with Biographies. 55th Annual International Society of Exploration Geophysicists Meeting, Washington, D. C., October 6-10*, pp. 143-145.
- Eller, E. E. and Conrad, R. W. (1976), "Introduction to Shock and Vibration Measurements," Chapter 12 in *Shock and Vibration Handbook*, Edited by C. M. Harris and C. E. Crede, 2nd ed., McGraw-Hill Book Company, New York.
- Ewing, W. M., Jardetzky, W. S., and Press, F. (1957), *Elastic Waves in Layered Media*, McGraw-Hill Book Company, New York, 380 pp.
- Grant, F. S. and West, G. F. (1965), *Interpretation Theory in Applied Geophysics*, McGraw-Hill Book Company, New York, 584 pp.
- Guericke, R. and Weinert, F. (1972), "The Behavior of Bituminous Mixtures in Laboratory Tests and Under Road Conditions," *Proceedings of the Third International Conference on the Structural Design of Asphalt Pavements, London, England, September 11-15*, pp. 233-246.
- Halvorsen, W. G. and Brown, D. L. (1977), "Impulse Technique for Structural Frequency Response Testing," *Sound and Vibration, Acoustical Publications, Inc., Bay Village, Ohio*, Vol. 11, No. 11, November, pp. 8-21.
- Hardin, B. O. and Black, W. L. (1968), "Vibration Modulus of Normally Consolidated Clay," *Journal of the Soil Mechanics and Foundations Division, ASCE*, Vol. 94, No. SM2, March, pp. 353-369.
- Hardin, B. O. and Drnevich, V. P. (1972), "Shear Modulus and Damping in Soils: Measurement and Parameter Effects," *Journal of the Soil Mechanics and Foundations Division, ASCE*, Vol. 98, No. SM6, June, pp. 603-624.
- Haakell, N. A. (1953), "The Dispersion of Surface Waves on Multilayered Media," *Bulletin of the Seismological Society of America*, Vol. 43, No. 1, January, pp. 17-34.
- Heisey, J. S., Stokoe, K. H. II, Hudson, W. R., and Meyer, A. H. (1982), "Determination of In Situ Shear Wave Velocities from Spectral Analysis of Surface Waves," *Research Report No. 256-2, Center for Transportation Research, The University of Texas at Austin, December*, 277 pp.
- Heisey, J. S., Stokoe, K. H. II, and Meyer, A. H. (1982), "Moduli of Pavement Systems From Spectral Analysis of Surface Waves," *Research Record No. 852, Transportation Research Board*, pp. 22-31.

- Heukelom, W. and Foster, C. R. (1960), "Dynamic Testing of Pavements," *Journal of the Soil Mechanics and Foundations Division, ASCE*, Vol. 86, No. SM1, February, pp. 1-28.
- Hewlett Packard Company (1977), "Digital Signal Analysis: Time and Frequency Domain Measurements," Application Note 240-0, August, 15 pp.
- Hewlett Packard Company (1985), "The Fundamentals of Signal Analysis," Application Note 243, Hewlett Packard Company, February, 57 pp.
- Hoar, R. J. (1982), "Field Measurement of Seismic Wave Velocity and Attenuation for Dynamic Analyses," Ph.D. Dissertation, The University of Texas at Austin, May, 478 pp.
- Jones, R. (1958), "In-Situ Measurement of the Dynamic Properties of Soil by Vibration Methods," *Geotechnique*, Vol. 8, No. 1, March, pp. 1-21.
- Jones, R. (1962), "Surface Wave Technique for Measuring the Elastic Properties and Thickness of Roads: Theoretical Development," *British Journal of Applied Physics*, Vol. 13, No. 1, January, pp. 21-29.
- Kallas, B. F. and Riley, J. C. (1967), "Mechanical Properties of Asphalt Pavement Materials," Proceedings of the Second International Conference on the Structural Design of Asphalt Pavements, University of Michigan, Ann Arbor, Michigan, August 7-11, pp. 931-952.
- Ludeling, R. (1977), "Shear Wave Measurements Using the Seismic Up-Hole Method," Proceedings of Dynamical Methods in Soil and Rock Mechanics, Institute of Soil and Rock Mechanics, Karlsruhe, Germany, Vol. 3, September 5-16, pp. 139-148.
- Lysmer, J. (1966), Personal communication with F. E. Richart, Jr., Cited in F. E. Richart, Jr., J. R. Hall, Jr., and R. D. Woods (1970), *Vibrations of Soils and Foundations*, Prentice-Hall, Inc., Englewood Cliffs, New Jersey, p. 91.
- Lytton, R. L., Moore, W. M., and Mahoney, J. P. (1975), "Pavement Evaluation: Phase I. Pavement Evaluation Equipment," Report No. FHWA-RD-75-78, Federal Highway Administration, 254 pp.
- Mamlouk, M. S. (1985), "Use of Dynamic Analysis in Predicting Field Multilayer Pavement Moduli," Research Record No. 1043, Transportation Research Board, Washington, D. C., pp. 113-119.
- Maxwell, A. A. and Fry, Z. B. (1967), "A Procedure for Determining Elastic Moduli of In Situ Soils by Dynamic Techniques," Proceedings of the International Symposium on Wave Propagation and Dynamic Properties of Earth Materials, University of New Mexico Press, Albuquerque, New Mexico, August 23-25, pp. 913-919.
- Miller, G. F. and Pursey, H. (1955), "On the Partition of Energy Between Elastic Waves in a Semi-Infinite Solid," Proceedings of the Royal Society, A, Vol. 233, pp. 55-69.
- Monismith, C. L. and Finn, F. N. (1984), "Overlay Design—A Synthesis of Methods," Proceedings of the Association of Asphalt Paving Technologists, Vol. 53, pp. 217-266.
- Moore, W. M., Hanson, D. I., and Hall, J. W., Jr. (1978), "An Introduction to Nondestructive Structural Evaluation of Pavements," Circular No. 189, Transportation Research Board, Washington, D. C., January.

- Nazarian, S. (1984), "In Situ Determination of Elastic Moduli of Soil Deposits and Pavement Systems by Spectral-Analysis-of-Surface-Waves Method," Ph.D. Dissertation, The University of Texas at Austin, 453 pp.
- Nazarian, S. and Stokoe, K. H. II (1983), "Evaluation of Moduli and Thicknesses of Pavement Systems by Spectral-Analysis-of-Surface-Waves Method," Research Report No. 256-4, Center for Transportation Research, The University of Texas at Austin, December, 123 pp.
- Nazarian, S. and Stokoe, K. H. II (1984), "Nondestructive Testing of Pavements Using Surface Waves," Research Record No. 993, Transportation Research Board, pp. 67-79.
- Nazarian, S. and Stokoe, K. H. II (1986), "Use of Surface Waves in Pavement Evaluation," Research Record No. 1070, Transportation Research Board, Washington, D. C., pp. 132-144.
- Nazarian, S., Stokoe, K. H. II, and Hudson, W. R. (1983), "Use of Spectral Analysis of Surface Waves Method for Determination of Moduli and Thicknesses of Pavement Systems," Research Record No. 930, Transportation Research Board, Washington, D. C., pp. 38-45.
- Patel, N. S. (1981), "Generation and Attenuation of Seismic Waves in Downhole Testing," Masters thesis, The University of Texas at Austin, May, 411 pp.
- Pell, P. S. and Brown, S. F. (1972), "The Characteristics of Materials for the Design of Flexible Pavement Structures," Proceedings of the Third International Conference on the Structural Design of Asphalt Pavements, London, England, September 11-15, pp. 326-342.
- Ramirez, R. W. (1985), *The FFT: Fundamentals and Concepts*, Prentice-Hall, Inc., Englewood Cliffs, New Jersey, 178 pp.
- Ramsey, K. A. (1976), "Effective Measurements for Structural Dynamics Testing," Sound and Vibration, Acoustical Publications, Inc., Bay Village, Ohio, Vol. 10, No. 4, April, pp. 18-31.
- Randall, R. B. (1977), *Application of B & K Equipment to Frequency Analysis*, 2nd ed. Bruel & Kjaer Instruments, Inc., Naerum, Denmark, September, 239 pp.
- Richart, F. E., Jr. (1977), "Field and Laboratory Measurements of Dynamic Soil Properties," Proceedings of Dynamical Methods in Soil and Rock Mechanics, Institute of Soil and Rock Mechanics, Karlsruhe, Germany, Vol. 1, September 5-16, pp. 3-36.
- Richart, F. E., Jr., Hall, J. R., Jr., and Woods, R. D. (1970), *Vibrations of Soils and Foundations*, Prentice-Hall, Inc., Englewood Cliffs, New Jersey, 414 pp.
- Rockland Systems Corporation (1977), "Spectrum Analysis—Theory, Implementation, and Applications," West Nyack, New York, 45 pp.
- Roesset, J. M. and Shao, K. (1985), "Dynamic Interpretation of Dynaflect and Falling Weight Deflectometer Tests," Research Record No. 1022, Transportation Research Board, Washington, D. C., pp. 7-16.

- Sanchez-Salineró, I., Roesset, J. M., Shao, K. Y., Stokoe, K. H. II, and Rix, G. J. (1987), "Analytical Evaluation of Variables Affecting Surface Wave Testing of Pavements," Paper Presented to Annual Meeting, Transportation Research Board, Washington, D. C., January.
- Shook, J. F. and Kallas, B. F. (1969), "Factors Influencing Dynamic Modulus of Asphalt Concrete," Proceedings of the Association of Asphalt Paving Technologists, Vol. 38, pp. 140-178.
- Sousa, J. B. and Monismith, C. L. (1987), "Dynamic Response of Paving Materials," Paper Presented to Annual Meeting," Transportation Research Board, Washington, D. C., January.
- Stokoe, K. H. II and Hoar, R. J. (1978), "Variables Affecting In Situ Seismic Measurements," Proceedings of the Earthquake Engineering and Soil Dynamics Conference, ASCE, Pasadena, California, Vol. II, June 19-21, pp. 919-938.
- Stokoe, K. H. II and Nazarian, S. (1983), "Effectiveness of Ground Improvement from Spectral Analysis of Surface Waves," Proceedings of the Eighth European Conference on Soil Mechanics and Foundation Engineering, Helsinki, Finland, May.
- Stokoe, K. H. II and Nazarian, S. (1985), "Use of Rayleigh Waves in Liquefaction Studies," Measurement and Use of Shear Wave Velocity for Evaluating Dynamic Soil Properties, Proceedings of a Geotechnical Engineering Division Session at ASCE Convention, Denver, Colorado, May 1, pp. 1-17.
- Stokoe, K. H. II and Woods, R. D. (1972), "In Situ Shear Wave Velocity by Cross-Hole Method," Journal of the Soil Mechanics and Foundations Division, ASCE, Vol. 98, No. SM5, May, pp. 443-460.
- Szendrei, M. E. and Freeme, C. R. (1970), "Road Responses to Vibration Tests," Journal of the Soil Mechanics and Foundations Division, ASCE, Vol. 96, No. SM6, November, pp. 2099-2124.
- Thomson, W. T. (1950), "Transmission of Elastic Waves Through a Stratified Soil Medium," Journal of Applied Physics, Vol. 21, No. 2, February, pp. 89-93.
- Thornhill, J. and Smith, C. C. (1980), *Fourier and Spectral Analysis: A Short Course*, IBM, Austin, Texas.
- Thrower, E. N. (1965), "The Computation of the Dispersion of Elastic Waves in Layered Media," Journal of Sound and Vibration, Academic Press, London, England, Vol. 2, No. 3, July, pp. 210-226.
- Troxell, G. E., Davis, H. E., and Kelly, J. W. (1968), *Composition and Properties of Concrete*, 2nd ed., McGraw-Hill Book Company, New York, 529 pp.
- Woods, R. D. (1978), "Measurement of Dynamic Soil Properties," Proceedings of the Earthquake Engineering and Soil Dynamics Conference, ASCE, Pasadena, California, Vol. I, June 19-21, pp. 91-178.
- Woods, R. D. (1986), "In Situ Tests for Foundation Vibrations," Use of In Situ Tests in Geotechnical Engineering, Geotechnical Special Publication No. 6, Proceedings of an ASCE Geotechnical Engineering Division Specialty Conference, Virginia Tech, Blacksburg, Virginia, June 23-25, pp. 336-375.